

VOLUME 75    FEBRUARY 18, 1971    NUMBER 4

JPCA<sub>x</sub>

---

THE JOURNAL OF

PHYSICAL  
CHEMISTRY

---

PUBLISHED BIWEEKLY BY THE AMERICAN CHEMICAL SOCIETY

# Keep pace with the new...

through these basic research journals of the American Chemical Society

## The Journal of the American Chemical Society

The premier American chemistry journal publishing original research papers in every field. Biweekly.

*ACS members: U.S. \$22.00	Canada, PUAS \$26.50	Other nations \$27.50
Nonmembers: U.S. \$44.00	Canada, PUAS \$48.50	Other nations \$49.50

## The Journal of Organic Chemistry

Embraces the field, from synthesis to structure to behavior. Biweekly publication.

*ACS members: U.S. \$20.00	Canada, PUAS \$24.50	Other nations \$25.50
Nonmembers: U.S. \$40.00	Canada, PUAS \$44.50	Other nations \$45.50

## The Journal of Physical Chemistry

Maintains a balance between classical areas of chemistry and modern structural quantum oriented areas. Biweekly.

*ACS members: U.S. \$20.00	Canada, PUAS \$24.00	Other nations \$25.00
Nonmembers: U.S. \$40.00	Canada, PUAS \$44.00	Other nations \$45.00

## Biochemistry

Covers enzymes, proteins, carbohydrates, lipids, nucleic acids and their metabolism, genetics, biosynthesis. Biweekly.

*ACS members: U.S. \$20.00	Canada, PUAS \$23.00	Other nations \$23.50
Nonmembers: U.S. \$40.00	Canada, PUAS \$43.00	Other nations \$43.50

## The Journal of Agricultural and Food Chemistry

Places special emphasis on the chemical aspects of agricultural and food chemistry. Bimonthly.

*ACS members: U.S. \$10.00	Canada, PUAS \$13.00	Other nations \$13.50
Nonmembers: U.S. \$20.00	Canada, PUAS \$23.00	Other nations \$23.50

## The Journal of Medicinal Chemistry

Emphasis is on synthesis, mode of action and pharmacology of medicinal agents. Monthly.

*ACS members: U.S. \$15.00	Canada, PUAS \$18.00	Other nations \$18.50
Nonmembers: U.S. \$30.00	Canada, PUAS \$33.00	Other nations \$33.50

## The Journal of Chemical and Engineering Data

Quarterly journal presenting data on properties and behavior of both new and known chemical systems.

*ACS members: U.S. \$15.00	Canada, PUAS \$18.00	Other nations \$18.50
Nonmembers: U.S. \$30.00	Canada, PUAS \$33.00	Other nations \$33.50

## Inorganic Chemistry

Publishes original research, both experimental and theoretical, in all phases of inorganic chemistry.

*ACS members: U.S. \$18.00	Canada, PUAS \$21.00	Other nations \$21.50
Nonmembers: U.S. \$36.00	Canada, PUAS \$39.00	Other nations \$39.50

## Macromolecules

Presents original research on all fundamental aspects of polymer chemistry. Bimonthly publication.

*ACS members: U.S. \$12.00	Canada, PUAS \$15.00	Other nations \$15.50
Nonmembers: U.S. \$24.00	Canada, PUAS \$27.00	Other nations \$27.50

American Chemical Society / 1155 Sixteenth Street, N.W., Washington, D.C. 20036

Please enter a one year subscription for the following journals:

1 _____	2 _____	3 _____
4 _____	5 _____	6 _____
7 _____	8 _____	9 _____
name _____	position _____	
address _____		
city _____	state/country _____	zip _____
your company _____	nature of company's business _____	

I am an ACS member     I am not an ACS member     Bill me for \$ \_\_\_\_\_

Payment enclosed (*payable to American Chemical Society*) in the amount of \$ \_\_\_\_\_. Payment must be made in U.S. currency, by international money order, UNESCO coupons, or U.S. bank draft; or order through your book dealer.

\* NOTE: Subscriptions at ACS member rates are for personal use only.

# THE JOURNAL OF PHYSICAL CHEMISTRY

---

**BRYCE CRAWFORD, Jr.**, *Editor*

STEPHEN PRAGER, *Associate Editor*

ROBERT W. CARR, Jr., FREDERIC A. VAN CATLEDGE, *Assistant Editors*

**EDITORIAL BOARD:** A. O. ALLEN (1970-1974), R. BERSOHN (1967-1971), J. R. BOLTON (1971-1975), S. BRUNAUER (1967-1971), M. FIXMAN (1970-1974), H. S. FRANK (1970-1974), J. R. HUIZENGA (1969-1973), M. KASHA (1967-1971), W. J. KAUZMANN (1969-1973), W. R. KRIGBAUM (1969-1973), R. A. MARCUS (1968-1972), W. J. MOORE (1969-1973), J. A. POPLE (1971-1975), B. S. RABINOVITCH (1971-1975), H. REISS (1970-1974), S. A. RICE (1969-1975), R. E. RICHARDS (1967-1971), F. S. ROWLAND (1968-1972), R. L. SCOTT (1968-1972), R. SEIFERT (1968-1972)

---

CHARLES R. BERTSCH, *Manager, Editorial Production*

---

AMERICAN CHEMICAL SOCIETY, PUBLICATIONS DIVISION,  
1155 Sixteenth St., N.W., Washington, D. C. 20036

RICHARD L. KENYON, *Director*

JOSEPH H. KUNEY, *Director of Business Operations and Director of Publications Research*

DAVID E. GUSHEE, *Publication Manager, Journals*

©Copyright, 1971, by the American Chemical Society. Published biweekly by the American Chemical Society at 20th and Northampton Sts., Easton, Pa. 18042. Second-class postage paid at Easton, Pa.

All manuscripts should be sent to *The Journal of Physical Chemistry*, Department of Chemistry, University of Minnesota, Minneapolis, Minn. 55455.

*Additions and Corrections* are published once yearly in the final issue. See Volume 74, Number 26 for the proper form.

*Extensive or unusual alterations in an article after it has been set in type are made at the author's expense*, and it is understood that by requesting such alterations the author agrees to defray the cost thereof.

The American Chemical Society and the Editor of *The Journal of Physical Chemistry* assume no responsibility for the statements and opinions advanced by contributors.

Correspondence regarding accepted copy, proofs, and reprints should be directed to Editorial Production Office, American Chemical Society, 20th and Northampton Sts., Easton, Pa. 18042. Manager: CHARLES R. BERTSCH. Assistant Editor: EDWARD A. BORGER. Editorial Assistant: EVELYN J. UHLER.

Advertising Office: Century Communications Corporation, 142 East Avenue, Norwalk, Conn. 06851.

#### **Business and Subscription Information**

Remittances and orders for subscriptions and for single copies,

notices of changes of address and new professional connections, and claims for missing numbers should be sent to the Subscription Service Department, American Chemical Society, 1155 Sixteenth St., N.W., Washington, D. C. 20036. Allow 4 weeks for changes of address. Please include an old address label with the notification.

Claims for missing numbers will not be allowed (1) if received more than sixty days from date of issue, (2) if loss was due to failure of notice of change of address to be received before the date specified in the preceding paragraph, or (3) if the reason for the claim is "missing from files."

Subscription rates (1971): members of the American Chemical Society, \$20.00 for 1 year; to nonmembers, \$40.00 for 1 year. Those interested in becoming members should write to the Admissions Department, American Chemical Society, 1155 Sixteenth St., N.W., Washington, D. C. 20036. Postage to Canada and countries in the Pan-American Union, \$4.00; all other countries, \$5.00. Single copies for current year: \$2.00. Rates for back issues from Volume 56 to date are available from the Special Issues Sales Department, 1155 Sixteenth St., N.W., Washington, D. C. 20036.

This publication and the other ACS periodical publications are now available on microfilm. For information write to: MICROFILM, Special Issues Sales Department, 1155 Sixteenth St., N.W., Washington, D. C. 20036.

# The Range of Research in Physical And So Is the List of Books

## REACTIONS UNDER PLASMA CONDITIONS Volume I

Edited by MUNDIYATH VENUGOPALAN,  
*Western Illinois University*

This is the first part of an important new two-volume survey of the fundamental physical theories and properties of matter in the plasma state. Volume I emphasizes plasma physics and plasma diagnostics, making it particularly valuable to physicists. The volumes deal with the types of reactions that can be achieved in a plasma medium—with special emphasis on the reaction-kinetical process—and the practical methods that can be applied for their investigation in both natural and laboratory physics.

1971 In press

## PHYSICAL CHEMISTRY OF ADHESION

By D. H. KAELBLE, *North American Rockwell Corporation*

This book treats the fields of thermodynamics, surface chemistry, polymer physics, rheology, and specialized topics in the mechanics of fracture. The book is intended to introduce, develop, and interconnect these outwardly unrelated subjects in relation to adhesion and cohesion, and to familiarize the chemist and physicist with the basic concepts and theories in these fields. The author has included historical discussions to acquaint the reader with classical viewpoints, and introduces new theoretical propositions and derivations.

1971 528 pages In press

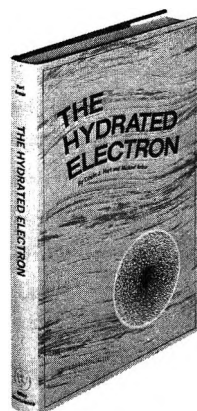
## MOLECULAR PHOTOELECTRON SPECTROSCOPY

### A Handbook of the He584 Spectra

By D. W. TURNER, *University of Oxford, England*; C. BAKER, *B. P. Chemicals, Surrey, England*; A. D. BAKER, *Swansea University, England*; and C. R. BRUNDLE, *Bell Telephone Laboratories, New Jersey*

A convenient reference book for researchers, this is essentially an account of the work done by a pioneering group of workers in the field of photoelectron spectroscopy. In the basic format of a handbook, it presents over 300 D.E. spectra using the Helium Resonance Line. It gives a general account of the underlying physical nature of the processes involved and of the experimental techniques developed by the authors in the course of their work. This volume is the first extensive compilation of the photoelectron spectra of gaseous molecules ranging from atoms and diatomic molecules through complex organic and inorganic systems.

1970 386 pages \$19.50



## THE HYDRATED ELECTRON

By EDWIN J. HART, *Argonne National Laboratory*; and MICHAEL ANBAR, *Stanford Research Institute*

“Discovered by radiation chemists within the last decade, the hydrated electron ranks with the hydrogen and hydroxide ions as fundamental species of aqueous solutions. . . .”

—from the Preface

Devoted to the present and potential importance of the hydrated electron, this monograph concentrates on its physical and chemical characteristics. It also reviews the peripheral topics of radiation chemistry, solvated electrons, and pulse radiolysis. With comprehensive coverage of this new field, the book will be an indispensable aid to researchers working in this or related fields. 1970 267 pages \$12.95

## SURFACE AND COLLOID SCIENCE

### Volume 3

Edited by EGON MATIJEVIĆ, *Clarkson College of Technology*

“On the whole, these volumes comprise a good beginning for the fulfillment of the editors’ aim of providing a comprehensive treatise on surface and colloid science. It is hoped that future volumes will continue to maintain the standards set here. . . .”—from a review of Volumes 1 and 2 in *Science*

Volume 3, the most recent volume in this series, continues the high standards and comprehensive coverage of its predecessors. Since the field of surface and colloid science covers a wide range of topics, the articles include many interdisciplinary aspects of physics, chemistry, biology, and engineering. 1971 320 pages \$16.95

## CHEMICAL AND MECHANICAL BEHAVIOR OF INORGANIC MATERIALS

Edited by ALAN W. SEARCY, *University of California, Berkeley*; DAVID V. RAGONE, *Carnegie-Mellon University*; and UMBERTO COLOMBO, *Montecatini Edison Company, Novara, Italy*

Of value to all workers in the fields of materials science, this is a comprehensive review of the present status of many specialty fields in this research area. The articles cover such topics as the evaporation of inorganic materials, thermodynamics and kinetics, dislocations and fracture, and the kinetics of densification. The papers comprising the book come from the two-week advanced course on ceramic science presented at the first International Conference on Materials Science, sponsored by *Accademia Nazionale del Lincei*, at Tremezzo, Italy, in 1968.

1970 715 pages \$27.50

# Chemistry Is Rapidly Expanding. We Have to Help Researchers.

## ABSOLUTE CONFIGURATION OF METAL COMPLEXES

By CLIFFORD J. HAWKINS,  
*University of Queensland, Australia*

*A volume in the series, Interscience Monographs on Chemistry, Inorganic Chemistry Section, edited by F. Albert Cotton and G. Wilkinson*

This is the first in-depth application of conformational analysis to the structure of coordination compounds. The author discusses various methods for the determination of the absolute configuration of metal complexes, using circular dichroism, nuclear magnetic resonance spectroscopy, and x-ray crystallography. Geometric isomers are important preliminaries to many absolute configuration studies, and because of this the methods used to differentiate geometric isomers are also briefly reviewed.

1971 368 pages \$19.50

## FITTING EQUATIONS TO DATA

### Computer Analysis of Multifactor Data for Scientists and Engineers

By CUTHBERT DANIEL, *Consultant*, and FRED S. WOOD, *American Oil Company*

With the assistance of John W. Gorman and Robert J. Toman.

This manual was designed to show the scientist and engineer some new ways of interpreting multifactor data. The authors have arranged their material to help the data analyst recognize the strengths and limitations of his data, test the assumptions implicit in the least-squares methods used, select appropriate forms of the variables, judge which combinations of variables are most influential, and state the conditions under which the fitted equations are applicable. Two computer programs (for linear and non-linear equations) implement the new methods proposed in addition to using standard least squares.

1971 304 pages \$12.95 (tent.)

## TRANSFER AND STORAGE OF ENERGY BY MOLECULES

### Volume 3, Rotational Energy

Edited by GEORGE M. BURNETT, *University of Aberdeen*, and ALASTAIR M. NORTH, *University of Strathclyde, Glasgow*

"... useful both as a compendium of current knowledge and as providing... a spur to the imaginative theorists and experimentalists who will make possible the much-needed major conceptual advances."—from a review of Volume 1 in *Science*

This is the third in this highly specialized and comprehensive five-volume set. Each of the volumes concentrates on a particular aspect of the subject, and this most recent addition covers the significance of molecular rotation in a variety of apparently unrelated phenomena.

1971 324 pages \$16.50 (tent.)

## ORGANIC SOLVENTS

### Physical Properties and Methods of Purification Third Edition

By JOHN A. RIDDICK, *formerly of the Commercial Solvents Corporation*; and WILLIAM B. BUNGER, *Indiana State University*

*Volume 2 in the series, Techniques of Chemistry, edited by A. Weissberger*

The newest edition of this book covers the physical properties and methods of purification of more than 350 solvents. Up-dated and revised to cover recent data, it includes the criteria of purity, methods of preparation and purification, purity and toxicology of classes of compounds and of specific solvents.

1971 1072 pages \$24.95

## FUEL CELLS

### Modern Processes for the Electrochemical Production of Energy

By WOLF VIELSTICH, *Institut für Physikalische Chemie der Universität Bonn, Germany*. Translated by D. J. G. Ives, *University of London, England*

This book charts the progress of research to the end of 1968 in the field of direct generation of electrical energy by electrochemical processes. The author starts with an explanatory introduction for the benefit of non-specialists, and then goes on to treat the largest field of research, the kinetics of electrode processes. The material is handled in such a way as to interest a wider group of electrochemists and physicists than those working directly on fuel cells.

1970 501 pages \$25.00

## VALENCE THEORY

### Second Edition

By J. N. MURRELL, *University of Sussex, England*; S. F. A. KETTLE, *University of Sheffield, England*; and J. M. TEDDER, *University of St. Andrews, Scotland*

As in its earlier edition, this second edition of *Valence Theory* deals with the main aspects of quantum chemistry as applied to valency, filling the gap between elementary and advanced texts. Much of the material has been revised, to be consistent with and to reflect recent advances. The authors have also added material on numerical problems encountered in a non-empirical SCFMO calculation, and have described the method of calculating overlap integrals.

1970 428 pages \$9.75

Prices subject to change without notice.

**wiley**

WILEY-INTERSCIENCE  
a division of JOHN WILEY & SONS, Inc.  
605 Third Avenue,  
New York, N.Y. 10016  
In Canada:  
22 Worcester Road, Rexdale, Ontario

You Are Cordially Invited  
 To Become  
 A Charter Subscriber  
 To The American Chemical Society's  
 Newest Publication  
**CHEMICAL TECHNOLOGY**

Cutting across all disciplines, the new monthly publication CHEMICAL TECHNOLOGY is written expressly for those charged with industrial innovation. Chemists and chemical engineers in industry will welcome its pragmatic approach.

Designed to be a highly readable, current awareness magazine, CHEMICAL TECHNOLOGY is a valuable addition to existing ACS publications.

Its articles range over areas of immediate interest, while monthly features deal with many facets of industrial life through interviews, articles, stories and anecdotes.

To start CHEMICAL TECHNOLOGY on its way to you, just complete and return the form at the right. You'll get a new outlook on the world of industrial chemistry.

American Chemical Society  
 1155-16th Street, N.W., Washington, D.C. 20036  
 Please start my one-year subscription to CHEMICAL TECHNOLOGY at the rate I have checked below.

Nonmember    U.S.    Canada, PUAS    Other Nations  
 Rate:     \$18.00     \$20.50     \$21.50

All ACS members have the opportunity, through June 1971, to examine copies of CHEMICAL TECHNOLOGY on a complimentary basis.

Name \_\_\_\_\_

Position \_\_\_\_\_  
(Specify title, please)

Address:     Home  
                    Business \_\_\_\_\_

City \_\_\_\_\_

State/Country \_\_\_\_\_ Zip \_\_\_\_\_

Your employer \_\_\_\_\_

Nature of your                    Manufacturing  
 employer's business:     or processing     Other \_\_\_\_\_  
(Please indicate)

If manufacturer,  
 type of products produced \_\_\_\_\_

I2A

# THE JOURNAL OF PHYSICAL CHEMISTRY

Volume 75, Number 4 February 18, 1971

On the Rate Constants for Reaction of Hydrogen Atoms in Aqueous Solutions P. Neta, G. R. Holdren, and Robert H. Schuler	449
The Radiation Chemistry of Aqueous Solutions of $\text{CFCl}_3$ , $\text{CF}_2\text{Cl}_2$ , and $\text{CF}_3\text{Cl}$ Turgut I. Balkas, J. H. Fendler, and Robert H. Schuler	455
Origin of Complex Electron Spin Resonance Spectra of $\gamma$ -Irradiated Polycrystalline <i>n</i> -Alkyl Iodides with Even Number of Carbon Atoms per Molecule R. J. Eglund, P. J. Ogren, and J. E. Willard	467
Growth and Decay of Alkyl Radicals in $\gamma$ -Irradiated Alkyl Iodides at 77°K H. W. Fenrick, N. B. Nazhat, P. J. Ogren, and J. E. Willard	472
Dissociative Electron Capture Process of Methyl Vinyl Ether in Organic Glasses Masahiro Irie, Koichiro Hayashi, Seizo Okamura, and Hiroshi Yoshida	476
Photoisomerization of Maleate Radical Anions Produced in 2-Methyltetrahydrofuran by $\gamma$ Irradiation at 77°K Ayako Torikai, Toshimi Suzuki, Tetsuo Miyazaki, Kenji Fueki, and Zen-ichiro Kuri	482
Butene Isomerization over Zinc Oxide A. L. Dent and R. J. Kokes	487
Catalytic Decomposition of Perchloric Acid Vapor on Zinc Oxide F. Solymosi and L. Gera	491
Solvent Effects on the Fluoroform Nuclear Magnetic Resonance Spectra William B. Smith and Arthur M. Ihrig	497
Structure of Nitroform in Various Solvents H. P. Marshall, F. G. Borgardt, Paul Noble, Jr., and N. S. Bhacca	499
Nuclear Magnetic Resonance Study of the Conformations of Valine and Phenylalanine Derivatives Richard A. Newmark and Max A. Miller	505
Correlation Times and Reorientation Activation Energies for Tetraalkylammonium Ions in Aqueous Solutions David W. Larsen	509
Spectroscopy of Rare Earth Oxide Molecules in Inert Matrices at 4°K Roger L. DeKock and William Weltner, Jr.	514
The Influence of Thermal Pretreatment on the Infrared Spectrum of Carbon Dioxide Adsorbed on Alumina N. D. Parkyns	526
Dielectric Absorption of Adsorbed Sulfur Dioxide in the Microwave Region Tsvia Ron and M. Folman	532
The Effect of the Emulsifying Agent on the Dielectric Properties of Water-in-Oil Emulsions I. D. Chapman	537
Molecular Association and the Dielectric Constant of Long-Chain Alkylammonium Salts in Benzene O. Levy, G. Markovits, and A. S. Kertes	542
Investigation of Micelle Structure by Fluorine Magnetic Resonance. IV. Fluorine-Labeled Nonionic Detergents Norbert Muller and Frank E. Platko	547
Electrochemical Behavior of Liquid Anion Membranes. Bionic Potentials with the $\text{NO}_3^-$ - $\text{Cl}^-$ , $\text{NO}_3^-$ - $\text{Br}^-$ , $\text{Br}^-$ - $\text{Cl}^-$ Couples P. R. Danesi, F. Salvemini, G. Scibona, and B. Scuppa	554
Electrochemical Investigations on the Spectral Sensitization of Gallium Phosphide Electrodes R. Memming and H. Tributsch	562
Kinetics of Copper(II)- and Copper(I)-Catalyzed Deuterium Exchange in Sulfuric and Perchloric Acid Solutions H. E. A. von Hahn and E. Peters	571

## NOTES

Photochemical Behavior of Isocyanides B. K. Dunning, D. H. Shaw, and H. O. Pritchard	580
Spectra and Cis-Trans Isomerism in Highly Bipolar Derivatives of Azobenzene G. Gabor and E. Fischer	581

On the Liquid Film Which Occurs in a Draining Vessel . . . . .	John A. Tallmadge	583
Dipolar Contributions to Carbon-13 Relaxation Times . . . . .	James R. Lyerla, Jr., David M. Grant, and Robin K. Harris	585
The Photochemistry of Solid Layers. Reaction Rates . . . . .	E. L. Simmons	588
Kinetics of Chemical Ionization. I. Reaction of <i>tert</i> -C <sub>4</sub> H <sub>9</sub> <sup>+</sup> with Benzyl Acetate . . . . .	S. Vredenberg, L. Wojcik, and J. H. Futrell	590
Spectrophotometric Study of the Equilibrium between Copper(I) Bromide, Copper(II) Bromide, and Bromine . . . . .	David L. Hilden and N. W. Gregory	592
Solvent Effect on Anthracene Monosulfonates in the First Excited State . . . . .	K. K. Rohatgi and B. P. Singh	595
Correlation between Translational and Rotational Relaxation Times for Ion Pairs in Solution . . . . .	Govind S. Darbari and Sergio Petrucci	598
Axial Coordination in the Vanadyl Ion . . . . .	Amos J. Leffler	599

#### COMMUNICATIONS TO THE EDITOR

Scavenging of the Molecular Hydrogen Yield from Water Irradiated with Tritium $\beta$ Particles . . . . .	A. Appleby and W. F. Gagnon	601
--	-----------------------------	-----

#### AUTHOR INDEX

Appleby, A., 601	Fischer, E., 581	Kertes, A. S., 542	Newmark, R. A., 505	Shaw, D. H., 580
Balkas, T. I., 455	Folman, M., 532	Kokes, R. J., 487	Noble, P., Jr., 499	Simmons, E. L., 588
Bhacca, N. S., 499	Fueki, K., 482	Kuri, Z., 482	Ogren, P. J., 467, 472	Singh, B. P., 595
Borgardt, F. G., 499	Futrell, J. H., 590	Larsen, D. W., 509	Okamura, S., 476	Smith, W. B., 497
Chapman, I. D., 537	Gabor, G., 581	Leffler, A. J., 599	Parkyns, N. D., 526	Solymosi, F., 491
Danesi, P. R., 554	Gagnon, W. F., 601	Levy, O., 542	Peters, E., 571	Suzuki, T., 482
Darbari, G. S., 598	Gera, L., 491	Lyerla, J. R., Jr., 585	Petrucci, S., 598	Tallmadge, J. A., 583
DeKock, R. L., 514	Grant, D. M., 585	Markovits, G., 542	Platko, F. E., 547	Torikai, A., 482
Dent, A. L., 487	Gregory, N. W., 592	Marshall, H. P., 499	Pritchard, H. O., 580	Tributsch, H., 562
Dunning, B. K., 580	Harris, R. K., 585	Memming, R., 562	Rohatgi, K. K., 595	von Hahn, H. E. A., 571
Egland, R. J., 467	Hayashi, K., 476	Miller, M. A., 505	Ron, T., 532	Vredenberg, S., 590
Fendler, J. H., 455	Hilden, D. L., 592	Miyazaki, T., 482	Salvemini, F., 554	Weltner, W., Jr., 514
Fenrick, H. W., 472	Holdren, G. R., 449	Muller, N., 547	Schuler, R. H., 449, 455	Willard, J. E., 467, 472
	Ihrig, A. M., 497	Nazhat, N. B., 472	Scibona, G., 554	Wojcik, L., 590
	Irie, M., 476	Neta, P., 449	Scuppa, B., 554	Yoshida, H., 476

## On the Rate Constants for Reaction of Hydrogen Atoms in

Aqueous Solutions<sup>1</sup>

by P. Neta, G. R. Holdren, and Robert H. Schuler\*

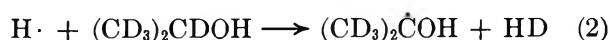
*Radiation Research Laboratories and Department of Chemistry, Mellon Institute of Science, Carnegie-Mellon University, Pittsburgh, Pennsylvania 15213 (Received October 16, 1970)**Publication costs assisted by the Carnegie-Mellon University and the U. S. Atomic Energy Commission*

The rates for the abstraction and addition reaction of the hydrogen atoms produced in the irradiation of aqueous solutions have been measured at pH 1 for 18 organic solutes. The rates were measured relative to the rate of formation of HD from deuterioisopropyl alcohol solutions in competitive experiments and put on an absolute scale by reference to the known rate for addition of hydrogen atoms to benzoic acid. A comparison is made with values measured previously on seven of the systems. The overall agreement is reasonable, and it is noted, in particular, that the relative rates measured by different methods agree quite well.

Recently we have undertaken extensive esr investigations of the relative rates for reaction of hydrogen



atoms with various organic substrates in aqueous solutions.<sup>2</sup> This work covers a range for the rate constant of reaction 1 of between  $10^5$  and  $10^9 M^{-1} \text{sec}^{-1}$  with the optimum region for study being  $\sim 10^7 M^{-1} \text{sec}^{-1}$ . Unfortunately there is very little in the way of reliable information on absolute rate constants in this region with which to establish the scale for the esr measurements. Anbar and Neta<sup>3</sup> have compiled the information available on hydrogen atom rate constants up to 1967 and have attempted to put all the literature values on a common scale. This compilation reveals a number of discrepancies in the literature values and reemphasizes the need both for determining accurate relative rates and for establishing the absolute scale for a number of reference reactions. We wish to report here the results of chemical experiments involving the competition between reaction 1 and abstraction of deuterium from deuterioisopropyl alcohol (reaction 2)



for some 18 solutes for which esr information is also available.<sup>2</sup> In general there is good agreement between the relative rates as determined by these two types of measurements, but this topic will be treated elsewhere.<sup>2</sup> The present work includes a comparison between the rate of reaction 2 and that for addition of hydrogen atoms to benzoic acid where the rate constant has been measured to be  $(1.00 \pm 0.15) \times 10^9 M^{-1} \text{sec}^{-1}$  by direct observation of the formation of the carboxycyclohexadienyl radical in pulse experiments.<sup>4</sup> Most of the relative rates reported here appear to be reliable to  $\pm 10\%$  or better so that, by reference to this previous result on benzoic acid, the absolute rates are believed to be accurate to  $\pm 20\%$ .

### Experimental Section

Hydrogen atoms were produced in aqueous solution by irradiating 0.1 *M* perchloric acid. At this acidity

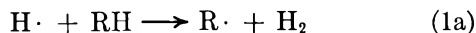
(1) Supported in part by the U. S. Atomic Energy Commission.

(2) P. Neta, R. W. Fessenden, and R. H. Schuler, submitted for publication in *J. Phys. Chem.*

(3) M. Anbar and P. Neta, *Int. J. Appl. Radiat. Isotopes*, **18**, 493 (1967).

(4) P. Neta and L. M. Dorfman, *J. Phys. Chem.*, **73**, 413 (1969).

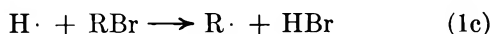
the electrons are rapidly converted to hydrogen atoms, and a total yield of hydrogen atoms  $\sim 3.6$  is expected. The reaction of these hydrogen atoms with various solutes has been studied in competition with their reaction with deuterioisopropyl alcohol. The absolute yield for the production of HD has been used as the reference in all cases. The competitions are of two types. The first is with saturated systems where  $H_2$  is produced



Studies of this type have previously been carried out using deuterium abstraction from deuterated sodium formate,<sup>5</sup> isopropyl alcohol, or methanol<sup>6,7</sup> as the reference reaction. In most cases, however, only the ratio HD/ $H_2$  was measured. The second type involves either addition of hydrogen to an unsaturated system, *e.g.*



or abstraction of halogen, *e.g.*



so that hydrogen is not produced. Previously relative rates for reactions of the type (1b) and (1c) with respect to (1a) were measured by observing the decrease in  $G(H_2)$ .<sup>8,9</sup> Since small amounts of HD can be measured in the presence of  $H_2$  the present work, in which reactions 1b and 1c have been studied in competition with reaction 2, permits more accurate measurements on this type of system.

The deuterioisopropyl alcohol used ( $C_3D_7OH$  Stohler Isotope Chemicals) was  $>99\%$  deuterated. Because of the large isotope effect favoring hydrogen abstraction, the small amount of protium impurity present results in an observed contribution  $\sim 0.2$  to  $G(H_2)$ , but this contribution could be easily corrected for by measurements on the pure solute. Benzoic acid, methanol, and most of the other second solutes were Baker Analyzed reagents. Ethanol was Rossville Gold Shield absolute alcohol. Solutions were prepared in triply distilled water containing  $0.1 M$  Baker Analyzed perchloric acid. Samples (10 ml) were outgassed by freeze-pump methods in irradiation cells with attached break seals.

Irradiations were carried out in a  $^{60}Co$  Gamma Cell 220 at a dose rate of  $1.8 \times 10^{16} \text{ eV g}^{-1} \text{ sec}^{-1}$ . Total absorbed doses were, in most cases,  $3.5 \times 10^{18} \text{ eV/g}$  at which dose  $\sim 2 \mu\text{mol}$  of hydrogen are produced from 10 ml of the isopropyl alcohol solution.

After irradiation the cells were opened on a vacuum line, and the gases volatile at liquid nitrogen temperature were pumped to a measuring volume. The  $H_2$  and HD content of this sample was then determined on a consolidated 21-103C mass spectrometer. The sensitivities of the instrument for  $H_2$ , HD, and  $D_2$  were determined along with each set of analyses. The sensi-

tivity of HD is  $\sim 5\%$  greater than that for  $H_2$ . In none of the experiments reported here was any significant yield of  $D_2$  observed [ $G(D_2) < 0.003$ ]. A correction of  $1.07\%$  (empirically determined) of the mass 3 peak was applied to the intensity observed at mass 2 to correct for the interference of  $D^+$  ion with  $H_2^+$ . The ratio  $G(HD)/G(H_2)$  should be, in general, accurate to a few per cent or better even in cases where the HD represents only  $\sim 5\%$  of the hydrogen. A somewhat larger error is involved in the determination of the absolute yields.

## Results and Discussion

The results obtained in experiments on deuterioisopropyl alcohol solutions given in Table I, which were made throughout the course of the work on different solutions, illustrate the reproducibility of the measurements. The observed total yield of hydrogen (3.7) is  $\sim 10\%$  lower than the expected initial yield [*i.e.*, the sum of 3.6 from the H atom abstraction reactions and 0.4 from the molecular yield ( $G_{H_2}$ )], to a large extent as a result of competition by  $H_2O_2$  formed in the irradiation. The  $G(H_2)$  is  $\sim 0.2$  units higher than  $G_{H_2}$  because of the protium impurity in the isopropyl alcohol. As mentioned above the presence of a small protium impurity is emphasized because of the large isotope effect involved (factor of  $\sim 7$ ).<sup>6</sup> In what follows an empirical correction is made on the assumption that this component is  $7\%$  of the observed HD yield.

For competition with saturated systems the relative rates can be described by

$$\frac{\text{rate of reaction 2}}{\text{rate of reaction 1a}} = \frac{G_H \cdot \frac{k_2 [C_3D_7CH]}{k_2 [C_3D_7OH] + k_{1a} [S] + k_x [X]}}{G_H \cdot \frac{k_{1a} [S]}{k_2 [C_3D_7OH] + k_{1a} [S] + k_x [X]}} \quad (I)$$

$$= \frac{k_2 [C_3D_7OH]}{k_{1a} [S]} \quad (II)$$

where  $k_2 [C_3D_7OH]$  describes the rate for reaction of hydrogen atoms with the deuterioisopropyl alcohol to produce HD,  $k_{1a} [S]$  the rate for reaction with the solute of interest to produce  $H_2$ , and  $k_x [X]$  the rate for reaction with the protium impurity in the deuterioisopropyl alcohol and any other impurity or radiation by-product

(5) A. Appleby, G. Scholes, and M. Simic, *J. Amer. Chem. Soc.*, **85**, 3891 (1963); G. Scholes and M. Simic, *J. Phys. Chem.*, **68**, 1738 (1964).

(6) M. Anbar and D. Meyerstein, *ibid.*, **68**, 3184 (1964).

(7) M. Anbar, D. Meyerstein, and P. Neta, *J. Chem. Soc. A*, 572 (1966).

(8) M. Anbar, D. Meyerstein, and P. Neta, *Nature*, **209**, 1348 (1966).

(9) M. Anbar and P. Neta, *J. Chem. Soc. A*, 834 (1967).

**Table I:**  $G(\text{H}_2)$  and  $G(\text{HD})$  from Irradiated Aqueous Solutions Containing Deuterioisopropyl Alcohol and Additives at pH 1<sup>a</sup>

Additive (S)	[S]	[(CD <sub>3</sub> ) <sub>2</sub> CDOH]	[(CD <sub>3</sub> ) <sub>2</sub> CDOH] [S]	$G(\text{H}_2)$	$G(\text{HD})$	$G(\text{total hydrogen})$	$\frac{G(\text{HD})^b}{G(\text{reaction 1})}$	$\frac{k_{\text{H} + (\text{CD}_3)_2\text{CDOH}^c}}{k_{\text{H} + \text{S}}}$
		0.01		0.61	3.05	3.66		
		0.01		0.64	3.01	3.66		
		0.01		0.67	2.91	3.58		
		0.01		0.62	3.10	3.72		
Isopropyl alcohol	0.0003	0.001	3.33	3.25	0.14	3.39 <sup>d</sup>	0.50	0.150 <sup>e</sup>
	0.001	0.0033	3.33	2.78	0.96	3.74	0.42	0.126 <sup>e</sup>
	0.001	0.01	10.0	1.87	1.85	3.72	1.41	0.141
	0.003	0.01	3.33	3.03	1.12	4.15	0.444	0.133
	0.01	0.01	1.0	3.65	0.42	4.07	0.132	0.132
	0.01	0.0333	3.33	3.02	1.03	4.05	0.410	0.123
	0.03	0.01	0.333	3.86	0.15	4.01	0.439	0.132
	0.10	0.01	0.1	4.15	0.052	4.20	0.0140	0.140
								0.134 ± 0.006 <sup>f</sup>
Benzoic acid	0.0003	0.03	100	0.589 <sup>g</sup>	1.59	2.18	0.921	0.0092 <sup>e</sup>
	0.0005	0.01	20	0.529 <sup>g</sup>	0.587	1.12	0.210	0.0105
	0.001	0.01	10	0.465 <sup>g</sup>	0.318	0.78	0.097	0.0097
	0.001	0.03	30	0.506 <sup>g</sup>	0.836	1.34	0.309	0.0103
	0.002	0.01	5	0.468 <sup>g</sup>	0.201	0.67	0.0585	0.0117
								0.0105 ± 0.0007 <sup>f</sup>

<sup>a</sup> At a total dose of  $3.5 \times 10^{18}$  eV/g. <sup>b</sup>  $G(\text{reaction 1})$  calculated as  $G(\text{H}_2) - [G_{\text{H}_2} + 0.07 G(\text{HD})]$  in the case of isopropyl alcohol solutions and  $G(\text{H}_2)_{k[\text{S}]} - G(\text{HD}) - [G_{\text{H}_2} + 0.07 G(\text{HD})]$  in the case of benzoic acid solutions. <sup>c</sup> For isopropyl alcohol calculated from eq III and for benzoic acid calculated from eq IV. <sup>d</sup> In this case it is estimated that the hydrogen yield should be decreased by  $\sim 0.6$  as a result of the competitive reaction of hydrogen atoms with the radiolytically produced  $\text{H}_2\text{O}_2$ . <sup>e</sup> Not included in the average because of the low solute concentration. Depletion effects will reduce the relative concentration of isopropyl alcohol somewhat more rapidly than that of deuterioisopropyl alcohol. Corrections for these effects lead to the approximate rate constant ratios of 0.10 and 0.12 in these two cases. <sup>f</sup> RMS deviations. <sup>g</sup> Reducing these numbers by 7% of the observed  $G(\text{HD})$  we obtain yields, respectively, of 0.477, 0.488, 0.443, 0.447, and 0.454. The average 0.46 can be compared with the average 0.43 obtained similarly in the absence of benzoic acid indicating that H abstraction from benzoic acid contributes not more than 1% of the hydrogen atom reactions.

present. It is seen that where abstraction occurs the  $k_x[\text{X}]$  terms have no significance in the determination of the relative rates. As long as hydrogen is not produced by reaction with the impurities the relative rates for reactions 2 and 1a can be taken, respectively, as  $G(\text{HD})$  and  $G(\text{H}_2) - [G_{\text{H}_2} + 0.07 G(\text{HD})]$  where  $G(\text{HD})$  and  $G(\text{H}_2)$  are the observed yields and  $G_{\text{H}_2}$  is the molecular yield which is taken here as 0.43. In terms of the experimental observables one can write

$$\frac{k_2}{k_{1a}} = \frac{[\text{S}]}{[\text{C}_3\text{D}_7\text{OH}]} \frac{G(\text{HD})}{G(\text{H}_2) - [G_{\text{H}_2} + 0.07 G(\text{HD})]} \quad (\text{III})$$

Eight experiments were carried out with mixtures of isopropyl alcohol and deuterioisopropyl alcohol and the results are given in Table I. From the constancy of the rate constant ratios determined from eq III, as reported in the last column, it is seen that this equation describes the relative rates very well over a factor of 100 variation in solute concentration ratio. The isotope effect measured here,  $k_{\text{H} + (\text{CH}_3)_2\text{CHOH}}/k_{\text{H} + (\text{CD}_3)_2\text{CDOH}}$ , is 7.5, in agreement with the value of 7.5 determined for  $\alpha$ -hydrogen abstraction from  $(\text{CH}_3)_2\text{CDOH}$ .<sup>6</sup>

The results of five experiments with benzoic acid are also given in Table I. First, it is noted that hydrogen atom abstraction reactions from the benzoic acid do not

measurably contribute to the observed  $G(\text{H}_2)$ . For this case, where reaction with the second solute is entirely *via* reaction 1a, the analog of eq III is

$$\frac{k_2}{k_{1b}} = \frac{[\text{S}]}{[\text{C}_3\text{D}_7\text{OH}]} \times \frac{G(\text{HD})}{G(\text{H}_2)_{k[\text{S}]} - G(\text{HD}) - [G_{\text{H}_2} + 0.07 G(\text{HD})]} \quad (\text{IV})$$

where  $G(\text{H}_2)_{k[\text{S}]}$  can be taken as the yield observed for hydrogen production in cases where hydrogen is produced by reaction with the solute at the same value of  $\Sigma k_i[\text{S}_i]$ . Because of the high reactivity of the benzoic acid all of these experiments were carried out at high effective solute concentrations where from the isopropyl alcohol experiments  $G(\text{H}_2)_{k[\text{S}]}$  is in the range 3.9–4.1.

Because of the large range of concentration ratios examined it is convenient, in examining the individual data points, to plot the ratio of  $G(\text{HD})$  to the calculated yield for reaction 1 *vs.* the solute concentration ratio logarithmically as shown in Figure 1. For simple competition the experimental points are expected to fall on lines of unit slope. The lines are, of course, translated on the concentration axis by the relative rates of

the reactions. The results obtained for methanol and ethanol are given in addition to those for isopropyl alcohol and benzoic acid. A similar treatment of the data on the other systems investigated shows a linear dependence on the concentration ratio from which the relative rate constants can be derived. The absolute rate constants given in Table II were calculated from

**Table II:** Rate Constants for the Reaction of Hydrogen Atoms with Organic Compounds in Aqueous Solutions at pH 1<sup>a</sup>

Compd	Rate constant $\times 10^{-7}$ ( $M^{-1} \text{ sec}^{-1}$ )
Acetic acid	0.013 <sup>b</sup>
Acetamide	0.019 <sup>c</sup>
Oxalic acid	0.03 <sup>d</sup>
Malonic acid	0.044
Acetone	0.17 <sup>e</sup>
Succinic acid	0.23
Acetonitrile	0.27 <sup>d</sup>
Methanol	0.29
Propionic acid	0.59
Butyric acid	0.74
Deuterioisopropyl alcohol	1.05
Ethanol	2.5
Propanol	2.7
Butanol	3.7
Isobutyl alcohol	5.0
Isopropyl alcohol	7.8
sec-Butyl alcohol	9.5
Bromoacetic acid	34 <sup>d</sup>
Benzoic acid	(100) <sup>a, d</sup>

<sup>a</sup> Absolute rate constants calculated from the observed relative rate constants assuming that for benzoic acid is  $1.0 \times 10^9 M^{-1} \text{ sec}^{-1}$ .<sup>4</sup> <sup>b</sup> An upper limit to the total rate of 0.020 is estimated if addition reaction is important (see text). <sup>c</sup> An upper limit of 0.03 is estimated in this case (see text). <sup>d</sup> Rate constant for the addition reaction. All other rate constants are for abstraction only. <sup>e</sup> Rate for abstraction only. A total rate constant of 0.26 is estimated in this case.

these relative rates by reference to the measured absolute rate for reaction of hydrogen atoms with benzoic acid.<sup>4</sup> Comments on the individual systems follow.

The total hydrogen yields observed from solutions of the alcohols (except for isobutyl alcohol) and propionic and succinic acid were all in the range 3.7–4.1. The interpretation of the data seems to be quite straightforward in that all of the hydrogen atoms appear to react either by reaction 1a or 2. In each of three experiments with isobutyl alcohol the total hydrogen yields were only 3.1. In this case, abstraction of hydrogen (both by H and OH) leads mainly to the formation of the tertiary radical  $(\text{CH}_3)_2\dot{\text{C}}\text{CH}_2\text{OH}$ . Although impurities in the alcohol might be responsible, buildup of olefin from disproportionation processes can lead to a pronounced scavenging of hydrogen atoms in secondary processes and the resultant observed reduction in  $G(\text{H}_2)$ . As noted above the complications introduced

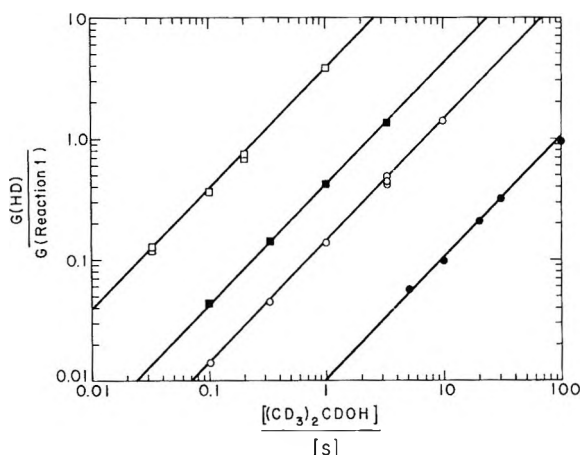


Figure 1. Logarithmic plot of relative yields of reactions 2 and 1 as a function of solute concentration ratio. Rates are measured relative to abstraction from deuterioisopropyl alcohol for benzoic acid ( $\bullet$ ), isopropyl alcohol ( $\circ$ ), ethanol ( $\blacksquare$ ), and methanol ( $\square$ ). The yield of reaction 2 is taken as measured directly by HD formation. The yield of reaction 1 as  $G(\text{H}_2) - [G_{\text{H}_2} + 0.07G(\text{HD})]$  for methanol, ethanol, and isopropyl alcohol and as  $G(\text{H}_2)_{\text{H}(\text{S})} - G(\text{HD}) - [G_{\text{H}_2} + 0.07G(\text{HD})]$  for benzoic acid (see eq III and IV). The lines of unit slope correspond to the dependences expected for simple competition between reactions 1 and 2. The relative rates for reaction of hydrogen atoms with the various substrates correspond to the factors translating the lines along the abscissa.

in either way should cancel, and no difficulty should be encountered in interpretation of the data according to eq III. The three measurements made, in fact, show a constant ratio of  $k_2/k_{1a}$ , and the rate constant calculated from this ratio is given in Table II. The total hydrogen yields observed from butyric acid solutions were anomalously low ( $\sim 2.8$ ). Because it is not obvious why the yields here should be lower than for propionic acid one suspects the presence of an impurity in this case. The relative rate constant was calculated on the assumption that no hydrogen was produced by reactions with the impurity which parallel those responsible for the reduction in the hydrogen yield and that, thus, eq III applies.

Of the solutes studied bromoacetic acid and acetonitrile follow the example of benzoic acid given above in that little hydrogen is produced by abstraction processes. For these two solutes treatment of the data according to eq IV gives constant values for  $k_2/k_{1a}$ , and the absolute rate constants obtained from such an interpretation are given in Table II. If, in the case of bromoacetic acid, the observed values for  $G(\text{H}_2)$  are corrected by 7%  $G(\text{HD})$ , the residual yield of hydrogen will be 0.412 and 0.407. These values are within experimental error identical with the expected molecular yield. Abstraction accounts for less than 1% of the hydrogen atom reactions, in agreement with the value of less than 0.1% estimated in a previous observation.<sup>9</sup> For acetonitrile values of 0.513 and 0.506 were observed for  $G(\text{H}_2) - 0.07G(\text{HD})$ . These values indicate that only  $3 \pm 1\%$  of the hydrogen atom reactions involve

abstraction. From this result the rate constant for abstraction from acetonitrile can be estimated as  $0.03 \times 2.7 \times 10^6 = 8 \times 10^4 M^{-1} \text{ sec}^{-1}$ . This value is essentially identical with that observed in acetic acid ( $13 \times 10^4 M^{-1} \text{ sec}^{-1}$ ). It is expected that a similar rate should also apply to abstraction from bromoacetic acid so that only a fraction  $10^5/3 \times 10^8 (= 0.03\%)$  of the hydrogen atoms should react *via* this path in agreement with the above-mentioned findings.

Acetone is more complicated in that both abstraction and addition reactions occur at comparable rates.<sup>10</sup> Treatment of the relative yields of HD and H<sub>2</sub> according to eq III gives the rate for the abstraction reaction in a quite straightforward way, and this value is reported in Table II. Determination of the rate of the addition reaction involves proper consideration of the reduction in the total hydrogen yield. This situation is complicated by the fact that, at the concentrations of acetone used, a significant fraction of the electrons react with the acetone so that the yield of hydrogen atoms is reduced. Correcting the observed reduction for this effect (assuming that  $k_{e_{aq}^- + \text{acetone}} = 0.26k_{e_{aq}^- + \text{H}^+}$ )<sup>3</sup> we obtain an estimate that the rate for the addition reaction is a factor of  $0.5 \pm 0.2$  times that for the abstraction process. The total rate constant for reaction of hydrogen atoms with acetone can, therefore, be given as  $(2.6 \pm 0.3) \times 10^6 M^{-1} \text{ sec}^{-1}$ .

Acetic acid and acetamide are very unreactive toward hydrogen atoms and as a result had to be studied at very high concentrations (0.5 to 1.0 M). Impurity effects will be emphasized and direct action on the solute becomes important [ $G(\text{CH}_4) = 0.2$  was measured for a 1.0 M acetic acid solution]. In both cases hydrogen atoms react mainly *via* abstraction (total yields of hydrogen were  $\sim 3$ ). Treating the observed  $G(\text{HD})$  and  $G(\text{H}_2)$  according to eq III we obtain the rate constants for abstraction given in Table II. If the observed reductions in the hydrogen yield result from addition reactions, we estimate that these reactions may contribute an additional 50% to the total rate but the effect is small and it is difficult to discount impurity problems. For example, the observed decreases can be accounted for by the presence of 0.01% unsaturated impurity in the solute so that this estimate of the addition rate must be regarded as an upper limit. This result indicates that addition to the carboxyl group is very slow ( $\sim 10^5 M^{-1} \text{ sec}^{-1}$  or less) and should not contribute to any measurable extent in the case of the higher aliphatic acids where abstraction is much more rapid.

The remaining two examples in the table, oxalic and malonic acid, are more complex in that at the concentrations of these solutes required for study of the hydrogen atom reactions, appreciable reaction with electrons occurs. In order to properly consider the data an estimate must be made of the resultant decrease in the hydrogen atom yield. It is noted, for example, that in

the case of oxalic acid, values for  $G(\text{H}_2)$  of only 0.35 and 0.26 were observed for 0.2 and 0.4 M solutions (0.27 and 0.23 if one corrects for the hydrogen from the C<sub>3</sub>HD<sub>6</sub>-OH). These yields are considerably lower than the accepted values of the molecular yield and can be explained only if electron scavenging occurs within the spurs. Similar low values of  $G(\text{H}_2)$  were also observed by Mičić and Draganić in studies of this system.<sup>11</sup> The fact that scavenging within the spurs is so important implies that the rate constant for the reaction of electrons with oxalic acid is very high. Hydrogen production by abstraction is, of course, not expected in this case. If we take the rate constant for  $e_{aq}^- + (\text{COOH})_2$  as  $2.5 \times 10^{10} M^{-1} \text{ sec}^{-1}$  at pH 1<sup>11</sup> then hydrogen atom yields of 1.55 and 1.16 can be estimated for 0.2 and 0.4 M solutions. Using these values and the experimentally measured yields of HD a rate constant of  $3 \times 10^6 M^{-1} \text{ sec}^{-1}$  for the addition reaction is obtained. A large error must be assigned to this value, however, because of possible effects of impurities (which could make  $k$  lower) and the assumptions in the calculations (*e.g.*, if the electron rate constant were taken as  $10^{10} M^{-1} \text{ sec}^{-1}$  the calculated  $k$  would be increased to  $5 \times 10^5 M^{-1} \text{ sec}^{-1}$ ). The rate constant for the addition to the carboxyl groups of oxalic acid appears to be somewhat higher than addition in the case of that given above for monobasic acids (*cf.* acetic acid). Such a higher value may very well reflect the mutual effect of the carboxyl groups on each other.

Malonic acid is even more complex because its rate for reaction with electrons at pH 1 is not presently known. In this case values for  $G(\text{H}_2)$  of 1.64 and 1.44 were observed at 0.2 and 0.5 M in the presence of 0.01 M deuterioisopropyl alcohol [ $G(\text{HD}) = 1.31$  and 0.53, respectively]. Abstraction is quite important and, if we assume no decrease in the molecular hydrogen produced in the spurs, a rate constant of  $4.4 \times 10^5 M^{-1} \text{ sec}^{-1}$  is obtained for the abstraction process. It is seen that the total hydrogen yield decreases with increased malonic acid concentration. The observed values can be explained if the rate constant for  $e_{aq}^- + \text{malonic acid}$  is taken as  $6 \times 10^9 M^{-1} \text{ sec}^{-1}$  and no addition occurs. This value should represent an upper limit for  $k_{e_{aq}^-}$  at pH 1. If the electron reacts with malonic acid at the same rate as at pH 6 ( $2.4 \times 10^8 M^{-1} \text{ sec}^{-1}$ ) and the observed reduction in  $G(\text{H}_2)$  results from addition (and impurity effects are not present), then (as an upper limit) the total rate for reaction of hydrogen atoms with malonic acid is  $9 \times 10^5 M^{-1} \text{ sec}^{-1}$ . More realistically, one can assume that the rate for hydrogen atom addition is  $\sim 1 \times 10^5$  (*cf.* acetic acid) and that the total rate is  $5.4 \times 10^5 M^{-1} \text{ sec}^{-1}$ . With this addition rate the rate constant for  $e_{aq}^- + \text{malonic}$

(10) S. Nehari and J. Rabani, *J. Phys. Chem.*, **67**, 1609 (1963).

(11) O. Mičić and I. Draganić, *Int. J. Radiat. Phys. Chem.*, **1**, 287 (1969).

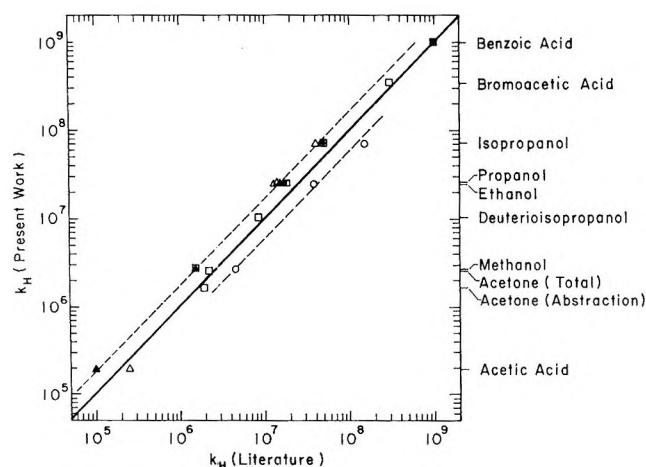


Figure 2. A comparison of the rate constants determined in this research with various literature values. The values of the present work are obtained by comparison with the absolute rate of  $1.0 \times 10^9 M^{-1} \text{sec}^{-1}$  given for benzoic acid (■) (see ref 4) and perfect correlation corresponds to the solid line of the figure. The literature values are grouped according to the method of determination: ○, competition with  $\text{OH}^-$ ; ●, competition with D-formate; △, competition with  $\text{Ag}^+$ ; ▲, competition with  $\text{Fe}^{3+}$ ; □, miscellaneous.

acid at pH 1 is estimated as  $\sim 1 \times 10^9 M^{-1} \text{sec}^{-1}$  which appears to be a reasonable value.

A comparison of the present results with the literature values listed in ref 3 is given in Figure 2. In many cases only relative rates were measured in the original work,

and it is seen that these relative rates agree quite well with those determined here. In ref 3 an attempt was made to put each of these sets of results on an absolute scale, and it is seen that in all cases there is agreement to within a factor of 2 with the present values which are believed to be accurate to  $\pm 20\%$ . Most previous measurements were made in near neutral solutions, but pH is not expected to have any appreciable effect in the cases compared in Figure 2. The discrepancies which exist can, to a large extent, be attributed to possible errors in the absolute rates for the reference reaction involved in the comparisons. In particular it is noted that, as given by the dashed lines in the figure, for those measurements where the rates were determined relative to reaction with  $\text{OH}^-$  (and which were ultimately compared to the rate of  $\text{H} + \text{O}_2$ ) the values are  $\sim 70\%$  higher than reported here and for those measured relative to reaction with  $\text{Ag}^+$ ,  $\text{Fe}^{3+}$ , or D-formate the rates are  $70\%$  lower. While it would appear that for many purposes the absolute rates of these reactions are sufficiently well known, it would be useful, for any detailed discussion, to have a number of additional measurements on the absolute rates of reference reactions in the range of  $10^5$ – $10^8 M^{-1} \text{sec}^{-1}$ .

*Acknowledgment.* The authors wish to thank Mr. G. K. Buzzard for his assistance with the mass spectrometric determinations.

(12) J. Rabani, *Advan. Chem. Ser.*, **50**, 242 (1965).

# The Radiation Chemistry of Aqueous Solutions of $\text{CFCl}_3$ , $\text{CF}_2\text{Cl}_2$ , and $\text{CF}_3\text{Cl}$ <sup>1</sup>

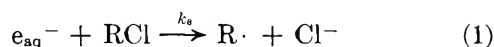
by Turgut I. Balkas, J. H. Fendler, and Robert H. Schuler\*

Radiation Research Laboratories and Department of Chemistry, Mellon Institute of Science, Carnegie-Mellon University, Pittsburgh, Pennsylvania 15213 and Chemistry Department, Middle East Technical University, Ankara, Turkey (Received October 29, 1970)

Publication costs assisted by the Carnegie-Mellon University and the U. S. Atomic Energy Commission

Radiation chemical studies of aqueous solutions of the three fluorochloromethanes show that the initial reaction occurs mainly *via* the attack of hydrated electrons on the solute to produce chloride ions. A rate constant of  $\sim 10^{10} M^{-1} \text{sec}^{-1}$  is observed for reaction of hydrated electrons with each of the solutes. In the absence of competing reactions the halogenated radical produced as the complement of the chloride ion undergoes secondary hydrolysis reactions. In the case of  $\text{CFCl}_3$ , one fluoride and three chloride ions are produced for each electron which reacts with the solute. Hydrolysis is complete except for experiments carried out at very high dose rates or in the presence of very reactive radical scavengers. The chloride ion yields from  $\text{CF}_2\text{Cl}_2$  and  $\text{CF}_3\text{Cl}$  are, respectively, twice and equal to the hydrated electron yield, with the yield from  $\text{CF}_3\text{Cl}$  being notably independent of dose, dose rate, or added radical scavenger. In these cases the fluoride ion yields exhibit a very pronounced dose rate dependence and complete hydrolysis occurs only at dose rates less than  $10^{13} \text{eV g}^{-1} \text{sec}^{-1}$ . A common dose rate dependence is observed for these two solutes, and this fact is taken to indicate that the rate-controlling steps involve the second-order reactions of a difluorinated radical, probably  $\text{CF}_2$ . The secondary hydrolysis reactions were studied on the  $10^{-6}$  to  $10^{-2}$  sec time scale using conductometric methods. In each case the second step in the hydrolysis occurs with a period of  $\sim 10 \mu\text{sec}$ . The third and fourth halide ions are produced in reactions which have periods  $\sim 1$  msec or longer. A number of effects which illustrate the minor importance of complicating side reactions are noted and discussed in some detail.

Radiation chemical studies on aqueous solutions of  $\text{CH}_3\text{Cl}$  have shown that this solute reacts selectively and rapidly with hydrated electrons. One equivalent of chloride ion<sup>2</sup> is produced for each electron scavenged by the  $\text{CH}_3\text{Cl}$  and the reaction responsible is presumably



We wish to report here the results of related studies on aqueous solutions of the three fluorochloromethanes in which large yields of halide ion are observed. In each case addition of ethylene suppresses the production of all but one chloride ion so that reaction 1 appears to be responsible for the initial attack on the solute. This reaction is then followed by secondary reactions which result, if competing reactions are unimportant, in the complete hydrolysis of the halide. In all three cases the solute was examined at a concentration sufficiently low that reaction is expected to be predominantly with electrons which have escaped from the spur, and the yield of reaction 1 can be expected to be close to the value of 2.75 observed in  $10^{-2} M$   $\text{CH}_3\text{Cl}$  solutions.<sup>2</sup> Complicating effects of competing secondary reactions at high dose rates have been explored. These studies are made possible by the availability of ion-selective electrodes which permit the ready analysis of both fluoride and chloride ions simultaneously produced. Auxiliary conductometric pulse-radiolysis experiments have been carried out to examine the secondary hydrolysis reactions on the  $10^{-6}$  to  $10^{-2}$  sec time scale.

## Experimental Section

For the steady-state experiments Matheson  $\text{CF}_3\text{Cl}$  (bp  $-81.4^\circ$ ),  $\text{CF}_2\text{Cl}_2$  (bp  $-29.8^\circ$ ), and  $\text{CFCl}_3$  (bp  $23.8^\circ$ ) were fractionated on a vacuum line at  $-80^\circ$  and known amounts (pressure-volume measurement) added to previously outgassed aqueous solutions. The solution concentrations were calculated from the solubility coefficients<sup>3</sup> and the known liquid and vapor volumes of the sealed sample tubes. In the case of  $\text{CFCl}_3$  (a liquid) the amount of added solute was less than the liquid phase solubility limit. For the pulse conductivity studies a flow system was employed, and measurements were made on solutions saturated at atmospheric pressure (saturation concentrations at  $25^\circ$ ;  $\text{CFCl}_3$ ,  $8 \times 10^{-3} M$ ,  $\text{CF}_2\text{Cl}_2$ ,  $2.3 \times 10^{-3} M$ ,  $\text{CF}_3\text{Cl}$ ,  $8.6 \times 10^{-4} M$ ).<sup>3</sup>

The analyses for fluoride and chloride ions were by means of ion-selective electrodes using methods completely identical with those employed in previous studies of  $\text{CH}_3\text{Cl}$  and  $\text{SF}_6$  solutions.<sup>2,4</sup> At the doses required for the chloride determinations sufficient hydrogen ion ( $\sim 10^{-4} M$ ) builds up in the irradiation of a neutral unbuffered solution that it competes significantly with the solute present at low concentration and

(1) Supported in part by the U. S. Atomic Energy Commission.

(2) T. I. Balkas, J. H. Fendler, and R. H. Schuler, *J. Phys. Chem.*, in press.

(3) "Matheson Gas Data Book," The Matheson Co., Inc., East Rutherford, N. J., 1966, pp 131, 159, 473.

(4) K.-D. Asmus and J. H. Fendler, *J. Phys. Chem.*, **72**, 4285 (1968).

the use of a buffer is necessary. Most solutions were buffered to pH 6.5 with sodium phosphate ( $2 \times 10^{-3} M Na_2HPO_4$  acidified slightly with  $H_2SO_4$ ). The buffer interferes with the use of the fluoride electrode at fluoride concentrations below  $10^{-5} M$ , but satisfactory results could be obtained at doses of  $10^{18} eV/g$  and greater at which the chloride was determined. In one series of experiments base was added to increase the initial pH to  $\sim 10$  so that the hydrogen ion would be neutralized as it was formed. Within experimental error the results of these experiments were identical with those obtained on the buffered solutions.

Irradiations were carried out both with  $^{60}Co$   $\gamma$  rays and with 2.8-MeV Van de Graaff electrons. The former covered the dose rate range of  $10^{13}$  to  $10^{16} eV g^{-1} sec^{-1}$ . Absorbed dose rates were determined in the  $\gamma$ -ray experiments by measurements on the Fricke system. Several experiments at moderately higher dose rates were carried out with an electron beam (current  $\sim 0.1 \mu A$ , duration 2–6 sec), and the fluoride yield was measured relative to the chloride yield. Since dose rate effects are very apparent in the  $CF_2Cl_2$  and  $CF_3Cl$  systems, pulse electron irradiations were used to examine the absolute yields for both fluoride and chloride production at very high dose rates. Currents up to 50 mA were used to produce absorbed dose rates up to  $2 \times 10^{23} eV g^{-1} sec^{-1}$ . Doses of  $3-5 \times 10^{18} eV/g$  were delivered in single pulses which were monitored by integration of the beam current with a pulse integrator. Dosimetry was in terms of chloride production from  $CH_3Cl$  ( $10^{-2} M$ ;  $G(Cl^-)$  taken as 2.8) with the observed effects interrelated by the electrical measurements. Two series of pulse irradiations were carried out at a beam current of 50 mA and a third series at a current two orders of magnitude lower. Because the irradiation geometry changed somewhat from series to series it was necessary, for comparison purposes, to normalize the integrated currents by factors determined from the relative effects on methyl chloride solutions. The methyl chloride results can, therefore, be compared only within each series but can in turn be compared to the results on  $CF_3Cl$  where a single chloride is also produced. In general, in spite of significant problems involving details of the irradiation geometry, the results within a single series of runs are reproducible to  $\pm 3\%$ . Together with the  $^{60}Co$  irradiations, these studies covered a ten order of magnitude variation in absorbed dose rate with essentially the same dose being delivered in periods which ranged from 25  $\mu sec$  to 5 days.

A large number of conductometric pulse-radiolysis experiments were carried out which were similar to those described by Beck<sup>5</sup> and also previously used in these laboratories in studies of  $CH_3Cl$  solutions.<sup>2</sup> Pure water was acidified slightly with perchloric acid to bring the pH to the desired value (usually  $\sim 6$ ). Relative conductivity yields were determined in terms of the experimental unit of mhos conductance per coulomb of

electron beam current collected from the conductivity cell (see ref 2). Absolute yields of ionized product were determined by reference to measurements on  $CH_3Cl$  solutions saturated at atmospheric pressure on the assumption that in this case the conductivity change results from the production of HCl with a yield of 3.14.<sup>2</sup> It is demonstrated here that reaction of hydrated electrons with  $CFCl_3$ ,  $CF_2Cl_2$ , and  $CF_3Cl$  first produces HCl so that direct comparison of the initial change with that observed in  $CH_3Cl$  solutions is possible. Since the rate constants are  $\sim 10^{10} M^{-1} sec^{-1}$ , this initial reaction must occur in the saturated solutions ( $\sim 10^{-3} M$ ) on the time scale of  $\sim 10^7$  sec and an abrupt change corresponding to the production of at least one equivalent of HCl is expected at the time of irradiation. Because the equivalent conductances of HF and HCl (395 and 425 mhos/equiv, respectively, at 25°) differ by only 7%, the order in which subsequent reactions occur will have little effect on the interpretation of the results (as long as one operates on the acid side of neutral as was done here).

The conductivity experiments carried out during the present study covered the dose range of  $2 \times 10^{15}$  to  $2 \times 10^{17} eV/g$  with pulses which were usually of  $\sim 1-\mu sec$  duration. The results represented in the dual-trace photographs of Figures 2, 5, and 6 were all at doses  $\sim 10^{16} eV/g$ . At these doses product concentrations of only  $\sim 10^{-6} M$  are produced. These doses are considerably less than in the case of the steady-state experiments so that certain secondary reactions may have a somewhat greater importance. In particular, hydrogen atoms will be removed by reaction with product oxygen at the higher doses of the steady-state experiments but may start to make a small contribution to the yields at the dose levels at which the conductivity experiments are carried out.

## Results and Discussion

*Summary of Rate Data.* For convenience in the following discussions the rate constants for the reactions of hydrated electrons ( $k_e$ ) and hydrogen atoms ( $k_H$ ) with the fluorochloromethanes and related compounds are given in Table I. The hydrogen atom data were obtained by measuring the concentration dependence of the decrease in the hydrogen atom signal in esr experiments<sup>6</sup> and the rates of the electron reactions with  $CFCl_3$  and  $CF_2Cl_2$  by competitive studies (present work—see below) and with  $CF_3Cl$  by pulse radiolysis.<sup>7</sup> Since the conductivity experiments described below were carried out on saturated solutions, the corresponding yields expected for the initial reaction of electrons with each of the solutes (calculated for the appropriate  $k_e[S]$  from the relation given in ref 2) are given in the final column.

(5) G. Beck, *Int. J. Radiat. Phys. Chem.*, **1**, 361 (1969).

(6) P. Neta, R. W. Fessenden, and R. H. Schuler, to be published.

(7) G. Bullock and R. Cooper, *Trans. Faraday Soc.*, **66**, 2055 (1970).

**Table I:** Rate Data and Expected Initial Yields

	Saturation <sup>a</sup> concn, <i>M</i>	Rate constants		$G(e_{aq}^-)_{M^c}$
		$k_H^b$	$k_e$	
CCl <sub>4</sub>	0.005	$4.4 \times 10^7$	$3.0 \times 10^{10}{}^e$	3.21
CFCl <sub>3</sub>	0.008	$1.5 \times 10^6$	$1.6 \times 10^{10}{}^f$	3.18
CF <sub>2</sub> Cl <sub>2</sub>	0.0023	$<10^6$	$1.4 \times 10^{10}{}^f$	2.92
CF <sub>3</sub> Cl	0.0009	$<10^6$	$4.4 \times 10^9{}^g$	2.73
CF <sub>4</sub>	0.0002	... <sup>d</sup>	... <sup>d</sup>	...
CH <sub>3</sub> Cl	0.1	$7 \times 10^4$	$1.1 \times 10^9{}^h$	3.14

<sup>a</sup> At atmosphere pressure. <sup>b</sup> From ref 6. <sup>c</sup> Yield of electrons expected to be scavenged at *M* (i.e., saturated solutions) from the relation developed for methyl chloride solutions (see ref 2). Initial yields of 2.82, 2.80, and 2.78 are expected, respectively, for  $10^{-3}$  *M* CFCl<sub>3</sub>, CF<sub>2</sub>Cl<sub>2</sub>, and CF<sub>3</sub>Cl. <sup>d</sup> No reaction of CF<sub>4</sub> with either H· atoms or electrons has been observed. <sup>e</sup> E. J. Hart, S. Gordon, and J. K. Thomas, *J. Phys. Chem.*, **68**, 1271 (1964). <sup>f</sup> This work. <sup>g</sup> Reference 7. <sup>h</sup> Reference 2.

*Effect of Ethylene on Halide Ion Yields.* As is shown in Table II each of the mixed halides gives a yield of both chloride and fluoride ion which is upwards of 2.7. Addition of  $6 \times 10^{-3}$  *M* ethylene suppresses the fluoride ion yield to less than 15% of the value observed for the ethylene-free solutions. At the same time, in each case the chloride ion yield is reduced to  $\sim 3$ . In partic-

**Table II:** Effect of C<sub>2</sub>H<sub>4</sub> on Halide Ion Yields<sup>a</sup>

	[C <sub>2</sub> H <sub>4</sub> ]	$G(Cl^-)$	$G(F^-)$
CFCl <sub>3</sub>	0	8.35	2.78
	$6 \times 10^{-3}$	3.90	0.35
CF <sub>2</sub> Cl <sub>2</sub>	0	5.46	3.98
	$6 \times 10^{-3}$	3.20	0.21
CF <sub>3</sub> Cl	0	2.74	6.78
	$6 \times 10^{-3}$	2.73	0.15

<sup>a</sup> Irradiated for 1 hr at a dose rate of  $1.34 \times 10^{15}$  eV g<sup>-1</sup> sec<sup>-1</sup>. Solute concentration  $\sim 10^{-3}$  *M* at pH 6.5.

ular it is noted that the chloride yield from CF<sub>3</sub>Cl is unaffected by the addition of ethylene while the fluoride yield is reduced by a factor of  $\sim 50$ . Ethylene is known to be very reactive toward CF<sub>3</sub>· radicals<sup>8</sup> so it is reasonable to assume that in this case the observed reduction in  $G(F^-)$  is the result of scavenging of CF<sub>3</sub>· radicals by the ethylene. It is concluded that the initial attack of the hydrated electron must be according to reaction 1. If one assumes similar initial reactions in the cases of CFCl<sub>3</sub> and CF<sub>2</sub>Cl<sub>2</sub>, then an approximate correction for lack of scavenging by the ethylene can be made to the observed  $G(Cl^-)$  by subtracting, respectively, twice and one-half the value of  $G(F^-)$ . The resultant corrected chloride yields, 3.20 and 3.10, are only  $\sim 0.4$  unit higher than  $G(Cl^-)$  observed from CF<sub>3</sub>Cl. A very slight partial hydrolysis, which selec-

tively gives chloride ion, seems to take place but this is relatively unimportant. For each of the three fluorochloromethanes, therefore, reaction 1 appears to be a formally correct description of the initial process and the halocarbon radical which would result from such a reaction seems to have at least a transitory existence. The additional halide ions observed in the absence of other solutes must then result from the hydrolysis of these latter radicals. Where hydrolysis is complete, the carbon must ultimately appear as an oxygenated product and must therefore be either further reduced to CO or be reoxidized to CO<sub>2</sub>.

*CFCl<sub>3</sub>.* Of the three solutes under discussion, CFCl<sub>3</sub> appears to be the most simple in that, except for the experiments at the highest absorbed dose rates or in the presence of ethylene, one fluoride and three chloride ions were produced for each electron which reacted with the CFCl<sub>3</sub>. Although its solubility is somewhat greater than that of the other fluorochloromethanes, most studies were carried out at a concentration of  $\sim 10^{-3}$  *M* in order to avoid the possibility of having a halocarbon phase present and to be in the range where reaction is expected to occur mainly with electrons which escape from the spurs. From the rate constant for reaction 1, this concentration of CFCl<sub>3</sub> is kinetically equivalent to  $10^{-3}$  *M* SF<sub>6</sub> or  $1.5 \times 10^{-2}$  *M* CH<sub>3</sub>Cl where the yields for scavenged electrons have been found to be 2.78 and 2.82, respectively.<sup>2,4</sup>

As is illustrated by typical data presented in Figure 1 both fluoride and chloride ions build up linearly with dose. Their yields were independent of dose rate over the range of  $10^{13}$  to  $2 \times 10^{16}$  eV g<sup>-1</sup> sec<sup>-1</sup> where direct comparison was made with the Fricke system. Twenty-nine runs were made over a variety of conditions and the means of the observed yields were  $G(Cl^-) = 8.34 \pm 0.10$  and  $G(F^-) = 2.77 \pm 0.10$  (root-mean-square deviations). The yield ratio is 3.01 with a probable error of 0.03. It is quite apparent in this case that once the solute reacts the resultant fragments are rapidly hydrolyzed. One can compare one-third of the chloride yield ( $2.78 \pm 0.03$ ) (or the fluoride yield) with the values  $\sim 2.8$  given above for the reaction of hydrated electrons with SF<sub>6</sub> and CH<sub>3</sub>Cl at the same value of  $k_s[S]$ . This yield is, in fact, only 1% lower than the value of 2.82 predicted from the empirical description of the results on methyl chloride solutions (see Table I). Such a comparison indicates that under the conditions of these experiments CFCl<sub>3</sub> reacts only with hydrated electrons. The specific nature of the reaction is confirmed by the results of competitive studies with H<sup>+</sup> and N<sub>2</sub>O given in Table III. A plot of  $G(X^-)/[G(X^-)_0 - G(X^-)]$  vs.  $1/[N_2O]$  extrapolates to a completely negligible ( $<0.02$ ) value at infinite N<sub>2</sub>O concentration showing that hydroxyl radicals do not

(8) R. A. Weir, P. P. Infelta, and R. H. Schuler, *J. Phys. Chem.*, **74**, 2596 (1970).

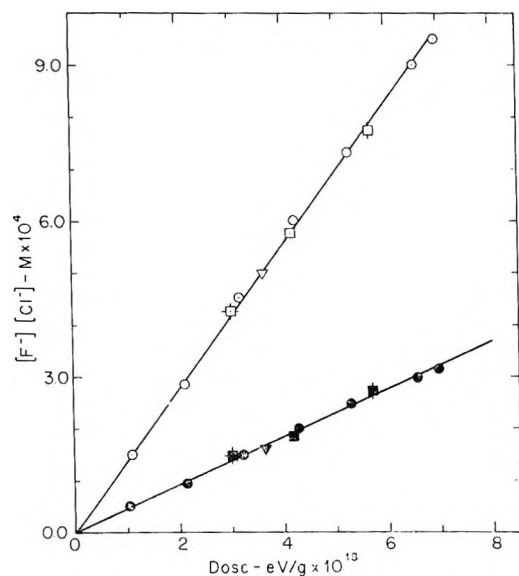


Figure 1. Production of chloride (open symbols) and fluoride (closed symbols) ions from  $10^{-3} M$   $CFCl_3$  as a function of dose at dose rates of  $1.3 \times 10^{15}$  ( $\circ, \bullet$ );  $2.0 \times 10^{13}$  ( $\nabla, \blacktriangledown$ );  $2.8 \times 10^{14}$  ( $\square, \blacksquare$ );  $7.5 \times 10^{15}$  ( $\square, \blacksquare$ ) and  $2.2 \times 10^{16}$  ( $\square, \blacksquare$ )  $eV g^{-1} sec^{-1}$ .

Table III: Effect of Solutes on Radiolysis of  $CFCl_3$  Solutions<sup>a</sup>

Solute	[S]	$G(Cl^-)$	$G(F^-)$	$G(Cl^-)/G(F^-)$
...	...	8.35	2.78	3.01
$CH_3OH$	$1.0 \times 10^{-2}$	8.25	2.80	2.94
$H^+$	$1.02 \times 10^{-3}$	3.11	1.04	2.99
	$2.04 \times 10^{-3}$	2.11	0.69	3.06
$N_2O$	$1.0 \times 10^{-3}$	5.28	1.72	3.07
	$2.0 \times 10^{-3}$	3.90	1.31	2.98
	$5.0 \times 10^{-3}$	2.21	0.69	3.20
	$8.1 \times 10^{-3}$	1.54	0.50	3.08

<sup>a</sup>  $1.0 \times 10^{-3} M$   $CFCl_3$ . Dose rate =  $1.3 \times 10^{15} eV g^{-1} sec^{-1}$ .

readily attack the halocarbon to produce halide ion. Similarly, the data for  $H^+$  indicate that at high acid concentrations where all the electrons have been converted into hydrogen atoms perhaps 5% of the latter may attack the  $CFCl_3$ . In the absence of acid only a negligible contribution to the yield ( $\sim 0.05 \times 0.6 = 0.03$ ) would result. The rate constant for reaction of hydrogen atoms with  $CFCl_3$  is given by esr measurements<sup>6</sup> as  $1.7 \times 10^6 M^{-1} sec^{-1}$  so that they are presumably removed by more rapid reactions with competing solutes or the peroxide and oxygen which build up to  $\sim 10^{-4} M$  during the course of these irradiations. As is shown in Table III, methanol has no effect on either  $Cl^-$  or  $F^-$  production. At very low doses in extremely pure water the hydrogen atoms can be expected to attack the  $CFCl_3$  and give a small additional yield of halide.

From the slopes of standard competition plots of the data of Table III the relative rate constants for reaction of hydrated electrons with  $CFCl_3$ ,  $H^+$  and  $N_2O$  are 1:1.50:0.56. Taking  $2.4$  and  $0.89 \times 10^{10} M^{-1} sec^{-1}$  as the absolute rate constants for the latter two reactions,<sup>9</sup>  $k_{CFCl_3}$  is, in both cases,  $1.6 \times 10^{10} M^{-1} sec^{-1}$ . It should be noted in the table that the ratio of 1:3 is maintained for  $G(F^-):G(Cl^-)$  in the presence of  $H^+$  and  $N_2O$ .

Results of experiments at the highest dose rates employed are given in Table IV. It is seen that the chloride and fluoride yields are, respectively, 91 and 86% of those observed at low dose rates. Since radicals seem to be important intermediates, it is indeed expected that for prolonged irradiations at high dose rates radical-radical reactions will compete with the hydrolysis reactions and a resultant decrease in the observed yield of halide ion should be observed. However, in the studies reported here the irradiations are of only short duration and the radicals build up only to concentrations of  $10^{-5}$  to  $10^{-4} M$  (depending on whether the combination reactions are fast or slow). At these levels the radical lifetimes will be at least a few microseconds. The initial hydrolysis reaction seems to compete effectively since only a small reduction is, in fact, observed. It is noted that if the observed chloride yield is corrected for the one equivalent expected from reaction 1 the residual ( $7.62 - 2.78 = 4.84$ ) is 87% of that found at low dose rates and twice the fluoride yield. It appears, therefore, that 13% of the  $CFCl_2\cdot$  radicals are lost by radical-radical reactions in these experiments. One additional pulse experiment at a dose rate of  $3 \times 10^{21} eV g^{-1} sec^{-1}$  gave absolute chloride and fluoride yields of 8.50 and 2.92 and a ratio of 2.91. These latter results are, within experimental error, identical with those at lower dose rates (which is as it should be since from the results at  $10^{21} eV g^{-1} sec^{-1}$ , one expects a drop of only one-tenth that at the higher dose rate or 1-2%).

Examination of the conductivity change of a saturated solution shows that for each electron scavenged by the  $CFCl_3$  one equivalent of  $HCl$  is formed immediately but that additional ionic species grow in over a period of  $\sim 5$  msec. A typical dual trace oscillogram is shown in Figure 2b and can be compared with the stepwise change in conductivity observed with methyl chloride (Figure 2a). Two regions of growth after the initial incremental change are apparent. First a rapid rise is observed in the region of  $10 \mu sec$ . This growth is essentially over in  $50 \mu sec$ . A longer growth is then observed on the millisecond time scale. This latter increase is exponential in character and has a half-period of 1.7 msec which was quite reproducible in a large number of experiments. Using pulses of 1- $\mu sec$  duration the conductivity change was measured as a

(9) S. Gordon, E. J. Hart, M. S. Matheson, J. Rabani, and J. K. Thomas, *Discussions Faraday Soc.*, **36**, 193 (1963).

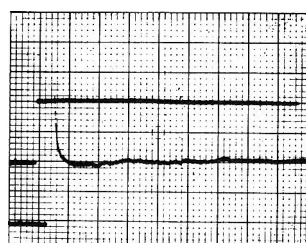
Table IV: Results of Pulse Experiments<sup>a</sup>

	Q-Integrated current, C × 10 <sup>8</sup>	Chloride produced, M × 10 <sup>4</sup>	[Cl <sup>-</sup> ]/Q	G(Cl <sup>-</sup> )	G(F <sup>-</sup> )	G[F <sup>-</sup> ]/G[Cl <sup>-</sup> ]
CH <sub>3</sub> Cl	0.645	1.90	2.95	(2.75) <sup>b</sup>	...	...
	0.505	1.42	2.81			
	0.580 <sup>c</sup>	1.65	2.85			
	0.640 <sup>c</sup>	1.85	2.89			
CFCl <sub>3</sub>	0.515	4.10	7.96	7.63	2.45	0.323
	0.695 <sup>c</sup>	5.50	7.92	7.60	2.35	0.309
CF <sub>2</sub> Cl <sub>2</sub>	0.625	3.01	4.82	4.62	1.10	0.240
	0.680	3.50	5.13	4.92	1.20	0.243
	0.750	3.70	4.94	4.73	<i>d</i>	<i>d</i>
	0.750 <sup>c</sup>	3.65	4.87	4.65	1.15	0.246
	0.770 <sup>c</sup>	3.40	4.42	4.25	1.07	0.250
CF <sub>3</sub> Cl	0.520	1.57	3.02	2.89	2.76	0.95
	0.520	1.55	2.98	2.85	2.91	1.02
	0.650	1.80	2.77	2.66	2.87	1.08

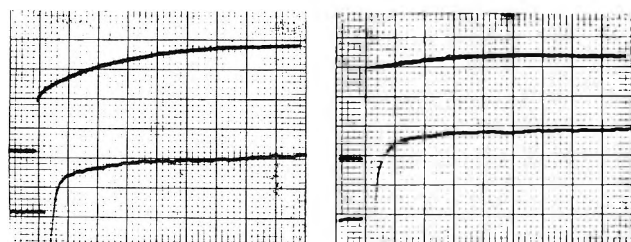
<sup>a</sup> Pulse currents  $\sim 50$  mA for 20  $\mu$ sec. Sample volume 2.0 cc. Doses  $\sim 3 \times 10^{18}$  eV g<sup>-1</sup> delivered at a dose rate  $\sim 10^{23}$  eV g<sup>-1</sup> sec<sup>-1</sup>. Methyl chloride concentration was  $10^{-2}$  M. All other solute concentrations were  $10^{-3}$  M. Sample buffered to pH 6.5. Absolute yields determined by comparing the halide ion produced per unit integrated current with the similar quantity for methyl chloride.

<sup>b</sup> Assumed. Absolute yield of 2.76 is calculated if it is assumed that 2.0 out of the 2.8 MeV per electron is absorbed in the sample.

<sup>c</sup> Series I. Integrated currents normalized by factor of 1.40. All other experiments series II. Methyl chloride results should be compared only within the separate series. <sup>d</sup> Not measured.



a



b

c

Figure 2. Oscilloscope recordings of the conductivity changes produced by the 1- $\mu$ sec pulse irradiation of solutions saturated with (a) CH<sub>3</sub>Cl, (b) CFCl<sub>3</sub>, and (c) both CFCl<sub>3</sub> and ethylene (0.0043 M) at pH 5.9. Time scale of lower traces is 10  $\mu$ sec/cm and upper traces is 1 msec/cm. Doses used were  $\sim 10^{18}$  eV/g and HX produced  $\sim 10^{-6}$  M. The yields corresponding to the plateaus of the upper curves are, respectively, 3.14 (assumed, cf. ref 2), 14.2, and 5.3. Initial spikes on lower traces are instrumental with recovery requiring  $\sim 5$   $\mu$ sec.

function of dose for doses up to  $10^{17}$  eV/g. Since the extrapolation to zero time is somewhat problematical, the changes observed at 50  $\mu$ sec (*i.e.*, on the first plateau on the lower curve of Figure 2b) were compared with

the changes observed in methyl chloride. The increase in conductivity was a linear function of dose with a slope of 440 units relative to a slope of 197 units for a saturated methyl chloride solution. This change at 50  $\mu$ sec corresponds to an HX yield of 7.0. Extrapolation of the growth curve back to zero time, as best one can, gives an estimate of one-half this value or 3.5 for the initial yield. For a solution 0.008 M in CFCl<sub>3</sub> the yield of reaction 1 is expected, from the results on methyl chloride, to be 3.2 so that it is clear that the second stage in the hydrolysis is essentially complete at 50  $\mu$ sec. The change observed at 10 msec was 875 units which, taking into account the slightly lower equivalent conductance of F<sup>-</sup>, corresponds to a final yield of 14.2. The secondary reactions which lead to the complete hydrolysis of the CFCl<sub>3</sub> must occur within the 10-msec time scale. The observed yield is  $\sim 10\%$  higher than the expected value of 12.8, but the difference can be real since, as pointed out above, the doses are very low and in the absence of competing reactants the hydrogen atoms can react with the CFCl<sub>3</sub>. From the rate constant for the H atom reaction mentioned above such attack should occur, at 0.008 M CFCl<sub>3</sub> and in the absence of competing reactions, with a half-period of  $\sim 50$   $\mu$ sec. The observed difference is, however, somewhat less than the  $4(0.6) = 2.4$  increase expected if all hydrogen atoms react in this way and so competing reactions for the hydrogen atoms appear to be present and the apparent half-life will be consequently reduced. An attempt to scavenge the hydrogen atoms with 0.1 M 2-propanol resulted in a 30% reduction of both the short- and long-lived components, presumably as a result of abstraction of hydrogen by

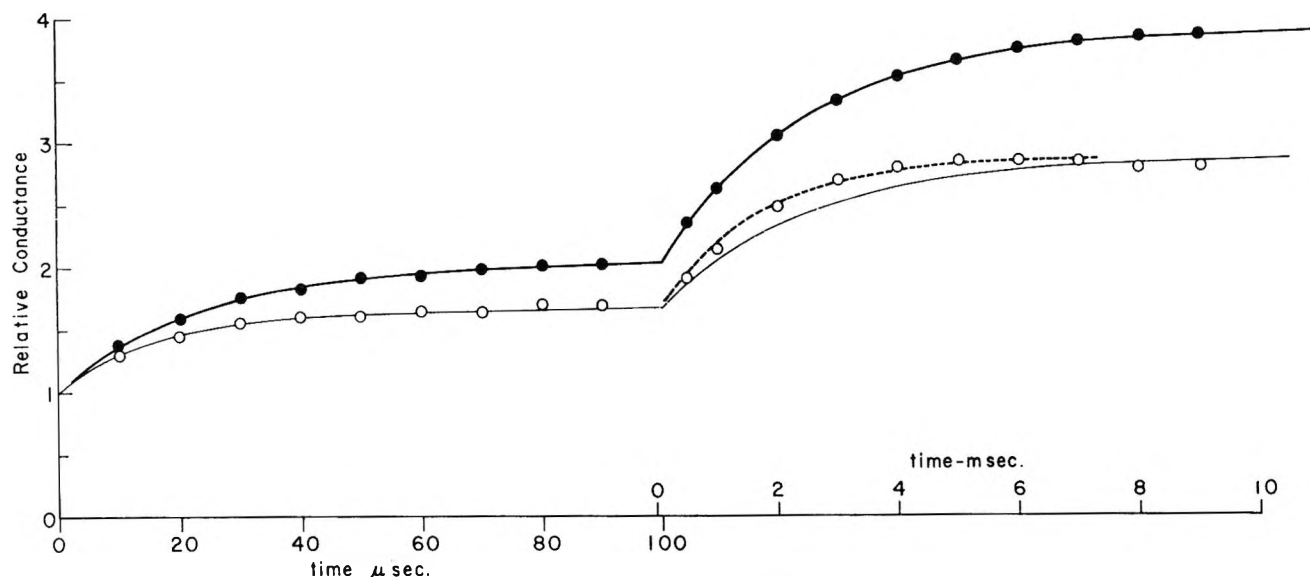


Figure 3. Relative conductance as a function of time calculated from eq I (solid curves) with rate constants as given in the text. Representative data for  $\text{CFCl}_3$  solutions (●) taken from Figure 2b. Similar data for  $\text{CFCl}_3$  solutions containing 0.1  $M$  2-propanol (○) show a 35% reduction in the yield from the secondary reactions and a corresponding decrease in the period of the initial stage. In this latter case the long-term reactions unexpectedly show a similar acceleration (dotted line) without, however, a corresponding reduction in the yield so that complications seem to be present.

the  $\text{CFCl}_2\cdot$  radical. A rate constant of  $2 \times 10^5 M^{-1} \text{sec}^{-1}$  for the abstraction process is required to account for the observed competition. In the type of results obtained here the details of hydrogen atom reactions will be completely obscured by the other secondary processes present.

Summarizing the conductivity results on  $\text{CFCl}_3$ , we can say that it appears that for each hydrated electron which reacts with the  $\text{CFCl}_3$ , as expected one molecule of  $\text{HCl}$  is produced immediately (*i.e.*, in times less than  $10^{-6}$  sec). A second molecule of  $\text{HX}$  (very probably  $\text{HCl}$ ) is then produced in a secondary reaction having a half-period  $\sim 15 \mu\text{sec}$  ( $k_2 = 46,000 \text{sec}^{-1}$ ) and a small additional component resulting from hydrogen atom attack may occur on this same time scale. Two additional molecules of  $\text{HX}$  are subsequently produced at much longer times in tertiary and quaternary reactions with rate constants  $k_3$  and  $k_4$ . From the exponential character of the growth, the third and fourth steps must occur essentially simultaneously, which implies that the third step is rate controlling; *i.e.*,  $k_4 \gg k_3 = 400 \text{sec}^{-1}$ . If we assume that hydrolysis occurs in this stepwise fashion, then, taking into account the growth and decay of the intermediate produced in the second step and the fact that the equivalent conductance of  $\text{HF}$  is 93% of that of  $\text{HCl}$ , the time dependence of the conductivity change relative to that for the initial reaction is given by

relative conductivity =

$$1 + f_s \left\{ 2.93(1 - e^{-(k_2/f_s)t}) - 1.93 \frac{k_2/f_s}{k_3 - k_2/f_s} (e^{-(k_2/f_s)t} - e^{-k_3 t}) \right\} \quad (\text{I})$$

where  $f_s$  is the fraction of the radicals produced in reaction 1 which undergo hydrolysis. This expression is plotted in Figure 3 (with  $k$ 's taken as given above) along with representative data from Figure 2b (normalized at 10 msec) and the curves and data for a 0.1  $M$  2-propanol solution where the secondary reactions are reduced by 35%. Although minor complications may be present in the form of parallel side reactions, the excellent agreement indicates that eq 2 gives a reasonably complete description of the time dependence of the hydrolysis.

The conductivity of a solution additionally saturated with ethylene (0.0043  $M$ ) was also examined, and atypical oscillogram is illustrated in Figure 2c. It is seen that the long-term growth has largely disappeared. The yield of  $\text{HX}$  at 50  $\mu\text{sec}$  is 4.6 and at 5 msec is 5.3. The latter value agrees well with the total of 5.2 estimated from the results of steady-state experiments (correcting the total of 4.25 given in Table I by 0.5 for the increased yield at 0.008  $M$   $\text{CFCl}_3$  and by 0.45 for the somewhat lower ethylene concentration). At 50  $\mu\text{sec}$  the excess over the initial value of the yield (estimated to be 3.1) is reduced to about 50% of the excess observed in the absence of ethylene, and the half-period of the increase in this region is reduced by roughly the same amount. Assuming that the scavenging reaction is



a crude estimate of  $10^4 M^{-1} \text{sec}^{-1}$  can be given for  $k_e$  by equating  $k_e[\text{C}_2\text{H}_4]$  with  $0.693/(17 \times 10^{-6})$ . It is interesting to note that while the extent of the increase on the millisecond time scale is only 10% of that found in the absence of ethylene, the growth period, itself,

does not appear to be reduced significantly. This fact implies that the  $\text{CFCl}_2\cdot$  radical hydrolyzes to a product which is responsible for the long-term growth but which does not react readily with ethylene. If this is so, then it would appear that a yield of 0.35 (*i.e.*, one-half of 0.7) of  $\text{CFCl}_2\cdot$  escapes scavenging by the ethylene (in agreement with the fluoride yield in the steady-state experiments) and that some parallel side reaction contributes to the short-term growth. This interpretation leads to an estimate of  $4 \times 10^7 M^{-1} \text{sec}^{-1}$  for  $k_e$ .

$\text{CF}_2\text{Cl}_2$ . It is seen in Table II that chloride ion is produced in the radiolysis of  $10^{-3} M$   $\text{CF}_2\text{Cl}_2$  solutions with a yield which is essentially twice the yield of solvated electrons. The simplest explanation is that the initial reaction occurs solely with solvated electrons and that, as with  $\text{CFCl}_3$ , hydrolysis of the secondary radical rapidly follows to produce quantitatively the second chloride. This explanation is borne out by the other observations reported here. The rate constant for reaction of hydrated electrons with  $\text{CF}_2\text{Cl}_2$  was determined by examining the reduction in the chloride yield produced by the addition of  $\text{N}_2\text{O}$  or  $\text{H}^+$ . Extrapolation of appropriate plots to infinite  $\text{N}_2\text{O}$  and  $\text{H}^+$  concentration shows that neither  $\text{H}\cdot$  nor  $\text{OH}\cdot$  attack contributes significantly to the chloride yield. Interpretation of the observed reduction in terms of simple competitive scavenging of hydrated electrons by the two solutes gives a value of  $1.4 \times 10^{10} M^{-1} \text{sec}^{-1}$  for the rate constant of reaction 1.

$\text{CF}_2\text{Cl}_2$  is, in many ways, the most complex of the three solutes. First it will be noted in Table II that although the yield of chloride ion from the ethylene-free solution is twice the yield of hydrated electrons, the fluoride ion yield is only 73% as great so that hydrolysis is not complete. Both yields are, however, linearly dependent on dose over the range of  $1$ – $10 \times 10^{18} \text{ eV/g}$ . Examination of the yields over a wide range of dose rates (but at approximately the same total dose) shows that a very interesting dose rate effect is present. A summary of the results obtained at dose rates up to  $10^{23} \text{ eV g}^{-1} \text{sec}^{-1}$  is given in Table V. The detailed data from pulse experiments, which were carried out parallel to those reported above for  $\text{CFCl}_3$ , are given in Table IV. The chloride yield is independent of dose rate up to  $10^{21} \text{ eV g}^{-1} \text{sec}^{-1}$  and drops off by only 10% in the experiments at  $10^{23} \text{ eV g}^{-1} \text{sec}^{-1}$  where combination of the  $\text{CF}_2\text{Cl}\cdot$  radicals is starting to become important. In general, it would appear that, except for experiments at very high dose rates or in the presence of a radical scavenger, hydrolysis of the chloride content is complete and that one can, as was done in the competitive studies, take one-half the chloride yield as a good measure of reaction 1. From the results of the  $\gamma$ -ray experiments this value is  $1/2(5.46) = 2.73$  or only slightly less than expected from the results on methyl chloride or  $\text{CFCl}_3$ .

At the lowest dose rates the fluoride yield is essen-

Table V: Dose Rate Dependence of Yields from  $\text{CF}_2\text{Cl}_2^a$

Dose rate, $\text{eV g}^{-1} \text{sec}^{-1}$	$G(\text{Cl}^-)$	$G(\text{F}^-)$	$G(\text{F}^-)/$ $G(\text{Cl}^-)$
$2.0 \times 10^{13}$	5.47	5.36	0.98
$1.1 \times 10^{14}$	5.43	5.05	0.93
$1.3 \times 10^{15}$	5.46 <sup>b</sup>	3.98 <sup>b</sup>	0.73
$7.5 \times 10^{15}$	5.53 <sup>b</sup>	3.81 <sup>b</sup>	0.69
$2.2 \times 10^{16}$	5.42	3.41	0.63
$6 \times 10^{17}$	(5.46) <sup>c</sup>	1.89	0.345
$2 \times 10^{18}$	(5.46) <sup>c</sup>	1.50	0.275
$3 \times 10^{21}$	5.28	1.49	0.282
$2 \times 10^{23}$	4.86	1.13	0.245

<sup>a</sup> At doses of  $\sim 3 \times 10^{18} \text{ eV/g}$ . <sup>b</sup> Yields are independent of dose from  $1$  to  $7 \times 10^{18} \text{ eV/g}$ . <sup>c</sup> Assumed. The results at higher dose rates indicate that there should be no significant dependence of the chloride yield on dose rate below dose rates of  $10^{20} \text{ eV g}^{-1} \text{sec}^{-1}$ .

tially identical with the chloride yield. However, the yield decreases as the dose rate is increased and at very high dose rates a very substantial reduction in the  $\text{F}^-:\text{Cl}^-$  ratio occurs. This decrease demonstrates that the secondary reactions proceed, for the most part, *via* the production of chloride ion in the second step and fluoride ions in the third and fourth steps. If fluoride ion was produced at the second step, the complementary fragment would be expected to be identical with that formed in the  $\text{CFCl}_3$  system. Since hydrolysis is known to be complete in the latter case, one would not expect a drop in fluoride production here. The fluoride yield does not, however, go to zero at very high dose rates as might be expected from the negligible yield observed in the presence of ethylene so that complications are unquestionably present. If the decrease observed in the region of  $10^{16} \text{ eV g}^{-1} \text{sec}^{-1}$  involves the competition between first- and second-order processes, then the second-order processes should be essentially complete at dose rates above  $10^{20} \text{ eV g}^{-1} \text{sec}^{-1}$ . The fluoride yields observed in the region of  $10^{18}$  to  $10^{22} \text{ eV g}^{-1} \text{sec}^{-1}$  are constant at about 1.5 and indicate that approximately 30% of the  $\text{CF}_2\text{Cl}\cdot$  radicals are completely hydrolyzed. The solid curve of Figure 4 is calculated on the assumption that 70% of the radicals produced in the secondary reaction undergo a second-order process which does not produce fluoride and that this reaction is in competition with a first-order hydrolysis with the rates being equal at a dose rate of  $10^{16} \text{ eV g}^{-1} \text{sec}^{-1}$ . The remaining 30% of the radicals are assumed to be hydrolyzed in all cases.

At dose rates above  $\sim 10^{23} \text{ eV g}^{-1} \text{sec}^{-1}$  an additional drop in fluoride production is expected because of the importance of  $\text{CF}_2\text{Cl}\cdot$  combination reactions (as is evidenced by the decreased chloride yield). The approximate effect expected is indicated in Figure 4 by the dashed curve calculated on the assumption that this effect is 50% complete at a dose rate of  $3 \times 10^{23} \text{ eV}$

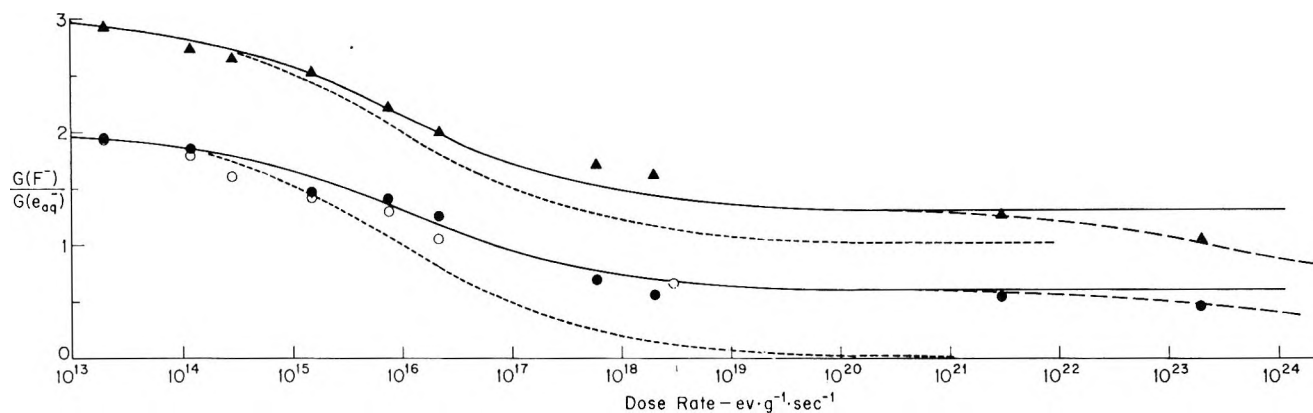


Figure 4. Effect of dose rate on the ratio of yield of fluoride ion produced to that for electrons scavenged for  $10^{-3} M$   $CF_2Cl_2$  (●),  $8 \times 10^{-3} M$   $CF_2Cl_2$  (○), and  $10^{-3} M$   $CF_3Cl$  (▲) solutions at pH 6.5. The absolute yields observed for the  $8 \times 10^{-3} M$   $CF_2Cl_2$  solutions are 15% greater than in the other cases because significant scavenging of electrons within the spurs occurs. The lower solid curve is calculated on the assumption that for 70% of the cases a second-order process removes the precursor of fluoride ion in competition with the first-order tertiary hydrolysis (with equal rates at  $10^{16} eV g^{-1} sec^{-1}$ ). The upper solid curve is similarly calculated on the assumption that fluoride ion is always produced in the secondary step and that 85% of the tertiary species undergo a competition similar to that for  $CF_2Cl_2$ . The dotted curves give the dose rate effects expected if the second-order reactions were 100% effective in removing the fluoride ion produced in the third and fourth steps. The dashed curves on the right represent crude estimates of the dose rate effects expected at high dose rates because of second-order reactions of the radicals produced in reaction 1.

$g^{-1} sec^{-1}$  and that combination of  $CF_2Cl\cdot$  with  $\cdot OH$  produces a limiting fluoride yield of 0.3.

At this point the principal question is as to the source of the fluoride observed in the region of  $10^{21} eV g^{-1} sec^{-1}$ . It would seem that experimental problems involving regions of space or time where the radical concentrations are low can be ruled out since only a trivial fraction (<1%) of the radicals can react under conditions resembling those present at low dose rates. Several mechanistic suggestions can be made. First it is noted that branching at the second step to produce fluoride ion and a chloro-fluoro species can occur. The latter, as indicated above, would be expected to hydrolyze. This explanation is, however, ruled out below. A second suggestion is that as radical-radical reactions become more important at the higher dose rates, some combination of  $CF_2Cl\cdot$  radicals with  $\cdot OH$  will occur. Any  $CF_2Cl(OH)$  produced from such reactions will, of course, rapidly hydrolyze, and a net yield of fluoride will be observed without any effect on the chloride production. From the lifetime ( $\sim 15 \mu sec$ ) of the  $CF_2Cl\cdot$  indicated by the conductivity experiments mentioned below, this effect may be of some small significance in the chemical experiments at dose rates  $\sim 10^{21} eV g^{-1} sec^{-1}$  where the OH lifetime is estimated to be  $\sim 30 \mu sec$ . At intermediate dose rates, other effects involving secondary hydrolysis of radiation-produced product are probably the most significant contributor, as will be discussed later.

We turn now to the conductivity measurements for further help and typical results obtained at pH 5.9 are illustrated in Figure 5a. It is seen that there is an appreciable growth over the first 100  $\mu sec$  with little further growth on the millisecond time scale. At 100

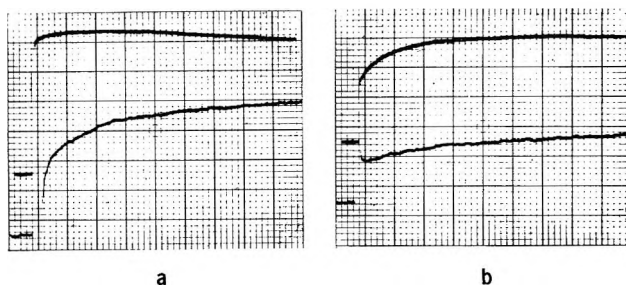


Figure 5. Conductivity changes observed in  $CF_2Cl_2$  saturated solutions (a) at pH 5.9, (b) at pH 5.1. Time scales are 100  $\mu sec/cm$  and 1 msec/cm. Slight drop at long time is the result of ac coupling in the amplifier.

$\mu sec$  the yield is 6.1 and at 5 msec 6.7. The latter is slightly less than the total of 7.0 expected from the yield observed in the steady-state experiments at the same dose rate if the increased solute concentration is taken into account. The growth up to 100  $\mu sec$  appears to be reasonably close to an exponential (with a half-life of  $\sim 15 \mu sec$ ) and can be extrapolated to an initial yield of 3.0. This value can be compared with the expected yield for reaction of hydrated electrons in a saturated solution (2.9). The yield of 6.1 present at 100  $\mu sec$  is twice the initial value showing that the second step in the hydrolysis is complete on this time scale. The growth at longer times corresponds to the production of a further yield of 0.2 equiv of halide ( $G = 0.6$ ) in reactions which have a period of the order to 500  $\mu sec$ . The source of this product is not completely obvious but is probably related to the similar observations on  $CF_3Cl$ , as discussed below, and also to the fluoride yield observed at high dose rates in the steady-state experiments. It is noted, however, that

there is no manifestation of growth with a period as long as the 1.7 msec observed for  $\text{CFCl}_3$ . It is concluded from this that no significant branching to produce fluoride ion occurs in the secondary reactions of  $\text{CF}_2\text{Cl}\cdot$  since such would result in the formation of the same tertiary species (and presumably a 1.7-msec component) as is produced in the case of  $\text{CFCl}_3$ .

Additional exploratory experiments were carried out at lower pH's in order to examine for possible catalytic effects on the hydrolysis rate. At pH 5.1 a very startling increase in lifetime is observed as is illustrated in Figure 5b. At 100  $\mu\text{sec}$  the yield (which was 6.1 at pH 5.9) is reduced to 4.2 and a long-term growth to a total yield of 6.4 occurs on the millisecond time scale ( $t_{1/2} \simeq 700 \mu\text{sec}$ ). In this case the lower curve can be readily extrapolated to zero time where the initial change corresponds to  $G(\text{HCl}) = 2.6$ . The curves of Figure 5b can be fit if one assumes that an additional HX yield of 1.3 is produced by reactions having a half-life of 25  $\mu\text{sec}$  which is then followed by the further production of a yield of 2.5 in reactions with a period of 700  $\mu\text{sec}$ . The large effect of the relatively small change in acid concentration (a factor of 6) on the lifetime cannot be simply a catalytic effect on the rate constant. Rather it would seem that the change in pH or some other unsuspected effect causes a change in the relative importance of two parallel reactions. The fast initial hydrolysis of  $\text{CF}_2\text{Cl}\cdot$  is suppressed in favor of a competing reaction but a mechanistic explanation is not obvious. On the surface it might appear that the hydrolysis reaction is base catalyzed at higher pH's. Such an explanation can, however, be ruled out at pH 5.9 since it would require an impossibly high rate constant ( $>10^{12} M^{-1} \text{sec}^{-1}$ ) to explain the growth period. Further chemical and conductometric studies on this point are obviously very much in order.

**$\text{CF}_3\text{Cl}$  Solutions.**  $\text{CF}_3\text{Cl}$  solutions are somewhat more simple in that, as shown by the negligible yield of fluoride observed in the presence of ethylene (Table II), only chloride ions are produced by the initial reactions of the hydrated electrons. In this case the secondary reactions unambiguously involve the production of fluoride ions. That  $\text{CF}_3\cdot$  radicals are produced and have a sufficient lifetime to be scavenged chemically is shown by esr experiments of Neta and Fessenden on  $\text{CF}_3\text{Cl}$  solutions where signals of the radical produced by their addition to fumaric acid (at  $10^{-3} M$ ) have been observed.<sup>10</sup> Bullock and Cooper<sup>7</sup> also have very recently reported that above pH 8 a yield of 2.4 of  $\text{CF}_3\text{H}$  is produced in the radiolysis of  $\text{CF}_3\text{Cl}$  solutions in the presence of 0.1  $M$  methanol.

A chloride yield of 2.74 ( $\pm 0.04$ ) was found in all experiments carried out in the present study. This yield was independent of dose (from 1 to  $10 \times 10^{18}$  eV/g), dose rate (from  $10^{13}$  to  $10^{23}$  eV  $\text{g}^{-1} \text{sec}^{-1}$ ) or added ethylene (from  $4 \times 10^{-4}$  to  $6 \times 10^{-3} M$ ). Since both hydrogen atoms and hydroxyl radicals should be

effectively eliminated by even low concentrations of ethylene, the lack of its effect on the chloride yield shows that neither of these species contributes to the initial yield. No competitive experiments were carried out but pulse-radiolysis measurements give the rate constant for reaction of hydrated electrons with this solute as  $4.4 \times 10^9 M^{-1} \text{sec}^{-1}$ .<sup>7</sup>

In spite of the simplicity of the initial reaction, some complexity in the subsequent chemistry is immediately apparent in Table I since the fluoride yield (6.78) is only 83% of the yield of 8.2 expected to result from complete hydrolysis. As with  $\text{CF}_2\text{Cl}_2$  this yield is independent of dose at a given dose rate but strongly dependent on dose rate (Table VI). As the dose rate is decreased  $G(\text{F}^-)/$

Table VI: Dose Rate Dependence of Yields from  $\text{CF}_3\text{Cl}^a$

Dose rate, eV $\text{g}^{-1} \text{sec}^{-1}$	$G(\text{Cl}^-)$	$G(\text{F}^-)$	$G(\text{F}^-)/$ $G(\text{Cl}^-)$
$2.0 \times 10^{13}$	2.76	8.00	2.90
$1.1 \times 10^{14}$	2.71	7.45	2.75
$2.8 \times 10^{14}$	2.72	7.21	2.65
$1.3 \times 10^{15}$	2.78 <sup>b</sup>	6.86 <sup>b</sup>	2.47
$7.5 \times 10^{15}$	2.73 <sup>b</sup>	6.06 <sup>b</sup>	2.22
$2.2 \times 10^{16}$	2.76	5.42	1.97
$6 \times 10^{17}$	(2.74) <sup>c</sup>	4.65	1.70
$2 \times 10^{18}$	(2.74) <sup>c</sup>	4.41	1.61
$3 \times 10^{21}$	2.74	3.46	1.26
$2 \times 10^{23}$	2.80	2.85	1.02

<sup>a</sup> At doses of  $\sim 3 \times 10^{18}$  eV/g. <sup>b</sup> Yields are independent of dose from 1 to  $7 \times 10^{18}$  eV/g. <sup>c</sup> Assumed.

$G(\text{Cl}^-)$  approaches a limiting ratio of 3 which corresponds to complete hydrolysis at very low dose rates. At very high dose rates this ratio appears to approach a limit of approximately 1 even though the ethylene experiments indicate that all of the fluoride can be scavenged. The first step in the hydrolysis of  $\text{CF}_3\cdot$  to produce the initial fluoride ion must be slow with respect to scavenging by ethylene but fast with respect to the reactions responsible for the dose rate dependence and subsequent secondary reactions must be considerably slower. It is noted in Figure 5 that the decrease with dose rate occurs in approximately the same region ( $10^{16}$  eV  $\text{g}^{-1} \text{sec}^{-1}$ ) as in the case of  $\text{CF}_2\text{Cl}_2$  and that, in fact, the curves for the two solutes parallel each other quite well. It is of course expected that if chloride ion is, as indicated above, eliminated in the second step in the case of  $\text{CF}_2\text{Cl}_2$ , then the same tertiary species will be produced in both systems and the similarity is not surprising. Since the second step in the present case can only involve production of fluoride ions, one expects the fluoride yield to approach the chloride yield at moderately high dose rates if the competitive processes solely

(10) P. Neta and R. W. Fessenden, private communication.

involve competitive first- and second-order reactions of a difluorinated intermediate, as described above for  $\text{CF}_2\text{Cl}_2$ . A further decrease should be observed as the dose rate is increased into the region where radical-radical reactions remove  $\text{CF}_3\cdot$ . This latter effect should be reasonably important at a dose rate of  $10^{23}$   $\text{eV g}^{-1} \text{sec}^{-1}$  (as it is for  $\text{CFCl}_3$  and  $\text{CF}_2\text{Cl}_2$ ) so the fact that the fluoride yield is observed to be equal to the yield of scavenged electrons at this dose rate appears to be somewhat of an artifact. There must be some source of excess fluoride which compensates for the  $\text{CF}_3$  removed by radical-radical reactions. This point is illustrated even better by the result at  $3 \times 10^{21}$   $\text{eV g}^{-1} \text{sec}^{-1}$  where the reactions responsible for the decreased fluoride yield should be, by arguments similar to those given above in the discussion of  $\text{CF}_2\text{Cl}_2$ , better than 99% complete but where a fluoride yield 26% in excess of the expected value is observed.

It would appear that  $\sim 15\%$  of the  $\cdot\text{CF}_3$  radicals always hydrolyze to give fluoride and that only  $\sim 85\%$  are subject to the competitive processes which cause the reduction in fluoride yield. The upper solid curve in Figure 5 is calculated on this basis (with the relative rates being assumed to be the same as for  $\text{CF}_2\text{Cl}_2$ ). A major difficulty in explaining this small residual fluoride now arises since that most readily advanced in the case of  $\text{CF}_2\text{Cl}_2$  (branching at the second step) cannot apply here (but then this was ruled out for  $\text{CF}_2\text{Cl}_2$  in the discussion of the observed conductivity changes). Reaction of  $\text{CF}_3\cdot$  with  $\cdot\text{OH}$  to produce  $\text{CF}_3\text{OH}$  (which would be followed by hydrolysis) probably contributes significantly at dose rates  $\sim 10^{23}$   $\text{eV g}^{-1} \text{sec}^{-1}$  but, as in the case of  $\text{CF}_2\text{Cl}_2$ , should be of relatively minor importance at  $10^{21}$   $\text{eV g}^{-1} \text{sec}^{-1}$ . Reaction of  $\text{OH}$  with tertiary and quaternary intermediates could be of some importance. Most of these explanations can, however, be ruled out on the basis of lifetime arguments, and at this point it is very probable that secondary reactions of radiation produced product are the most important contributing factor. Studies in the presence of radical scavengers should provide information on this point but are expected to be quite complex because of the high reactivity of the  $\text{CF}_3\cdot$  radicals.<sup>7</sup> If this trivial explanation is correct, then in the absence of complications the fluoride yields from  $\text{CF}_2\text{Cl}_2$  and  $\text{CF}_3\text{Cl}$  should approach 0 and 1 at high dose rates and be described in the intermediate region by the dotted curves in Figure 5. The principal conclusions arrived at here will, however, be unaffected.

The dose rate effect involves the fixing of fluoride in organic form and leaves very few possibilities for the ultimate products since oxygenated fluorides are expected to hydrolyze completely. Because  $\text{CF}_3\cdot$  radicals hydrolyze very rapidly (see below), the production of  $\text{C}_2\text{F}_6$  can be ruled out as being important at all except the highest dose rates. The only possible product which fits the bill would seem to be  $\text{C}_2\text{F}_4$ . The source

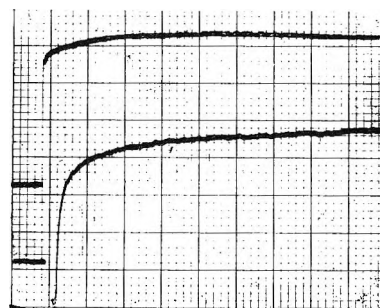


Figure 6. Conductivity change observed in  $\text{CF}_3\text{Cl}$  saturated solution at pH 5.9. Time scales are  $10 \mu\text{sec/cm}$  and  $1 \text{msec/cm}$ .

of this product would, of course, be the combination of  $\text{CF}_2$  radicals, and it seems very likely that any other fate of a difluorinated intermediate will ultimately result in fluoride production. Gas chromatographic analysis for  $\text{C}_2\text{F}_4$  was attempted in experiments carried out at a dose rate of  $7 \times 10^{15}$   $\text{eV g}^{-1} \text{sec}^{-1}$ , but none was detected ( $G(\text{C}_2\text{F}_4) < 0.2$ ). Either its yield is very low or (more likely) it is consumed in addition reactions during the course of the irradiation.

An example of the results of conductivity experiments is illustrated in Figure 6. Here the conductivity change at  $100 \mu\text{sec}$  corresponds to the full development of one equivalent of  $\text{HF}$  in addition to the initial  $\text{HCl}$  [ $(G(\text{HCl}) + G(\text{HF}))_{100 \mu\text{sec}} = 5.4$ ]. The lower curve of Figure 6 can be duplicated if it is assumed that a yield of  $\text{HCl}$  of 2.7 is initially present and that this is then followed by the production of one additional  $\text{HF}$  with  $t_{1/2} = 10 \mu\text{sec}$ . A 15% additional increase ( $\Delta G(\text{HF}) = 0.9$ ) is then observed on the millisecond time scale for a total yield of 6.3 which may be compared with the yield of 6.2 measured chemically at this dose rate.

Steady-state experiments in which the ethylene concentration was decreased to  $5 \times 10^{-4} M$  gave a fluoride yield of 0.48. This yield is only moderately increased over that given in Table II (at  $6 \times 10^{-3} M$ ) so that hydrolysis will compete with addition to ethylene on even terms only when the ethylene concentration is reduced to  $\sim 10^{-4} M$  or less. The addition reaction must be very rapid and if the results of the steady-state and conductivity experiments can be directly compared, then a rate constant of  $\sim 7 \times 10^8 M^{-1} \text{sec}^{-1}$  can be estimated. Bullock and Cooper<sup>7</sup> have obtained a rate constant of  $4 \times 10^7 M^{-1} \text{sec}^{-1}$  in alkaline solution by comparing the addition rate to that for abstraction of hydrogen from formate ion. The absolute rate of the latter was directly determined by observing the formation of  $\text{CO}_2^-$ . If this rate constant were to apply at the lower pH, then the reaction period at  $5 \times 10^{-4} M$  ethylene would be  $35 \mu\text{sec}$ . It is seen in Figure 6 that the second stage of hydrolysis is essentially complete at this time. A major discrepancy exists and the results of the two experiments are not easily reconcilable. Either there is a pronounced dependence of rate on

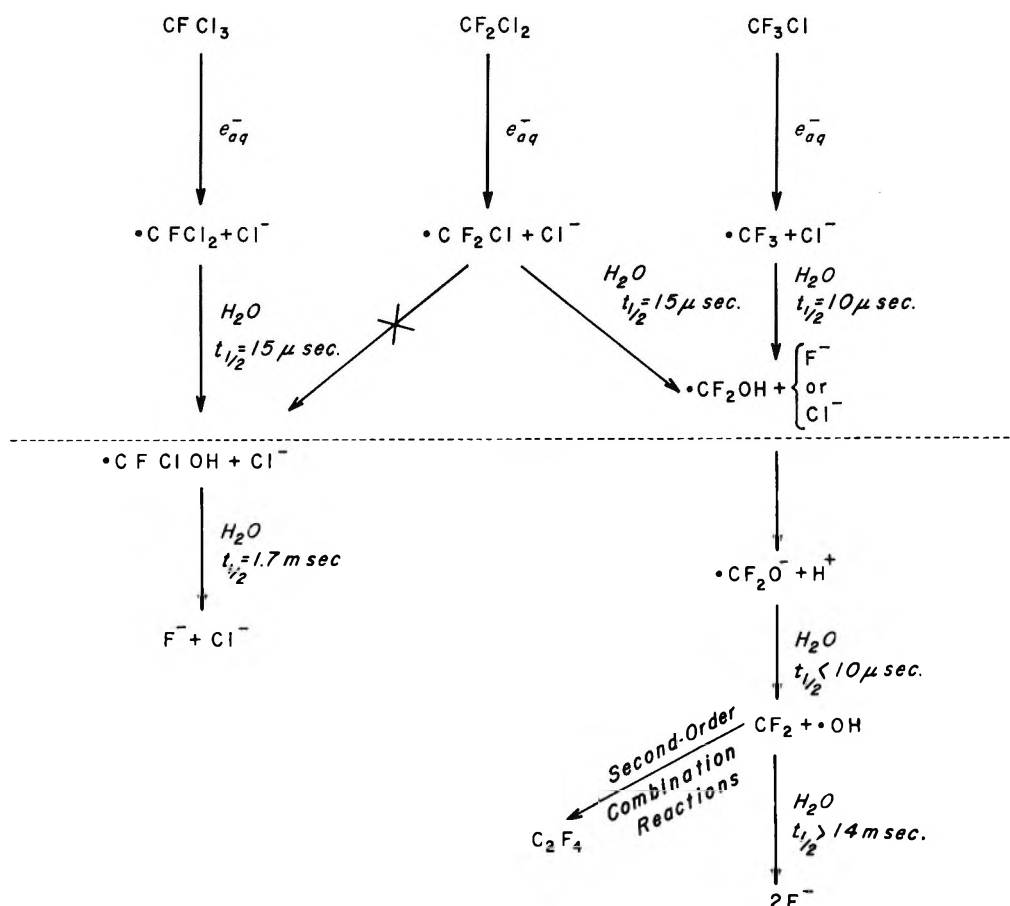


Figure 7. Summary of the major features of the radiation chemical reactions of  $\text{CFCl}_3$ ,  $\text{CF}_2\text{Cl}_2$ , and  $\text{CF}_3\text{Cl}$  in aqueous solutions at  $\text{pH} \sim 6$ . The reactions above the dashed line represent direct conclusions from the experimental observations and are reasonably certain. It is noted that  $\cdot\text{CF}_2\text{Cl}$  does not appear to hydrolyze significantly to  $\cdot\text{CFClOH}$  and  $\text{F}^-$ . The order in which the halide ions are produced from  $\cdot\text{CFCl}_2$  is unknown. The suggested path for the reactions of  $\cdot\text{CF}_2\text{OH}$  is speculative but conforms to the observed dose rate dependence of the fluoride yields from  $\text{CF}_2\text{Cl}_2$  and  $\text{CF}_3\text{Cl}$  and the fact that the conductivity observed on the microsecond time scale is explained entirely by the two equivalents of  $\text{HX}$  produced in the first two steps.

$\text{pH}$  or the results of one or both experiments are being misinterpreted.

The rate constant for the addition of  $\text{CF}_3\cdot$  radicals to ethylene has been given as  $3 \times 10^6 \text{ M}^{-1} \text{ sec}^{-1}$  in liquid hydrocarbons<sup>8</sup> and as  $3.5 \times 10^6 \text{ M}^{-1} \text{ sec}^{-1}$  in the vapor phase.<sup>11</sup> The rate constant for the addition reaction in aqueous solution simply cannot be as low as indicated by these latter values since such would require a  $\text{CF}_3\cdot$  lifetime of at least milliseconds to explain the highly efficient scavenging by the ethylene. It is seen quite clearly in Figure 6 that hydrolysis occurs on a much shorter time scale. A very pronounced increase (two orders of magnitude) in the rate of  $\text{CF}_3\cdot$  addition to ethylene in the aqueous system over that in hydrocarbon solution or in the gas phase is indicated.

### Summary

The major features of the above results seem to be quite clear although certain minor details are not completely understood at the present time and complete elucidation will require further study. The various steps are, as far as they are known, summarized in the

flow diagram of Figure 7. For all three solutes the initial reaction of the hydrated electrons appear to be exclusively according to reaction 1 to produce a chloride ion. The first step in the hydrolysis of the complementary radical then occurs with a period of the order of  $10 \mu\text{sec}$  and, if oxidation or reduction does not occur, material balance requires that the reaction be



The subsequent chemistry is more complex and several specific points are discussed here.

In the conductivity experiments the total doses were small even through the dose rates were moderately high and the radical concentrations built up to only a small fraction of those which would be present at steady state. For example, in the experiments of Figures 2, 5, and 6 the doses were  $\sim 10^{16} \text{ eV/g}$  and the radical concentrations produced were only  $\sim 5 \times 10^{-7} \text{ M}$ . Assuming a maximum second-order rate constant of

(11) J. M. Sangster and J. C. J. Thynne, *J. Phys. Chem.*, **73**, 2083 (1969).

$10^{10} M^{-1} \text{sec}^{-1}$  the radicals will have, at this concentration, a minimum mean lifetime toward combination of 200  $\mu\text{sec}$  and very little radical-radical reaction will occur before the initial stage of hydrolysis is complete. The products of this hydrolysis, however, appear to have a longer lifetime so that complicating effects are possible at later stages.

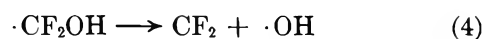
In the chemical experiments the total doses used were several orders of magnitude greater than in the conductivity experiments and the radical concentrations approached their steady-state values. In spite of this, the yields observed in the two types of experiments at a dose rate of  $10^{21} \text{eV g}^{-1} \text{sec}^{-1}$  are comparable and the reaction paths not obviously different. In the chemical experiments at the highest dose rates the mean radical lifetimes for diffusion-controlled processes will be comparable to the period of the initial hydrolysis so that formation of  $\text{CX}_3\text{CH}$  will undoubtedly occur and contribute to the observed yields. Because of this, fluoride production is not expected to go to zero at infinite dose rate. The effects expected for  $\text{CF}_2\text{Cl}_2$  and  $\text{CF}_3\text{Cl}$  at high dose rates are approximately described by the dashed curves of Figure 5 but an exact description depends in detail on reaction rate and mechanistic assumptions. In principle, the rate constant for  $\text{CF}_3\cdot$  combination should be determinable from such studies by referencing the drop in fluoride yield to the rate of the initial hydrolysis. Unfortunately, the complicating factors in the chemical experiments place a large uncertainty on such a determination. For the curves as drawn the rate constant is  $10^9 M^{-1} \text{sec}^{-1}$ . Further detailed chemical and conductometric studies in the presence of scavengers should help here.

The drop in fluoride yield observed in the region of  $10^{16} \text{eV g}^{-1} \text{sec}^{-1}$  is, as far as can be seen, common to  $\text{CF}_2\text{Cl}_2$  and  $\text{CF}_3\text{Cl}$  and seems unquestionably to result from the second-order reaction of a difluorinated species which hydrolyzes relatively slowly. It is suggested that this species is very probably  $\text{CF}_2$  and that combination reactions fix fluoride in an organic form (presumably  $\text{C}_2\text{F}_4$  since as indicated above any simple oxygenated product would ultimately hydrolyze). The production rate at a dose rate of  $10^{16} \text{eV g}^{-1} \text{sec}^{-1}$  is only  $5 \times 10^{-7} M \text{sec}^{-1}$  so that the half-period toward hydrolysis of the intermediate responsible for the dose rate effect must be 14 msec (assuming the rate constant of the competing second-order process to be  $10^{10} M^{-1}$

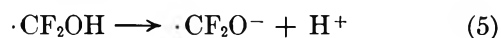
$\text{sec}^{-1}$ ) or greater. The sensitivity and low-frequency response characteristics of the conductivity apparatus are not suitable for direct observation of this reaction. Chemical experiments to demonstrate (and if possible make use of) this intermediate must be carried out under very critically controlled concentration and dose rate conditions in order to avoid the scavenging of its very reactive precursor.

It is noted that the electron-withdrawing properties of fluorine almost certainly ensure that  $\cdot\text{CF}_2\text{OH}$  is a moderately strong acid<sup>12</sup> and it should rapidly ionize at pH 6. No additional ions are, however, apparent in the conductivity experiments so that the lifetime of  $\cdot\text{CF}_2\text{OH}$  must be short with respect to its formation period, *i.e.*, 10  $\mu\text{sec}$ . Such a situation will greatly simplify the possible secondary paths in that complicating features involving second-order reactions of  $\cdot\text{CF}_2\text{OH}$  (which would almost certainly produce fluoride ion) will be eliminated. If this is the case, all intermediates except  $\text{CF}_2$ , H, and OH must have short lifetimes and the additional ionized products observed in the conductivity experiments on the millisecond time scale and the excess fluoride found in the chemical experiments must be the result of trivial reactions with radiation-produced product (probably  $\text{C}_2\text{F}_4$ ).

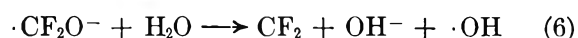
If  $\text{CF}_2$  is an important intermediate, the question arises as to how it is formed since further reduction of the carbon is required. Two possible paths, which are stoichiometrically equivalent, involve either the direct dissociation of  $\cdot\text{CF}_2\text{OH}$  (formed in reaction (3)) into  $\text{CF}_2$  and  $\cdot\text{OH}$



or, more probably, ionization



followed by oxidation of water



In both cases the driving force for the reaction would have to be the energy released in forming singlet  $\text{CF}_2$ . Further work obviously needs to be done to corroborate the identity of the species which follow the initial hydrolysis of the radical formed in reaction 1.

(12) By analogy with  $(\text{CF}_3)_2\dot{\text{C}}\text{OH}$  which G. Laroff and R. W. Fessenden (private communication) have found to have a  $pK < 2$ .

# Origin of Complex Electron Spin Resonance Spectra of $\gamma$ -Irradiated Polycrystalline *n*-Alkyl Iodides with Even Number of Carbon Atoms per Molecule<sup>1</sup>

by R. J. Eglund, P. J. Ogren, and J. E. Willard\*

Department of Chemistry, University of Wisconsin, Madison, Wisconsin 53706 (Received July 30, 1970)

Publication costs assisted by the University of Wisconsin

The esr spectra of six isotopically different  $\gamma$ -irradiated polycrystalline ethyl iodides ( $C_2H_5^{127}I$ ,  $C_2H_5^{129}I$ ,  $C_2D_5^{127}I$ ,  $C_2D_5^{129}I$ ,  $CH_3CD_2^{127}I$ , and  $CD_3CH_2^{127}I$ ) have been examined to assist in determining the origin of the unusual 1000-G wide pattern from  $C_2H_5I$ . Comparison of the spectra from  $C_2H_5I$ ,  $C_2D_5I$ ,  $CH_3CD_2I$ , and  $CD_3CH_2I$  confirms the contribution of hyperfine splitting by hydrogen and indicates that it is due primarily to the methyl hydrogen atoms with little or no contribution from the methylene hydrogens. Comparison of the X- and Q-band spectra of  $\gamma$ -irradiated polycrystalline  $C_2H_5I$  indicates that the great spectral width is not caused by anisotropic  $g$  values, reopening the question as to whether it may be the result of hyperfine splitting by iodine. This has been investigated by the substitution of  $^{129}I$  for  $^{127}I$ . Exposure of  $\gamma$ -irradiated polycrystalline  $C_2H_5I$  to near-infrared radiation converts the complex esr spectrum into the ethyl radical spectrum.  $\gamma$  irradiation of polycrystalline  $C_2H_4I_2$  does not produce the spectrum obtained from  $C_2H_5I$ .  $\gamma$  irradiation of all glassy and polycrystalline *n*-alkyl chlorides and bromides from  $C_2$  to  $C_6$ , as well as the glassy iodides and odd-carbon-number polycrystalline iodides, yields only the spectrum of the alkyl radical. The hypothesis that the complex spectra from the  $C_2$ ,  $C_4$ ,  $C_6$ , and  $C_8$  *n*-alkyl iodides result from physically trapped electrons is considered. In this case the breadth of the spectrum results from hyperfine splitting by iodine nuclei. The difference between the spectra observed for the alkyl halides with odd and even numbers of C atoms per molecule then indicates that the branching ratio between physical trapping and dissociative capture is controlled by small differences in the crystal structure of the matrix.

## Introduction

Polycrystalline  $C_2H_5I$  which has been  $\gamma$ -irradiated at 77°K gives an unexpectedly complex esr spectrum with more than 32 lines spread over 1000 G.<sup>2,3</sup> Similar complexity with varying spreads is found for the polycrystalline forms of other *n*-alkyl iodides having an even number of carbon atoms per molecule through  $C_8$ , but not for the odd-carbon-number species<sup>2</sup> or the glassy<sup>2-5</sup> forms. As a result of experiments with  $C_2D_5I$  which showed that hyperfine coupling with hydrogen contributes to the line structure, and with  $C_2H_5^{129}I$  which failed to show that hyperfine coupling with iodine is involved, it has been suggested that the breadth of the spectra results from coupling of the spin of the unpaired electron in a species such as  $C_2H_5I^+$  or  $C_2H_5I^-$  with orbital angular momentum on the iodine to give radicals with anisotropic  $g$  values.<sup>3</sup> To further test this hypothesis and obtain additional information on the "odd-even effect" we have compared the spectrum at 35-GHz microwave frequency with that at 9.5 GHz, eliminated the interfering signals from the irradiated quartz sample tube, observed the spectra from  $CD_3CH_2I$ ,  $CH_3CD_2I$ , and  $CD_3CD_2^{129}I$ , determined radiation  $G$  values, and compared the alkyl iodide spectra with those of alkyl bromides and chlorides. The added information leads to revised interpretations.

## Experimental Section<sup>6</sup>

$C_2D_5I$ ,  $CD_3CH_2Br$ ,  $CH_3CD_2I$ , and  $C_2D_5Br$ , of stated isotopic purity of 98% or higher, were used as received from Merck Sharpe and Dohme, Ltd., after drying over  $P_2O_5$  on the vacuum line.  $C_2D_5^{129}I$  and  $CD_3CH_2^{127}I$  were made from the bromides by the reaction  $3C_2D_5Br$  (or  $3CD_3CH_2Br$ ) +  $AlI_3 \rightarrow 3C_2D_5I$  (or  $CD_3CH_2I$ ) +  $AlBr_3$ ,<sup>7a</sup> under vacuum.  $AlI_3$  was formed by heating  $I_2$  with granular Al.  $^{129}I_2$  was prepared from an acidified  $Na^{129}I$  solution (Oak Ridge National Laboratory) by addition of  $PdCl_2$  followed by heating of the precipitated  $PdI_2$ . Deuterated ethyl bromide was allowed to react with  $AlI_3$  in the absence of air for 12 hr

(1) This work has been supported in part by the U. S. Atomic Energy Commission under Contract AT(11-1)-1715, by the W. F. Vilas Trust of the University of Wisconsin, and by NSF and Danforth Foundation fellowships held by P. J. Ogren.

(2) H. W. Fenrick, S. V. Filseth, A. L. Hanson, and J. E. Willard, *J. Amer. Chem. Soc.*, **85**, 3731 (1963).

(3) H. W. Fenrick and J. E. Willard, *ibid.*, **88**, 412 (1966).

(4) P. B. Ayscough and C. Thompson, *Trans. Faraday Soc.*, **58**, 1477 (1962).

(5) B. Smaller and M. S. Matheson, *J. Chem. Phys.*, **28**, 1169 (1958).

(6) Additional details are given by (a) P. J. Ogren, Ph.D. Thesis, University of Wisconsin (1968); (b) R. J. Eglund, Ph.D. Thesis, University of Wisconsin (1968).

(7) (a) H. C. Brown and W. J. Wallace, *J. Amer. Chem. Soc.*, **75**, 6279 (1953); (b) H. W. Harvey, J. C. Hoh, W. F. Podolski, and G. H. Youngquist, Proceedings of the 13th Conference on Remote Systems Technology, Hinsdale, Ill., 1965, p 152.

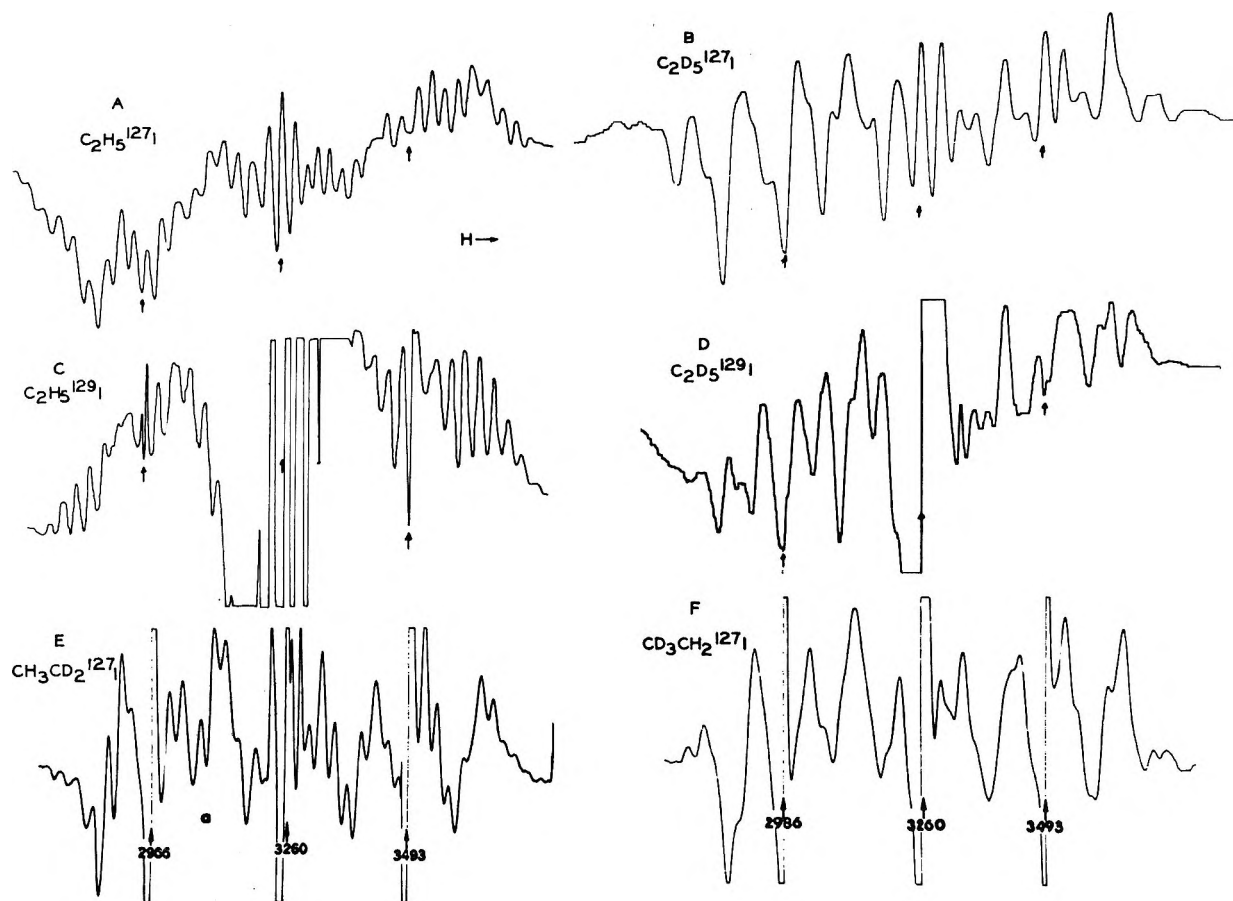


Figure 1. ESR spectra of  $\gamma$ -irradiated isotopically substituted polycrystalline ethyl iodides at 77°K:  $\gamma$  dose  $4 \times 10^{19}$  eV g<sup>-1</sup>, modulation amplitude (MA) 1250, signal level 200 to 800. (A) C<sub>2</sub>H<sub>5</sub><sup>127</sup>I removed from irradiation tube and mechanically randomized; (B) C<sub>2</sub>D<sub>5</sub><sup>127</sup>I removed from irradiation tube and mechanically randomized; (C) C<sub>2</sub>H<sub>5</sub><sup>129</sup>I in thin ordinary quartz tube; (D) C<sub>2</sub>D<sub>5</sub><sup>129</sup>I in thin ordinary quartz tube; (E) CH<sub>3</sub>CD<sub>2</sub><sup>127</sup>I in Suprasil; (F) CD<sub>3</sub>CH<sub>2</sub><sup>127</sup>I in Suprasil. In each section of the figure the three vertical arrows indicate the magnetic fields at which the hydrogen doublet and central signal from  $\gamma$ -irradiated ordinary quartz or Suprasil appear when the spectrum is taken without removing the sample tube. For the microwave frequency used, these signals are at 2986, 3260, and 3493 G. The intense group of lines in the center of the C<sub>2</sub>H<sub>5</sub><sup>129</sup>I spectrum is due to C<sub>2</sub>H<sub>5</sub> radicals produced from a small amount of (C<sub>2</sub>H<sub>5</sub>)<sub>4</sub>Sn remaining from the synthesis used for preparation of the C<sub>2</sub>H<sub>5</sub><sup>129</sup>I.

at 0°, following which the volatile material was distilled under vacuum and pumped on at -78°. The remaining ethyl iodide contained 1-2% C<sub>2</sub>H<sub>5</sub>Br, as measured by gas chromatography. Mass spectrometric analysis of CD<sub>3</sub>CH<sub>2</sub>I showed <2% C<sub>2</sub>HD<sub>4</sub>I and <7% C<sub>2</sub>H<sub>3</sub>D<sub>2</sub>I.

CH<sub>3</sub>CH<sub>2</sub><sup>129</sup>I was prepared by the reaction of tetraethyltin and <sup>129</sup>I<sub>2</sub> as described previously.<sup>3</sup> CH<sub>2</sub>-ICH<sub>2</sub>I (Aldrich) was recrystallized from ethanol. The other alkyl halides were Eastman White Label, dried over P<sub>2</sub>O<sub>5</sub> under vacuum.

X-Band esr measurements were made with a Varian 4500 spectrometer. The degassed samples in 3 mm i.d., 4 mm o.d. Suprasil tubes were measured under liquid N<sub>2</sub> at 77°K following  $\gamma$  irradiation at 77°K with a <sup>60</sup>Co source at a dose rate of  $2 \times 10^{18}$  eV g<sup>-1</sup> min<sup>-1</sup>. To avoid the esr signals from irradiated Suprasil, some irradiated samples were forced out of the broken tube under liquid nitrogen, with a wire, and allowed to fall

to the bottom of the esr dewar. In other experiments, the esr signal from H atoms was minimized by using very thin-walled sample tubes made of ordinary fused silica. (The H-atom signal induced in ordinary fused silica by  $\gamma$  irradiation is an order of magnitude smaller than that from Suprasil of the same thickness exposed to the same radiation dose, although the central "electron" signal is much larger.)

Measurements at 35.5 GHz (Q band) were made at the Chemistry Division of the Argonne National Laboratory, with the generous assistance of Dr. Peter Schindler in the laboratory of Dr. John Weil, using a Varian V-4566 cylindrical Q-band cavity, and a <sup>60</sup>Co source<sup>7b</sup> delivering  $3 \times 10^{19}$  eV g<sup>-1</sup> min<sup>-1</sup> to the samples which were in 2.5 mm o.d. thin-walled quartz tubes. The cavity was cooled by immersing the tuning rod at the bottom in liquid nitrogen. The decay rate of esr signals from samples in quartz tubes imbedded in Cry-Con high-heat conductivity grease in a recess in

the top of the tuning rod, at the bottom of the cavity, was similar to that of signals from samples known to have been held at 77°K in the X-band cavity.

## Results

**Effects of Isotopic Substitution.** The esr spectra of  $\gamma$ -irradiated polycrystalline  $C_2H_5^{127}I$ ,  $C_2D_5^{127}I$ ,  $C_2H_5^{129}I$ ,  $C_2D_5^{129}I$ ,  $CH_3CD_2^{127}I$ , and  $CD_3CH_2^{127}I$  are given in Figure 1. The first two of these were taken on samples which had been removed from the irradiation tubes and thus show the structure of the radical spectra in the regions previously<sup>2,3</sup> obscured by the hydrogen doublet and central signal from the irradiated Suprasil. The samples of  $C_2H_5^{129}I$  and  $C_2D_5^{129}I$  irradiated and observed in thin-walled ordinary quartz tubes gave a more favorable ratio of the H-atom doublet to the radical signals than had been achieved<sup>3</sup> in Suprasil.

**Comparison of X-Band and Q-Band Spectra.** If the unusual width of the 9.5-MHz (X band) spectrum of Figure 1 results from an anisotropic *g* tensor of I-containing radicals, the width of the spectrum measured in the Q band (35.5 GHz) could be as much as 4000 G, since the separation between esr lines associated with different *g* values is directly proportional to the microwave frequency. The Q-band spectrum of a sample of  $C_2D_5^{127}I$  in a Suprasil tube is shown in Figure 2. To a close approximation its width is the same as that of the "1000-G spectrum" observed in the X band. Thus *g* anisotropy does not make a major contribution to the width of these spectra.

**Mechanical Randomization of Oriented Crystals.** The spectra of Figures 1A and B were taken after breaking the irradiated samples into small pieces with a wire. Before pulverizing, the  $C_2H_5^{127}I$  spectrum showed major changes when the esr dewar was rotated 90° around its vertical axis. After pulverizing there was no such orientation effect. This confirms that there is net orientation of the crystallites formed by crystallization of ethyl iodide in an esr tube. In contrast to the  $C_2H_5I$  spectra the relatively broad lines from the  $\alpha,\beta$ - and  $\beta$ -deuterated samples changed only slightly when rotated. Consequently meaningful comparison of spectra B and D of Figure 1 was possible even though the latter had not been randomized.

**Ethyl Radicals in Polycrystalline  $C_2H_5I$ ; Photobleaching Effects.** Ethyl radicals contribute to the central portion of the esr signal of samples such as that of Figure 1A, the intensity of the ethyl sextet varying with the purity of the  $C_2H_5I$ . In samples with 5% impurity, the ratio of the sextet lines to the other lines was ten times larger than for the purified sample of Figure 1. The complex spectra of other even-C-number alkyl iodides tested were not sensitive to low levels of impurity.

Exposure of  $\gamma$ -irradiated polycrystalline  $C_2H_5I$  to a 630–1000-nm band of radiation from a tungsten lamp with filters has been shown by Calin Roy of our lab-

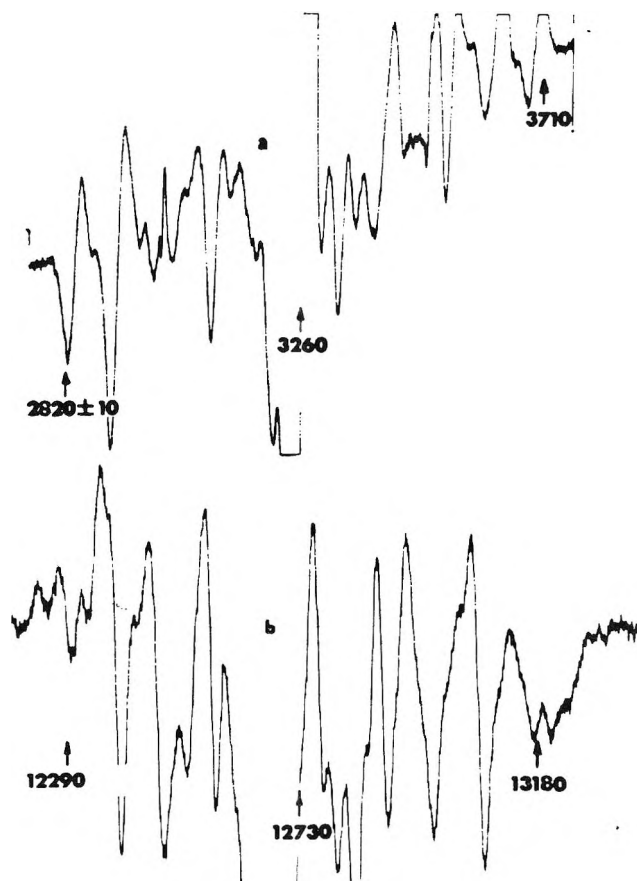


Figure 2. Q-Band esr spectrum of  $\gamma$ -irradiated polycrystalline  $C_2D_5I$  compared to X-band spectrum: dose  $6 \times 10^{19}$  eV  $g^{-1}$ . (a) X band, MA 1250; (b) Q band, MA 1000. The numbers indicate the magnetic fields in gauss corresponding to the positions of the arrows.

oratory to cause a decrease in most of the lines of the spectrum of Figure 1, but relatively little decrease in the lines attributed to the  $C_2H_5$  radical.

**Spectra of Polycrystalline Alkyl Halides Other Than Ethyl Iodide.** All  $\gamma$ -irradiated polycrystalline *n*-alkyl iodides with even C number from  $C_2H_5I$  through  $C_8H_{15}I$  show broader more complex esr spectra than would be produced by the alkyl radicals formed by rupture of the C–I bond.<sup>3</sup> The spectral breadth and complexity decrease with increasing carbon number. The present work shows a further decrease for  $\gamma$ -irradiated polycrystalline *n*- $C_{10}H_{21}I$  which gives an esr spectrum of six well-defined lines centered at the free electron *g* value with a splitting of about 25 G, with perhaps two very much weaker lines on each wing. All  $\gamma$ -irradiated polycrystalline *n*-alkyl bromides and chlorides from  $C_2$  to  $C_6$  have been tested,<sup>6b</sup> and, like the iodides with odd C number, all give the six-line spectrum characteristic of the corresponding alkyl radical and no evidence of an "odd-even effect."

$\gamma$ -Irradiated polycrystalline  $C_2H_4I_2$  gives a broad unresolved esr spectrum,<sup>6b</sup> unlike that from either glassy or polycrystalline  $C_2H_5I$ , suggesting that  $C_2H_4I$  is not responsible for the "1000-G signal" from  $C_2H_5I$ .

## Discussion

The most significant conclusions to be drawn from the experiments described above are (1)  $g$  anisotropy does not make a major contribution to the width of the "1000-G spectrum" of polycrystalline ethyl iodide, (2) the width and complexity of the spectrum is probably attributable to hyperfine splitting by iodine, and (3) the unpaired electrons responsible for the spectrum undergo hyperfine coupling with the  $\beta$ -hydrogen atoms of ethyl iodide but little or no interaction with the  $\alpha$ -hydrogen atoms. The first conclusion follows from the similar widths of the X-band and Q-band spectra, the second from the differences between the spectra of the  $^{127}\text{I}$  and  $^{129}\text{I}$  species, and the third from the similarity of the spectrum of  $\text{CH}_3\text{CD}_2\text{I}$  to that of  $\text{C}_2\text{H}_5\text{I}$ , and of that of  $\text{CD}_3\text{CH}_2\text{I}$  to that of  $\text{C}_2\text{D}_5\text{I}$ .

The differences between the spectra of the  $^{127}\text{I}$  and  $^{129}\text{I}$  species are most clearly illustrated by comparison of the  $\text{C}_2\text{D}_5^{127}\text{I}$  and  $\text{C}_2\text{D}_5^{129}\text{I}$  samples because their spectra do not show the large anisotropic effects with rotation which make meaningful comparisons of  $\text{C}_2\text{H}_5\text{I}$  samples difficult. The line structure of Figure 1D ( $\text{C}_2\text{D}_5^{129}\text{I}$ ) is distinctly different from that of Figure 1B ( $\text{C}_2\text{D}_5^{127}\text{I}$ ) indicating hyperfine splitting by iodine. If complete resolution were achieved, the ratio of number of lines for the  $^{127}\text{I}$  and  $^{129}\text{I}$  samples would be 0.75 (the spins are 5/2 and 7/2). It is not surprising that this difference is obscured, as is much of the hydrogen hyperfine splitting, by the unresolved broad lines of the deuterated samples. Another criterion of hyperfine splitting by iodine is a difference of total spectral breadths for the  $^{127}\text{I}$  and  $^{129}\text{I}$  samples. The ratio should be the ratio of nuclear magnetic moments, which is 1.08. The widths of all the spectra of the  $^{127}\text{I}$  samples examined appear to be greater than those of the  $^{129}\text{I}$  samples, consistent with the predicted ratio.

If there is hyperfine coupling with iodine, the 1000-G breadth of the spectrum is not unexpected, since the esr spectrum of free I atoms in the gas phase is 2000 G wide.<sup>8</sup> The number of lines (*ca.* 40 in Figure 1A) is more surprising. Free  $^{127}\text{I}$  and  $^{129}\text{I}$  atoms in a condensed phase would give six and eight lines, respectively. Splitting of each of these lines by equal coupling with three H atoms on the methyl group of the  $\text{C}_2\text{H}_5\text{I}$  would lead to 24 and 32 lines. The larger number of lines observed suggests coupling with more than one I atom or methyl group, small  $g$  anisotropies resulting from spin-orbit coupling, or anisotropic hyperfine coupling to I.

It has been reasoned<sup>3</sup> that the most plausible species to account for the observed spectrum from  $\gamma$ -irradiated polycrystalline  $\text{C}_2\text{H}_5\text{I}$  is  $\text{C}_2\text{H}_5\text{I}^+$  or  $\text{C}_2\text{H}_5\text{I}^-$ . The evidence (Figures 1E and 1F) that the unpaired electron couples with the  $\beta$ -hydrogen atoms but not the  $\alpha$ -hydrogen atoms of the  $\text{C}_2\text{H}_5\text{I}$  molecule argues against this conclusion. The species responsible for the spectrum

must be consistent with the following observations: (1) hyperfine splitting by iodine, (2) hyperfine splitting by the  $\beta$ - but not the  $\alpha$ -hydrogen atoms, (3) production of  $\text{C}_2\text{H}_5$  radicals by "momentary anneal" at 147°K of crystals formed by rapid crystallization, (4) production of the broad type of spectrum in  $n$ -alkyl iodides with even numbers of C atoms up to  $\text{C}_8$  and not higher, but not in those with odd numbers of C atoms.

The failure of  $\gamma$  irradiation to produce alkyl radicals in polycrystalline alkyl iodides of even-C-number indicates that the electrons from the irradiation must undergo a fate other than the dissociative electron capture typical of electrons in the presence of alkyl halides. The  $G$  value of  $\text{C}_2\text{H}_5$  radicals in the radiolysis of  $\text{C}_2\text{H}_5\text{I}$  glass at 77°K is well established to be *ca.* 2, values of 1.5,<sup>9</sup>  $2.0 \pm 0.4$ ,<sup>4</sup>  $2.2 \pm 0.5$ ,<sup>6a</sup> and  $2.2 \pm 0.4$ <sup>6b</sup> having been reported. The  $G$  value for the species giving the complex spectrum in polycrystalline  $\text{C}_2\text{H}_5\text{I}$  is not as well established. The early estimates of 0.33<sup>9</sup> and *ca.* 0.01<sup>2</sup> were undoubtedly much too low. Our current best estimate of *ca.* 3 is subject to uncertainties in the integration of the complex spectrum, and power saturation differences between the glass and crystal but is similar to the yield of alkyl radicals in the glasses.

The fate of the electrons in the even-C-number polycrystalline alkyl iodides must be either prompt neutralization, formation of  $\text{RI}^-$  without dissociation, or physical trapping. On the basis of the facts now available, we postulate that the fate is physical trapping and that this trapping accounts for the complex spectra by allowing coupling with I atoms and  $\beta$ -hydrogen atoms of the  $\text{C}_2\text{H}_5\text{I}$ . This hypothesis is similar to the well-supported conclusion of Williams and coworkers<sup>10</sup> that electrons can be physically trapped and coupled with two nitrogen atoms in  $\text{CD}_3\text{CN}$ , and that when photochemically released they react by dissociative capture to give  $\text{CD}_3$  radicals ( $\text{CD}_3\text{CN} + e \rightarrow \text{CD}_3 + \text{CN}^-$ ), or form  $\text{CD}_3\text{CN}^-$ . According to the hypothesis the molecular packing of all the glassy  $n$ -alkyl halides and the polycrystalline  $n$ -alkyl halides except the iodides with two, four, six, and eight carbon atoms is such that electrons readily undergo dissociative capture, as they do in liquid alkyl halides<sup>11a</sup> and with alkyl halides present as solutes in hydrocarbon glasses.<sup>11b</sup> In the two-, four-, six-, and eight-carbon normal iodides the crystal structure is such that the energetics or kinetics of dissociative capture and physical trapping are altered to favor the latter.

(8) S. Aditya and J. E. Willard, *J. Chem. Phys.*, **44**, 833 (1966).

(9) G. L. Hermann and L. A. Harrah, Technical Report AFML-TR-65-333, 1966.

(10) (a) M. A. Bonin, K. Tsuji, and F. Williams, *Nature*, **218**, 946 (1968); (b) M. A. Bonin, K. Takeda, K. Tsuji, and F. Williams, *Chem. Phys. Lett.*, **2**, 363 (1968); (c) M. A. Bonin, K. Takeda, and F. Williams, *J. Chem. Phys.*, **50**, 5423 (1969); (d) K. Takeda and F. Williams, *J. Phys. Chem.*, in press.

(11) (a) P. R. Geissler and J. E. Willard, *J. Amer. Chem. Soc.*, **84**, 4627 (1962); (b) R. F. C. Claridge and J. E. Willard, *ibid.*, **87**, 4992 (1965).

Whereas physically trapped electrons have been observed in a variety of hydrocarbon glasses, trapping yields in low-molecular-weight polycrystalline hydrocarbons are much lower, or nonexistent. This has been attributed to the absence of suitable voids in the ordered crystalline structure,<sup>10b</sup> or to a greater mobility of positive charge.<sup>12</sup> Williams and coworkers<sup>10b</sup> conclude that the mechanism of electron trapping in crystalline organic cyanides is dependent on the dipole fields of the individual molecules and specific features of the crystalline structure. They suggest that the phenomenon may be of general occurrence in molecular crystals.

Reasons may be advanced for believing that the trapping in acetonitrile is as the anionic dimer  $(\text{CD}_3\text{CN})_2^-$  rather than as more delocalized electrons.<sup>13</sup> The distinction between physically trapped electrons and anions in the crystalline nitriles and the organic iodides probably cannot be correctly made as "either-or." Rather there may exist a range of trapping situations varying in extent of unpaired electron delocalization. The complexity of the polycrystalline ethyl iodide spectrum, containing both iodine and proton hyperfine structure, precludes a decision as to how many nuclei contribute to the hyperfine interaction. The hyperfine anisotropy of the broad spectrum (as shown by the "orientation effect") implies a well-defined molecular orbital, rather than the isotropic delocalized orbital characteristic of electrons trapped in glasses.

There are dramatic indications in several systems that small differences in reaction matrices may cause major effects on reaction rates or mechanisms. These

include (1) the very slow rates of recombination of alkyl radicals with geminate partners in perdeuterated as compared to perprotiated hydrocarbon<sup>14</sup> and ethyl iodide<sup>15</sup> glasses at 77°K; (2) the inability of 3-methylpentane-*h*<sub>14</sub> glass to trap hydrogen atoms, whereas they are trapped in 3MP-*d*<sub>14</sub>;<sup>16</sup> (3) the differences in product yields from radiolysis of glassy and polycrystalline ethyl iodide.<sup>17</sup> In this context it is not surprising that odd- and even-carbon-number iodides might show differences in electron trapping capability. No information is available on the crystal structure of the alkyl iodides used in this work, but it is known that some alkyl halides<sup>18</sup> and alkanes<sup>6b,19</sup> show systematic odd-even differences in thermodynamic properties and types of molecular packing within the crystals.

- (12) A. Ekstrom and J. E. Willard, *J. Phys. Chem.*, **74**, 1708 (1970)  
(13) E. J. Eglund and M. C. R. Symons, *J. Chem. Soc. A*, 1326 (1970).  
(14) W. G. French and J. E. Willard, *J. Phys. Chem.*, **72**, 4604 (1968).  
(15) H. W. Fenrick, N. B. Nazhat, P. J. Ogren, and J. E. Willard, *ibid.*, **75**, 472 (1971).  
(16) (a) D. Timm and J. E. Willard, *J. Amer. Chem. Soc.*, **91**, 3406 (1969); (b) M. A. Long and J. E. Willard, *J. Phys. Chem.*, **74**, 1207 (1970).  
(17) H. J. Anikar and J. E. Willard, *Radiat. Res.*, **30**, 204 (1967).  
(18) (a) T. Malkin, *J. Chem. Soc.*, 1976 (1931); (b) T. Malkin, *Trans. Faraday Soc.*, **29**, 977 (1933); (c) J. D. Meyer and E. E. Reid, *J. Amer. Chem. Soc.*, **55**, 1574 (1933); (d) R. W. Crowe and C. P. Smyth, *ibid.*, **72**, 1098 (1950); (e) A. Müller, *Proc. Roy. Soc.*, **124**, 317 (1929).  
(19) For a review see M. G. Broadhurst, *J. Res. Nat. Bur. Stand. Sect. A*, **66**, 241 (1962).

## Growth and Decay of Alkyl Radicals in $\gamma$ -Irradiated Alkyl Iodides at 77°K<sup>1,2</sup>

by H. W. Fenrick, N. B. Nazhat, P. J. Ogren, and J. E. Willard\*

Department of Chemistry, University of Wisconsin, Madison, Wisconsin 53706 (Received August 7, 1970)

Publication costs assisted by the University of Wisconsin

During  $\gamma$  irradiation of glassy ethyl iodide at 77°K the concentration of trapped ethyl radicals grows to a steady state where the rate of radical production is balanced by the rate of thermal decay plus radiation induced decay. In the absence of radiation, the fraction of the radicals which decays per unit time is independent of the initial radical concentration, but decreases with time. This and other evidence indicates that the decay is by geminate recombination of  $C_2H_5 + I^-$  pairs formed by dissociative electron capture and possibly also of  $C_2H_5 + I$  pairs. The rates of decay of  $C_2H_5$  and  $C_2D_5$  in a  $C_2H_5I-C_2D_5I$  mixed matrix are equal, but decay is much slower in a  $C_2D_5I$  matrix than a  $C_2H_5I$  matrix. The inhibiting effect of matrix deuteration on decay, coupled with the relatively small effect of the chain length of the matrix molecules (from  $C_2H_5I$  to  $C_6H_{13}I$ ) is further evidence that radical decay in the alkyl iodide glasses is controlled by molecular vibration or rotation processes rather than by diffusion. Experiments using  $CH_3^{13}CH_2I$  suggest that the isomerization  $CH_3^{13}CH_2 \rightarrow CH_2^{13}CH_3$  does not occur in glassy ethyl iodide.

### Introduction

This paper reports evidence on the mechanisms of decay of *n*-alkyl radicals in  $\gamma$ -irradiated alkyl iodide glasses. It is part of a program of investigation of radiation-induced reactions of alkyl halides in the liquid<sup>3</sup> and solid states<sup>4</sup> and a broader study of the mechanisms of radical production and decay in organic glasses.<sup>5</sup>

### Experimental Procedures<sup>6</sup>

The purification procedures and esr techniques employed and the methods for forming and distinguishing glassy and polycrystalline samples have been described previously.<sup>4a,b</sup> Ethyl iodide-1-<sup>13</sup>C (stated isotopic content 50%) and  $C_2D_5I$  (stated isotopic purity > 99%) were used as received from Merck Sharp and Dohme. Relative radical concentrations during decay of the alkyl iodides were determined from the peak heights of the first derivative esr spectra.

### Results and Discussion

**Radical Production As a Function of  $\gamma$  Dose.** During prolonged  $\gamma$  irradiation of  $C_2H_5I$  glass at 77°K, the concentration of  $C_2H_5$  radicals increases until a steady state is reached (Figure 1). When irradiation is stopped, the rate of decay of the radicals is 30 to 50% less than the rate of production during irradiation (determined from the initial slope of the growth curve), indicating that radiation-induced decay, as well as thermal decay, competes with radical production to achieve the steady state. Further investigations of the kinetics of the radical growth are described elsewhere.<sup>6a</sup>

**Radical Decay Kinetics in Ethyl Iodide Glass.** The concentration of  $C_2H_5$  radicals in  $\gamma$ -irradiated  $C_2H_5I$  glass at 77°K decayed by a factor of ca.  $10^3$  in 12 months, the reciprocal of the concentration being linear with time, suggesting a random combination of diffusing

radicals. However, this is misleading. When the data for samples with widely different initial radical concentration (resulting from different  $\gamma$  doses) are normalized for dose, the decay curves superimpose (Figure 2) for at least 20 days, at which time the radical concentration has decreased by 98%. Normalized data for samples which received 30- and 45-min irradiations at  $3 \times 10^{18}$  eV g<sup>-1</sup> min<sup>-1</sup> and 40 min at  $10^{17}$  eV g<sup>-1</sup> min<sup>-1</sup> likewise fall on the curve of Figure 2. Thus, the fractional decay per unit time is independent of the initial concentration. A plot of the logarithm of the radical concentration vs. time shows curvature convex to the origin, rather than the straight line of a "pure" first-order decay. The results indicate that (a)  $C_2H_5$  radicals do not decay by random encounter with  $C_2H_5$  radicals or other radiation produced species; (b)

(1) This work was supported in part by the U. S. Atomic Energy Commission under Contract AT(11-1)-1715 and by the W. F. Vilas Trust of the University of Wisconsin.

(2) Fellowship support from the Danforth Foundation, the Iraqi Ministry of Education, and the National Science Foundation is acknowledged with appreciation.

(3) (a) E. O. Hornig and J. E. Willard, *J. Amer. Chem. Soc.*, **79**, 2429 (1957); (b) R. J. Hanrahan and J. E. Willard, *ibid.*, **79**, 2434 (1957).

(4) (a) H. W. Fenrick, S. V. Filseth, A. L. Hanson, and J. E. Willard, *ibid.*, **85**, 3731 (1963); (b) H. W. Fenrick and J. E. Willard, *ibid.*, **88**, 412 (1966); (c) H. J. Arnikar and J. E. Willard, *Radiat. Res.*, **30**, 204 (1967); (d) R. F. C. Claridge and J. E. Willard, *J. Amer. Chem. Soc.*, **88**, 2404 (1966); (e) R. J. Eglund and J. E. Willard, *J. Phys. Chem.*, **71**, 4158 (1967); (f) R. J. Eglund, P. J. Ogren, and J. E. Willard, *ibid.*, **75**, 467 (1971); (g) T. O. Jones, R. H. Luebke, Jr., J. R. Wilson, and J. E. Willard, *ibid.*, **62**, 9 (1958); (h) G. L. Hermann and L. A. Harrah, Technical Report AFML-TR-65-333, 1966.

(5) (a) R. F. C. Claridge and J. E. Willard, *J. Amer. Chem. Soc.*, **87**, 4992 (1965); (b) M. Shirom and J. E. Willard, *J. Phys. Chem.*, **72**, 1702 (1968); (c) W. G. French and J. E. Willard, *ibid.*, **72**, 4604 (1968).

(6) Further details are given in the Ph.D. theses of (a) P. J. Ogren, University of Wisconsin, 1968, and (b) H. W. Fenrick, University of Wisconsin, 1966.

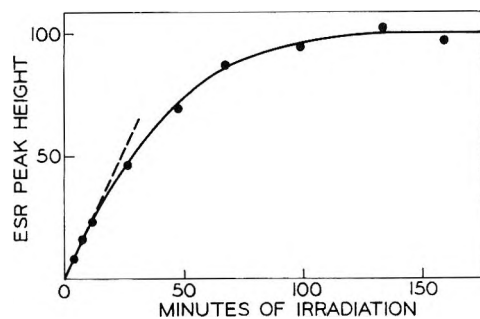


Figure 1. Growth of  $C_2H_5$  radicals during  $\gamma$  irradiation of  $C_2H_5I$  glass at  $77^\circ K$ . Dose rate  $2 \times 10^{18} \text{ eV g}^{-1} \text{ min}^{-1}$ . Initial rate  $= 1 \times 10^{-3} \text{ mol \% min}^{-1}$  and the steady-state concentration  $= 5 \times 10^{-2} \text{ mol \%}$ , assuming  $G(C_2H_5)_{\text{initial}} = 2.0$ . The interruption of irradiation for each esr examination was 10 min or less.

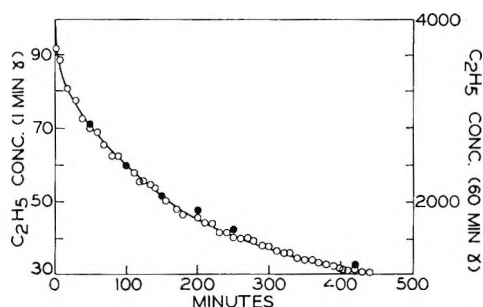


Figure 2. Decay of  $C_2H_5$  radicals in  $C_2H_5I$  glass at  $77^\circ K$ . O, following 1-min  $\gamma$  irradiation at  $2 \times 10^{18} \text{ eV g}^{-1} \text{ min}^{-1}$ ; ●, following 60-min  $\gamma$  irradiation at  $2 \times 10^{18} \text{ eV g}^{-1} \text{ min}^{-1}$ . 100 units  $= 1.1 \times 10^{-3} \text{ mol \%}$ .

each radical must disappear by combination with a predestined partner; (c) steric configuration factors must cause different radicals to have different probabilities per unit time for combination with their predestined partners. Combination with a geminate partner, rather than random combination with other reactive fragments within the same spur is required to explain the data because first-order dependence on the initial radical concentration holds for 98% or more of the decay. The probability that intraspur encounters by diffusion could remove the radicals with loss of no more than 2% to random diffusion is vanishingly small, unless diffusion within the radiation-damaged spur is much easier than diffusion through the walls of the spur.

Such "composite first-order" decay has been observed for alkyl radicals produced by dissociative electron capture from alkyl halides in 3-methylpentane (3MP) glass at  $77^\circ K$ , and also for 3-methylpentyl radicals produced in proximity to I atoms during photolysis of HI in 3MP.<sup>5a,c</sup> In these systems each radical is adjacent to a geminate partner, but far removed from other reactive species, *i.e.*, there is no spur.

It seems probable that the  $C_2H_5$  radicals observed in the radiolysis of  $C_2H_5I$  result predominantly from the

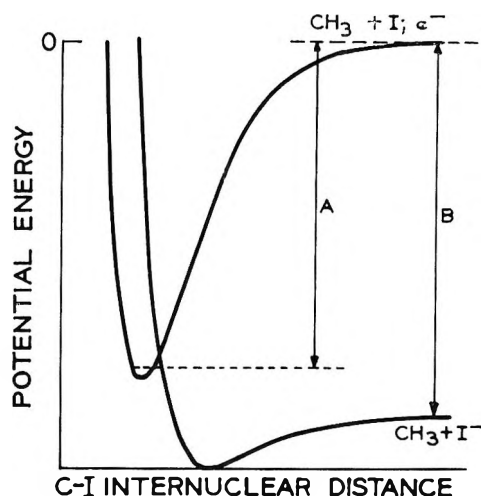


Figure 3. Potential energy diagram representing the potential energy minimum which allows  $CH_3I^-$  formation following loss of the excess energy from the dissociative capture process. Arrow A represents the dissociation energy of the  $CH_3-I$  bond and B the electron affinity of the iodine atom.

reaction  $C_2H_5I + e^- \rightarrow C_2H_5 + I^-$  and that they decay by geminate recombination ( $C_2H_5 + I^- \rightarrow C_2H_5I^-$ ). Figure 3 illustrates the type of energy relationships<sup>7</sup> which allow the occurrence of both dissociative capture and recombination to form trapped  $C_2H_5I^-$ , with the excess energy of the dissociative capture process being lost to the matrix.  $C_2H_5I^-$  is paramagnetic but the absence of an esr signal for it does not exclude its presence since line broadening effects may make esr spectra unobservable, as previously noted.<sup>5a,c,8</sup> Halogen-containing radicals are known to give broad spectra with correspondingly low intensities of the individual lines relative to those of alkyl radicals.<sup>4b,9</sup>

Geminate recombination is the simplest model of ethyl radical decay suggested by the decay kinetics. However, the overall radiation chemistry of the glass is complex and ethyl radicals may also undergo other reactions. Some five trapped intermediates have been observed at  $77^\circ K$ ,<sup>4d,e</sup> and the stable products formed on warming include  $C_2H_4$  and  $C_2H_6$ , which are produced with  $G$  values greater than unity.<sup>4h,9</sup>

Radiation-sensitized decomposition of  $C_2H_5I$  to  $C_2H_5 + I$ , as well as dissociative electron capture, may contribute to the yield of ethyl radicals ( $G = ca. 2$ )<sup>6a,10</sup> in  $\gamma$ -irradiated  $C_2H_5I$  glass. However, the  $G$  value for  $C_2H_5$  production from 1 mol %  $C_2H_5I$  in 3MP glass at  $77^\circ K$  by dissociative electron capture is 1.1,<sup>5b</sup> and the yield would be expected to be higher in 100%  $C_2H_5I$ . The decay characteristics of geminate  $CH_3-I$  pairs

(7) W. E. Wentworth, E. Chen, and J. C. Steelhammer, *J. Phys. Chem.* **72**, 2671 (1968).

(8) S. Aditya and J. E. Willard, *J. Chem. Phys.*, **44**, 833 (1966).

(9) R. Eglund and J. E. Willard, *J. Phys. Chem.*, **71**, 4158 (1967).

(10) P. B. Ayscough and C. Thomson, *Trans. Faraday Soc.*, **58**, 1477 (1962).

produced by photodissociation of  $\text{CH}_3\text{I}$  in 3MP glass are identical with those of  $\text{CH}_3\cdot\text{I}^-$  pairs produced by dissociative capture.<sup>6a</sup> Whether such identity between the reactions of neutral and charged partners exists in other systems must depend on the relative energetics of the processes that produce I and  $\text{I}^-$  and matrix factors controlling the recombination.

On the basis of the decay results it might be expected that a sample which has received a 60-min irradiation, during which radical decay occurs simultaneously with radical production, should have a much higher percentage of slower decaying radicals than a sample which has received a 1-min irradiation. The data of Figure 2 show that this is not the case. It appears that the radiation-induced decay processes, discussed in the previous section, must selectively remove those radicals which have the longest residence times for thermal decay. For sufficiently long times of irradiation the predicted increase in the fraction of slower decaying radicals is observed. For example, a sample irradiated for 36 hr at  $10^{16} \text{ eV g}^{-1} \text{ min}^{-1}$  required 300 min for 50% decay of the radicals present immediately after irradiation, as compared to *ca.* 150 min for the experiments of Figure 2. A sample which received five 4-min irradiations at  $2 \times 10^{18} \text{ eV g}^{-1} \text{ min}^{-1}$ , interspersed with 4-hr decay periods, required 300 min for 50% decay of the radicals present after the fifth irradiation.

**Radical Decay in Other Alkyl Iodide Glasses.** The predominant free radical produced by  $\gamma$  irradiation of alkyl iodide glasses at 77°K is the alkyl radical of the original iodide.<sup>10</sup> Curves for the decay at 77°K of five such radicals are shown in Figure 4. The approximate times for 90% decay, the approximate temperatures at which the radicals disappear within 5 min, the melting points of the crystalline form, and the ratios of the temperatures of rapid decay to these melting points are shown in Table I.

**Table I:** Decay of Alkyl Radicals in  $\gamma$ -Irradiated Alkyl Iodide Glasses at 77°K

Glassy matrix	Approx time for 90% decay, days	Approx $T$ for decay in 5 min, °K	Mp of crystalline compd	$T/T_m$
$\text{C}_2\text{H}_5\text{I}$	2	101	165	0.61
$\text{C}_2\text{D}_5\text{I}$	700	105	165	0.64
$n\text{-C}_3\text{H}_7\text{I}$	6	108	172	0.63
$n\text{-C}_4\text{H}_9\text{I}$	2	106	170	0.63
$n\text{-C}_5\text{H}_{11}\text{I}$	2	118	187	0.64
$n\text{-C}_6\text{H}_{13}\text{I}$	27	123	205	0.60

From the qualitative similarity of the curves for the other radicals to that for ethyl iodide, coupled with the data of Figure 2 and the probability that the mechanism of production for all the radicals is similar, it is

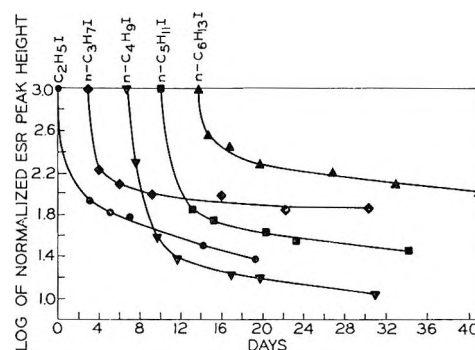


Figure 4. Decay of alkyl radicals in  $\gamma$ -irradiated normal  $\text{C}_2\text{H}_5\text{I}$ ,  $\text{C}_3\text{H}_7\text{I}$ ,  $\text{C}_4\text{H}_9\text{I}$ ,  $\text{C}_5\text{H}_{11}\text{I}$ , and  $\text{C}_6\text{H}_{13}\text{I}$  glasses at 77°K. Each sample had received a dose of *ca.*  $7 \times 10^{19} \text{ eV g}^{-1}$ . Decay measurements were started immediately after irradiation. Initial peak heights have been normalized.

plausible to assume that the decays of the different radicals in the different matrices are all composite first order. Differences in the dynamics of radical rearrangement necessary to allow geminate recombination are reflected by differences in the ratios of the fast-decaying to slow-decaying populations. However, the similarity of decay rates for these radicals and matrices, which vary in chain length from  $\text{C}_2$  to  $\text{C}_6$ , indicates that factors other than chain length predominate in controlling the rate of decay. These factors are believed to be vibrations or rotations of groups necessary to assist the radicals in achieving the configuration needed for recombination with geminate partners.

The constancy of the ratio of the temperature of rapid decay in the glass to the melting point of the crystals is of interest. Diffusion in the glass must be slow at the temperature of rapid decay, since the systems do not crystallize, although the crystalline forms are more stable. Rapid decay in crystals does not occur below about  $T_m = 0.9$ .

**Matrix Isotope Effect.**  $\text{C}_2\text{D}_5$  radicals produced in  $\text{C}_2\text{D}_5\text{I}$  glass at 77°K decay much more slowly than  $\text{C}_2\text{H}_5$  radicals in  $\text{C}_2\text{H}_5\text{I}$  glass. The intensity of the  $\text{C}_2\text{D}_5$  spectrum in  $\text{C}_2\text{D}_5\text{I}$  requires 12 days for 50% decay and 2 years for 90% decay, as compared to 150 min for 50% decay and *ca.* 3 days for 90% decay of  $\text{C}_2\text{H}_5$  in  $\text{C}_2\text{H}_5\text{I}$ .  $\gamma$  Irradiation of a glass composed of 50 mol %  $\text{C}_2\text{H}_5\text{I}$  and 50 mol %  $\text{C}_2\text{D}_5\text{I}$  produces the esr spectrum of a mixture of  $\text{C}_2\text{D}_5$  and  $\text{C}_2\text{H}_5$  radicals. During 7 days of observation this spectrum decayed without change in shape to 20% of its initial intensity, while  $\text{C}_2\text{H}_5$  and  $\text{C}_2\text{D}_5$  radicals in pure  $\text{C}_2\text{H}_5\text{I}$  and  $\text{C}_2\text{D}_5\text{I}$  samples decayed to 6 and 60%, respectively, of their initial values. These results indicate that  $\text{C}_2\text{H}_5$  and  $\text{C}_2\text{D}_5$  radicals decay at equal rates in a given matrix, but that decay is much slower in a deuterated than in a protiated matrix.

Studies of the rates of geminate recombination of  $\text{CH}_3$  and  $\text{CD}_3$  with halide ions in 3MP-*h*<sub>14</sub> and 3MP-*d*<sub>14</sub> have shown that such processes are also insensitive to

deuteration of the radical but sensitive to deuteration of the matrix.<sup>5a</sup> Other examples of reduced decay rates of radicals in deuterated as compared to protiated matrices have been reported.<sup>5c,11</sup> The greater reduction in decay rates by matrix deuteration than by increasing the radical size from  $C_2H_5$  to  $C_6H_{13}$  and in the size of the matrix molecules from  $C_2H_5I$  to  $C_6H_{13}I$  is clearly consistent with the conclusion that the rate-controlling step in decay is not translational diffusion of radicals but molecular rearrangements with rates controlled by vibrational frequencies and amplitudes or by moments of inertia of rotation of  $CH_3$  groups or other groups of the matrix molecules.

*Absence of Radical Isomerization.* Isomerization by a hydrogen atom shift occurs for some trapped radicals at 77°K.<sup>10</sup> Such isomerization must lead to a change in geometry of the radical relative to potential reaction partners with which it may combine. This change might contribute to the falling off in fractional decay rate relative to "pure" first-order decay. However, for the propyl through amyl systems, the constancy of the esr spectral structure with time rules against shifts from primary to secondary radicals, since such shifts would alter the number of protons with which the unpaired electron could couple. In the case of ethyl iodide,  $CH_3^{13}CH_2I$  has been used to test for isomerization. If the rearrangement  $CE_3^{13}CH_2 \rightarrow CH_2^{13}CH_3$  occurred on the same time scale as the radical decay, the different isotropic  $\alpha$ - and  $\beta$ - $^{13}C$  splittings (40 and 13 G, respectively<sup>12</sup>) should produce observa-

ble changes in the decaying ethyl radical esr spectrum. The observed spectrum decayed without change in structure.

*Radical Decay in Polycrystalline Alkyl Iodides.* In contrast to  $\gamma$ -irradiated alkyl iodide glasses, where there is a single type of radical which decays with no significant formation of other types, the corresponding polycrystalline systems are complex.<sup>6b</sup>  $\gamma$  Irradiation of fast frozen polycrystalline ethyl iodide at 77°K produces a central esr spectrum of more than 30 lines extending over 1000 G. Brief annealing at 147°K causes this to diminish while the six-line spectrum of  $C_2H_5$  appears.<sup>4b</sup> Polycrystalline *n*-butyl, *n*-hexyl, and *n*-octyl iodides yield complex spectra which change to simpler spectra on either ageing at 77°K or warming. The normal alkyl iodides with uneven number of C atoms per molecule from  $C_3$  to  $C_7$  all produce six- or seven-line esr spectra when the polycrystalline form is  $\gamma$ -irradiated at 77°K. In each case changes in the relative intensities or the number of lines occur on warming. In all polycrystalline samples examined the decay of the total radical signal is much slower than in the corresponding glassy samples, 50% decay at 77°K requiring of the order of 20 days. Rapid decay (disappearance in 5 min) does not occur at temperatures less than 0.9 of the melting point.

(11) (a) P. J. Sullivan and W. J. Koski, *J. Amer. Chem. Soc.*, **85**, 384 (1963); **86**, 159 (1964); (b) H. S. Judekeis and S. Siegel, *J. Chem. Phys.*, **43**, 3625 (1965).

(12) R. W. Fessenden, *J. Phys. Chem.*, **71**, 74 (1967).

# Dissociative Electron Capture Process of Methyl Vinyl Ether

## in Organic Glasses

by Masahiro Irie,\* Koichiro Hayashi, Seizo Okamura,

*Department of Polymer Chemistry, Kyoto University, Kyoto, Japan*

and Hiroshi Yoshida

*Research Reactor Institute, Kyoto University, Osaka, Japan (Received September 21, 1970)*

*Publication costs assisted by Kyoto University and Hokkaido University*

Dissociative electron capture by methyl vinyl ether has been studied by electron spin resonance in 3-methylhexane and 2-methyltetrahydrofuran glasses containing methyl vinyl ether irradiated by  $^{60}\text{Co}$   $\gamma$  rays at 77°K. The yield of trapped electrons increases remarkably with increasing concentration of methyl vinyl ether in the 3-methylhexane glass, while the increase is insignificant in the 2-methyltetrahydrofuran glass. The rate of photobleaching of the trapped electrons induced by visible light decreases with the addition of methyl vinyl ether to 3-methylhexane, while it increases in 2-methyltetrahydrofuran. The bleaching of the trapped electrons results in the formation of methyl radicals by the dissociative electron capture process,  $\text{CH}_3\text{OCH}=\text{CH}_2 + e \rightarrow \cdot\text{CH}_3 + \text{CH}_2=\text{CHO}^-$ . In contrast to alkyl halides which capture electrons dissociatively during the  $\gamma$  irradiation, the dissociative electron capture process of methyl vinyl ether occurs only when the electrons are liberated from their physical traps by visible light. This is attributed to the fact that the cross section of methyl vinyl ether for physical electron trapping is larger than that for dissociative electron capture and that, under the visible light illumination, the electrons are detrapped and trapped repeatedly and finally captured by methyl vinyl ether to give methyl radicals.

### Introduction

Electrons formed by ionizing radiations are physically trapped in organic glasses at low temperature.<sup>1,2</sup> These trapped electrons are readily liberated thermally or by visible or infrared light and give rise to chemical reactions. The reactions of electrons in organic glasses are classified into three classes: recombination reaction with cationic species, formation of anionic species, and dissociative capture reaction.

Recombination reactions occur most generally in organic glasses and have been extensively studied by measurements of optical absorption,<sup>2c,d</sup> electron spin resonance,<sup>3</sup> radiation-induced luminescence,<sup>4</sup> and radiation-induced electrical conductivity.<sup>5</sup> When an appropriate solute is added to the glasses, formation of anionic species and dissociative electron capture by the solute compete with the recombination reaction. By optical absorption measurement, the correlation between photobleaching of trapped electrons and formation of anion radicals was studied in irradiated 2-methyltetrahydrofuran<sup>2a</sup> and 3-methylpentane glass.<sup>2c</sup> However, the study of the correlation between photobleaching of electrons and formation of free radicals by the dissociative electron capture process is rather difficult because of the large cross section of the process.<sup>6,7</sup> Even immediately after irradiation only the free radicals are observable, and no trapped electrons, at the concentration of solute used.<sup>8-11</sup>

The present authors investigated, in a previous re-

port,<sup>11</sup> the charge recombination processes and formation of anion radicals in 3-methylpentane glass containing vinyl ethers as solutes. In the present investigation, the dissociative electron capture process of methyl vinyl ether in  $\gamma$ -irradiated 3-methylhexane (nonpolar solvent) and 2-methyltetrahydrofuran (polar solvent) glasses are studied by esr. Methyl vinyl

\* Address correspondence to this author at the Faculty of Engineering, Hokkaido University, Sapporo, Japan.

(1) For example, (a) D. R. Smith, F. Okenka, and J. J. Pieroni, *Can. J. Chem.*, **45**, 833 (1967); (b) K. Tsuji, H. Yoshida, and K. Hayashi, *J. Chem. Phys.*, **46**, 810 (1967); (c) K. Tsuji and F. Williams, *J. Amer. Chem. Soc.*, **89**, 1526 (1967); (d) H. Tsujikawa, K. Fueki, and Z. Kuri, *J. Chem. Phys.*, **47**, 256 (1967).

(2) For example, (a) P. J. Dyne and O. A. Miller, *Can. J. Chem.*, **43**, 2696 (1965); (b) F. S. Dainton and G. A. Salmon, *Proc. Roy. Soc., Ser. A*, **285**, 319 (1965); (c) J. B. Guarino and W. H. Hamill, *J. Chem. Phys.*, **44**, 1279 (1966); (d) D. W. Skelly and W. H. Hamill, *ibid.*, **44**, 2893 (1966).

(3) M. Irie, K. Hayashi, S. Okamura, and H. Yoshida, *ibid.*, **48**, 922 (1968).

(4) O. Janessen and K. Funabashi, *ibid.*, **46**, 101 (1967).

(5) B. Wiseal and J. E. Willard, *ibid.*, **46**, 4387 (1967).

(6) W. H. Hamill, J. P. Guarino, N. R. Ronayne, and J. A. Ward, *Discuss. Faraday Soc.*, **36**, 169 (1963).

(7) J. B. Gallivan and W. H. Hamill, *Trans. Faraday Soc.*, **61**, 1960 (1965).

(8) R. F. C. Claridge and J. E. Willard, *J. Amer. Chem. Soc.*, **87**, 4992 (1965).

(9) D. W. Skelly, R. G. Hayes, and W. H. Hamill, *J. Chem. Phys.*, **43**, 2795 (1965).

(10) M. Shirom and J. E. Willard, *J. Phys. Chem.*, **72**, 1702 (1968).

(11) M. Irie, K. Hayashi, S. Okamura, and H. Yoshida, *Int. J. Radiat. Phys. Chem.*, **1**, 297 (1969).

ether captures electrons not only physically, but also chemically. In addition to the fact that it provides trapping sites for electrons in nonpolar glass, it captures electrons dissociatively.<sup>11</sup> Therefore, methyl vinyl ether used as a solute makes it possible to elucidate the dissociative electron capture process in detail, by observing both electrons and product free radicals.

### Experimental Section

Purification of 3-methylhexane was as described previously for 3-methylpentane.<sup>11</sup> 2-Methyltetrahydrofuran was fractionally distilled three times from sodium and distilled *in vacuo* into a sodium-potassium mirrored vessel until the mirror was no longer damaged. Methyl vinyl ether was passed through a column of potassium hydroxide, dried with calcium hydride, and distilled *in vacuo* five times into a sodium-potassium mirrored vessel.

The above samples were distilled into esr sample tubes of quartz glass (Spectrosil, Thermal Syndicate Co.), sealed under a vacuum of less than  $10^{-4}$  Torr, irradiated with  $^{60}\text{Co}$   $\gamma$  rays at 77°K in the dark, and measured by a conventional esr spectrometer as in the previous investigation.<sup>3</sup>

The photobleaching was carried out with light from a tungsten lamp through a Toshiba filter V-Y46 ( $\lambda > 460$  nm).

### Results and Discussion

(i) *Yield of Trapped Electrons.* 3-Methylhexane and 2-methyltetrahydrofuran glasses containing methyl vinyl ether show after  $\gamma$  irradiation at 77°K electron spin resonance signals as shown in Figure 1 (solid lines). In the former glass the signal is composed of a sextet spectrum due to 3-methylhexyl radicals,<sup>12</sup> a broad central portion due to cation radicals of methyl vinyl ether, and a sharp singlet spectrum due to trapped electrons, similar to the case of 3-methylpentane glass containing methyl vinyl ether as solute.<sup>11</sup> In the latter glass, a septet spectrum and a sharp singlet spectrum are observed which are attributed, respectively, to 2-methyltetrahydrofuran radicals<sup>13</sup> and the trapped electrons. The absence of cation radicals of the solute contained in the glass is in accord with the previous results obtained by optical absorption measurements.<sup>2</sup>

The intensity of the singlet spectrum from 3-methylhexane glass increases remarkably with the increasing concentration of added methyl vinyl ether. For 2-methyltetrahydrofuran glass, however, the increase in the intensity is insignificant as shown in Figure 2. These facts imply that the added polar solute (methyl vinyl ether) provides physical trapping sites for electrons in a nonpolar glass, while it provides an insignificant number of new trapping sites for electrons in a polar glass. This latter may be due to a smaller polarity of the solute than that of the solvent or alternatively due to such a small number of trapping sites provided

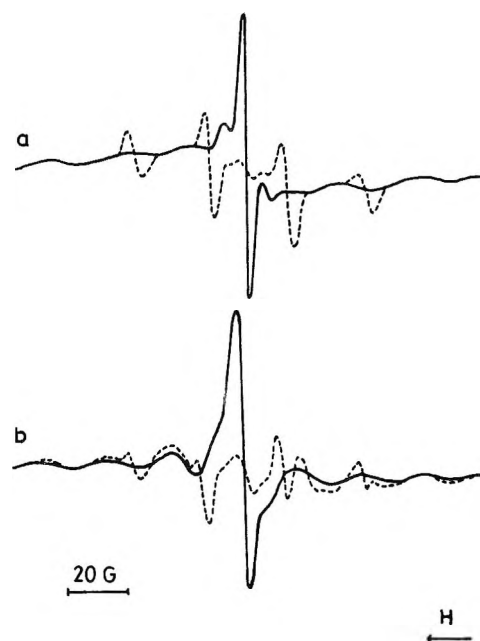


Figure 1. (a) ESR spectrum of 3-methylhexane glass containing 9.1 mol % methyl vinyl ether irradiated to a dose of  $5.2 \times 10^{18}$  eV/g at 77°K. Solid line, 10 min after irradiation; broken line, after photobleaching of the trapped electrons. (b) ESR spectrum of 2-methyltetrahydrofuran glass containing 8.0 mol % methyl vinyl ether irradiated to a dose of  $5.2 \times 10^{18}$  eV/g at 77°K. Solid line, 10 min after irradiation; broken line, after photobleaching of the trapped electrons.

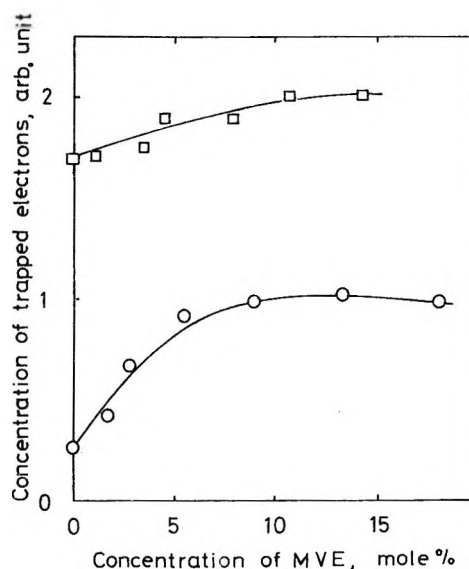


Figure 2. Dependence of the concentration of trapped electrons in 3-methylhexane glass and 2-methyltetrahydrofuran glass, irradiated by  $\gamma$  rays at 77°K to a dose of  $5.2 \times 10^{18}$  eV/g, on the concentration of methyl vinyl ether added to the glasses. Two curves are on the same scale: O, trapped electrons in 3-methylhexane glass; □, trapped electrons in 2-methyltetrahydrofuran glass.

(12) K. Tsuji and F. Williams, *J. Phys. Chem.*, **72**, 3884 (1968).

(13) D. R. Smith and J. J. Pieroni, *Can. J. Chem.*, **43**, 876, 2141 (1965).

by the solute that their contribution is insignificant in comparison with the trapping sites already present in a polar solvent before the addition of the solute.

(ii) *Photobleaching of Trapped Electrons.* The singlet spectrum due to the trapped electrons in pure 3-methylhexane and 2-methyltetrahydrofuran glasses is readily bleached by visible light. The half lifetimes are independent of the initial concentration of the trapped electrons within the range of radiation dose examined ( $5.2 \times 10^{18} \sim 7.0 \times 10^{19}$  eV/g). This fact implies that the electrons disappear by recombining with predestined positive charges, as is the case for the thermal decay of trapped electrons in 3-methylpentane<sup>3</sup> and 2-methyltetrahydrofuran glasses.<sup>13</sup>

In the presence of methyl vinyl ether, the singlet spectrum is replaced by a quartet spectrum due to methyl radicals, as shown in Figure 1, when the trapped electrons are bleached by visible light. Figure 3 shows the representative curves of photo-decay of the trapped electrons, which fit well an exponential decay, showing that, after an early period, the trapped electrons disappear by first-order reactions.

Figure 4 shows the dependence of the photo-induced first-order decay rate constants on the concentration of methyl vinyl ether added to the glass. In 3-methylhexane glasses the decay rate decreases with increasing concentration of methyl vinyl ether. In 2-methyltetrahydrofuran, on the contrary, it increases with increasing concentration of methyl vinyl ether. These facts suggest that methyl vinyl ether has a different behavior in the reaction with electrons depending on the polarity of solvent. Trapping sites in 3-methylhexane formed by methyl vinyl ethers retard the recombination and the formation of the methyl radicals, whereas in 2-methyltetrahydrofuran methyl vinyl ether acts as an electron capturing reagent to yield methyl radicals, accelerating the decay of electrons.

(iii) *Recombination Reaction and Dissociative Electron Capture Reaction.* 3-Methylhexane and 2-methyltetrahydrofuran glasses containing methyl vinyl ether irradiated at 77°K in the dark show a prominent singlet spectrum due to trapped electrons. When the samples are bleached with visible light, the singlet spectrum decreases and the quartet spectrum, due to methyl radicals, appears clearly as described previously. The electrons formed by photoionization of *NN,N',N'*-tetramethyl-*p*-phenylenediamine in the glasses react with methyl vinyl ether to yield methyl radicals too, which adds evidence that the methyl radicals are formed through the dissociative electron capture of neutral methyl vinyl ether molecules.

Figure 5 shows the correlation between the photobleaching of the trapped electrons and the simultaneous formation of methyl radicals in the  $\gamma$ -irradiated 3-methylhexane and 2-methyltetrahydrofuran glasses at 77°K. Tables I and II indicate the dependence of conversion efficiency from the trapped electrons to the

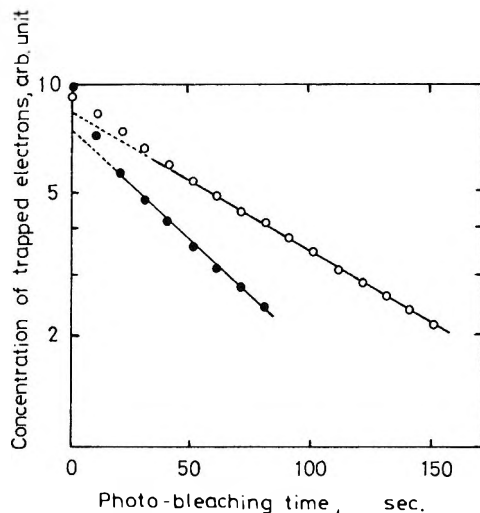


Figure 3. Photo-induced decay at 77°K of trapped electrons: (O) in 3-methylhexane glass containing 5.6 mol % methyl vinyl ether and (●) in 2-methyltetrahydrofuran glass containing 7.96 mol % methyl vinyl ether, irradiated by  $\gamma$  rays to a dose of  $5.2 \times 10^{18}$  eV/g at 77°K. The light intensity used on 2-methyltetrahydrofuran glass is 8.05 times as high as that used on 3-methylhexane glass.

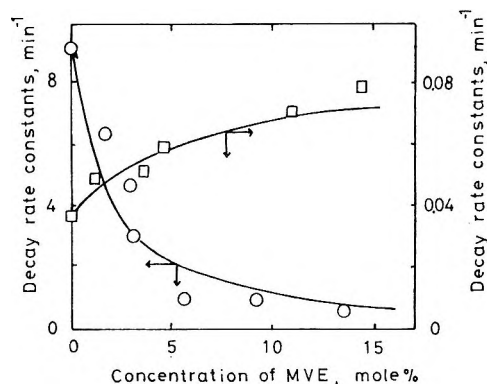


Figure 4. Dependence of the photo-induced first-order decay constant of trapped electrons: (O) in 3-methylhexane glass and (□) in 2-methyltetrahydrofuran glass at 77°K, irradiated by  $\gamma$  rays to a dose of  $5.2 \times 10^{18}$  eV/g, on the concentration of methyl vinyl ether (MVE) added to the glasses.

methyl radicals on the concentration of methyl vinyl ether in 3-methylhexane and 2-methyltetrahydrofuran, respectively. For instance, 73% of the trapped electrons are converted to methyl radicals in 3-methylhexane containing 13.4 mol % of methyl vinyl ether and 28% of the trapped electrons are converted to methyl radicals in 2-methyltetrahydrofuran containing 10.8 mol % of methyl vinyl ether. The efficiency of conversion is independent of the concentration of the trapped electrons but depends on the concentration of added methyl vinyl ether.

The thermal decay of methyl radicals at 77°K fits second-order kinetics both in the 2-methyltetrahydrofuran and 3-methylhexane glasses in the range of decay examined, as shown in Figure 6. The decay behavior is

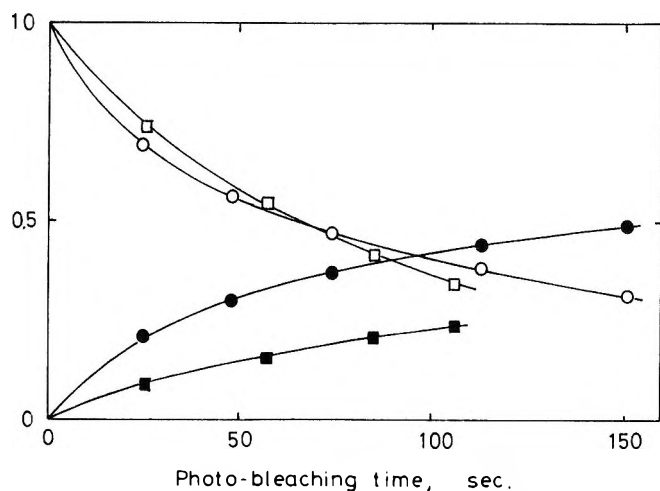


Figure 5. Correlation between photobleaching of trapped electrons and formation of trapped methyl radicals in 3-methylhexane glass containing 13.4 mol % methyl vinyl ether and in 2-methyltetrahydrofuran glass containing 14.3 mol % methyl vinyl ether, both irradiated by  $\gamma$  rays to a dose of  $5.2 \times 10^{18}$  eV/g at 77°K. The light intensity for 2-methyltetrahydrofuran glass is 8.05 times as high as that for 3-methylhexane glass. The curves for the trapped electrons and the methyl radicals are on the same scale:  $\circ$ , trapped electrons in 3-methylhexane glass;  $\square$ , trapped electrons in 2-methyltetrahydrofuran glass;  $\bullet$ , product methyl radicals in 3-methylhexane glass;  $\blacksquare$ , product methyl radicals in 2-methyltetrahydrofuran glass. Ordinate: concentration of trapped electrons and methyl radicals, arbitrary units.

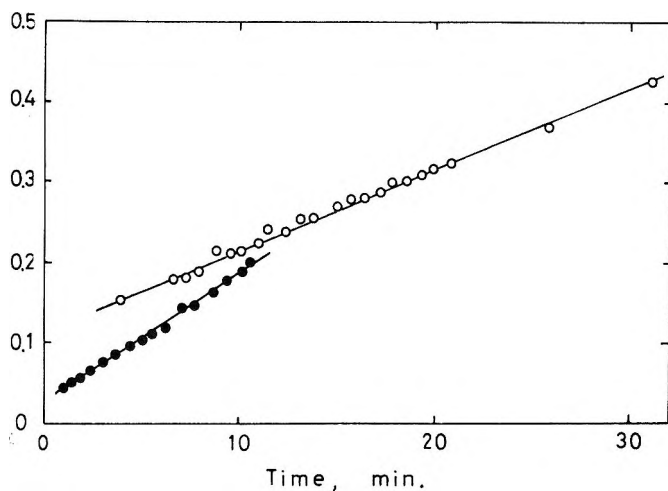


Figure 6. The decay of methyl radicals ( $\circ$ ) in 3-methylhexane glass and ( $\bullet$ ) in 2-methyltetrahydrofuran glass at 77°K. Ordinate: (concentration of methyl radicals)<sup>-1</sup>.

different from that of methyl radicals produced from methyl iodide in 3-methylpentane where they disappear following the first-order kinetics.<sup>8,9</sup> The decay rate is faster in 2-methyltetrahydrofuran than in 3-methylhexane, even when the initial concentrations are the same. The observed decay was taken into account for calculating the yield of the methyl radicals (Figure 6, Table I and II).

Table I: Conversion of the Trapped Electrons in 3-Methylhexane Glass at 77°K to Methyl Radicals

Concentration of methyl vinyl ether, mol %	Yield, G, of trapped electrons	Yield, G, of methyl radicals <sup>a</sup>
0	0.26	
1.8	0.41	0.014
2.9	0.67	0.16
5.6	0.91	0.34
9.1	0.98	0.60
13.4	1.02	0.73

<sup>a</sup> After complete photobleaching of the trapped electrons.

Table II: Conversion of the Trapped Electrons in 2-Methyltetrahydrofuran Glass at 77°K to Methyl Radicals

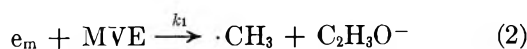
Concentration of methyl vinyl ether, mol %	Yield, G, of trapped electrons	Yield, G, of trapped methyl radicals <sup>a</sup>	Increase of 2-methyltetrahydrofuran radicals
0	1.70		-1.63
1.2	1.72	$\approx 0$	-0.64
3.5	1.76	0.18	0.46
4.6	1.90	0.37	0.75
8.0	1.90	0.48	1.17
10.8	2.12	0.58	1.47

<sup>a</sup> After complete photobleaching of the trapped electrons.

Photobleaching of trapped electrons in pure 3-methylhexane did not induce any change in the concentration of the 3-methylhexyl radicals. In 2-methyltetrahydrofuran, however, the photobleaching of the trapped electrons reduces the concentration of 2-methyltetrahydrofuran radicals to one-half. Smith and Pieroni reported the reduction to one-third of the initial concentration,<sup>13</sup> which is in contrast to the finding of other laboratories.<sup>10,14</sup> The reduction in the radical concentration is suppressed when methyl vinyl ether is added to 2-methyltetrahydrofuran glass, and at the concentration of more than 3 mol %, the radicals increase in concentration as shown in Table II. The formation of 2-methyltetrahydrofuran radicals is brought about by the hydrogen abstraction from 2-methyltetrahydrofuran molecules by "reactive" methyl radicals produced by the dissociative electron capture process. Thermal decay of trapped methyl radicals results in no subsequent change in the 2-methyltetrahydrofuran radical concentration.

The photo-illumination of the irradiated 3-methylhexane and 2-methyltetrahydrofuran glasses gives rise to the following reactions of the trapped electrons in the presence of methyl vinyl ether at 77°K.

(14) F. S. Dainton, J. P. Keene, T. J. Kemp, G. A. Salmon, and J. Tepley, *Proc. Chem. Soc.*, 265 (1964).



where  $e_t$  and  $e_m$  represent the trapped electron and the electron liberated from the trap under the influence of light, the mobile electron, respectively, MVE represents methyl vinyl ether, and  $k$ 's are corresponding rate constants.

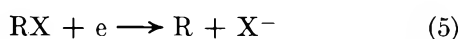
Methyl radicals react with the matrix molecules of 2-methyltetrahydrofuran to give new 2-methyltetrahydrofuran radicals immediately after their formation by photobleaching of trapped electrons by process 2, whereas they cause no further formation of the 2-methyltetrahydrofuran radicals when they are once trapped and then react thermally. A fraction of the methyl radicals having an excess energy is thought to abstract hydrogen atoms from 2-methyltetrahydrofuran molecules and the rest are thermalized, being trapped and recombining with each other. Willard, *et al.*<sup>10</sup> reported that the hot methyl radical can abstract a hydrogen from saturated hydrocarbons. However, the excess energy seems to be so small in the present case that the methyl radicals can abstract hydrogen from 2-methyltetrahydrofuran but not from 3-methylhexane.<sup>15</sup>

The conversion efficiency of the trapped electrons to methyl radicals (including both trapped and "reactive" methyl radicals<sup>16</sup>), according to process 2 above, depends on the concentration of methyl vinyl ether. The efficiency increases with the added amount of methyl vinyl ether and it reaches about 1.0 at 8.0 mol % in the 2-methyltetrahydrofuran glass. At low concentration, the efficiency in 2-methyltetrahydrofuran glass is about 3.3 times as high as that in 3-methylhexane glass. The mobile electrons liberated from their traps by photo-illumination react with either methyl vinyl ether or positively charged species according to the processes 2 and 3. The conversion should follow eq 4

$$\frac{[e_t]}{[\text{CH}_3^{\text{all}}]} = 1 + \frac{k_2}{k_1[\text{MVE}]} \quad (4)$$

$[e_t]/[\text{CH}_3^{\text{all}}]$  is plotted in Figure 7, being proportional to the reciprocal concentration of methyl vinyl ether as expected from eq 4. The ratio of  $k_2$  to  $k_1$  is 0.028 in 2-methyltetrahydrofuran and is 0.10 in 3-methylhexane. The charge neutralization is interrupted by the dissociative electron capture more considerably in polar glass than in nonpolar glass.

In gas phase, it is well known that the dissociative electron capture process



can occur when  $A(X) + E(e) > B(\text{R-X})$ , where  $A$ ,

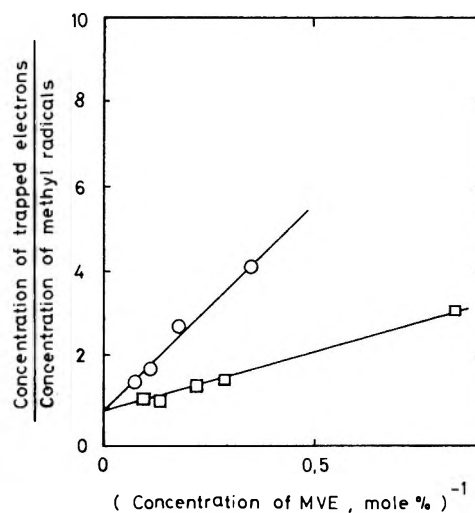
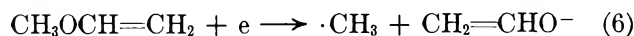


Figure 7. Dependence of  $[e_t]/[\text{CH}_3^{\text{all}}]$  on the reciprocal concentration of methyl vinyl ether added to 3-methylhexane glass and 2-methyltetrahydrofuran glass: ○,  $[e_t]/[\text{CH}_3^{\text{all}}]$  in 3-methylhexane glass; □,  $[e_t]/[\text{CH}_3^{\text{all}}]$  in 2-methyltetrahydrofuran glass;  $[e_t]$  is the concentration of trapped electrons;  $[\text{CH}_3^{\text{all}}] = 1/2([e_t] + [\Delta\text{MTHF}] + [\text{CH}_3^{\text{trapped}}])$ , where  $[\Delta\text{MTHF}]$  and  $[\text{CH}_3^{\text{trapped}}]$  are the increase in the 2-methyltetrahydrofuran radical concentration and the concentration of trapped methyl radicals, respectively.

$E$ , and  $B$  are electron affinity, electron energy (or appearance potential), and bond energy (or dissociation energy), respectively.<sup>7</sup> In the present study,  $R$  is  $\text{CH}_3$  and  $X$  is  $\text{CH}_2=\text{CHO}$



The bond energy between carbon and oxygen is 84 kcal/mol. Although the electron affinities of  $\text{C}_2\text{H}_5\text{O}$  and  $\text{OCOCH}_3$  are estimated to be 60 and 76 kcal/mol, respectively,<sup>7</sup> that of  $\text{C}_2\text{H}_5\text{O}$  has not yet been determined. It is thought to be a little smaller or nearly equal to the bond energy between carbon and oxygen. This value suggests that the dissociative electron capture process is not a fast process in the glass at 77°K.

Let us consider the behavior of electrons in the 3-methylhexane glass. The electrons ejected by  $\gamma$  rays

(15) Dissociation energies ( $D$ ) of H-C bond of similar compounds were obtained as follows:  $D(\text{H}-\text{CH}_2\text{CH}_3) = 98.3 \text{ kcal/mol}^{15b}$  and  $D(\text{H}-\text{CH}_2\text{OCH}_3) = 82 \pm 3 \text{ kcal/mol}^{15c}$  or  $91.1 \pm 1.0 \text{ kcal/mol}^{15d}$  (b) A. F. Trompman-Dickenson, *Chem. Ind. (London)*, 379 (1965); (c) R. H. Martin, F. W. Lampe, and R. W. Tafz, *J. Amer. Chem. Soc.*, **88**, 1353 (1966); (d) L. F. Loucles and K. J. Laidler, *Can. J. Chem.*, **45**, 2785 (1967).

(16) In pure 2-methyltetrahydrofuran, each trapped electron eliminates a 2-methyltetrahydrofuran radical, when photobleached, as shown in Table II. This is interpreted as being due to recombination between the radical (septet spectrum) and hydrogen atom which results from charge neutralization of the electron with a positive charge. In the presence of methyl vinyl ether only a fraction of the trapped electrons,  $[e_t] - [\text{CH}_3^{\text{all}}]$ , eliminate the radicals and the rest react with methyl vinyl ether to form "reactive" and trapped methyl radicals. Therefore the observed change in the 2-methyltetrahydrofuran radical concentration ( $[\Delta\text{MTHF}]$ ), when all the trapped electrons are bleached, is

$$[\Delta\text{MTHF}] = ([\text{CH}_3^{\text{all}}] - [\text{CH}_3^{\text{trapped}}]) - ([e_t] - [\text{CH}_3^{\text{all}}])$$

$$[\text{CH}_3^{\text{all}}] = 1/2([e_t] + [\Delta\text{MTHF}] + [\text{CH}_3^{\text{trapped}}])$$

are physically captured either by the trapping sites intrinsic to 3-methylhexane glass or by those due to added methyl vinyl ether, or captured dissociatively by methyl vinyl ether. We denote the cross sections of methyl vinyl ether for dissociative electron capture and for physical electron trap by  $\sigma_d$  and  $\sigma_p$ , respectively, and that of solvent for physical electron trap by  $\sigma_{p'}$ .<sup>17</sup> The fact that only the trapped electrons and no methyl radicals are observed immediately after the irradiation is due to  $\sigma_p N + \sigma_{p'}(1 - N) > \sigma_d N$ , where  $N$  is the mole fraction of methyl vinyl ether, since methyl vinyl ether acts simultaneously as an electron capture reagent and physical trapping site for electron. The electrons liberated from their trapping sites by photoillumination collide with methyl vinyl ether several times before they encounter their predestined positive charge and recombine with it. Photobleaching of electrons produces methyl radicals only when  $nN\sigma_d$  is larger than  $\sigma_r$  ( $nN$  is the mean ratio of the number of collisions made with methyl vinyl ether to positive charge and  $\sigma_r$  is the cross section of a positive charge for an electron). Therefore, in 3-methylhexane glass with added methyl vinyl ether

$$\sigma_p N + \sigma_{p'}(1 - N) > \sigma_d N > \frac{\sigma_r}{n} \quad (7)$$

In 3-methylpentane glasses containing 0.4 mol % of alkyl halides, however, only alkyl radicals are observed immediately after irradiation and no trapped electrons are detected.<sup>9</sup> In these glasses,  $\sigma_d$  of alkyl halides is larger than  $\sigma_p + \sigma_{p'}(1/N - 1)$  and most of the ejected electrons are not physically trapped but dissociatively captured by alkyl halides. Williams, *et al.*,<sup>18</sup> reported that the dissociative electron capture of acetonitrile in

2-methyltetrahydrofuran glass was not observed under  $\gamma$  irradiation, but subsequent photobleaching of the trapped electrons induced the reaction. They interpreted the different reactivity of electron with acetonitrile, under  $\gamma$ -irradiation and under subsequent photoillumination, by the new concept of "photo-excited" electrons. The different reactivity of electrons may be attributed alternatively, as in the present investigation, to  $\sigma_{p'}(1 - N) > \sigma_d N$ , where  $\sigma_{p'}$  and  $\sigma_d$  are the cross section of 2-methyltetrahydrofuran for physical electron trap and that of acetonitrile for dissociative electron capture, respectively, and  $N$  is the mole fraction of acetonitrile, without introducing the concept of "photo-excited" electron. In this case  $\sigma_p N$  is negligibly small in comparison with  $\sigma_{p'}(1 - N)$ . The fact that dissociative electron capture process occurs by photobleaching of trapped electrons is interpreted by  $nN\sigma_d > \sigma_r$ .

In condensed phases, the electrons liberated from trapping sites by photoillumination lose the excess kinetic energy quickly and reach thermal energy. If  $A(X) \approx B(R-X)$ , the thermalized electron can give rise to the dissociative electron capture reaction. If the reaction occurs under the condition of  $A(X) < B(R-X)$ , it is necessarily caused by the electrons having an excess energy, which may be termed as "photo-excited" electrons. The kinetic treatments, as in the present investigation, are still valid essentially, even though the "photo-excited" electrons are involved in the dissociative electron capture process.

(17) This does not necessarily mean that a physical trap is formed by a single matrix molecule.

(18) M. A. Bonin, J. Lin, K. Tsuji, and F. Williams, *Advan. Chem. Ser.*, No. 82, 269 (1968).

## Photoisomerization of Maleate Radical Anions Produced in 2-Methyltetrahydrofuran by $\gamma$ Irradiation at 77°K

by Ayako Torikai,\* Toshimi Suzuki, Tetsuo Miyazaki, Kenji Fueki, and Zen-ichiro Kuri

Department of Synthetic Chemistry, Faculty of Engineering,  
Nagoya University, Chikusa-ku, Nagoya, Japan (Received August 21, 1970)

Publication costs assisted by the Faculty of Engineering, Nagoya University

Photoisomerization of  $\gamma$ -ray-induced maleate radical anions in MTHF has been studied by electron spin resonance (esr), optical absorption measurements, and product analysis.  $\gamma$  Irradiation of MTHF glasses of maleic acid, dimethyl and diethyl maleate at 77°K yields the corresponding radical anions. These species change into the fumaric acid radical anion and dimethyl and diethyl fumarate radical anions, respectively, by illumination of light. Upon illumination of  $\gamma$ -irradiated dimethyl maleate in MTHF glass with visible light, neither the formation of new radicals nor the change of solvent radicals is observed, and any gaseous or liquid products other than dimethyl fumarate do not increase in their amounts. The experimental results obtained indicate that other reactions than the cis  $\rightarrow$  trans isomerization are not involved in this case.

### Introduction

Product analysis and observation of reaction intermediates are two complementary methods used for the study of reaction mechanisms. We have applied both methods to several organic systems at 77°K in order to understand their radiolysis mechanisms: the reaction of nitrous oxide with electrons in organic glass,<sup>1</sup> the radiolysis of phenyl acetate,<sup>2</sup> and the radiolysis of isobutane.<sup>3</sup>

Photochemical cis-trans isomerization of molecules has been studied extensively by many investigators. Photoisomerization of radical anions, however, has not been reported previously, except that of the stilbene radical anion, as studied by optical absorption spectroscopy.<sup>4</sup> Reactions of excited radical anions brought about by light illumination can be studied by optical absorption spectroscopy or esr, but there remains some uncertainty about their overall mechanisms. In this work, we have studied, by esr and optical absorption spectroscopy as well as product analysis, the photochemical reaction of maleate radical anions, which are produced by  $\gamma$  irradiation of maleic acid esters in 2-methyltetrahydrofuran glass at 77°K.

### Experimental Section

Dimethyl maleate (DMM; *cis*-CH<sub>3</sub>OCOCH=CHCOOCH<sub>3</sub>), diethyl maleate (DEM; *cis*-C<sub>2</sub>H<sub>5</sub>OCOCH=CHCOOC<sub>2</sub>H<sub>5</sub>), diethyl fumarate (DEF; *trans*-C<sub>2</sub>H<sub>5</sub>OCOCH=CHCOOC<sub>2</sub>H<sub>5</sub>) were of high purity and were used after degassing and distillation on a vacuum line. Maleic acid (MA; *cis*-HOCOCH=CHCOOH), fumaric acid (FA; *trans*-HOCOCH=CHCOOH), and dimethyl fumarate (DMF; *trans*-CH<sub>3</sub>OCOCH=CHCOOCH<sub>3</sub>) were of high purity and were used without further purification. 2-Methyltetrahydrofuran (MTHF) was purified by passage through an alumina column after having

been fractionally distilled and dried over a sodium mirror. Biphenyl (Ph<sub>2</sub>) was purified by recrystallization.

Samples were irradiated with  $\gamma$  rays from a <sup>60</sup>Co source at 77°K and in most cases at a dose rate of  $6.86 \times 10^{18}$  eV/g hr for absorption studies and at a dose rate of  $5.36 \times 10^{19}$  eV/g hr for esr and product analysis experiments. Photobleaching of  $\gamma$ -irradiated samples was carried out at 77°K with a tungsten light or ultraviolet light from a medium-pressure mercury lamp. The wavelength of the light from the mercury lamp ranged mainly from 230 to 450 nm.

Esr and optical absorption spectra of irradiated samples were measured at 77°K on a JES-3BX esr spectrometer or a Hitachi EPU-2A spectrophotometer, respectively. Final products were analyzed by a Hitachi K 53 gas chromatograph with a flame ionization detector (polyethylene glycol column, 2 m long, at 150°).

### Results and Discussion

**Optical Absorption Spectra.** The spectrum obtained by  $\gamma$ -ray irradiation of a MTHF solution containing DMM at a low concentration is shown in Figure 1a. This spectrum has an absorption maximum at  $\lambda_{\max}$  345 nm. The absorption band shifts to the shorter wavelength region by illumination with uv light, and its absorption maximum appears at  $\lambda_{\max}$  335 nm (Figure 1b). The 335-nm band is bleached by further illumination with uv light (Figure 1c).

(1) T. Wakayama, T. Kimura, T. Miyazaki, K. Fueki, and Z. Kuri, *Bull. Chem. Soc. Jap.*, **42**, 266 (1969).

(2) Y. Noro, M. Ochiai, T. Miyazaki, A. Torikai, K. Fueki, and Z. Kuri, *J. Phys. Chem.*, **74**, 63 (1970).

(3) T. Wakayama, T. Kimura, T. Miyazaki, K. Fueki, and Z. Kuri, *Bull. Chem. Soc. Jap.*, **43**, 1017 (1970).

(4) T. Shida and W. H. Hamill, *J. Chem. Phys.*, **44**, 4372 (1966).

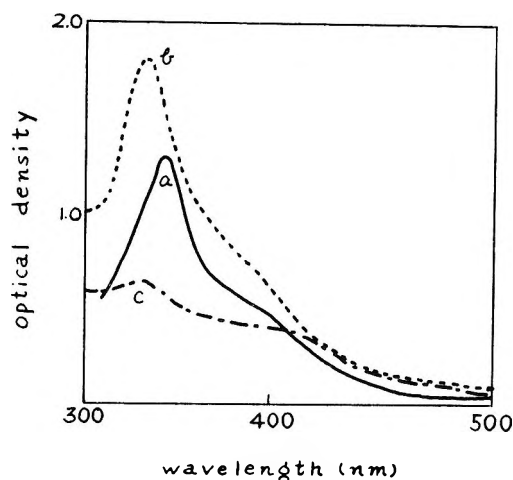


Figure 1. Absorption spectra of  $\gamma$ -irradiated 1 mol % DMM in MTHF at 77°K: a, irradiation dose,  $1.18 \times 10^{18}$  eV/g; b, the same sample as a, after 2 min illumination with uv light; c, the same sample as a, after 5 min illumination with uv light.

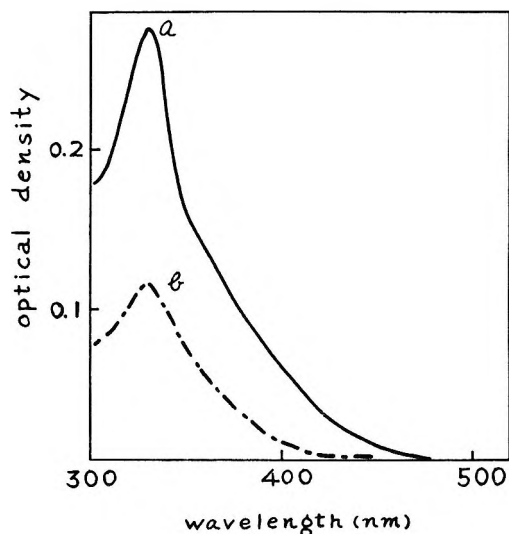


Figure 2. Absorption spectra of  $\gamma$ -irradiated 0.02 mol % DMF in MTHF at 77°K: a, irradiation dose,  $1.87 \times 10^{18}$  eV/g; b, the same sample as a, after 5 min illumination with uv light.

The spectrum shown in Figure 1b coincides with that of a  $\gamma$ -irradiated MTHF solution containing DMF (Figure 2a). This band is also photobleachable with uv light (Figure 2b). In the case of the irradiated DMF-MTHF solutions, only the 335-nm band is observed before and after illumination with uv light. The 335- and 345-nm bands were not observed when MTHF glasses containing DMM or DMF were irradiated by uv light without  $\gamma$  irradiation.

Similar results were obtained for DEM and DEF (Figures 3 and 4).

The bands at 345 and 335 nm may be attributable to the DMM and DMF radical anions, respectively, for the following reasons: (1) the solvated electron

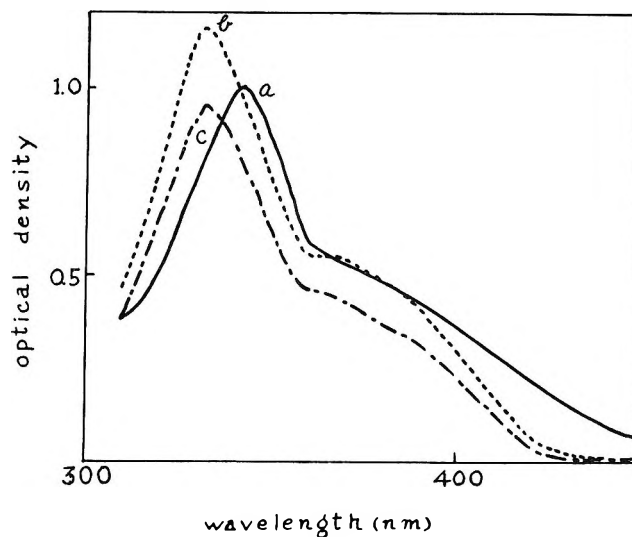


Figure 3. Absorption spectra of  $\gamma$ -irradiated 0.93 mol % DEM in MTHF at 77°K: a, irradiation dose,  $1.87 \times 10^{18}$  eV/g; b, the same sample as a, after 2 min illumination with uv light; c, the same sample as a, after 5 min illumination with uv light.

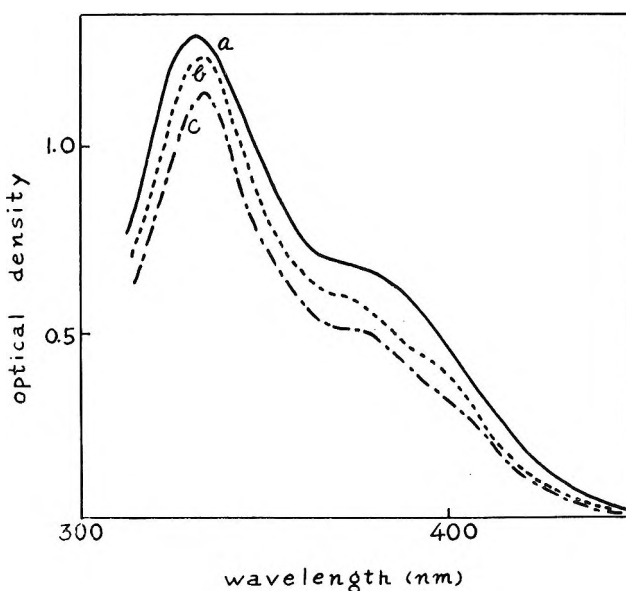


Figure 4. Absorption spectra of  $\gamma$ -irradiated 0.93 mol % DEF in MTHF at 77°K: a, irradiation dose,  $1.87 \times 10^{18}$  eV/g; b, the same sample as a, after 2 min illumination with uv light; c, the same sample as a, after 5 min illumination with uv light.

band of MTHF at 1300 nm could not be found in this case; (2) these bands can be photobleached with uv or visible light. These assignments are also supported by the fact that the competitive reaction between biphenyl and DMM takes place in MTHF glass (Figure 5).  $\gamma$ -Ray irradiation of a MTHF solution of Ph<sub>2</sub>-DMM produced the Ph<sub>2</sub><sup>-</sup> band at 408 nm<sup>5</sup> and the DMM-

(5) J. P. Guarino, M. R. Ronayne, and W. H. Hamill, *Radiat. Res.*, **17**, 379 (1962).

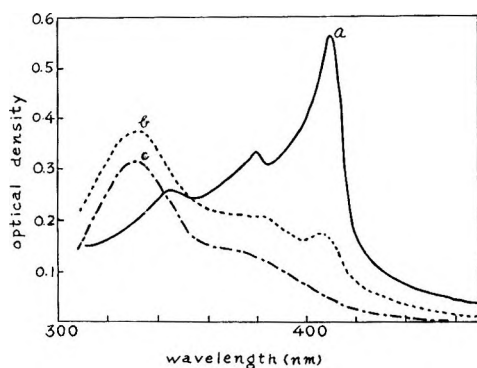
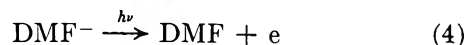
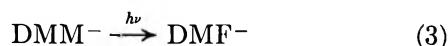
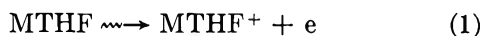


Figure 5. Absorption spectra of  $\gamma$ -irradiated biphenyl and DMM in MTHF at 77°K; concentration of biphenyl, 1 mol %, concentration of DMM, 0.2 mol %: a, irradiation dose,  $1.25 \times 10^{18}$  eV/g; b, the same sample as a, after exposure to tungsten light ( $\lambda > 350$  nm); c, the same sample as b, after exposure to tungsten light (nonfilter).

band at 345 nm. Upon illumination of light ( $\lambda > 350$  nm), the 408-nm band diminished in its intensity and the 335-nm band appeared. The 335-nm band can be photobleachable with further illumination of the light. In the competitive reaction experiment, it was found that the efficiency of electron capture by DMM is 5–10 times as high as that of biphenyl.

These results show the *cis*  $\rightarrow$  *trans* photoisomerization of maleate radical anions produced by  $\gamma$  irradiation. The photoisomerization also occurs by irradiation of maleate radical anions with visible light. Irradiation by uv light of wavelength near 340 nm causes more noticeable changes in the spectra.

The following reaction mechanism is presented based on the experimental results.



The molar extinction coefficient ( $\epsilon$ ) at 335 nm was roughly estimated from the competitive reaction experiment to be  $\epsilon \approx 1.5 \times 10^4$  l. mol  $\text{cm}^{-1}$ . Using this value of  $\epsilon$ , the *G* value for the formation of fumarate radical anion is calculated to be 2.4.

The experiment on the photoisomerization of maleic acid radical anions to fumaric acid radical anions was also carried out. The *cis*  $\rightarrow$  *trans* photoisomerization of the acid radical anions was observed in this case.

*Esr Spectra.* The esr spectra of  $\gamma$ -irradiated MTHF glasses containing DMM or DMF are shown in Figures 6 and 7.

The narrow singlet due to the trapped electron in MTHF was not observed in these cases. The competitive reaction between biphenyl and DMM was studied by esr measurement. The  $\gamma$  irradiation of

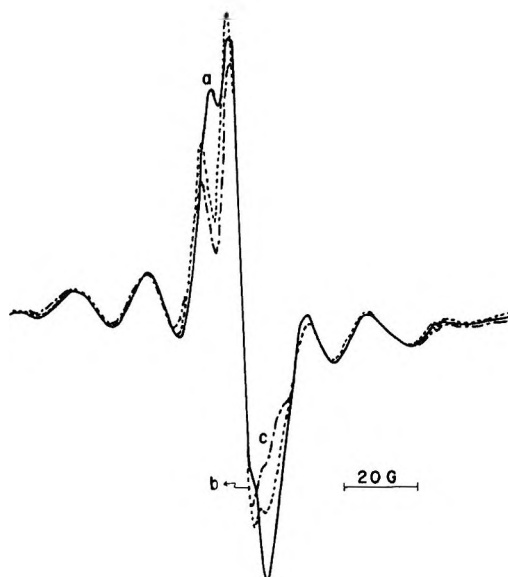


Figure 6. ESR spectra of  $\gamma$ -irradiated 1 mol % DMM in MTHF at 77°K: a, irradiation dose,  $8.74 \times 10^{18}$  eV/g; b, the same sample as a, after 5 min illumination with uv light; c, the same sample as a, after 10 min illumination with uv light.

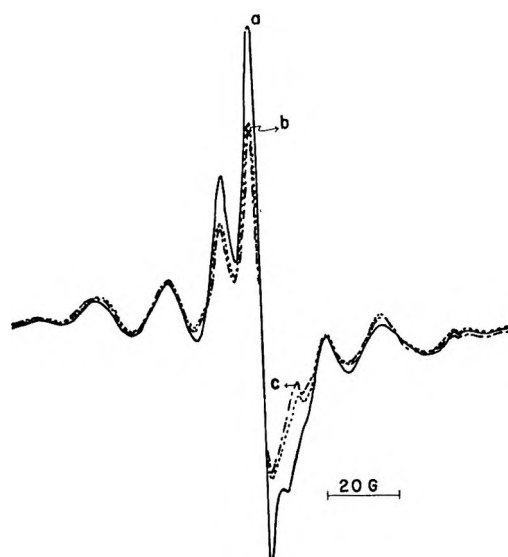


Figure 7. ESR spectra of  $\gamma$ -irradiated 0.3 mol % DMF in MTHF at 77°K: a, irradiation dose,  $8.74 \times 10^{18}$  eV/g; b, the same sample as a, after 5 min illumination with uv light; c, the same sample as a, after 10 min illumination with uv light.

$\text{Ph}_2\text{-DMM}$  systems produces the biphenyl radical anion as shown in Figure 8a. This esr spectrum changes with illumination by visible light ( $\lambda > 350$  nm) into the spectrum which is identical with that obtained by  $\gamma$  irradiation of DMF in MTHF (Figure 8b). From these results, the esr spectrum in Figure 8a may be attributable to an anionic species.

$\gamma$ -Irradiated MTHF solutions containing maleic acid give a three-line esr spectrum as shown in Figure

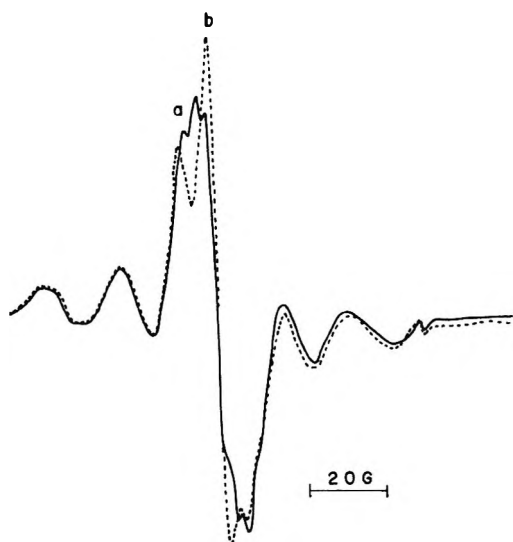


Figure 8. ESR spectra of  $\gamma$ -irradiated biphenyl and DMM in MTHF at 77°K; concentration of biphenyl, 1 mol %, concentration of DMM, 0.2 mol %; a, irradiation dose,  $6.24 \times 10^{18}$  eV/g; b, the same sample as a, after exposure to tungsten light ( $\lambda > 350$  nm).

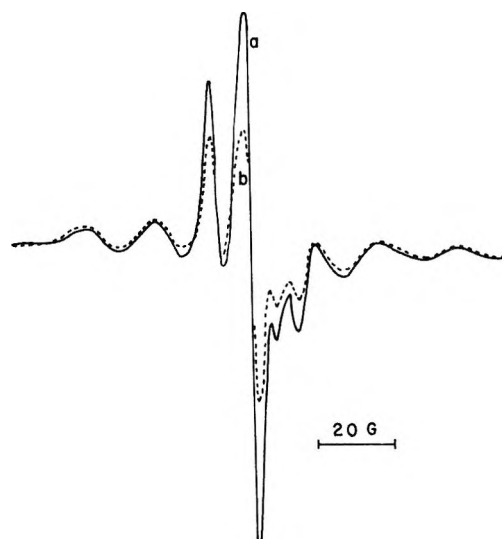


Figure 10. ESR spectra of  $\gamma$ -irradiated 1 mol % FA in MTHF at 77°K: a, irradiation dose,  $8.74 \times 10^{18}$  eV/g; b, the same sample as a, after 15 min illumination with uv light.

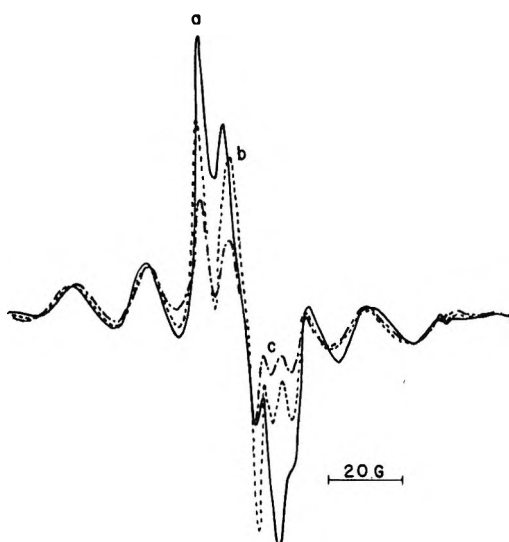


Figure 9. ESR spectra of  $\gamma$ -irradiated 1 mol % MA in MTHF at 77°K: a, irradiation dose,  $8.74 \times 10^{18}$  eV/g; b, the same sample as a, after 20 min illumination with uv light; c, the same sample as a, after 45 min illumination with uv light.

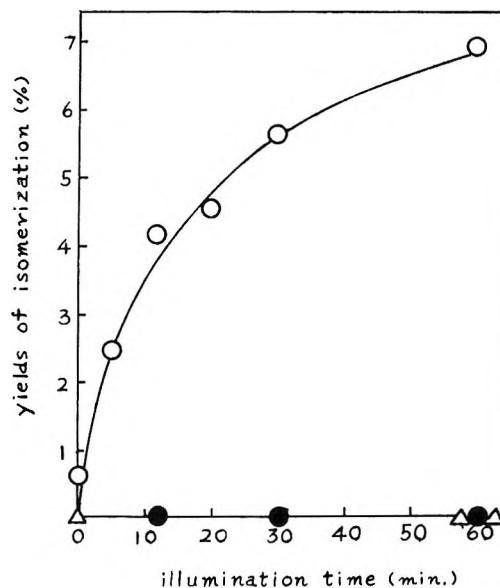


Figure 11. Photoisomerization of DMM anion and DMF anion with tungsten light at 77°K: concentration of DMM or DMF, 0.81 mol % in MTHF: O, illumination with tungsten light to DMM in MTHF after  $\gamma$  irradiation (irradiation dose,  $7.98 \times 10^{20}$  eV/g); ●, illumination with tungsten light only, to DMM in MTHF; Δ, illumination with tungsten light to DMF in MTHF after  $\gamma$  irradiation (irradiation dose,  $7.98 \times 10^{20}$  eV/g).

9a. This spectrum changes into a different spectrum by illumination with uv light (Figure 9b), and it is gradually bleached by further illumination of uv light (Figure 9c). The spectrum shown in Figure 9b coincides with that of a  $\gamma$ -irradiated MTHF solution containing fumaric acid (Figure 10a). Such a spectral change also occurred with the illumination of visible light.

Photobleaching of the radical anions causes neither the formation of new radicals nor the change in yield of solvent radicals. Thus the bond rupture, addition reac-

tion, or decarboxylation does not take place in this case. These esr results, together with the results of product analysis and optical absorption measurements on maleic acid esters, seem to be attributable to the cis  $\rightarrow$  trans isomerization of maleic acid radical anions to fumaric acid radical anions.

The three-line esr spectrum of maleic acid radical anions with a line separation of about 10 G may be interpreted in terms of the splitting by the two hydrogen

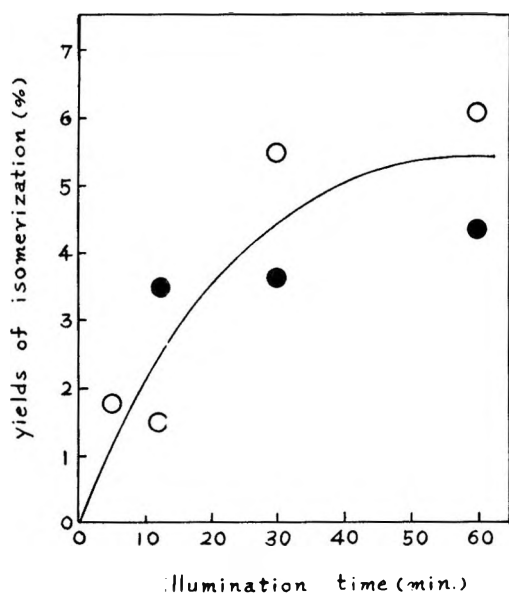


Figure 12. Photoisomerization of DMM and DMF in MTHF at 77°K with uv light only: ○, concentration of DMM, 0.81 mol %; ●, concentration of DMF, 0.81 mol %.

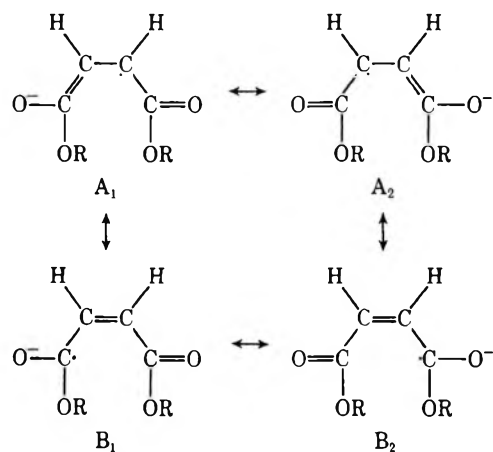
atoms attached to the C=C double bond (Figure 9a). The unpaired electron density on a carbon atom is roughly estimated to be 0.4.

**Product Analysis.** The yield of isomerization of DMM or DMF by illumination of visible light is shown in Figure 11. When DMM is  $\gamma$ -irradiated in MTHF glass at 77°K, DMF is produced in a rather small amount, but its yield increases appreciably by illumination of the  $\gamma$ -irradiated sample with visible light at 77°K. As shown in Figure 11, DMM in MTHF glass, which is not  $\gamma$ -irradiated, does not isomerize at all by illumination of visible light at 77°K, because the DMM molecule does not absorb the light of wavelengths longer than 300 nm. Therefore the photoisomerization of  $\gamma$ -irradiated DMM in MTHF glass cannot be attributed to the isomerization of neutral DMM molecules but to that of the species produced by  $\gamma$  irradiation. Since trapped electrons are not observed by esr in a  $\gamma$ -irradiated MTHF glass containing DMM, the trapped electrons do not contribute to the effect of illumination of visible light. It has been recognized that the solute cation is not formed in a  $\gamma$ -irradiated MTHF glass containing solute. As discussed in the previous section, the species which has an absorption band in the range of wavelengths longer than 300 nm is only the DMM radical anion in  $\gamma$ -irradiated MTHF containing DMM. Therefore the photoisomerization should arise from the change of the DMM radical anion into the DMF radical anion (reaction 3). This is based on the following observations. First, any gaseous or liquid products other than DMF do not increase in their yields by illumination of  $\gamma$ -irradiated DMM in MTHF glass with visible light at 77°K. Sec-

only, the isomerization of DMF does not occur at all by illumination of  $\gamma$ -irradiated DMF in MTHF glass with visible light at 77°K (Figure 11). It can be considered that the further illumination of light probably causes photo-detachment of an electron from the DMF radical anion (reaction 4).

It will be interesting to compare the isomerization of an anion with that of the parent molecule. When DMM or DMF in MTHF glass at 77°K is illuminated by uv light, the isomerization occurs in both cases (Figure 12). Therefore, the isomerization *via* the excited molecule is possible for both the starting materials, DMM (cis-type) and DMF (trans-type). On the contrary, the isomerization by way of the excited radical anion occurs selectively for the starting material of cis-type only. The similar selectivity in the isomerization reaction of radical anion was also observed in the case of stilbene anion.<sup>4</sup>

The maleate anion may be expressed as a resonance hybrid of the following structures



where R represents H, CH<sub>3</sub>, or C<sub>2</sub>H<sub>5</sub>. Since the unpaired electron density on the carbon atom attached to each hydrogen atom is estimated roughly to be 0.4 from the esr spectrum of maleic acid radical anions, the contribution of A<sub>1</sub> and A<sub>2</sub> to the structure of maleate anion is about four times as great as that of B<sub>1</sub> and B<sub>2</sub>. Therefore the chemical bond between the two carbon atoms attached to the hydrogen atoms has partly a character of single bond. If it is assumed that such a single bond character increases further in the excited maleate radical anion, the isomerization would occur easily. Since the negative charge may be mainly localized on the two oxygen atoms of the carbonyl groups and the distance between the two oxygen atoms of cis-type is shorter than that of trans-type, the energy of Coulomb repulsion between the two oxygen atoms of cis-type may be greater than that of trans-type and the radical anion of trans-type becomes more stable than that of cis-type. Thus the radical anion of trans-type may be selectively produced in the isomerization by way of the excited radical anion.

## Butene Isomerization over Zinc Oxide

by A. L. Dent and R. J. Kokes\*

Department of Chemistry, The Johns Hopkins University, Baltimore, Maryland 21218 (Received August 14, 1970)

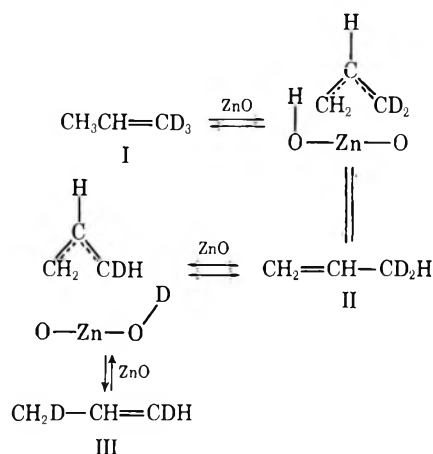
Publication costs assisted by the Petroleum Research Fund

Infrared and traditional techniques have been used to examine butene-1 and *cis*-butene isomerization over zinc oxide. On a per unit area basis it is found that zinc oxide is comparable to alumina as an isomerization catalyst. *cis*-Butene isomerization occurs readily between room temperature and 100° with an activation energy of about 18 kcal. Infrared studies of adsorbed butene show that adsorption occurs with dissociation; it is concluded that adsorbed butene forms a  $\pi$ -bonded allylic species. This species, which can occur in two forms, favors the species which is the precursor to *cis*-butene. The isomerization of *cis*-butene (and presumably butene-1) appears to occur by simultaneous isomerization to both isomeric forms, *i.e.*, *trans*- and 1-butene. It is suggested that the  $\pi$ -allyl form of butene is likely to be the intermediate in isomerization.

### Introduction

Details of double-bond isomerization of olefins over metals<sup>1</sup> and many transition metal complexes<sup>2</sup> are consistent with a sequence involving reversible addition of a hydrogen atom to form a  $\sigma$ -bonded alkyl from complexed or adsorbed olefins. Over many metal oxides,<sup>3-5</sup> however, alkyl formation from olefins is irreversible; hence, alkyl reversal cannot be the mechanism of isomerization. Kinetic evidence suggests<sup>5,6</sup> that allyl species may be formed as intermediates over these oxides. To date, however, the best evidence that these species are in fact intermediates in the isomerization of butene and the higher olefins remains mechanistic inference.

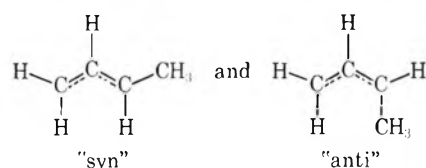
Recently,<sup>7,8</sup> we presented evidence based on ir studies that propylene adsorbs dissociatively on zinc oxide to form a symmetric allyl species analogous to those formed as ligands in transition metal complexes.<sup>9</sup> The proposed site for adsorption is a zinc ion surrounded by oxide ions. In this picture adsorption of  $\text{CH}_3\text{CHCD}_2$  is presumed to involve the following steps



wherein the species shown without zinc oxide are a loosely bound " $\pi$ -complex" nearly in equilibrium with the gas phase. Kinetic studies<sup>10</sup> in which I was circu-

lated over zinc oxide support this picture inasmuch as they show that II was the initial product and the central CH bond is undisturbed. Similarly, related reactions of propylene are consistent with this picture.

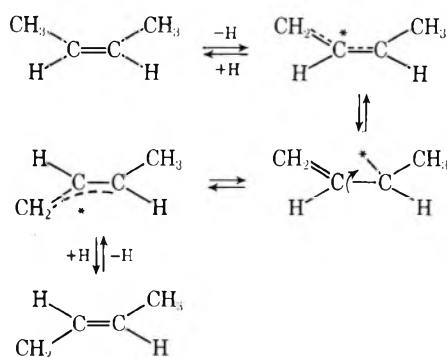
Isomerization of butene *via* a  $\pi$ -allyl species introduces some new stereochemical features. The  $\pi$ -allyl species formed from propylene is presumed to be planar with its plane approximately parallel to the surface. Since it is attached to the electropositive zinc, it may have considerable carbanion character. A corresponding structure for adsorbed butene would lead to two isomeric forms, *viz.*



*cis*-Butene should lead initially to the anti form; *trans*-butene should lead initially to the syn form, and 1-butene should give rise initially to both. The equilibrium distribution of syn and anti forms usually differs

- (1) G. C. Bond, "Catalysis by Metals," Academic Press, New York, N. Y., 1962.
- (2) R. Cramer, *Accounts Chem. Res.*, **1**, 186 (1968).
- (3) W. C. Conner, R. A. Innes, and R. J. Kokes, *J. Amer. Chem. Soc.*, **90**, 6858 (1968).
- (4) A. L. Dent and R. J. Kokes, *J. Phys. Chem.*, **73**, 3772, 3781 (1969).
- (5) R. L. Burwell, Jr., G. L. Haller, K. C. Taylor, and J. F. Read, *Advan. Catal.*, **20**, 1 (1969).
- (6) H. H. Voge and C. R. Adams, *ibid.*, **17**, 151 (1967).
- (7) A. L. Dent and R. J. Kokes, *J. Amer. Chem. Soc.*, **92**, 1092 (1970).
- (8) A. L. Dent and R. J. Kokes, *ibid.*, **92**, 6709 (1970).
- (9) (a) W. R. McClellan, H. H. Hoen, H. N. Cripps, E. L. Muetterties, and B. W. Howk, *ibid.*, **83**, 1601 (1961); (b) G. Wilke, B. Bogdanovic, P. Hardt, P. Heimbach, W. Keim, M. Kröner, W. Oberkirch, K. Tanaka, E. Steinrücke, D. Walter, and H. Zimmermann, *Angew. Chem., Int. Ed. Engl.*, **5**, 151 (1966).
- (10) A. L. Dent and R. J. Kokes, *J. Amer. Chem. Soc.*, **92**, 6718 (1970).

greatly from the equilibrium distribution of *cis*- and *trans*-butene; for cobalt complexes<sup>11</sup> the syn form precursor of *trans*-butene is by far the most stable. By way of contrast for the corresponding carbanion, the *cis* anion seems by far the more stable.<sup>12</sup> In the base-catalyzed isomerization of more complex *cis*-olefins (*cis*- $\alpha$ -methylstilbene) the ions corresponding to syn and anti are not interconvertible and *cis*-*trans* isomerization involves the  $\alpha$ -olefin as an intermediate;<sup>13</sup> for the simpler *cis*-olefins (*cis*-butene) heterogeneous base-catalyzed *cis*-*trans* isomerization is direct and the  $\alpha$ -olefin is not an intermediate.<sup>14</sup> Isomerization *via*  $\pi$ -allyl ligands of transition metal complexes may be important in some cases<sup>15</sup> but it has not been established if the syn-anti conversion is direct. The observation that many  $\pi$ -allyls are "dynamic"<sup>9b</sup> and undergo rapid  $\sigma$  to  $\pi$ -allyl interconversion suggests the possibility of a mechanism for *cis* to *trans* conversion which does not involve butene-1 as an intermediate



where \* represents the complexed atom. Thus, in the isomerization of *cis*-butene over oxide catalysts wherein surface  $\pi$ -allyls are intermediates, one can expect either the sequential pathway



or the simultaneous conversion of *cis*-butene to 1- and *trans*-butene.

This paper deals with three questions. (1) Does butene form  $\pi$ -allyl species over zinc oxide? (2) Is zinc oxide an effective isomerization catalyst for butenes? (3) Is butene-1 an intermediate in the *cis*-*trans* isomerization? In view of the results with propylene<sup>7,8</sup> question 1 may seem fatuous. This is not true. Steric restrictions on surface species are often severe;<sup>16</sup> the presence of the additional methyl group in butene may inhibit formation of the  $\pi$ -allyl species. In our approach to these questions we shall utilize ir criteria developed for propylene to judge if a  $\pi$ -allyl species is formed and shall use traditional mechanistic techniques to answer the remaining questions.

## Experimental Section

The infrared techniques, materials (Kadox-25), and pretreatment have been described in detail elsewhere.<sup>4,7,8,10</sup> Kinetic runs were carried out in a closed

circulating system with a volume of about 100 cm<sup>3</sup>. Small samples of gas were withdrawn periodically for chromatographic analysis. Runs at room temperature were made with a 10.0-g sample of zinc oxide; runs at elevated temperature were made with a 1.0-g sample of zinc oxide. No detailed studies were made of the life of the catalyst during repeated isomerization runs. Nevertheless, the fact that the results of the room temperature run (on one catalyst sample) coupled with results on runs at 100 and 68° (in that order) yielded a good Arrhenius plot suggests that poisoning is not severe and the reported rates are reasonably reliable.

## Results and Discussion

**Infrared Studies.** Figure 1 shows the spectrum in the OH region for zinc oxide after admission of butene-1 at a pressure of about 8 mm. Spectrum a, taken after 8 min of exposure, shows two features: first, the strong surface hydroxyl band at 3615 cm<sup>-1</sup> is shifted about 5 cm<sup>-1</sup> to lower frequencies; second, a new band appears at about 3587 cm<sup>-1</sup>. This new band, clearly an OH, appears to arise from dissociation of the adsorbed butene. Spectrum b shows this region after exposure to the gas phase for 1 hr. It is clear that the OH band formed from butene grows with time; detailed studies, however, reveal that there is little change after the first 20 min. Spectrum c shows the results after 20 min evacuation. Two features are evident from this spectrum; first, we find that in the absence of the gas phase

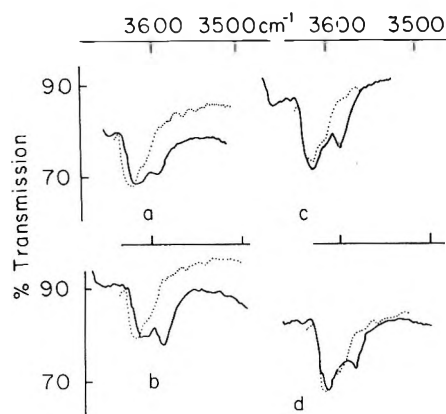


Figure 1. Spectra of zinc oxide in the OH region in butene-1 background is shown as a dotted line: a, 8 min after exposure to butene-1 at 8 mm; b, 60 min after exposure to butene-1 at 8 mm; c, 70 min of exposure to butene-1 followed by 20 min of degassing; d, c after 90 min degassing.

(11) C. L. Aldridge, H. B. Jonassen, and E. Pulkkinen, *Chem. Ind. (London)*, 374 (1960); D. W. Moore, H. B. Jonassen, T. B. Joyner, and A. J. Bertrand, *ibid.*, 1304 (1960).

(12) S. Bank, A. Schriesheim, and C. A. Rowe, Jr., *J. Amer. Chem. Soc.*, **87**, 3244 (1965).

(13) D. H. Hunter and D. J. Cram, *ibid.*, **86**, 5478 (1964).

(14) W. O. Haag and H. Pines, *ibid.*, **82**, 387 (1960).

(15) J. F. Harrod and A. J. Chalk, *ibid.*, **88**, 3491 (1966).

(16) E. F. Meyer and R. L. Burwell, Jr., *ibid.*, **85**, 2881 (1963).

the hydroxyl band of the zinc oxide has shifted back its previous position; second, the OH band formed from butene is reduced somewhat in intensity. Spectrum d shows the result after degassing for 90 min; further reduction in the band intensity due to the adsorbed species is evident. When the sample was degassed a total of 16 hr, this band intensity decreased by roughly an additional 20%.

These results are similar to those with propylene insofar as they indicate dissociative adsorption of the olefin. The hydrogen in butene which yields the hydroxyl has not been identified but the tracer results with propylene make it reasonable to suppose that the allylic hydrogen is lost. Results with butene, however, differ from those with propylene in two respects: first, the dissociation (as evidenced by the OH band) is rapid but not instantaneous as found for propylene; second, dissociatively adsorbed butene is more easily removed by room temperature evacuation than dissociatively adsorbed propylene. These facts suggest that steric effects may be present and that the driving force for formation of adsorbed methyl allyl species is not as great as for the allyl species. Accordingly, the kinetic behavior of these two species may be quite different.

Figure 2a shows the CH region of the spectrum about 10 min (solid line) and 60 min (dotted line) after admission of 8 mm of butene-1 to a sample of zinc oxide. These spectra, which are primarily due to physically adsorbed and gas-phase butenes, show that sizeable changes occur as a function of time. Table I compares

**Table I:** Dominant Bands in Spectrum of Zinc Oxide plus Butene-1

Initial, <sup>a</sup> cm <sup>-1</sup>	Final, <sup>b</sup> cm <sup>-1</sup>	Butene-1, <sup>c</sup> cm <sup>-1</sup>	<i>cis</i> - Butene, <sup>e</sup> cm <sup>-1</sup>	<i>trans</i> - Butene, <sup>e</sup> cm <sup>-1</sup>
3082		3086		
	3035 3020		3030	3021
			2985	
2972		2976		
	2972			2967
2945	2945 <sup>c</sup>	2941		2941
	2925		2932	2924
		2903		
			1660	1676 <sup>d</sup>
1655		1645		
1630	1630			
1610				
1550-1570 <sup>c</sup>	1550-1570 <sup>c</sup>			

<sup>a</sup> This scan was begun after 10 min of exposure to butene-1; the region near 1600 was scanned after 20 min of exposure.

<sup>b</sup> This scan was begun after 60 min of exposure to butene-1; the region near 1600 was scanned after 70 min of exposure.

<sup>c</sup> There may be more than one band. <sup>d</sup> Infrared inactive.

<sup>e</sup> See ref 17.

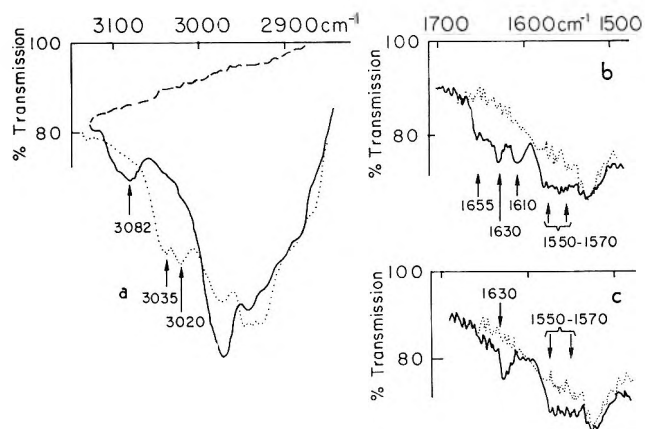


**Figure 2.** Spectra of zinc oxide in the presence of butene-1. Background is shown as a dashed line in a and as a dotted line in b and c: a, solid line, after 10 min of exposure to butene-1 (8 mm); dotted line, after 60 min of exposure to butene-1 (8 mm); b, after 20 min of exposure to butene-1 (8 mm); c, after 70 min of exposure to butene-1 (8 mm). Arrows mark positions of peaks referred to in text.

the dominant bands for the initial and final spectrum with the corresponding region for the *n*-butene isomers.<sup>17</sup> The region above 3000 cm<sup>-1</sup> is particularly clear cut. Initially, a band is observed only at 3082 cm<sup>-1</sup>; this corresponds quite closely to the 3086 cm<sup>-1</sup> band for gaseous butene-1. After 1 hr the band at 3082 cm<sup>-1</sup> is gone and two new bands (above 3000 cm<sup>-1</sup>) have appeared at 3035 and 3018 cm<sup>-1</sup> which correspond within the experimental uncertainty to the expected bands for *cis*-butene (3030 cm<sup>-1</sup>) and *trans*-butene (3021 cm<sup>-1</sup>). Other bands listed suggest similar behavior. Thus, it is evident that double bond isomerization has occurred.

Figure 2b and c show the spectrum in the double bond region after 20 and 70 min of exposure to the gas phase, respectively. Bands due to adsorbed species dominate this region of the spectrum. The initial spectrum (b) shows at least four bands at about 1650, 1630, 1610, and 1550-1570 cm<sup>-1</sup>. Of these only the band at about 1650 cm<sup>-1</sup> can be assigned to the gas phase and the most reasonable assignment is to gaseous butene-1. In the spectrum after 70 min of exposure, the bands at about 1650 and 1610 cm<sup>-1</sup> are no longer prominent. No bands due to gaseous species are observed. This is not unexpected if the composition of the gas phase has approached equilibrium. At equilibrium the dominant species is *trans*-butene (77%<sup>18</sup>) which shows no ir active C=C band and the *cis*-butene (20% at equilibrium<sup>18</sup>) has a much weaker C=C band than the butene-1<sup>19</sup> (3% at equilibrium<sup>18</sup>).

(17) N. Sheppard and D. M. Simpson, *Quart. Rev. Chem. Soc.*, **6**, 1 (1952).

(18) D. M. Golden, K. W. Eggers, and S. W. Benson, *J. Amer. Chem. Soc.*, **86**, 5416 (1964).

(19) L. J. Bellamy, "The Infrared Spectra of Complex Molecules," Wiley, New York, N. Y., 1958, p 39; R. T. Conley, "Infrared Spectroscopy," Allyn and Bacon, Boston, Mass., 1966, p 97.

Firm assignments for these C=C bands require more detailed experiments but a tentative assignment can be made based on analogies with propylene.<sup>7,8</sup> The bands at 1550–1570  $\text{cm}^{-1}$ , we believe, are due to a  $\pi$ -allyl species; the shift from the double bond region for butenes is about 100  $\text{cm}^{-1}$  compared to the shift of 107  $\text{cm}^{-1}$  observed for the  $\pi$ -allyl formed from propylene. In addition to such species for propylene, we also observed a " $\pi$ -complex" in which the shift in C=C stretch was about 30  $\text{cm}^{-1}$ . We believe the band at 1610  $\text{cm}^{-1}$  seen in the initial spectrum represents a butene-1 " $\pi$ -complex;" disappearance of this band in time is consistent with this assignment. Similarly, the band at 1630  $\text{cm}^{-1}$ , which persists and may intensify after 70 min, may be tentatively assigned to  $\pi$ -complexed butene-2 (cis and/or trans).

Some support for the above assignments is offered by the behavior of the bands at 1630, band A, and 1550–1570  $\text{cm}^{-1}$ , band B, on degassing. Both bands are still present after a brief degassing. In time, however, both bands decrease in intensity. Band A, which is presumably due to the more weakly held  $\pi$ -complex, decreases on degassing much faster than band B, which is presumably due to the more strongly held  $\pi$ -allyl species. After 90 min of degassing band A is gone but band B persists. After 16 hr of degassing, however, the intensity of band B is less than half that at the start of degassing. This decrease in band B is qualitatively similar to that observed for the OH band formed on adsorption; hence, it offers some support for assignment of band B to a  $\pi$ -allyl species which gives rise to the dissociative adsorption.

Bands in the CH stretching region due to adsorbed species are relatively weak. No prominent bands are evident above 3000  $\text{cm}^{-1}$ , the region diagnostic for olefins. Were the assignment based on the CH stretching region alone, one might conclude only saturated species were present. Nevertheless, the correlation of the decrease on degassing of bands in this region to the decrease on degassing of band B suggests that all bands in the CH stretching region stem from olefinic species.

*Isomerization of cis-Butene.* Figure 3 shows the course of *cis*-butene isomerization as a function of time at room temperature. Similar data were also obtained at 68 and 100°. The initial rates conformed well to an Arrhenius plot and yielded an activation energy of about 18 kcal/mol. On a per unit area basis the rate at room temperature is  $4 \times 10^{10}$  (molecules/sec)/ $\text{cm}^2$ . Data of Hightower and Hall<sup>20</sup> for GA48 alumina yield an initial rate of  $14 \times 10^{10}$  (molecules/sec)/ $\text{cm}^2$ . Since the activation energy for alumina is less than that found for zinc oxide, this means that zinc oxide is comparable (on a per unit area basis) to alumina as an isomerization catalyst between room temperature and 100°. At the lower temperature zinc oxide is less active and at the higher temperature it is more active.

Extrapolation of the rate data in Figure 3 to zero

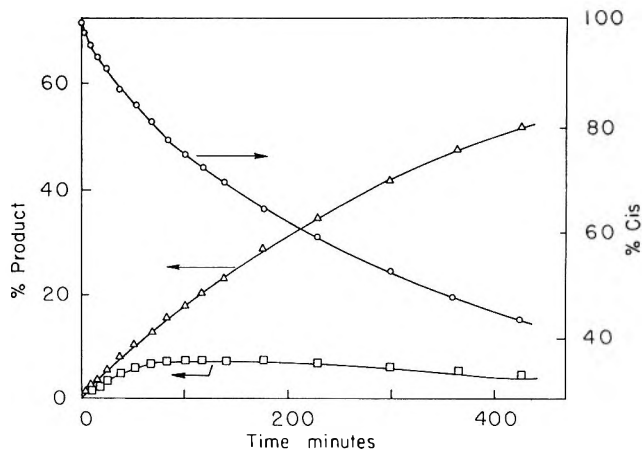


Figure 3. *cis*-Butene isomerization over zinc oxide: O, *cis*-butene (right-hand ordinate); Δ, *trans*-butene; □, butene-1.

conversion shows that the initial ratio of butene-1 to *trans*-butene formation is about unity. Above room temperature the ratio is somewhat less than unity. Thus, butene-1 is not an intermediate in the *cis*-*trans* isomerization as one finds for the homogeneous base catalyzed isomerization of more complex ions.<sup>13</sup> Thus, in this respect, zinc oxide is similar to heterogeneous base-catalyzed isomerization.<sup>14</sup>

An attempt was made to see if the surface species on the catalyst showed a strong preference for the precursor of *cis*- or *trans*-butene by flash desorption. In this experiment at the end of the room temperature run before gas-phase equilibrium was achieved (gas phase composition 31% *cis*, 65% *trans*, 4.0% butene-1) the catalyst was evacuated for 1 hr to remove the bulk of the  $\pi$ -complexed butene. Then it was stored *in vacuo* 2 days to permit further equilibration of the surface species. After further evacuation at room temperature for 1 hr, the catalyst was rapidly heated to 150°, a temperature shown to be sufficient to completely remove the adsorbed butenes. The composition of the evolved gas is compared in Table II to the computed equilibrium values at room temperature and 150°. It seems clear from these data that the equilibrated strongly held butene favors the precursor of *cis*-butene to an extent greater than that in the equilibrated gas

Table II: Composition of Butenes

	Flash desorbed, %	Equilibrium <sup>18</sup> 25°, %	Equilibrium <sup>18</sup> 150°, %
Butene-1	7	3	10
<i>cis</i> -Butene	37	20	28
<i>trans</i> -Butene	56	77	62

(20) J. W. Hightower and W. K. Hall, *J. Amer. Chem. Soc.*, **89**, 778 (1967).

phase or even the gas phase at the end of the run two days earlier. This preference, most evident for the strongly held butene, may explain the stereochemical preference for *cis*-butene found in butene-1 isomerization over oxide catalysts.<sup>20</sup>

**Conclusions.** It appears that butene adsorbs dissociatively on zinc oxide to form a species analogous to the  $\pi$ -allyl formed from propylene.<sup>7,8</sup> In addition it forms  $\pi$ -complexed species analogous to those formed by propylene.<sup>8</sup> The equilibrated strongly held butenes corresponding to  $\pi$ -allyls preferentially form *cis*-butenes on desorption compared to the corresponding equilibrium distribution in the gas phase. Zinc oxide is a catalyst for the isomerization of butenes comparable in activity on a per unit area basis to alumina. In *cis*-butene isomerization both *cis*-*trans* and double bond

migration take place simultaneously; *i.e.*, butene-1 is not an intermediate in *cis*-*trans* isomerization as has been found in homogeneous base-catalyzed isomerizations.<sup>13</sup> The results show that  $\pi$ -allyls form readily and that isomerization occurs readily on zinc oxide; hence, it is plausible to conclude that  $\pi$ -allyls are intermediates in isomerization over zinc oxide but until further data are available, it must be noted that this conclusion is tentative and as yet not proven.

**Acknowledgment.** Acknowledgment is made to the donors of the Petroleum Research Fund, administered by the American Chemical Society, for support of this research. The authors also wish to express their gratitude to C. C. Chang who rechecked the spectra in Figures 1 and 2.

## Catalytic Decomposition of Perchloric Acid Vapor on Zinc Oxide

by F. Solymosi\* and L. Gera

*Gas Kinetics Research Group of the Hungarian Academy of Sciences, Szeged, Hungary (Received August 21, 1970)*

*Publication costs borne completely by The Journal of Physical Chemistry*

The effect of zinc oxide was studied on the vapor-phase decomposition of perchloric acid. The interaction between the catalyst and the substrate was investigated by infrared spectroscopy, electric conductivity, thermal and chemical analysis. The interaction was most pronounced at 250° when a great amount of zinc perchlorate was formed. Zinc oxide catalyzed the decomposition of perchloric acid above 310°. The reaction followed first-order kinetics. The value of the activation energy was 45 kcal/mol. Experiments were performed with magnesium and cadmium oxides too; however, both oxides were found to be inactive substances. Taking into account the stability of perchlorate salts and the activity order of the oxides, the conclusion was drawn that the formation and decomposition of surface perchlorate may play an important role in the catalytic decomposition of perchloric acid. Measurements were also carried out on the catalysis of the gas-phase decomposition of ammonium perchlorate; in this process zinc oxide was found to be an outstanding catalyst.

### Introduction

In order to elucidate the role of catalysts used in propellents containing ammonium perchlorate (AP) it seems very important to know their influence on the thermal stability of perchloric acid. The first direct evidence showing that oxides are able to catalyze the decomposition of perchloric acid was published in 1968.<sup>1</sup> Chromium oxide was found to be the most active catalyst, and its effect has recently been studied in more detail.<sup>2</sup> Its excellent catalytic effect was exhibited even if a small amount of it was incorporated into the surface layer of tin dioxide, a considerably less active catalyst.<sup>3</sup>

The present paper will deal primarily with the effect of zinc oxide. In its presence AP was found to decompose

at a measurable rate at a temperature as low as 200° and its ignition occurred at a temperature lower by 200° than in the case of the pure substance.<sup>4</sup> For the purpose of comparison, the behavior of cadmium oxide and of magnesium oxide was also examined. The effects of these on the stability of AP were commensurable with that of zinc oxide.<sup>5,6</sup>

(1) F. Solymosi, S. Börcsök, and E. Lazar, *Combust. Flame*, **12**, 397 (1968).

(2) F. Solymosi and S. Börcsök, *J. Chem. Soc. A*, 601 (1970).

(3) F. Solymosi and T. Bánsági, Proceedings of the 2nd International Conference on Space Engineering, D. Reidel Publ. Co., Dordrecht, Holland, 1970, p 145.

(4) F. Solymosi and L. Révész, *Nature*, **192**, 64 (1961); *Z. Anorg. Chem.*, **322**, 86 (1963).

## Experimental Section

**Materials.** Zinc oxide was obtained as a product of the decomposition of zinc oxalate prepared in our laboratory by mixing A.G. zinc chloride and ammonium oxalate at 60°. The substance so obtained was washed and dried at 120° for 3 hr and was finally decomposed at 500° for 5 hr. Cadmium oxide was prepared by decomposing cadmium hydroxide at 400° for 5 hr. Magnesium oxide was of A.G. purity supplied by Merck. Pellets of 8 mm diameter and 2 mm thickness were prepared at a pressure of 2700 kg/cm<sup>2</sup> from the finely pulverized oxides and were treated at a temperature of 800° for 5 hr. In the catalytic experiment two pellets of approximately 0.2–0.3 g each were used.

The perchloric acid (BDH) used was of 70% purity. It was concentrated to azeotropic composition (73.6%) by passage of nitrogen at 100° for a considerable length of time. The catalytic investigations were carried out in a flow system described earlier.<sup>2</sup> The reaction products and the undecomposed perchloric acid were absorbed in gas-washing bottles containing sodium hydroxide or potassium iodide and their amounts determined by chemical analysis. In most cases, the flow rate of nitrogen was 156 ml/min, and the amount of perchloric acid passed varied from 2.5 to 3.0 × 10<sup>-5</sup> mol/min. The residence time of the perchloric acid in the reaction zone was 0.28 sec. When detailed kinetic studies were carried out, this time was varied between 0.695 and 0.114 sec by changing the rate of flow of nitrogen. The decomposition of Zn(ClO<sub>4</sub>)<sub>2</sub>·5H<sub>2</sub>O was studied under similar conditions. The flow rate of nitrogen was 156 ml/min in this case too. The weight of zinc perchlorate samples was 100 mg; the amount of chlorine formed was determined at various intervals by iodometric analysis.

The electric conductivity of the catalysts was measured during the catalytic reaction in an enlarged catalytic reactor. Differential thermal analysis and infrared spectroscopic measurements were carried out with a MOM-type derivatograph and a UNICAM SP 100 spectrophotometer.

The gas-phase catalytic decomposition of AP was studied in a vacuum. Finely pulverized AP (50 mg), pretreated at 300° for 1–3 hr, was placed in the lower part of a 10-mm diameter glass tube (divided into two parts by a sealed-in sintered glass disk) which was then sealed with a micro flame (Figure 1). The catalyst (100 mg) in the form of powder or pellet was placed on the sintered glass. By means of a platinum wire the sample holder prepared in this manner was fixed to the end of a joint that extended into the reaction vessel and was placed into the cold zone of the reaction tube. The reaction vessel was heated up to the required temperature and after about 1 hr pumping (10<sup>-4</sup> Torr) the sample holder was lowered into the hot zone by rotating the joint. The condensable gases

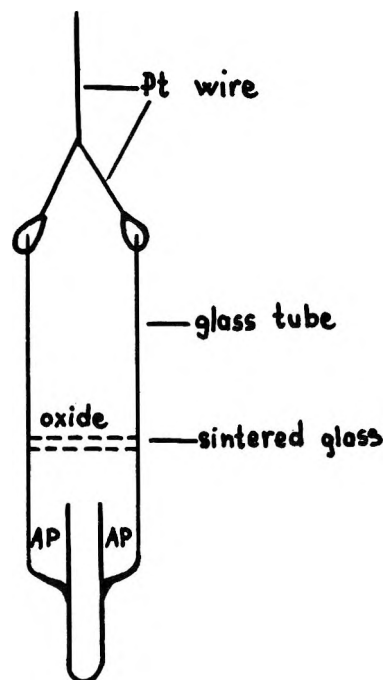


Figure 1. Sample holder for studying the catalytic decomposition of ammonium perchlorate in the gas phase.

were frozen out in a trap cooled by liquid air, and the pressures of the permanent gases were measured with a sensitive oil manometer. At the end of the experiment, the amounts of decomposed AP and of frozen-out chlorine and chlorine dioxide formed were determined.

## Results and Discussion

**Reaction Products and Constancy of the Catalytic Activity.** According to our exploratory experiments, the decomposition of perchloric acid on zinc oxide takes place at a measurable rate above 315°. The highest temperature where the catalytic effect of the reaction vessel can be neglected is 370°. Chemical analysis revealed that the catalytic decomposition of perchloric acid on zinc oxide takes place mainly according to the reaction



Chlorine dioxide was present only as an impurity (<1%) even in the case when, by the alteration of the reaction vessel, the residence time of the reaction products in the hot zone was decreased from 0.28 to 0.023 sec. Some hydrochloric acid was also observed, which indicated the slight occurrence of the reaction



The extent of this reaction was practically constant (8–10% of the decomposed HClO<sub>4</sub>) in the experimental

(5) F. Solymosi and K. Fónagy, *Symp. (Int) Combustion Proc. 11th*, 429 (1967).

(6) F. Solymosi, *Magy. Kém. Foly.*, 73, 358 (1967).

temperature range. Hence our experiments were mainly directed to reaction 1.

Prior to kinetic measurements, the changes in the activity of the catalysts were investigated (Table I).

**Table I:** Change in the Activity of ZnO

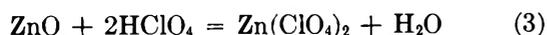
Time, min	—Percentage decomposition/min—	
	325°	350°
15	3.25	12.25
30	3.5	12.7
45	3.1	12.5
60	2.8	12.15
75	2.5	11.85
90	2.45	11.5
105		11.4
120		11.2
135	2.1	10.85
150	2.25	10.8
165	2.25	10.65
180	2.20	10.65

The activity of the oxides, *i.e.*, the percentage decomposition of perchloric acid, was measured at time intervals of 15 min. From the results it can be seen that the activity of the catalyst first decreases to a small extent, but after a certain time no appreciable change can be observed.

*Interaction between Zinc Oxide and Perchloric Acid.* To know more about the interaction between catalysts and perchloric acid, electric conductivity measurements, infrared spectroscopy, differential thermal analysis, and chemical analysis were used. The spectra of samples treated below 300° are in good agreement with the infrared spectrum of zinc perchlorate. Above 300°, where a rapid decomposition of perchloric acid occurs on zinc oxide, no changes can be observed in the spectra of the oxide.

Thermoanalytical studies lead to similar results. DTA curves of the catalysts, treated below 300°, are similar to those of zinc perchlorate, while those of substances treated above 300° show no changes characteristic of the decomposition of zinc perchlorate.

From the results of chemical analysis of substances treated with perchloric acid at various temperatures it appeared that perchloric acid reacts with zinc oxide below 300°



The analytical results are summarized in Table II.

The formation of zinc perchlorate began at 180°; the extent of the reaction increased up to 250°, and then decreased; above 300° the presence of zinc perchlorate could no longer be shown by chemical analysis.

Electric conductivity measurements also support the existence of a considerable interaction between perchloric acid and zinc oxide. At the temperature of

**Table II:** Formation of  $\text{Zn}(\text{ClO}_4)_2$  at Different Temperatures<sup>a</sup>

Temp, °C	Amount of ZnO used, mg	Zn(ClO <sub>4</sub> ) <sub>2</sub> formed, %
150	286.1	0.72
180	218.4	4.47
200	267.0	11.23
250	266.9	15.84
270	290.5	7.37
280	291.5	4.13
290	252.5	1.23
300	175.0	0.26
310	437.0	0.06
335	300.7	0.01

<sup>a</sup> Reaction time was 2 hr. The amount of perchloric acid passed per min was  $2.8 \times 10^{-6}$  mol.

the catalytic decomposition of perchloric acid (350°), the conductivity of zinc oxide measured in nitrogen decreased by about 4 orders of magnitude within a few minutes. After this, however, there was no or only a slight change (Figure 2).

When the nitrogen gas containing perchloric acid was replaced by pure nitrogen, the original state could not be reestablished, and only a minimal increase in conductivity occurred. This observation reveals that the excess zinc in the surface layer of zinc oxide under-

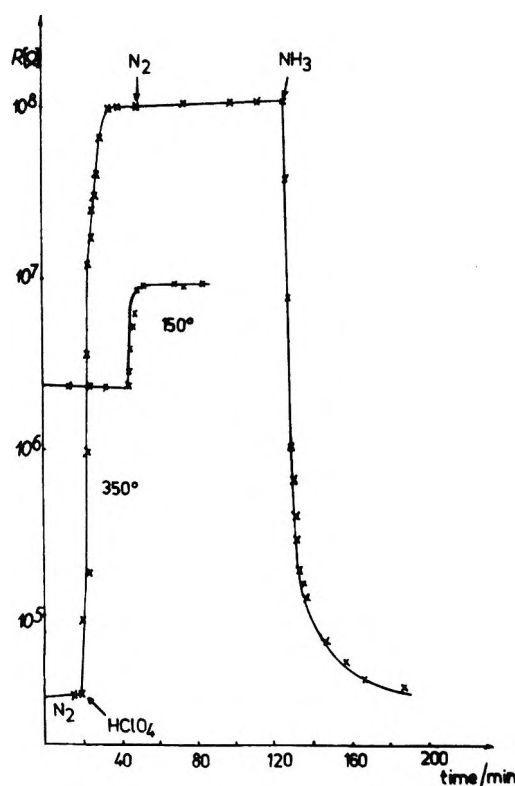


Figure 2. The effect of  $\text{HClO}_4$  and  $\text{NH}_3$  on the electric resistivity of  $\text{ZnO}$  at 350° and 150°.

goes an irreversible oxidation due to perchloric acid and/or the decomposition products.

Taking into consideration that reductive ammonia is formed in the dissociation of AP in addition to perchloric acid, it seemed interesting to investigate whether the original state of the catalyst could be reestablished with ammonia at the same temperatures. In order to get a true comparison, the ammonia content of the nitrogen carrier gas was made virtually equal to that of the perchloric acid. The addition of ammonia increased the conductivity of the perchloric acid-treated zinc oxide. The conductivity of the oxide rapidly attained its original value, and moreover, after further treatment with ammonia, became lower than that of the initial substance.

Measurements were also carried out in the temperature range 200–280°, where perchloric acid does not decompose, and thus the effect of decomposition products could be avoided. The conductivity of the sample increased by about 2.0–2.5 orders of magnitude in this case too; after 15–20 min, however, it changed irregularly as a result of the formation and melting of zinc perchlorate.

The adsorption of perchloric acid exerted a considerably smaller influence on the electric conductivity of ZnO at 150° (Figure 2). In 30 min 1.06 mg of HClO<sub>4</sub> adsorbed on 1 g of zinc oxide, irreversibly. An interesting behavior was exhibited when the oxide treated with HClO<sub>4</sub> at 150° was heated up to higher temperatures in pure nitrogen. The electric resistivity first decreased up to 330°, which corresponds to the temperature of catalytic reaction, then suddenly increased by about 2–2.5 orders of magnitude and on further heating decreased again. This behavior can be explained by taking into account that at 330° the chemisorbed perchloric acid decomposes and simultaneously the surface of zinc oxide becomes oxidized, this leading to a great increase of its resistivity. The results of these experiments are shown in Figure 3. For comparison the dependence of the electric resistance of untreated zinc oxide, which behaves regularly, is also shown.

Detailed conductivity measurements were carried out at 300 and 350° in the presence of the vapors produced from AP. These exerted a similar influence on the conductivity of zinc oxide as did perchloric acid. These findings indicate that zinc oxide also undergoes an irreversible change in the case of AP decomposition. The reducing action of ammonia formed in the dissociation of AP could not be manifested possibly due to the high oxygen content of perchloric acid.

*The Effect of Cadmium Oxide and Magnesium Oxide.* Similar measurements to the above were carried out with cadmium and magnesium oxides. In both cases chemical reaction occurred between the oxides and perchloric acid. The formation of cadmium perchlorate from perchloric acid and cadmium oxide was observed

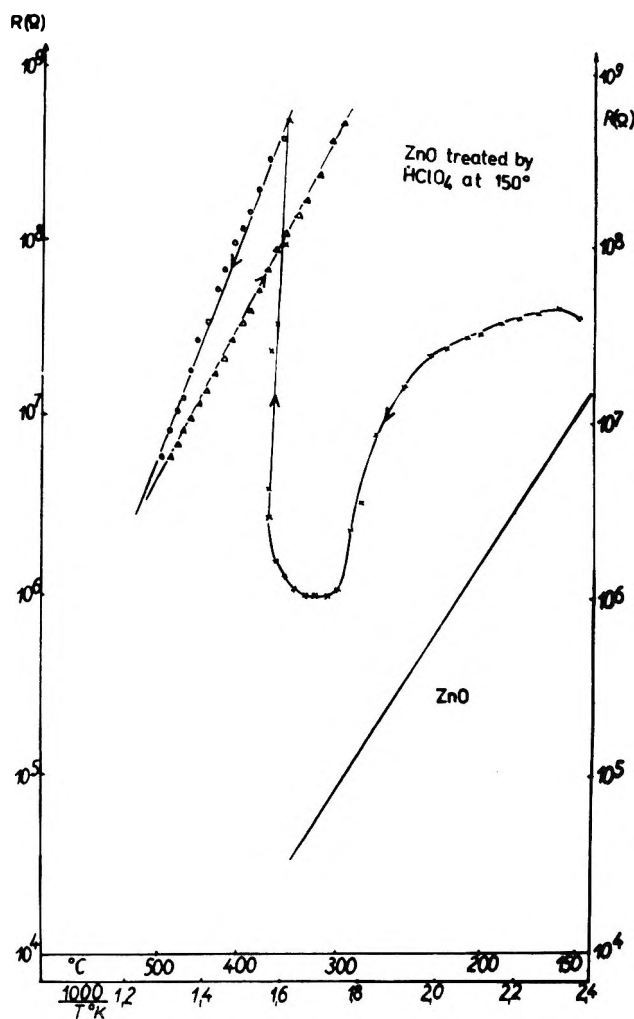


Figure 3. The effect of temperature on the electric resistivity of ZnO pretreated with HClO<sub>4</sub> at 150°.

at a temperature as low as 200°. The extent of the reaction increased with increasing temperature. The catalytic decomposition of perchloric acid remained at a very low level even between 350 and 400°. Taking into consideration the decomposition occurring in the empty reactor the percentage decomposition of perchloric acid at 380° on cadmium oxide amounted only to 1–2%.

The reaction between magnesium oxide and perchloric acid took place at 300° under the experimental conditions. The extent of this reaction was smaller than that in the case of cadmium oxide. The catalytic effect of magnesium oxide was noticeable only above 350°. However, even at this temperature the amount of perchloric acid catalytically decomposed was greater by only 1–1.5% than that in an empty reactor.

*Kinetic Measurements.* The value of the activation energy of the catalytic decomposition was determined initially from the temperature dependence of the percentage conversion in the temperature range 315–350°, first by a decreasing, then by an increasing temperature

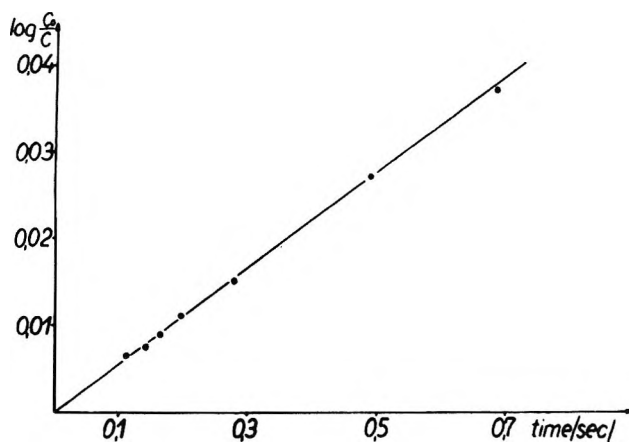


Figure 4. The applicability of the first-order rate equation: temperature  $340^{\circ}$ ;  $C_0$  = initial concentration of  $\text{HClO}_4$ ;  $C = C_0 - X$ ;  $X$  = decomposed  $\text{HClO}_4$ ;  $\tau$  = residence time of  $\text{HClO}_4$

program; afterward this procedure was repeated with a fresh catalyst, but in the reverse order. Two measurements, lasting for 15 min, were made at all temperatures and the values obtained were averaged.

The values of the two series of measurements fall practically on the same straight line; hysteresis cannot be observed. The activation energy was calculated to be  $45.6 \pm 1.5$  kcal/mol.

From the detailed kinetic measurements it appeared that the reaction follows first-order kinetics. This is shown by the data of Figure 4.

The rate constants at each temperature were determined several times and were well reproducible. The value of the activation energy was found to be  $45 \pm 1.5$  kcal/mol (Table III).

Table III: Kinetic Data for the Catalytic Decomposition of  $\text{HClO}_4^a$

Temp, $^{\circ}\text{C}$	$k_{\text{app.}}$ $\text{min}^{-1} \text{m}^{-2}$
355	29.49
350	23.17
345	17.21
340	11.58
335	9.69
330	6.02

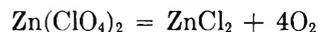
<sup>a</sup> The surface area of  $\text{ZnO}$  is  $1.64 \text{ m}^2/\text{g}$ . Activation energy in  $\text{kcal mol}^{-1}$  is  $45.6 \pm 1.5$ .

On the basis of kinetic measurements we assume that in the temperature range studied, the slow, rate determining process of the catalytic decomposition is the chemisorption of perchloric acid on the surface of the catalyst. Taking the above into consideration, it seems very likely that the decomposition of perchloric acid takes place through the surface formation and decomposition of perchlorate ion. According to our

earlier investigations,<sup>7</sup> the decomposition of the partially dehydrated zinc perchlorate



occurred at  $280$ – $315^{\circ}$  under vacuum under isothermal conditions and gave almost identical gaseous products as did the zinc oxide-catalyzed decomposition of perchloric acid. The reaction producing zinc chloride



occurred only to a small extent. From the kinetic data, based on oxygen pressure measurements, the activation energy was calculated to be  $40$  kcal/mol. For the sake of completeness the decomposition of zinc perchlorate was also studied under the experimental conditions applied in the case of the catalytic decomposition of perchloric acid by measuring the amount of chlorine evolved. The initial rapid chlorine evolution is due to a fast reaction in the molten phase. After this the substance solidified and the decomposition slowed down. The rate constants of the slow decomposition of zinc perchlorate were calculated using the monomolecular decay equation. The activation energy of the reaction was  $39.7$  kcal/mol. The solid residue contained zinc oxide and chloride in a  $5:1$  mole ratio.

On the basis of the available data it seems very likely that the effectiveness of an oxide in the decomposition of perchloric acid is closely connected with the stability of its perchlorate salt. This assumption is supported by the fact that neither cadmium oxide nor magnesium oxide showed any catalytic effect. The perchlorate salts of these two metals are considerably more stable than zinc perchlorate; their decompositions commenced at  $380$  and  $400^{\circ}$ , respectively.<sup>7</sup> Chromium oxide, on the other hand, efficiently catalyzed the decomposition of perchloric acid even at a temperature as low as  $140^{\circ}$ ; this catalyzing ability of the oxide is presumably due to the high instability of chromium perchlorate.<sup>2</sup>

*Effect of Oxides on the Vapor-Phase Decomposition of AP.* One of the aims of these investigations was to obtain data for the elucidation of the mechanism of the catalytic decomposition of AP. Hence it is reasonable to interpret the results from this point of view. The fact that of the three oxides studied only zinc oxide catalyzed the decomposition of perchloric acid, while in the slow decomposition and ignition of AP all the three exerted practically the same catalytic effect, led us to conclude that the role of the oxides in the decomposition of AP is not only the catalysis of the decomposition of perchloric acid formed in the dissociation of AP, as was assumed in the case of the copper chromite catalyst.<sup>8</sup> If this were the case, it could then be ex-

(7) F. Solymosi, *Acta Chim. Acad. Sci. Hung.*, **57**, 35 (1968).

(8) P. W. M. Jacobs and A. Russel-Jones, *Symp. (Int) Combustion*, **11th**, 457 (1967).

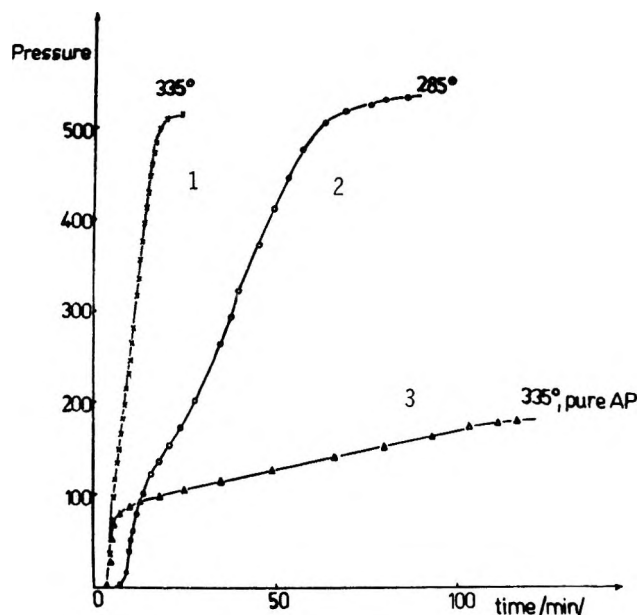


Figure 5. The effect of ZnO on the vapor-phase decomposition of  $\text{NH}_4\text{ClO}_4$ : 1,  $335^\circ$ ; 2,  $285^\circ$ ; 3, pure AP at  $335^\circ$ .

pected that the activities of the oxides might be commensurable in the decomposition of perchloric acid.

As ammonia is formed in addition to perchloric acid in the dissociation of AP, the effects of the oxides were also investigated in the gas-phase decomposition of AP. Zinc oxide exerted a pronounced effect, whereas with cadmium or magnesium oxides the extent of decomposition was scarcely greater than in the absence of the catalysts. The catalytic effect of zinc oxide was exhibited even at  $265^\circ$ , where the pure AP, pretreated at  $300^\circ$ , underwent only sublimation and its decomposition was negligible. Some of the experimental results are shown in Figure 5.

It is worth mentioning that according to our investigations carried out under similar experimental conditions, the effects of transition metal oxides ( $\text{NiO}$ ,  $\text{Cr}_2\text{O}_3$ ,  $\text{CuO}$ ) on the gas-phase decomposition of AP were far below that of zinc oxide, in spite of the fact that these oxides are more effective catalysts in the decomposition of perchloric acid than is zinc oxide.<sup>9</sup> The considerable catalytic effect of zinc oxide observed in the temperature range  $260$ – $280^\circ$  is rather surprising since, as was shown by our earlier measurements, perchloric acid scarcely decomposes on zinc oxide below  $300^\circ$ ; the only product is zinc perchlorate. (It must be taken into account, however, that when the catalysis of the decomposition of perchloric acid was studied, the measurements were carried out with  $\text{HClO}_4 \cdot 2\text{H}_2\text{O}$  using nitrogen as carrier gas, while in the dissociation of AP anhydrous perchloric acid was formed, which is more unstable than the dihydrate.)

From the above it appears that the behavior of oxides is different in perchloric acid vapor than in gaseous AP; hence the conclusion can be drawn that in the catalysis of the decomposition of gaseous AP the essential factor is not merely the promotion of the decomposition of perchloric acid, but also the conditions for the oxidation of ammonia; consequently, the catalyst plays a double role. From our measurements it appears that this requirement can best be fulfilled by zinc oxide, in spite of the fact that both in the oxidation of ammonia and the decomposition of perchloric acid it proved to be a far worse catalyst than the oxides of the transition metals. Investigations concerning the role of zinc oxide in the gas-phase decomposition of AP are in progress.

(9) F. Solymosi, L. Gera, and S. Börcsök, *Symp. (Int) Combustion*, 13th, in press.

# Solvent Effects on the Fluoroform Nuclear Magnetic Resonance Spectra

by William B. Smith\* and Arthur M. Ihrig

Department of Chemistry, Texas Christian University, Fort Worth, Texas 76129 (Received July 29, 1970)

Publication costs assisted by The Robert A. Welch Foundation

The proton and fluoride chemical shifts of fluoroform in a variety of solvents have been determined. These results are compared with those reported in the literature for chloroform. The chemical shifts for the proton, in general, move downfield with increasing polarity of the solvent while the fluorine chemical shift moves upfield. The operation of a solvent "reaction field" is indicated. Specific complexation of the fluoroform to benzene was suggested by the marked upfield shifts of both the proton and fluorine chemical shifts.

Recently, Lichter and Roberts have reported on the proton and  $^{13}\text{C}$  chemical shifts of chloroform in a variety of solvents.<sup>1</sup> It was their conclusion that the primary effect producing solvent-induced chemical shifts was the known hydrogen bonding propensities of the solute rather than such effects as the solvent "reaction field." Their results in benzene were consistent with the idea of a 1:1 complex in which the CH bond axis of the solute lies along the sixfold axis of the solvent molecule.

The investigation of solvent-induced chemical shifts has been a subject of considerable interest as a means of studying weak interactions.<sup>2</sup> However, as Lichter and Roberts<sup>1</sup> point out, few solvent studies involving nuclei other than protons have appeared. Because of the greater polarity of fluoroform (1.6 D as opposed to 1.1 D<sup>3</sup>) as a solute, the study of solvent effects on both proton and fluorine chemical shifts seemed a worthwhile extension of the chloroform work.

## Experimental Section

A sample of fluoroform was obtained from the Matheson Company. Reagent and spectral grade solvents were used, and in no case were any impurities detected. Proton and fluorine spectra were taken on a Varian HA-100 spectrometer operating at 100 and 94.1 MHz. Gaseous fluoroform was condensed and measured as a liquid and then distilled into an appropriate quantity of solvent to give ca. 5 mol % solution. These samples were degassed by the usual freeze-thaw techniques and sealed under vacuum. Two sets of samples containing tetramethylsilane and 1,1,2,2-tetrachloro-3,3,4,4-tetrafluorocyclobutane<sup>4</sup> as internal references were prepared for the proton and fluorine investigations, respectively. The proton spectra were calibrated in frequency sweep mode with the final line positions representing an average of at least five independent scans. The fluorine spectra were calibrated in the HR mode by superimposing audiofrequency side bands generated with a Hewlett-Packard 200 CD oscillator on each of the transitions in the fluorine spectra. The fluorine chemical shifts represent an average of at least five independent measurements with an estimated accuracy of  $\pm 0.5$  Hz.

## Results and Discussion

The chemical shifts on the protons and fluorines in fluoroform in a variety of solvents are given in Table I as are the values of the HF coupling constant. It has been noted before<sup>5</sup> that the fluoroform HF coupling

Table I: Nmr Data for Fluoroform in Various Solvents

Solvent	H, ppm	F, ppm	$J_{\text{HF}}$ , Hz
1. Cyclohexane	6.25	35.96	79.31
2. Carbon tetrachloride	6.46	35.69	79.23
3. Benzene	5.31	35.73	79.27
4. Anisole	5.89	35.78	79.26
5. Chloroform	6.47	35.45	79.25
6. Methylene chloride	6.54	35.25	79.35
7. Acetone	7.04	34.70	79.40
8. Nitrobenzene	6.83	35.35	79.32
9. Dimethylformamide	7.32	34.63	79.37
10. Acetonitrile	6.75	34.39	79.38
11. Nitromethane	6.74	34.83	79.38

constant is to a large extent solvent independent. That trend is confirmed in Table I and stands in contrast to the observations of Lichter and Roberts<sup>1</sup> that the CH coupling of chloroform follows the proton chemical shift in a linear fashion.

With the exceptions of benzene and anisole all proton chemical shifts are downfield from the value in the least polar solvent, cyclohexane. This observation is in accord with those of Lichter and Roberts<sup>1</sup> for chloroform. However, in contrast to the carbon chemical

(1) R. L. Lichter and J. D. Roberts, *J. Phys. Chem.*, **74**, 912 (1970).

(2) (a) P. Laszlo, *Progr. Nucl. Magn. Resonance Spectrosc.*, **3** (1968); (b) J. Ronayne and D. H. Williams, *Ann. Rev. NMR (Nucl. Magn. Resonance) Spectrosc.*, **2** (1969).

(3) A. L. McClellan, "Tables of Experimental Dipole Moments," W. H. Freeman, San Francisco, Calif., 1963.

(4) R. W. Taft, E. Price, I. R. Fox, I. C. Lewis, K. K. Anderson, and G. T. Davis, *J. Amer. Chem. Soc.*, **85**, 709 (1963), have adequately established the suitability of the cyclobutane as an internal standard for fluorine chemical shifts.

(5) R. H. Cox and S. L. Smith, *J. Magn. Resonance*, **1**, 432 (1969).

shifts in the chloroform study, the chemical shifts of the fluoroform fluorines are all upfield in all solvents compared with cyclohexane. There is only a very rough linear correlation between the proton chemical shifts for fluoroform and chloroform in the same solvents.

Solvent-induced chemical shifts may be caused by the operation of a number of different effects.<sup>2</sup> Presumably the effects of bulk susceptibility are eliminated by the use of an internal standard. Similarly, one may suppose that van der Waals effects and anisotropy of randomly oriented solvent molecules are of little importance. Lichter and Roberts<sup>1</sup> suggest that the major causative factor for solvent-induced chemical shift effects (excluding the specific complexation with aromatic solvents such as benzene) is the hydrogen bonding interaction of chloroform with the solvent. They found no reason to propose the operation of the solvent "reaction field" effect. A similar conclusion had been reached previously by Kuntz and Johnson<sup>6</sup> for a series of alkyl halides and polyhalides.<sup>7</sup>

However, the general downfield shift of the proton and the concomitant upfield shift of the fluorine chemical shifts in solvents of increasing polarity suggests the operation of the "reaction field" effect. Petrakis and Bernstein<sup>8</sup> have observed the proton and fluorine chemical shifts in the gas phase of fluoroform in gas mixtures of various polar "perturbers." They concluded that the effects of the perturbing fields of the gaseous diluents operated in opposite senses on ends of the fluoroform dipole; *i.e.*, with increasing polarity of the medium the proton will be deshielded while the fluorines will be shielded. Our results in solution concur with their vapor phase measurements. Furthermore, excepting the aromatic solvents, there are rough linear correlations between such solvent parameters as  $(\epsilon - 1) / (\epsilon + 1)$ , as shown in Figure 1, and the solvent molar transition energies  $E_T$  of Dimroth, Reichardt, Siepmann, and Bohlmann.<sup>9</sup> No doubt hydrogen bonding and more specific complexation interactions operate with fluoroform, but this more polar solute allows the "reaction field" effect of the solvents to be seen.

It is now generally accepted that chloroform hydrogen bonds weakly to benzene forming a 1:1 complex with the C-H bond along the sixfold symmetry axis of the benzene. Lichter and Roberts<sup>1</sup> have calculated a separation of about 3.8 Å for the difference between the center of the ring and the chloroform proton. Given the greater electronegativity of fluorine over chlorine and the greater polarity of fluoroform, one might expect

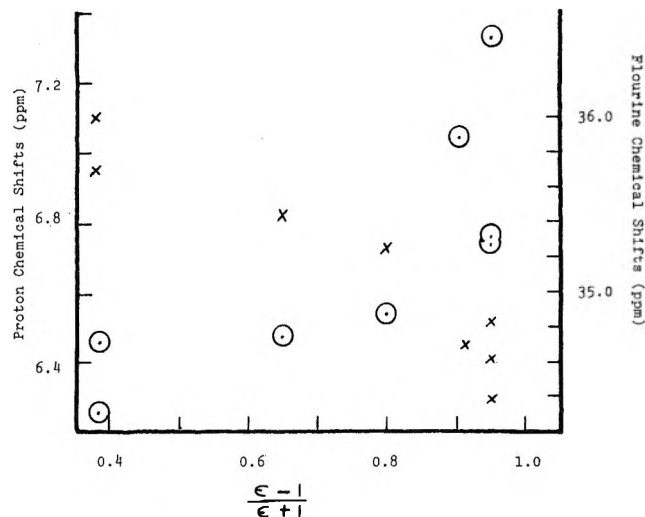


Figure 1. Plot of the proton (circles) and fluorine (X) chemical shifts in various solvents (aromatics excluded) vs. the solvent dielectric constant function.

fluoroform to complex more closely to the benzene. Using Johnson-Bovey tables for the calculation of anisotropic effect of the solvent on the fluoroform proton yields a range of 3.6–3.8 Å for the separation.<sup>10</sup> As the confirmation of these values one can calculate that the fluorine should experience an upfield of *ca.* 0.23 ppm on going from cyclohexane to benzene,<sup>11</sup> a value in good agreement with the experimental value of 0.33 ppm and suggestive of the correctness of the geometry of the complex.

*Acknowledgment.* This work was supported by the Robert A. Welch Foundation. We wish to express our gratitude to the Foundation. A. M. I. wishes to express his appreciation to the T. C. U. Research Foundation for a Postdoctoral Fellowship.

(6) I. D. Kuntz and M. D. Johnson, *J. Amer. Chem. Soc.*, **89**, 6008 (1967).

(7) A referee has pointed out that the behavior of the protons in our system is not dissimilar from that recently observed for  $\alpha$ -chloroacetonitrile in a series of solvents [R. L. Schmidt, R. S. Butler, and J. H. Goldstein, *J. Phys. Chem.*, **73**, 1117 (1969)]. Collision complexes were evoked as the best explanation for the latter system.

(8) L. Petrakis and H. J. Bernstein, *J. Chem. Phys.*, **38**, 1562 (1963).

(9) See C. Reichardt, *Angew. Chem., Int. Ed. Engl.*, **4**, 29 (1965).

(10) Lichter and Roberts<sup>1</sup> chose a chemical shift value for the chloroform proton in a nonpolar-isotropic solvent from the linear relationship of the chemical shift and  $J_{13CH}$ . Their value was 0.16 ppm upfield from the experimental value in cyclohexane. Our calculations were made from the data in cyclohexane and with a 0.16 ppm correction added in. The latter gave the separation of 3.6 Å.

(11) The geometry of the fluoroform molecule was taken from R. A. Berheim, D. J. Hoy, T. R. Krugh, and B. J. Lavery, *J. Chem. Phys.*, **50**, 1350 (1969).

Structure of Nitroform in Various Solvents<sup>1a,b</sup>

by H. P. Marshall,\* F. G. Borgardt, Paul Noble, Jr., and N. S. Bhacca

Lockheed Palo Alto Research Laboratory, Palo Alto, California 94304 (Received June 29, 1970)

Publication costs assisted by the Lockheed Palo Alto Research Laboratory

Proton exchange rates were determined for nitroform in D<sub>2</sub>O–D<sub>2</sub>SO<sub>4</sub> solvent up to an analytical mole fraction of D<sub>2</sub>O = 0.5. The proton exchange rate for an analytical mole fraction of 0.159 of D<sub>2</sub>O in D<sub>2</sub>SO<sub>4</sub>–D<sub>2</sub>O is given by  $\log k$  (sec<sup>-1</sup>) = 9.38 – 19,200/2.303RT ( $\Delta S^\ddagger$  at 55° is –17 eu) for the temperature range of 40–70°. Further, the log of the rate constants was found to be proportional to the analytical mole fraction of D<sub>2</sub>O in D<sub>2</sub>SO<sub>4</sub>. A mechanism for the proton exchange reaction is proposed. Proton chemical shifts for nitroform, 1,1-dinitroethane, and 1,1-dinitropropane were determined in a series of solvents. The chemical shift of nitroform ranges from  $\delta$  (ppm) of 7.40 in CCl<sub>4</sub> to  $\delta$  (ppm) of 9.18 in acetone; in the latter solvent, complex formation occurs with a  $K_{eq} = 10$  (~37°) (concentration in mole fraction). Rapid proton exchange occurs between water, methanol, and 12 N HCl and nitroform. Proton chemical shifts of 1,1-dinitroethane and 1,1-dinitropropane for the C-1 proton are shifted downfield by ~0.7 (ppm) in changing solvent from CCl<sub>4</sub> to acetone. Small shifts (~0.04 ppm) downfield were observed for the C-2 protons. Coupling constants were determined for the various protons in the dinitroalkanes and found to be independent of the solvent system.

## Introduction

For some time, this laboratory has been involved in studies of the synthesis, reactions, physical properties, and structure of the polynitroalkanes. As part of these studies, an nmr investigation was carried out to obtain an insight into the structure, H-bonding, complex formation, and proton exchange rates for several polynitroalkanes.

Previous studies have shown nitroform to have some of the properties of strong protic acids, also to occur as a colorless to intensely yellow substance depending upon the nature of the solvent, and to undergo addition reactions with  $\alpha,\beta$ -unsaturated carbonyl compounds in which either C- or O-alkylation can occur. This paper is concerned with defining the structure of nitroform and other 1,1-dinitroalkane species in various solvent systems.

## Experimental Section

**Materials.** Nitroform (HNF) was prepared by a modification of the procedure<sup>2</sup> used in the course of preparation of trinitroethanol. Tetranitromethane was titrated with alcoholic KOH to give KC(NO<sub>2</sub>)<sub>3</sub>, which upon acidification with HCl yielded an aqueous slurry. Extraction of this slurry with CCl<sub>4</sub>, followed by drying and evaporation, yielded reasonably pure HNF. Final purification of the HNF just before use was achieved by fractional sublimation.

The polynitroalkanes, 1,1-dinitroethane and 1,1-dinitropropane, were prepared by the method of Schechter and Kaplan.<sup>3</sup> These materials were purified by fractional distillation at reduced pressure. The purity was 99+% as indicated by gas-phase chromatography. The dioxane–nitroform complex, C<sub>4</sub>H<sub>8</sub>O<sub>2</sub>·

2HC(NO<sub>2</sub>)<sub>3</sub>, was prepared as previously described by Shechter and Cates.<sup>4</sup>

**Solvents.** The acetone, acetonitrile, and carbon tetrachloride were commercial spectral grade solvents. Acetone-*d*<sub>6</sub> (purchased from Varian) was used as received. Methanol was dried by a procedure described by Wiberg.<sup>5</sup> Trifluoroacetic acid, commercial grade (Peninsular Chemical Co., Gainesville, Fla.), was purified by distillation. Deuterated acetic acid (CH<sub>3</sub>-COOD) was prepared by reaction of purified CH<sub>3</sub>COCl with D<sub>2</sub>O followed by fractional distillation. Proton magnetic resonance spectra showed the presence of only a trace of CH<sub>3</sub>COOH.

Deuteriosulfuric acid was prepared in an all-glass vacuum system. Purified SO<sub>3</sub> was slowly distilled into D<sub>2</sub>O until a slight excess of SO<sub>3</sub> was attained. Then the D<sub>2</sub>SO<sub>4</sub> was distilled into a glass container for storage. The proton magnetic resonance spectra of the D<sub>2</sub>SO<sub>4</sub> showed the presence of only a trace of HDSO<sub>4</sub>.

Solutions of various analytical mole fraction<sup>6</sup> of

(1) (a) This work has been carried out as part of the Lockheed Independent Research Program; (b) portions of this paper were presented before the Division of Physical Chemistry at the 153rd National Meeting of the American Chemical Society, Miami, Fla., April 1967.

(2) F. G. Borgardt, A. K. Seeler, and P. Noble, Jr., *J. Org. Chem.*, **31**, 2806 (1966).

(3) R. B. Kaplan and H. Shechter, *J. Amer. Chem. Soc.*, **83**, 3535 (1961).

(4) H. Shechter and H. L. Cates, Jr., *J. Org. Chem.*, **26**, 51 (1961).

(5) K. Wiberg, "Laboratory Techniques in Organic Chemistry," McGraw-Hill, New York, N. Y., 1960.

(6) Throughout this paper analytical mole fraction (*X*) refers to the composition of the solvent in terms of the original amount of reagents employed for its preparation; thus for D<sub>2</sub>O,  $X_{D_2O}$  = moles of D<sub>2</sub>O / (moles of D<sub>2</sub>O + moles of D<sub>2</sub>SO<sub>4</sub>). No attempts are made to calculate actual mole fractions of various species after equilibration or complex formation has occurred.

$D_2O(X_{D_2O})$  with the  $D_2SO_4$  were prepared gravimetrically. The composition of the  $D_2SO_4$  solutions at several  $X_{D_2O}$  was checked by titration with standard base and was found to be within 0.2% of the calculated  $X_{D_2O}$  values.

All proton spectra were determined at 60 Mc/sec using a Varian A-60 spectrometer equipped with a variable temperature probe. Tetramethylsilane was used as an internal standard unless otherwise indicated.

Ultraviolet spectra of the HNF in various solvents were determined with a Cary-14 spectrophotometer.

### Results and Discussion

The chemical shifts of HNF were determined in  $D_2O$ - $D_2SO_4$  solvent at various mole fractions of  $D_2O$  ( $X_{D_2O}$ ). These data are summarized in Table I and plotted in Figure 1. The chemical shift of HNF increased from 8.18 ppm to 8.60 ppm as the  $X_{D_2O}$  was increased from  $\sim 0$  to 0.5. The chemical shifts of the  $HDSO_4$  were essentially the same for the pure solvent as in the presence of the HNF. The absorption peaks for the HNF and  $HDSO_4$  were very sharp up to an  $X_{D_2O} \approx 0.5$  with a single peak observable for  $X_{D_2O} > 0.5$ .

**Table I:** Chemical Shift of HNF in  $D_2O$ - $D_2SO_4$ <sup>a</sup>

Analytical mole fraction of water, $X_{D_2O}$	Chemical shift	
	$\delta_{HNF}$ , ppm	$\delta_{HDSO_4}$ , ppm
0.0072 <sup>b,d</sup>	8.18	11.18
0.143	8.27	11.15
0.191	8.28	11.70
0.298	8.33	11.98
0.370	8.42	12.09
0.430	8.42	12.13
0.472	8.61 <sup>c</sup>	12.13
0.487 <sup>e</sup>	8.58 <sup>c</sup>	12.12
0.491	8.60 <sup>c</sup>	12.05
0.493	8.60 <sup>c</sup>	12.07
0.495	8.60 <sup>c</sup>	12.13
0.497	8.58 <sup>c</sup>	12.13
0.498		12.09
0.499	8.60 <sup>c</sup>	12.11
0.598		11.72
0.659		11.34
0.718		10.85
0.749		10.45

<sup>a</sup> TMS used as an external standard. <sup>b</sup> All solutions were prepared on a weight basis; concentration of solutions at several  $D_2SO_4$  were checked by titrations with standard base. <sup>c</sup>  $\delta_{HNF}$  signal observed only at spectrum amplitude of 80. <sup>d</sup> In the absence of HNF, the chemical shift for the pure solvent was 11.24. <sup>e</sup> In the absence of HNF, the chemical shift for the pure solvent was 12.16.

The proton exchange rates of HNF in  $D_2O$ - $D_2SO_4$  were determined as a function of  $X_{D_2O}$ . The rate constants,  $k_1$ , were calculated using a first-order rate expression for which the concentration of HNF was as-

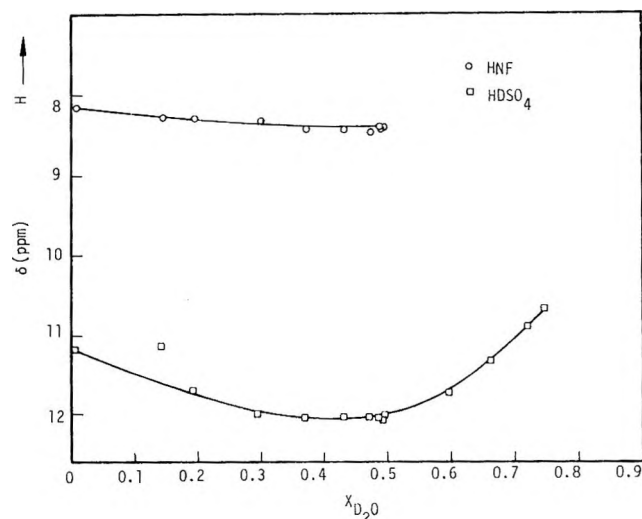


**Figure 1.** Chemical shift of HNF and  $HDSO_4$  in  $D_2O$ - $D_2SO_4$  as a function of analytical mole fraction of  $D_2O$ .

sumed to be proportional to the line intensity of the proton resonance peak of the HNF. The same values of rate constants were obtained, within experimental error, when the areas of the proton resonance peaks were used to estimate the HNF concentrations. The kinetic data are given in Table II. At an  $X_{D_2O}$  of 0.159, the proton exchange rates were determined as a function of temperature and gave for the energy of activation,  $\Delta E^\ddagger$ , 19.2 kcal/mol and for the entropy of activation,  $\Delta S^\ddagger$ , -17 eu at 55°.

The exchange rate is relatively slow and increases as  $X_{D_2O}$  is increased. A forty-fold increase in  $k_1$  was observed as  $X_{D_2O}$  was increased from 0.159 to 0.468.

The proton exchange reaction occurring between HNF and the  $D_2O$ - $D_2SO_4$  solvent is probably a bimolecular reaction involving HNF and  $D_2O$ . Thus the rate of disappearance of HNF may be expressed by

$$-d(\text{HNF})/dt = k_2(a_{\text{HNF}})(a_{D_2O}) \quad (1)$$

where  $k_2$  is the bimolecular rate constant and  $a_{\text{HNF}}$  and  $a_{D_2O}$  are the activities of HNF and  $D_2O$ , respectively. The  $k_1$ 's reported in Table II were obtained by eq 2, namely

$$-d(\text{HNF})/dt = k_1(\text{HNF}) \quad (2)$$

Strictly speaking, the rates should have been computed using the activities of HNF as given by

$$-d(\text{HNF})/dt = k_1(a_{\text{HNF}}) = k_1(\text{HNF})(\gamma_{\text{HNF}}) \quad (3)$$

$\gamma_{\text{HNF}}$  being the activity coefficient for nitroform.

The activity of HNF is assumed to be proportional to its concentration, which implies that  $\gamma_{\text{HNF}}$  is a constant during the course of a kinetic run. This is a reasonable assumption since the total concentration of nitroform species (sum of the concentration of nitroform and deuterionitroform) during a run is constant. Thus eq 1-3 can be combined giving eq 4.

**Table II:** Kinetic Data for HNF Proton Exchange in D<sub>2</sub>O-D<sub>2</sub>SO<sub>4</sub>

Run	Temperature, °C	Mole fraction of D <sub>2</sub> O, X <sub>D<sub>2</sub>O</sub>	First-order rate constant		Initial concn of HNF (g of HNF)/(g of D <sub>2</sub> O-D <sub>2</sub> SO <sub>4</sub> ) solvent	ΔE <sup>†</sup> , kcal/mol	ΔS <sup>†</sup> , eu
			k <sub>1</sub> , sec <sup>-1</sup> (% error) <sup>a</sup>	η <sup>b</sup>			
11	40	0.159	9.58 × 10 <sup>-6</sup> (12)	5	0.0967		
10	40	0.159	1.08 × 10 <sup>-4</sup> (16)	5	0.0702		
1	55	0.159	4.48 × 10 <sup>-4</sup> (3)	22	0.0806	19.2	-17
2	55	0.159	4.08 × 10 <sup>-4</sup> (3)	13	0.1151		
12	70	0.159	1.39 × 10 <sup>-3</sup> (3)	9	0.0836		
13	70	0.159	1.61 × 10 <sup>-3</sup> (6)	10	0.0801		
3	55	0.260	1.34 × 10 <sup>-3</sup> (2)	6	0.0506		
4	55	0.260	1.13 × 10 <sup>-3</sup> (5)	11	0.0502		
5	55	0.365	4.45 × 10 <sup>-3</sup> (7)	6	0.0576		
6	55	0.365	5.97 × 10 <sup>-3</sup> (4)	4	0.0533		
7	55	0.468	1.87 × 10 <sup>-2</sup> (7)	8	0.0536		
8	55	0.468	1.60 × 10 <sup>-2</sup> (4)	8	0.0460		
9	55	0.468	1.68 × 10 <sup>-2</sup> (9)	9	0.0561		

<sup>a</sup> Average error in *k*'s. <sup>b</sup> Number of points used in determining each *k*<sub>1</sub>.

$$k_1 = k_2(a_{D_2O}) \quad (4)$$

The *a*<sub>D<sub>2</sub>O</sub> in the D<sub>2</sub>O-D<sub>2</sub>SO<sub>4</sub> was assumed to be the same as the activity of water (*a*<sub>w</sub>) in H<sub>2</sub>O-H<sub>2</sub>SO<sub>4</sub> at the same concentration. The assumption that *a*<sub>w</sub> = *a*<sub>D<sub>2</sub>O</sub> is quite valid since it has been shown that the acidity functions of H<sub>0</sub> and D<sub>0</sub> are very similar.<sup>7</sup> The *a*<sub>w</sub> (molar units) were computed from the data of Giauque,<sup>8</sup> for the densities of D<sub>2</sub>O-D<sub>2</sub>SO<sub>4</sub>, the values of the densities of H<sub>2</sub>O-H<sub>2</sub>SO<sub>4</sub> were used.<sup>9</sup> The value of *k*<sub>2</sub> computed for this reaction is 14 l. mol<sup>-1</sup> sec<sup>-1</sup> (Table III).

**Table III:** Calculated Second-Order Rate Constants for Proton Exchange of HNF in D<sub>2</sub>SO<sub>4</sub>-D<sub>2</sub>O at 55°

X <sub>D<sub>2</sub>O</sub>	g/cc <sup>a</sup>	<i>k</i> <sub>1</sub> , sec <sup>-1</sup> <sup>b</sup>	<i>a</i> <sub>w</sub> <sup>c</sup>	<i>k</i> <sub>2</sub> , l. mol <sup>-1</sup> sec <sup>-1</sup>
0.159	1.84	4.28 × 10 <sup>-4</sup>	2.58 × 10 <sup>-5</sup>	16
0.260	1.83	1.24 × 10 <sup>-3</sup>	9.53 × 10 <sup>-5</sup>	13
0.365	1.82	5.21 × 10 <sup>-3</sup>	3.78 × 10 <sup>-4</sup>	14
0.468	1.78	1.72 × 10 <sup>-2</sup>	1.41 × 10 <sup>-4</sup>	12

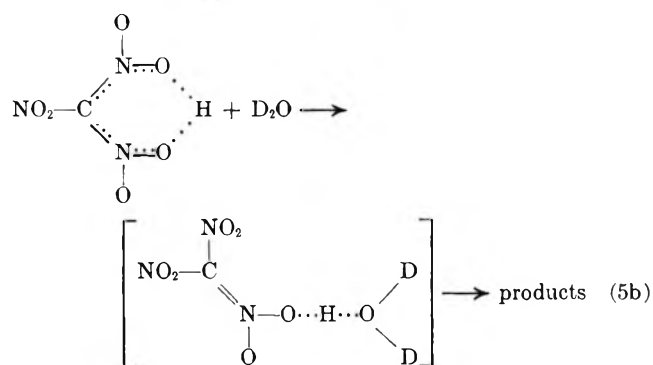
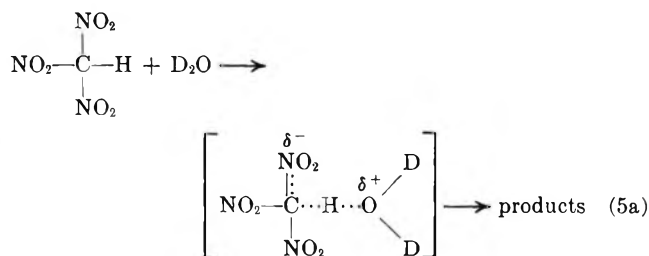
Av 14

<sup>a</sup> Density of H<sub>2</sub>O-H<sub>2</sub>SO<sub>4</sub> solutions at same X<sub>H<sub>2</sub>O</sub> as X<sub>D<sub>2</sub>O</sub>.

<sup>b</sup> Average value from duplicate runs, Table IV. <sup>c</sup> Data calculated from ref 16 (molar units).

The reaction appears to represent a monotonic function of the solvent composition; *i.e.*, the rate of reaction is related directly to the activity of water in the concentrated acid.<sup>10</sup>

The reaction can be envisioned to be proceeding as indicated in eq 5, where the species in the brackets is the activated complex.



In either case, 5a or 5b, ion-pair formation could occur followed by collapse to the deuterated species. Also, the HD<sub>2</sub>O<sup>+</sup> could leave the vicinity of the nitroform anion followed by reaction with the D<sub>2</sub>O-D<sub>2</sub>SO<sub>4</sub> solvent.

Further information bearing on the structure of the nitroform species was obtained by determining the uv spectra of HNF in H<sub>2</sub>O-H<sub>2</sub>SO<sub>4</sub>. The pertinent data are summarized in Table IV.

No significant change in the uv spectra was observed

(7) E. Hogfeldt and J. Biegeleisen, *J. Amer. Chem. Soc.*, **82**, 15 (1960).

(8) W. F. Giauque, E. W. Hornung, J. E. Kunzler, and T. R. Rubin, *ibid.*, **82**, 62 (1960).

(9) "Handbook of Chemistry and Physics," 45th ed, The Chemical Rubber Publishing Co., Cleveland, Ohio, 1963.

(10) J. Leffler and E. Grunwald, "Rates and Equilibrium of Organic Reactions," Wiley, New York, N. Y., 1963.

Table IV: Ultraviolet Absorption Bands for HNF in Various Solvents

Solvent	Concn of HNF, mol/l. $\times 10^3$	Absorbance, $A$	$\lambda_{\max}$	$\epsilon_{\max}$
H <sub>2</sub> O-H <sub>2</sub> SO <sub>4</sub> , $X_{\text{H}_2\text{O}} = 0.21$	11.06	0.832	278	75
H <sub>2</sub> O-H <sub>2</sub> SO <sub>4</sub> , $X_{\text{H}_2\text{O}} = 0.35$	6.95	0.595	276	86
H <sub>2</sub> O-H <sub>2</sub> SO <sub>4</sub> , $X_{\text{H}_2\text{O}} = 0.46$	5.79	0.424	278	73
H <sub>2</sub> O-H <sub>2</sub> SO <sub>4</sub> , $X_{\text{H}_2\text{O}} = 0.55$	6.32	0.517	277	81
H <sub>2</sub> O-H <sub>2</sub> SO <sub>4</sub> , $X_{\text{H}_2\text{O}} = 0.62$	5.69	0.097	280	17
H <sub>2</sub> O-H <sub>2</sub> SO <sub>4</sub> , $X_{\text{H}_2\text{O}} = 0.71$	7.68	0.202	276	26
H <sub>2</sub> O-H <sub>2</sub> SO <sub>4</sub> , $X_{\text{H}_2\text{O}} = 0.79$	8.61	0.650	277	75
H <sub>2</sub> O-H <sub>2</sub> SO <sub>4</sub> , $X_{\text{H}_2\text{O}} = 0.92$	6.59	(0.57)	270-280 <sup>a</sup>	(86)
H <sub>2</sub> O <sup>d</sup>	0.0315	0.22	350	7,000
H <sub>2</sub> O <sup>d</sup>	3.77	1.818	290-310 <sup>a</sup>	480
CH <sub>3</sub> COCH <sub>3</sub>	2.62	0.54	341	206
CH <sub>3</sub> COOH	2.84	0.30	275(s) <sup>b</sup>	105
CH <sub>3</sub> CN	2.76	2.08	350	754
CCl <sub>4</sub>	4.21	0.42	280	100 <sup>c</sup>
Hexane	2.83	0.31	281(s) <sup>b</sup>	110
0.5 N NaOH <sup>d</sup>			351	16,000 <sup>d</sup>

<sup>a</sup> Broad band. <sup>b</sup> Shoulder. <sup>c</sup> Reported  $\lambda_{\max} = 280$  and  $\epsilon_{\max} = 110$  in isoctane; V. N. Slovetskii, V. A. Shlyapochnikov, K. K. Babievskii, and S. S. Novikov, *Izv. Akad. Nauk SSSR, Otd. Khim. Nauk*, 1709 (1960). <sup>d</sup> Approximate value; we found some variation of  $\lambda_{\max}$  with concentration; HNF is unstable in aqueous solvents; M. Kamlet, private communication.

Table V: Solvent Effect on Chemical Shifts of Polynitroalkane Protons

Solvent <sup>a</sup>	Compd, ppm						
	HC(NO <sub>2</sub> ) <sub>3</sub>	C <sub>4</sub> H <sub>9</sub> O <sub>2</sub> ·2HC(NO <sub>2</sub> ) <sub>3</sub>	CH <sub>3</sub> CH(NO <sub>2</sub> ) <sub>2</sub>		CH <sub>2</sub> CH <sub>2</sub> CH(NO <sub>2</sub> ) <sub>2</sub>		CH <sub>3</sub> (J, cps)
			CH (J, cps)	CH <sub>3</sub> (J, cps)	CH (J, cps)	CH <sub>2</sub> (J, cps)	CH <sub>3</sub> (J, cps)
CCl <sub>4</sub>	7.40	7.82 (7.70) <sup>c</sup>	6.19 (6.6) <sup>d</sup>	2.16 (6.6) <sup>d</sup>	6.14 (7.0) <sup>d</sup>	2.55 (7.5) <sup>d</sup>	1.15 (7.5) <sup>d</sup>
CF <sub>3</sub> COOH	7.40						
Neat	7.83		6.55	2.22	6.35	2.59	1.15
H <sub>2</sub> SO <sub>4</sub> (98%)	8.2						
CH <sub>3</sub> CN	8.35	8.34	6.60	2.13	6.47	2.52	1.07
CH <sub>3</sub> COOD	8.68						
CH <sub>3</sub> OH	Exchange <sup>b</sup>	Exchange <sup>b</sup>	6.80	2.11	6.66	2.55	1.12
CH <sub>3</sub> COCH <sub>3</sub>	9.18 <sup>e</sup>		6.95	2.19	6.81	2.59	1.14
		8.62					

<sup>a</sup> Concentration of polynitroalkanes about 10%. <sup>b</sup> HNF exchanges rapidly in water, 12 N HCl, and slowly in concentrated D<sub>2</sub>SO<sub>4</sub>. <sup>c</sup> Concentration about 5%; no shift of CH<sub>3</sub> proton of dioxane occurs on changing the concentration. <sup>d</sup> No observable change of  $J$  with solvent change. <sup>e</sup> In acetone-*d*<sub>6</sub>,  $\delta$  is 9.23.

as the  $X_{\text{H}_2\text{O}}$  was varied from  $\sim 0$  to 1.0. A decrease of the extinction coefficient for  $X_{\text{H}_2\text{O}}$  in the range of 0.55 and 0.79 and a shift of  $\lambda_{\max}$  toward the visible as  $X_{\text{H}_2\text{O}}$  approached a value of 1.0 were noted. These spectra of HNF in H<sub>2</sub>O-H<sub>2</sub>SO<sub>4</sub> solutions (similar spectra would be obtained for HNF in D<sub>2</sub>O-D<sub>2</sub>SO<sub>4</sub> system) lead one to conclude that the preponderance of the HNF is in the state with H bonded directly to carbon. This would indicate that a reaction scheme shown by eq 5a is the favored reaction path for the proton exchange process. The data indicate the exchange in the H<sub>2</sub>O-H<sub>2</sub>SO<sub>4</sub> system is a specific base (H<sub>2</sub>O or D<sub>2</sub>O) catalyzed reaction.

Further insight into the behavior and structure of HNF was obtained in the determination of the proton resonance spectra in a series of solvents. Also, proton resonance spectra for several other polynitro com-

pounds were determined. The chemical shifts derived from these spectra are given in Table V with some coupling constants for the polynitroalkane compounds.

In Figure 2 the chemical shift of nitroform in CCl<sub>4</sub> and in acetone is plotted as a function of the analytical mole fraction of HNF. In CCl<sub>4</sub>, the proton resonance is shifted upfield essentially linearly to a value of  $\sim 7.25$  ppm as  $X_{\text{HNF}}$  approaches zero. The upfield shift probably results from a lowering of the dielectric constant of the medium in going from  $X_{\text{HNF}}$  of 1.0 to 0.

In acetone, the proton resonance of the HNF is shifted downfield by  $\sim 1.4$  ppm as the  $X_{\text{HNF}}$  is varied from 1.0 to 0. The chemical shift of the proton resonance of the HNF is probably associated with complex formation between HNF and acetone by hydrogen bonding<sup>11</sup> with rapid exchange occurring between the complex and the "free" HNF. The equilibrium con-

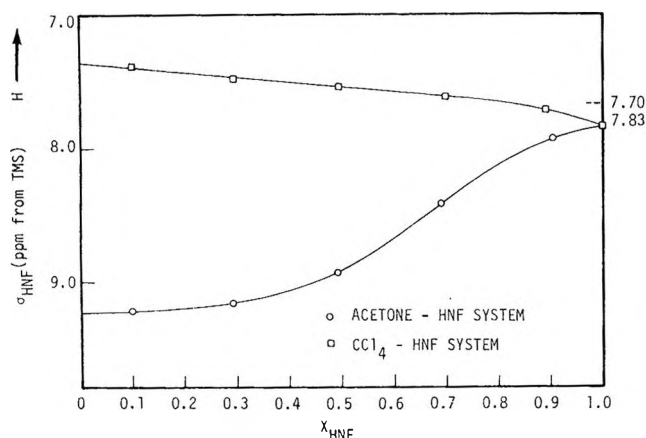
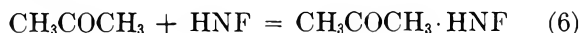
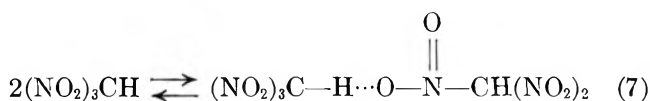


Figure 2. Chemical shift of nitroform in  $\text{CCl}_4$  and acetone as a function of analytical mole fraction of HNF.

stant for complex formation between acetone and HNF (eq 6) was calculated as 10 (concentration in mole fraction) at  $37^\circ$ .

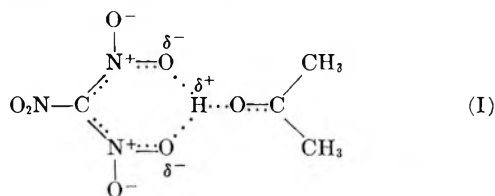


The procedure, described in the literature,<sup>12</sup> gave for the chemical shift of the complex a value of 9.35 ppm. The proton absorption peak due to the HNF-HNF-acetone complex was very sharp over almost the entire range of concentration. Some line broadening of the signal was observed at  $X_{\text{HNF}}$  of 0.0987. The chemical shifts of the acetone methyl protons varied from 2.06 to 2.24 ppm (extrapolated values) linearly as  $X_{\text{HNF}}$  was increased from 0 to 1.0, with no proton exchange occurring between HNF and  $\text{CH}_3$  group in acetone as indicated by no change in the line intensity of  $\text{CHD}_2$  absorption whenever acetone- $d_6$  was used as the solvent. Some self-association of the HNF may take place, but probably is very small. Equilibria such as shown in eq 7 are certainly plausible and would account for the



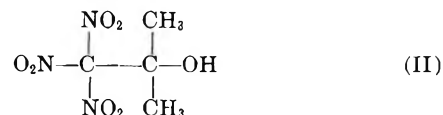
slight line broadening that was observed as well as the difference in chemical shift between the neat liquid and its solutions in  $\text{CCl}_4$ . (Differences between the viscosity of the neat liquid and the  $\text{CCl}_4$  solution are not responsible for the observed line broadening.)

The structure of the complex between HNF and acetone may be represented by structure I



wherein the proton of HNF is still strongly bound to the NH (nitroform anion) group. The complex repre-

sented by structure I would be resonance stabilized as is apparent from the number of resonant structures possible for this complex. This structure is compatible with the observed uv spectra of HNF in acetone (see Table IV): The  $\lambda_{\text{max}}$  of HNF in acetone is shifted toward the visible and  $\epsilon_{\text{max}}$  is larger than that observed for HNF in nonhydrogen bonding solvents such as  $\text{CCl}_4$  and hexane. This structure is also strongly favored based on the proposed structures for the activated complex for the proton exchange reaction between HNF and  $\text{D}_2\text{O}-\text{D}_2\text{SO}_4$ . Another possibility is the formation of a compound as indicated by structure II



as a result of the Henry reaction.<sup>13</sup>

Several arguments against structure II for the HNF-acetone complex are as follows. (a) Hall<sup>14</sup> was not able to prepare 2,2,2-trinitro-1,1-dimethylethanol (II); however its existence in acetone solution could be argued. (b) Compound II would be expected to be a strong acid even in acetone and exist mostly as the individual ions, part of the driving force for ionization being obtained from steric interactions of the methyl groups with the nitro groups. The  $\text{pK}'\text{s}$  in  $\text{H}_2\text{O}$ <sup>14</sup> of 2,2,2-trinitroethanol and 2,2,2-trinitro-1-methyl-ethanol are 6.1 and 3.6, respectively. Substitution of another methyl group would further increase the acid strength by several orders of magnitude yielding highly acidic solution which should promote proton exchange between HNF and acetone- $d_6$ . This was not observed. (c) Also, the uv spectra are more compatible with structure I than II (see Table IV).

In other solvents (data in Table V) the proton resonance of the HNF is shifted to lower fields as compared to the neat solution; the noticeable exceptions are the upfield shifts observed in  $\text{F}_3\text{CCOOH}$  and in  $\text{CCl}_4$  (discussed above) and for the rapid proton exchange occurring in  $\text{CH}_3\text{OH}$ . We believe that the downfield shifts are due to complex formation through hydrogen bonding as discussed for the behavior of HNF in acetone.

In  $\text{CH}_3\text{COOD}$  and in trifluoroacetic acid two sharp absorption peaks are observed in each case, indicating that proton exchange between these solvents and the HNF, if it is taking place, does so slowly. In trifluoroacetic acid the proton resonance due to the HNF is observed at 7.40 ppm, *i.e.*, upfield of that for the neat solution. The upfield shift is probably not due to a lowering of the dielectric constant of the medium (for

(11) A. Loewenstein and Y. Margalit, *J. Phys. Chem.*, **69**, 4152 (1965).

(12) The NMR-EPR staff of Varian Associates, "NMR and EPR Spectroscopy," Pergamon Press, New York, N. Y.

(13) For a resume of the Henry reaction, see P. Noble, Jr., F. G. Borgardt, and W. L. Reed, *Chem. Rev.*, **64**, 19 (1964).

(14) T. N. Hall, *Tetrahedron*, **19** (1), 115 (1963).

$\text{CF}_3\text{COOH}$ , the dielectric constant<sup>15</sup> is 43 at 25°), but probably is due to the lower basicity of the solvent, trifluoroacetic acid, compared to the other solvents.

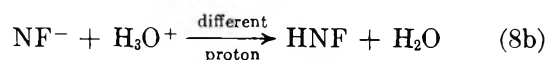
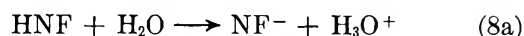
The effect of various solvents on the chemical shifts of the protons in the other polynitro compounds and the molecular complex, dioxane·2HNF, were studied and the findings are summarized in Table V. Good agreement was obtained with the data of Hoffman<sup>16</sup> for studies carried out in the same solvent systems.

The chemical shift of dinitroethane and dinitropropane are similar in character to those observed for HNF in the same solvents, the notable exception being that no rapid exchange occurred in methanol. The resonance absorption peaks were very pronounced with no noticeable line broadening. The coupling constants for the various protons of the two dinitro compounds were found to remain constant with change of solvent.

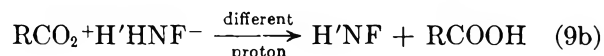
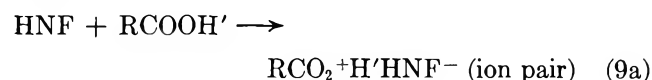
The chemical shift of HNF was found to be essentially independent of temperature in acetic acid ( $\text{CH}_3\text{COOD}$ ) and in acetonitrile, as is evident from the data presented in Table VI. The change in chemical shift was only 0.05 and 0.1 ppm for a temperature change of 45° in acetic acid and acetonitrile, respectively. Slow proton exchange takes place between the acetic acid and the HNF since the spectra showed two sharp resonance peaks at 37°, one for the HNF and the other due to the

acidic proton of acetic acid. Increased line broadening of the HNF resonance absorption was observed with increased temperature.

A few further comments must be made relative to the behavior of HNF in various solvents. It has been shown experimentally that the proton exchange between HNF and methanol, water, concentrated HCl, and  $\text{D}_2\text{O}-\text{D}_2\text{SO}_4$  for  $X_{\text{D}_2\text{O}} \geq 0.5$  occurs quite rapidly. On the other hand, slow proton exchange occurs between HNF and  $\text{CH}_3\text{COOH}$ ,  $\text{CF}_3\text{COOH}$ , and  $\text{D}_2\text{O}-\text{D}_2\text{SO}_4$  for  $X_{\text{D}_2\text{O}} \leq 0.5$ . Proton exchange in these solvents is the result of acid dissociation of HNF. In water, a strongly basic solvent, the acid dissociation proceeds as shown in eq 8a



followed by the reverse reaction, eq 8b. In carboxylic acid solvents (weak base) the acid dissociation proceeds as shown in eq 9a



probably proceeding through an ion pair, followed by collapse of the ion pair to starting materials. Steps 8a and 9a are probably rate determining. The relative rates of proton exchange of HNF in the various solvents appear to be a function of the specific basicity of the solvent.

*Acknowledgment.* The authors are grateful to Professor E. Grunwald for some helpful suggestions in the preparation of this manuscript.

(15) J. H. Simons and K. E. Larentzen, *J. Amer. Chem. Soc.*, **72**, 1426 (1950).

(16) W. Hoffman, L. Stefanak, T. Urbanski, and M. Witanowsky, *ibid.*, **86**, 54 (1964).

**Table VI:** Effect of Temperature on Chemical Shift of HNF in Acetic Acid and Acetonitrile

Temp. °C	Chemical shift, HNF, ppm	
	$\text{CH}_3\text{COOD}$	$\text{CH}_3\text{CN}$
38	8.70 <sup>a</sup>	8.35
60	8.62	8.32
70		8.30
80	8.60	8.30
100	8.56	
110	8.53	

<sup>a</sup> Same value of  $\delta$  (ppm) obtained after cooling sample from 110°.

# Nuclear Magnetic Resonance Study of the Conformations of Valine and Phenylalanine Derivatives<sup>1</sup>

by Richard A. Newmark<sup>2,\*</sup> and Max A. Miller<sup>3</sup>

Central Research Laboratory, 3M Company, St. Paul, Minnesota 55101  
and Department of Chemistry, University of Colorado, Boulder, Colorado 80907 (Received August 10, 1970)

Publication costs assisted by the 3M Company

The nmr spectra of *N*-acetylalanine methyl ester, *N*-acetylvaline methyl ester, and *N*-acetylphenylalanine ethyl ester have been studied in several solvents. The variation of the vicinal coupling constants is used to calculate qualitative changes in the population of the side-chain rotamers. The vicinal coupling constants in glycyphenylalanyl-glycine and in phenylalanine showed little variation with temperature in neutral aqueous solution. Comparison of our data with results on other oligopeptides suggests that intramolecular interactions are more important than the dielectric constant of the medium in determining the relative energies of the rotamers.

## Introduction

Prediction of the three-dimensional structure of polypeptides or proteins requires knowledge of the relative stabilities of the amino acid conformers.<sup>4,5</sup> Nuclear magnetic resonance has been used to determine the relative energies for the three staggered conformations of several amino acid side chains.<sup>6-11</sup> In almost all cases charged amino acids have been studied, although neutral species provide a more general model for the conformations within a protein. Since the interior of large proteins is an environment in which highly polar water molecules are excluded, information on the conformer energies of uncharged amino acid derivatives in different media is desirable. Several extensive studies of the solvent dependence of vicinal coupling constants in substituted ethanes have been performed to show the usefulness of this technique for determining the relative stability of ethane rotamers,<sup>12-14</sup> but no systematic studies of the solvent dependence of coupling constants in amino acids have been reported.

## Experimental Section

Glycyphenylalanyl-glycine (Gly-Phe-Gly), L-phenylalanine (Phe), *N*-acetyl-L-alanine methyl ester (NAAME), *N*-acetyl-L-phenylalanine ethyl ester (NAPEE), *N*-acetyl-L-valine methyl ester (NAVME), *N*-acetyl-DL-phenylalanine amide (NAP amide), and L-valine (Val) were used as received from Cyclo Chemical Co. The NAVME solutions were degassed under nitrogen; solutions of NAPEE in organic solvents were prepared by distillation of the solvent onto the solid compound in a vacuum line. Aqueous solutions of phenylalanine derivatives were prepared using equal amounts of NaH<sub>2</sub>PO<sub>4</sub> and Na<sub>2</sub>HPO<sub>4</sub> buffer to give a pH about 6.9. The solutions were lyophilized twice from D<sub>2</sub>O to mini-

mize the H<sub>2</sub>O resonance. Perdeuteriodimethyl sulfoxide (DMSO) was stored over molecular sieves.

The spectra of NAAME and NAVME were obtained on a Varian A-60 calibrated with audio side bands. The other spectra were taken in the internal lock, frequency sweep mode on a Varian HA-100 spectrometer. Corrections for the nonlinearity of the recorder sweep were made using the procedure of Newmark, *et al.*<sup>15</sup> Spectra of a saturated solution (about 0.02 *M*) of Gly-Phe-Gly and of 0.02 *M* Phe solutions were accumulated for several hours on a Varian C-1024 CAT. Spectra were generally taken of 0.2 *M* solutions to obtain reasonable signal strengths. A concentration study from 0.1 to 0.4 *M* of NAPEE in DMSO revealed no concentration effects on the coupling constants within experimental error. Since the line widths of the  $\beta$  proton peak in phenylalanine are about 0.8 Hz due to coupling

(1) This investigation was supported in part by a research grant, GM 16264, from the United States Public Health Service.

(2) To whom inquiries should be addressed at 3M.

(3) National Science Foundation Undergraduate Research Participant.

(4) T. Ooi, R. A. Scott, G. Vanderkooi, and H. A. Scheraga, *J. Chem. Phys.*, **46**, 4410 (1967).

(5) A. J. Hopfinger and A. G. Walton, *Biopolymers*, **9**, 29 (1970).

(6) K. G. R. Pachler, *Spectrochim. Acta*, **20**, 581 (1964).

(7) K. G. R. Pachler, *Z. Anal. Chem.*, **224**, 211 (1966).

(8) R. B. Martin and R. Mathur, *J. Amer. Chem. Soc.*, **87**, 1065 (1965).

(9) H. Ogura, Y. Arata, and S. Fujiwara, *J. Mol. Spectrosc.*, **23**, 76 (1967).

(10) J. R. Cavanaugh, *J. Amer. Chem. Soc.*, **89**, 1558 (1967).

(11) J. R. Cavanaugh, *ibid.*, **90**, 4533 (1968).

(12) R. J. Abraham and G. Gatti, *J. Chem. Soc. B*, 961 (1969).

(13) F. Heatley and G. Allen, *Mol. Phys.*, **16**, 77 (1969).

(14) W. F. Reynolds and D. J. Wood, *Can. J. Chem.*, **47**, 1295 (1969).

(15) R. A. Newmark, G. R. Apai, and R. O. Michael, *J. Magn. Resonance*, **1**, 418 (1969).

to the aromatic protons,<sup>16</sup> the errors in the vicinal coupling constants are estimated at about 0.1 Hz.

## Results

The vicinal coupling in NAAME was determined from the first-order splitting of the methyl doublet of the  $\beta$  carbon. The coupling constant and chemical shifts of the protons are given in Table I. The chemical shift of the NH proton was about  $3\tau$  in the non-aqueous solutions, but could not be accurately determined because of broadening by the <sup>14</sup>N quadrupole moment. It is clear from Table I that the chemical shifts are extremely sensitive to the medium but that the coupling constant is almost unchanged.

**Table I:** Chemical Shifts and  $J_{\alpha\beta}$  Coupling Constant in NAAME

	Chemical shifts <sup>a</sup>				$J_{\alpha\beta}$ (Hz)
	C $\alpha$ H	CO $_2$ CH $_3$	COCH $_3$	C $\beta$ H $_3$	
CDCl $_3$	5.39	6.23	7.98	8.59	7.13
C $_6$ D $_6$	5.33	6.68	8.30	8.80	7.14
CCl $_4$	5.52	6.28	8.05	8.54	7.15
CD $_3$ COCD $_3$	5.56	6.32	8.08	8.67	7.12
CH $_3$ OH		6.27	8.03	8.62	7.14
CD $_3$ CN	5.63	6.33	8.11	8.70	7.11
DMSO	5.73	6.38	8.17	8.76	7.15
D $_2$ O <sup>b</sup>	5.61	6.24	7.97	8.61	7.26

<sup>a</sup>  $\tau$  units; reference is internal tetramethylsilane. <sup>b</sup> Reference is sodium 2,2-dimethyl-2-silapentane sulfonate.

The general features of the ABX proton spectrum of phenylalanine in aqueous solution have been discussed previously.<sup>10</sup> In organic solvents coupling of the  $\alpha$  proton to the amide proton makes precise determination of the X proton lines impossible, and the coupling constants were determined from the analysis of the AB octet of the  $\beta$  protons. The poor signal/noise on the 0.2 M solutions made it difficult to locate the four outer octet lines more precisely than 0.2 Hz, but each outer line is separated by  $J_{AB}$  from a strong inner line. The data were analyzed by first using all 8 lines to assign the transitions and determine  $J_{AB}$ , and then iterating over the four strong lines using a modified version of LA-OCN3.<sup>17</sup> The  $\alpha$  proton chemical shift was measured directly in the nonaqueous solutions, but was masked by the residual HDO signal in aqueous solutions of Gly-Phe-Gly and NAP amide. Spin tickling was used to determine the shift in the latter cases. The results are given in Table II.

In NAVME the  $\alpha$  proton is a quartet from splitting by the NH and  $\beta$  proton, but unlike NAPEE, the lines were well resolved. The vicinal coupling constants are given in Table III.

Since internal rotation between the three staggered conformations of substituted amino acids is rapid at all

accessible temperatures in the solvents studied, the observed coupling constants are weighted averages

$$J_{ij} = p^a J_{ij}^a + p^b J_{ij}^b + p^c J_{ij}^c$$

where  $p^k$  is the population and  $J_{ij}^k$  is the coupling constant in rotamer  $k$ . Following Pachler<sup>6</sup> and Cavanaugh,<sup>10,11</sup> we assume  $J_g$  and  $J_t$ , the gauche and trans coupling constants, are 2.60 and 13.56 Hz, respectively, and that the rotamers are always in their staggered conformations. The above equation can then be used to calculate the relative populations of the rotamers given in Tables II and III.

## Discussion

A possible systematic error in the interpretation of the data is the variation of the gauche and trans couplings with solvent. Abraham<sup>18</sup> and Smith and Cox<sup>19</sup> have shown vicinal proton couplings across saturated carbon-carbon bonds are independent of solvent. In alanine the three rotamers must have the same energy by symmetry, and our results on NAAME (Table I) in several organic solvents show  $J = 7.15 \pm 0.03$  Hz. However, the coupling in D $_2$ O was 7.25 Hz. Thus, the coupling constants in the amino acids appear independent of solvent for organic liquids, and the shift observed in water is relatively small. On the other hand, the chemical shifts in NAAME (Table I) changed over 0.3 ppm with solvent, and detailed analysis of the chemical shifts in NAVME or NAPEE for conformational effects was not attempted.

The variation with solvent of the vicinal coupling constants in NAPEE and NAVME is over an order of magnitude greater than the experimental error and qualitatively shows that a substantial change is occurring in the relative populations of the rotamers as the medium is changed. Although the coupling constants tend to increase with increasing dielectric constant of the solvent, the trend is not monotonic, and other factors besides solvent polarity must be responsible for the changes in the population of the conformers.

It is not possible to assign the chemical shifts of the two  $\beta$  protons in phenylalanine to the individual nuclei from comparison with other molecules. Since Gly-Phe-Gly crystallizes with the phenyl ring trans to the amide linkage (rotamer I, Figure 1),<sup>20,21</sup> it is probable that I remains the favored conformer in solution.<sup>22</sup> The relative populations of the three rotamers given in Table II provide a qualitative indication of the popula-

(16) M. P. Williamson, R. J. Kostelnik, and S. J. Castellano, *J. Chem. Phys.*, **49**, 2218 (1968).

(17) S. Castellano and A. A. Bothner-By, *ibid.*, **41**, 3863 (1964).

(18) R. J. Abraham, *J. Phys. Chem.*, **73**, 1192 (1969).

(19) S. L. Smith and R. H. Cox, *ibid.*, **72**, 198 (1968).

(20) R. E. Marsh and J. P. Glusker, *Acta Crystallogr.*, **14**, 1110 (1961).

(21) A. V. Lakshminarayanan, V. Sasisekharan, and G. N. Ramachandran in "Conformation of Biopolymers," G. N. Ramachandran, Ed., Academic Press, New York, N. Y., 1967, p 61.

**Table II:** Coupling Constants and Rotamer Populations of Phenylalanine Derivatives<sup>a</sup>

	Solvent <sup>b</sup>	$\epsilon^c$	Coupling constants		Fractional populations <sup>a,d</sup>		
			$J_{AX}$	$J_{BX}$	$p_I$	$p_{II}$	$p_{III}$
NAPEE	CCl <sub>4</sub> <sup>e</sup>	2.2	(6.06)		(0.63)		
	C <sub>6</sub> H <sub>5</sub> CH <sub>3</sub> , 5°	2.4	6.16	6.76	0.38	0.32	0.30
	C <sub>6</sub> H <sub>5</sub> CH <sub>3</sub>	2.4	6.20	6.38	0.34	0.33	0.33
	C <sub>6</sub> H <sub>5</sub> CH <sub>3</sub> , 98°	2.2	6.48	6.01	0.31	0.35	0.34
	CDCl <sub>3</sub> <sup>e</sup>	4.7	(5.95)		(0.60)		
	CD <sub>3</sub> COCD <sub>3</sub>	21.0	6.06	7.80	0.47	0.32	0.21
	C <sub>2</sub> D <sub>5</sub> OD	24.0	6.33	8.31	0.52	0.34	0.14
	CD <sub>3</sub> OD	33.0	5.83	8.54	0.54	0.29	0.17
	CD <sub>3</sub> CN	38.0	5.98	7.82	0.48	0.31	0.21
	DMSO	45.0	5.96	8.98	0.58	0.31	0.11
Phenylalanine	D <sub>2</sub> O	76.0	6.06	8.25	0.52	0.32	0.16
	D <sub>2</sub> O	76.0	5.21	8.10	0.50	0.24	0.26
	D <sub>2</sub> O, 80°	61.0	5.43	7.90	0.48	0.26	0.26
NAP amide	D <sub>2</sub> O	76.0	6.02	8.93	0.58	0.31	0.11
	D <sub>2</sub> O, 82°	62.0	6.05	8.72	0.56	0.31	0.13
Gly-Phe-Gly	D <sub>2</sub> O	76.0	5.72	9.06	0.59	0.29	0.12
	D <sub>2</sub> O, 87°	59.0	5.81	8.70	0.56	0.29	0.15
DD-NAP-Ala ME <sup>f</sup>	DMSO	45.0	4.40	9.80	0.66	0.16	0.18
DL-NAP-Ala ME <sup>f</sup>	CDCl <sub>3</sub>	4.7	5.93	8.49	0.54	0.30	0.16
	DMSO	45.0	5.41	9.34	0.61	0.26	0.13
c-Gly-Phe <sup>g</sup>	DMSO	45.0	4.7	5.3	0.25	0.19	0.56

<sup>a</sup> The values given assume rotamer I has a lower energy than rotamer II. If II has a lower energy (see text), then  $J_{AX}$  and  $J_{BX}$ , and  $p_I$  and  $p_{III}$ , should be interchanged. <sup>b</sup> Temperature is 32° unless specified otherwise. Concentrations are 0.02 M for NAPEE in D<sub>2</sub>O, phenylalanine, and Gly-Phe-Gly. All other solutions are about 0.2 M. <sup>c</sup> Solvent dielectric constant. <sup>d</sup> Rotamers are designated in Figure 1. <sup>e</sup> Deceptively simple spectrum. Only the average vicinal coupling constant and the sum of  $p_I + p_{III}$  can be determined. <sup>f</sup> Reference 27. <sup>g</sup> Reference 23.

**Table III:** Coupling Constants and Rotamer Populations in Valine Derivatives

	Solvent	$\epsilon^a$	$J_{\alpha\beta}$	$J_{HNCH}$	$p_{III}^b$
NAVME	CCl <sub>4</sub>	2.2	5.07	8.86	0.23
	CDCl <sub>3</sub>	4.9	5.15	8.86	0.23
	CH <sub>2</sub> Cl <sub>2</sub>	8.2	5.37	8.76	0.25
	CD <sub>3</sub> COCD <sub>3</sub>	19.0	5.9	<sup>c</sup>	0.30
	CD <sub>3</sub> OD	33.0	6.11	<sup>c</sup>	0.32
	CD <sub>3</sub> CN	38.0	5.91	8.39	0.30
	DMSO	45.0	6.52	8.14	0.36
	D <sub>2</sub> O	76.0	5.98	<sup>c</sup>	0.31
	C <sub>6</sub> D <sub>6</sub>	2.4	5.35	8.72	0.25
	C <sub>6</sub> H <sub>5</sub> CH <sub>3</sub>	2.4	5.30	8.71	0.25
	C <sub>6</sub> H <sub>5</sub> Cl	5.7	5.09	8.65	0.23
	C <sub>6</sub> H <sub>5</sub> CHO	19.0	5.49	8.60	0.26
	C <sub>6</sub> H <sub>5</sub> NO <sub>2</sub>	35.0	5.40	8.56	0.26
Valine	D <sub>2</sub> O	76.0	4.41	<sup>c</sup>	0.16
Gramieiden S <sup>d</sup>	DMSO	45.0	9.0	9.0	0.59
c-Gly-Val <sup>e</sup>	DMSO	45.0	4.2	<sup>c</sup>	0.15
	D <sub>2</sub> O	76.0	3.7	<sup>c</sup>	0.10

<sup>a</sup> Dielectric constant of solvent. <sup>b</sup> Fractional population of rotamer III, Figure 2. <sup>c</sup> Exchange of amide proton with solvent occurs. <sup>d</sup> Reference 24. <sup>e</sup> Reference 23.

tion changes necessary to give the observed variation in the coupling constants but cannot be used in quantitative calculations because of the approximations inherent in the use of the equation above. The more sterically hindered form III is favored in media of low

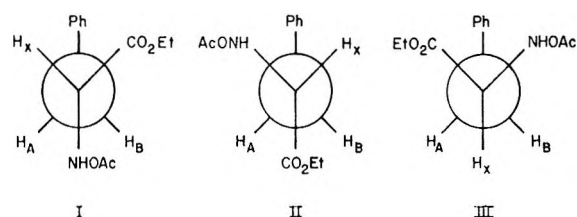


Figure 1. Newman projections about the  $\alpha\beta$  bond for the three rotamers of NAPEE. The projections for Gly-Phe-Gly are identical, but with OEt and OAc replaced by glycine residues.

dielectric constant. This suggests that in III the aromatic ring might interact with the gauche ester or amide groups to minimize the dipole moment.

The results of the variable temperature measurements on the phenylalanine derivatives (Table II) showed that the changes of the coupling constant with temperature were much smaller than the changes with solvent. Apparent changes in rotamer populations with temperature are barely outside of experimental error for the aqueous solutions. In toluene, the trans rotamer I of NAPEE is favored at low temperatures.

(22) The other alternative is that II has a lower energy; then the values of  $J_{AX}$  and  $J_{BX}$ , and  $p_I$  and  $p_{III}$ , should be interchanged in Table II. The populations of rotamer III are independent of this assumption, which may be invalid because of hydrogen bonding effects in the solid favoring rotamer I.

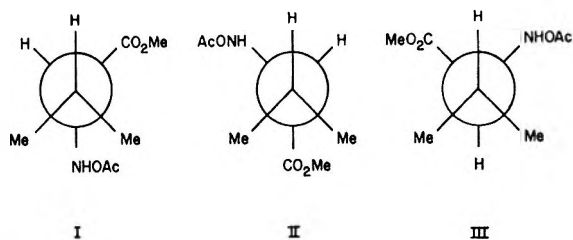


Figure 2. Three rotamers of NAVME.

As the temperature is raised, the populations of the three rotamers equalize and then diverge.

Since valine has only two vicinal protons, only one coupling is observed. The low value of this coupling in valine and cycloglycylvaline<sup>23</sup> in aqueous solution shows that the trans valine rotamer (III, Figure 2) is considerably higher in energy than one of the gauche rotamers, but it is not possible to determine the relative populations of the gauche rotamers. The gauche rotamer(s) is also favored in nonaqueous media of low dielectric constant. The coupling constant is significantly higher for NAVME in alcohol, DMSO, and water; the relative population of the trans rotamer increases to 0.31, 50% higher than in  $\text{CDCl}_3$  or  $\text{CCl}_4$ . Stern, *et al.*,<sup>24</sup> found the coupling constant of the valine residue in Gramicidin S was 9 Hz, indicating 60% of the molecules were trans. In line with this result, Blake, *et al.*,<sup>25</sup> found valine in the trans form in three of the five valine residues of lysozyme that crystallized in one particular rotameric form.

The constant value of the coupling constant for NAVME observed in aromatic solvents (Table III) suggests that intermolecular interactions with the aromatic ring are more important than the effective dielectric constant of the medium in determining rotamer stability.

Vicinal HNCN coupling constants are also a function of dihedral angle.<sup>26-28</sup> The relative constancy of this coupling at 8.5 Hz for NAVME in the nonaqueous solutions suggests no significant conformational changes about the C-N bond are occurring.

## Conclusions

In both phenylalanine and valine there is a substan-

tial increase in the coupling constants in going from the dipolar ion to the *N*-acetyl ester in aqueous solutions, indicating an appreciable change in the relative populations of the conformers. The similarity of the couplings in methanol, ethanol, and water suggests that hydrogen bonding from the solvent plays an important role in the preferential solvation of the conformers. Our results suggest considerable caution should be exercised in using the published rotamer energies of the amino acids in calculations on the structure of polypeptides or proteins, and the concentration study of Cavanaugh<sup>11</sup> further shows that the rotamer energies in the charged amino acids in aqueous solutions are very sensitive to concentration.

The solvent studies of NAPEE and NAVME show that reasonable changes in the populations of the three rotamers are observed, but that intramolecular interactions are more important than the medium in determining the relative populations of the conformers. Thus, cyclophenylalanylglycine shows a strong preference for the gauche rotamer (III, Figure 1) in which the benzene ring is folded over the piperazinedione ring of the cyclic dipeptide, but in all the other derivatives of phenylalanine that have been studied a trans isomer is favored in DMSO or aqueous solutions.

The nmr results on valine in aqueous solutions would suggest minimal population of the trans isomer, whereas the results for NAVME indicate the trans isomer should be found one-third of the time in DMSO or water. Comparison of these predictions with the experimental results in lysozyme or Gramicidin S show that even NAVME is not a good model for the interactions of the side chains of the amino acid.

(23) K. D. Kopple and M. Ohnishi, *J. Amer. Chem. Soc.*, **91**, 962 (1969).

(24) A. Stern, W. A. Gibbons, and L. C. Craig, *Proc. Nat. Acad. Sci. U. S.*, **61**, 734 (1968).

(25) C. C. F. Blake, G. A. Mair, A. C. T. North, D. C. Phillips, and V. R. Sarma, *Proc. Roy. Soc. B*, **167**, 365 (1967).

(26) A. A. Bothner-By and R. H. Cox, *J. Phys. Chem.*, **73**, 1830 (1969).

(27) V. F. Bystrov, S. L. Portnova, T. A. Balashova, V. I. Tsetlin, V. T. Ivanov, P. V. Kostetzky, and A. O. Yu, *Tetrahedron Lett.*, 5225 (1969).

(28) V. F. Bystrov, S. L. Portnova, V. I. Tsetlin, V. T. Ivanov, and A. O. Yu, *Tetrahedron*, **25**, 493 (1969).

## Correlation Times and Reorientation Activation Energies for

### Tetraalkylammonium Ions in Aqueous Solutions

by David W. Larsen

Department of Chemistry, University of Missouri—St. Louis, St. Louis, Missouri 63121 (Received July 8, 1970)

Publication costs assisted by the Office of Water Resources Research

Proton nmr line shapes are presented for aqueous solutions of ions of the type  $(\text{CH}_3)_3\text{NR}^+$  where R is methyl, ethyl, isopropyl, *tert*-butyl, and where R is straight alkyl chains of various length. The line shapes of these cations are governed by the rate of  $^{14}\text{N}$  quadrupole relaxation. The line shapes were fitted within experimental error using modified equations of the type proposed by Pople and Sack. The observed ordering of the  $^{14}\text{N}$  relaxation rates for the cations  $(\text{CH}_3)_3\text{NR}^+$  is methyl < *tert*-butyl < isopropyl < ethyl; the ordering is rationalized in terms of the bond angles in the cations.  $^{14}\text{N}$  quadrupole relaxation rates were determined as a function of temperature, from which estimates of activation energies for correlation decay processes were made. Rotational tumbling of the cation is the correlation decay mechanism. The activation energy for the process is very low for short R groups, but it is found to increase with the length of the alkyl chain. For long alkyl chains, when micelles are present, the activation energy is again very low, which indicates that the head groups undergo a concerted reorientation on the surface of the micelle.

#### Introduction

Nmr studies on the ions  $(\text{CH}_3)_4\text{N}^+$  and  $(\text{CH}_3)_3\text{NCH}_2\text{-CH}_3^+$  in the solvents  $\text{D}_2\text{O}$  and dimethyl sulfoxide- $d_6$  ( $\text{DMSO-}d_6$ ) were reported<sup>1</sup> recently by us. Conclusions concerning interactions of the cations with anions and with solvent molecules were drawn from the observed line shapes. The line shapes were found to be governed primarily by the rate of  $^{14}\text{N}$  nuclear quadrupole relaxation in the presence of fluctuating electric field gradients. Transition probabilities were estimated by comparing the observed line shapes with line shapes calculated using the theory of quadrupolar relaxation postulated by Pople<sup>2</sup> and Sack.<sup>3</sup> The estimated transition probabilities were crude because there are qualitative differences between the observed line shapes and those calculated using the Pople-Sack equations.<sup>2,3</sup>

It was concluded<sup>1</sup> that the different values of the transition probabilities for the two ions  $(\text{CH}_3)_4\text{N}^+$  and  $(\text{CH}_3)_3\text{NCH}_2\text{CH}_3^+$  in aqueous solution are due primarily to electric field gradients caused by differences in the N-C bonds. The temperature dependence of the spectra indicates that the correlation decay mechanism is a low activation energy process, and it was proposed that rotational tumbling of the cations is the process which modulates the electric field gradients.

This work uses modified Pople-Sack equations<sup>2-3</sup> to calculate line shapes which fit the observed nmr line shapes within experimental error. Also presented are nmr studies of two series of ions of the type  $(\text{CH}_3)_3\text{NR}^+$ . The first series of cations contained short R groups, both straight and branched chains. The study was made (1) to determine the relative importance of internal structural factors of the cation which influence

quadrupole coupling constants (QCC): C-N-C bond angles or electronic distributions within N-C bonds (inductive effects), and (2) to determine the activation energies for correlation decay for this series of cations. The second series of cations contained straight chain R groups of various length. This study was made to investigate the  $^{14}\text{N}$  transition probabilities and activation energies for correlation decay as a function of chain length. Cations containing R groups of sufficient length to exist primarily as micelles were included in this series in order to determine the differences in  $^{14}\text{N}$  transition probabilities and correlation decay activation energies between single ions and micelles.

#### Experimental Section

**Tetraalkylammonium Salts.** The noncommercially available salts were prepared by allowing trimethylamine to react with the appropriate alkyl iodide in water solution over silver oxide for extended periods of time. The solutions were then carefully filtered, neutralized with hydriodic acid, and evaporated to dryness. The salts were recrystallized before use.

**Nmr Measurements.** Aqueous solutions 0.05 M in tetraalkylammonium halide were prepared. Nmr spectra of the solutions were recorded as previously indicated,<sup>1</sup> using a Perkin-Elmer R-20 nmr spectrometer operating at 60 MHz. The resolution was carefully adjusted before recording each separate spectrum. An average of 15 spectra were recorded for each sample to obtain optimum nmr line shapes for study. The

(1) D. W. Larsen, *J. Phys. Chem.*, **74**, 3380 (1970).

(2) J. A. Pople, *Mol. Phys.*, **1**, 168 (1958).

(3) R. A. Sack, *ibid.*, **1**, 163 (1958).

spectra were fitted by comparison of appropriate line shape parameters (such as line width) with corresponding parameters from calculated line shapes. The spectra reported herein are examples; the experimental parameters used were averages over all spectra for a given sample.

## Results and Discussion

The nmr spectra of ions of the type  $(\text{CH}_3)_3\text{NR}^+$ , where R = methyl, ethyl, isopropyl, and *tert*-butyl, are presented in Figure 1. The spectra are shown for the ions in aqueous solution at two temperatures.

The nmr spectra of ions of the type  $(\text{CH}_3)_3\text{NR}^+$ , where R = *n*-hexyl, *n*-octyl, *n*-decyl, and *n*-hexadecyl, are presented in Figure 2. The spectra are shown for ions in aqueous solution at two temperatures.

*Calculated Line Shapes.* The Pople-Sack treatment<sup>2,3</sup> gives the spectral line shape of the nmr absorption of protons coupled to a nucleus with  $I = 1$  ( $^{14}\text{N}$ ) by

$$I(\omega) \propto \text{Re} \mathbf{W} \cdot (i\omega \mathbf{E}_n - i\Omega - \mathbf{\Pi})^{-1} \cdot \mathbf{1} \quad (1)$$

where  $\mathbf{W}$  is a row vector with elements proportional to occupation probabilities of the sites in equilibrium,  $\mathbf{1}$  is a column vector with all components equal to unity,  $\mathbf{E}_n$  is the unit matrix of order  $n$ ,  $\Omega$  is a diagonal matrix with elements  $\omega_j$  (Larmor frequencies for the  $n$  sites), and  $\mathbf{\Pi}$  is a matrix with elements  $\pi_{jk} = p_{kj}$  and  $\pi_{jj} = -\sum_k p_{jk}$  ( $j \neq k$ ) where  $p_{jk}$  is the transition probability between site  $j$  and site  $k$ . The treatment is the Bloch equations (for the slow passage, nonsaturation case) in matrix notation. The line shapes given by Pople<sup>2</sup> are for the three site case ( $^{14}\text{N}$  spin states) with the rate of proton transverse relaxation ( $1/T_2$ ) assumed to be zero. Figure 3 presents the observed line shapes and those calculated from the Pople-Sack equations.<sup>2,3</sup> It can be seen that the agreement between calculated and observed line shapes is rather poor. In the present case, the natural

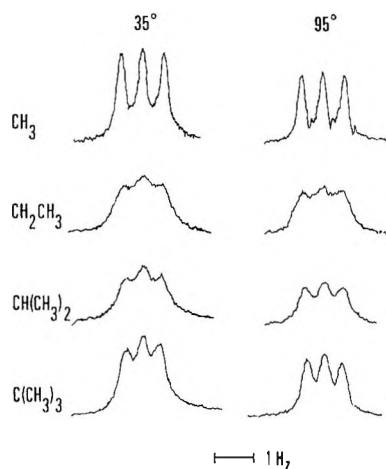


Figure 1. Observed methyl proton resonance spectra for  $(\text{CH}_3)_3\text{NR}^+\text{I}^-$  at two temperatures in  $\text{D}_2\text{O}$  solution.

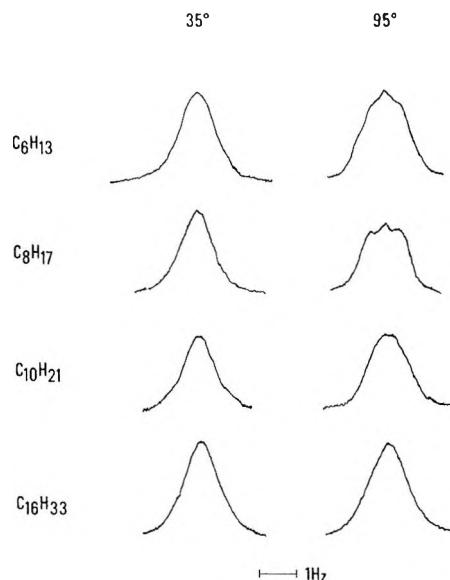


Figure 2. Observed methyl proton resonance spectra for  $(\text{CH}_3)_3\text{NR}^+\text{Cl}^-$  at two temperatures in  $\text{D}_2\text{O}$  solution.

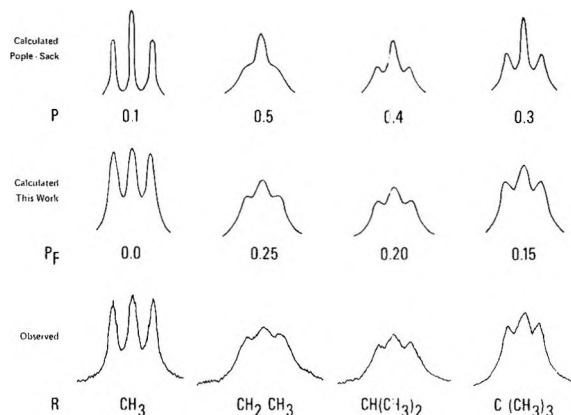


Figure 3. Observed and calculated methyl proton resonance spectra for  $(\text{CH}_3)_3\text{NR}^+\text{I}^-$  at  $35^\circ$  in  $\text{D}_2\text{O}$  solution. Values of transition probabilities used in the calculations are given in the figures.

line width is always an appreciable part of the observed line width. Also, the ion-paired cation will presumably be in a different environment (with respect to chemical shift and electric field gradient) from the free solvated cation. Equation 1 can be easily modified<sup>4,5</sup> to include effects of proton natural line width and chemical exchange between free ion and ion-paired environments (six site case).

Equation 1 is modified according to the following procedure. A  $6 \times 6$  matrix  $(i\omega \mathbf{E}_n - i\Omega - \mathbf{\Pi})$  is constructed, which allows the  $\text{R}_4\text{N}^+$  ion to occupy two chemical sites with three  $^{14}\text{N}$  spin states in each site. The two chemical sites correspond to free  $\text{R}_4\text{N}^+$  and ion paired  $\text{R}_4\text{N}^+$ . Proton natural line width is ac-

(4) H. S. Gutowsky, R. L. Vold, and E. J. Wells, *J. Chem. Phys.*, **43**, 4107 (1965).

(5) E. S. Gore and H. S. Gutowsky, *J. Phys. Chem.*, **73**, 2515 (1969).

counted for by addition of a matrix  $1/T_2 \mathbf{E}_n$  to the  $6 \times 6$  matrix. This assumes that proton natural line width is the same in all 6 sites. Two separate transition probabilities for unit change of  $^{14}\text{N}$  spin state are introduced into  $\mathbf{\Omega}$ ; these are  $p_F$  and  $p_P$  which refer to free  $\text{R}_4\text{N}^+$  and ion-paired  $\text{R}_4\text{N}^+$ , respectively. Two chemical exchange probabilities are introduced into  $\mathbf{\Omega}$ ; these are  $1/\tau_F$  and  $1/\tau_P$  which refer to free  $\text{R}_4\text{N}^+$  and ion-paired  $\text{R}_4\text{N}^+$ , respectively. It is assumed that chemical exchange occurs without change in  $^{14}\text{N}$  spin state, since in general  $1/\tau_F, 1/\tau_P \gg p_F, p_P$ . The vector  $\mathbf{W}$  has three components  $w_F$  and three components  $w_P$  corresponding to fractions of free  $\text{R}_4\text{N}^+$  and ion-paired  $\text{R}_4\text{N}^+$ , respectively. The steady-state requirement for chemical exchange is  $w_F/\tau_F = w_P/\tau_P$ . The modified equations are identical with those of Gore and Gutowsky;<sup>5</sup> however, our notation is that of Pople<sup>2</sup> and Sack.<sup>3</sup>

Line shape functions  $I(\omega)$  were calculated using the modified eq 1 with  $1/T_2, p_F, p_P, 1/\tau_F,$  and  $w_F$  as parameters. The process involved numerical calculations of  $I(\omega) = f(\omega)$ , which required inversion of  $6 \times 6$  complex matrices. This was done using an IBM 1130 computer.

It was possible to reproduce the observed spectra within experimental error; the calculated line shapes are shown in Figure 3. The values of parameters used in calculating the spectra were determined as follows. (1) The natural line width was estimated to be 0.2–0.3 Hz from the solvent and the well resolved  $(\text{CH}_3)_4\text{N}^+$  spectra. A value of  $1/T_2 = 1.0$  rad/sec was found to provide the best overall fit for the ions in Figure 1. This value represents an upper limit, and a slightly smaller value ( $\sim 0.8$  rad/sec) gives a better fit of the  $(\text{CH}_3)_4\text{N}^+$  spectrum. Natural line widths were assumed to be equal for all  $(\text{CH}_3)_3\text{NR}^+$  ions, but small variations in  $T_2$  with the R groups are to be expected.<sup>6</sup> (2) Lifetimes of these ion pairs and free ions, as estimated from ultrasonic absorption measurements,<sup>7</sup> are typically  $10^{-6}$  to  $10^{-9}$  sec. A value  $1/\tau_F = 10^5$  sec $^{-1}$  was used in the calculation. This value was chosen arbitrarily for the calculation; the exact value used for  $1/\tau_F$  is unimportant since the restriction that ensures complete averaging over the two chemical environments is  $1/\tau_F > 10^4$  sec $^{-1}$ . Values of  $1/\tau_F \sim 10^2$  to  $10^3$  sec $^{-1}$  would be necessary for broadening effects due to chemical exchange to be present in the spectra. (3) The ion-pair resonance was assumed to be chemically shifted from that of the free ion. Ion-pair resonances are typically shifted<sup>8</sup> 10 Hz relative to free ions in these systems. A chemical shift difference  $|\nu_P - \nu_F|$  of 10 Hz was used in the calculations; however, a value of 100 Hz gives identical line shapes, since  $\tau_F$  is small enough that the criterion  $\tau_F|\nu_P - \nu_F| \ll 1$  is still satisfied. (4) Evidence was presented in the previous study<sup>1</sup> that  $p_P \approx p_F$  for aqueous solution of  $\text{R}_4\text{N}^+$ ; thus  $p_P = p_F + 0.01$  was used arbitrarily in the

calculation. (5) Evidence was also presented in the previous study<sup>1</sup> that at the concentrations used in the present study,  $w_F \gg w_P$ ; thus fractions of ion pairs and free ions used in the vector  $\mathbf{W}$  were 0.01 and 0.99, respectively. It was found by systematic variation of the parameters  $p_F, p_P,$  and  $w_F$ , that the calculation is insensitive to the difference between  $p_F$  and  $p_P$  provided that the difference is small, and also that the calculation is insensitive to the value of  $w_P$  provided that it is small. (6) The value of  $J_{\text{N-CH}_3} = 0.55$  Hz was assumed to be constant for all ions. Some variation in  $J$  as a function of R group is likely, but the variation is expected to be small.<sup>9</sup>

The values of  $p_F$  used in the calculations of line shapes in Figure 3 are given in Table I. As stated above,

**Table I:**  $^{14}\text{N}$  Transition Probabilities for  $(\text{CH}_3)_3\text{NR}^+$  Ions in  $\text{D}_2\text{O}$  Solution at 35°

R group	Ion	$p_F,^a$ sec $^{-1}$
$\text{CH}_3$	$(\text{CH}_3)_4\text{N}^+$	0
$\text{CH}_2\text{CH}_3$	$(\text{CH}_3)_3\text{NCH}_2\text{CH}_3^+$	0.25
$\text{CH}(\text{CH}_3)_2$	$(\text{CH}_3)_3\text{NCH}(\text{CH}_3)_2^+$	0.20
$\text{C}(\text{CH}_3)_3$	$(\text{CH}_3)_3\text{NC}(\text{CH}_3)_3^+$	0.15

<sup>a</sup> Estimated limit of error  $\pm 0.02$  sec $^{-1}$ .

$1/T_2 = 1.0$  rad/sec provides the best overall fit for the ions. If allowance is made for small variation in  $1/T_2$ , a slightly better fit is obtained for the  $(\text{CH}_3)_4\text{N}^+$  spectrum. The calculations show that  $p_F \approx 0$  for  $(\text{CH}_3)_4\text{N}^+$  in  $\text{D}_2\text{O}$  solution which is expected for perfect tetrahedral symmetry. The numerical values of the  $^{14}\text{N}$  transition probabilities presently reported are consistently lower than those previously reported;<sup>1</sup> however, the validity of the previous arguments and conclusions remains unchanged if the presently reported  $p_F$  values are taken to be correct.

The spectra of  $(\text{CH}_3)_4\text{N}^+$  in  $\text{DMSO}-d_6$  solution<sup>1</sup> were also satisfactorily fitted by eq 1;  $w_P$  (fraction of ion pairs) was assumed to vary between 0.1 (at 75°) and 0.9 (at 12°) with  $p_F = 0.05, p_P = 0.40,$  and  $1/\tau_F = 10^5$  sec $^{-1}$ . The calculated and observed spectra are presented in Figure 4. Again, the numerical values of  $p_F$  and  $p_P$  are slightly lower than previously reported but the previous conclusions remain valid.

The line shapes for the ions shown in Figure 2 were also fitted using the above procedure with  $1/T_2 =$

(6) H. G. Hertz and M. D. Zeidler, *Ber. Bunsenges. Phys. Chem.*, **68**, 821 (1964).

(7) G. Atkinson, R. Garnsey, and M. J. Tait, *Hydrogen-Bonded Solvent Syst. Proc. Symp.*, 161 (1968); *Chem. Abstr.*, **70**, 118729t (1969).

(8) D. W. Larsen and A. C. Wahl, *Inorg. Chem.*, **4**, 1281 (1965).

(9) P. G. Gassman and D. C. Heckert, *J. Org. Chem.*, **30**, 2859 (1965).

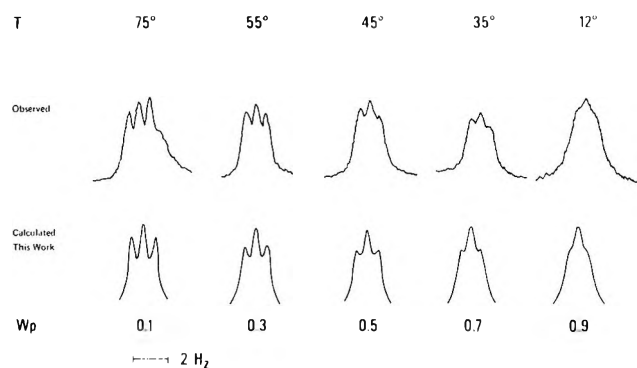


Figure 4. Observed and calculated methyl proton resonance spectra for  $(\text{CH}_3)_4\text{N}^+$  in dimethyl sulfoxide- $d_6$  over a range of temperatures. Values of transition probabilities used in the calculations are given in the figure. The 75° spectrum shows a small peak due to residual water.

1.0 rad/sec. Values of  $p_F$  determined from the best fits are presented in Table II; the  $(\text{CH}_3)_3\text{NCH}_2\text{CH}_3^+$  is included in Table II for comparison. Also presented in Table II are estimates of activation energies ( $E_a$ ) for the correlation decay process which were determined from the temperature dependences of the  $p_F$  values.

Table II:  $^{14}\text{N}$  Transition Probabilities and Reorientation Activation Energies for  $(\text{CH}_3)_3\text{NR}^+$  Ions in  $\text{D}_2\text{O}$  Solution

R group	$p_F$ (35°), sec $^{-1}$	$p_F$ (95°), sec $^{-1}$	$E_a$ , kcal
Ethyl	$0.25 \pm 0.02^a$	$0.25 \pm 0.02^a$	$\sim 0$
n-Hexyl	$0.57 \pm 0.04$	$0.37 \pm 0.03$	$1.6 \pm 0.5^b$
n-Octyl	$0.77 \pm 0.05$	$0.31 \pm 0.03$	$3.4 \pm 0.6$
n-Decyl	$0.91 \pm 0.05$	$0.51 \pm 0.04$	$2.2 \pm 0.6$
n-Hexadecyl	$0.54 \pm 0.04$	$0.52 \pm 0.04$	$\sim 0$

<sup>a</sup> Estimated limit of error. <sup>b</sup> Estimated limit of error.

**Quadrupole Coupling Constants.** The values of the transition probability,  $p$ , for transitions between adjacent spin states of an  $I = 1$  nucleus are given by<sup>2</sup>

$$p = \frac{3}{40} \left( \frac{e^2 Qq}{\hbar} \right)^2 \tau_c \quad (2)$$

where  $(e^2 Qq/\hbar)$  is the quadrupole coupling constant (QCC), and  $\tau_c$  is the correlation time. The transition probability  $p$  depends upon the product  $(\text{QCC})^2 \tau_c$ , both quantities being variable parameters in the  $(\text{CH}_3)_3\text{NR}^+$  ions. Since the measurement of a  $p$  value does not allow separation of factors QCC and  $\tau_c$ , it is necessary to consider the relationship of each separate factor to the experimentally variable parameters.

Evidence has been presented<sup>1</sup> which indicates that for aqueous  $(\text{CH}_3)_3\text{NR}^+$  with  $\text{R} = \text{CH}_3$  and  $\text{CH}_2\text{CH}_3$ , the QCC values depend exclusively upon the nature of R (internal structure of the cation) and that water

molecules and anions contribute negligibly to QCC. It was also concluded<sup>1</sup> that the difference in  $p$  values for the two cations depends primarily upon the difference in QCC values and that  $\tau_c$  values are essentially identical. The  $p_F$  values in Table I are consistent with this view, and in addition they shed light upon the origin of QCC. For all ions except  $(\text{CH}_3)_4\text{N}^+$ , the spectra were found to be independent of solvent, concentration, and added electrolyte; furthermore, for aqueous  $(\text{CH}_3)_4\text{N}^+$ ,  $p_F \approx 0$ . Thus factors external to the ions in Table I have a negligible effect on  $p_F$ . This leaves three factors which could contribute to the observed  $p_F$  variation in Table I:  $\tau_c$ , C-N-C bond angles, and inductive effects. Values of  $\tau_c$  should follow the ordering  $\text{CH}_3 < \text{CH}_2\text{CH}_3 < \text{CH}(\text{CH}_3)_2 < \text{C}(\text{CH}_3)_3$ , as should inductive effects on QCC. However, C-N-C bond angle variation<sup>10</sup> could account for the observed ordering, *i.e.*, the groups in  $(\text{CH}_3)_4\text{N}^+$  have tetrahedral symmetry (QCC  $\approx 0$ ) and the groups in  $(\text{CH}_3)_3\text{NCH}_2\text{CH}_3^+$  exhibit the largest departure from tetrahedral symmetry (largest QCC). These considerations suggest that for aqueous  $\text{R}_4\text{N}^+$  with short R groups,  $\tau_c$  values are similar and QCC differences due to bond angle variation are the primary cause of the observed variation in  $p_F$ .

**Correlation Times.** The nmr spectra for the ions in Figure 1 exhibit almost no temperature dependence, and thus the correlation decay mechanism is a low activation energy process. It was concluded previously that the modulation of the electric field gradient at the  $^{14}\text{N}$  occurs by cation rotation and that correlation times for  $(\text{CH}_3)_4\text{N}^+$  and  $(\text{CH}_3)_3\text{NCH}_2\text{CH}_3^+$  ions are essentially identical. This view appears to be valid for the series of ions in Figure 1.

For aqueous  $(\text{CH}_3)_3\text{NR}^+$  where R is a long straight alkyl chain, the C-N-C bond angles and N-C bonds are expected to be essentially independent of chain length. If QCC values are determined by internal cation structure at  $^{14}\text{N}$  for long R groups, as is apparently true for short R groups, then QCC values are essentially identical for the ions in Table II. The following two studies were made to test this possibility. (1) It was observed that the nmr line shapes are independent of added electrolyte concentration and nature of the anion. (2) The line shapes are also independent of cation concentration over the concentration range which can be studied by nmr. Unfortunately, the range is not large enough to provide conclusive evidence because of the limited solubility of the larger cation salts. These observations<sup>11-13</sup> along with those

(10) C. T. O'Konski and Tae-Kyn Ha, *J. Chem. Phys.*, **49**, 5354 (1968).

(11) In themselves, the observations for cations with long R groups do not rule out a collision modulated field gradient contribution to  $T_1$  for  $^{14}\text{N}$ , in which solvent collisions play a dominant role. This mechanism would be of the type postulated for  $^{129}\text{Xe}$  (see ref 12 and 13). However, this mechanism has been ruled out (see ref 1) for cations with short R groups.

(12) H. C. Torrey, *Phys. Rev.*, **130**, 2306 (1963).

made on short R cations indicate that the QCC values are not measurably affected by changes in parameters external to the cation (*i.e.*, ion pairing and micelle formation). Once it is established that QCC values are determined primarily by internal structural features of the cations, it then follows that the transition probabilities in Table II are measures of relative correlation times.

It is evident that both  $p_F$  values and  $E_a$  values pass through maxima for the ions studied. This behavior can be explained on the basis of two contributing factors. First, the correlation decay mechanism that has been proposed<sup>1</sup> for  $R_4N^+$  ions is rotational tumbling. Thus both  $p_F$  and  $E_a$  values should, in general, increase with chain length; *i.e.*, the reorientation which destroys correlation is less favorable for long alkyl chains than for short alkyl chains. This general increase in  $p_F$  and  $E_a$  values with chain length can be seen for the ions (except hexadecyl) in Table II. Second, the decyl and hexadecyl salts exist partially as micelles. The hexadecyl salt is well above the critical micelle concentration<sup>14</sup> (cmc) and exists almost completely as micelles. Thus there is a second process associated with micelles which destroys correlation. This process is characterized by a smaller  $\tau_c$  and a smaller  $E_a$  than is the process for single ions in solution, which accounts for the maxima in Table II. The concentration of the decyl salt is just above the cmc in this study.<sup>14</sup> However, the conversion of single ions to micelles occurs over a rather wide concentration range for the decyl salts,<sup>14</sup> and thus the observed  $E_a$  value for the decyl salt must reflect contributions from both single ions and micelles.

Proton  $T_1$  measurements<sup>15</sup> on micelle systems indicate

that the heads extend two to three  $CH_2$  groups beyond the micelle surface, and the greater relaxation rate in the micelle interior was attributed to an electrostatic anchoring of the heads on the micelle surface. The present quadrupole relaxation studies (in which the electric field gradient seen by  $^{14}N$  is determined by the internal structural features of the cation) indicate that the heads on the micelle surface undergo rapid motion, characterized by a low activation energy. Quadrupole relaxation rates reflect motion which modulates the electric field gradient, whereas the proton  $T_1$  values reflect motion which changes the relative positions of the protons (magnetic dipoles). In the present case, highly concerted motion which changes the direction of the internal electric field gradient (head motion) would be expected to have some influence upon the motion of chains in the micelle interior. It is surprising that the net result of rapid head motion on the surface is an increase in interior proton  $T_1$  correlation times. However, the important point is that if "anchoring" of heads on the micelle surface implies restricted motion it must also imply motion more rapid than in the single ions.

*Acknowledgements.* Support of the Office of Water Resources Research through Grant A-022-MO is gratefully acknowledged.

(13) I. Oppenheim, M. Bloom, and H. C. Torrey, *Can. J. Phys.*, **42**, 70 (1964).

(14) H. S. Harned and B. B. Owen, "The Physical Chemistry of Electrolytic Solutions," Reinhold, New York, N. Y., 1958, pp 529-531.

(15) J. Clifford, *Trans. Faraday Soc.*, **61**, 1276 (1965).

# Spectroscopy of Rare Earth Oxide Molecules in Inert Matrices at 4°K<sup>1</sup>

by Roger L. DeKock and William Weltner, Jr.\*

Department of Chemistry, University of Florida, Gainesville, Florida 32601 (Received October 12, 1970)

Publication costs assisted by the Air Force Office of Scientific Research and the National Science Foundation

The monoxide and dioxide molecules vaporizing from the solid rare earth oxides in the range of 2100–2900°K have been trapped in solid argon and neon at 4°K. Monoxide molecules with ground-state vibrational frequencies between 808 and 832 cm<sup>-1</sup> were observed in the infrared for all of the metals except Yb and Eu. The small variation in  $\nu''$  is in sharp contrast to the transition metal monoxides. Electronic spectra of the monoxides and metal atoms were also obtained and comparison made with gas-phase data where available. The dioxides of Ce, Pr, and Tb were trapped and their stretching frequencies observed in the infrared. CeO<sub>2</sub> in neon, argon, and nitrogen emits strongly in the region of 4900–6500 Å with a lifetime of about 200 msec, indicating probably a triplet-singlet transition.

## Introduction

It is well known that the spectroscopy of the rare earth metal atoms and compounds is difficult and that it is in a relatively retarded state compared to the transition metals. This research was begun with the hope that the matrix-isolation technique could be of some aid in the clarification of at least one small group of rare earth molecules, the diatomic and triatomic oxides. The complexity of the gas-phase spectra of these species is evident from the large number of tabulated band heads<sup>2a</sup> and the few cases in which a rotational analysis has been made.

Most of the oxide molecules can be generated by vaporization of the corresponding solid oxide at temperatures above 2000°K. Mass spectrometric work<sup>2b–c</sup> indicates that for the majority of these compounds the only molecular species in the vapor are the monoxides and in some cases the dioxides. They can then be trapped in solid neon or argon at 4°K and their optical spectra observed throughout the infrared, visible, and ultraviolet regions. The vibrational spectra in the infrared are usually easily interpretable, particularly with the aid of isotopic <sup>18</sup>O substitution, but the electronic spectra are still quite complex. Attempts have also been made to observe emission spectra without any real success except in the case of the CeO<sub>2</sub> molecule. Here a readily analyzed yellow-green phosphorescence (*i.e.*, long-lived emission) is obtained.

This research then comprises essentially a survey of the spectra of the monoxide and dioxide molecules of the rare earths at 4°K. Further work is needed to clarify even these simplified spectra.

## Experimental Section

The furnace and dewar arrangement used in the matrix isolation work have been described previously.<sup>3</sup> All of the compounds were vaporized from tungsten cells with dimensions of 1 in. in length, 0.010-in. walls, and 0.25-in. o.d. These cells were resistively heated by

passing several hundred amperes of current through them at about 6 V. The windows in the dewar were of cesium iodide.

The infrared spectra were recorded from 4000 to 200 cm<sup>-1</sup> on a Perkin-Elmer 621 grating infrared spectrophotometer with an accuracy of  $\pm 1$  cm<sup>-1</sup>. The electronic spectra were recorded on a Jarrel Ash 0.5-m Ebert scanning spectrometer with appropriate photomultiplier tubes and gratings to cover the various spectral regions. Emission spectra were carried out by exciting through a lithium fluoride window with an AH-6 high-pressure mercury lamp. Some emission spectra were examined by exciting with an Oriel Optics Corporation 1000-W xenon lamp equipped with an F11-20 monochromator.

The rare earth oxides were purchased from Spex Industries, Inc. and attain a purity of 99.9+%. A sample of Ce<sub>2</sub>O<sub>3</sub> was obtained from K & K Laboratories, Inc. and a high-purity sample of Eu<sub>2</sub>O<sub>3</sub> (99.999%) was purchased from American Potash and Chemical Corporation. Enriched oxygen <sup>18</sup>O<sub>2</sub> (91.1%) was obtained from Miles Laboratories, Inc.

The rare gases argon and neon were Airco research grade. The rare gas flow rate was maintained at 0.5 l. atm/hr and the rare gas was precooled with a liquid nitrogen bath immediately before entering the dewar. The window was cooled with liquid helium so that the trapping temperature was always near 4.2°K.

The solid oxides CeO<sub>2</sub>, Ce<sub>2</sub>O<sub>3</sub>, Pr<sub>6</sub>O<sub>11</sub>, Tb<sub>4</sub>O<sub>7</sub>, and the

(1) The support of the Air Force Office of Scientific Research and the National Science Foundation is gratefully acknowledged.

(2) (a) A. Gatterer, J. Junkes, E. W. Salt peter, and B. Rosen, "Molecular Spectra of Metallic Oxides," The Vatican Press, Vatican City, 1957; (b) D. White, P. N. Walsh, L. L. Ames, and H. W. Goldstein in *Thermodyn. Nucl. Mater. Proc. Symp.*, 417 (1962); (c) L. L. Ames, P. N. Walsh, and D. White, *J. Phys. Chem.*, **71**, 2707 (1967); (d) J. A. Fries and E. D. Cater, Mass Spectrometric Determination of Dissociation Energies of PrS, GdS, and PrO, U. S. Atomic Energy Comm., 1969, COO-1182-27, 43 pp. (Eng.) Avail. Dep.; CFSTI; (e) M. P. Panish, *J. Chem. Phys.*, **34**, 2197 (1961).  
(3) W. Weltner, Jr., and D. McLeod, Jr., *ibid.*, **45**, 3096 (1966).

sesquioxides of the remaining eleven rare earths were vaporized at temperatures ranging from 2150 to 2900°K, generally increasing from cerium to lutetium oxide. Each of the samples was outgassed for at least 30 min at or near the final operating temperature prior to the experiment. The average deposition time employed was 30 min.

*Infrared Spectra. Nd, Sm, Gd, Dy, Ho, Er, Tm, and Lu Monoxide Molecules.* The observed infrared absorptions and the most probable assignments are given in Table I along with known gas-phase values. As is normally found, the absorptions in neon occur at slightly higher energy than in argon and are in closer agreement with the gas phase values. For the oxides of Nd, Sm, Gd, Dy, Ho, Er, Tm, and Lu only a single

major infrared absorption near 820  $\text{cm}^{-1}$  is observed. As indicated in Table I, several of the bands actually consist of multiplets which are attributed to different sites in the rare gas lattice. Occasionally bands appeared between 900 and 1000  $\text{cm}^{-1}$  arising from tungsten oxide species produced by interaction with the cell material.<sup>4</sup> Also, in a few cases, dimers or cluster bands were formed which increased in intensity upon diffusion. In the SmO spectrum in argon such a band appeared at 657  $\text{cm}^{-1}$ ; in a GdO-argon matrix a band at 773  $\text{cm}^{-1}$  reacted similarly.

The behavior of LuO in neon is puzzling since the dilute matrix exhibited its strongest ir frequency at 811  $\text{cm}^{-1}$ , 14  $\text{cm}^{-1}$  lower than the argon value. This shift is in the opposite direction to that expected or observed in the other rare earths. It is difficult to attribute this to site effects.

*Ce, Pr, and Tb Monoxide and Dioxide Molecules.* The oxides of Ce, Pr, and Tb give an infrared absorption near 820  $\text{cm}^{-1}$  which is assigned to the monoxide in analogy with the location of this band for the other rare earth oxides. However, as indicated in Table I, other bands are observed in the region 700–800  $\text{cm}^{-1}$  which can be assigned to the dioxides.

In the case of Ce, if the original sample of cerium oxide (either  $\text{Ce}_2\text{O}_3$  or  $\text{CeO}_2$ ) is not sufficiently outgassed prior to matrix deposition an absorption is observed at 808  $\text{cm}^{-1}$  in argon, plus other bands in the 750- $\text{cm}^{-1}$  region. This absorption band alone has been observed when a sample of cerium metal was vaporized from a tantalum cell. Presumably oxygen is obtained from surface oxidation of the metal or from the cell material and in this strongly reducing atmosphere leads to the preferential vaporization of the  $\text{CeO}$  molecule. On this basis and with the knowledge that the gas phase frequency<sup>5</sup> is  $830 \pm 40 \text{ cm}^{-1}$ , the 808- $\text{cm}^{-1}$  band is assigned to  $\text{CeO}$ .

For a bent triatomic molecule, two stretching frequencies are allowed in the ir, a symmetric stretch  $\nu_1$  and an asymmetric stretch  $\nu_3$ ; only  $\nu_3$  is allowed for a linear symmetrical triatomic molecule. A bending frequency is also infrared active but is presumed to lie below our lower limit of investigation, 200  $\text{cm}^{-1}$ . In the case of  $\text{CeO}_2$ , the molecule is known to be bent from electric deflection experiments,<sup>6</sup> so that both  $\nu_1$  and  $\nu_3$  will be infrared active. Samples of  $\text{CeO}_2$  and  $\text{Ce}_2\text{O}_3$  gave identical results upon vaporization, consistent with the observations of White, *et al.*,<sup>2b</sup> that the composition of  $\text{CeO}_2$  moves toward  $\text{Ce}_2\text{O}_3$  as material is vaporized. The spectrum in argon is presented in Figure 1. The 736- $\text{cm}^{-1}$  band is assigned to  $\nu_3$  since it is more intense, and the 756- $\text{cm}^{-1}$  band to  $\nu_1$ . Strong annealing of the

**Table I:** Observed Infrared Bands of Rare Earth Oxide Molecules

Starting solid material	Molecule	Observed bands, $\text{cm}^{-1}$ <sup>a</sup>		Gas phase $\Delta G''_{1/2}$ , $\text{cm}^{-1}$
		Argon matrix	Neon matrix	
$\text{CeO}_2, \text{Ce}_2\text{O}_3$	$\text{CeO}_2$	736 s	759 s	
		756 w	756 m <sup>d</sup> 777 w 785 vw	
Ce	$\text{CeO}$	808	820	830 <sup>b</sup>
		$\text{Pr}_6\text{O}_{11}$	$\text{PrO}$	818 s 812 w <sup>d</sup> 731 s 732 m <sup>d</sup>
$\text{Nd}_2\text{O}_3$	$\text{NdO}$	815 s	823	
		809 w <sup>d</sup>		
$\text{Sm}_2\text{O}_3$	$\text{SmO}$	808	819	
		$\text{Eu}_2\text{O}_3$	?	950 w 913 s 788 s 718 m 669 s 482 m
$\text{Gd}_2\text{O}_3$	$\text{GdO}$	813	824	825 <sup>c</sup>
		$\text{Tb}_4\text{O}_7$	$\text{TbO}$	824 s 738 m 718 m
$\text{Dy}_2\text{O}_3$	$\text{DyO}$	829 m		
		826 w <sup>d</sup>		
$\text{Ho}_2\text{O}_3$	$\text{HoO}$	829 m		834 <sup>c</sup>
		826 w <sup>d</sup> 823 vw <sup>d</sup>		
$\text{Er}_2\text{O}_3$	$\text{ErO}$	829 m		
		826 w <sup>d</sup>		
$\text{Tm}_2\text{O}_3$	$\text{TmO}$	832 m		
		829 w <sup>d</sup>		
$\text{Yb}_2\text{O}_3$	$\text{LuO}$	None	None	
		$\text{Lu}_2\text{O}_3$		827 w <sup>d</sup> 825 m 821 w <sup>d</sup>

<sup>a</sup> Intensities are indicated by s, strong; m, medium; w, weak; vw, very weak. <sup>b</sup> Reference 5, uncertainty in this frequency is  $\pm 40 \text{ cm}^{-1}$ . <sup>c</sup> Reference 1, see discussion of electronic spectrum of this molecule in text. <sup>d</sup> Matrix sites. <sup>e</sup> No ir bands although WO bands were observed in the visible region.

(4) W. Weltner, Jr., and D. McLeod, Jr., *J. Mol. Spectrosc.*, **17**, 276 (1965).

(5) L. L. Ames and R. F. Barrow, *Proc. Phys. Soc.*, **90**, 869 (1967).

(6) M. Kaufman, J. Muenter, and W. Klemperer, *J. Chem. Phys.*, **47**, 3365 (1967).

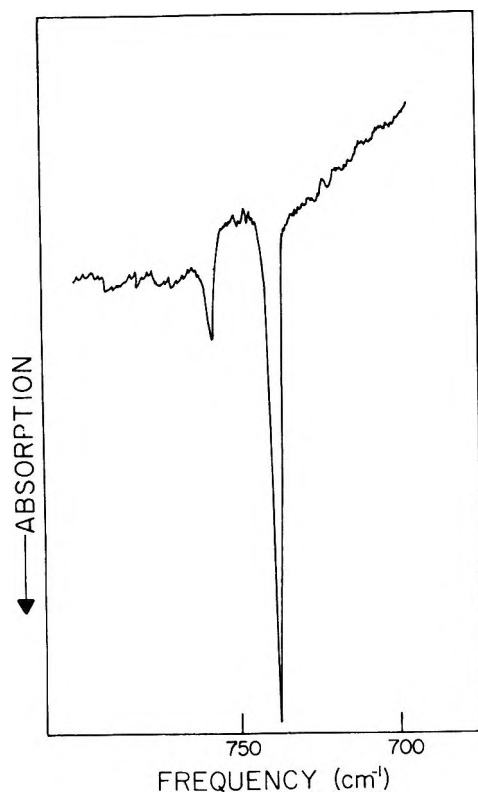


Figure 1. Infrared spectrum of  $\text{CeO}_2$  in an argon matrix at  $4^\circ\text{K}$ .

$\text{CeO}_2$ :Ar matrix results in a decrease in intensity of the bands at  $756$  and  $736\text{ cm}^{-1}$  and a concomitant increase in two bands at  $571$  and  $483\text{ cm}^{-1}$ . Therefore, these bands are assigned to dimers or aggregates of  $\text{CeO}_2$ . The isotopic labeling data with  $^{18}\text{O}$  support this assignment (see below).

$\text{CeO}_2$  has also been trapped in a nitrogen matrix, and the infrared spectrum is presented in Figure 2. The strong  $719\text{-cm}^{-1}$  band is assigned to  $\nu_3$ , and either the  $761\text{-}$  or the  $714\text{-cm}^{-1}$  band could be  $\nu_1$ . In analogy with the argon spectrum one would tend to assign  $\nu_1 = 761\text{ cm}^{-1}$ , but other evidence is against that choice. The  $719\text{--}714$  bands decrease together as the matrix is strongly diffused, whereas the  $761\text{-cm}^{-1}$  band does not. Also, as discussed later, the emission spectrum of  $\text{CeO}_2$  in  $\text{N}_2$  exhibits a vibrational progression near  $715\text{ cm}^{-1}$ , and for a symmetric triatomic molecule that frequency should be  $\nu_1$  in the ground state. One must conclude that  $\nu_1$  is much more affected by the nitrogen environment than  $\nu_3$  since  $\nu_1$  shifts from  $756$  to  $714\text{ cm}^{-1}$  from an argon to a nitrogen matrix while  $\nu_3$  shifts from only  $736$  to  $719\text{ cm}^{-1}$ . (Nitrogen is known to be a more perturbing medium than solid neon or argon)<sup>7</sup>. Further annealing of the nitrogen matrix causes two bands to appear at  $568$  and  $483\text{ cm}^{-1}$ ; these are analogs of the  $571\text{-}$  and  $483\text{-cm}^{-1}$  bands observed in argon.

Isotopic labeling with  $^{18}\text{O}$  was carried out by passing  $^{18}\text{O}_2$  over cerium metal at about  $1600^\circ\text{K}$ . After the formation of the oxide was completed, the temperature

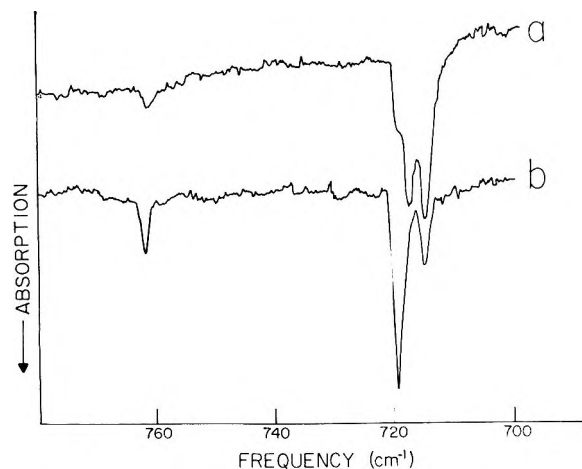


Figure 2. Infrared spectrum of  $\text{CeO}_2$  in a nitrogen matrix; (a) is before and (b) after annealing.

was raised to  $2150^\circ\text{K}$  and the matrix deposition was carried out. The presence of  $^{16}\text{O}_2$  in the  $^{18}\text{O}_2$  (about 9%) and as an impurity in the Ce metal or tungsten cell (see discussion above on production of  $\text{CeO}$ ) made it impossible to eliminate  $^{16}\text{O}$  from the vaporizing molecules so that  $\text{Ce}^{16}\text{O}_2$  and  $\text{Ce}^{16}\text{O}^{18}\text{O}$  would also be expected to appear in the spectrum.

The ir spectrum in argon is presented in Figure 3 and shows that, in addition to the  $\text{Ce}^{16}\text{O}_2$  bands at  $756$  and  $736\text{ cm}^{-1}$ , new bands appear at  $745$ ,  $707$ , and  $702\text{ cm}^{-1}$ . Runs in which the amount of  $^{18}\text{O}_2$  passed into the cell was varied indicated that these new bands all arose from molecules containing  $^{18}\text{O}$ . One expects to observe, for a mixture of three such isotopically substituted species, three weak bands due to  $\nu_1$  and three strong bands due to  $\nu_3$ , with the mixed-isotope molecule producing the middle band in each triplet. This is clearly not observed here. Our interpretation of the observed spectra depends partially upon two other pieces of evidence: First, the emission spectrum of the matrix in Figure 3 exhibits a progression of frequency difference about  $700\text{ cm}^{-1}$  (see Table VI and a later discussion) which must be interpreted as  $\nu_1''$  for  $\text{Ce}^{18}\text{O}_2$ . Also, in all ir spectra there is a weak shoulder at this frequency and in one very well annealed matrix the shoulder is resolved.

For  $\text{Ce}^{18}\text{O}_2$  we then assign  $\nu_1$  to the weak band at  $\sim 700\text{ cm}^{-1}$  and  $\nu_3$  to the strong band at  $707\text{ cm}^{-1}$ . For  $\text{Ce}^{16}\text{O}^{18}\text{O}$  we would then expect to find  $\nu_1$  as a weak band about midway between  $756$  and  $700$ , and  $\nu_3$  as a strong band between  $736$  and  $707\text{ cm}^{-1}$ . Instead we find two medium intensity bands at  $745$  and  $702\text{ cm}^{-1}$ . It seems likely that these are the mixed  $\nu_1$  and  $\nu_3$  frequencies occurring in  $\text{Ce}^{16}\text{O}^{18}\text{O}$  which, of course, now

(7) See G. C. Pimentel and S. W. Charles, *Pure Appl. Chem.*, **7**, 111 (1963). Relatively large shifts have been observed from argon to nitrogen matrices; for example, for  $\text{FeCl}_2$   $\nu_3$  shifts from  $490\text{ cm}^{-1}$  in argon to  $447\text{ cm}^{-1}$  in  $\text{N}_2$  [M. E. Jacox and D. E. Milligan, *J. Chem. Phys.*, **51**, 4143 (1969).]

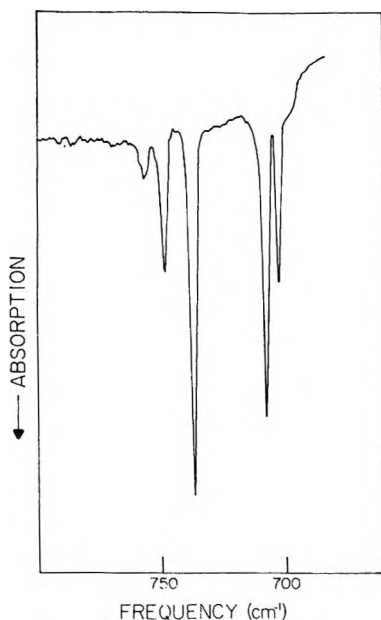


Figure 3. Infrared spectrum of  $\text{Ce}^{16}\text{O}_2$ ,  $\text{Ce}^{18}\text{O}^{16}\text{O}$ , and  $\text{Ce}^{18}\text{O}_2$  in an argon matrix at  $4^\circ\text{K}$ .

has only a plane of symmetry so that  $\nu_1$  and  $\nu_3$  can interact.

Although the Teller-Redlich product rule<sup>8</sup> cannot be applied explicitly for a triatomic molecule without knowledge of the geometry and the bending frequency  $\nu_2$ , estimates of the expected isotopic shift can be made. In the  $a_1$  representation of  $C_{2v}$  symmetry, to which  $\nu_1$  and  $\nu_2$  belong, the apex angle O-Ce-O does not enter into the product ( $\nu_1^f \nu_2^f / \nu_1 \nu_2$ ). For  $\text{CeO}_2$  this ratio is calculated to be 0.8989. The experimental ratio of  $\nu_1^f / \nu_1 = 700/756 = 0.9259$  but the bending frequencies are not known. For  $\nu_3$  the isotopic shift depends upon the apex angle; however, the dependence is small. The ratio  $\nu_3^f / \nu_3$  changes from 0.9536 to 0.9487 in going from linear  $\text{CeO}_2$  to an apex angle of  $90^\circ$ . The experimental value is  $707/736 = 0.9606$  which, considering anharmonicity, implies a nearly linear  $\text{CeO}_2$ . This is in accord with the weak intensity of the observed  $\nu_1$  in the ir spectrum in Figure 1.

The substitution of  $^{18}\text{O}$  in  $\text{CeO}_2$  is helpful in the assignment of the bands at 571, 483  $\text{cm}^{-1}$  in argon and 568, 483  $\text{cm}^{-1}$  in nitrogen. In each matrix, each of these bands formed a definite triplet in the  $^{18}\text{O}$  experiment. The spectrum is presented in nitrogen in Figure 4 since not enough intensity was achieved in the argon run. The absorptions appear at 568, 555, 542  $\text{cm}^{-1}$  and 483, 469, 459  $\text{cm}^{-1}$ . These bands can be analyzed assuming a  $D_{2h}$  structure involving bridging oxygen atoms. In  $D_{2h}$  symmetry we have a total of six allowed infrared modes with symmetries  $B_{1u}$  ( $\nu_7, \nu_8$ ),  $B_{2u}$  ( $\nu_9, \nu_{10}$ ), and  $B_{3u}$  ( $\nu_{11}, \nu_{12}$ ).  $\nu_7$  and  $\nu_8$  can be described as out-of-plane ring bending motions;  $\nu_{10}$ , as an outer bond bending in the plane;  $\nu_9$  and  $\nu_{11}$ , as bridge-bond stretchings; and  $\nu_{12}$ , as an outer bond stretching.<sup>9,10</sup> On the basis of

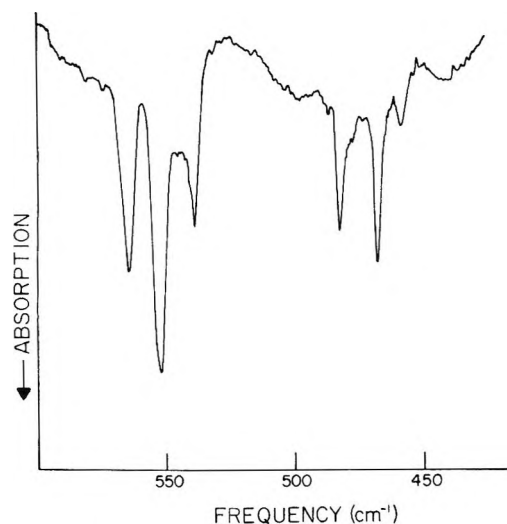


Figure 4. Infrared spectrum of a strongly diffused nitrogen matrix at  $4^\circ\text{K}$  originally containing  $\text{Ce}^{16}\text{O}_2$ ,  $\text{Ce}^{18}\text{O}^{16}\text{O}$ , and  $\text{Ce}^{18}\text{O}_2$ . Observed bands are attributed to dimers.

infrared studies<sup>10</sup> of  $(\text{MCl}_2)_2$  where M is a first-row transition metal, we expect  $\nu_9$  and  $\nu_{12}$  to be the two highest energy modes. The outer oxygen stretchings  $\nu_{12}$  in the dimer involving  $^{16}\text{O}$ ,  $^{18}\text{O}$ , and the mixed isotopes are then assigned to 568, 542, and 555  $\text{cm}^{-1}$ , respectively. The assumption is made here that the motion of the ring oxygens mixes very little with this stretching so that the various isotopic substitutions in the ring only cause these bands to be somewhat broadened. Correspondingly, the ring stretchings  $\nu_9$  are assigned to 483, 459, and 469  $\text{cm}^{-1}$ .

For  $\text{TbO}_2$  two bands of nearly equal intensity are observed at 718 and 783  $\text{cm}^{-1}$ , in addition to the band at 824  $\text{cm}^{-1}$  which is assigned to  $\text{TbO}$ . Vaporization of  $\text{Pr}_6\text{O}_{11}$  gives a band at 818  $\text{cm}^{-1}$  which is assigned to  $\text{PrO}$  and another strong band at 731  $\text{cm}^{-1}$  which is probably  $\nu_3$  of  $\text{PrO}_2$ . Since no band is observed which can be assigned to  $\nu_1$  we assume that either  $\text{PrO}_2$  is linear or only slightly bent.

**Eu Oxide Molecules.** In comparison to the simplicity of the infrared spectra of the preceding rare earth oxides, the spectra of europium oxide vapor is quite complex (see Figure 5). In an argon matrix, six distinct absorptions appear while in neon five bands are observed, none of which can be assigned to tungsten oxide or to other rare earth oxide molecules. To remove the possibility of impurity bands, 99.999% pure material was vaporized at 2250°K and yielded the same spectra. Annealing the argon matrix to about 30°K did not produce significant changes.

(8) G. Herzberg, "Molecular Spectra and Molecular Structure. II. Infrared and Raman Spectra of Polyatomic Molecules," D. Van Nostrand, Princeton, N. J., 1945, p 228.

(9) K. R. Thompson and K. D. Carlson, *J. Chem. Phys.*, **49**, 4379 (1968).

(10) G. E. Leroi, T. C. James, J. T. Hougen, and W. Klemperer, *ibid.*, **36**, 2879 (1962), and references given in ref 9.

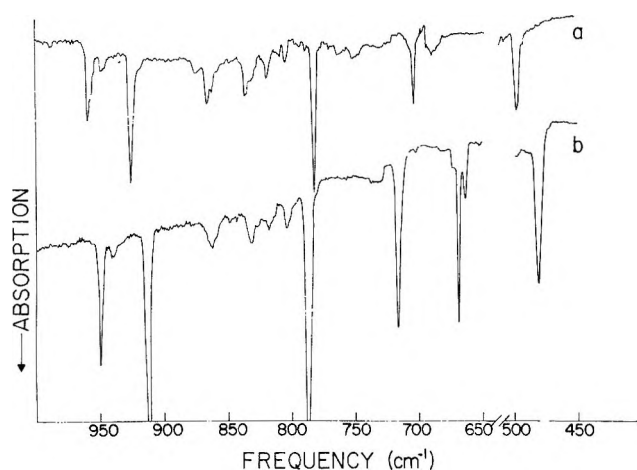


Figure 5. Infrared spectrum of matrices containing the vapor from solid  $\text{Eu}_2\text{O}_3$  trapped at  $4^\circ\text{K}$ : (a) neon matrix; (b) argon matrix.

Mass spectrometric work<sup>2b-e,11</sup> indicates that only the monoxide and Eu atoms should be present in the vapor phase in a ratio of about  $\text{MO}/\text{M} = 0.1$ . One then suspects that the window was not at  $4^\circ\text{K}$  during the preparation of the matrices shown in Figure 5. However, several runs were made separated by many months and by other successful trapping experiments which refute that suspicion. At present these bands cannot be assigned and further work is needed to clarify the situation.

**Electronic Spectra. Survey of Absorption Spectra.** The spectrum of each of the rare earth oxide vapors in matrices at  $4^\circ\text{K}$  was measured in the general region of  $8500\text{--}2000 \text{ \AA}$ . We will give here a brief discussion of these spectra and, where possible, a correlation with gas-phase data. Representative spectra will be shown in figures but usually reference will be made to the prominent bands listed in tables. The  $4^\circ\text{K}$  spectra have aided the gas-phase spectroscopist in the investigation of the transition metal oxides<sup>12</sup> and perhaps this will also be true for the rare earth oxides.

The mass spectrometric data of Ames, *et al.*,<sup>2b</sup> indicates the species expected in the vapor and in almost all cases our ir spectra are in agreement with their observations. Their measurements also give a ratio of  $\text{MO}/\text{M}$ , diatomic molecules to atoms, in the vapor, and generally these species are present in comparable amounts. One then often expects to see electronic transitions of both atoms and molecules in the matrix spectra. In one case, that of  $\text{Yb}_2\text{O}_3$ , only atoms are observed since no ir band is detected. For all of the other rare earths there will be atoms present along with the diatomics so that the spectrum of the atoms should also be determined to clarify the assignments. This has only been done in the cases of Ce, Nd, and Lu since considerable effort was required to measure the spectra for all of the rare earth oxides. In some of the spectra the different shapes of atom and molecule bands makes a distinction,

but not always an identification, possible. Unfortunately, the long vibrational progressions occurring in the spectra of the transition metal diatomics hardly ever occur in the rare earths; usually only (0,0) bands are observed accompanied perhaps by weak (1,0) bands.

Past work with the transition metal oxides indicates that electronic transitions are generally shifted to higher frequencies in a neon matrix and to lower frequencies in argon, but the size of the shift depends upon the molecule and the transition considered. Neon does have the advantage that the bands are almost always narrower than in other matrices. The indications are that in the heavier diatomic oxides the electronic transitions are shifted further from the gas values in neon than in argon, and this seems to apply to the rare earth oxides. It does seem clear, if we may take LaO as a relevant example, that the rare earth oxide transitions can be expected to be shifted by 300 to  $500 \text{ cm}^{-1}$  toward higher frequencies in neon. The data that we will discuss below also indicate that the transitions in argon may be much closer to the gas-phase values and may lie at higher or lower frequencies.

Except for  $\text{CeO}_2$ , the emission spectra of these matrices were generally weak. Strong emission of Tm atoms did occur from an argon matrix made by trapping the vapor over solid  $\text{Tm}_2\text{O}_3$ .

**CeO.** The vaporization of Ce metal apparently is also accompanied by the formation of CeO molecules, as evidenced by the observation of a large ir band at  $820 \text{ cm}^{-1}$  in neon (see above). The electronic spectrum of that matrix shows numerous absorption bands in the region from  $8000$  to  $3500 \text{ \AA}$ . Vaporization of a well outgassed sample of  $\text{CeO}_2$  yielded no absorption bands throughout this region, and the ir indicates that only  $\text{CeO}_2$  is trapped. The bands resulting from the vaporization of metal are then only due to Ce atoms and CeO, but unfortunately there is no reliable way to distinguish them in the spectrum.

Gatterer, *et al.*,<sup>2a</sup> list at least nine possible CeO systems in the gas-phase spectra extending from  $8600$  to  $4600 \text{ \AA}$ . Ames and Barrow<sup>5</sup> have recently made a rotational analysis of four strong absorption bands, presumably (0,0) bands which include three of those listed by Gatterer. They conclude that these four bands (at  $7937$ ,  $7242$ ,  $4931$ , and  $4798 \text{ \AA}$ ) all originate from sub-states of a probable  $^3\Phi$  ground state. At  $4^\circ\text{K}$  only transitions from the  $^3\Phi_2$  substate would be observed, that is, only the bands at  $7937$  and  $4931 \text{ \AA}$  should be seen in the matrix spectra.

Figure 6 shows the neon matrix spectrum between  $6800$  and  $8100 \text{ \AA}$ . The very strong  $7846 \text{ \AA}$  band probably corresponds to Ames and Barrow's  $7937\text{-\AA}$  gas band; the shift is to the blue in a neon matrix, as ex-

(11) J. M. Haschke and H. A. Eick, *J. Phys. Chem.*, **73**, 374 (1969).

(12) W. Weltner, Jr., *Science*, **155**, 155 (1967).

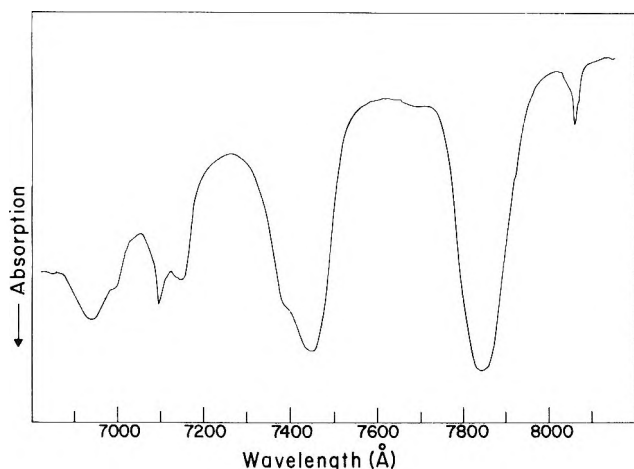


Figure 6. A portion of the absorption spectrum of CeO plus atomic Ce in a neon matrix at 4°K.

pected. Shoulders at 7395 and 6994 Å may be the (1,0) and (2,0) transitions of this system in the matrix, yielding  $\Delta G'_{1/2} = 777 \text{ cm}^{-1}$ ,  $\Delta G'_{3/2} = 775 \text{ cm}^{-1}$  in satisfactory agreement with the gas<sup>5</sup>  $\omega$  value of  $751 \pm 32 \text{ cm}^{-1}$ . From the general similarity of the shapes of bands in this region, it also appears likely that other (0,0) bands occur at 7445, 7144, and 6936 Å in neon. The first two of these may correspond to the (0,0) gas bands near 7570 and 7297 Å listed by Gatterer.

We have looked in the region of 4900 Å in the matrix spectra for Ames and Barrow's second system but can find no satisfactory counterpart. A strong band occurs at 4983 Å in the matrix, but this is unlikely to correspond to a gas band at 4931 Å. Our spectrum then indicates that the gas system observed by those authors does not begin from the  $X^3\Phi_2$  state.

The matrix spectra are very rich in bands of almost the same intensity. These have been listed in Table II.

*PrO.* An argon matrix which showed strong ir bands at 818 and 731  $\text{cm}^{-1}$  (assigned here to PrO and PrO<sub>2</sub>) yielded an absorption spectrum containing the prominent bands listed in Table II. If the strongest bands at 5914 and 5592 Å (see Figure 7) are assigned as (0,0) bands then the (1,0) may be chosen to lie at 5656 and 5370 Å, respectively, and the excited-state frequencies are found to be 771 and 749  $\text{cm}^{-1}$  in the two systems. It is possible that the (2,0) band of the 5914-Å system occurs at 5416 Å.

Gatterer, *et al.*,<sup>2a</sup> list four systems in the gas spectrum at 6018.9 (VIII), 5763.4 (IX), 5691.0 (X), and 5352.0 Å (XI) which could possibly be identified with these two matrix progressions. The two systems VIII and X have lower state vibrational frequencies near 826  $\text{cm}^{-1}$  which is in agreement with the neon matrix ir band. The  $\nu''$  of system IX is not known. Then the most likely assignment would match the 5914- and 5592-Å matrix systems with VIII and X in the gas spectrum.

Table II: Positions of Prominent Bands<sup>a</sup> between 8000 and 3500 Å

CeO + Ce neon $\lambda$ , Å	PrO argon $\lambda$ , Å	NdO		Nd atoms	
		Neon $\lambda$ , Å	Argon $\lambda$ , Å	Neon $\lambda$ , Å	Argon $\lambda$ , Å
7846 s	7052	6868 s		4784	4830 vs
7445 s	6832	6802 vs	7026 vs	4772 <sup>vs</sup>	4764 vs
7395 s	6504	6467 m	6674 m	4718 <sup>vs</sup>	4653 m
7144 m	5914 s	6174 w	5830 vs	4713 <sup>br</sup>	4529 m
6936 m	5656 m	5668 vs	5608 m	4615 s	4514 m
6602 s	5592 s	5510 w	5508 w	4610 s	4455 m
6510 s	5416 w	5445 m	5476 m	4574 s	4366 m
6358 s	5370 w	5281 m	5367 w	4555 s	4072 w
6130 s	4832 w	5233 m	5200 w	4488 vs	4059 w
6032 s	4505 vw	5068 m	5054 m	4414 s	3839 w
5970 s	4451 vw	4930 m	4188 m	4333 s	3826 w
5734 s	4367 w	4201 w	4068 w	4247 s	
5481 s	4303 w	4116 w		4038 s	
5186 s	4188 w			3937 s	
5108 s	4162 w				
4983 s	4048 w				
4728 s	4014 w				
4632 s	3972 w				
4416 s	3887 w				
4228 s	3788 w				
4086 s					
3834 s					
3704 s					
3645 s					
3537 s					
3512 s					
3355 s					
3268 s					
3164 m					
3068 s					
3031 s					
2949 s					
2869 s					
2662 s					

<sup>a</sup> Intensities of bands are indicated by: vs, very strong; s, strong; m, medium; w, weak; vw, very weak. Line widths are indicated by sh, sharp; br, broad.

(Matching with IX and X would give opposite shifts for the gas-matrix effect of the two systems.) The excited state  $\nu'$  derived from the band heads in the gas spectra are 781  $\text{cm}^{-1}$  (VIII) and 783  $\text{cm}^{-1}$  (X) and the latter does not correspond with  $\nu' = 749 \text{ cm}^{-1}$  for the 5592-Å matrix system. This leaves only the 5914-Å system in argon to correspond to the 6018.9 Å (VIII) in the gas, a matrix shift of 294  $\text{cm}^{-1}$  to higher energy. This is not a very satisfying shift since it is more expected for a neon than an argon matrix, and it seems likely that both transitions VIII and X are not being observed at 4°K. This means that, although they both probably terminate in the ground state, it is not the lowest substate.

The large number of systems seen in the gas phase in the near-ir, out to 8500 Å, were not observed in the matrix spectra except for perhaps the three absorptions

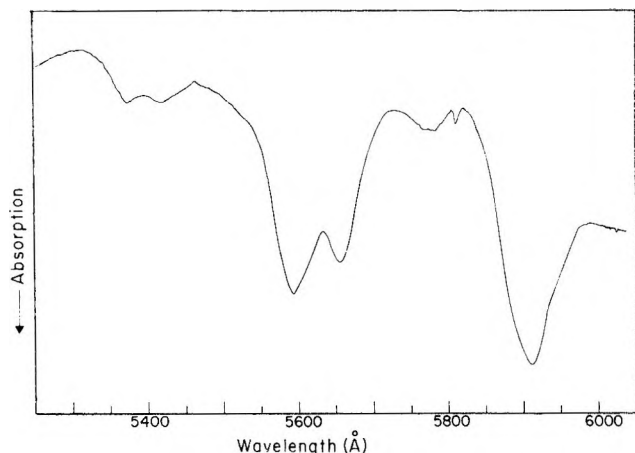


Figure 7. A portion of the absorption spectrum of PrO in an argon matrix at 4°K.

between 6500 and 7100 Å given in Table II. However, it is difficult to find a correspondence with the gas systems.<sup>2a</sup>

*NdO*. In spite of the mass spectrometric<sup>2c</sup> results that  $(M/O/M) > 100$  in the vapor, strong atomic bands were observed in neon and argon matrices when the vapor over solid  $Nd_2O_3$  was trapped. Nd atoms were then also isolated in neon and argon in order to be able to distinguish the NdO spectrum in each matrix. Figure 8 shows a portion of the spectrum of NdO and Nd atoms in neon at 4°K with the NdO bands indicated. There are bands throughout the 3500–8500-Å region with two very strong ones at 6802 and 5668 Å. The (1,0) band of the 6802-Å system appears at 6467 Å yielding a  $\Delta G'_{1/2} = 762 \text{ cm}^{-1}$ . The (1,0) band for the 5668-Å system may lie at 5445 Å (see Figure 8) so that  $\Delta G'_{1/2} = 722 \text{ cm}^{-1}$ , but this is a very uncertain assignment. The prominent bands of NdO observed in neon are listed in Table II.

Gatterer, *et al.*,<sup>2a</sup> list band heads between 8700 and 6300 Å in the gas emission spectrum, but no vibrational or rotational analyses have been made. These band heads are so numerous that it is difficult to guess as to which corresponds to the 6802-Å head observed in neon. Taking account of the blue shift in neon, it probably lies among the band heads between 6934 and 6894 Å in the gas.

*SmO*. The absorption spectrum of a neon matrix containing a large amount of SmO and some Sm atoms exhibited bands between 6400 and 3500 Å. (A large number of WO and TaO bands.<sup>4,13</sup> were observed in accord with the findings of Ames, *et al.*, for the vaporization of  $Sm_2O_3$ .) There appear to be two sets of bands, some sharp and others rounded, which vary in intensity relative to each other (see Table III). The rounded bands appear to become relatively more intense at a higher temperature of vaporization and are perhaps Sm atoms.<sup>2c</sup>

Gatterer<sup>2a</sup> gives (0,0) bands for four systems in the

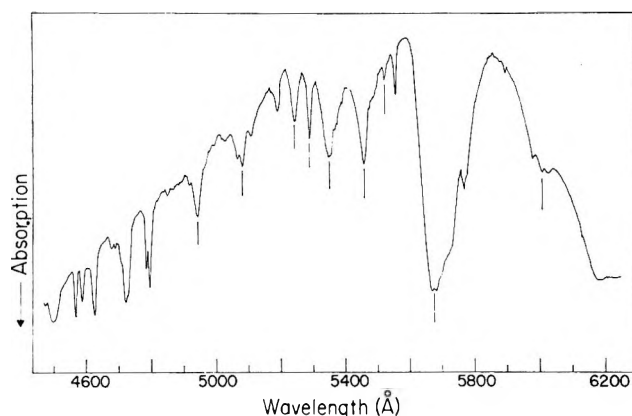


Figure 8. A portion of the absorption spectrum of NdO plus atomic Nd in a neon matrix at 4°K. NdO bands are indicated by vertical lines.

Table III: Positions of Prominent Bands<sup>a</sup> between 8000 and 3500 Å

SmO neon λ, Å	EuO neon λ, Å	GdO neon λ, Å	TbO argon λ, Å	DyO argon λ, Å	HoO argon λ, Å
6262 br	5746 vw	5936 vs	6009 m	7028 w	5618} vs
6085 br	5438 w	5745 w	5860 w	6760 w	5582} vs
5735 br	5074 vw	5633 m	5735 vw	6368 m	5350 w
5718 br	4476	5558 m	5598 vw	6115 m	5038} vs
5566 br	4434 vs	5414 s	5339 m	6021 m	4968} vs
5550 sh	4400	5178 m	5264 s	5750 vs	4767 vw
5480 sh		4948 vw	5072 w	5482 m	4677 w
5369 br		4385 s	4768 w	5373 m	4484 vw
4959 sh		4246 m	4607 w	5348 m	4312 w
4561 br		4132 w	4442 w	5150 vs	4143 w
4396 br			4326 w	4935 vs	4025 m
4326 sh			4208 w	4890 vs	4003 m
4256 sh			4072 w	4649 m	3947 m
4191 br				4613 m	3899 m
3755 sh				4478 s	3862 m
3709 sh				4401 w	3831 m
3689 sh				4330 m	3604 w
				4305 m	3499 vw
				4000 s	3176 w

<sup>a</sup> Intensities of bands are indicated by: vs, very strong; s, strong; m, medium; w, weak; vw, very weak. Line widths are indicated by sh, sharp; br, broad.

gas spectrum, but only for the A system at 3747.7 Å are vibrational spacings given. However, the vibrational frequencies derived from the assigned (1,0) and (0,1) bands for the A system are much too high to be correct for SmO. The other (0,0) bands are given at 4650, 4282.0, and 4154.7 Å (?). Possible (0,0) bands in the neon matrix spectrum are at 5550, 4959, 4326, 4256, 3755, 3709, and 3689 Å. The 5550-Å band has a possible (1,0) band at 5319 Å, yielding  $\Delta G'_{1/2} = 782 \text{ cm}^{-1}$ . The 4256-Å band may also have a weak (1,0)

(13) W. Weltner, Jr., and D. McLeod, Jr., *J. Chem. Phys.*, **42**, 882 (1965).

at 4282 Å so that  $\Delta G'_{1/2} = 785 \text{ cm}^{-1}$ . None of the observed gas systems is matched very well by a matrix band when the expected 200-Å blue shift is taken into consideration.

*EuO*. As discussed earlier, the ir spectra are anomalous in exhibiting many absorption bands in both neon and argon matrices. The behavior in the visible and uv in these two matrices is again very similar and in each case only a very intense band is observed at about 4400 Å with a number of very weak bands at longer wavelengths. The bands observed are listed in Table III. The 4400-Å band is a triplet in neon matrices.

Gatterer, *et al.*,<sup>2a</sup> list a few band heads observed in the gas phase between 5900 and 6500 Å but no assignments have been made. It appears that it would be worthwhile to examine the region near 4500 Å in the gas phase where a transition involving the ground state should occur corresponding to the very intense 4400-Å band in the matrix.

*GdO*. There is only one gas-phase emission system<sup>2a,14</sup> which has been definitely shown to terminate in the ground state. This is the system at 4615.6 Å ( $\Delta G'_{1/2} = 824.70 \text{ cm}^{-1}$ ).<sup>14</sup> The only band in our neon spectrum (see Figure 9) which can correspond to this lies at 4385 Å, which is a very large matrix shift of 1140  $\text{cm}^{-1}$ . (A large GdO ir band at 824  $\text{cm}^{-1}$  is observed for this matrix so there is no doubt of the presence of the diatomic molecule in large concentration.) However, if one does accept the 4385-Å band as a (0,0) band, then the 4246 band may be the (1,0) yielding  $\Delta G'_{1/2} = 746 \text{ cm}^{-1}$  in good agreement with 743  $\text{cm}^{-1}$  from the gas data. The (2,0) may also occur at about 4132 Å but that band is difficult to measure because of the two overlapping WO bands (see Figure 9). A gas-neon matrix shift might be as large as 500  $\text{cm}^{-1}$ , and the observed discrepancy probably indicates that the gas transition does not terminate in the lowest sublevel of the ground state of GdO.

The observed matrix bands, all rather broad, are listed in Table III.

*TbO*. Argon matrix spectra were measured between 8000 and 4000 Å, but broad bands only appeared below 6000 Å. The strongest band is at 5264 Å and a weak band at 5072 Å may be (1,0). This yields a reasonable value,  $\Delta G'_{1/2} = 719 \text{ cm}^{-1}$ , for the excited state vibrational frequency. All of the matrix bands are broad (width at half-height of 5264-Å band is  $\sim 500 \text{ cm}^{-1}$ ) and are listed in Table III. According to mass spectrometric data and our ir spectra, these electronic transitions could arise from both TbO and TbO<sub>2</sub> (see Table I). Gatterer, *et al.*,<sup>2a</sup> give emission bands for TbO between 6500 and 5200 Å but no vibrational assignments.

*DyO*. The electronic spectrum was measured between 8000 and 3500 Å in an argon matrix. An ir band was also observed at 829  $\text{cm}^{-1}$  indicating a high concentration of DyO molecules. The prominent

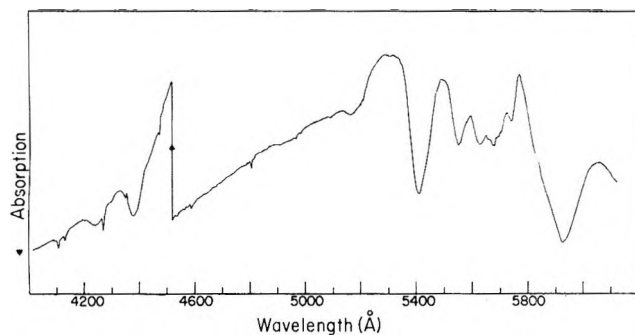


Figure 9. A portion of the absorption spectrum of GdO in a neon matrix at 4°K. The arrow indicates a change of slits.

bands are listed in Table III; all are of rounded shape. Gatterer, *et al.*,<sup>2a</sup> list bands between 6500 and 4500 Å, but the only vibrational assignment has been made by Piccardi<sup>15</sup> of a system at 5263.4 Å. There is no obvious system in the matrix which matches that. Ames, *et al.*,<sup>2c</sup> indicate that the MO/M ratio in the gas phase is about 2 in the mass spectrometer so that some of our observed bands could be atomic. There are two bands at 4649 and 4613 Å whose width is narrow and therefore might be in that category.

*HoO*. The spectra were observed between 7300 and 3300 Å in argon matrices where an intense HoO absorption band was observed in the ir. Two very strong doublets ( $\sim 700 \text{ cm}^{-1}$  wide at half-height) appear at 5582–5618 and 4968–5038 Å. Corresponding very weak bands appear at 5350 and 4767 Å which may be the (1,0) bands.  $\Delta G'_{1/2}$  values would then be 776 and 859  $\text{cm}^{-1}$ , respectively, but there is considerable uncertainty in these values because of the breadth of the bands and the difficulty in determining their peaks. Other prominent bands in the argon spectrum are listed in Table III.

Gatterer, *et al.*,<sup>2a</sup> list four gas systems but only two of them have vibrational frequencies (about 834  $\text{cm}^{-1}$ ) in the lower state near that observed in an argon matrix. These are his systems I at 5591.1 Å and II at 5319.1 Å. System I probably corresponds to our matrix system at 5582–5618, which is a doublet because of matrix sites. System II may very well be terminating in a higher lying substate of the ground electronic level which would not be populated at 4°K. The gas transition at 5319.1 Å would then not be seen in the matrix absorption spectrum. The matrix spectra suggest that there should be another system of transitions to the ground state in the gas spectrum with a (0,0) at about 4980 Å. Gatterer does not give an assignment of bands between 5070 and 4617 Å.

*ErO*. Figure 10 shows a portion of the spectrum in an argon matrix in which a large ir band was observed at 829  $\text{cm}^{-1}$ . An ir band was not observed in neon

(14) C. B. Suarez and R. Grinfeld, *J. Chem. Phys.*, **53**, 1110 (1970).

(15) G. Piccardi, *Spectrochim. Acta*, **1**, 533 (1941).

indicating that there was some difficulty with trapping in this particular case. This is puzzling since weak WO electronic transitions were observed in neon. Spectra were measured between 7300 and 3500 Å but most of the intense bands appear between 5900 and 4700 Å (see Table IV). There are both broad and sharp bands in the spectrum which could arise from a mixture of molecules and metal atoms. The mass spectrometric work<sup>2c</sup> indicates that MO/M = 2, supporting such a premise. None of the relatively sharp bands are TaO or WO.

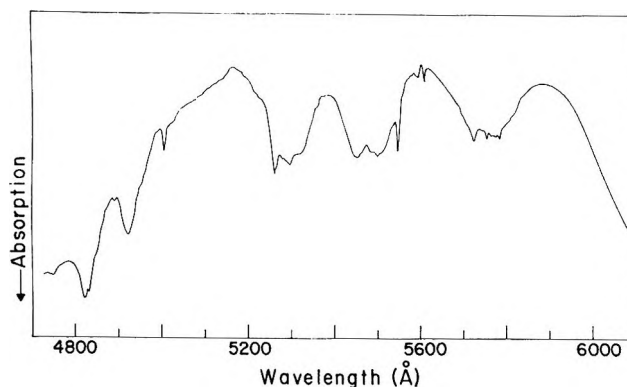


Figure 10. A portion of the absorption spectrum of ErO in an argon matrix at 4°K.

Table IV: Positions of Prominent Bands<sup>a</sup> between 8000 and 3500 Å

ErO argon, Å	TmO argon, Å	Yb argon, Å	LuO neon, Å	Lu neon, Å
5789 s	5830 m	5580 m	8116 vs	8435 m
5733 s	5477 m	5358 m	7882 vw	5507 } <sub>s</sub>
5614 w	5423 vs	5268 s	7708 w	5432 } <sub>s</sub>
5552 s	5304 s	5083 m	7100 vs	5189 m
5504 s	4859 ) <sup>w</sup>	4688 vw	6908 w	5017 m
5452 s	4829 ) <sup>w</sup>	4328 w	6764 w	4984 m
5300 s	4664 m	3900 vs	6631 m	4745 m
5264 s	4420 m	3765 w	6377 vw	4618 w
4924 s	4258 m	3628 w	5985 s	4440 m
4824 s	4193 vs		5937 ) <sup>s</sup>	4346 s
4693 ) <sup>m</sup>	4110 vs		5928 ) <sup>s</sup>	3786 w
4669 ) <sup>m</sup>	3916 s		5748 m	
4190 m	3837 s		5504 m	
4158 m	3787 m		5200 w	
3995 m	3766 m		4978 s	
3914 m	3678 vs (br)		4730 w	
3880 m	3586 m		4435 m	
3738 m	3443 m		4280 m	
3701 m	3281 w		4155 w	
3376 m	3265 w		4099 w	
	3208 m		4048 w	
	3195 m		3977 w	
	3097 w			
	3062 m			
	2986 m			
	2910 w			

<sup>a</sup> Intensities of bands are indicated by: vs, very strong; s, strong; m, medium; w, weak; vw, very weak. Line widths are indicated by: sh, sharp; br, broad.

Gatterer lists numerous emission bands between 5800 and 5000 Å, but no rotational or vibrational analysis has been done. There are no obvious correlations between matrix and gas data and no obvious progressions in the matrix spectra.

**TmO.** When the ir band of TmO at 832 cm<sup>-1</sup> appeared strongly in an argon matrix, the visible absorption spectrum was intense over the entire region and into the ultraviolet. (The matrix appeared dark red.) Decreasing the vaporization temperature to the point where bands could be observed still left an intense

absorption in the region of 3500 to 4300 Å; however, the concentration of TmO was so low that an ir band was not observed. This indicates that the electronically absorbing species is Tm atoms which according to the mass spectrometric data<sup>2c</sup> should be present in a concentration ten times that of TmO. Excitation with high-pressure mercury light produced extensive emission bands which were also very likely atomic since no vibrational progressions could be found. Prominent bands are listed in Table IV.

**Yb.** In agreement with mass spectrometry,<sup>2c</sup> any molecules vaporized are present in very small concentration since no ir bands were observed in an argon matrix. Between 8000 and 3500 Å, the only broad atomic bands observed are listed in Table IV.

**LuO.** This molecule is isoelectronic with LaO so that a comparison with the earlier matrix work<sup>16</sup> on that molecule can be made. However, the gas-phase data are in much worse condition than those for LaO since no rotational analyses are available. Gatterer, *et al.*,<sup>2a</sup> list only two (0,0) bands at 5170.1 (A) and 4661 Å (B).

As mentioned earlier, the relative positions of ir bands in neon and argon matrices are not as expected for LuO, but they all do appear in the neighborhood of 820 cm<sup>-1</sup>, as generally found for these diatomic oxides. We give here only the electronic spectrum in neon (see Figure 11) since this was the matrix in which LaO was trapped; the argon results are difficult to correlate with those in neon. Lu metal was also vaporized and the atom bands accounted for in the spectra. One atom band is shown in Figure 11 at 8435 Å. Prominent LuO and Lu bands in neon are listed in Table IV.

The two very strong bands of LuO at 8116 and 7100 Å correspond to those at 7706 and 7188 Å for LaO and are therefore to be associated with the A<sup>2</sup>Π<sub>r</sub> ← X<sup>2</sup>Σ transition. If the (1,0) transitions are the weak bands at 7708 and 6764 Å then the excited state vibrational

(16) W. Weltner, Jr., D. McLeod, Jr., and P. H. Kasai, *J. Chem. Phys.*, **46**, 3172 (1967).

**Table V:** Emission Bands of CeO<sub>2</sub> in Various Matrices at 4°K

$\nu''_1$	Argon matrix			Nitrogen matrix			Neon matrix		
	$\lambda$ , Å ± 1	$\nu$ , cm <sup>-1</sup> ± 10	$\Delta\nu$ , cm <sup>-1</sup>	$\lambda$ , Å ± 1	$\nu$ , cm <sup>-1</sup> ± 10	$\Delta\nu$ , cm <sup>-1</sup>	$\lambda$ , Å ± 2	$\nu$ , cm <sup>-1</sup> ± 15	$\Delta\nu$ , cm <sup>-1</sup>
0	5040	19,836		5191	19,259		4982	20,067	
	5070	19,718				5011	19,951		
	5101	19,599				5038	19,844		
	5129	19,492				5054	19,783		
	5161	19,371							
1	5239	19,082	754	5333	18,746		5146	19,427	
	5272	18,963	755	5342	18,714		5183	19,289	778
	5305	18,845	754	5371	18,613		5213	19,178	773
	5336	18,735	757	5379	18,586		5237	19,082	762
	5370	18,617	754	5385	18,565		5261	19,003	780
2	5455	18,327	755	5544	18,022	712	5360	18,652	775
	5490	18,210	753	5553	18,003	711	5396	18,527	752
	5524	18,098	747	5585	17,900	713	5430	18,411	767
	5559	17,984	751	5593	17,875	711	5455	18,327	755
	5596	17,865	752	5601	17,849	716			
3				5608	17,827	710			
	5679	17,604		5767	17,335	698	5589	17,887	755
	5686	17,582	745	5777	17,305	698	5627	17,767	760
	5718	17,484		5812	17,201	699	5662	17,659	752
	5725	17,462	748	5821	17,174	701	5693	17,561	766
	5758	17,362	736	5830	17,148	701			
	5796	17,248	736	5839	17,121	706			
	5930	16,859	745	6009	16,637	698	5840	17,118	769
	5938	16,836	746	6020	16,607	698	5877	17,011	766
	5971	16,743	741	6057	16,505	696	5911	16,913	746
4	5980	16,718	744	6065	16,483	691	5945	16,816	745
	6013	16,626	736	6076	16,454	694			
	6053	16,516	732	6086	16,427	694			
	6205	16,112	747	6273	15,937	700	6153	16,248	763
	6212	16,093	743	6323	15,811	694	6183	16,169	744
	6249	15,998	745						
	6257	15,978	740						
5	6292	15,889	737						
	6502	15,372	740				6448	15,504	744
	6511	15,354	739				6484	15,418	751
	6551	15,261	737						
	6561	15,237	741						
	6598	15,152	737						

frequencies are found to be  $\Delta G'_{1/2}(^2\Pi_{1/2}) \cong 650 \text{ cm}^{-1}$  and  $\Delta G'_{1/2}(^2\Pi_{3/2}) \cong 700 \text{ cm}^{-1}$ . These frequencies are rather low when compared to those for the excited states of the other rare earth oxides so that the assignment of these (1,0) bands is doubtful.

Other, relatively strong, broad bands occur at 5985, 5748, 5504, 4978, 4435, 4280, and 4099 Å as shown in Figure 11. The two gas-phase bands at 5170 and 4661 Å probably correspond to the 4978 and 4435-Å bands in neon. This is about the matrix shift expected from LaO in neon.<sup>16</sup> The (1,0) band of the 4435 Å system appears to be hidden under the 4280 Å band; this may be part of the  $C^2\Pi \leftarrow X^2\Sigma$  system appearing at 4152 Å for LaO in neon. The remaining five matrix bands are presumably (0,0) transitions of other systems.

The sharp bands at 6631 and 5928–5937 Å are reminiscent of those that grew in (at 5592 Å) during the exposure of a LaO neon matrix to tungsten light.<sup>16</sup> There

they were conjectured to arise from LaO in other sites. The LuO sharp bands do not “grow in” and the only noticeable variation is from matrix to matrix where the 5930-Å doublet varies in intensity relative to the underlying broad 5985-Å band. These distinctive sharp bands did not arise in the LuO–argon matrices, so that they may again be site effects in neon.

*Emission of CeO<sub>2</sub>.* A well outgassed sample of solid CeO<sub>2</sub> produced a matrix exhibiting no absorption bands; however, a strong yellow-green emission was observed in neon, argon, and nitrogen matrices (see Figures 12 and 13). It was always necessary to anneal the matrices in order to obtain sharp emission bands; Figure 13 indicates the effect of annealing in a nitrogen matrix. A large amount of structure, attributed to matrix sites, is evident on each of the seven bands in the Franck–Condon envelope. The bands were considerably more rounded in a neon matrix.

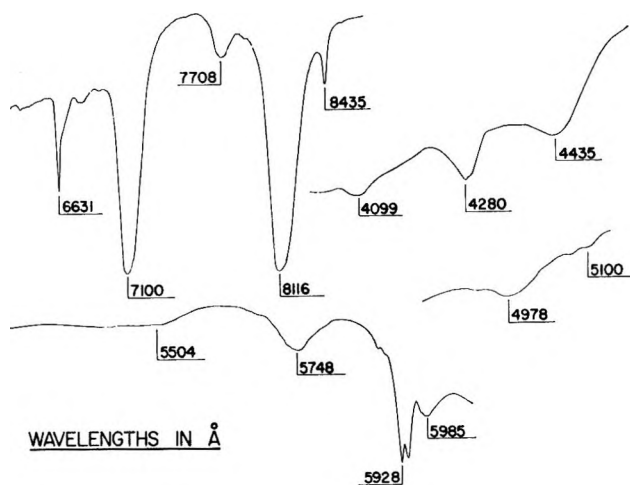


Figure 11. The absorption bands of LuO in a neon matrix at 4°K.

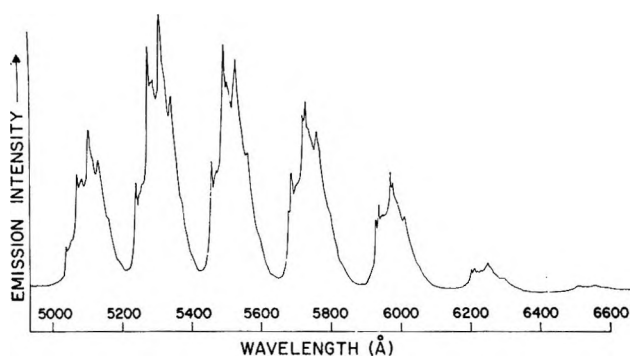


Figure 12. Emission spectrum of CeO<sub>2</sub> in an argon matrix at 4°K.

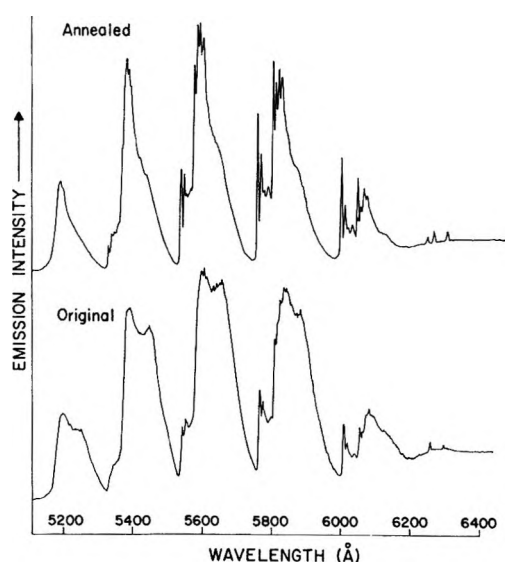


Figure 13. Emission spectra of CeO<sub>2</sub> in a nitrogen matrix at 4°K showing the effect of annealing.

The half-life of the emission from an argon matrix was found to be  $200 \pm 50$  msec, indicating that it is a highly forbidden transition. If the ground state of

CeO<sub>2</sub> is singlet this is probably a spin-forbidden triplet  $\rightarrow$  singlet transition.

The emission peaks in neon, argon, and nitrogen matrices are tabulated in Table V. The differences between band peaks indicates that there is one vibrational mode involved with  $\Delta G''_{1/2} = 770$  cm<sup>-1</sup> in neon, 755 cm<sup>-1</sup> in argon, and 715 cm<sup>-1</sup> in nitrogen. Since it is likely that the molecule is of C<sub>2v</sub> symmetry in both the ground and excited states, this frequency then corresponds to  $\nu''_1$ . These values are in satisfactory agreement with 777, 756, and 714 cm<sup>-1</sup>, respectively, observed for this vibrational mode in the ir. In a nitrogen matrix no fine structure is evident on the (0,0) band so that  $\Delta G''_{1/2}$  was estimated assuming an anharmonicity of 5 cm<sup>-1</sup> (see Table V). There is no ambiguity concerning the head of the emission system since the Franck-Condon maximum occurs near the (0,0) band. One estimates from the neon and argon spectra that the (0,0) band would lie at about 5000 Å in the gas phase.

As mentioned in the discussion of the ir spectra, isotopic labeling with <sup>18</sup>O resulted in bands due to Ce<sup>16</sup>O<sub>2</sub>, Ce<sup>18</sup>O<sub>2</sub>, and Ce<sup>16</sup>O<sup>18</sup>O. The emission from all of these molecules leads to complications in the observed spectra, but a careful analysis of the (1,0), (2,0), and (3,0) bands in argon verifies that the  $\nu''_1$  frequencies for all of these molecules are involved in the spectrum (see Table VI). The many overlapping bands and the

Table VI: Emission of Isotopically Substituted CeO<sub>2</sub> in Argon at 4°K

$\nu''$	Ce <sup>16</sup> O <sub>2</sub>		Ce <sup>18</sup> O <sub>2</sub>		Ce <sup>16</sup> O <sup>18</sup> O	
	$\nu$ , cm <sup>-1</sup>	$\Delta\nu$ , cm <sup>-1</sup>	$\nu$ , cm <sup>-1</sup>	$\Delta\nu$ , cm <sup>-1</sup>	$\nu$ , cm <sup>-1</sup>	$\Delta\nu$ , cm <sup>-1</sup>
0	19,836					
	19,718					
	19,599					
	19,492					
1	19,082	754	19,137	699	19,090	746
	18,963	755	19,013	705	18,974	748
	18,845	754	18,902	697	18,853	746
	18,735	757	18,799	693		
2	18,327	755	18,425	712	18,389	701
	18,210	753	18,305	708	18,346	744
	18,098	747			18,271	703
	17,984	751			18,231	743
					18,154	699
					18,118	735
3	17,582	745	17,731	694	17,683	706
	17,462	748	17,613	692	17,646	743
	17,362	736				700
	17,248	736				

fact that the Ce<sup>18</sup>O<sub>2</sub> frequency at about 700 cm<sup>-1</sup> is essentially the same as one of the Ce<sup>16</sup>O<sup>18</sup>O frequencies makes the analysis difficult.

## Discussion

Except for the case of europium oxide, all of the above infrared results are those expected from mass spectrometric work<sup>2b-e</sup> on these compounds. That is, the monoxides are observed in each case except Yb and the dioxides are also observed for CeO<sub>2</sub>, PrO<sub>2</sub>, and TbO<sub>2</sub>. Small amounts of NdO<sub>2</sub> have recently been detected<sup>17</sup> but only if the sample was in an oxidizing atmosphere brought about by the addition of O<sub>2</sub>.

For the monoxides, there is very little difference among the frequencies. If one excludes the assignment of EuO as being uncertain due to the complexity of the spectrum, the total spread in frequencies (in argon) is from 832 cm<sup>-1</sup> for TmO to 808 cm<sup>-1</sup> for CeO. This is in distinct contrast to the analogous first-row transition metal oxides where the spread in gas-phase frequencies is from 1012 cm<sup>-1</sup> for VO to 628 cm<sup>-1</sup> for CuO.<sup>18</sup> Also the observed neon matrix values for the series HfO, TaO, and WO are 974,<sup>19</sup> 1028,<sup>13</sup> and 1055 cm<sup>-1</sup>.<sup>4</sup> This difference between the trends in stretching frequencies of the rare earth monoxides and transition metal oxides is undoubtedly due to the fact that the d electrons of the transition metal atoms are in more diffuse orbitals and are more involved in the bonding than the analogous f electrons of the rare earth atoms.

There appears to be no relationship between the observed infrared stretching frequencies for the rare earth monoxides reported here and the dissociation energies.<sup>2c,20</sup> However, this effect is not uncommon for the transition metal monoxides either. For example, the dissociation energies of HfO, TaO, and WO are 183, 194, and 155 kcal/mol, whereas their respective stretching frequencies are 974, 1020, and 1055 cm<sup>-1</sup> in a neon matrix.

It now seems clear that the general rule<sup>21</sup> that  $\nu_3$  is larger than  $\nu_1$  in triatomic molecules applies only to light molecules. While in relatively heavy SrF<sub>2</sub> and BaF<sub>2</sub><sup>22</sup> this rule seems still to apply, in TaO<sub>2</sub>,<sup>13</sup> ThO<sub>2</sub>, and ZrO<sub>2</sub>,<sup>23</sup> an assignment of  $\nu_1 > \nu_3$  has been made. In all of these cases the assignments were based upon either intensity relationships or isotopic shifts. More definitive evidence can be provided by emission spectra where  $\nu''_1$  can be directly observed. In the case of Ce<sup>16</sup>O<sub>2</sub>, the emission indicates  $\nu''_1 = 756$  cm<sup>-1</sup> in argon so that  $\nu_1 > \nu_3 = 736$  cm<sup>-1</sup>, but this is reversed in Ce<sup>18</sup>O<sub>2</sub> where  $\nu_3 = 707$  cm<sup>-1</sup>  $>$   $\nu_1 = 700$  cm<sup>-1</sup>. It is possible, of course, that the lower electronic state in emission is not the ground state, but the agreement between the ir and optical frequency for Ce<sup>16</sup>O<sub>2</sub> would seem to preclude that here. It may be noted that the choice of  $\nu_1 > \nu_3$ , or *vice versa*, has very little effect upon the calculated value of the metal-oxygen stretching force constant, regardless of the apex angle in the molecule.

The translation of matrix electronic spectra into gas-phase data has often been straightforward: witness TiO<sup>19</sup> or TaO.<sup>13</sup> Unfortunately, the shifts are much larger for LaO<sup>16</sup> and also appear to be large for the rare earth oxides. The (0,0) bands for LaO in neon are about  $400 \pm 100$  cm<sup>-1</sup> higher in energy than in the gas phase, and if ScO may be used as evidence, argon matrix data may actually be more useful for the prediction of the positions of electronic (but not vibrational) transitions in the gas phase. This seems to be justified by some of our observations on the rare earth oxides. For example, in HoO, the (0,0) band of system I at 5591.1 Å in the gas phase appears to shift very little in an argon matrix where it is a strong, broad doublet at 5582-5618 Å. Also, for NdO where neon and argon data have been obtained, the positions of the two strong bands shift by  $480 \pm 10$  cm<sup>-1</sup> toward lower energy in the heavier matrix, thereby probably just about canceling the predictable blue shift when the gas molecule is placed in a solid neon environment. It is on the basis of these approximate conclusions that we have tried, in the earlier discussions of individual molecules, to predict the positions of (0,0) bands in the gas.

Because of the large spin-orbit coupling in these molecules the multiplets in the ground electronic state are widely separated. Of course, transitions at 4°K take place from the lowest substate, but the gas emission spectra do not necessarily terminate in that state; indeed, matrix spectra often indicate that this is not the case. The transitions from various substates of the ground state vary widely in energy (see, for example, the CeO gas-phase absorption data<sup>5</sup>) so that matrix spectra, in spite of their shift, should be of aid in determining which transition is from the lowest substate.

The most perplexing molecule studied here was EuO where there was a large discrepancy between the matrix ir spectra and the expectations from the mass spectral data.<sup>2c</sup>

*Acknowledgment.* The authors are grateful to D. McLeod, Jr., for his spectra of Lu and LuO in matrices.

(17) H. G. Staley and J. H. Norman, *Int. J. Mass Spectrom. Ion Phys.*, **2**, 35 (1969).

(18) C. J. Cheetham and R. F. Barrow, *Advan. High Temp. Chem.*, **1**, 7 (1967).

(19) W. Weltner, Jr., and D. McLeod, Jr., *J. Phys. Chem.*, **69**, 3488 (1965).

(20) J. Drowart and P. Goldfinger, *Angew. Chem., Int. Ed. Engl.*, **6**, 581 (1967).

(21) See Table II-5 and II-7, K. Nakamoto, "Infrared Spectra of Inorganic and Coordination Compounds," Wiley, New York, N. Y., 1963.

(22) V. Calder, D. E. Mann, K. S. Seshadri, M. Allavena, and D. White, *J. Chem. Phys.*, **51**, 2093 (1969).

(23) M. J. Linevsky, "Proceedings of the Third Meeting of the Interagency Chemical Rocket Propulsion Group on Thermochemistry, El Segundo, California, 1965," Vol. 1, Chemical Propulsion Information Agency, Silver Spring, Md., p 71.

# The Influence of Thermal Pretreatment on the Infrared Spectrum of Carbon Dioxide Adsorbed on Alumina

by N. D. Parkyns

Gas Council, London Research Station, Michael Road, London, S.W.6., Great Britain (Received October 30, 1970)

Publication costs assisted by the Gas Council (London, England)

The effect of heating different aluminas from 400 to 1000° on the infrared spectrum of adsorbed carbon dioxide has been investigated and shown to be the major cause of discrepancies of data previously published on this system. The aluminas used were almost entirely dehydroxylated by heating at 800°. As a result, the bicarbonate bands, which appear when carbon dioxide is added after lower temperature treatments, do not appear, but are replaced by uncoordinated, uni- and bidentate carbonate ion bands. Other bands, attributed to "organic-type" carbonate species, are affected to a far lesser extent.

## Introduction

Recently, four papers dealing with the infrared spectra of carbon dioxide adsorbed on alumina have appeared.<sup>1-4</sup> When these are considered together with earlier studies,<sup>5-7</sup> certain discrepancies and mutually contradictory features are observed. Table I shows the main spectra features which appear at pressures of about 1-2 Torr, the degassing conditions used, and the phase of the alumina under study.

Table I gives only an outline of the observed spectra. When the conditions of adsorption (CO<sub>2</sub> pressure a few Torr, adsorption temperature 20-25°) were departed from, new bands appeared in several instances. In addition, bands at 2350-2370 cm<sup>-1</sup> were also observed in all cases: there is general agreement among the authors that these are due to some form of physically adsorbed carbon dioxide. Without making detailed comparisons between the spectra, we can separate them into two or three main classes.

(a) Rea and Lindquist,<sup>7</sup> Fink,<sup>4</sup> Peri,<sup>6</sup> and Parkyns,<sup>3</sup> all agree in finding a key band at 3610 ± 5 cm<sup>-1</sup> (2667 cm<sup>-1</sup> for deuterated surfaces) which is ascribed to the hydroxyl stretching mode of a surface bicarbonate group. Parkyns further showed that the sharp and intense bands at 1640, 1480, and 1232 cm<sup>-1</sup> were all different modes of the bicarbonate species.

(b) As a rule, two or three bands of variable intensity are found between 1740 and 1870 cm<sup>-1</sup> but assignments which have been made to particular species are much less certain than for the bicarbonate bands. Neither Gregg and Ramsay<sup>1</sup> nor Yakerson, *et al.*,<sup>2</sup> observed bands in this region.

(c) Gregg and Ramsay observed no bicarbonate bands at all but described their spectra in terms of uncoordinated and bidentate carbonate ions.

The purpose of the present paper is to show how the nature of the spectra of adsorbed carbon dioxide on alumina is influenced by increasing the degassing tem-

perature prior to adsorption and to see whether these results can be used to reconcile the observed differences in the spectra hitherto published.

## Experimental Section

The spectroscopic and other apparatus were as previously described.<sup>3,8</sup> Alumina samples used were: (A) A very pure alumina, made by P. Spence and Sons, Widnes, England, described as "Gibbsite-rich." This was similar to the material used by Gregg and Ramsay.<sup>1</sup> After calcination in air at 600° before use (to remove organic matter) it was in the  $\chi$  phase. The BET surface area as determined by the manufacturers was 420 m<sup>2</sup>/g after heating at 400°. (B) Alumina, as above, which had been heated for 2 hr at 1000° *in vacuo* and then allowed to rehydrate by exposure to the air for a few weeks. After the conclusion of experiments, which entailed a final further heating to 1000°, the surface area was 122 m<sup>2</sup>/g and a mixture of  $\delta$ -,  $\chi$ -,  $\theta$ -, and  $\kappa$ -alumina was found by X-ray diffraction. (C) Alumina, type "C" from Degussa (Germany) was as described previously.<sup>8</sup> The surface area, after degassing at room temperature, was 96 m<sup>2</sup>/g, but after 2 hr evacuation at 900° rose to 103 m<sup>2</sup>/g. It was found to be in the  $\gamma$  phase. The three types of sample were activated by stepwise heating *in vacuo* for 2 hr, starting at 400°. The carbon dioxide was added to a pressure

(1) S. J. Gregg and J. D. F. Ramsay, *J. Phys. Chem.*, **73**, 1243 (1969).

(2) V. I. Yakerson, L. I. Lafer, V. Ya. Danyushevskii, and A. M. Rubenstein, *Izv. Akad. Nauk SSSR Ser. Khim.*, **19**, (1969).

(3) N. D. Parkyns, *J. Chem. Soc. A*, 410 (1969).

(4) P. Fink, *Z. Chem.*, **7**, 324 (1967).

(5) L. H. Little and C. H. Amberg, *Can. J. Chem.*, **40**, 1997 (1962).

(6) J. B. Peri, *J. Phys. Chem.*, **70**, 3168 (1966).

(7) D. G. Rea and R. H. Lindquist, paper presented to the 136th National Meeting of the American Chemical Society, Atlantic City, N. J., Sept 1959.

(8) N. D. Parkyns, *J. Chem. Soc. A*, 1910 (1967).

Table I: Infrared Spectra of Carbon Dioxide on Alumina

Ref	Degassing temp and phase of Al <sub>2</sub> O <sub>3</sub> , °C	Adsorption bands and intensities					
2	450 (γ) <sup>a</sup>	2650 (m)		1645 (m), 1600 (w)	1440 (s), 1370 (w)	1230 (m)	
3	400 (γ + χ)	3605 (m)	1820 and 1780 (m)	1640 (s)	1480 (s)	1232 (s)	1180 (m)
3	400 (γ + χ) <sup>a</sup>	2666	1820 and 1780	1615	1475	<1000	1180
1	1000 (κ)			1652 (s)	1460 (s)	1234 (m)	
4	500 (γ)	3615 (m)	1790 (m)	1645 (s)	1490 (s)	1240 (m)	1200 (m)
5	(γ)		1750	1635	1500	1235	
6	800 (γ)	3610	1870–1800	1650 (s)	"Others in this region"		
7	b (γ)	3610 (m)	1825 and 1790 (m)	1639 (s)	1490 (s)	1236 (m)	1210 (m)
	c (γ)		1856 (m)	1652 (m)	1525 (m), 1460 (m)		1210 (m)

<sup>a</sup> Deuterated surface. Lindquist and Rea also obtained results on deuterated surface which for the sake of brevity are not given here. <sup>b</sup> "Alkaline" surface, temperature of degassing not stated. <sup>c</sup> "Low alkaline" surface, obtained by heating in CO<sub>2</sub>.

of about 2 Torr and the spectrum was taken. After evacuation of the sample for about 1 hr, the spectrum was rerun. The activation temperature was then raised 200° until the maximum of 1000° was reached, this being the practical limit of the furnace used: carbon dioxide was added as described above after each period of heating.

The spectra published in this paper were obtained by digitizing the wavelength-transmittance curves obtained from the spectrometer with a D-Mac Curve Digitizer. The digitized spectrum was fed into an IBM 1130 computer and converted to the wave number-absorbance presentation by a suitable program (written by Mrs. B. J. Gillett of this laboratory). The spectrum of the alumina after evacuation, but before addition of carbon dioxide, was used as the reference  $I_0$  value: absorbance values were obtained at a given frequency by taking the logarithm of the value of  $I$ , obtained after addition of carbon dioxide, divided by the corresponding value of  $I_0$ . The curves were plotted automatically on a Benson-Lehner plotter. The whole process introduced a certain amount of noise which was not present on the original spectra: it did, however, reveal features in the spectrum which were otherwise obscured by alumina bands, notably at 1200–1400 cm<sup>-1</sup>.

## Results

*Surface Groups of Aluminas.* Peri<sup>9</sup> has described in detail the effect of increasing temperature on the infrared spectrum of alumina aerogel, in particular, on that of the hydroxyl groups. Alumina A showed progressive dehydroxylation on heating, no hydroxyl groups being detectable after heating at 800°; aerogels still have appreciable numbers present after the same treatment. The limit of detection was governed by lack of balance between the beams of the spectrometer, due to water vapor, in this absorption region (3800–3600 cm<sup>-1</sup>). This was about ±0.5% transmittance, corresponding to an absorbance of 0.005. Comparison

with the peak absorbance of the hydroxyl groups before the heat treatment showed that this limit of detection was equivalent to <1% of the initial concentration.

The concentration of hydroxyl groups on samples B and C was similar after heating both at 400 and at 600°, *i.e.*, about 33% of that on sample A after similar treatment. As before, heating to 800° was sufficient to remove all spectroscopic traces of the hydroxyl groups.

The strong sharp band at 1370 cm<sup>-1</sup> which seems characteristic of transition-phase aluminas<sup>3</sup> was irreversibly removed by heating at 1000° and was replaced by a very broad band at about the same frequency.

*Band Due to Physically Adsorbed Carbon Dioxide.* The absorption band near the  $\nu_3$  vibration of gaseous carbon dioxide (2349 cm<sup>-1</sup>) has been generally attributed to physically adsorbed gas. An unusual feature is the increase in frequency which occurs on adsorption, particularly on samples which have been heated to 600° or more. Peri<sup>6</sup> has discussed the nature of adsorption sites ( $\alpha$  sites) responsible for this increase (about 21 cm<sup>-1</sup>): his observations have been generally confirmed although the extent of the increase is not usually so great: Gregg and Ramsay<sup>1</sup> as well as Fink<sup>4</sup> give 2365 cm<sup>-1</sup> for the band in question. In the present work, the Spence alumina (A), which had not previously been heated to 600°, showed a maximum at 2346 cm<sup>-1</sup> after evacuation at 400°; this increased to 2362 ± 2 cm<sup>-1</sup> after evacuation at 600° and thereafter remained constant, all experiments being carried out at a final equilibrium pressure of about 2 Torr.

In an experiment to see whether the equilibrium pressure had a marked effect on the frequency, a sample of alumina C was heated to 800°. On addition of the carbon dioxide, the absorption frequency declined from 2367 cm<sup>-1</sup> at 0.12 Torr final pressure (absorbance 0.04) to 2362 cm<sup>-1</sup> at 1.23 Torr ( $A = 0.20$ ) and finally 2356 cm<sup>-1</sup> at 36.1 Torr ( $A = 0.38$ ).

(9) J. B. Peri, *J. Phys. Chem.*, **69**, 211 (1965).

The effect of the degassing temperature on the intensity of the band of adsorbed  $\text{CO}_2$  is shown in Table II. In all cases, the intensity rises to a maximum after heating at 600–800°. All samples were of the same thickness (25 mg/cm<sup>2</sup>).

**Table II:** Absorbance of Physically Adsorbed Carbon Dioxide Band after Heating Alumina to the Temperature Shown

Sample	Temperature of degassing, °C				Equilibrium pressure, Torr
	400	600	800	1000	
A	0.13	0.34	0.33	0.14	1.95 ± 0.05
B	0.07	0.17	0.26	0.20	2.05 ± 0.08
C	0.06	0.18	0.18	0.09	2.22 ± 0.02

*Absorption Bands Due to Chemisorbed Carbonate and Bicarbonate Groups.* Samples which showed absorption bands of surface hydroxyl groups, *i.e.*, those heated only to 400 and 600°, gave the characteristic bands of the bicarbonate group (3605, 1642, 1480, and 1236 cm<sup>-1</sup>) on addition of  $\text{CO}_2$  (Figures 1 and 2). This behavior is in accordance with the previous work of Parkyns<sup>3</sup> and Fink<sup>4</sup> for samples where the maximum outgassing temperature was 500°.

In addition, a small band appeared at 1455 cm<sup>-1</sup> for samples B and C at temperatures of 600° and above. In sample A it appeared after heating at 400° but not at 600° but then reappeared at 800 and 1000°. The band was broad in all cases. It is probably to be assigned to the vibration of the uncoordinated carbonate ion.<sup>10</sup>

When all hydroxyl groups are removed from the aluminas, by heating to 800° or above, the character of the spectra obtained on addition of carbon dioxide is completely altered. No bicarbonate bands are observed (with the possible exception of a very weak one at 1236 cm<sup>-1</sup>) but instead a rather broad band central at 1660 ± 10 cm<sup>-1</sup> appears, together with a weaker band at 1530 ± 10 cm<sup>-1</sup> and another between 1360 and 1406 cm<sup>-1</sup> (Figure 1). These bands appear for all samples, the intensity in the case of alumina A being about twice that of alumina B and C: that of the latter aluminas is about the same. Because the bands are all broad and have much lower absorbances than the bicarbonate bands, it is difficult to be precise about relative intensities. The position of the bands is slightly dependent on the evacuation temperature.

The variation in intensity of these bands with pressure of  $\text{CO}_2$  added was investigated for a sample of alumina C, previously heated to 800°. The intensity of all bands (Figure 3) approximately doubles when the pressure increases from 0.12 Torr to a maximum of 36.1 Torr. At higher pressures, small broad bands at 1235 and 1270 cm<sup>-1</sup> become more evident.

It is relatively easy to distinguish between the bicar-

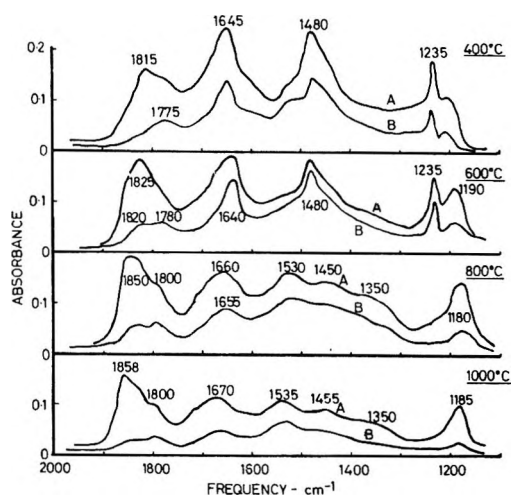


Figure 1. Spectrum of carbon dioxide adsorbed on alumina B after evacuation at 400, 600, 800, and 1000°, respectively: A, after addition of 2.0 Torr of carbon dioxide; B, after evacuation to 10<sup>-5</sup> Torr at room temperature.

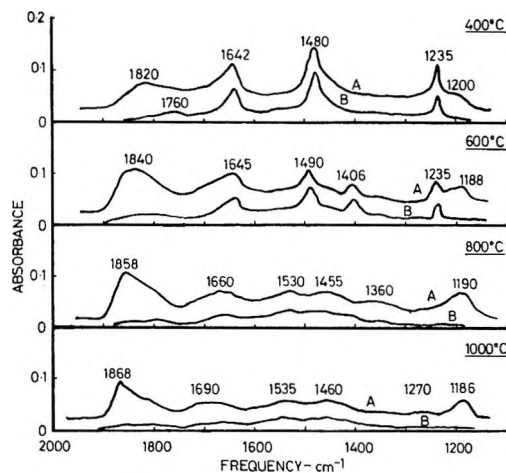


Figure 2. Spectrum of carbon dioxide adsorbed on alumina C after evacuation at 400, 600, 800, and 1000°, respectively: A, after addition of 2.0 Torr of carbon dioxide; B, after evacuation to 10<sup>-5</sup> Torr at room temperature.

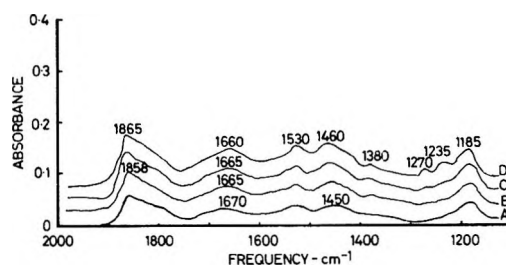


Figure 3. Spectrum of carbon dioxide adsorbed on alumina C after heating at 800°: A, final pressure 0.12 Torr; B, final pressure 1.23 Torr; C, final pressure 9.84 Torr; D, final pressure 36.1 Torr.

(10) K. Nakamoto, "IR Spectra of Inorganic and Co-ordination Compounds," Wiley, New York, N. Y., 1963.

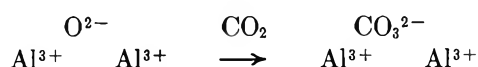
bonate bands and the others because the former are much sharper: in cases where the two types appear simultaneously (see Figure 1C), the sharp bicarbonate band at 1640 cm<sup>-1</sup> has a "tail" due to the broader band at 1650 cm<sup>-1</sup>.

*Bands in the 1800-cm<sup>-1</sup> Region.* The absorption bands in this region are similar to those found in earlier work, where their assignments were discussed at length.<sup>3</sup> At least two bands are found; the first at higher frequency increasing from 1820 cm<sup>-1</sup> (400° degas) to 1868 cm<sup>-1</sup> (1000° degas) (Figure 2); the second, which generally appears as an inflection on the first, appearing at 1800–1820 cm<sup>-1</sup>. On evacuation of the system at room temperature a small band remains at 1750–1790 cm<sup>-1</sup>. The intensity of this group of bands increases as the temperature of sample pretreatment is raised and behaves quite independently of the carbonate and bicarbonate groups. Also, as in previous work, a rather broad band appears at 1180–1200 cm<sup>-1</sup>, whose intensity correlates fairly well with that of the 1800-cm<sup>-1</sup> bands. This correlation is confirmed by the results of Fink<sup>4</sup> and Rea and Lindquist.<sup>7</sup>

## Discussion

*Spectra of Adsorbed Carbon Dioxide.* The results presented here show that the character of the spectrum of carbon dioxide adsorbed on alumina is radically changed by pretreatment at high temperatures. The similarity of the results for aluminas C (a  $\gamma$ -phase structure) and B (a mixture of transition phases) shows that the crystal structure has only a limited influence, if any, on the spectrum. The most noticeable effect of increasing temperature is on the hydroxyl groups. Heating to 800° removes the hydroxyl groups completely from all the samples used (although Peri<sup>6,9</sup> showed that some still remained on aerogel samples at this temperature) and naturally, when carbon dioxide is added, no bicarbonate groups are formed (Figure 1C and D). Both Rea and Lindquist<sup>7</sup> and Parkyns<sup>3</sup> observed that only the groups of highest frequency interacted with adsorbed carbon dioxide to form bicarbonate groups. Rea and Lindquist found that they could remove the high-frequency surface hydroxyl groups selectively, by heating their alumina samples in carbon dioxide at 500–600°. After this treatment they observed no bands due to bicarbonate groups on addition of CO<sub>2</sub> (see Table I results for "low alkaline" surface).

At the same time, as the concentration of bicarbonate groups is reduced by removing the active hydroxyl groups, we see that a band (assigned to free carbonate ions) appears at 1445 cm<sup>-1</sup>. Presumably, this is produced by a reaction of the carbon dioxide molecule with a surface oxide ion.



The appearance of the free, uncoordinated carbonate ion, argues a high degree of local symmetry so that such adsorption sites probably occur in regions where a high degree of surface dehydration has occurred, and where the crystal surface is flat and free of anion or cation defects.

Gregg and Ramsay<sup>1</sup> found, in addition to the carbonate ion band at 1460 cm<sup>-1</sup>, an equally strong band at 1652 cm<sup>-1</sup> and another at 1234 cm<sup>-1</sup> which they ascribed to the bidentate carbonate ion. The development of the 1655–1670-cm<sup>-1</sup> band found in our spectra, is seen in Figure 1 to begin at 600° and increase to a maximum at 800°. The corresponding low-frequency band (1235 cm<sup>-1</sup>) is not so definite because of the possibility of confusion with the bicarbonate band at 1235 cm<sup>-1</sup>. However, adsorption of CO<sub>2</sub> at higher pressures (Figure 3) shows that the band, although much weaker than that at 1660 cm<sup>-1</sup>, is fairly definite. Furthermore, another band is observed at 1270 cm<sup>-1</sup>. In addition to the bidentate ion, Figure 1 shows evidence of bands belonging to the unidentate ion at 1530 and 1350 cm<sup>-1</sup>. Unfortunately, all these carbonate ion bands are very broad and the overlap makes it difficult to be precise about the exact band maxima. Examination of the spectra in Gregg and Ramsay's paper shows that there are also indications of the bands due to the unidentate ion. Nakamoto<sup>10</sup> gives examples of unidentate ions having bands at 1360 (s) and 1460 (m) ( $\nu_1$  and  $\nu_6$ , respectively) and of a bidentate ion with bands at 1590 (vs) and 1320 cm<sup>-1</sup> (m) ( $\nu_1$  and  $\nu_5$ ). The agreement with the position of the bands, although not good, is at least good enough to make the suggested assignments plausible.

Formation of uni- and bidentate carbonate ions is most likely to occur at positions where an oxide ion is exposed, e.g., "steps" in the crystal faces; the degree of local crystal coordination determines which type of bonding occurs.

The behavior of the bands at around 1800 cm<sup>-1</sup> (and 1180 cm<sup>-1</sup>) is quite different from, and independent of, that of the carbonate bands. The intensity of the former increases progressively with the temperature of pretreatment, but that of the latter tends to fall. The correlation of the 1800-cm<sup>-1</sup> bands with that at about 1180 cm<sup>-1</sup>, observed previously,<sup>3</sup> was confirmed by the present work, although it is not possible to be quite certain which of the two (or possibly three bands) at 1800–1870 cm<sup>-1</sup> is involved. In view of the relative broadness of the band at 1180 cm<sup>-1</sup>, whose position does, in fact, vary between 1170 and 1200 cm<sup>-1</sup>, it may be possible that this band consists of two symmetrical overlapping ones. Whether this is so or not, the assignment given previously<sup>3</sup> of the "organic" carbonate type structure fits in better with the observed frequencies rather than that of Fink,<sup>4</sup> who gives a sort of bidentate carbonate structure as being responsible for bands at 1785 and 1200 cm<sup>-1</sup>. These bands fall rather outside

the limits observed either for uni- or bidentate carbonate ions; the bands observed between 1350 and 1650  $\text{cm}^{-1}$  in the present work correspond somewhat better to this type of bonding.

The question of the number of adsorption sites is raised by the intensity of the band due to adsorbed carbon dioxide at 2350–2370  $\text{cm}^{-1}$ . In all the samples investigated the intensity of this band for a given pressure, increased to a fairly broad maximum between 600 and 800° and then fell off again fairly sharply after heating to 1000° (Table II). At the highest pressures used in this work (36.1 Torr, Figure 2)  $p/p_0 < 10^{-5}$ ; at 2 Torr it is  $< 10^{-6}$ , so that physical adsorption on the BET model is more or less ruled out. Furthermore, alumina C which is nonmicroporous<sup>11</sup> gives a band of comparable intensity to that on alumina A which is microporous. Thus, enhancement of adsorption by microporosity is not the sole cause. Previous explanations have included the presence of specially active sites ( $\alpha$  sites)<sup>6</sup> and of dipole interaction (carbon monoxide on metal oxides).<sup>5,12</sup> Both have had to take into account the raising of the stretching frequency of the adsorbed  $\text{CO}_2$  and  $\text{CO}$ , respectively. Pink and his coworkers<sup>13</sup> have reported that heating alumina produces sites which chemisorb anthracene and in the presence of oxygen give a strong esr signal. The maximum signal occurs after heating to 900° after which temperature intensity falls off. Thus, there is at least a first approximation to the behavior of the intensity of the band due to adsorbed carbon dioxide and it is possible that the same or similar sites are active in both cases.

The surface area of the very pure alumina used (sample A) falls steadily from the initial value of 400  $\text{m}^2/\text{g}$  to 122  $\text{m}^2/\text{g}$  after heating to 1000° (sample B). We might suppose that this would reduce the number of sites available for adsorption by carbon dioxide, but when we look at sample C, which shows no reduction in BET surface area and yet gives the same sort of behavior on adding  $\text{CO}_2$  as samples A and B, we realize that there is no obvious correlation between surface area and band intensity. There is an analogy in fact with the results of Ross, *et al.*,<sup>14</sup> for the decomposition of ethanol on alumina. They found that although the BET surface area of alumina fell when it was heated, the ratio of catalytic activity to surface area increased. Specifically, there was a particularly marked increase after heating to 800°. The relatively limited results presented in this present paper do not justify extended discussion on the topic of specific physical adsorption of carbon dioxide but enough has been said to show that they do relate fairly well with the findings of workers using other techniques.

*Nature of Sites for Chemisorption of Carbon Dioxide.* Practically all the structures that have been proposed for the chemisorbed species of adsorbed carbon dioxide on alumina have involved surface hydroxyl and oxide

groups. Removal of the active hydroxyl groups, by heating *in vacuo* or at lower temperatures in carbon dioxide gas,<sup>7</sup> removes the bicarbonate species. The mechanism of the formation of the surface bicarbonate groups has been discussed previously.<sup>3</sup> The formation of bicarbonate groups takes precedence over that of carbonate groups whether the latter are uni- or bidentate or uncoordinated. Obviously, as dehydroxylation proceeds, some areas of the surface appear where hydroxyl groups have been completely removed, leading to carbonate ion formation; at the same time bicarbonate ions are formed on areas where active hydroxyl groups remain.

The nature of the sites for the formation of carbonate-type species can now be considered. Stoichiometry demands that an oxide ion be involved in forming  $\text{CO}_3^{2-}$  from  $\text{CO}_2$ , but the question is, are all surface oxide ions equally active as adsorption sites? Gregg and Ramsay<sup>1</sup> state that the adsorption of  $\text{CO}_2$  on alumina at 150° (following degassing at 1000°) and at 12 Torr is just under  $15 \times 10^{-3} \text{ cm}^3 \text{ m}^{-2}$ . This corresponds to a figure of  $40 \times 10^{12}$  molecules/ $\text{cm}^2$  of surface or 0.4 molecules/100  $\text{Å}^2$ .  $20 \times 10^{12}$  molecules  $\text{cm}^{-2}$  (0.2/100  $\text{Å}^2$ ) remained on desorption, corresponding to carbon dioxide strongly held by chemisorption. The quantity ( $40 \times 10^{12}$ ) may contain a contribution from carbon dioxide molecules physically adsorbed. In addition, Figure 2 shows that the concentration of carbonate species on the surface increases with pressure, at least up to 36 Torr, at room temperature. Thus, these quantities must be taken as order of magnitude ones only, but it is instructive to compare them with the 6.25 oxide ions/100  $\text{Å}^2$  assumed by Peri for the 100 surface of  $\gamma$  alumina. The van der Waals radius of a free carbonate ion is 2.4  $\text{Å}$ , corresponding to an area of 14  $\text{Å}^2$  so that the steric factor would, in any case, limit the number of molecules adsorbed to, say, 6/100  $\text{Å}^2$ . This is still at least 10 times as high as the figure given by Gregg and Ramsay, indicating that only 1 in 10 oxide ions is in fact active for carbon dioxide chemisorption.

Finally, it is relevant to note that treatment of alumina aerogels with fluoride ions completely inhibits the chemisorption of carbon dioxide.<sup>15</sup> Molecular adsorption remains relatively unaffected except for an increased shift of the  $\nu_3$  band up to 2387  $\text{cm}^{-1}$  and the appearance of the normally forbidden  $\nu_1$  band at 1380  $\text{cm}^{-1}$ . Peri proposed that adsorption sites which are normally active on unfluorided alumina react with fluoride ions as

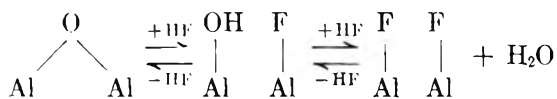
(11) D. A. Payne and K. S. W. Sing, *Chem Ind. (London)*, 918 (1969).

(12) D. A. Seanor and C. H. Amberg, *J. Chem. Phys.*, **42**, 2967 (1965); *Proc. Int. Congr. Catal. 3rd*, 540 (1965).

(13) B. D. Flockhart, J. A. N. Scott, and R. C. Pink, *Trans. Faraday Soc.*, **62**, 730 (1966).

(14) D. E. R. Bennett and R. A. Ross, *J. Chem. Soc. A*, 1524 (1968).

(15) J. B. Peri, *J. Phys. Chem.*, **72**, 2917 (1968).



Hydroxyl groups can be removed either by heating or by direct reaction with HF, while the oxide ions (perhaps more strictly Al-O-Al sites) react to give fluorided alumina cations. The  $\alpha$  sites are not removed by the treatment.

### Conclusions

1. The main discrepancies between the observed spectra of carbon dioxide adsorbed on alumina can be accounted for by the effect on the surface of different degrees of heat pretreatment.

For relatively low "activation" temperatures (<500°) a relatively large hydroxyl concentration remains on the surface and the main chemisorption is due to bicarbonate groups, having absorption bands at 3605, 1640, 1480, and 1235 cm<sup>-1</sup>. These bands are strong, sharp, and well defined. There are also some ill-defined bands in the 1800-cm<sup>-1</sup> region.

At intermediate temperatures (500–700°), more of the active (high frequency) hydroxyl groups are removed and the intensity of the bicarbonate groups falls. On the other hand, rather poorly defined bands due to carbonate ions in varying degrees of coordination appear at 1200–1650 cm<sup>-1</sup>. The intensity and absorption frequency of the bands at around 1800 cm<sup>-1</sup> rises and a broad band is observed at ~1180 cm<sup>-1</sup> which is associated with at least one of the former.

At high temperatures (800–1000°), hydroxyl groups are more or less completely removed (<1% of original intensity) and bicarbonate groups are no longer observed. The carbonate bands are no longer obscured

by the bicarbonate ones although their intensity is no higher than after thermal activation at lower temperatures. Tentative assignments are uncoordinated carbonate ion, 1445–1470 cm<sup>-1</sup>, unidentate, 1530 and 1370 cm<sup>-1</sup>, and bidentate, 1660 and 1230 cm<sup>-1</sup> (or 1270 cm<sup>-1</sup>). These bands are very broad and overlap considerably. Bands at 1800 cm<sup>-1</sup> increase to a maximum of intensity after 800° activation and thereafter decline a little.

2. A large band in the region 2340–2370 cm<sup>-1</sup> is attributed, as in previous work, to physically adsorbed, nondissociated carbon dioxide molecules. The intensity of this band is strongly pressure dependent but for a given pressure tends to rise with activation temperature to a maximum between 600 and 800° and falls again at 1000°. The interaction between the alumina surface and the adsorbed carbon dioxide is probably specific and may involve more than one type of site, as shown by apparent frequency shift on higher temperature activation.

3. The effect of the solid phase of the alumina on the observed spectra is secondary at most;  $\gamma^-$ ,  $\chi^-$ , and a mixture of  $\delta^-$ ,  $\chi^-$ ,  $\theta^-$ , and  $\kappa^-$  aluminas all behaving in much the same way.

Much further and more detailed work remains to be done on the alumina-CO<sub>2</sub> system. In this work, at least seven species of adsorbed carbon dioxide have been detected from their characteristic infrared absorption bands and there may be even more. Thus, great caution should be observed when interpreting results on this system obtained by other techniques.

*Acknowledgments.* I wish to thank Mrs. B. J. Gillett for experimental assistance and for processing spectral data on the computer. I am grateful to the Gas Council for permission to publish this paper.

## Dielectric Absorption of Adsorbed Sulfur Dioxide in the Microwave Region

by Tsvia Ron and M. Folman\*

Department of Chemistry, Technion-Israel Institute of Technology, Haifa, Israel (Received September 21, 1970)

Publication costs borne completely by The Journal of Physical Chemistry

Dielectric absorptions in the microwave region at two different frequencies (23,500 and 3000 MHz) were studied on SO<sub>2</sub> adsorbed on porous Vycor glass. Using a solution-like model for the composite adsorbate-adsorbent system, relaxation times and free energy of activation for orientation of the adsorbate were calculated. Good agreement between results at the two frequencies was found.

In previous work from this laboratory dielectric absorptions in the microwave region of adsorbed molecules were described.<sup>1-3</sup> Except for one instance, where a mucopolysaccharide was employed,<sup>4</sup> the adsorbents were of silica type. The present work is concerned with SO<sub>2</sub> adsorbed on porous Vycor glass. The measurements were performed at two different frequencies, 3000 and 23,500 MHz, and for a whole range of temperatures. The absorptions found are of Debye type, two maxima of unequal intensity appearing in the  $T \tan \delta$  vs. temperature plots. From these, relaxation times and potential barriers for orientation were calculated by assuming a solution-like model.

### Experimental Section

The measurements were performed by employing two different microwave systems operating at 3000 and 23,500 MHz. The high-frequency system and the method of measurement have been described previously.<sup>1</sup> For the lower frequency the method remained basically the same, the apparatus being based on a sensitive heterodyne beat method in which the solid adsorbent is placed inside a resonance cavity. The difference was in the operation mode and construction of the cavity. Whereas the high-frequency system operates in the TE<sub>01n</sub> mode, the low-frequency one was constructed to operate in the TH<sub>01</sub> mode. This enabled the use of a cavity of reasonably small dimensions. The cavity itself was of transmission type, made of brass, and silver plated on the inside (Figure 1). The cavity was coupled to the microwave system with loops of silver wire passing through vacuum-tight Teflon leads.

The adsorbent sample was placed along the axis of the cavity where electric field is concentrated in the TH<sub>01</sub> mode. A Vycor glass rod, 50 mm long and 3 mm in diameter served as adsorbent. The upper end of the rod (slightly thicker) was kept inside an iron holder, which could be lifted together with the adsorbent by means of small magnet, and hooked inside a quartz tube vacuum-sealed to the cover of the cavity. During desorption of the sample an electric furnace was placed around the tube containing the adsorbent. The desorption temperature was regulated by means of a

thermocouple and a Variac transformer. The cavity was connected to a conventional vacuum system through a copper tube sealed to the cover. Most measurements were carried out in the temperature range 270–130°K. The whole cavity was immersed in a thermostat bath controlled to within 0.5°K. A mixture of Freon 12 with ethanol was used as bath liquid and was cooled by a stream of liquid air circulating in a copper coil.

*Theory of the Measurement.* In order to calculate the loss tangent, expressions derived by Jackson, *et al.*,<sup>5</sup> for a partially filled cavity, were used. For such a case the expression  $\tan \delta = (1/Q - 1/Q_1)$  is modified by a factor  $K$  and becomes

$$\tan \delta = K \left( \frac{1}{Q} - \frac{1}{Q_1} \right) \quad (1)$$

where  $Q$  and  $Q_1$  are the quality factors of the cavity containing the adsorbent + adsorbate and of the adsorbent, respectively.

$K$  is given by

$$K = \frac{\left(\frac{a}{b}\right)^2 + F^2 \left(\frac{\epsilon_1}{\epsilon_0} - 1\right)}{\frac{\epsilon_1}{\epsilon_0} F^2 \left(1 + \frac{J_1^2(\beta_1 b)}{J_0^2(\beta_1 b)}\right)} \quad (2)$$

where  $a$  is the radius of the cavity,  $b$  is the radius of the adsorbent sample, and  $\epsilon_1$  and  $\epsilon_0$  are the dielectric constants of the sample and of free space, respectively.  $J_1$  and  $J_0$  are Bessel functions of the first order,  $\beta_1 = 2\pi/\lambda_0(\epsilon_1/\epsilon_0)$ ,  $\lambda_0$  is the free space wavelength, and  $F$  is defined by

$$F = [Y_0(\beta_0 a)J_0(\beta_0 b) - Y_0(\beta_0 b)J_0(\beta_0 a)] \frac{\beta_0 \pi a}{2} \quad (3)$$

(1) U. Feldman, Ch. Schonfeld, and M. Folman, *Trans. Faraday Soc.*, **53**, 2394 (1963).

(2) U. Feldman and M. Folman, *ibid.*, **60**, 440 (1964).

(3) I. Lubezki, U. Feldman, and M. Folman, *ibid.*, **61**, 940 (1965).

(4) I. Lubezki, F. A. Bettelheim, and M. Folman, *ibid.*, **63**, 1794 (1967).

(5) F. Horner, T. A. Taylor, R. Dunsmuir, J. Lamb, and W. Jackson, *J.I.E.E.*, Part 3, **93**, 53 (1946).

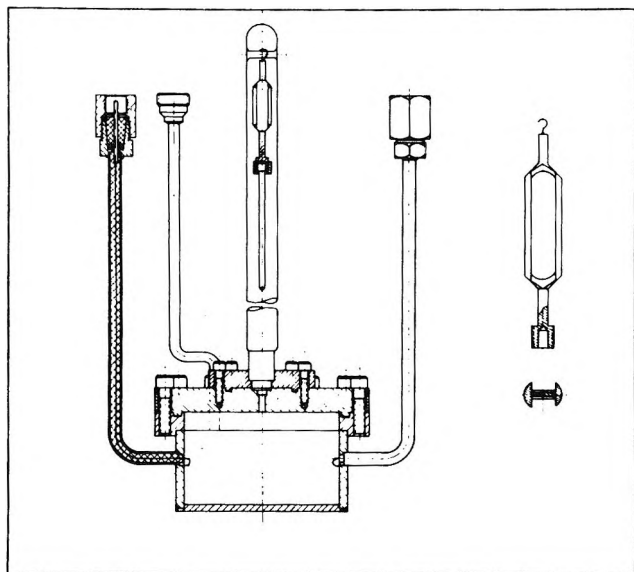


Figure 1. The resonance cavity for adsorption and  $\tan \delta$  measurements at 3000-MHz  $TH_0$  mode.

where  $Y_0$  is the second-order Bessel function,  $\beta_0 = 2\pi/\lambda_0$ . The ratio  $\epsilon_1/\epsilon_0$  is a complicated function of  $a$  and  $b$ . However, in the case  $a \gg b$  a simpler expression for this ratio is obtained

$$\frac{\epsilon_1}{\epsilon_0} = 1 + 1.04 \frac{\Delta\omega}{\omega_0} \frac{a^2}{b^2} \frac{1}{F} \quad (4)$$

where  $\omega_0$  is the resonance frequency and  $\Delta\omega$  is the change of resonance frequency that occurs after insertion of the adsorbent.

The  $Q$  factor of the loaded cavity was obtained from its resonance curve displayed on a double-beam oscilloscope, the half-power being measured by frequency markers using a highly stabilized cw oscillator. Subsequent changes in  $Q$  due to adsorption were obtained by adjusting a calibrated precision attenuator connected in series with the cavity, so that the transmitted power was maintained at constant level. In the region where the crystal detector obeys the square law the relation

$$\frac{Q_1}{Q} = \left(\frac{P_1}{P}\right)^{1/2} \quad (5)$$

holds, where  $P_1$  and  $P$  are the signal intensities recorded on the scope. Finally,  $\tan \delta$  becomes

$$\tan \delta = K \left( \frac{1}{Q} - \frac{1}{Q_1} \right) = \frac{K}{Q_1} \left( \frac{Q_1}{Q} - 1 \right) = \frac{K}{Q_1} \left( \sqrt{\frac{P_1}{P}} - 1 \right) = \frac{K}{Q_1} (10^{\Delta/20} - 1) \quad (6)$$

where  $\Delta$  is the difference in readings of the attenuator.

In order to check the validity of the described procedure, the dielectric constant and loss of NaCl were obtained by inserting a rod-shaped sample of known

dimensions into the center of the cavity and measuring the shift in resonance frequency and the change in  $Q$  factor. Using the equations given above,  $\tan \delta$  and  $\epsilon$  of the sample were calculated and found to be in agreement with values cited in the literature.

**Materials and Sample Preparations.** The porous Vycor glass was obtained from the manufacturer (Corning Glass Works, Corning, N. Y.) in shapes of rods and plates. It was polished to the desired thickness and freed from any adsorbed impurities by burning in a stream of oxygen at 723°K.

The surface area of the sample measured by low-temperature adsorption of argon was 124 m<sup>2</sup>/g for the rod-shaped sample and 180 m<sup>2</sup>/g for the disk.

SO<sub>2</sub> of spectroscopic grade was supplied by J. N. Matheson and Co. It was further purified by bulb to bulb distillation and multiple freezing.

## Results and Discussion

The adsorption isotherms of SO<sub>2</sub> on the two different samples of porous Vycor glass are given in Figures 2 and 3. The measurements were performed at low surface coverages ( $\theta_{max} \approx 0.28$ ), much below the capillary condensations region. In this region no real hysteresis is expected despite the fact that attainment of final equilibrium on desorption requires longer times than on adsorption. From these isotherms isosteric heats of adsorption were calculated. For the rod sample the  $q^{st}$  was 8.5 kcal/mol for low coverages and decreased to 6.4 kcal/mol in the region of higher coverages. These figures correspond to previous findings for a similar system.<sup>6</sup> For the disk sample the isosteric heat was initially higher, close to 9 kcal/mol and remained fairly constant down to a coverage of 8 ml/g; only for higher coverages it decreased to 7.0 kcal/mol.

The difference in the isosteric heat between the two samples seems to be real. The higher value was ob-

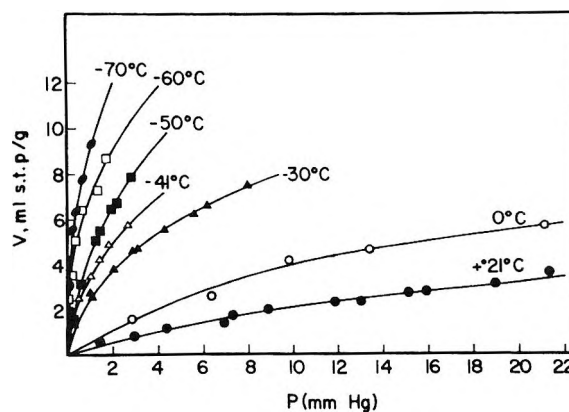


Figure 2. Adsorption isotherms of SO<sub>2</sub> on a porous silica glass rod for the temperature range between 124 and 234°K.

(6) M. Folman and D. J. C. Yates, *Trans. Faraday Soc.*, **54**, 429 (1958).

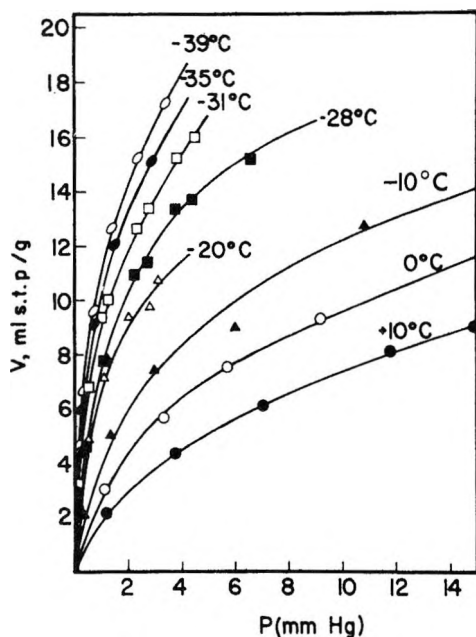


Figure 3. Adsorption isotherms of  $\text{SO}_2$  on a porous silica glass disk for temperature range between 234 and 294°K.

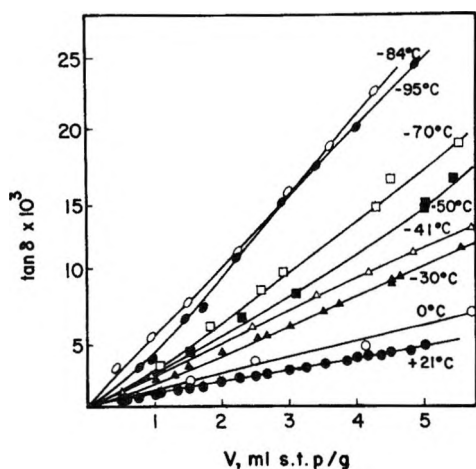


Figure 4. Plots of  $\tan \delta$  vs. volume of  $\text{SO}_2$  adsorbed on a porous silica glass rod at 3000 MHz.

tained for the disk sample the surface area of which is larger than that of the rod by 45%. Such a difference in surface area is connected with the structure of the two samples; the mean pore radius in the disk sample must be considerably smaller. This should cause higher heats of adsorption in the disk sample since the adsorbate is located on sites where the molecules are under the influence of the surface fields from surrounding walls.

$\tan \delta$  vs.  $V$  (amount adsorbed) plots are shown in Figures 4 and 5 for the temperature range between 142 and 294°K for the rod sample at 3000 MHz. The results obtained at 23,500 MHz and the temperature range between 234 and 294°K are shown in Figures 6 and 7.

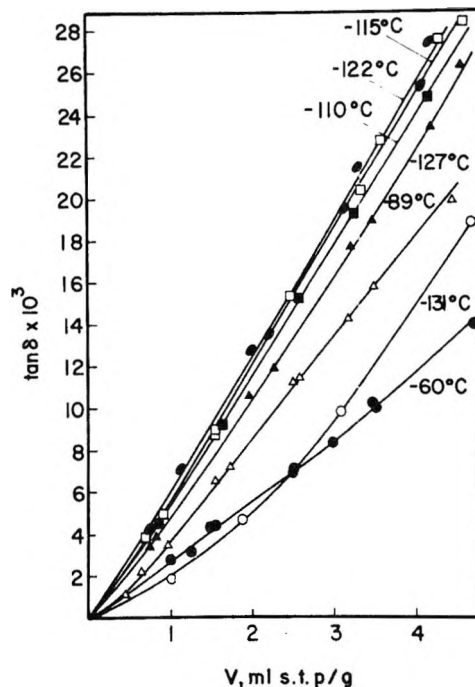


Figure 5. Plots of  $\tan \delta$  vs. volume of  $\text{SO}_2$  adsorbed on a porous silica glass rod at 3000 MHz.

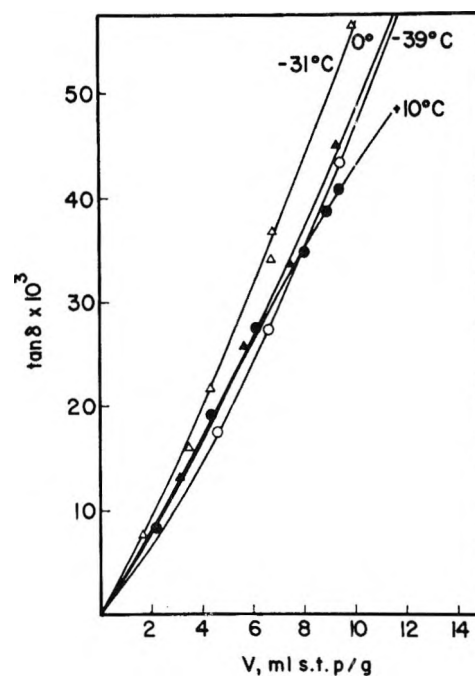


Figure 6. Plots of  $\tan \delta$  vs. volume of  $\text{SO}_2$  adsorbed on a porous silica glass disk at 23,500 MHz.

In the microwave region it is difficult to work within a wide range of frequencies since a narrow frequency band only can be covered by a single system. Instead it is possible to work at one or two selected frequencies and at different temperatures and to obtain relaxation times from plots of  $T \tan \delta$  against temperature. If the adsorbent-adsorbate system is treated as a two-

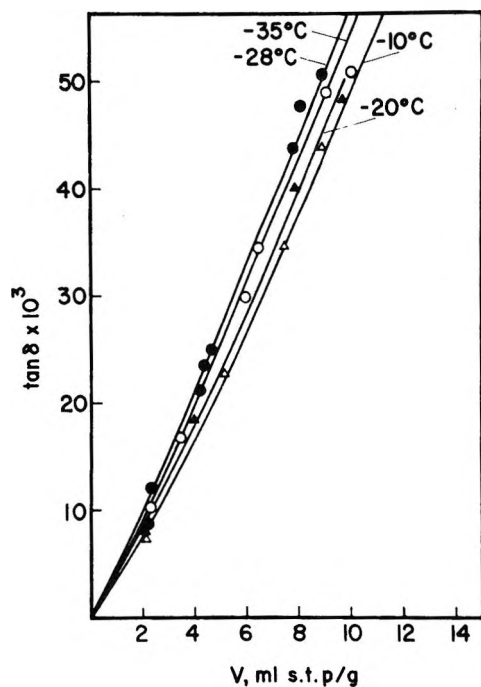


Figure 7. Plots of  $\tan \delta$  vs. volume of  $\text{SO}_2$  adsorbed on a porous silica glass disk at 23.500 MHz.

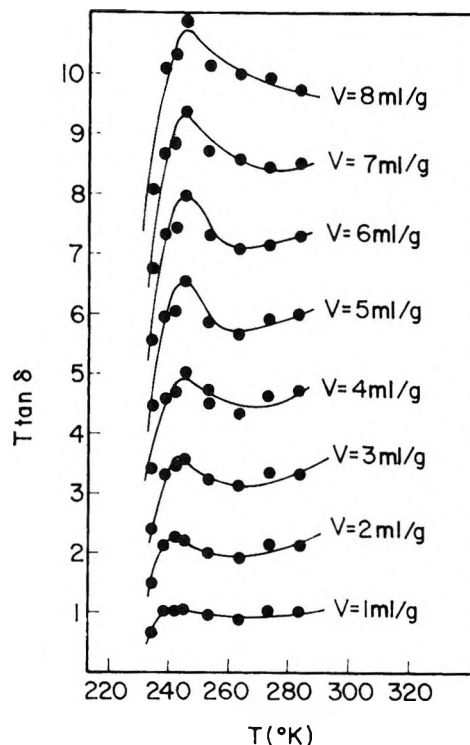


Figure 9.  $T \tan \delta$  vs. temperature plots at 23.500 MHz for  $\text{SO}_2$  adsorbed on porous silica glass disk, at constant coverages.

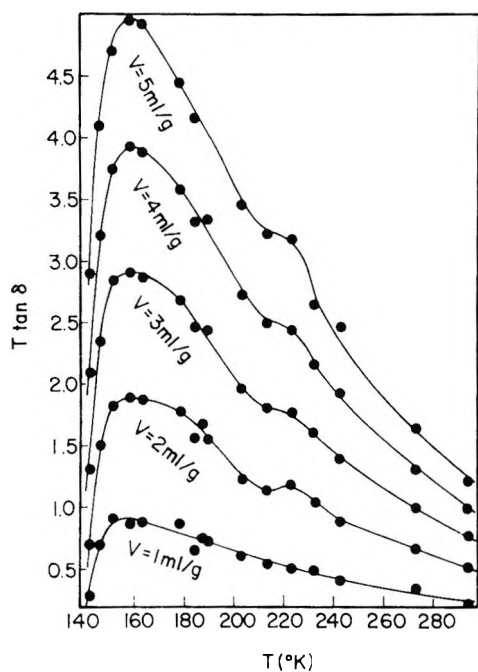


Figure 8.  $T \tan \delta$  vs. temperature plots at 3000 MHz for  $\text{SO}_2$  adsorbed on porous silica glass rod at constant coverages.

component solution, the Debye equation for solutions may be applied to obtain the relaxation time of the adsorbate.

The expression for the loss tangent is then

$$\tan \delta = \frac{(\epsilon + 2)^2}{\epsilon} \frac{4\pi\mu^2}{27kT} cN \frac{\omega\tau}{1 + \omega^2\tau^2} \quad (7)$$

where  $\epsilon$  is the dielectric constant of the adsorbate-

adsorbent system,  $k$  the Boltzmann constant,  $\mu$  the dipole moment, and  $c$  the concentration in mol/ml. Equation 7 was originally derived for polar solutes in nonpolar lossless solvents; in our case the adsorbent is not entirely loss-free. Nevertheless, its losses are not high and it is believed that after allowing for  $\tan \delta$  of the solid adsorbent, no large error is introduced.

Graphs of  $T \tan \delta$  against temperature, constructed for constant coverages, are shown in Figures 8 and 9. Both graphs show presence of maxima. At the peak  $\omega\tau = 1$ ,  $\omega\tau/(1 + \omega^2\tau^2) = 1/2$  and the height of the maximum is given by  $((\epsilon + 2)^2/2\epsilon) (4\pi\mu^2 Nc/27 kT)$ . For the 3000-MHz frequency, the maximum is obtained at 158°K and for 23,500 MHz at 245°K. The free energy of activation for the orientation process is obtained using the expression of reaction rate theory

$$\tau = \frac{h}{kT} e^{\Delta F^\ddagger/RT} \quad (8)$$

where  $\tau$  is the relaxation time and  $\Delta F^\ddagger$  the free energy of activation. This equation is similar to that obtained from an expression applicable to restricted rotation about a single axis. The  $\Delta F^\ddagger$  values obtained from measurements at 3000 and 23,500 MHz are very close indeed and equal 1.60 and 1.70 kcal/mol, respectively.

A more careful examination of the plot in Figure 8 reveals that there exists at 233°K another, very weak maximum. Repeated measurements confirmed this

finding.  $\Delta F^\ddagger$  corresponding to this maximum equals 2.50 kcal/mol.

In order to find a corresponding absorption in the high-frequency region, measurements should be extended above 320°K. This, however, cannot be done since at such a temperature  $\text{SO}_2$  is scarcely adsorbed.

To find out whether the absorptions considered are of Debye type, theoretical curves of  $T \tan \delta$  vs.  $T$  were calculated by means of eq 7, after adopting the experimental value of  $\Delta F^\ddagger$ . The results of these calculations are shown in Figure 10 as the dashed lines. It may be seen that these lines do not fit the experimental points well. A similar computation, made after assuming the existence of two partially superimposed absorptions, resulted in the solid lines in Figure 10. This time the calculated curves fitted the experimental points well; therefore the existence of a second absorption region seems to be established.

From the relative intensities of the two absorptions the ratio of the number of molecules contributing to these absorptions was obtained as 0.77:0.23. This was obtained by assuming that the dipole moment of the

$\text{SO}_2$  molecule in the adsorbed state does not differ from the gas-phase value. This assumption may seem somewhat arbitrary, since the surface field certainly induces a moment in the adsorbate. However, it is believed that this moment is small in comparison with the permanent one; moreover, it is not clear to what extent, if at all, the induced moment contributes to the absorption. Its direction is parallel to the surface field; therefore its contribution to orientation polarization may be small or negligible. It is possible to assume that these absorptions are connected with two different adsorption sites. Since the surface of the Vycor glass adsorbent has a high concentration of OH groups,<sup>7</sup> these certainly serve as sites for the  $\text{SO}_2$  adsorbate. The nature of the second site is not known. Since the barrier for orientation of the adsorbate located on these sites is considerably higher than the other one, it may be connected with adsorption inside the smallest capillaries and cracks. In this respect a correspondence exists between the orientation barrier and the heat of adsorption. The ratio of the initial and final adsorption heat values corresponds roughly to the ratio of the two potential barriers for orientation.

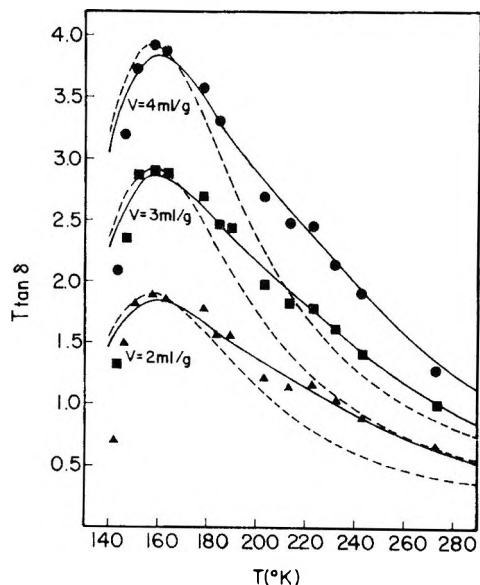


Figure 10.  $T \tan \delta$  vs. temperature plots at 3000 MHz for  $\text{SO}_2$  adsorbed on porous silica glass: ●, ■, ▲, experimental values; dashed line, Debye curve calculated on the assumption of one absorption region; solid line, superposition of two Debye curves.

### Summary

Dielectric absorptions of the  $\text{SO}_2$ -porous Vycor glass system were measured at different microwave frequencies and temperatures and for different surface coverages. Close agreement was found between the values of free energy of activation for orientation obtained using microwave systems operating not only at different frequencies but in different modes. This proves the validity of equations employed in calculating the  $\tan \delta$  values from measurements in the  $\text{TH}_{01}$  mode.

The close correspondence between the experimental absorption curve and the one constructed relying on the Debye equation and under the assumption that there exist two maxima indicates that the absorptions are of Debye type and that for the system considered two different adsorption sites are present. Assuming that the dipole moment of the  $\text{SO}_2$  adsorbate does not differ considerably from the gas-phase value, it was found that the two sites were populated in the proportion 0.77:0.23.

(7) M. E. Nordberg, *J. Amer. Ceram. Soc.*, 27, 299 (1944).

# The Effect of the Emulsifying Agent on the Dielectric Properties of Water-in-Oil Emulsions

by I. D. Chapman

Department of Chemistry, Trent University, Peterborough, Ontario, Canada (Received July 24, 1970)

Publication costs assisted by the National Research Council of Canada

The dielectric properties of w/o (water-in-oil) emulsions are dependent upon the nature of the emulsifier. In emulsions stabilized with nonionic emulsifiers such as Span 80 the water droplets aggregate together resulting in anomalous dielectric behavior. Magnesium stearate used as an emulsifier gives emulsions in which the droplets do not aggregate significantly and whose dielectric behavior can be closely predicted by classical Maxwell-Wagner equations for interfacial polarization. The polarization arises from a frequency-independent surface conductivity in the former type of emulsions and, in the latter emulsion type, from bulk conductivity produced by ionization of the hydrolysis products of magnesium stearate.

## Introduction

During recent studies<sup>1</sup> on the dielectric properties of water-in-oil emulsions stabilized with an anionic emulsifying agent, magnesium stearate, it was noted that the observations differed quite markedly from those of Hanai<sup>2</sup> with similar emulsions, but stabilized with nonionic emulsifiers. In particular, the low-frequency dielectric constants of emulsions with an identical per cent of water could differ by a factor of 2 or more.

The electrical properties of emulsions and suspensions have been reviewed recently by Hanai.<sup>3</sup> He pointed out that dielectric dispersion due to interfacial polarization could be expected for w/o emulsions. He found the high-frequency dielectric constant ( $\epsilon_h$ ) could be adequately calculated from the Bruggeman<sup>4</sup> equation, while the low-frequency dielectric constant ( $\epsilon_l$ ) was found best calculated from an extension of Wagner's equation<sup>5</sup> developed by Hanai<sup>6</sup> using the mathematical techniques employed in Bruggeman's approach. However, agreement between theory and observation was not good even at low concentrations of water. Hanai also observed that his values of  $\epsilon_l$  fell toward the calculated values if a shearing force was applied to the emulsion; this led him to suggest that aggregation of the water droplets in the emulsion might explain his high  $\epsilon_l$  values.

It was decided, therefore, to compare the dielectric properties of the two emulsion types, particularly the theoretical and observed values for  $\epsilon_l$ .

## Experimental Section

The dielectric investigations extended from 50 Hz to 100 MHz in two ranges; the first, up to 100 kHz, was covered by a General Radio Type 1650 B bridge and the second, from 500 kHz onward, was covered by a Hewlett-Packard RX bridge. This latter bridge was modified by the addition of a noninductive 50-kilohm

resistor in parallel with the measuring arm of the bridge. This was found to be necessary given the particular range of values of  $R_p$  and  $C_p$  developed by the cell and systems under investigation.

Two cells were used due to the quite different capacitance ranges of the bridges. The first cell, used with the GR bridge, was made of two concentric stainless steel cylinders, the inner cylinder being insulated from the outer one. The inner cylinder was made in three sections, the middle section being insulated by very thin Teflon spacers from the upper and lower sections which were electrically connected. The signal was applied to the middle section, the two end sections acting as guard plates. With this arrangement end capacitances were completely removed and the dielectric constants could be calculated directly from the ratio of the measured capacitance to that of the empty cell as calculated from measurements made with calibrating liquids. With the length of the middle section 7.89 cm and a gap of 0.40 cm between it and the outer electrode, the measured capacitance with air was 23.0 pF.

The second cell was an adaptation of one described by O'Konski and Edwards.<sup>7</sup> The cell was made of stainless steel and consisted of a central electrode of 0.320-cm diameter which protruded through a Teflon support and silicone O rings 1.397 cm into a small cylindrical outer electrode of 0.805-cm i.d. The cell was directly attached to a GR874 connector which could be

- (1) I. D. Chapman, *J. Phys. Chem.*, **72**, 33 (1968).
- (2) T. Hanai, *Kolloid-Z.*, **177**, 57 (1961).
- (3) T. Hanai, "Emulsion Science," P. Sherman, Ed., Academic Press, New York, N. Y., 1968, Chapter 5.
- (4) D. A. G. Bruggeman, *Ann. Phys.*, **24**, 636 (1935).
- (5) K. W. Wagner, *Arch. Electrotech. (Berlin)*, **2**, 371 (1914).
- (6) T. Hanai, *Kolloid-Z.*, **171**, 23 (1960).
- (7) C. T. O'Konski and A. Edwards, *Rev. Sci. Instrum.*, **39**, 1456 (1968).

mounted on the terminals of the RX bridge by means of a coaxial flange. The cell was calibrated with dry air, benzene, and 1,2-dichloroethane. The measured cell capacitance was related to the permittivity by the relation

$$C_p = \epsilon C_0 + C_{\text{end}}$$

where  $C_0$  and  $C_{\text{end}}$  were determined by least-squares analysis to be 0.953 and 3.87 pF, respectively. Dielectric constants calculated for emulsions at low frequencies on the RX bridge where dielectric dispersion was not significant compared well with those calculated at high frequencies on the GR bridge.

Emulsions were made from distilled and deionized water (specific conductivity  $< 10^{-6}$  ohm $^{-1}$  cm $^{-1}$ ) and paraffin oil (density at  $+10^\circ$ , 0.85 g cc $^{-1}$ ) using ultrasonic techniques. The emulsifiers used in this work were Span 80 (sorbitan monooleate) and magnesium stearate at 1% concentration in the oil. Other emulsifiers of the two general types were also used and gave similar results but were generally less stable. The emulsions with magnesium stearate as an emulsifier were mixed, allowed to stand for 24 hr, beaten, and then dielectric properties were measured at  $+10^\circ$ . These emulsions were stable at this temperature for a few hours. Emulsions using Span 80 as an emulsifier were stable over long periods of time after mixing as judged by their dielectric properties.

## Results and Discussion

The dielectric results can be classed into two groups: those of emulsions made with the nonionic emulsifier (Sorbitan monooleate, Span 80) and those of emulsions stabilized with the ionic emulsifier (magnesium stearate). Figures 1 and 2 show results from a study of a 20% water-in-oil Span-stabilized emulsion (hereafter referred to as SSE). They are typical of all such emulsions and are similar to those results reported by Hanai.<sup>2</sup> These can be compared with the results from a study at the same temperature of a 20% water-in-oil emulsion stabilized by magnesium stearate (MSSE). This latter system differs from the former in the following points: (1) there appear to be no low-frequency losses due to ionic conduction; (2) the value of  $\epsilon'$  is lower; and (3) ( $\epsilon''$ ) max occurs at a higher frequency.

*Low-Frequency Values of the Dielectric Constant ( $\epsilon_1$ ).* Figure 3 shows the values of  $\epsilon_1$  as a function of per cent water in the two types of emulsions. The values of  $\epsilon_1$  for SSE are higher than those for MSSE. Hanai has suggested that the high values for  $\epsilon_1$  for emulsions stabilized with nonionic emulsifiers arose from the aggregation of the water droplets; he observed that  $\epsilon_1$  fell as increasingly large shearing forces were applied.<sup>2</sup> The two photomicrographs of Figure 4 clearly show that the droplets in the SSE are clustered together in large areas while there appears to be little aggregation and a wider range of particle size in the MSSE. Possi-

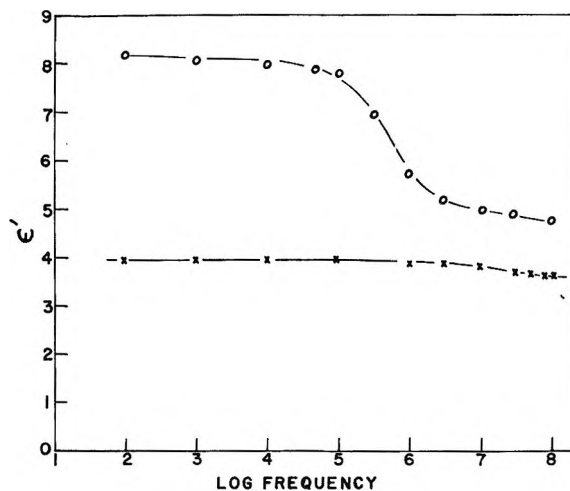


Figure 1. Real part of the dielectric constant of 20% w/o emulsions plotted against log frequency at  $+10^\circ$ : O, SSE; X, MSSE.

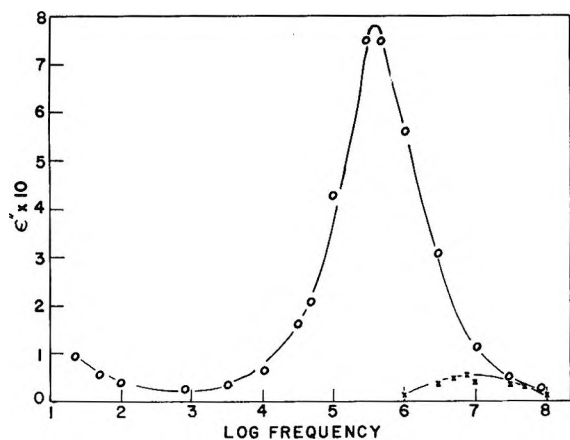


Figure 2. Imaginary part of the dielectric constant of 20% w/o emulsions plotted against log frequency at  $+10^\circ$ : O, SSE; X, MSSE.

ble reasons for this difference in behavior are discussed later.

The study of heterogeneous dielectrics until recently has concentrated on attempting to express the dielectric constants of such systems in terms of the dielectric constants of the constituent phases.<sup>3</sup> In his excellent review of the electrical properties of emulsions, Hanai<sup>3</sup> discussed the derivation of a number of those equations. The derivations follow two approaches.

Wagner<sup>5</sup> presented a theory of interfacial polarization for a system of spherical droplets sparsely distributed in a dispersing medium. By considering the potential outside a spherical region of a collection of such spheres and assuming that this was equal to the potential outside a sphere of the same size having a dielectric constant  $\epsilon^*$ , he showed that the dielectric properties of the system could be represented by

(8) L. H. K. van Beek, "Progress in Dielectrics," Vol. 7, J. B. Birks, Ed., Heywood, London, 1967.

$$\frac{\epsilon^* - \epsilon_m^*}{\epsilon^* + 2\epsilon_m^*} = \frac{\epsilon_p^* - \epsilon_m^*}{\epsilon_p^* + 2\epsilon_m^*} \phi$$

where  $\epsilon^*$ ,  $\epsilon_p^*$ , and  $\epsilon_m^*$  are the complex dielectric constants of the system, the dispersed phase, and the dispersing medium.  $\phi$  is the volume fraction of the dispersed phase. For the special case of a w/o emulsion, this reduces to

$$\epsilon_1 = \epsilon_m \frac{1 + 2\phi}{1 - \phi} \quad (1)$$

Equation 1 is strictly only applicable to dilute concentrations of dispersed phase.

Hanai<sup>9</sup> extended Wagner's theory to higher concentrations by using a mathematical procedure employed by Bruggeman.<sup>4</sup> In the special case of a w/o emulsion where the conductivity of the dispersed phase,  $\kappa_p$  is greater than the conductivity of the dispersing medium  $\kappa_m$  and  $\kappa_p$  is greater than the conductivity of the system at low frequencies,  $\kappa_1$ , his equations reduce to

$$\epsilon_1 = \epsilon_m \frac{1}{(1 - \phi)^3} \quad (2)$$

In his own studies of w/o emulsions stabilized with nonionic emulsifiers (a mixture of sorbitan esters of fatty acids), Hanai<sup>2</sup> showed that neither eq 1 or 2 compared well with his observed values of  $\epsilon_1$  even at comparatively large values of shearing stress, although eq 2 was closer in predicting values for  $\epsilon_1$ . Pearce<sup>9</sup> measured the dielectric constants of sea water in fuel oil at concentrations up to 63% water and at 1 kHz (corresponding to  $\epsilon_1$  at this frequency and conductivity of dispersed phase). Equation 2 was found to agree well with his results. However, it is difficult to judge his work in the context of this study as he did not use any emulsifier; suitable but unknown molecular species were probably present in the fuel oil.

Figure 3 shows the calculated values for  $\epsilon_1$  from the two equations. Equation 1 better predicts the observed results for MSSE at these concentrations of the dispersed phase. As noted by Hanai, neither equation is at all applicable to SSE. However, as Pearce pointed out, the degree of randomness of distribution of the droplets is implicit in the derivation of both types of equations, ranging from an ordered situation in Wagner's approach to a disordered one in equations of the Bruggeman type. The rather close agreement in the case of MSSE with eq 1 might therefore be grounds for believing that the droplets in such emulsions are relatively discrete and are in an orderly distribution, such order arising from sedimentation, for example, since the density of water is greater than that of oil.

**Mechanism of Dielectric Loss.** *a. SSE.* The results shown in Figures 1 and 2 for SSE are typical of a heterogeneous system where the dielectric relaxation effect is due to the time-dependent polarization of the inter-

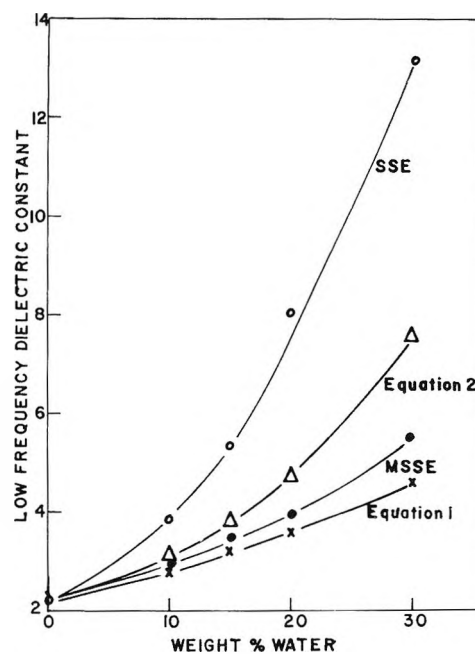


Figure 3. Experimental and calculated values of the low-frequency dielectric constant as a function of weight per cent water. Determined at  $+10^\circ$  and 1 kHz.

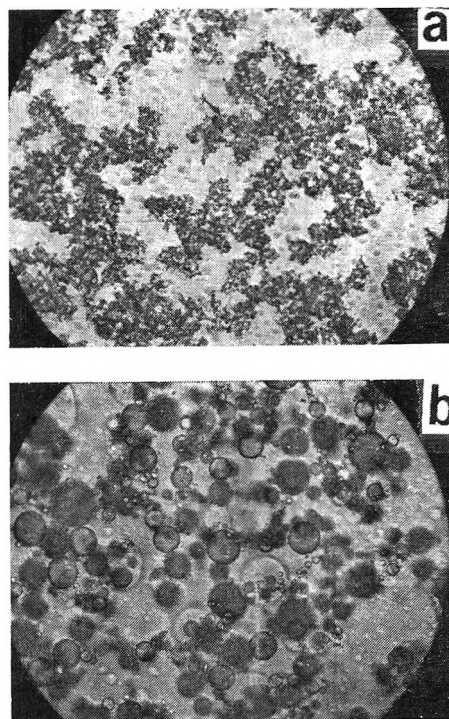


Figure 4. Photomicrographs of 20% w/o emulsions: a, stabilized with Span 80; b, stabilized with magnesium stearate.

faces between the suspended particles and the surrounding medium.

Pauly and Schwan<sup>10</sup> have derived an expression for

(9) C. A. R. Pearce, *Brit. J. Appl. Phys.*, **6**, 113 (1955).

(10) H. Pauly and H. P. Schwan, *Z. Naturforsch. A*, **14**, 125 (1959).

the relaxation time constant  $T$  for large volume fractions of suspended particles

$$T = \frac{1}{2\omega f_0} = \frac{\epsilon_p + 2\epsilon_m - \phi(\epsilon_p - \epsilon_m)}{\kappa_p + 2\kappa_m - \phi(\kappa_p - \kappa_m)} \epsilon_v \quad (3)$$

where  $f_0$  is the frequency corresponding to the maximum in the  $\epsilon''$  vs.  $\log f$  plot and  $\epsilon_v$  is the dielectric constant in a vacuum,  $8.8514 \times 10^{-14}$  F cm<sup>-1</sup>. From Figure 2,  $f_0$  was calculated to be 600 kHz for the SSE. Given that  $\kappa_m$  is  $\ll \kappa_p$ ,  $\epsilon_p = 84$ ,  $\epsilon_m = 2.18$ , and  $\phi = 0.18$ , one can calculate that  $\kappa_p$  would have to be of the order of  $3 \times 10^{-5}$  ohm<sup>-1</sup> cm<sup>-1</sup>. The emulsion had been made with water whose conductivity was  $< 10^{-6}$  ohm<sup>-1</sup> cm<sup>-1</sup> so the possibility that the system had picked up ionic impurities was investigated. An emulsion was made in the normal fashion and was then broken by centrifuging at 20,000 rpm for 6 hr at 40°. The aqueous phase was separated and its conductivity was found to be  $3 \times 10^{-5}$  ohm<sup>-1</sup> cm<sup>-1</sup>, thus confirming the presence of ionic impurities. Placing the stainless steel vessels and the ultrasonic probe in contact with water under conditions similar to those used during the preparation of the emulsions did not give rise to any ionic impurities in the water. This led to the investigation of the Span as a source of impurity. The usual amount of Span beaten directly with water alone gave a conductivity reading for the aqueous phase of  $3 \times 10^{-5}$  ohm<sup>-1</sup> cm<sup>-1</sup>. Possible impurities in Span are sorbitols, anhydrosorbitols, and oleic acid. Oleic acid in small amounts beaten with water also gave rise to conductivities of the order of  $10^{-5}$  ohm<sup>-1</sup> cm<sup>-1</sup>. The oleic acid was removed from the Span by washing first with dilute sodium bicarbonate solution, then with water. The Span was then extracted with ether. The Span recovered after removing the ether was beaten with water; the conductivity of the aqueous phase was  $2 \times 10^{-6}$  ohm<sup>-1</sup> cm<sup>-1</sup>. An emulsion was then prepared using the acid-free Span. The dielectric properties of this emulsion were identical with those shown in Figure 2. Given the new value for  $\kappa_p$  which would predict a value of  $f_0$  at around 40 kHz, the mechanism of dielectric loss could not therefore be due to bulk conductivity in the water phase.

A number of theories of emulsion stability have been advanced; of these, theories involving the concept of the electrical double layer have received much attention. The double layer theory postulates a nonuniform distribution of ions near an interface while bulk neutrality is maintained. The distribution of ions in the double layer causes the electrical potential in the layer to decrease with distance from the interface, the most commonly measured potential being the  $\zeta$  potential which is a measure of the potential at the plane of shear. In liquid-liquid systems such as emulsions, double layers may exist on both sides of the interface.

SSE's were investigated by Verwey.<sup>11</sup> He showed that the  $\zeta$  potential in the water phase ( $\zeta_w$ ) which is

very small and negative in the absence of Span will increase considerably in the presence of added Span, while  $\zeta_o$ , the  $\zeta$  potential in the oil phase which was large and positive will decrease and become very small. Rigole and van der Wee<sup>12</sup> studied the effect of added ions on the electrokinetic mobility of w/o emulsions stabilized with Span 80 and noted HCl had a considerable effect. They explained their observation by suggesting that the Span molecules tend to accumulate at the water-oil interface with the sorbitan group facing the water. In the oil phase there is little tendency for dissociation to occur, but some H<sup>+</sup> will enter the water. This would give rise to a layer of negative charges at the interface and a diffuse layer mainly formed from positive charges in the water. Following Verwey's arguments they ignored  $\zeta_o$  and so calculated values for  $\zeta_w$ . They confirmed that  $\zeta_w$  was negative and the diffuse part of the double layer was built of positive charges. The addition of H<sup>+</sup> would decrease the dissociation and the value of  $\zeta_w$  as observed and could even, at higher concentrations of H<sup>+</sup>, reverse the sign of  $\zeta_w$  by forming OH<sub>2</sub><sup>+</sup> groups of the sorbitan part of the molecule. This work suggests that the mechanism of dielectric polarization in these emulsions could involve surface conductivity arising from H<sup>+</sup> in the very thin double layer in the water.

Even if oleic acid is present in the Span, this mechanism cannot be discounted since the oleic acid would also concentrate and orient itself at the interface, thus giving rise to the possibility of the same process of double layer formation. Interestingly, it was noted that the acid-free Span did not give as stable an emulsion as had the unpurified Span.

Various models of the effect of a frequency-independent purely conductive surface layer on the dielectric properties of suspended particles have been advanced and applied to experimental data by O'Konski<sup>13</sup> and Schwan, *et al.*<sup>14</sup> Both showed that this treatment for spheres is equivalent to one involving bulk conductivity alone, *i.e.*, eq 3 would apply if the bulk conductivity term  $\kappa_p$  was changed to a surface conductivity term  $\kappa_s$ .  $\kappa_s = \kappa_p + \kappa_s'$  and  $\kappa_s' = 2\lambda/a$ .  $\lambda$  is the surface conductance and  $a$  is the radius of the sphere. Equation 3 would predict a value of  $10^{-4}$  to  $10^{-5}$  ohm<sup>-1</sup> cm<sup>-1</sup> for  $\kappa_s$ . The diameter of the majority of the droplets was found to be 10  $\mu$  by microscopic examination. Thus, neglecting  $\kappa_p$ , the surface conductance would be around  $10^{-8}$  ohm<sup>-1</sup>, which is the magnitude usually found.<sup>14</sup>

Other theories of dielectric polarization involving surface conductivity, *e.g.*, Schwarz,<sup>15</sup> can be neglected.

(11) E. J. W. Verwey, *Proc. Kon. Ned. Akad. Wetensch.*, **53**, 382 (1950).

(12) W. Rigole and P. Van der Wee, *J. Colloid Sci.*, **20**, 145 (1965).

(13) C. T. O'Konski, *J. Phys. Chem.*, **64**, 605 (1960).

(14) H. P. Schwan, G. Schwarz, J. Maczuk, and H. Pauly, *ibid.*, **66**, 2626 (1962).

Schwarz's theory involves the diffusion-controlled relaxation of a surface capacitance, but making reasonable estimates of surface charge density and mobility of  $H^+$  for the SSE,  $f_0$  was calculated to be below 1 kHz, and the dielectric enhancement ( $\epsilon_1 - \epsilon_h$ ) would be  $>10^3$ . As Schwan, *et al.*,<sup>14</sup> showed, any explanation of the dielectric polarization based on electrophoretic movements of the water droplets can also be rejected since it would give rise to a change in the dielectric constant which is opposite to that which is experimentally observed.

b. MSSE. The observed value of  $f_0$  for the MSSE (10 MHz), (Figure 2) would be predicted by a conductivity value  $\kappa_p$  of between  $10^{-4}$  and  $10^{-3}$  ohm $^{-1}$  cm $^{-1}$ . An MSSE demulsified by centrifuging gave an aqueous phase with conductivity  $6 \times 10^{-4}$  ohm $^{-1}$  cm $^{-1}$ . As in the previous case the source of impurity must lie with the emulsifier. Again both bulk and surface conductivity can be advanced as possible mechanisms for the dielectric loss. A study by Albers and Overbeek<sup>16</sup> suggests the former is more likely in this case. In a study of emulsion stability, Albers and Overbeek measured the electrokinetic mobility of water-in-benzene emulsions. Their emulsions were stabilized with ionic emulsifiers. Emulsions stabilized with magnesium oleate were quite stable. However, the  $\zeta$  potential (which they identified with the surface potential) was much lower for these emulsions than it was for other less stable emulsions stabilized with other salts of oleic acid, contrary to hitherto accepted theory, which predicted that the higher the surface potential, the more stable the emulsions. They suggested that the stability might arise from a solid-like film at the water-benzene interface produced by hydrolysis of the magnesium oleate. They analyzed the interfacial film and found it to be chemically consistent with an  $Mg \cdot (OL \cdot OH)$  or an  $Mg(OH)_2 \cdot Mg(OL)_2$  complex.

In support of Albers and Overbeek's work, it was noticed that the dielectric properties of freshly made MSSE changed with time,  $\epsilon_1$  tending to fall and more importantly,  $f_0$  tending to increase until 24 hr or so had

passed. This was not the simple "falling out" of an emulsion which would cause drastic changes in its dielectric properties. If, as Albers and Overbeek and this work suggests, hydrolysis does occur in those emulsions stabilized with magnesium salts of long chain acids, then the ionization of the hydrolysis products is more likely to give rise to bulk conductivity than to surface conductivity.

The dielectric increment predicted by Pauly and Schwan<sup>10</sup> on the basis of bulk conductivity in the water phase and Maxwell-Wagner dispersion is given by

$$\epsilon_1 - \epsilon_h = \frac{9\phi(1 - \phi)(\epsilon_m\kappa_p - \epsilon_p\kappa_m)^2}{[(\epsilon_p + 2\epsilon_m) - \phi(\epsilon_p - \epsilon_m)] \times [(\kappa_p + 2\kappa_m) - \phi(\kappa_p - \kappa_m)]^2}$$

Here  $\epsilon_m = 2.18$ ,  $\epsilon_p = 84$ ,  $\kappa_p = 10^{-4}$  ohm $^{-1}$  cm $^{-1}$  ( $\gg \kappa_m$ ),  $\phi = 0.18$ . The calculated value of  $(\epsilon_1 - \epsilon_h) = 0.5$ , in good agreement with the observed value of 0.35.

The lack of aggregation noticed in MSSE probably arises from the thick film of partial hydrolyzates in the interface. As Kitchener and Mussellwhite<sup>17</sup> point out, such shells may act as a barrier preventing close approach of the dispersed droplets which may then be kept out of the range at which London-van der Waals forces become strong. Albers and Overbeek<sup>18</sup> showed that the charge on the droplets is not a significant factor in stabilizing w/o emulsions by repulsion. Therefore the SSE are not prevented by charge stabilization from aggregating together.

*Acknowledgments.* The author wishes to thank the National Research Council of Canada and Trent University for their generous financial support of this work.

(15) G. Schwarz, *J. Phys. Chem.*, **66**, 2636 (1962).

(16) W. Albers and J. Th. G. Overbeek, *J. Colloid Sci.*, **14**, 501 (1959).

(17) J. A. Kitchener and P. F. Mussellwhite, "Emulsion Science," P. Sherman, Ed., Academic Press, New York, N. Y., 1968, p 101.

(18) W. Albers and J. Th. G. Overbeek, *J. Colloid Sci.*, **14**, 510 (1959).

## Molecular Association and the Dielectric Constant of Long-Chain

### Alkylammonium Salts in Benzene

by O. Levy, G. Markovits, and A. S. Kertes\*

*Department of Inorganic Chemistry, The Hebrew University, Jerusalem, Israel (Received May 27, 1970)*

*Publication costs borne completely by The Journal of Physical Chemistry*

Dielectric constant measurements were performed in benzene solutions of tridodecylammonium and tetraheptylammonium salts and some of their mixtures in order to determine the extent of dipole-dipole interaction leading to the formation of molecular associates. The best fits of experimental data were found for the monomer-dimer equilibrium model in the case of tertiary ammonium salts and a monomer-trimer model for the quaternary salts. The dipole moment of the monomers and the oligomers and the appropriate aggregation constants were calculated. Dipole moments of similar compounds found in the literature have been discussed and recalculated on the assumption of a monomer-dimer equilibrium.

Previous vapor pressure lowering (osmometric) measurements in solutions of tridodecyl<sup>1,2</sup> and tetraheptylammonium<sup>2</sup> salts and some of their mixtures<sup>3</sup> in benzene have been interpreted in terms of intermolecular association. It has been suggested that in benzene and other nonpolar, zero dipole moment hydrocarbons, strong dipole-dipole attraction forces are responsible for the formation of dimers, trimers, and higher oligomers. The next logical step was to measure the dielectric behavior of these solutions and to evaluate the effective dipole moment of the monomeric ion pairs and possibly that of the higher molecular aggregates formed.

A variety of conductance and dielectric studies<sup>4-12</sup> provides enough evidence that short-chain (five carbon atoms per chain or less) alkylammonium salts when dissolved in nonpolar solvents exist not only in the form of electrically neutral undissociated ion pairs but also in the form of quadrupoles (dimers), even at low solute concentrations, and become more complex, in terms of higher aggregates, as the concentration increases. Bauge and Smith<sup>10,11</sup> also provided quantitative information for a number of tertiary and quaternary ammonium salts on the extent of such intermolecular association and evaluated the dipole moments of the dimers formed.

Except for some fragmentary information of alkylamine extracts of mineral acids<sup>13,14</sup> (containing water and possibly also excess of either the amine or the acid) and our preliminary report,<sup>15</sup> no dielectric measurements seem to have been reported on strictly binary systems consisting of a water-immiscible nonpolar hydrocarbon and long-chain (eight or more carbon atoms per chain for the tertiary and six or more for the quaternary amines) alkylammonium salts. In the past decade or so, high molecular weight tertiary and quaternary alkylamine salts received much attention as

excellent "liquid anion exchanger" in solvent extraction of inorganic compounds.<sup>16</sup>

#### Experimental Section

Tetra-*n*-heptylammonium chloride and bromide were Eastman Kodak White Label products. The tri-*n*-dodecylammonium chloride, perchlorate, and bisulfate<sup>17</sup> and the tetrahaloferrates<sup>18</sup> of both tertiary and quaternary amines were prepared and purified as described previously. Benzene was an Analytical Reagent Møllinckrodt product.

- (1) A. S. Kertes and G. Markovits, *J. Phys. Chem.*, **72**, 4202 (1968).
- (2) A. S. Kertes, O. Levy, and G. Markovits, *ibid.*, **74**, 3568 (1970).
- (3) O. Levy, G. Markovits, and A. S. Kertes, *J. Inorg. Nucl. Chem.*, in press.
- (4) J. A. Geddes and C. A. Kraus, *Trans. Faraday Soc.*, **32**, 585 (1936).
- (5) C. A. Kraus, *J. Phys. Chem.*, **60**, 129 (1956).
- (6) E. A. Richardson and K. H. Stern, *J. Amer. Chem. Soc.*, **82**, 1296 (1960).
- (7) A. A. Maryott, *J. Res. Nat. Bur. Stand.*, **41**, 1 (1948).
- (8) M. Davies and G. Williams, *Trans. Faraday Soc.*, **56**, 1619 (1960).
- (9) M. Davies and G. Johansson, *Acta Chem. Scand.*, **18**, 1171 (1964).
- (10) K. Bauge and J. W. Smith, *J. Chem. Soc.*, 4244 (1964).
- (11) K. Bauge and J. W. Smith, *J. Chem. Soc. A*, 616 (1966).
- (12) G. S. Hooper and C. A. Kraus, *J. Amer. Chem. Soc.*, **56**, 2265 (1934).
- (13) W. J. McDowell and K. A. Allen, *J. Phys. Chem.*, **63**, 747 (1959).
- (14) V. M. Bobrik, *Russ. J. Inorg. Chem.*, **13**, 113 (1968).
- (15) A. S. Kertes, O. Levy, and G. Markovits in "Solvent Extraction Research," A. S. Kertes and Y. Marcus, Ed., Wiley-Interscience, New York, N. Y., 1969, p 177.
- (16) Y. Marcus and A. S. Kertes, "Ion Exchange and Solvent Extraction of Metal Complexes," Wiley-Interscience, London, 1969, Chapter 10.
- (17) A. S. Kertes, H. Gutmann, O. Levy, and G. Markovits, *Israel J. Chem.*, **6**, 421 (1968).
- (18) O. Levy and A. S. Kertes, *J. Inorg. Nucl. Chem.*, **31**, 888 (1969).

Densities of the benzene solutions, prepared on a molar basis, were determined using a 63-ml pycnometer with expansion cap to minimize evaporation losses. In the concentration range studied,  $10^{-3}$  to  $10^{-2}$  M, densities vary linearly with the molar concentration  $c$ , and the coefficients  $B$  of the function  $\rho = \rho_0 + Bc$  are given in Table I.  $\rho_0$ , the density of pure benzene at  $30^\circ$ , was

**Table I:** Values of the Coefficient  $B$  in the Density Equation at  $30^\circ$

$(C_{12}H_{25})_3NHCl^a$	-0.003	$(C_7H_{15})_4NCl$	0.027
$(C_{12}H_{25})_3NHClO_4$	0.030	$(C_7H_{15})_4NBr$	0.070
$(C_{12}H_{25})_3NH_2SO_4^a$	0.030	$(C_7H_{15})_4NFeCl_4$	0.117
$(C_{12}H_{25})_3NHFeCl_4$	0.144	$(C_7H_{15})_4NFeBr_4$	0.250
$(C_{12}H_{25})_3NHFeBr_4$	0.285		

<sup>a</sup> At  $25^\circ$ .

$\rho_0 = 0.86836$  (0.87368 at  $25^\circ$ ) and its dielectric constant  $\epsilon_0 = 2.2650$  (2.2740 at  $25^\circ$ ).

The instrument was a modification of that used in the heterodyne beat method.<sup>19</sup> The reference crystal oscillator was held at a constant frequency of 1 Mc/sec. The sample arm consisted of a sample cell and a factory calibrated General Radio Type 1422 D variable precision capacitor of a maximum capacity of 1150 pF. The measuring cell of 60 pF capacitance with air, requiring 25 ml of solution and calibrated with benzene, permitted measuring the dielectric constant with an internal consistency within 0.0002 unit, essential for the type of systems and solute concentration range used in this work, where the maximum  $\Delta\epsilon$  observed was less than 0.2 unit. The temperature of the cell was kept constant by circulating water from a bath controlled at  $30^\circ \pm 0.01$ .

## Results

Figures 1 and 2 show the experimental data, plotted as  $\Delta\epsilon/w = (\epsilon - \epsilon_0)/w$  against  $w$ , the total solute concentration on the weight fraction scale, for benzene solutions of the tertiary and quaternary alkylammonium salts studied. In all cases, the lack of a linear function reflects the departure of the solutes from the condition of a simple ion pair and suggests the formation of higher aggregates on account of ion pairs.

A previously<sup>10,20</sup> used method of calculation, slightly modified here, allows for the dipole moment of the monomeric ion pair to be independent of the presence of dimers or higher aggregates in equilibrium and yields simultaneously the aggregation constant  $\beta_n$  of the reaction



where  $R^+$  stands for either the  $(C_{12}H_{25})_3NH^+$  or the  $(C_7H_{15})_4N^+$  cation and  $A^-$  for the anionic part of the ion pair. The measured dielectric constant,  $\epsilon$ , is pro-

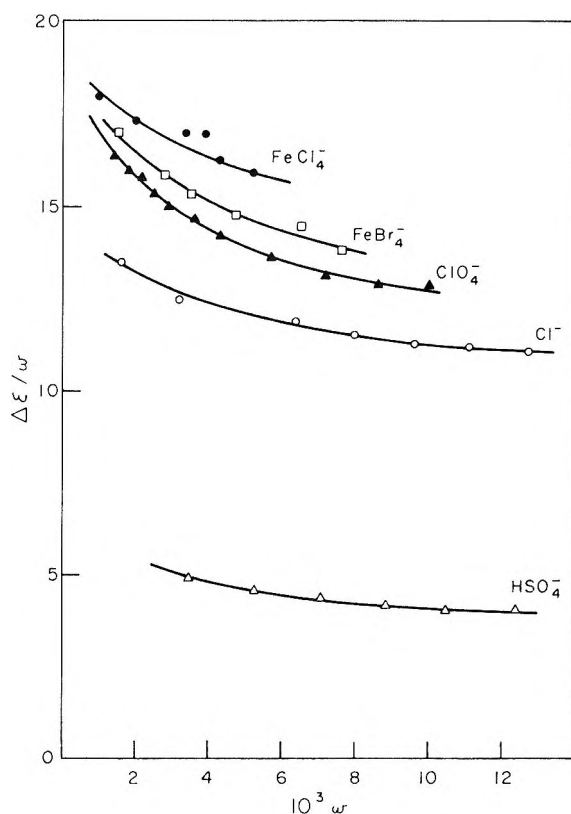


Figure 1. Dielectric constant of tridodecylammonium salts in benzene.

portional to the weight fraction of the monomer,  $w_1$ , and the oligomer,  $w_n$ , and through the experimental polarizability,  $\Delta\epsilon/w = \alpha$  ( $\Delta\epsilon_1/w_1 = \alpha_1$ ;  $\Delta\epsilon_n/w_n = \alpha_n$ ), the aggregation constant of reaction 1 is given by

$$\beta_n = \frac{(\alpha_1 - \alpha)(\alpha_1 - \alpha_n)}{(\alpha - \alpha_n)^n} \frac{M^{n-1}}{n(\rho w)^{n-1}} \quad (2)$$

where  $M$  is the formula weight of the solute,  $w = w_1 + w_n$ , and  $\rho$  is the density of solution with dielectric constant  $\epsilon$  and solute concentration  $w$ , for any particular system where the difference  $(\alpha_1 - \alpha_n)$  remains constant. Expressing eq 2 through the experimentally accessible polarizability,  $\alpha$

$$\alpha = \alpha_1 - \frac{n\beta_n(\alpha - \alpha_n)^n (\rho w)^{n-1}}{(\alpha_1 - \alpha_n)^n M^{n-1}} \quad (3)$$

a plot of  $\alpha$  against  $(\alpha - \alpha_n)^n (\rho w)^{n-1}$  should result in a straight line for the proper value of  $\alpha_n$ , the intercept at  $w = 0$  yielding  $\alpha_1$ , and from the slope,  $\beta_n$  can be calculated. Equation 3 was solved by a nonlinear least-square program (CDC 6400 computer), and the dipole moments deduced, as given by Smith (ref 19, chapter 1), using the molar polarizability  $\alpha_0 = 3[R]M/4\pi N$  values which have been calculated from atomic and bond

(19) C. P. Smith, "Dielectric Behavior and Structure," McGraw-Hill, New York, N. Y., 1955, Chapter 2.

(20) H. A. Pohl, M. E. Hobbs, and P. M. Gross, *J. Chem. Phys.*, **9**, 408 (1941).

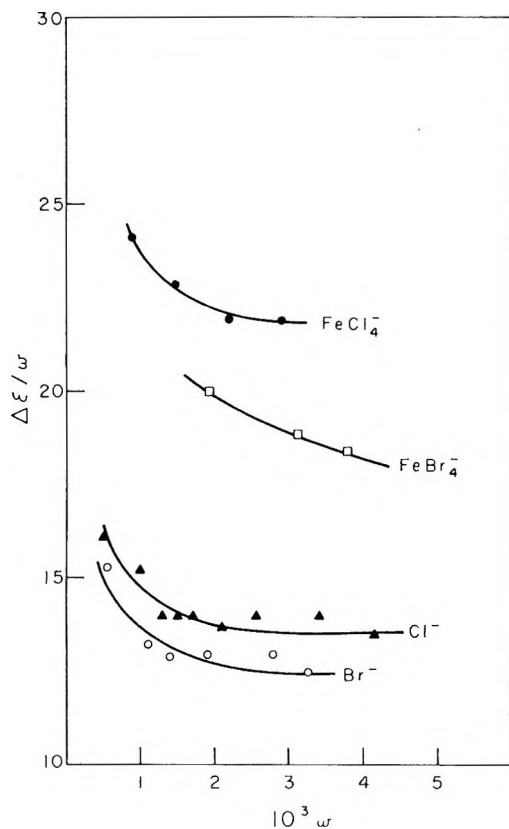


Figure 2. Dielectric constant of tetraheptylammonium salts in benzene.

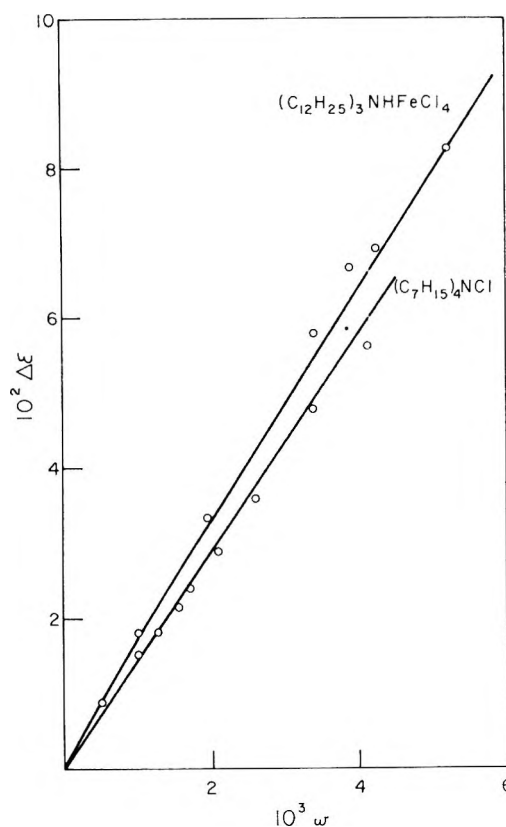


Figure 3. Experimental (O) and calculated (—) dielectric constants.

Table II: Dipole Moments, Aggregation Constants, and Interionic Distances of Alkylammonium Salts at 30°

Salt	$\mu_1$ , D	$n$	$\mu_n$ , D	$\beta_n$ , (mol/ lit) <sup>-n+1</sup>	$\alpha_0 \times$ 10 <sup>24</sup> , cc	$r$ , Å
(C <sub>12</sub> H <sub>25</sub> ) <sub>3</sub> NHCl <sup>a</sup>	7.6	2	7.8	14.1	71	4.7
(C <sub>12</sub> H <sub>25</sub> ) <sub>3</sub> NHClO <sub>4</sub>	10.1	2	8.7	77.0	74	5.0
(C <sub>12</sub> H <sub>25</sub> ) <sub>3</sub> NH <sub>2</sub> SO <sub>4</sub> <sup>a</sup>	6.4	2	5.8	1,270	74	4.6
(C <sub>12</sub> H <sub>25</sub> ) <sub>3</sub> NHFeCl <sub>4</sub>	11.2	2	10.7	82.7	78	5.2
(C <sub>12</sub> H <sub>25</sub> ) <sub>3</sub> NHFeBr <sub>4</sub>	12.3	2	12.5	220	83	5.4
(C <sub>7</sub> H <sub>15</sub> ) <sub>4</sub> NCl	8.3	3	13.0	1,200	59	4.6
(C <sub>7</sub> H <sub>15</sub> ) <sub>4</sub> NBr	8.5	3	13.7	2,000	60	4.6
(C <sub>7</sub> H <sub>15</sub> ) <sub>4</sub> NFeCl <sub>4</sub>	12.3	3	19.4	20,000	68	5.1
(C <sub>7</sub> H <sub>15</sub> ) <sub>4</sub> NFeBr <sub>4</sub>	12.8	3	21.6	5,300	71	5.2

<sup>a</sup> At 25°.

refractions given in the literature<sup>21</sup> (Table II). For the tertiary ammonium salts the best fit was obtained with  $n = 2$ , whereas for the quaternary salts,  $n = 3$  gave the most satisfactory fit of the experimental data. The calculated values are compiled in Table II; the  $\beta_n$  values are expressed on a molar concentration scale rather than on the weight fraction scale.

Table II also shows the interionic distances,  $r$ , in the ion pairs estimated from the relationship<sup>8</sup>

$$\mu_1 = er(1 - \alpha_0/r^3) \quad (4)$$

where  $e$  is the electronic charge. This, a somewhat simplified relationship, probably gives slightly low<sup>10</sup> values for  $r$ , but still higher than the charge separation estimated from conductivity measurements, which for (C<sub>12</sub>H<sub>25</sub>)<sub>3</sub>NHClO<sub>4</sub> was found to be 4.2 Å<sup>22</sup> and 4.9 Å for (C<sub>12</sub>H<sub>25</sub>)<sub>3</sub>NHFeCl<sub>4</sub>.<sup>23</sup>

In order to check the derived dipole moments and association constants, the molecular Debye-Clausius-Mossotti expression (ref 19, chapter 1) for mixtures containing the solvent ( $s$ ), the monomer, and the oligomer (the concentration of the solutes in  $w$  rather than in  $N$ , numbers of molecules per unit volume, as that for the solvent)

$$\frac{\epsilon - 1}{\epsilon + 2} = \frac{4\pi}{3} N_s \alpha_s + \frac{4\pi N}{3} \frac{\rho}{M} (w_1 \alpha_1 + w_n \alpha_n / n) \quad (5)$$

has been applied to evaluate  $\Delta\epsilon_{\text{calcd}}$ . The agreement with the experimental  $\Delta\epsilon$ 's is satisfactory (Figure 3). The first term on the right hand of eq 5 is practically constant in the solute concentration range studied and has the value of 0.2966.

Before turning now to the dielectric constant measurements of ternary systems containing two solutes,

(21) B. V. Yoffe, "Rukovodstvo po refraktometriidlya khimikov," Izdatelstvo Univerziteta, Leningrad, 1956.

(22) G. Markovits, Ph.D. Thesis, Hebrew University, 1969.

(23) O. Levy, Ph.D. Thesis, Hebrew University, 1970.

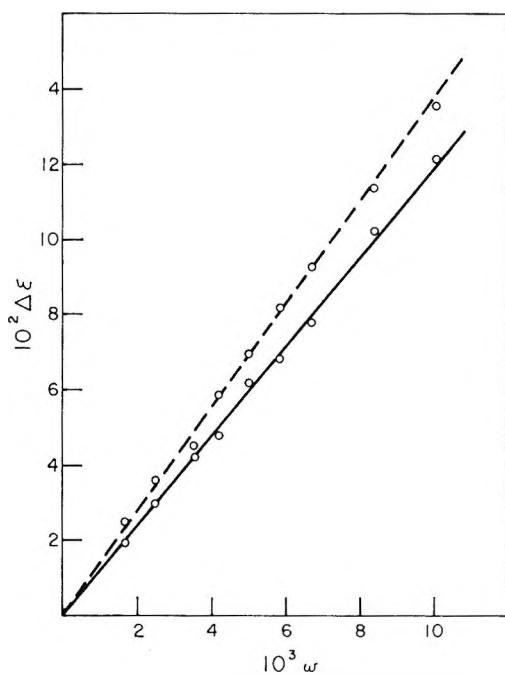
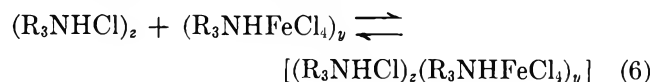


Figure 4. Effective (—) and calculated (---) dielectric constants of mixtures of tridodecylammonium chloride and tetrachloroferrate.

$(C_{12}H_{25})_3NHCl$  and  $(C_{12}H_{25})_3NHFeCl_4$ , we shall recall that earlier osmometric data<sup>3</sup> revealed that in addition to the homogeneous oligomers of both solutes a heterogeneous aggregate is formed according to the reaction



with an equilibrium constant  $\beta_{zy}$  when benzene solutions of the two solutes are mixed in varying molar ratios. It has been found that  $z = y = 1$  fitted the experimental data, giving a value of  $\log \beta_{11} = 2.82$ .

We have now measured the effective dielectric constant of solutions obtained by mixing benzene solutions of the components at a constant 1:1 molar ratio but at an increasing overall concentration. The experimental  $\Delta\epsilon$  values are plotted in Figure 4 as a function of the weight fraction of the total solute concentration, along with  $\Delta\epsilon_{\text{calcd}}$  calculated on the basis of additivity of  $\Delta\epsilon$  increments obtained previously in the individual systems. The lack of additivity may again be explained as due to the formation of a new species, mixed aggregate, in terms of equilibrium 6 with a higher dipole moment, thus confirming the conclusion of previous vapor pressure data.<sup>3</sup>

In order to calculate  $z$ ,  $y$ , and  $\beta_{zy}$  on the assumption that no change in the composition of the homogeneous oligomers takes place, eq 5 has been extended to

$$\frac{\epsilon - 1}{\epsilon + 2} = \frac{4\pi}{3} N_s \alpha_s + \frac{4\pi N \rho}{3} \left( \frac{w_1 \alpha_1}{M} + \frac{w_2 \alpha_2}{2M} + \frac{w_1' \alpha_1'}{M'} + \frac{w_2' \alpha_2'}{2M'} + \frac{w_{zy} \alpha_{zy}}{zM + yM'} \right) \quad (7)$$

where the unprimed and primed quantities stand for the previously derived values from the individual  $R_3NHCl$  ( $\alpha_1 = 53.86 \times 10^{-23}$  cc,  $\alpha_2 = 63.41 \times 10^{-23}$ ) and  $R_3NHFeCl_4$  ( $\alpha_1' = 109.27 \times 10^{-23}$ ,  $\alpha_2' = 108.21 \times 10^{-23}$ ) systems, respectively. Using the material balance equations

$$w = w_1 + w_2 + w_{zy} = w_1 + 2\beta_2 w_1^2 + \beta_{zy} w_1^z w_1'^y$$

$$w' = w_1' + w_2' + w_{zy}' =$$

$$w_1' + 2\beta_2 w_1'^2 + \beta_{zy} w_1^z w_1'^y \quad (8)$$

the Debye-Clausius-Mossotti eq 7 has been solved by means of a nonlinear least-square program. The best fit of the experimental dielectric constant data was obtained for  $x = y = 1$  and  $\log \beta_{11} = 2.92$  which compares reasonably well with the value obtained osmometrically.<sup>3</sup> The dipole moment of the heterogeneous dimer, calculated according to Smith (ref 19, chapter 1), was found to have a value  $\mu_{11} = 15.0$  D.

## Discussion

We shall start the discussion by a comparison of the results obtained using the two techniques, vapor pressure lowering and dielectric constant. Interpreting the osmometric data,<sup>1,2</sup> equilibria involving aggregates higher than the dimer (or trimer) have been invoked on account of a solute concentration higher by at least one order of magnitude. Calculated on the basis of the osmometrically derived aggregation constants of the high oligomers ( $n = 8$  and 16 for tridodecylammonium perchlorate, 6 for the bisulfate, 8 and 22 for the tetrachloroferrate, and 18 or 24 for the tetraheptylammonium salts), their fraction becomes very low ( $<0.01$  mol fraction) at the solute concentration level investigated by the dielectric constant measurements. Nevertheless, while the  $\beta_2$  values for the tertiary ammonium salts derived now are in reasonable agreement with those found osmometrically, the present  $\beta_3$  values for the quaternary ammonium salts differ by as much as two orders of magnitude. Figure 5 shows the mean aggregation number,  $n$ , for the tridodecylammonium chloride and tetrachloroferrate systems, as calculated from the data obtained by both methods in the partially overlapping concentration range. Obviously, a similar plot for the quaternary salts is less satisfactory.

Speaking in thermodynamic terms, however, the lack of complete agreement in the  $\beta_n$  values derived from the two types of measurements is likely to be due to the fact that the common basic assumption made in deriving the mass action law equations is not fully justified. In both types of calculations it has been assumed, namely, that the deviation of the systems from an ideal behavior is entirely due to the specific solute-solute interaction leading to the formation of oligomers. This assumption implies in turn that the activity coefficient of all species in equilibrium, the monomer and the different oligomers,<sup>15</sup> is unity. This

Table III: Recalculated Dipole Moments of Monomeric and Dimeric Alkylammonium Salts in Benzene Solutions

Compd	Concn range, $10^{3w}$	$\mu_1$ reported	$\mu_1$ calcd	$\mu_2$ calcd	$\beta_2$ calcd
$\text{Bu}_3\text{NHCl}^a$	0.07–0.45	7.17	7.17	10.1	(29)
$\text{Bu}_3\text{NHB}_1^a$	0.06–0.22	7.61	7.56	10.6	(78)
$\text{Bu}_3\text{NHB}_1^b$	0.86–6.40	8.5	8.3	16.7	6
$\text{Bu}_3\text{NHI}^a$	0.036–0.29	8.09	8.12	11.5	460
$\text{Bu}_3\text{NHPic}^a$	0.022–0.33	13.1	12.9	14.3	960
$\text{Bu}_3\text{NHPic}^c$	0.038–0.50	11.9	11.4	16.9	(6)
$\text{Bu}_3\text{NHPic}^b$	0.12–6.48	11.79	11.52	16.3	14
$i\text{-Am}_3\text{NHPic}^a$	0.02–0.37	13.3	13.4	9.0	248
$i\text{-Am}_3\text{NHPic}^b$	0.040–0.13	11.9	11.7	16.6	9
$i\text{-Am}_3\text{NHPic}^d$	0.08–0.86	13.9	13.6	13.4	(616)
$\text{Bu}_4\text{NBr}^a$	0.02–0.35	11.6	10.4	14.6	13
$\text{Bu}_4\text{NBr}^e$	0.23–5.22	13.9	(5.4)	(7.6)	(53)
$\text{Bu}_4\text{NI}^f$	0.05–0.48	12.7	9.5	13.3	520
$\text{Bu}_4\text{NClO}_4^a$	0.02–0.32	14.1	11.2	15.5	91
$\text{Bu}_4\text{NPic}^a$	0.023–0.20	17.8	17.8		196
$\text{Bu}_4\text{NPic}^e$	0.05–2.23	20.8	17.2	17.0	287
$\text{Bu}_4\text{NPic}^f$	0.12–1.01	15.1	15.2	21.5	82
$i\text{-Am}_4\text{NBr}^d$	0.05–0.54	>14.0	7.3	10.3	187
$i\text{-Am}_4\text{NCNS}^a$	0.016–0.42	15.4	14.1		723
$i\text{-Am}_4\text{NPic}^a$	0.012–0.19	18.3	18.6	20.4	1400
$i\text{-Am}_4\text{NPic}^d$	0.01–0.54	19.4	18.4	12.6	382

<sup>a</sup> Reference 4. <sup>b</sup> Reference 11. <sup>c</sup> Reference 7. <sup>d</sup> Reference 12. <sup>e</sup> Reference 6. <sup>f</sup> Reference 10.

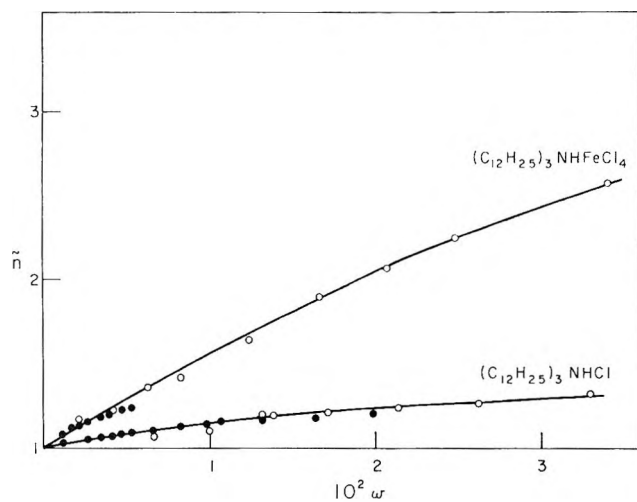


Figure 5. Mean aggregation number of tridodecylammonium salts in benzene: osmometry (○); dielectric constant (●).

very frequently made<sup>16</sup> assumption may not be entirely correct and the deviation of the systems under consideration from ideality is apparently due to both specific and nonspecific nonidealities.

The other point we wish to discuss concerns the dipole moments of the alkylammonium salts derived here and their comparison with those of similar compounds reported in the literature.<sup>4–12</sup> The existence of rather large permanent dipole moments of dimeric molecules in nonpolar media is not new. Effective dipole moments have been reported for dimeric alcohols,<sup>24</sup> carboxylic acids,<sup>20</sup> and acid amides,<sup>25</sup> in addition

to the permanent dipole moments of alkylammonium salts found by Bauge and Smith,<sup>10</sup> and Maryott.<sup>7</sup>

For the most widely studied quaternary ammonium salts, the consensus is that aggregates with several times the formula weight are formed even at concentration as low as 0.001 *M*.<sup>5</sup> Tertiary alkylammonium salts exhibit a smaller tendency toward aggregation, a possible reason being<sup>5</sup> a smaller dipole moment of their monomer. This indeed seems to be reflected by the literature data reported (Table III).

The  $\mu_1$  values for the salts investigated now do not show significant difference between the values for the two classes of alkylammonium salts, the largest difference being about 1 debye unit. However, they may not be directly comparable due to a difference in the alkyl chain length. It is felt that the large  $\mu_1$  values for the quaternary ammonium salts are essentially due to the fact that no corrections for the contribution of the dipole moments of the dimer (or other higher aggregate) have been considered in evaluating the dipole moment of the monomer; thus, they may represent the dipole moment of a monomer–dimer mixture with a mean aggregation number  $\bar{n}$ . This may be considered as a substantial failure unless the experimental data refer to a very low concentration range<sup>4</sup> (see Table III). In other cases, the actually

(24) D. A. Ibbitson and L. F. Moore, *J. Chem. Soc. B*, 76 (1967); 80 (1967), and references therein.

(25) M. E. Hobbs and W. W. Bates, *J. Amer. Chem. Soc.*, **74**, 746 (1952).

applied procedure which consists of an evaluation of  $\mu_1$  from the experimental data in the apparently linear fraction of the  $\Delta\epsilon$  vs. concentration plot and disregarding the lack of linearity at increased concentrations may not be rigorous enough.<sup>24</sup>

In order to verify whether there is an effect of the presence of a dimer with its own permanent dipole upon that of the monomer, we have now recalculated literature data where detailed experimental information was provided for a number of butyl and isoamylammonium salts, using the model of a monomer-dimer equilibrium. It should be emphasized that in this recalculation the computer program is such as to give equal weight to the experimentally determined  $\epsilon$ 's over the whole concentration range, rather than weighing the results in favor of the dilute solutions, which is the way of calculation in the extrapolation procedure.

The results of recalculation are compiled in Table III, along with the  $\mu_1$  values originally reported.

An examination of the numerical values suggests that if the solute concentration range is low enough and where the contribution of complex species is not significant, the monomer-dimer model does not affect the  $\mu_1$  values originally computed. In the case of tertiary ammonium salts, where the  $\beta_2$  values are generally low, the reported and recalculated  $\mu_1$  values are again not much different. On the other hand, differences become apparent when the reported  $\mu_1$  values were obtained from data in a concentration range where appreciable aggregation takes place. In these cases the recalculated  $\mu_1$  values are lower by several debye units, though only in a few cases  $\text{Bu}_4\text{NPic}^{4,6}$  and  $i\text{-Am}_4\text{NPic}^{4,12}$  bring the recalculated  $\mu_1$  values closer to one another.

## Investigation of Micelle Structure by Fluorine Magnetic Resonance.

### IV. Fluorine-Labeled Nonionic Detergents<sup>1</sup>

by Norbert Muller\* and Frank E. Platko

Department of Chemistry, Purdue University, Lafayette, Indiana 47907 (Received August 31, 1970)

Publication costs assisted by the National Science Foundation

The nonionic surfactants 8,8,8-trifluorooctyl hexaoxyethylene glycol monoether (**1**) and 8,8,8-trifluorooctyl methyl sulfoxide (**2**) have been prepared and their fluorine chemical shifts measured in water and aqueous urea solutions as a function of concentration and temperature. Chemical shifts for the monomeric and micellized materials were found to be nearly the same as corresponding values for anionic trifluoroalkyl detergents. When the aggregation numbers are less than about 25 they can be evaluated from the nmr data, assuming a simple mass action model. For **1** the aggregation number in water is 16 at 27° and changes only slightly with changing temperature below 42°. At higher temperatures or with added urea the micelles are considerably larger, and precise values for the aggregation numbers cannot be found. Derived values of the free energies, enthalpies, and entropies of micellization are in good agreement with available data for the unfluorinated analogs of **1** and **2**. For every trifluoroalkyl detergent so far studied, the free energy of micellization is about 0.4 kcal/mol less favorable than for the related alkyl compound. Micellization of **1** involves a substantial negative heat capacity change which becomes smaller when urea is added. Consequently urea addition reduces the positive enthalpy of micellization at low temperatures but increases it at temperatures above 43°. Some observations of the effect of dioxane and tetrahydrofuran on the micellization of **2** are also reported.

#### Introduction

As reported in the preceding papers,<sup>2-4</sup> fluorine nuclear magnetic resonance (nmr) measurements on several anionic surfactants having hydrocarbon chains with a terminal trifluoromethyl group readily yielded values of the chemical shifts for the monomeric ions and the micellar material and of the critical micelle

concentrations (cmc) as well as limited information about micellar size. The cmc's of the trifluoro com-

(1) Financial support from the National Science Foundation under Grant G. P. 8370 is gratefully acknowledged.

(2) N. Muller and R. H. Birkhahn, *J. Phys. Chem.*, **71**, 957 (1967).

(3) N. Muller and R. H. Birkhahn, *ibid.*, **72**, 583 (1968).

(4) N. Muller and T. W. Johnson, *ibid.*, **73**, 2042 (1969).

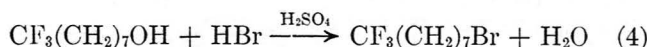
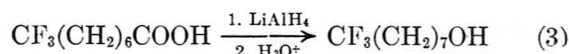
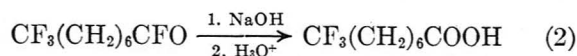
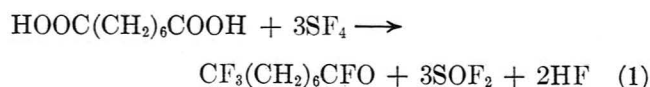
pounds were consistently about twice as large as those of the corresponding nonfluorinated materials. The effects of temperature changes and of addition of simple electrolytes or organic cosolvents on the micellization of the fluorinated compounds were closely similar to the known effects of such perturbations on ordinary anionic detergents.<sup>5</sup> Inevitably, detailed interpretation of the results was made more difficult by the fact that all observed properties depend on the behavior of both the surfactant ions and their counterions.

Although it is generally agreed that the interior of a micelle resembles a tiny drop of liquid hydrocarbon, the fluorine shift of a micellized detergent,  $\delta(S_m)$ , differs considerably from the value characteristic of a  $\text{CF}_3(\text{CH}_2)_n$  group in a typical hydrocarbon solvent (essentially independent of  $n$  when  $n \geq 6$ ). Instead,  $\delta(S_m)$  is nearly midway between this value and the shift,  $\delta(S)$ , for the monomeric ion in water. This finding cannot be ascribed to the fact that the alkyl chains in the micelle are partially fluorinated, because the shift for  $\text{CF}_3(\text{CH}_2)_n$  compounds using  $\text{CF}_3(\text{CH}_2)_8\text{CF}_3$  as the solvent is nearly the same as that in hexane. It was therefore suggested that the  $\text{CF}_3$  groups in the micelles are in an environment which is at least partly aqueous in nature. However, it was noted also that the aqueous monomer shifts were appreciably altered by added electrolytes, raising the possibility that the  $\delta(S_m)$  values might be controlled in part by interactions between  $\text{CF}_3$  groups and charged moieties at the micellar surface.

These considerations prompted us to undertake the nmr study of two fluorine-labeled nonionic detergents described here. The compounds, S,S,S-trifluorooctyl hexaoxyethylene glycol monoether,  $\text{CF}_3(\text{CH}_2)_7\text{O}(\text{C}_2\text{H}_4\text{O})_6\text{H}$  (hereafter designated **1**), and S,S,S-trifluorooctyl methyl sulfoxide,  $\text{CF}_3(\text{CH}_2)_7\text{S}(\text{O})\text{CH}_3$  (hereafter **2**), were selected because they are relatively easy to prepare and purify, because they allow the effect of a large change in headgroup size to be evaluated, and because a considerable body of information about their unfluorinated analogs is available.<sup>6-12</sup> We determined the fluorine chemical shift of **1** as a function of concentration and temperature in water, 2.0 M urea, and 4.0 M urea. Compound **2** is only slightly soluble in water, and we studied it in aqueous urea solutions, 2.0 M aqueous 1,4-dioxane, and 2.0 M tetrahydrofuran.

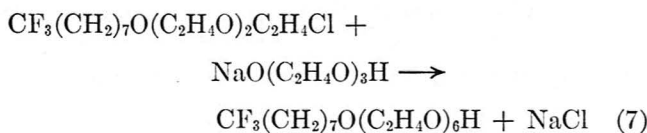
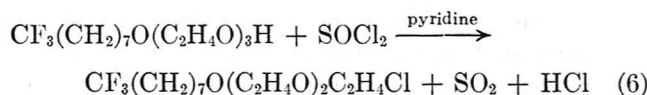
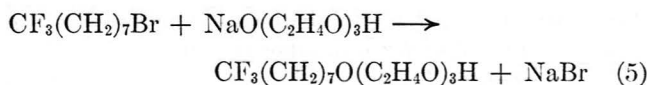
### Experimental Section

The starting material for the preparation of both fluorinated detergents was 8,8,8-trifluoro-1-bromooctane, which was made from suberic acid using the following sequence of well-known reactions<sup>13</sup>



The trifluorobromooctane was isolated as a colorless liquid, bp 60° (2 mm).

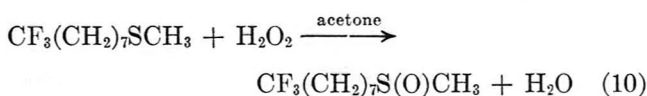
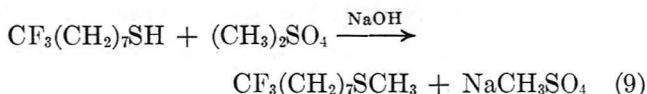
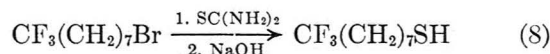
The reaction scheme for the synthesis of **1** was essentially the same as one given in ref 6, *i.e.*



Compound **1** was isolated from the reaction mixture and distilled from charcoal in a molecular still at 10<sup>-4</sup> mm. The product was a colorless oil which solidified when chilled, mp 10.5°.

*Anal.* Calcd for **1**: C, 53.56; H, 8.77; F, 12.71; mol wt 448.5. Found: C, 53.65; H, 8.80; F, 12.93; mol wt 444.2.

The reaction sequence used for the preparation of **2** was as follows



Compound **2** was isolated, twice sublimed under vacuum, and then twice recrystallized from hexane. It was a white solid, mp 36.5–37.5°.

*Anal.* Calcd for **2**: C, 46.93; H, 7.44; F, 24.75; S, 13.92; mol wt 230.3. Found: C, 46.95; H, 7.36; F, 24.90; S, 13.79; mol wt 233.

(5) M. F. Emerson and A. Holtzer, *J. Phys. Chem.*, **71**, 3320 (1967).

(6) J. M. Corkill, J. F. Goodman, and R. H. Ottewill, *Trans. Faraday Soc.*, **57**, 1627 (1961).

(7) J. M. Corkill, J. F. Goodman, and S. P. Harrold, *ibid.*, **60**, 202 (1964).

(8) J. M. Corkill, J. F. Goodman, and J. R. Tate, *ibid.*, **60**, 996 (1964).

(9) J. S. Clunie, J. M. Corkill, J. F. Goodman, P. C. Symons, and J. R. Tate, *ibid.*, **63**, 2839 (1967).

(10) J. M. Corkill, J. F. Goodman, P. Robson, and J. R. Tate, *ibid.*, **62**, 987 (1966).

(11) T. Walker, personal communication.

(12) J. M. Corkill, J. F. Goodman, and J. R. Tate, *Hydrogen-Bonded Solvent Syst. Proc. Symp.*, 181 (1968).

(13) For additional details see F. E. Platko, Ph.D. Thesis, Purdue University, 1970.

Tetrahydrofuran (Baker AR) and 1,4-dioxane (Lynn, Pure Bulk) were distilled before use because they were found to produce slightly turbid solutions in water unless this was done. Water from the laboratory distilled water supply was redistilled from alkaline permanganate. Urea (Mallinckrodt Reagent grade) was used without further purification.

Nmr samples were made by methods essentially similar to those described earlier,<sup>4</sup> except that the solutions containing urea, dioxane, or tetrahydrofuran were made keeping the molarity of additive constant for each set of samples. Spectra were obtained with a Varian HA-60-IL spectrometer operated at 56.445 MHz. The reference capillaries contained a mixture of 98% 1,1,2-trichlorotrifluoropropane and 2% 1,2-difluorotetrachloroethane. Shifts were measured from the  $C_3F_3Cl_3$  peak, and are related to previously reported shifts based on benzotrifluoride as a reference by the formula<sup>14</sup>

$$\delta(C_3F_3Cl_3) = \delta(C_6H_5CF_3) + 2.253 + 2.9 \times 10^{-4}t \quad (11)$$

where  $t$  is the centigrade temperature. The position of the  $CFCl_2CFCl_2$  peak was used to find the temperature,<sup>15</sup> controlled with a Varian V-4341/V-6057 variable temperature accessory. A Varian C-1024 time-averaging computer was used for sensitivity enhancement with the more dilute samples as needed. Reproducibility of the chemical shift determinations varied somewhat as the temperature was changed, but the deviations seldom exceeded  $\pm 0.01$  ppm.

## Results

The fluorine spectra of the two nonionic detergents closely resemble those of several previously examined compounds of the type  $CF_3(CH_2)_nX$ , where  $n \geq 6$  and  $X$  is any one of a number of functional groups including  $CF_3$ ,  $COOH$ , and  $SO_3Na$ . Short-range proton-fluorine spin-spin interaction splits the fluorine peak into a triplet with a spacing of 10.5 Hz. Each component has a width of slightly over 2 Hz because of unresolved longer range spin-spin interactions. For pure liquid **1** the shift decreases somewhat nonlinearly as the temperature is raised, as follows

Temp, °C	13.1	19.8	38.2	51.5	66.0
Shift, ppm	4.75	4.72	4.62	4.53	4.43

In solution each detergent again produces a triplet fluorine signal (except in the immediate vicinity of the cloud point; see below) indicating that exchange of monomeric and micellar material is rapid on the nmr time scale. Typical data for **1** in water at two temperatures are given in Figure 1 as plots of the chemical shift against the reciprocal of the overall detergent concentration,  $S_0$ . Micelle shifts are obtained by extrapolating the high-concentration data to  $1/S_0 = 0$ ;

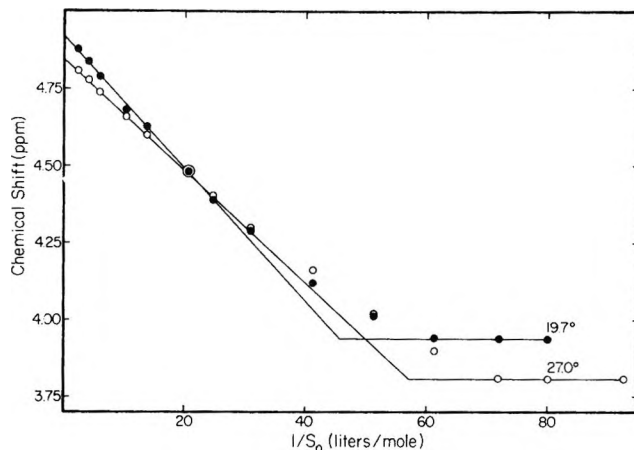


Figure 1. Chemical shift as a function of the reciprocal of the total detergent concentration for 8,8,8-trifluorooctyl hexaoxyethylene glycol monoether in water at 19.7 and 27.0°.

monomer shifts are the limiting values attained in the most dilute solutions; cmc's are found by extrapolating the two linear portions of the  $\delta$  vs.  $1/S_0$  plots until they intersect.<sup>2</sup> Since the  $\delta(S)$  values are directly measured, they should be accurate to within  $\pm 0.01$  ppm. It is more difficult to specify the accuracy of the  $\delta(S_m)$  and cmc values because they are found by graphical extrapolation and the reliability varies from one set of data to the next, depending on the number of points in the linear region of the plot, their scatter, and the slope of the line. We estimate that errors in the  $\delta(S_m)$  values should not exceed  $\pm 0.02$  ppm and that the accuracy of the cmc's justifies reporting two significant figures.

Results at various temperatures for **1** in water and 2.0 and 4.0 *M* urea appear in Table I. The upper limit of the temperature range is set by the cloud point, which is near 65° or about 7° below the value reported<sup>9</sup> for unfluorinated *n*-octylhexaoxyethylene glycol monoether. Solutions with  $S_0 > 0.04$  *M* examined at 64.8° gave two fluorine resonances, apparently owing to separation of the samples into a detergent-rich phase with  $\delta \cong 4.49$  and a water-rich phase with  $\delta \cong 4.22$ . Values of  $\delta(S_m)$  and cmc reported for this temperature were found using only the data for the less concentrated solutions, which fall on a normal dilution curve. Addition of urea slightly raises the cloud point.

Results for **2** dissolved in water, 2.0 and 4.0 *M* urea, 2.0 *M* dioxane, and 2.0 *M* tetrahydrofuran are collected in Table II. In water, only  $\delta(S)$  values are given because the compound is too insoluble to allow  $\delta(S_m)$  or cmc to be determined. Organic additives increase the solubility enough for typical dilution curves to be obtained.

## Discussion

*Chemical Shifts.* At each temperature, both non-

(14) T. W. Johnson, Ph.D. Thesis, Purdue University, 1970.

(15) N. Muller and T. W. Johnson, *J. Phys. Chem.*, **73**, 2460 (1969).

**Table I:** Nmr Results for Trifluorooctyl Hexaoxyethylene Glycol Monoether in Water and Aqueous Urea Solutions

Solvent	Temp, °C	Monomer shift, ppm	Micelle shift, ppm	Critical micelle concn, $M \times 10^2$
Water	1.5	4.30	5.07	4.3
	10.2	4.11	5.02	3.1
	19.7	3.94	4.92	2.2
	27.0	3.81	4.85	1.8
	32.5	3.71	4.81	1.5
	42.0	3.55	4.73	1.3
	52.0	3.40	4.64	1.2
	64.8	3.23	4.47	1.1
2.0 M urea	2.6	4.15	5.03	5.9
	16.6	3.90	4.92	3.9
	29.8	3.67	4.79	2.8
	43.9	3.46	4.67	2.2
	57.6	3.26	4.55	1.9
	71.1	3.09	4.42	1.8
4.0 M urea	3.6	4.02	5.00	7.4
	14.2	3.88	4.92	5.8
	29.0	3.64	4.77	4.0
	47.7	3.35	4.63	3.1
	59.8	3.19	4.52	2.7
	73.1	3.02	4.37	2.5

**Table II:** Nmr Results for Trifluorooctyl Methyl Sulfoxide in Water and Mixed Aqueous Solvents

Solvent	Temp, °C	Monomer shift, ppm	Micelle shift, ppm	Critical micelle concn, $M \times 10^2$
Water	2.0	4.31		
	9.6	4.15		
	15.3	4.04		
	23.4	3.88		
	30.2	3.76		
	35.8	3.67		
2.0 M urea	2.1	4.16	5.12	8.7
	7.2	4.09	5.06	8.2
	14.3	3.95	5.00	7.5
4.0 M urea	3.2	4.07	5.03	10.5
	10.2	3.95	5.00	9.8
	17.4	3.85	4.94	9.1
	22.9	3.74	4.89	8.5
	28.0	3.67	4.84	8.1
	35.0	3.56	4.77	7.8
2.0 M dioxane	28.1	3.85	4.83	7.5
2.0 M tetrahydrofuran	27.6	3.94	5.10	5.5

ionic detergents yield the same  $\delta(S)$ , and the value found is identical with that reported earlier<sup>2-4,14</sup> for several anionic detergents of the type  $\text{CF}_3(\text{CH}_2)_n\text{X}$ . The immediate environment of the  $\text{CF}_3$  group thus appears to be quite unaffected by changes in the size, chemical constitution, or electrical charge of the solubilizing group. We had anticipated that **1** might exist at least in part in a form in which the 19-atom hexa-

oxyethylene chain is folded back over the hydrocarbon tail and that this would lead to a change in the fluorine shift, but there is no evidence of such behavior. The results suggest that in water the hydrocarbon chains exist primarily in the extended zigzag conformation, preventing the  $\text{CF}_3$  groups from coming close to the solubilizing moiety. An alternative interpretation is that in each case the head group is so strongly hydrated that a shell of solvent molecules keeps the  $\text{CF}_3$  group from coming in contact with it.

The micelle shifts in water are given in Table I for compound **1**. Since Table I and the results in ref 4 show that urea causes only a slight decrease in  $\delta(S_m)$ , it is estimated from the data in Table II that  $\delta(S_m)$  for **2** at a given temperature is perhaps 0.1 ppm larger than for **1**. Considering these values together with those reported for anionic surfactants<sup>2-4,14</sup> it appears that there are real variations in  $\delta(S_m)$  as the nature of the head group is changed, but perhaps the most significant finding is that these variations are so small. This implies that the micelle shifts for the anionic detergents are affected little or not at all by the electrical charges at the micellar surface and strengthens the supposition that the shifts reflect exposure of the  $\text{CF}_3$  groups to an environment of partly aqueous and partly hydrocarbon character. This environment apparently changes only slightly when rather drastic changes are made in the size or charge type of the solubilizing group.

At first glance it might seem surprising that  $\delta(S_m)$  for **1** is larger than the shift found for the pure liquid, but this can be rationalized as follows. In the pure liquid, a  $\text{CF}_3$  group may be adjacent either to a hydrocarbon or to a hexaoxyethylene chain. It should therefore exhibit a shift between that found for  $\text{CF}_3(\text{CH}_2)_n\text{X}$  compounds in hexane (about 6.3 ppm at 27°) and that found in polyethylene glycols (4.0 ppm in triethylene glycol at 27°), and the observed value (4.7 ppm at 27°) is in this range. In the micelle, the molecules are likely to be so arranged that contact between  $\text{CF}_3$  groups and hexaoxyethylene chains is minimal; the  $\text{CF}_3$  groups are then adjacent either to other  $\text{CF}_3(\text{CH}_2)_7$  chains or to water molecules, and exhibit a typical micelle shift.

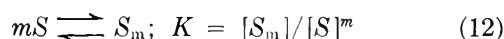
The effects of additives on  $\delta(S)$  and  $\delta(S_m)$  are similar to those reported for sodium trifluorododecylsulfate.<sup>4</sup>

**Micelle Size.** On the basis of light-scattering experiments it has been reported repeatedly that aggregation numbers ( $m$ ) of nonionic detergents increase as the temperature is raised. For some materials,  $\log m$  appears to be a linear function of the temperature over the whole accessible range,<sup>16</sup> while for others this behavior is found above a transition temperature, and  $m$  is roughly constant at lower temperatures.<sup>17,18</sup> Simple

(16) R. R. Balmbra, J. S. Clunie, J. M. Corkill, and J. F. Goodman, *Trans. Faraday Soc.*, **58**, 1661 (1962).

calculations show<sup>4</sup> that in the absence of complicating counterion effects nmr dilution curves should make it possible to determine  $m$  values with moderate accuracy if the degree of aggregation is not too large. Accordingly, we undertook to explore the temperature dependence of the micelle size for compound **1** by this method.

If micellization is assumed to be governed by a simple mass-action expression



one may write

$$\log m[S_m] - m \log [S] = \log mK = \text{constant} \quad (13)$$

and therefore a plot of  $\log m[S_m]$  against  $\log [S]$  should be linear with a slope equal to  $m$ . For a sample with known  $[S_0]$  and chemical shift  $\delta$ , the required quantities are readily evaluated using

$$[S] = [S_0][\delta(S_m) - \delta]/[\delta(S_m) - \delta(S)] \quad (14)$$

and

$$m[S_m] = [S_0] - [S] \quad (15)$$

When the data for the aqueous solutions of **1** are treated in this way, using values of  $\delta(S_m)$  and  $\delta(S)$  from Table I, the plots are strongly curved, and indeed the values of  $[S]$  pass through a maximum as  $[S_0]$  increases, which is not consistent with eq 12. This apparent anomaly seems to be caused by the fact that at high concentrations, where the quantity  $[\delta(S_m) - \delta]$  is small, the calculated  $[S]$  is extremely dependent on the exact value adopted for  $\delta(S_m)$ . Consequently, a very small adjustment of  $\delta(S_m)$  suffices to eliminate the curvature, as illustrated in Figure 2, which shows two sets of points based on the data for **1** at 27°, one taking  $\delta(S_m) = 4.850$  and the other  $\delta(S_m) = 4.865$ . The latter set defines a reasonably good straight line with a slope of 16.

With suitably adjusted  $\delta(S_m)$  values, similar plots using the data at temperatures below 42° gave the following results

Temp, °C	1.5	10.2	19.7	27.0	32.5
$m$	18	13	14	16	19

In each case, the slope is well enough defined to suggest that the uncertainty in  $m$  should not exceed  $\pm 2$ . At 42° the plot shows rather severe scatter and a steeper slope suggesting that  $m$  is approximately 30. At the higher temperatures,  $m$  appears to be still larger, and the plots are so steep that no meaningful value can be assigned to the slopes. The slow change in  $m$  with temperature below 42°, followed by a sharp rise above 42°, is quite similar to the behavior reported by Elworthy and McDonald for hexadecyl polyoxyethylene glycol monoethers.<sup>17</sup>

In view of the results obtained using an approach based on a simple mass-action model, it appears that it would not be profitable to adopt a more elaborate

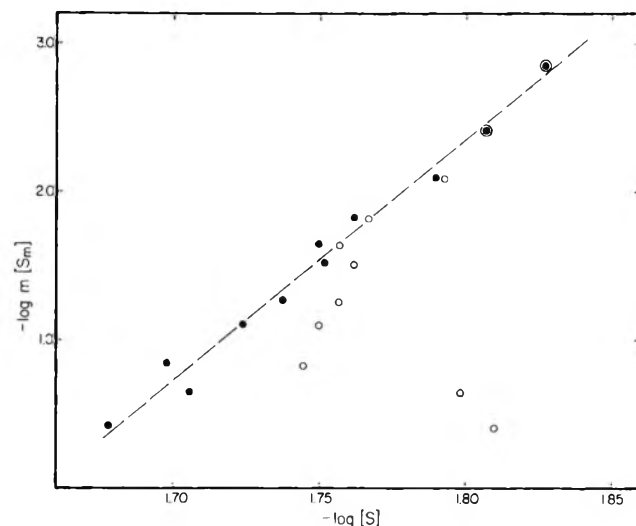


Figure 2. Plot of  $\log m[S_m]$  vs.  $\log [S]$  for aqueous 8,8,8-trifluorooctyl hexaoxyethylene glycol monoether at 27°. Open circles, points calculated taking  $\delta(S_m) = 4.850$ , filled circles with  $\delta(S_m) = 4.865$ . The dashed line has a slope of 16.2.

procedure based on a multiple-equilibrium model.<sup>19</sup> Such a model is valuable when there is reason to believe that  $m$  will change with increasing detergent concentration. Our data provide no evidence for such changes. Indeed a marked concentration dependence of  $m$  seems unlikely *a priori* for a nonionic detergent since, above the cmc,  $[S]$  is very nearly constant and hence the only major effect of further increasing  $[S_0]$  is to reduce the average distance between micelles. Unless this distance is made very small, it seems implausible that merely changing the separation between the electrically neutral micelles could cause significant changes in the average micelle size.

Addition of urea to solutions of **1** causes an increase in the aggregation number, but since the nmr procedure yields well defined  $m$  values only when  $m$  is small, no quantitative conclusion about this effect can be drawn. It is noteworthy that addition of urea to sodium trifluorododecylsulfate solutions caused a *reduction* in the micelle size.<sup>4</sup> Micelles of **2** in aqueous urea are also too large to allow  $m$  to be determined. In 2.0 *M* dioxane, they are perhaps somewhat smaller than in 2.0 *M* urea, and in 2.0 *M* tetrahydrofuran they are smaller still ( $m \cong 10$ ). This trend is similar to that found<sup>4</sup> with sodium trifluorododecylsulfate, but the lowering of the aggregation number by tetrahydrofuran is less extreme for **2** than for the sodium salt.

*Thermodynamics of Micelle Formation.* The standard free energy of micellization per mole of monomer is given by

(17) P. H. Elworthy and C. McDonald, *Kolloid Z.*, **195**, 16 (1964).

(18) P. Becher and H. Arai, *J. Colloid Interface Sci.*, **27**, 634 (1968).

(19) J. M. Corkill, J. F. Goodman, T. Walker, and J. Wyer, *Proc. Roy. Soc., Ser. A*, **312**, 243 (1969).

$$\Delta G_m^\circ = RT \ln X_0 \quad (16)$$

where  $X_0$  is the cmc in mole fraction units. Results are presented in Table III; conversions from molarities to mole fractions were made taking densities of 1.00, 1.03, and 1.06 g/cm<sup>3</sup>, respectively, for the solutions in water and 2.0 and 4.0 *M* urea. The nonionic detergents resemble the anionics in that introducing the three fluorine atoms approximately doubles the cmc. Accordingly, the  $\Delta G_m^\circ$  values for **1** and **2** are less negative than those of their nonfluorinated analogs<sup>8,10</sup> by about 0.4 kcal/mol. The difference presumably arises from a favorable interaction between the polar CF<sub>3</sub> groups and neighboring water molecules, which stabilizes the monomeric more than the micellized form.

**Table III:** Thermodynamic Variables of Micellization for 8,8,8-Trifluorooctyl Hexaoxyethylene Glycol Monoether (**1**) and 8,8,8-Trifluorooctyl Methyl Sulfoxide (**2**)<sup>a</sup>

Compd	Solvent	Temp, °C	$-\Delta G_m^\circ$ , kcal/mol	$\Delta H_m^\circ$ , kcal/mol	$\Delta S_m^\circ$ , cal/mol deg
<b>1</b>	Water	5	4.0	6.7	39
<b>1</b>	Water	25	4.7 (5.1)	4.9 (4.8)	32 (33)
<b>1</b>	Water	40	5.2 (5.6)	3.4 (3.5)	27 (29)
<b>1</b>	Water	60	5.7	1.4	21
<b>1</b>	2.0 <i>M</i> urea	5	3.8	5.0	32
<b>1</b>	2.0 <i>M</i> urea	25	4.4 (4.9)	4.2 (3.4)	29 (28)
<b>1</b>	2.0 <i>M</i> urea	40	4.8	3.1	25
<b>1</b>	2.0 <i>M</i> urea	60	5.3	1.6	21
<b>1</b>	4.0 <i>M</i> urea	5	3.6	4.2	28
<b>1</b>	4.0 <i>M</i> urea	25	4.2	3.8	27
<b>1</b>	4.0 <i>M</i> urea	40	4.5	2.9	24
<b>1</b>	4.0 <i>M</i> urea	60	5.0	1.9	21
<b>2</b>	Water	25	-(4.6)	-(1.7)	-(21)
<b>2</b>	2.0 <i>M</i> urea	10	3.6	1.9	20
<b>2</b>	4.0 <i>M</i> urea	10	3.5	1.8	19
<b>2</b>	4.0 <i>M</i> urea	28	3.8	1.5	18

<sup>a</sup> The numbers in parentheses are values for the unfluorinated analogs of **1** and **2** from ref 8, 10, and 12.

For **1**, the cmc is lower by about a factor of 20 than the value one would estimate for an anionic detergent with the same hydrophobic group. Such a difference is in line with the finding that the ratio (cmc)<sub>ionic</sub>:(cmc)<sub>nonionic</sub> is about 100 for detergents with twelve-carbon chains<sup>6</sup> and decreases when the alkyl chain is shortened.<sup>20</sup> It is often inferred that these differences simply reflect the presence or absence of electrostatic repulsions which hinder the micellization of ionic species. This reasoning, however, implies that the enthalpy of micellization should be more favorable for nonionics than for ionics, and we find (and others have shown for other surfactants<sup>7,8,10</sup>) that the opposite is true.

A common procedure for the evaluation of enthalpies of micellization is to plot log cmc vs.  $1/T$  and to use the relation<sup>21</sup>

$$\Delta H_m^\circ = 2.303R d(\log \text{cmc})/d(1/T) \quad (17)$$

Figure 3 shows our results plotted in this way. Similar data have sometimes been treated with the assumption that these plots should be linear,<sup>22</sup> but we find that they are strongly curved, showing that  $\Delta H_m^\circ$  decreases at higher temperatures. Table III contains  $\Delta H_m^\circ$  values at several temperatures obtained by drawing tangents to the smooth curves in Figure 3, and, for comparison, calorimetric  $\Delta H_m^\circ$  values for unfluorinated *n*-octyl hexaoxyethylene glycol monoether.<sup>8</sup> Procedures using eq 17 have often been criticized, especially when applied to ionic detergents.<sup>23</sup> For nonionics, however,

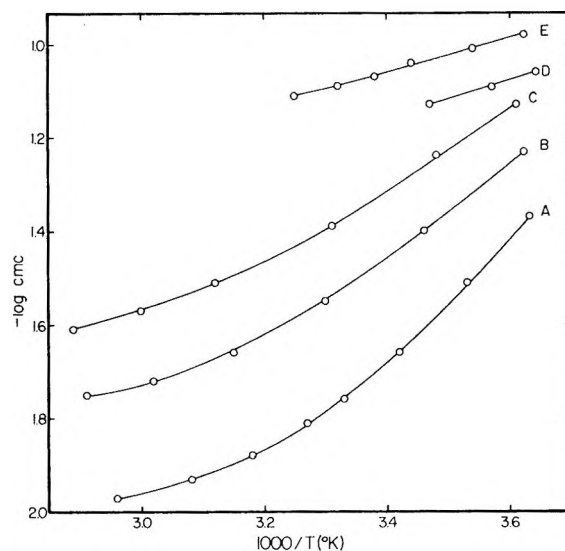


Figure 3. Temperature dependence of the critical micelle concentration for 8,8,8-trifluorooctyl hexaoxyethylene glycol monoether in water (A), 2.0 *M* urea (B), and 4.0 *M* urea (C), and for 8,8,8-trifluorooctyl methyl sulfoxide in 2.0 *M* urea (D) and 4.0 *M* urea (E).

the available evidence suggests that Stainsby and Alexander's approach yields acceptable results, though perhaps of lesser accuracy than calorimetric  $\Delta H_m^\circ$  values.<sup>8</sup> Although caution should be used when comparing  $\Delta H_m^\circ$  values for fluorinated and unfluorinated materials, the agreement between the sets of values in Table III supports the validity of the Stainsby and Alexander method and shows that it does not necessarily yield less accurate results than the calorimetric measurements.

The temperature dependence of  $\Delta H_m^\circ$  implies that micellization of **1** is accompanied by a heat capacity change  $\Delta C_p^\circ \cong -1.0 \times 10^2$  cal/deg per mol of monomer, with the magnitude of  $\Delta C_p^\circ$  increasing some-

(20) K. W. Herrmann, *J. Phys. Chem.*, **66**, 295 (1962).

(21) G. Stainsby and A. E. Alexander, *Trans. Faraday Soc.*, **46**, 587 (1950).

(22) M. J. Schick, *J. Phys. Chem.*, **67**, 1796 (1963).

(23) P. White and G. C. Benson, *Trans. Faraday Soc.*, **55**, 1052 (1959).

what as the temperature rises. This is consistent with the supposition that water structure is enhanced around the hydrophobic groups and that the headgroups are extensively hydrated through hydrogen bond formation between water molecules and the ether oxygens. Both mechanisms cause the water surrounding the detergent monomers to be in a state of low enthalpy and entropy, as compared with bulk water. That at least some of this water is "set free" when the detergent aggregates is shown also by the positive  $\Delta S_m^\circ$  values (from  $\Delta G_m^\circ = \Delta H_m^\circ - T\Delta S_m^\circ$ ) included in Table III. Very similar arguments have been used to account for the positive  $\Delta C_p$ 's of denaturation often found for proteins.<sup>24, 25</sup>

Thermochemical quantities for the micellization of **2** are also included in Table III. Again, the favorable free energy of micellization arises from an entropy term which overpowers a large unfavorable enthalpic contribution. The magnitudes of  $\Delta H_m^\circ$  and  $\Delta S_m^\circ$  change drastically when the headgroup is changed, but these changes are mutually compensating to such an extent that  $\Delta G_m^\circ$  is almost unaffected.

Urea increases the cmc of **1**, that is reduces the favorable free energy of micellization, over the whole temperature range, but its effect on the enthalpy and entropy is less simple. At low temperatures,  $\Delta H_m^\circ$  falls with rising urea concentration, and the net reduction in the magnitude of  $\Delta G_m^\circ$  may be attributed to an accompanying decrease in the  $T\Delta S_m^\circ$  term. Quite similar re-

sults were reported for the micellization of octylsulfanyl alcohols in the presence of urea.<sup>26</sup> However,  $\Delta C_p^\circ$  for **1** is much less negative in the presence of urea than water, *i.e.*,  $\Delta H_m^\circ$  in the urea solutions decreases less rapidly with rising temperature than in water. Consequently,  $\Delta H_m^\circ$  is independent of the concentration of added urea at about 43°, and above this temperature it is increased by urea addition. These findings are not consistent with the suggestion<sup>27</sup> that "addition of urea to polyoxyethylene surfactants increases the hydration of the ethylene oxide chains and consequently raises the cmc values of these solutions." Indeed, our results are not unambiguously interpretable on the basis of any simple model of the role played by urea in these systems.

The changes in  $\Delta H_m^\circ$ ,  $\Delta S_m^\circ$ , and  $\Delta G_m^\circ$  produced by urea addition are much smaller for **2** than for **1** at temperatures near 10° (see Table III). Evidently, the additive strongly modifies the interaction of the solvent both with the headgroups and with the hydrophobic chains, and these effects cannot be separated in the absence of data for related detergents having hydrophobic chains of varying length.<sup>26</sup>

(24) C. Tanford, *Advan. Protein Chem.*, **23**, 121 (1968); **24**, 1 (1970).

(25) J. F. Brandts in "Structure and Stability of Biological Macromolecules," S. N. Timasheff and G. D. Fasman, Ed., Marcel Dekker, New York, N. Y., 1969 p 213.

(26) J. M. Corkill, J. F. Goodman, S. P. Harrold, and J. R. Tate, *Trans. Faraday Soc.*, **63**, 240 (1967).

(27) M. J. Schick, *J. Phys. Chem.*, **68**, 3585 (1964).

## Electrochemical Behavior of Liquid Anion Membranes. Biionic Potentials

with the  $\text{NO}_3^-$ - $\text{Cl}^-$ ,  $\text{NO}_3^-$ - $\text{Br}^-$ ,  $\text{Br}^-$ - $\text{Cl}^-$  Couples

by P. R. Danesi, F. Salvemini, G. Scibona,\* and B. Scuppa

Industrial Chemistry Laboratory, C.N.E.N., CSN-Casaccia, Rome, Italy (Received January 16, 1970)

Publication costs assisted by C.N.E.N., CSN-Casaccia

The membrane potentials of benzene solutions of nitrate, chloride, and bromide salts of tetraheptylammonium interposed between two aqueous electrolyte solutions are reported. In the case of biionic potentials with the  $\text{NO}_3^-$ - $\text{Cl}^-$ ,  $\text{NO}_3^-$ - $\text{Br}^-$ ,  $\text{Cl}^-$ - $\text{Br}^-$  couples a quantitative correlation between the measured potential, the ion-exchange constants, the ion-pair formation constants, and the ionic mobilities is discussed. The existence of a transient potential is also analyzed and correlated to both the solubility of the alkylammonium salt in the water phase and to the ion-exchange rate (in the case of biionic potentials).

### Introduction

The electrochemical properties of low dielectric constant solutions of liquid ion exchangers interposed between two aqueous electrolyte solutions containing ions to which the organic phase is permeable have been reported<sup>1-4</sup> mainly for the case of monoionic potentials.

In the present paper both monoionic and biionic potential measurements for such systems (also known as liquid membrane electrodes) are reported and discussed at the light of the current state of the available theory with the aim to contribute to a better understanding of the potential originating mechanism and then to the design of highly selective liquid membrane electrodes.

### Experimental Section

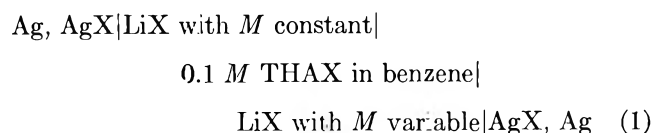
**Reagents.** HCl, HBr,  $\text{HNO}_3$ , LiBr, LiCl, and  $\text{LiNO}_3$  of analytical grade purity, supplied by Carlo Erba, have been used in the experiments. Benzene of the same type of purity, supplied by Carlo Erba, has been used. Tetraheptylammonium iodide (THAI) supplied by Eastman Kodak has been used to prepare the other alkylammonium salts. The preparation of THACl and  $\text{THANO}_3$  has been already reported.<sup>5</sup> THABr has been prepared following the same procedure used for THACl. To take into account possible concentration variations due to solubilization of the alkylammonium salt or exchange reactions (in the case of biionic potentials), all aqueous and organic solutions have been analyzed by standard analytical procedures before and after the membrane potential measurements. Silver-silver chloride, silver-silver bromide, and saturated calomel electrodes have been prepared according to ref 6 and 7.

**Solubility.** The solubility of the THACl salt in LiCl solutions has been determined by measuring potentiometrically the chloride concentration in the aqueous

phase before and after the equilibration of the aqueous solutions with the benzene solutions of THACl (phase ratio 1:1).

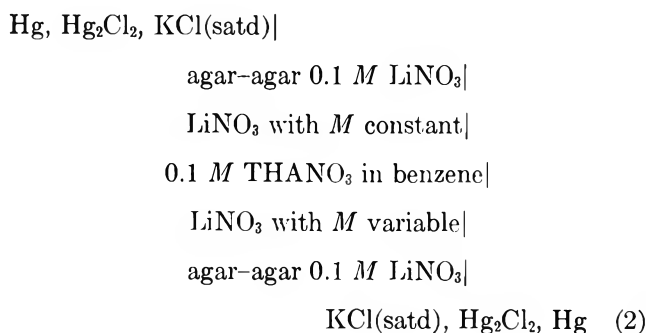
**Interfacial Tension Measurements.** The measurements have been performed following the procedure reported in ref 8.

**Membrane Potential Measurements. Monoionic Potentials.** All the membrane potential measurements have been performed by using cells with stirred organic and aqueous phases unless differently indicated. In the case of the halide ions the membrane potentials have been measured by means of the cell

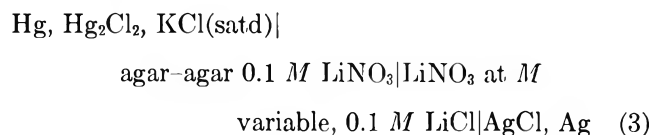


where  $\text{X}^- = \text{Br}^-$  or  $\text{Cl}^-$ . The emf of this cell is given by  $E = V_0 - RT/F \ln (a_x'/a_x'')$  where  $a_x$  stands for the mean aqueous activity of the ions,  $V_0$  represents the membrane potential, and the symbols ' and '' refer to the two aqueous sides of the cell. In the case of the  $\text{NO}_3^-$  anion, the membrane potential has been measured by means of the cell

- (1) G. Eisenman, *Anal. Chem.*, **40**, 310 (1968).
- (2) C. S. Coetze and H. Freiser, *ibid.*, **40**, 2071 (1968).
- (3) C. S. Coetze and H. Freiser, *ibid.*, **41**, 1128 (1969).
- (4) (a) C. Botrè and G. Scibona, *Ann. Chim. (Rome)*, **52**, 1199 (1962); (b) J. W. Ross, Jr., *Science*, **155**, 1378 (1967); (c) J. W. Ross, Jr., Orion Research Inc. Bulletin 92-81.
- (5) P. R. Danesi, M. Magini, and G. Scibona, "Progress in Coordination Chemistry," Elsevier, Amsterdam, 1968, paper J-19.
- (6) J. Janz, "Reference Electrodes," Academic Press, New York, N. Y., 1961, Chapter 4.
- (7) A. S. Brown, *J. Amer. Chem. Soc.*, **56**, 646 (1934).
- (8) K. Reilly and L. Rae, "Physico Chemical Methods," Vol. 1, Methuen, London, 1943, and bibliography therein.



The emf of cell 2 is given by  $E = V_0 + \Delta E_j$  where  $\Delta E_j$  is the difference between the two junction potentials at the agar-solution ' and agar-solution '' interfaces.  $\Delta E_j$  has been evaluated by means of emf measurements with cells of the type

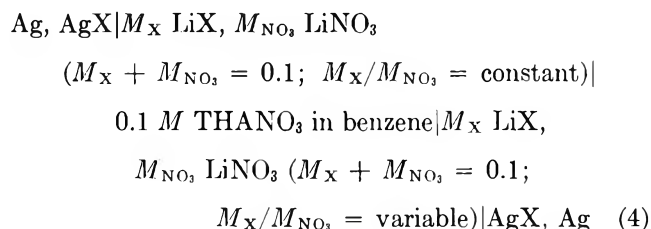


In this case the emf of the cell will be given by

$$E = E_0 - RT/F \ln a_{\text{Cl}^-} + E_j$$

Straight lines have been obtained by plotting the data in the form  $E + RT/F \ln a_{\text{Cl}^-}$  vs.  $M$ . Therefore the liquid junction potential function is of the form  $E_j = a + bM$  with  $a$  and  $b$  constants and the  $\Delta E_j$  contribution to the liquid membrane potential can be accounted for. The organic and the aqueous phases used in the cells had been previously preequilibrated. The organic phase was preequilibrated with the most diluted aqueous electrolyte solution and the aqueous phase with a THAX 0.1  $M$  benzene solution (with the  $X^- = \text{Cl}^-$ ,  $\text{Br}^-$ , or  $\text{NO}_3^-$  according to the cell type). In the equilibrations the phase ratio was the same as the one used in the electrochemical cells.

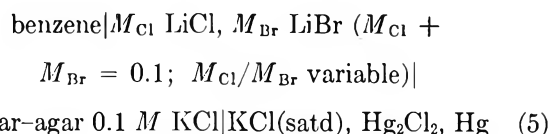
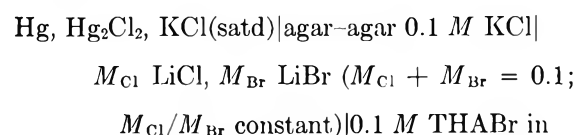
**Biionic Potentials.** The biionic membrane potential measurements have been performed with stirred (organic and aqueous phase) cells of the type



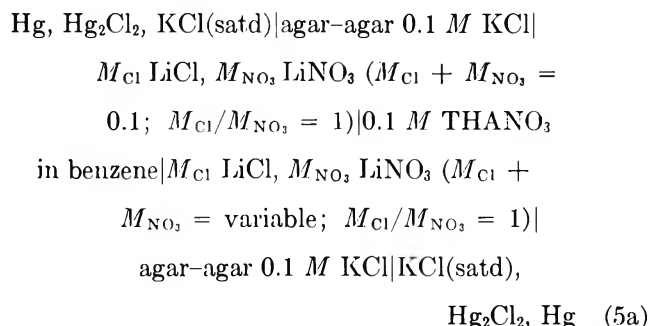
where  $X^- = \text{Cl}^-$  or  $\text{Br}^-$ . The emf of this cell is given by

$$E = V_0 - RT/F \ln (a_{X'}/a_{X''})$$

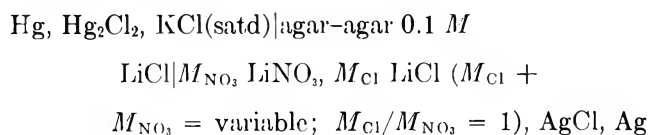
In the  $\text{Br}^- \text{Cl}^-$  case the following cell has been used



In the  $\text{NO}_3^- \text{Cl}^-$  case some measurements have been also performed by using the cell



The emf of cell 5 is given by  $E = V_0$ . The difference between the two junction potentials at the two agar-solution interfaces is, in fact, negligible. The emf of cell 5a is given by  $E = V_0 + \Delta E_j$ . As in the case of monoionic potential measurements, previously described,  $\Delta E_j$  has been evaluated by means of emf measurements with cells of the type



In this case the emf of the cell will be given by  $E = E_0 - (RT/F) \ln a_{\text{Cl}^-} + E_j$ . Also in this case the data have been plotted in the form  $E + (RT/F) \ln a_{\text{Cl}^-}$  vs.  $M_{\text{Cl}}$ . The obtained straight lines have indicated that the liquid junction potential is of the form  $E_j = a + b(M_{\text{Cl}} + M_{\text{NO}_3})$ . The  $\Delta E_j$  contribution to the liquid membrane potential can be so accounted for.

The organic and aqueous solutions used in the cells had been previously equilibrated: the organic phase with the aqueous solution containing the lowest  $\text{LiX}$  (for cell 4) and  $\text{LiCl}$  (for cell 5 and 5a) concentrations, the aqueous phases with the benzene solution of THAX 0.1  $M$  (with  $X^- = \text{NO}_3^-$  or  $\text{Br}^-$  according to the cell type). The emf values have been measured by using a Cary 31 vibrating reed electrode electrometer at  $25 \pm 1^\circ$ . As a consequence of the high impedance of the system the electrochemical cells were placed inside a copper Faraday cage to perform noiseless electrical potential measurements.

## Results and Discussion

In Figure 1 the membrane potential,  $V_0$ , of cells 1 and 2 is reported as function of the logarithm of the mean activity,  $a_X$ , for nitrate, bromide, and chloride ions. The experimental data (at  $25^\circ$ ) satisfy the relation

$$V_0 = A \log (a_{X'}/a_{X''}) \quad (6)$$

with  $A = (59 \pm 1) \text{ mV}$ .

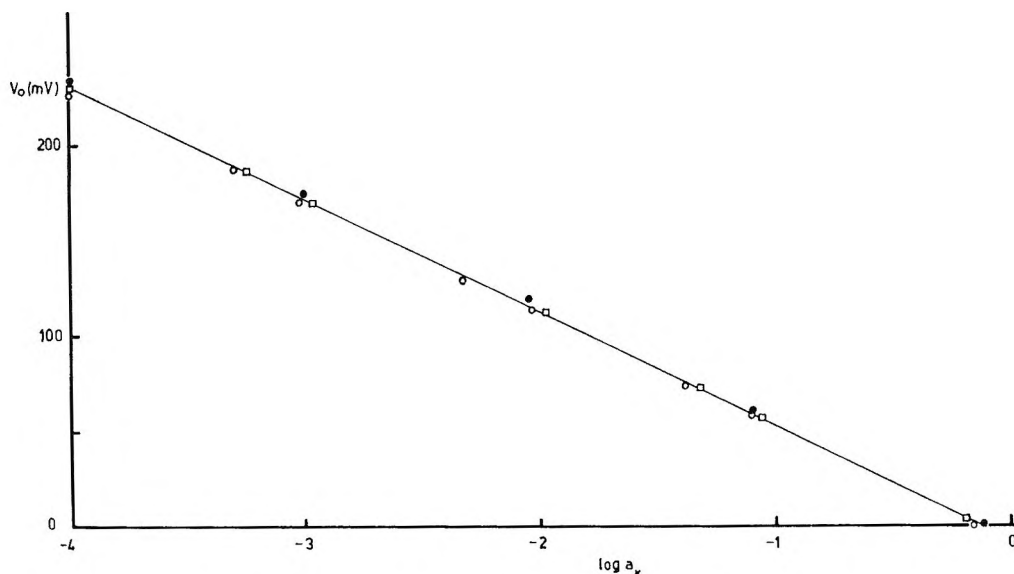


Figure 1. Membrane potential  $V_0$  (mV) vs. logarithm of mean anion activity,  $a_x$ , for  $\text{Br}^-$  ( $\square$ ),  $\text{Cl}^-$  ( $\bullet$ ), and  $\text{NO}_3^-$  ( $\circ$ ) ions.

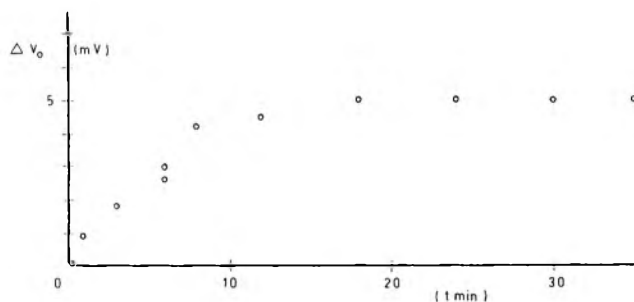


Figure 2. Variation of the membrane potential,  $\Delta V_0$  (mV), with time  $t$  in minutes in the case of the  $\text{Cl}^-$  ion.

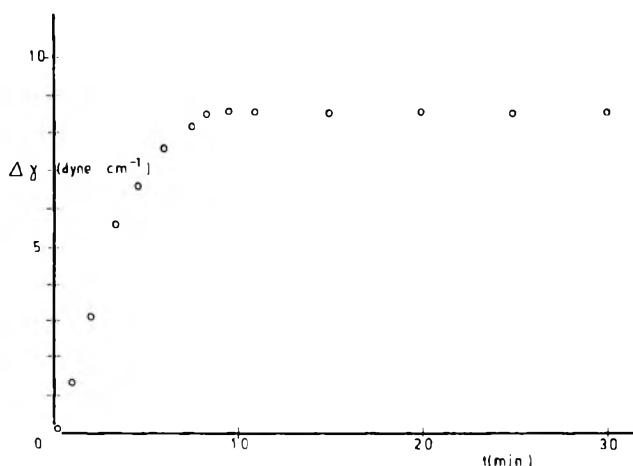


Figure 3. Variation of the interfacial tension,  $\Delta\gamma$  ( $\text{dyn cm}^{-1}$ ), with time for the system  $0.1 M$  THACl in benzene solution- $0.1 M$  LiCl in aqueous solution.

A transient potential was observed when nonpre-equilibrated aqueous solutions were used. In Figure 2 the variation with time of the potential of cell 1 with  $\text{X}^- = \text{Cl}^-$  is reported. The variation with time of the inter-

facial tension of a benzene solution of  $0.1 M$  THACl in contact with an aqueous solution of  $0.1 M$  LiCl is reported in Figure 3.  $\Delta V_0$  and  $\Delta\gamma$  represent the differences between the potential (Figure 2) and the interfacial tension (Figure 3) values at time  $t$  and time zero. Both the variations are due to the solubilization of THACl in the aqueous electrolyte solution. In fact by using aqueous solutions pre-equilibrated with the organic phase both the potential and the interfacial tension become independent of time.

The solubility of  $\text{THANO}_3$  and  $\text{THABr}$  is very similar to that of THACl. Although a detailed solubility study has not been carried out for these two salts the same considerations which apply to THACl also hold for  $\text{THANO}_3$  and  $\text{THABr}$ .

In Figures 4 and 5 the potential,  $E$ , of cells 4, 5, and 5a, is reported as function of the logarithm of concentration of the  $\text{NO}_3^-$  and  $\text{Br}^-$  ions for the couples  $\text{Br}^-$ - $\text{Cl}^-$ ,  $\text{NO}_3^-$ - $\text{Br}^-$ ,  $\text{NO}_3^-$ - $\text{Cl}^-$ . All the measurements (at  $25^\circ$ ) satisfy the relation

$$V_0 = 59 \log (a_1' + P_{2,1}a_2') / (a_1'' + P_{2,1}a_2'') \quad (7)$$

with  $P_{2,1} = 33 \pm 5$  for the  $\text{NO}_3^-$ - $\text{Cl}^-$ ,  $P_{2,1} = 5 \pm 2$  for the  $\text{NO}_3^-$ - $\text{Br}^-$ , and  $P_{2,1} = 8 \pm 2$  for the  $\text{Br}^-$ - $\text{Cl}^-$  couples.  $a_2$  represents the primary ion activity ( $\text{NO}_3^-$  for the  $\text{NO}_3^-$ - $\text{Br}^-$ ,  $\text{NO}_3^-$ - $\text{Cl}^-$  couples and  $\text{Br}^-$  for the  $\text{Br}^-$ - $\text{Cl}^-$  one). When a constant ionic strength ( $0.1 M$ ) has been used, the activities have been replaced by the concentrations. Therefore the  $P_{2,1}$  values must be multiplied by the ratio of the activity coefficients of the two ions. However this ratio has been neglected in the calculation since it is very close to one in the experimental conditions used. In the case of cell 5a the activity coefficients have been calculated through the relationship

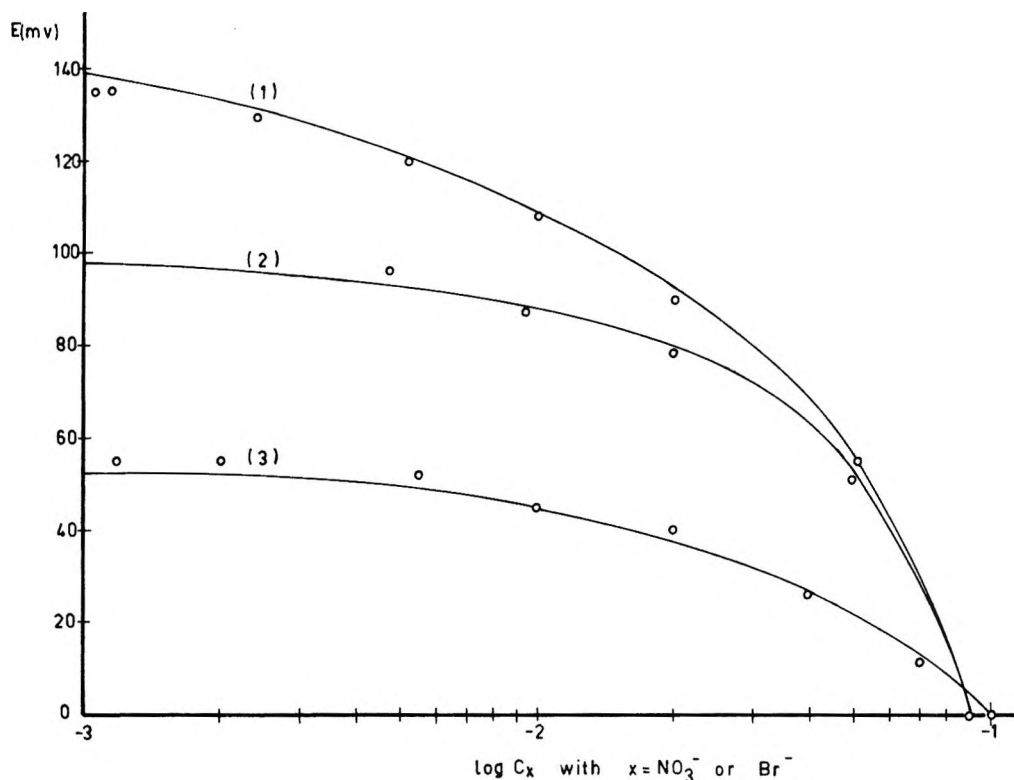


Figure 4. Potential values,  $E$  (mV), of cells 4 and 5 vs. logarithm of  $\text{NO}_3^-$  and  $\text{Br}^-$  concentration in biionic membrane potential determinations for the couples:  $\text{NO}_3^-$ - $\text{Cl}^-$  (1),  $\text{NO}_3^-$ - $\text{Br}^-$  (2),  $\text{Br}^-$ - $\text{Cl}^-$  (3). The solid lines have been calculated with the following  $P_{2,1}$  values:  $P_{\text{NO}_3, \text{Cl}} = 33$ ,  $P_{\text{NO}_3, \text{Br}} = 5$ ,  $P_{\text{Br}, \text{Cl}} = 8$ .

$$\log \gamma_{\text{LiNO}_3(\text{LiCl})} = \log \gamma_{\text{LiCl}(\text{LiNO}_3)} = \frac{1}{2}(\log \gamma_{\text{LiCl}} + \log \gamma_{\text{LiNO}_3})$$

$P_{2,1}$  has been calculated by solving, for each experimental point, eq 7 with respect to  $P_{2,1}$  and then averaging the results. In the case of cell 4 the  $E$  values have been previously transformed into  $V_0$  values by subtracting the term due to the halide ion activities. Experimental  $P_{2,1}$  values have been already reported<sup>9</sup> for couples similar to those of this paper. However since the chemical characteristics of the liquid membranes used are not described, no quantitative comparison between the  $P_{2,1}$  values can be performed. In the case of biionic potentials a change in composition of the organic phase (with respect to the initial one) can take place during the measurements. Such a change is due to biphasic exchange reactions. Therefore when the electrochemical cells 4, 5, and 5a are used the presence of some chloride or bromide salt in the organic phase has to be expected after some time. In Figure 6 the dashed line represents the molarity of  $\text{THACl}$  ( $\bar{C}_{\text{Cl}}$ ) present in the organic phase as function of the  $\text{Cl}^-/\text{NO}_3^-$  ratio in the aqueous solution for a membrane (0.1  $M$   $\text{THANO}_3$  in benzene) interposed between two aqueous solutions (one with a  $\text{Cl}^-/\text{NO}_3^-$  concentration ratio of 0.1 and the other with the same ratio variable from 0.1 to 100). The data are steady-state values. After 2 min the composition of the organic phase reaches a constant value that does not change for several hours.

The straight (continuous) line of Figure 6 represents the molarity of  $\text{THACl}$  in the organic phase (benzene solution of 0.1  $M$   $\text{THANO}_3$ ) in equilibrium with an aqueous electrolyte solution with a total molarity of 0.1 and variable  $\text{Cl}^-/\text{NO}_3^-$  concentration ratio. From these curves it can be observed that the chloride concentrations in the organic phase equilibrated with aqueous electrolyte solutions with  $\text{Cl}^-/\text{NO}_3^-$  concentration ratios of 0.1 and of 100 are, respectively,  $5 \times 10^{-5}$  and  $2.9 \times 10^{-2}$ . The value of  $3.3 \times 10^{-3}$ , obtained in steady-state conditions for a membrane interposed between aqueous electrolyte solutions with  $\text{Cl}^-/\text{NO}_3^-$  concentration ratio of 0.1 and 100, is then intermediate between these two values. Owing to the change in composition a transient potential of about 2 min is therefore observed during the biionic potential determinations.

**Steady-State Potentials.** Equations 6 and 7 describe the experimental results for monoionic and biionic potential measurements. The form of the equations is similar to that used in the case of solid membranes. However in the case of liquid membranes the mobility of both cations and anions and of the associated species in solution has to be considered. As far as the origin of membrane potential is concerned both the ion distribution at the boundary and the ion diffusion across the membrane can contribute to the potential.

(9) K. Srinivasan and G. Rechnitz, *Anal. Chem.*, **41**, 1203 (1969).

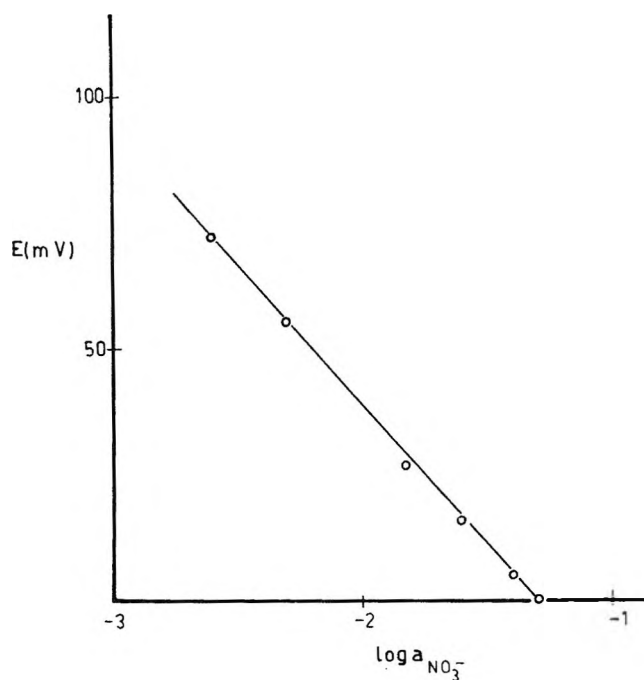


Figure 5. Potential values,  $E$  (mV), of cell 5a vs. logarithm of  $\text{NO}_3^-$  activity in biionic membrane potential determinations for the couple  $\text{NO}_3^-/\text{Cl}^-$ . The solid line has been calculated with  $P_{\text{NO}_3, \text{Cl}} = 33$ .

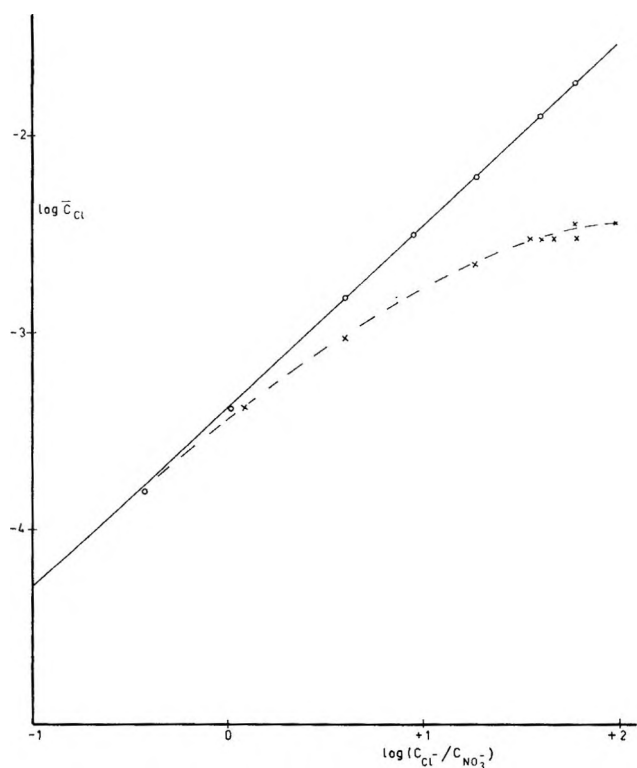


Figure 6. Log-log plot of organic chloride molarity,  $\bar{c}_{\text{Cl}}$ , vs. the aqueous concentration ratio  $C_{\text{Cl}^-}/C_{\text{NO}_3^-}$ .  $C_{\text{Cl}^-} + C_{\text{NO}_3^-}$  was kept constant to 0.1 M. See text for explanation of dashed and solid lines.

In the literature steady-state liquid membrane potentials have been explained either in terms of pure diffusive

processes<sup>10-12</sup> or of boundary equilibria arising from the distribution of ions at the water-membrane interface.<sup>13-18</sup> A review of these works is given in ref 19.

In ref 4a the potential measurements with liquid membranes consisting of benzene solutions of alkylammonium salts have been treated by using the quasi thermodynamic approach of Scatchard. Other works with the same type of membranes have treated the potential as arising from ion distribution equilibria.<sup>20,21</sup> In this case the liquid membrane has been assumed as having constant chemical properties (isotropic) in all the space it occupies. Recent theoretical and experimental work<sup>22-24</sup> has shown that both boundary equilibria (ion-exchange reactions) and nonequilibrium processes (diffusion-migration) can contribute to the potential and to the liquid electrode specificity. Since in low dielectric constant media associated species can exist their contribution to the membrane potential has been theoretically considered.<sup>23,24</sup> Following ref 23 the membrane potential is given by

$$(Fz_i/RT)V_0 = -\ln \left[ \frac{(\sum u_i K_i a_i')}{(\sum u_i K_i a_i'')} \right] - \int_1 - \int_2 \quad (8)$$

where  $u_i$ ,  $a_i$ ,  $z_i$ , and  $K_i$  represent the mobility in the oil phase, the aqueous activity, the charge, and the distribution constant between oil and water phases of the  $i$ th charged species. The integrals  $\int_1$  and  $\int_2$  account for the contribution of the ion pair to the membrane potential. Equation 8 is based on the assumption that (i) only ions and ion pairs are present in solution; (ii) ions and ions pairs behave as independent units in the diffusion-migration process; (iii) the uptake of co-ions in the organic phase is excluded; (iv) the flux of the site

- (10) V. H. Meyer, H. Hauptman, and J. F. Sievers, *Helv. Chim. Acta*, **19**, 946 (1936).
- (11) M. Dupeyrat, *J. Chim. Phys.*, **61**, 303 (1964).
- (12) N. Nernst and E. H. Riesenfeld, *Ann. Phys.*, **8**, 600 (1902).
- (13) F. Haber and Z. Klemensiewicz, *Z. Phys. Chem. (Leipzig)*, **67**, 385 (1909).
- (14) F. Haber and R. Beutner, *Ann. Phys.*, (4) **26**, 327 (1908).
- (15) F. Haber, *ibid.*, **4** (26), 927 (1908).
- (16) F. M. Kerpfen and J. E. B. Randles, *Trans. Faraday Soc.*, **49**, 823 (1953).
- (17) L. Michaelis, "Hydrogen Ion Concentration," Williams and Wilkins Co., Baltimore, Md., 1926.
- (18) R. Beutner, "Physical Chemistry of Living Tissues and Life Processes," Williams and Wilkins Co., Baltimore, Md., 1944.
- (19) K. Sollner, *Ann. N. Y. Acad. Sci.*, **148**, 154 (1968).
- (20) K. Sollner and G. Shean, *J. Amer. Chem. Soc.*, **86**, 1901 (1964).
- (21) O. D. Bonner and D. C. Lunney, *J. Phys. Chem.*, **70**, 1140 (1964).
- (22) G. Eisenman, "The Ion Exchange Characteristics of the Hydrated Surface in Selective Glass Electrodes" in Symposium on Microelectrodes, M. Lavaller, Ed., Wiley-Interscience, New York, N. Y., 1967.
- (23) J. Sandblom, G. Eisenman, and J. L. Walker, *J. Phys. Chem.*, **71**, 3862 (1967).
- (24) J. L. Walker, G. Eisenman, and J. P. Sandblom, *ibid.*, **72**, 978 (1968).

(the anion in the case of a cation exchangers or the cation in the case of an anion exchanger) at the water-membrane boundaries is zero. Since eq 8 has been obtained without the restraints of steady-state conditions, it applies to both initial and steady-state membrane potentials. In our experimental conditions a solubility of the tetraheptylammonium ion occurs, and the condition of zero flux of the site (the alkylammonium radical  $\text{THA}^+$ ) is not respected. Moreover by means of vapor pressure lowering and light scattering measurements the possible existence of a monomer (ion pair), of a 3-mer, and of a 25-mer has been pointed out for both the  $\text{THANO}_3$  and  $\text{THACl}$  salts in benzene solutions.<sup>5</sup> Although no quantitative information is available for benzene solutions of the  $\text{THABr}$  salt, it is expected that also this salt forms aggregates. The presence of mixed aggregates (one cation and two anions present in the aggregate) has been pointed out<sup>25</sup> in the case of  $\text{NO}_3^-$  and  $\text{UO}_2(\text{NO}_3)_3^-$ . No information is at this moment available on the aggregation behavior of the mixtures  $\text{THANO}_3$ - $\text{THACl}$ ,  $\text{THANO}_3$ - $\text{THABr}$ , and  $\text{THABr}$ - $\text{THACl}$ . However the presence of mixed aggregates is highly probable also in these systems. Therefore an expression accounting for both the cation mobility and for the presence of higher associated species than the ion pair in the organic phase is needed.

In a paper<sup>26</sup> dealing with the irreversible thermodynamic processes in liquid ion-exchange membranes, with no limitation regarding the species present in the organic phase, the membrane diffusion potential,  $\Delta\psi_0$ , in steady state (for  $z_i = 1$ ) is given by the equation

$$(F/RT)\Delta\psi_0 = - \int_1'' \sum_{i=1}^k \bar{l}_i/z_i d \ln \bar{a}_i - F \int_3 \quad (9)$$

with

$$\int_3 = \int_1'' \sum_{i=k+1}^n \bar{l}_i d \ln \bar{a}_i$$

where  $i = 1, \dots, k$  refers to charged species (simple ions and charged aggregates),  $i = k + 1, \dots, n$  to the uncharged species,  $\bar{l}_i$  is the transport number in the membrane (if water is the  $n - 1$  component,  $\bar{l}_{n-1}$  is its reduced transport number), and  $\bar{a}_i$  are the activities in the membrane.

Equation 9 applies only to steady-state conditions. However it accounts for the mobility of cations, anions, and associated species in the organic phase. It has to be noted that when the transport number of the cation in the organic phase is negligible,  $\bar{l}_c \simeq 0$ , eq 9 can be rewritten to obtain an equation similar to eq 8. In fact by combining the membrane diffusion potential (eq 9 with  $\bar{l}_c \simeq 0$ ) with the distribution potential obtained from the continuity equations of the electrochemical potential the following equation for the total membrane potential,  $V_0$ , is obtained

$$(F/RT)V_0 = -\ln [(\sum u_i K_i a_i') / (\sum u_i K_i a_i'')] - \int_3 \quad (10)$$

where the transport number has been expressed in terms of mobilities  $u_i$  and the membrane concentration,  $\bar{C}_i$ , has been expressed in terms of aqueous activity,  $a_i$ , by means of the boundary equilibrium condition  $\bar{C}_i/\bar{C}_s = a_i K_i / \sum a_i K_i$  (see ref 23) and  $z_i$  has been set equal to one.

It has to be noted that when  $\bar{l}_c \simeq 0$  it is highly probable also that the transport number of the associated species is negligible. In these conditions ( $\bar{l}_c \simeq 0$ ) and with stirred membranes it is  $\int_3 = 0$  and  $\int_1$  and  $\int_2 = 0$ . Therefore both eq 8 and 10 reduce to the first term, and there is no difference between strongly associated and completely dissociated systems. Equations 6 and 7 find then a logical explanation in the framework of current theory of the membrane potential if the assumption of a negligible mobility of the cation in the organic phase with respect to the anion is verified. In the case of monoionic potentials when  $\bar{l}_c \simeq 0$  eq 10 turns into eq 6 and a slope ( $A$  of eq 6) of  $59 \pm 1$  mV is obtained (Figure 1) for the  $\text{NO}_3^-$ ,  $\text{Br}^-$ , and  $\text{Cl}^-$  ions. To have such a numerical value for the slope  $\bar{l}_c$  has to be  $\leq 0.01$ .

For benzene solutions of methyltri-*n*-octylammonium nitrate a transport number  $\bar{l}_c = 0.08$  has been reported.<sup>27</sup> However, due to the approximations present in the treatment of the data, this value must be taken only as indicative and a value of 0.01 could be equally realistic. The small value of  $\bar{l}_c$  could then justify the assumption of a very small  $u_c$ . Similar values of  $\bar{l}_c$  can also be expected for  $\text{THANO}_3$ ,  $\text{THABr}$ , and  $\text{THACl}$ . In fact all these tetraheptylammonium salts are formed by a cation having an ionic radius larger than the one of the anion. Also in the case of biionic potential  $\bar{l}_c \simeq 0$  can be expected. Then  $\int_3 \simeq 0$  and eq 10 turns into eq 7.

*Transient Value.* In the experimental conditions used (stirred cells) the transient potentials are due to the solubilization of the long-chain alkylammonium salt in water (when nonpreequilibrated solutions are used) and to the change in composition of the organic phase. This latter transient potential depends on the exchange constant ( $K_{2,1}$ ) values. In fact when the  $K_{2,1}$  value is such to make negligible the amount of the other anion in the organic phase ( $K_{2,1} > 1000$ ), no transient potential will be observed if the solubilization phenomena have been accounted for by means of suitable preequilibrations of both the phases. As far as the building up of the steady state through the membrane is concerned, it is evident that when the membrane phase

(25) G. Scibona, *J. Phys. Chem.*, **70**, 1365 (1966).

(26) G. Scibona, *ibid.*, to be published.

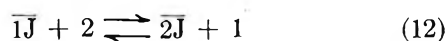
(27) G. Scibona and B. Scuppa, *ibid.*, **68**, 2003 (1964).

is stirred no gradient of ions inside the membrane bulk can exist. The flux of ions takes place through the boundaries in the stagnant layers at both the oil and aqueous sides of the interface and a short time (of the order of seconds) is required to build up a concentration gradient. In this condition  $\mathcal{J}_2$  of eq 8 is zero and both eq 8 and 10 represent the initial and the steady-state values of the membrane potential. When unstirred membranes are used, but the system is not convection free (as it is in the case of horizontal and thin membrane phases), both eq 8 and 9 still represent the initial and the steady-state values of the membrane potential. These observations agree with the experiments. In the case of monoionic potential determinations with no convection-free cells and with the solubilization phenomena accounted for, the same value for the membrane potential is in fact observed with stirred and unstirred membranes. The same comments hold for biionic or multiionic potential determinations.

*Considerations on the Selectivity of the Electrode.* Expressions for  $P_{2,1}$  have been already reported.<sup>23</sup> In the case of two ions from eq 7, 8, and 10 (with  $\mathcal{J}_1, \mathcal{J}_2$ , and  $\mathcal{J}_3 \approx 0$ ) it follows that

$$P_{2,1} = K_2 u_2 / K_1 u_1 \quad (11)$$

To obtain the ratio of the ion distribution constants  $K_2/K_1$  let us consider the equilibrium constant,  $K_{2,1}$ , for the biphasic exchange reaction



( $\bar{1}\bar{J}$  and  $\bar{2}\bar{J}$  indicate the organic salt formed between the cation J and the anions 1 and 2, the bar refers to the organic phase) and the ion-pair equilibrium  $\bar{1} + \bar{J} \rightleftharpoons \bar{1}\bar{J}$ , with  $K_{1J}$  equilibrium constant. The following relation is therefore easily obtained.

$$\frac{K_{2J}}{K_{1J}} \frac{K_2}{K_1} = K_{2,1} \quad (13)$$

By introducing the ratio  $K_2/K_1$  from eq 13 into eq 11 we obtain

$$P_{2,1} = K_{2,1} T_{1,2} (u_2/u_1) = K_{2,1}^* (u_2/u_1) \quad (14)$$

with  $T_{1,2} = K_{1J}/K_{2J}$  and  $K_{2,1}^* = K_{2,1} T_{1,2}$ . The  $P_{2,1}$  values therefore depend on both the ion distribution between the two phases and the diffusion-migration process. The  $K_2, K_1, K_{1J}, K_{2J}$ , and  $K_{2,1}$  are thermodynamic quantities and thus independent of the alkylammonium salt concentration (unless of structural changes of the oil phase with the concentration). However since the dielectric constant of the oil phase depends on the alkylammonium salt concentration the free energy of distribution of the ions can be concentration dependent. Also the  $u_2$  and  $u_1$  values can of course be affected by structural changes of the oil phase, but its ratio is probably less sensitive than  $K_2/K_1$  to these changes. A dependence of  $P_{2,1}$  on the alkylammonium salt concentration is therefore expected.<sup>28</sup> Of course

the dependence of the electrical potential on the liquid anion exchanger concentration has to be expected only in the case of multiionic potentials (in the case of monoionic potentials the ion distribution free-energy term does not appear in the potential equation). Let us now analyze the parameters that affect the  $P_{2,1}$  values. It has been shown<sup>29</sup> that the exchange constant  $K_{2,1}$  for long-chain alkylammonium salts depends on two main processes: (i) the water structure-breaking factor of the ions; (ii) the ion-ion, ion-dipole, dipole-dipole interactions in the membrane phase.

Large ions strongly disturb the water structure and are pulled away from the water phase. Therefore although the smaller ion gives a higher ion-pair formation constant the larger ion is preferred in the membrane phase. In first approximation the  $K_{2,1}$  values will then increase with the difference of ionic radius in solution  $\Delta r_i$ , as shown in Table I. Since the ion-pair formation

Table I

	System		
	NO <sub>3</sub> -Cl	Br-Cl	NO <sub>3</sub> -Br
$K_{2,1}^a$	75	21	3.7
$P_{2,1}$	33 ± 5	8 ± 2	5 ± 2
$\Delta r_i$	0.21	0.14	0.08
$T_{1,2}$	1.78	1.41	1.26
$K_{2,1}^*$	133.5	29.6	4.66
$P_{2,1}/K_{2,1}^*$	0.25 ± 0.04	0.27 ± 0.07	1.1 ± 0.4
S	0.74	0.66	1.1

<sup>a</sup> G. Scibona, J. F. Byrum, K. Kimura, and J. W. Irvine, Jr., "Solvent Extraction Chemistry," North-Holland, Amsterdam, 1967, pp 398-407.

constant  $K_{iJ}$  decreases with the ion radius, the  $T_{1,2}$  factor will increase with  $\Delta r_i$ . The  $K_{2,1}$  values have then to increase in the order  $K_{NO_3,Cl} > K_{Br,Cl} > K_{NO_3,Br}$  that is in the same order of  $\Delta r_i$ . To obtain some figures for  $T_{1,2}$  it is necessary to know  $K_{iJ}$ . Approximate calculations of the ion-pair formation constant  $K_{iJ}$  can be performed by using the simplified equation  $K_{iJ} = e^{q/R^2 T}$  with  $q = 336/D r_{iJ}$ , with  $r_{iJ}$  the closest approach distance of the ion pair and  $D$  the dielectric constant of the medium. By using  $D = 2.27$ ,  $r_{RBr} = 9.13 \text{ \AA}$ ,  $r_{RNO_3} = 9.21 \text{ \AA}$ , and  $r_{RCl} = 9.0 \text{ \AA}$  the  $T_{1,2}$  and the  $K_{2,1}^*$  values reported in Table I have been obtained.<sup>30</sup> As far as the exchange properties are concerned ( $K_{2,1}$

(28) P. R. Danesi and G. Scibona, *J. Phys. Chem.*, to be published.

(29) G. Scibona, F. Orlandini, and P. R. Danesi, *J. Inorg. Nucl. Chem.*, **28**, 1701 (1966).

(30) The  $r_{iJ}$  values are obtained by the sum of the cation radius ( $r = 7.16 \text{ \AA}$ , from extrapolation of Stokes radii of alkylammonium cations of ref 31) and the anion radius ( $r_{Cl} = 1.84 \text{ \AA}$ ,  $r_{Br} = 1.92 \text{ \AA}$ , and  $r_{NO_3} = 2.03 \text{ \AA}$  from ref 32).

(31) R. A. Robinson and R. H. Stokes, "Electrolyte Solutions," Butterworths, Washington, D. C., and New York, N. Y., 1959, p 125.

parameters) the electrode specificity has to depend on  $\Delta r_i$ . The  $P_{2,1}$  values have to increase in the same order as  $K_{2,1}$  and  $\Delta r_i$ , that is  $P_{\text{NO}_3, \text{Cl}} > P_{\text{Br}, \text{Cl}} > P_{\text{NO}_3, \text{Br}}$ . However to give a complete description of the electrode specificity the ratio of the mobilities,  $u_2/u_1$ , has also to be evaluated. The mobility of an ion depends on its size, its shape, and its interactions with the environment. On shape and size considerations it can be expected that the larger ion has a smaller mobility; on the other hand it has to be considered that smaller ions can affect the polarizability of benzene molecules to a greater extent.<sup>33</sup> Therefore a local polarization of the solvent (induced dipole alignment) is possible with an increase of local viscosity and a decrease of the ion mobility. On which of these factors the  $u_2/u_1$  ratio depends, in our experimental conditions, is a hard question to answer. However it is possible to obtain some information on this point by considering the  $K_{2,1}^*$  and  $P_{2,1}$  figures of Table I. The ratio  $P_{2,1}/K_{2,1}^* = u_2/u_1$  gives values of 0.25, 0.27, and 1.1 for the  $\text{NO}_3^-$ - $\text{Cl}^-$ ,  $\text{Br}^-$ - $\text{Cl}^-$ , and  $\text{NO}_3^-$ - $\text{Br}^-$  systems. A simple explanation to these figures could be given by considering the lower mobility of the nitrate and bromide ions with respect to the chloride. Some figures can also be obtained theoretically by considering that the mobility,  $u_i$ , is correlated to the diffusion coefficient by means of the well-known Nernst-Einstein relation

$$D/KT = u \quad (15)$$

A theoretical expression, based on statistical mechanics,<sup>36</sup> for the diffusion coefficient is given by

$$D = \frac{d^2}{V_f^{1/3}} (KT/2\pi m)^{1/2} \exp(-E_0/RT) \quad (16)$$

where  $d$  is the distance between successive equilibrium positions of the diffusing particle,  $V_f$  is the free volume of the ion,  $m$  is the mass of the ion, and  $E_0$  is the potential energy difference between the particle in the liquid and in the gas state, that is the interaction energy between the ion and the solvent molecules. By using eq 15 and 16 the following relation is obtained

$$S = u_2/u_1 = (m_1/m_2)^{1/2} (V_{f(1)}/V_{f(2)})^{1/3} \exp[-(E_2 - E_1)KT] \quad (17)$$

The  $S$  values reported in Table I support the hypothesis that the mobility of the nitrate and bromide ions is lower than that of the chloride. The calculations have been performed by neglecting the exponential. The ion free volume,  $V_f$ , is in first approximation given by  $V_f = 8(V_s^{1/3} - r_i)^3$  with  $V_s$  the free volume per molecule of sol-

vent.  $V_{\text{C}_6\text{H}_6} = 1.5 \times 10^{-22} \text{ cm}^3$  has been used in the calculations. In conclusion for the case of THACl, THABr, and THANO<sub>3</sub> the difference in ionic radii  $\Delta r_i$ , contributes positively to the electrode specificity through its influence on the ion-exchange properties of the long-chain alkylammonium salts. However as far as the mobility ratio is concerned the difference in ionic radii decreases the electrode specificity since larger and heavier ions have lower mobility. An influence of the long-chain alkylammonium salt concentration on the electrode specificity is also expected through the dielectric constant changes of the oil phase with the salt concentration.

### Summary

The detailed analysis of the electrochemical behavior at zero current of some liquid membrane electrodes has shown that both ion distribution and diffusion processes contribute to the membrane potential. In fact, the membrane potential values have been quantitatively correlated to the ion-exchange equilibrium constants and to the ion mobilities in the membrane phase. Such correlations have been possible since the equilibrium thermodynamics of the exchange processes between aqueous electrolyte solutions and the liquid membrane (benzene solutions of tetraheptylammonium salts) is known for the salts that have been studied. Further the choice of a large cation (the tetralkylammonium ion) makes negligible the contribute of the cation and of the associated species to the membrane potential. In these conditions the strongly associated membrane behaves as a completely dissociated one. Finally it has been shown that both the solubilization of the alkylammonium salt in water (when nonpre-equilibrated solutions are used) and the change in composition of the membrane phase (biionic potential case) are processes which contribute to the transient potentials. The latter process (change in composition of the organic phase) depends on the value of the ion-exchange equilibrium constants. When this constant has a large value the rate of ion exchange is a second-order effect.

(32) C. B. Monk, "Electrolytic Dissociation," Academic Press, New York, N. Y., 1961, p 271.

(33) It is known that<sup>34</sup> at a distance of 3 Å from an electronic charge the field strength is of 160 million V cm<sup>-1</sup>. The polarizability of benzene increases a great deal at field strength of the order of 100 million V cm<sup>-1</sup>.<sup>35</sup>

(34) J. O. Hirschfelder, C. F. Curtis, and R. B. Bird, "Molecular Theory of Gases and Liquids," Wiley, New York, N. Y., 1964.

(35) C. A. Coulson, A. Maccolle, and L. Sutton, *Trans. Faraday Soc.*, **46**, 106 (1952).

(36) W. Jost, "Diffusion," Academic Press, New York, N. Y., 1960, p 467.

# Electrochemical Investigations on the Spectral Sensitization of Gallium Phosphide Electrodes

by R. Memming\*

*Philips Zentrallaboratorium GmbH, Laboratorium Hamburg, Hamburg, Germany*

and H. Tributsch

*Physikalisch Chemisches Institut, Technische Hochschule, Munich, Germany (Received June 2, 1970)*

*Publication costs assisted by Philips Zentrallaboratorium*

The spectral sensitization of gallium phosphide electrodes in contact with an electrolyte was studied using cryptocyanine, pseudoisocyanine, methylene blue, rhodamine B, rose bengal, and crystal violet as sensitizing dyes. A sensitized cathodic photocurrent was observed with n- and p-type electrodes. It is caused by an electron transfer from the valence band of GaP to the ground level of the dye. In certain cases (rhodamin B, rose bengal, crystal violet) it is postulated that, besides charge transfer, energy transfer also takes place. The influence of O<sub>2</sub> and H<sub>2</sub>O<sub>2</sub> on the sensitization is discussed and the results compared with those obtained with ZnO electrodes.

## Introduction

In most semiconductors the conductivity can be increased by light absorption. The energy of the incident light must be sufficiently large for electrons to be excited from the valence into the conduction band. Photoconduction was also observed at lower energies if light was absorbed by a dye being in contact with the semiconductor.<sup>1-4</sup> Similar effects were also studied at semiconductor/electrolyte interfaces. The rate of certain electrochemical reactions can be influenced by varying the concentration of electrons and holes in the semiconductor electrode, e.g., by light absorption within the crystal. As shown for ZnO, electrode processes may also be sensitized by light absorption in the dye which is adsorbed on ZnO electrodes.<sup>5,6</sup>

In all papers on sensitization effects at surfaces, the problem is discussed whether the sensitization is caused by energy or charge transfer. The mechanism is still not completely understood. It is rather difficult to solve this problem with semiconductors being in contact with a gas atmosphere because only the space charge at the semiconductor surface is varied by a transfer of electrons between dye and crystal as shown by photopotential and photoconductivity measurements.<sup>1-4</sup> More information can be obtained with semiconductor/electrolyte interfaces since charge carriers transferred from the dye to the crystal or *vice versa* can be removed from the surface by ionic conductance in the electrolyte. As shown for the ZnO/dye/electrolyte interface, electrons excited in the dye from its ground to a higher energy state are transferred into the conduction band of ZnO.<sup>6</sup> Investigations on the supersensitization by reducing agents support the charge-transfer mechanism.<sup>7</sup>

In order to get more information about transfer mechanisms we studied the spectral sensitization of GaP electrodes. The band gap of GaP (2.25 eV) is sufficiently large to permit sensitization experiments with a variety of dyes. A further advantage of GaP is the fact that n- and p-type crystals are available. The electrochemical behavior of GaP<sup>8</sup> and several reaction mechanisms of redox systems<sup>9,10</sup> have previously been studied in detail.

## Experimental Section

The investigations were performed with single crystals of GaP as electrode materials. We used n- and p-type material doped with Te and Zn, respectively. The crystals showed a conductivity of about 1 ohm-cm (carrier density 10<sup>17</sup> cm<sup>-3</sup>). They were glued in Araldite (Ciba) sockets and connected with a Teflon rod. For the measurements a Teflon cell having a glass window on the bottom was used. The Teflon

- (1) R. C. Nelson, *J. Opt. Soc. Amer.*, **46**, 13, 1016 (1956); **51**, 1182, 1186 (1961).
- (2) A. Terinin and I. Akimov, *Z. Phys. Chem. (Leipzig)*, **217**, 307 (1961); *J. Phys. Chem.*, **69**, 732 (1965); *Dokl. Akad. Nauk SSSR*, **172**, 23 (1967).
- (3) H. Meier, "Die Photochemie der organischen Farbstoffe," Springer, Berlin, 1963.
- (4) I. Akimov, "Collection: Elementary Photoprocesses in Molecules," *Nauka*, 397 (1966).
- (5) E. Michel-Beyerle, H. Gerischer, F. Rebenrost, and H. Tributsch, *Electrochim. Acta*, **13**, 1509 (1968).
- (6) H. Gerischer and H. Tributsch, *Ber. Bunsenges. Phys. Chem.*, **72**, 437 (1968).
- (7) H. Tributsch and H. Gerischer, *ibid.*, **73**, 251 (1969).
- (8) R. Memming and G. Schwandt, *Electrochim. Acta*, **13**, 1299 (1968).
- (9) K. H. Beckmann and R. Memming, *J. Electrochem. Soc.*, **116**, 368 (1969).
- (10) R. Memming, *ibid.*, **116**, 785 (1969).

rod with the GaP-electrode could be shifted towards the cell window so that any distance between the two could be adjusted. In order to avoid light absorption within the electrolyte this distance was kept very small ( $<0.2$  mm).

All measurements were performed under potentiostatic conditions. A saturated calomel electrode was used as a reference electrode. The GaP electrode was illuminated with monochromatic light (Zeiss monochromator), the light source being a 500-W xenon lamp. The corresponding photocurrents were measured using a picoamperemeter (Hewlett-Packard) or in the case of chopped light (13 cps) a lock-in amplifier.

Before each measurement the electrode was polished ( $10 \mu$  diamond paste) and etched in HCl. The solutions were not buffered since buffer substances lead to side reactions in dye solutions which interfere with the main process.

## Results

**Spectral Distribution of Sensitization.** As shown in Figure 1 for p-type GaP electrodes the cathodic current (hydrogen evolution) and for n-type GaP the anodic current (dissolution) is limited. In both cases these currents may be increased by illuminating the electrodes (dashed curves). The spectral distribution of the corresponding photocurrents ("intrinsic photocurrent") is given in Figures 2a and b (dashed lines).

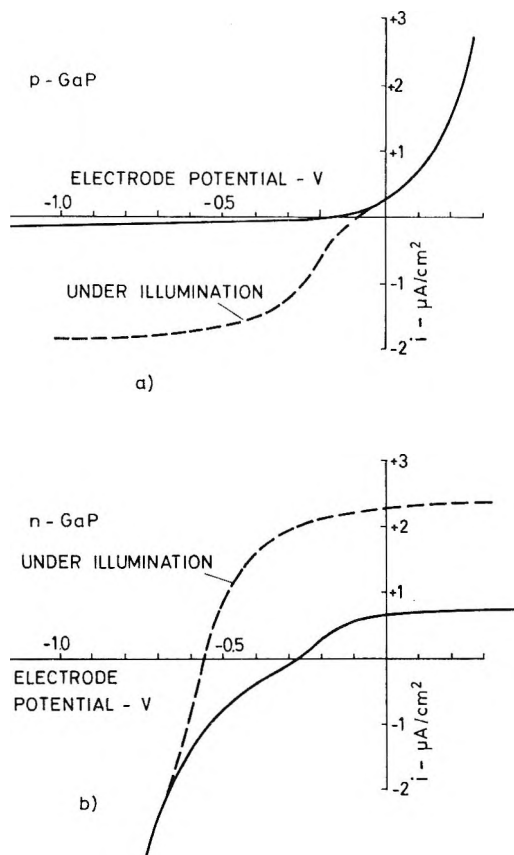


Figure 1. Interfacial current vs. electrode potential in 1 N KCl.

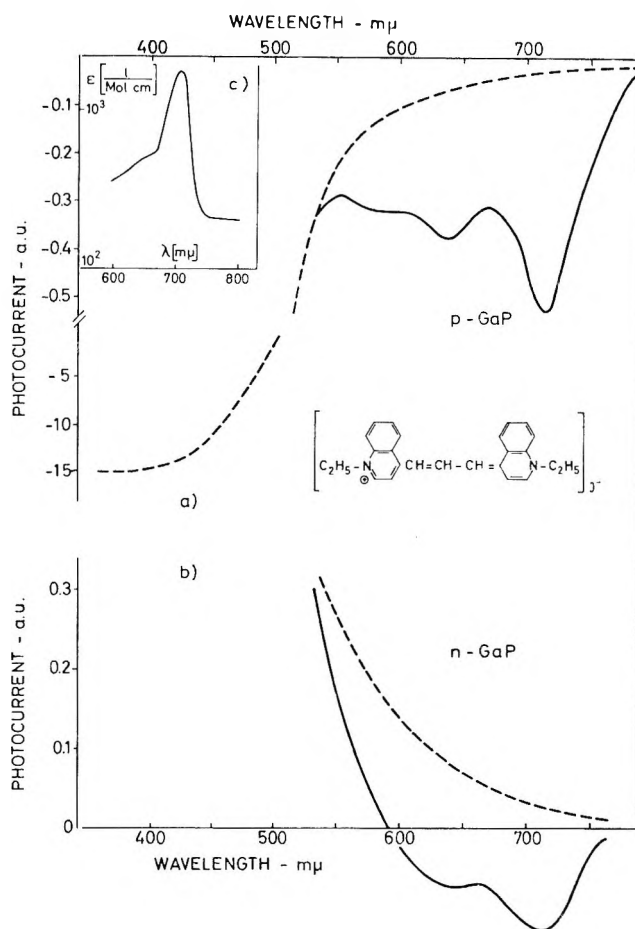


Figure 2. Spectral distribution (normalized to unit intensity) of the photocurrent for  $10^{-4}$  M cryptocyanine in 1 N KCl (not oxygen free) at an electrode potential  $U_E = -0.7$  V (dashed line: without dye) (lock-in technique); a.u. = arbitrary units; (c) absorption spectrum of the dye.

The intrinsic photocurrents set in at about  $\lambda$  570  $m\mu$  which corresponds to the band gap (indirect transition) of GaP. Since in the case of p-type GaP the cathodic current is increased by illumination we plotted this photocurrent as a negative current in order to distinguish between anodic and cathodic processes.

Adding a certain dye, as *e.g.*, cryptocyanine, to the electrolyte an additional cathodic current peak occurs in the spectral distribution (Figures 2a and b). For comparison we also plotted the absorption spectrum of cryptocyanine (Figure 2c). The shapes of the sensitization and absorption spectra are essentially identical. The height of the sensitization peak depends very much on the pretreatment of the electrode surface. Whereas with very well polished ( $1 \mu$  diamond paste) and weakly etched electrodes only a small current peak was observed, electrodes with a rougher surface obtained by etching sufficiently long showed much larger sensitization effect. Therefore, we used for all further experiments only electrodes prepared in this manner.

Similar results were obtained with other dyes such as pseudoisocyanine and methylene blue. The absorption

**Table I:** Comparison between Absorption and Sensitization Maxima

Dye	Absorption max, $\lambda$ , $m\mu$	Sensitization max, $\lambda$ , $m\mu$	Comments to sensitization
Cryptocyanine	710	710 <sup>a</sup>	
Pseudoisocyanine	{525 (monomer) 570 (polymer)}	570	Polymer band only
Methylene blue	{660 (monomer) 600 (dimer)}	{660 (very weak) 600 (strong)}	Dimer band dominates
Rhodamine B	550	570 <sup>b</sup>	Cutoff at shorter wavelengths
Rose bengal	550	570 <sup>c</sup>	Cutoff at shorter wavelengths
Crystal violet	{620 (monomer) 550 (dimer)}	620 <sup>d</sup>	Cutoff at shorter wavelengths

<sup>a</sup> Figure 2. <sup>b</sup> Figure 3. <sup>c</sup> Figure 4. <sup>d</sup> Figure 5.

and sensitization maxima are indicated in Table I. In these cases we also obtained a cathodic sensitization current for p- and n-type GaP, and the spectral distribution coincides at least with certain absorption bands: for methylene blue in the spectral distribution the dimer band, and for pseudoisocyanine the polymer band, dominates considerably (see Table I). According to absorption measurements of aqueous dye solutions the dimer<sup>11</sup> band of methylene and the polymer band of pseudoisocyanine<sup>12</sup> were only observed at much higher concentrations.

The absorption of the dyes reported above does not overlap with the fundamental absorption of GaP. On the other hand, using dyes with an absorption at lower wavelengths we also observed a cathodic sensitization current, but in the spectral distribution a rather sharp cutoff appears at the short wavelength side. This was found for rhodamine B (Figure 3), rose bengal (Table I), and crystal violet. For comparison we also measured the sensitization spectra of the same dyes using ZnO as an electrode as demonstrated for rose bengal in Figure 4 and crystal violet in Figure 5. The measurements with GaP and ZnO were performed successively in the same electrolyte. Whereas for ZnO the spectral distribution agrees very well with the absorption spectrum of the dye, a cutoff appears with GaP electrodes. It should be mentioned that all these spectra were measured using solutions containing oxygen.

In all cases, besides methylene blue, we found a cathodic sensitization with p- as well as with n-type electrodes. The photocurrents with n-type electrodes, however, were always smaller than with p-type. These results may be connected with the potential dependence of the sensitization current. This is demonstrated in Figures 6 and 7 using cryptocyanine and rhodamine B as sensitizing dyes. The adsorbed dye was excited by light of a wavelength of 720 and 570  $m\mu$ , respectively (maximum value of photocurrents in Figures 2 and 3). In the case of p-type GaP the photocurrent rises at about +0.4 V and reaches a saturation value which remains constant over a large cathodic potential

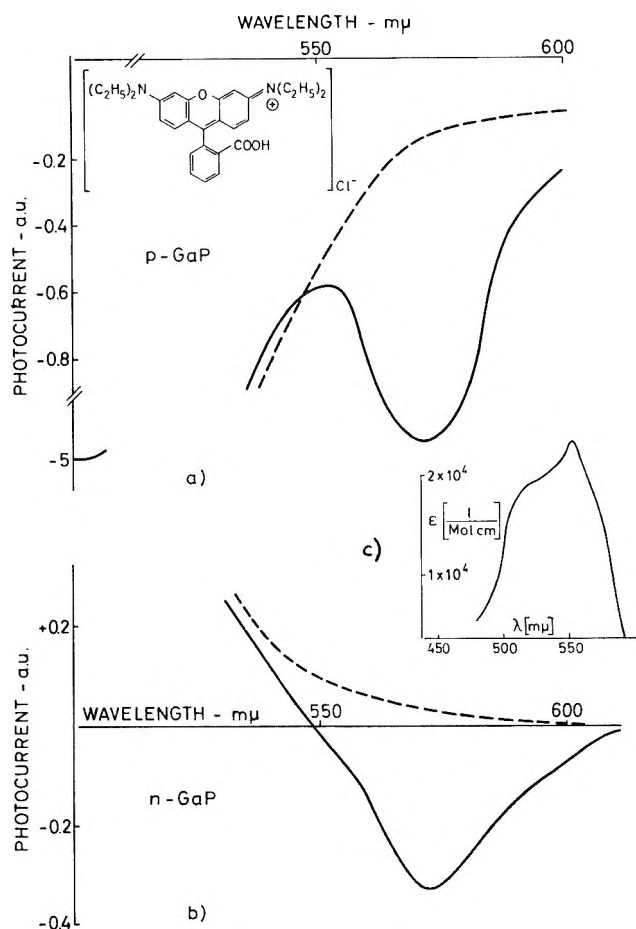


Figure 3. Spectral distribution of the photocurrent for  $5 \times 10^{-5} M$  rhodamine B in 1 N KCl (not oxygen free) at  $U_E = -0.6$  V (dashed line, without dye): (a) p-GaP (lock-in technique); (b) n-GaP (dc method); (c) absorption spectrum.

range (Figure 6). With n-type GaP, on the other hand, the sensitization sets in at more cathodic potentials (Figure 7b). For comparison we also plotted the

(11) (a) Th. Förster, "Fluoreszenz organischer Verbindungen," Vandenhoeck and Ruprecht, Göttingen, 1951; (b) Th. Förster, *Discuss. Faraday Soc.*, 27, 7 (1959).

(12) G. Scheibe, A. Schöntag, and F. Katheder, *Naturwissenschaften*, 29, 499 (1939).

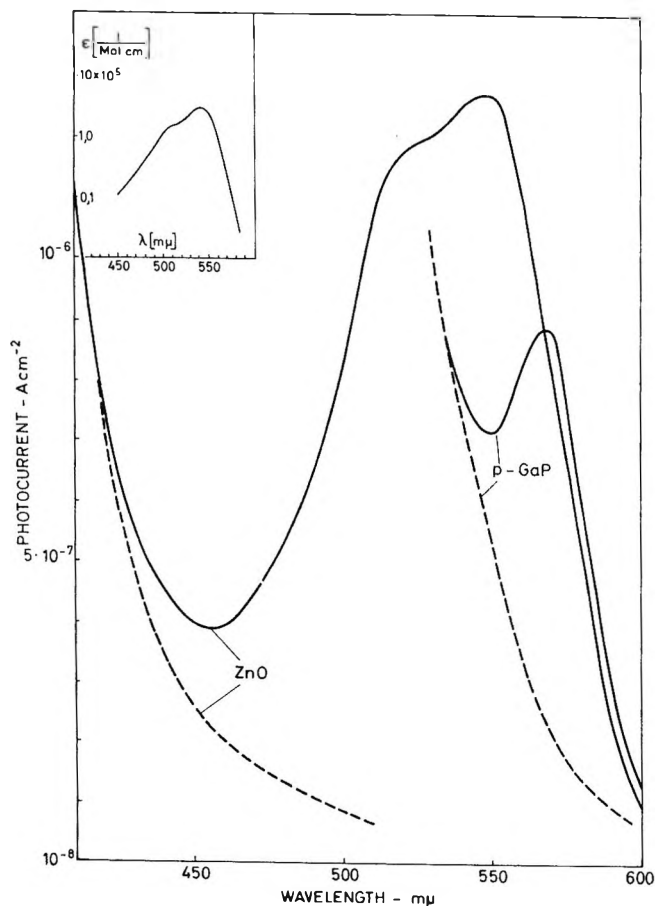


Figure 4. Spectral distribution of the photocurrent at n-ZnO and p-GaP for  $5 \times 10^{-5} M$  rose bengal in 1 N KCl (not oxygen free) at  $U_E = -0.1 V$  (dashed line: without dye) (lock-in technique).

dark currents as obtained with both electrodes. Whereas no influence of most of the dyes was observed, a reduction peak of rhodamine B is visible at an n-GaP electrode near 1.1 V. In the case of rhodamine B obviously the sensitization current is reduced (Figure 7c) as soon as the reduction of the dye sets in. With p-GaP no reduction of the dye was observed in the dark current. We only used these p-electrodes which show a dark current below  $10^{-2}$  to  $10^{-1} \mu A$ . The dark current with n-GaP depends very much on the potential, especially at large cathodic potentials the dark current increases rapidly due to hydrogen evolution. In this range the photocurrent is not constant, since hydrogen reduces the dye.

In connection with this problem methylene blue seems to be an exception, since in this case also with p-type material a maximum in potential dependence of the sensitization current was observed. The position of the maximum is independent from the pH value.

A further difference between p- and n-type GaP occurs in the relaxation times of the corresponding sensitization currents. For the experiments a shutter with a rise time of about 1 msec was used and the results for the transient processes are plotted in Figure 8.

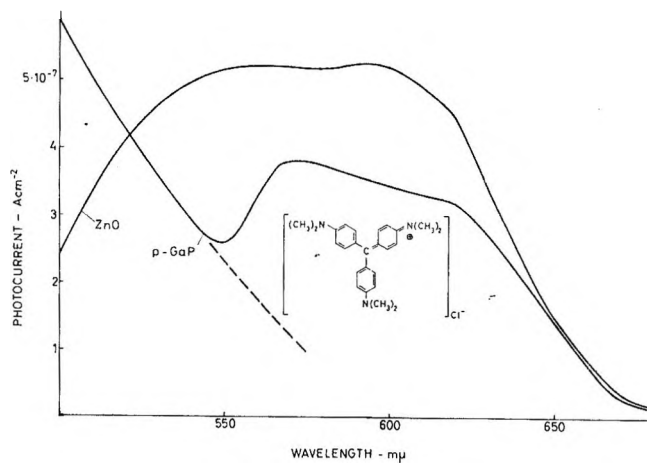


Figure 5. Spectral distribution of the photocurrent at n-ZnO and p-GaP for  $5 \times 10^{-5} M$  crystal violet in 1 N KCl (not oxygen free) at  $U_E = -0.1 V$  (dashed line: without dye).

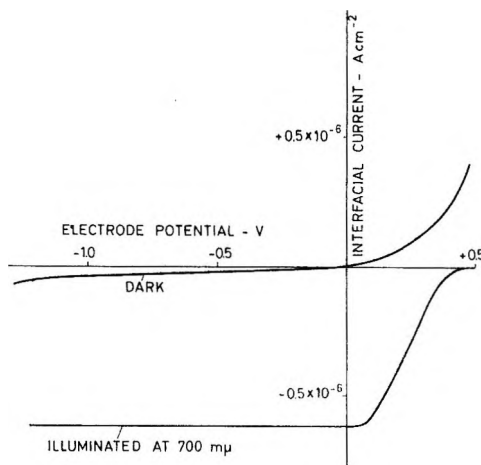


Figure 6. Interfacial current vs. electrode potential for p-GaP in  $5 \times 10^{-5} M$  rhodamine B solution, excitation at  $\lambda 570 m\mu$ .

As shown by curves b and c the relaxation process is very fast for p-GaP. In the case of n-GaP the intrinsic photocurrent (without dye) (curve d) also rises rapidly but decreases again within about 100 msec. The latter effect was only observed during cathodic polarization and not at anodic potentials (see dashed curve in curve d). After addition of the dye to the solution sensitization occurs. The sensitization current increases also slowly as shown in Figure 8e. The relaxation times are identical after turning on and off the light.

These experiments demonstrate that measurements performed with chopped light and using lock-in technique may lead to errors. Therefore we used for measurement with n-GaP mainly the dc method (unchopped light). This is important especially for measurements of the potential dependence.

*Addition of Redox Systems.* Adding  $H_2O_2$  to the dye solution the sensitization current decreases. Such a desensitization was observed with rhodamine B, rose

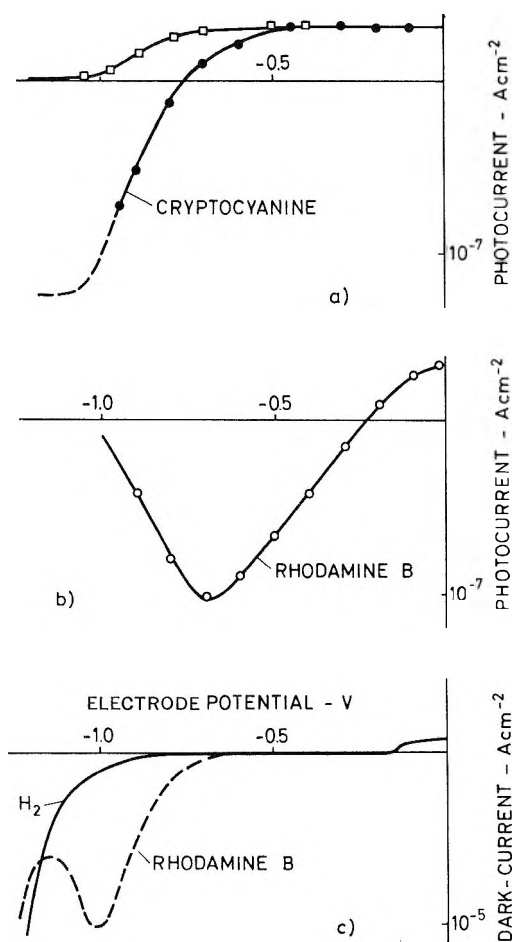


Figure 7. Dark and photocurrent vs. electrode potential for n-GaP in various dye solutions ( $5 \times 10^{-6} M$ ), excitation at maximum value of sensitization.

bengal, and methylene blue for both types of electrodes (n- and p-type). Oxygen dissolved in the electrolyte, on the other hand, leads to an enhancement of the sensitization. This is demonstrated by passing nitrogen and oxygen successively through the electrolyte (Figure 9). The spectral distribution remains unchanged. A variety of other oxidizing and reducing agents including  $Fe^{2+}$  (methylene blue), hydroquinone (rose bengal), allylthiourea (rhodamine B), and others were tested. With all these systems no effect could be detected.

### Discussion

*Charge and Energy Transfer.* As demonstrated in Figures 2 and 3 cathodic photocurrents always were observed if light was absorbed by dye adsorbed on GaP. The question arises whether the primary step is a charge or an energy transfer. In both cases first an electron is excited in the dye from the ground state into its lowest excited singlet state. An electron could then be transferred from the GaP electrode to the empty ground state thus leading to a reduction of the dye (charge-transfer mechanism). Since a cathodic sensitization

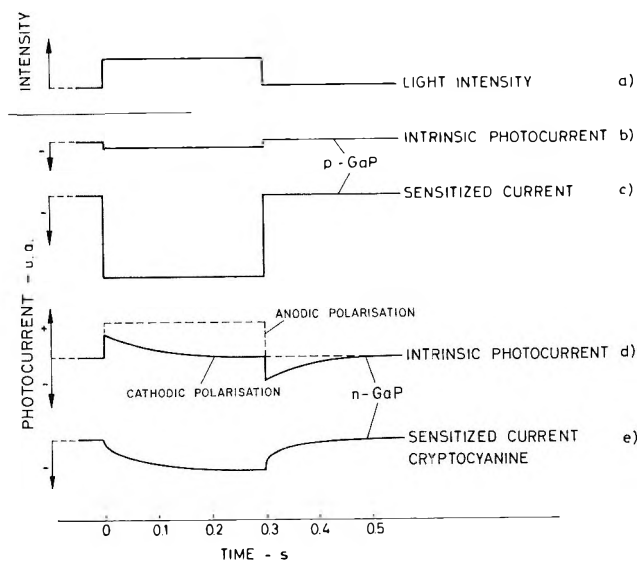


Figure 8. Relaxation of the photocurrents.

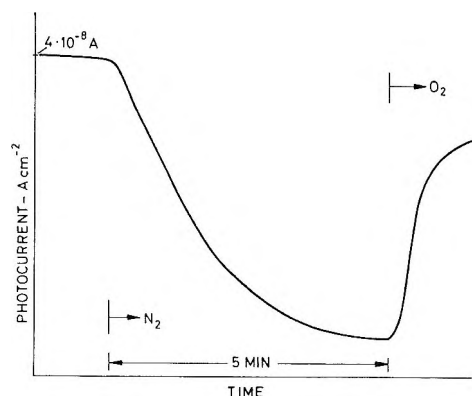


Figure 9. Influence of  $O_2$  and  $N_2$  on the sensitization current of rhodamine B ( $5 \times 10^{-5} M$ ), excitation at  $\lambda 570 m\mu$ .

current was also observed with p-type GaP only electrons from the valence band are available for this process. From this it follows that the ground level of the dye must overlap with the valence band of GaP as demonstrated in Figure 10a. Assuming that an electron is directly transferred from the valence band of GaP to the ground level of the dye, a hole is formed in the valence band which moves under the action of the electric field of the space charge region towards the interior of the electrode.

In the case of a direct transfer of the excitation energy from the dye to GaP, however, we have to postulate that in GaP there exist energy levels of the same energy difference as those between excited singlet and ground state in the dye. This is principally possible if corresponding energy levels at the GaP surface are present. In this case an energy transfer results in an excitation of an electron from the valence band to an acceptor level. The hole thus formed in the valence band then moves under cathodic polarization towards the interior, whereas the electron is transferred from the

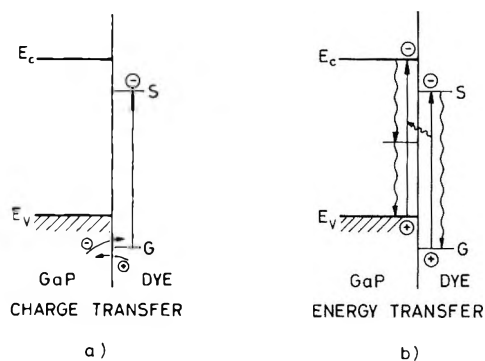


Figure 10. Schematic diagram of: (a) charge transfer; (b) energy transfer.

acceptor level to the dye (cathodic current). This model would also explain the sensitization current. Moreover, the reaction product, the reduced dye species, would be identical in the charge- and energy-transfer mechanism.

On the other hand, if the excitation energy is transferred from the dye to the solid so that an electron is excited from the valence band to an acceptor level, then the electron may also recombine with the corresponding hole. In this case the excitation energy is dissipated to the lattice. Since the surface recombination rate of electron-hole pairs in GaP is rather high<sup>9</sup> the quantum yield for the sensitization current should be low. According to our measurements, however, the quantum yield is rather large, estimating as follows: illuminating a p-type GaP electrode by light of a wavelength below  $\lambda \sim 570 \text{ m}\mu$  electrons are excited directly into the conduction band and are consumed for hydrogen evolution (intrinsic "photocurrent"). For a low penetration depth a quantum yield of about 1% was found for this process.<sup>9</sup> On the other hand, the sensitization current in certain cases (*e.g.*, rhodamine B) reaches values of the same order of magnitude as the intrinsic photocurrent (see *e.g.*, Figure 3), although a monolayer of rhodamine B absorbs only about 1% of the incident light. According to these values the quantum yield for the sensitization current is of the order of 10 to 30%. This estimate indicates that a charge-transfer mechanism is mainly responsible for the sensitization. The quantum yield decreases by factor of 5–10 eliminating oxygen from the solution. This effect will be discussed later on.

This does not mean that energy transfer should generally be excluded. As already mentioned above the efficiency for energy transfer depends on the density of energy levels of the proper energy difference within the semiconductor electrode. The greatest number of energy states are available in the conduction and valence band of GaP, *i.e.*, if such a dye is so adsorbed on the surface that its energy difference between the ground and excited singlet state is equal to or larger than the band gap, then the probability of energy transfer should

be much higher. More precisely speaking energy transfer is expected if the fluorescence spectra of the donor (excited dye) and the absorption spectra of the acceptor (semiconductor) overlap.<sup>11a,b</sup> In this case an energy transfer should be much faster than charge transfer since in any charge transfer a certain activation energy is required. As already lined out above in the case of energy transfer the sensitization current is expected to be very small because of the high surface recombination rate of electron-hole pairs in GaP.

A suitable donor for energy transfer to p-GaP is eosin which shows a fluorescence at about  $550 \text{ m}\mu$ , *i.e.*, at a wavelength where absorption already occurs in GaP. Corresponding measurements with p-GaP have shown that the sensitization current is negligibly small. This result indicates indeed that energy is transferred from eosin to GaP. This assumption is supported by the fact that with other p-type semiconductors with a much larger band than GaP, as *e.g.*, p-SiC, a large sensitization current was observed with eosin.

On the other hand, we also observed a decrease of the sensitization current if the absorption spectra of the dye and GaP overlap. This was shown for rhodamine B, rose bengal, and crystal violet. According to Figures 3–5 a strong sensitization was observed but on the short wavelength side of the sensitization spectra a sharp decrease of the photocurrent occurs. This cutoff is more evident comparing the sensitization spectra of rose bengal and crystal violet as obtained with p-GaP and n-ZnO electrodes (Figures 4 and 5). The same effect occurs with rhodamine B. From Figures 4 and 5 it must be concluded that the sensitization decreases rapidly as soon as the energy of the incident light corresponds to the energy of the band gap of GaP. This effect may also be interpreted by assuming a change in the transfer mechanism, *i.e.* at higher energies of incident light, energy instead of charge is transferred from the dye to GaP so that electron-hole pairs are formed in the crystal. These electron-hole pairs, as mentioned above, recombine *via* surface states so that the sensitization is quenched. In this case it has to be assumed, however, that energy transfer does not only occur with excited molecules being in their lowest vibrational state but with those which are not in thermal equilibrium with the environment, *i.e.* the transfer of excitation energy must occur from a higher vibrational state of the molecule. This model implies that the transfer rate has to be of the order of  $10^{11}$  to  $10^{12} \text{ sec}^{-1}$ . In the present case we have to assume a strong coupling between semiconductor and dye, which seems to be reasonable since the dye is adsorbed on the electrode surface.

Such a spectral distribution leading to the interpretation that both energy and charge transfer occur was only found with GaP until now. Further investigations, especially with other semiconductors, are necessary to prove this model. This is also desirable since

the charge-transfer current depends strongly on the amount of oxygen dissolved in the electrolyte, although the spectral distribution is not changed by oxygen. Before we will discuss the supersensitization by oxygen in detail we have to consider the potential dependence of the photocurrents as obtained with n- and p-type GaP.

As far as the spectral distribution of the sensitization is concerned it should finally be mentioned that the dimer peaks dominate in some cases because the density of dye molecules in the adsorbed layer is larger than in the solution. The appearance of the polymer band can be explained in the same way. The sensitization effect of pseudoisocyanine has been studied already in detail with ZnO electrodes<sup>13</sup> and will not be discussed here.

**Potential Dependence of Sensitization.** For most dyes the same spectral distribution was found with p- and n-type electrodes. Differences between the two types of electrodes are found as far as the potential dependence of the sensitization current is concerned. As shown in Figures 6 and 7 a sensitization current occurs with n-type only at higher cathodic potentials than with p-type electrodes. The different behavior of these electrodes will be comprehensible considering the potential distribution at the interface for both types.

According to results obtained by capacity measurements the position of the Fermi level at the surface is identical for p- and n-type GaP electrodes.<sup>10</sup> Consequently the potential distribution is different in both cases, *i.e.*, the energy bands are bent downwards in p-type and upwards in n-type GaP as shown in Figure 11 for an electrode potential of  $-0.3$  V (against calomel) in neutral solutions. Flat band potential is reached with n-GaP at about  $-1.2$  V and with p-type at  $+0.9$  V.<sup>10</sup> According to the sign of the electric field within the space charge region in p-GaP a hole formed by transferring an electron from the valence band to the dye drifts towards the interior of the bulk. In this case the sensitization current depends only on the light intensity and remains constant over a large potential range as shown in Figure 6. In n-type GaP, on the other hand, the field is of opposite sign, so that injected holes are pushed back towards the surface (see Figure 11) and consumed for the anodic dissolution. In this case the cathodic sensitization current is compensated by an anodic current so that the net current is zero. This effect is field dependent, *i.e.*, at higher cathodic polarization holes may diffuse into the interior of the crystal and recombine with electrons from the conduction band. Then, a sensitization is detectable for n-type GaP and the corresponding current increases at higher cathodic potentials. This was observed with most dyes as shown for cryptocyanine in Figure 7a. One should expect a saturation current as indicated by the dotted line in this figure. Unfortunately, this could not be proved experimentally since hydrogen

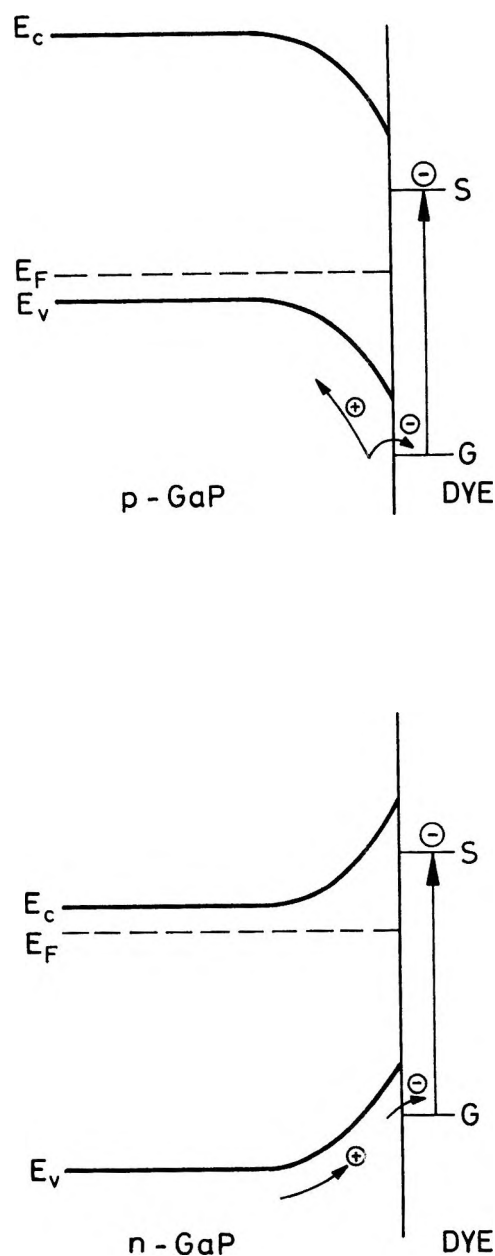


Figure 11. Potential distribution of the interface GaP/dye/electrolyte.

evolution made measurements in this potential range impossible.

The mechanism seems to be somewhat more complex, however, using rhodamine B or rose bengal instead of cryptocyanine as a sensitizing dye. Obviously in this case as well the electric field of the space charge is responsible for the potential dependence, but the photocurrent found with n-type GaP passes a maximum at  $-0.7$  V (Figure 7b). In this potential range, however, we also observed a reduction of rhodamine B without illumination as indicated in Figure 7c. From this result it may be concluded that the adsorbed monolayer is already reduced in the dark, *i.e.*, the sensitization

(13) H. Tributsch, *Ber. Bunsenges Phys. Chem.*, **73**, 582 (1969).

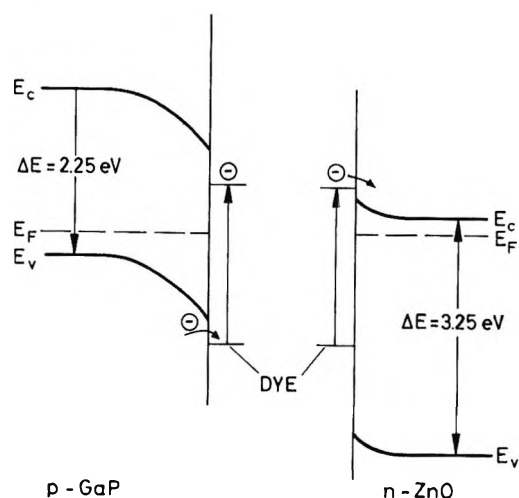


Figure 12. Comparison between GaP and ZnO surfaces.

disappears. Since no reduction was observed with p-type GaP, electrons from the conduction band are consumed for this process.

Moreover, there are certain particularities in the relaxation time of the sensitization current at cathodic potentials. All photocurrents measured with p-GaP (with and without dye) rise rapidly after the light has been turned on (Figure 8b and c). In the case of n-GaP the rise time of the sensitization current is much larger, about 50–100 msec (Figure 8e). Since also for the intrinsic photocurrent at cathodic potentials a relaxation time of the same order of magnitude was observed (Figure 8d) the origin of both relaxations seems to be identical. Their nature, however, is not yet understood.

*Comparison between GaP and ZnO.* As discussed above, charge transfer is the dominant mechanism. Although the potential dependence of the sensitization current is different for n- and p-GaP electrodes, electrons are only transferred from the valence band to the ground state of the excited dye (cathodic current). In contrast to GaP it was observed with ZnO electrodes that electrons are transferred from the excited dye to the conduction band of ZnO (anodic process). This difference between GaP and ZnO is caused by the fact that the positions of the energy band in an absolute energy scale are different for both compounds. In order to illustrate the charge-transfer mechanisms for GaP and ZnO we have to consider the potential distribution, keeping both electrodes at the same electrode potential, *i.e.*, with the Fermi levels of both electrodes identical, as shown in Figure 12 for an electrode potential  $U_E = -0.2$  V. The corresponding band bendings for GaP and ZnO were taken from capacity measurements.<sup>10,14</sup> Neglecting other double layer effects, the energy terms of the dye may be plotted on the same level for both interfaces (see Figure 12). Then, it is clear that the ground state of the dye only overlaps

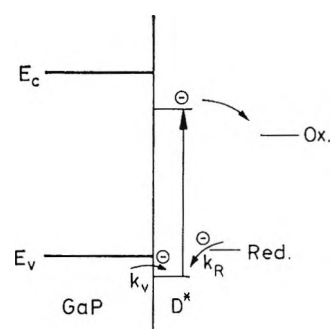


Figure 13. Schematic presentation of super- and desensitization at GaP electrodes.

with the valence band of GaP and the first excited singlet state with the conduction band of ZnO.

*Super- and Desensitization.* Experiments with ZnO have shown that reducing agents increase the anodic sensitization current.<sup>7</sup> This result was interpreted as an electron transfer from the reducing agent to the ground state of the excited dye. Since the ground state was then occupied the excited electron could not return from the upper singlet level to the ground level. Consequently, the probability of an electron transfer to the conduction band was much higher. According to this interpretation one should expect for GaP a desensitization after addition of a reducing agent. As illustrated in Figure 13 the ground level of the excited dye may trap an electron from the reducing agent, so that it is blocked for an electron transfer from the valence band of GaP. Whether a reducing agent works efficiently as a desensitizer depends on the two rate constants  $k_V$  and  $k_R$  (as defined in Figure 13). Since most reducing agents which enhanced the sensitization current with ZnO electrodes did not show any effect with GaP it must be concluded that the coupling between the valence band of GaP and the ground level of the dye is quite strong ( $k_V \gg k_R$ ). We only observed a desensitization with  $H_2O_2$ . Since the spectral distribution was not changed by  $H_2O_2$  we have to conclude that  $H_2O_2$  only influences the charge transfer. Obviously,  $H_2O_2$  acts as a reducing agent in this case. This result was surprising. It was checked that no reactions between  $H_2O_2$  and dye occurred already in the dark. We expected an enhancement of the sensitization by  $H_2O_2$  because an oxidizing agent could capture an electron from the excited singlet level of the dye, as also indicated in Figure 13. Obviously, the ground state of the dye seems to fit much better to the energy level of the redox system  $H_2O_2-O_2$  ( $U_E = +0.9$  V) than its excited level to that of  $H_2O_2-OH^-$  ( $U_E = +1.77$  V).

As mentioned above, an oxidizing agent should enhance the sensitization with GaP electrodes. Such an effect was observed with molecular oxygen (Figure

(14) F. Lohmann, *Ber. Bunsenges. Phys. Chem.*, **70**, 428 (1966).

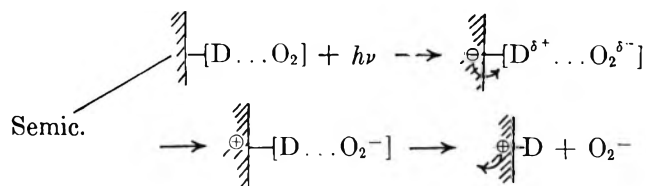
9). In this case the spectral distribution was independent of the amount of oxygen dissolved in the electrolyte, *i.e.*, we only observed a supersensitization in a wavelength range where charge transfer is postulated. The cutoff at the short wavelength side of the spectra as found with rhodamine B, rose bengal, and crystal violet is not affected by oxygen. This is reasonable since we postulated a fast energy transfer from higher vibrational levels of the excited molecules in the "cut-off region." In photochemical processes, oxygen, however, plays a special role since there are several possibilities for energy or charge transfer. Various mechanisms are discussed in the literature as follows.

a. The simplest interpretation is the assumption that oxygen is directly reduced by the excited dye.<sup>15</sup> According to recent investigations, however, this mechanism can be omitted.<sup>16</sup>

b. Kautsky<sup>17</sup> suggested an energy transfer from an excited dye to oxygen by which oxygen should be transferred from its triplet ground state to its excited singlet state. With certain sensitizers, *e.g.*, with a variety of fluorescein dyes, this mechanism could be proved.<sup>17</sup> In our case we had to assume that holes are injected from the excited oxygen ( $O_2^*$ ) into the valence band of GaP. Since we observed a supersensitization not only with fluorescein dyes but also with triphenylmethane dyes with which energy transfer to  $O_2$  never was found the Kautsky mechanism seems to be rather unlikely in our case.

c. The best possibility explaining the oxygen effect is afforded by the assumption of a charge-transfer com-

plex between sensitizer (D) and oxygen ( $O_2$ ). Kearns and Khan<sup>18</sup> have calculated the energies of various states of the system  $[D \dots O_2]$  complex as a function of intermolecular distance and have shown that a minimum of the potential energy exists for a charge-transfer complex  $[D^{\delta+} \dots O_2^{\delta-}]$ . Since the negative charge is shifted relatively towards oxygen an electron transfer from the valence band (V.B.) to the ground state of the dye is facilitated, as



The charge transfer is followed by a splitting of the complex and the  $O_2^-$  radical reacts further with the solution.

*Acknowledgments.* The authors are indebted to Professor Gerischer (T.H. Munich), Dr. Beckmann and Dr. Möllers (both Philips Hamburg) for many valuable discussions. Thanks are also due to Ir. Peters (Philips Nat. Lab. Eindhoven) for providing us with single crystals and to Ing. Kürsten for performing the experiments.

(15) J. Weiss, *Naturwissenschaften*, **23**, 610 (1935).

(16) K. Gollnick, *Advan. Photochem.*, **6**, 1 (1968).

(17) H. Kautsky and A. Hirsch, *Chem. Ber.*, **64**, 2677 (1931).

(18) A. K. Kahn and D. R. Kearns, *J. Chem. Phys.*, **48**, 3272 (1968).

# Kinetics of Copper(II)- and Copper(I)-Catalyzed Deuterium Exchange in Sulfuric and Perchloric Acid Solutions

by H. E. A. von Hahn and E. Peters\*

Department of Metallurgy, University of British Columbia, Vancouver 8, Canada (Received August 5, 1970)

Publication costs assisted by the National Research Council of Canada

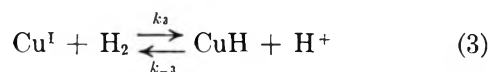
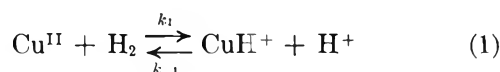
The cupric and cuprous ion-catalyzed exchange of deuterium with protium in sulfuric and perchloric acid solutions was studied at 160° and 5–15 atm of D<sub>2</sub> or H<sub>2</sub> pressure. Exchange occurred in both the D<sub>2</sub>-H<sub>2</sub>O and the H<sub>2</sub>-D<sub>2</sub>O systems. In the absence of copper ions no exchange took place. The Cu<sup>I</sup>-catalyzed exchange rates were markedly greater than the Cu<sup>II</sup>-catalyzed exchange rates. The exchange studies revealed a hitherto unobserved fast reaction between cuprous ions and dissolved hydrogen in perchloric acid solutions. The exchange rates were unexpectedly fast in low sulfuric acid solutions indicating the possible existence of reactive copper sulfate complexes. The rates of exchange and of Cu<sup>II</sup> reduction were measured at several levels of cuprous ion concentration. With these data and suitable derived equations, the four parameters  $k_1$ ,  $k_{-1}/k_2$ ,  $k_3$ , and  $k_{-3}/k_4$  of the Cu<sup>II</sup>-reduction rate law, *viz.*

$$-^{1/2} \frac{d[\text{Cu}^{\text{II}}]}{dt} = \frac{k_1[\text{Cu}^{\text{II}}]^2[\text{H}_2]}{\frac{k_{-1}}{k_2}[\text{H}^+] + [\text{Cu}^{\text{II}}]} + \frac{k_3[\text{Cu}^{\text{I}}][\text{Cu}^{\text{II}}]^2[\text{H}_2]}{\left[\frac{k_{-1}}{k_2}[\text{H}^+] + [\text{Cu}^{\text{II}}]\right] \left[\frac{k_{-3}}{k_4}[\text{H}^+] + [\text{Cu}^{\text{II}}]\right]}$$

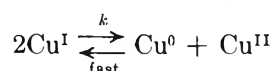
could be calculated for each exchange experiment. The values obtained were in satisfactory agreement with those obtained in previous studies in the H<sub>2</sub>-H<sub>2</sub>O system, when taking isotope effects into consideration.

## Introduction

The self-catalyzed reduction of cupric ions by hydrogen proceeds according to the mechanism



This mechanism was found to be valid for aqueous sulfuric acid solutions at elevated temperatures and pressures, *e.g.*, 160° and 5 atm of H<sub>2</sub>. At sufficiently high cuprous ion concentrations the following disproportionation reaction takes place.



This mechanism was first proposed by Dunning and Potter<sup>1</sup> and later confirmed by the present authors.<sup>2</sup> The latter developed the rate law of the Cu<sup>II</sup> reduction from this mechanism and demonstrated its validity experimentally. This law has the form

$$-^{1/2} \frac{d[\text{Cu}^{\text{II}}]}{dt} = \frac{k_1 [\text{Cu}^{\text{II}}]^2[\text{H}_2]}{\frac{k_{-1}}{k_2}[\text{H}^+] + [\text{Cu}^{\text{II}}]} + \frac{k_3[\text{Cu}^{\text{I}}][\text{Cu}^{\text{II}}]^2[\text{H}_2]}{\left[\frac{k_{-1}}{k_2}[\text{H}^+] + [\text{Cu}^{\text{II}}]\right] \left[\frac{k_{-3}}{k_4}[\text{H}^+] + [\text{Cu}^{\text{II}}]\right]} = R_{\text{Cu}^{\text{II}}} + R_{\text{Cu}^{\text{I}}} \quad (5)$$

The derived rate law indicates that the rate of Cu<sup>II</sup> reduction will be inhibited with increasing acidity as a result of the back reactions -1 and -3. If the acid effect occurs as indicated, its magnitude can be measured by means of deuterium exchange experiments by replacing either H<sub>2</sub> with D<sub>2</sub> or H<sub>2</sub>O with D<sub>2</sub>O in the reaction system. In the D<sub>2</sub>-H<sub>2</sub>O system, for example, HD will be formed in the back reactions as illustrated by the equations



An analogous scheme applies to reactions 3 and -3. Isotope exchange experiments have been done earlier by Potter,<sup>3</sup> who used H<sub>2</sub>-D<sub>2</sub> mixtures to reduce cupric

(1) W. J. Dunning and P. E. Potter, *Proc. Chem. Soc. London*, 244 (1960).

(2) E. A. von Hahn and E. Peters, *J. Phys. Chem.*, 69, 547 (1965).

ions and observed the appearance of HD in the gas phase. Webster and Halpern<sup>4</sup> used D<sub>2</sub>O-enriched water in the Ag<sup>+</sup>-catalyzed hydrogen reduction of dichromate ions in perchloric acid solutions and also observed the appearance of HD in the gas phase. They showed that the exchange rates increased with increasing acidity. However, in these studies no quantitative kinetic studies of the exchange reactions were made.

The present work is part of a kinetic study of Cu<sup>II</sup> reduction by hydrogen in sulfuric and perchloric acid solutions.<sup>5</sup> The main purpose was to obtain direct evidence of the acid effect as given by reactions -1 and -3. In addition, a quantitative evaluation of the kinetic data was to be attempted.

### Experimental Section

D<sub>2</sub> and D<sub>2</sub>O, both of 99.5 mol % purity, were obtained from the Liquid Carbonics Division of the General Dynamics Corporation. D<sub>2</sub> was supplied in a 2.8-l. cylinder at 500 psig, and D<sub>2</sub>O in 100-g lots in sealed ampoules. The main impurity in the D<sub>2</sub> was approximately 0.55 mol % HD. However, this amount was sufficiently small to be ignored in computing the amounts of HD produced in the exchange reactions.

Reagent grade chemicals and distilled water were used in preparing the experimental solutions. Stock solutions of cupric sulfate and cupric perchlorate were prepared by dissolving cupric oxide with stoichiometric amounts of the appropriate acids. Aliquots of these solutions were diluted with water and acid to the initial experimental volume of 1 l.

In preparing 1 l. of an acid CuSO<sub>4</sub> solution in D<sub>2</sub>O, 0.15 mol of CuO and 1.0 mol of H<sub>2</sub>SO<sub>4</sub> were added to part of the D<sub>2</sub>O, the CuO dissolved by gentle heating, and the solution made up to volume after cooling, with the remaining D<sub>2</sub>O. Although 2 mol of protons were thereby introduced into the heavy water solution, virtually all the acid hydrogens were D<sup>+</sup>, and any H<sup>+</sup> effects on the exchange results could be ignored.<sup>6-9</sup>

The exchange experiments were done in a 2-l. high-pressure autoclave made by the Parr Instrument Company. Details of the experimental apparatus including the solution sampling system and the experimental procedure have been described previously.<sup>10</sup> Both gas and solution samples were taken during the course of the experiments in order to measure the extents of both the exchange reactions and of the Cu<sup>II</sup> reduction.

The gas samples were taken into evacuated sampling bottles of about 1.5 ml capacity and analyzed mass-spectrometrically for HD, H<sub>2</sub>, and D<sub>2</sub>.<sup>11</sup> The solution samples were analyzed for Cu<sup>I</sup> concentration as previously described.<sup>10</sup>

The extent of the exchange reactions was measured in terms of moles of HD and H<sub>2</sub> produced per liter of solution. For the heavy water experiment (H<sub>2</sub>-D) the appearance of HD and D<sub>2</sub> was measured.

The total moles of HD and H<sub>2</sub> (or D<sub>2</sub>) produced

during the exchange experiments were calculated by cumulative addition of the differential numbers of moles of these gas species produced in the time intervals between successive gas samples. Since liquid samples were also taken, causing decreases in solution volume, these results were adjusted to the basis of one liter of solution. The differential numbers of moles of exchanged hydrogens were obtained by adding the amounts in the gas phase and in solution. About 95% of each hydrogen species was present in the gas phase. In calculating the amounts in the gas phase, the ideal gas law and Raoult's law of partial pressures were used. The amounts dissolved in solution were calculated with the solubility coefficient  $\alpha$  for hydrogen in pure water. The figure used was  $\alpha = 11.8 \times 10^{-4}$  mol/l. atm at 160°.<sup>12</sup> Gas and solution volumes were corrected for the changes caused by taking solution samples. The amounts of gases removed in the samples were disregarded. Also disregarded were the amounts of HD and H<sub>2</sub> (or D<sub>2</sub>) consumed in the reduction of Cu<sup>II</sup>, because the errors were tolerable, and considerable extra calculations would have been required to make these corrections.

### Results and Discussion

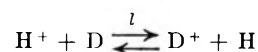
*Experimental Results.* The exchange experiments were done under the conditions shown in Table I. Deuterium exchange took place in each experiment except in experiment D<sub>2</sub>-E, where copper ions had not been added to the solution. This experiment showed thus that copper ions (Cu<sup>II</sup> and Cu<sup>I</sup>) are essential if the exchange reactions are to proceed and that the

(3) P. E. Potter, Ph.D. Thesis, The University of Bristol, 1958.

(4) A. H. Webster and J. Halpern, *J. Phys. Chem.*, **61**, 1239 (1957).

(5) E. A. Hahn, Ph.D. Thesis, The University of British Columbia, 1963.

(6) That this is a good approximation is shown by the following calculation: the equilibrium constant for the reaction



is  $l \approx 0.68$  at 25°.<sup>7</sup> Here D and H are solvent hydrogens. The initial light and heavy hydrogen concentrations before acid proton exchange were  $[\text{H}^+] = 0.71$  (see Table I),  $[\text{H}] = 1.29$  (assuming that at worst all HSO<sub>4</sub><sup>-</sup> converts rapidly to DSO<sub>4</sub><sup>-</sup>), and  $[\text{D}] = 105.0 - 1.29 = 103.71$  (used 950 ml D<sub>2</sub>O, sp gr 1.066). With these values and the given value of  $l$ , the equilibrium D<sup>+</sup> concentration was calculated to be 0.70 mol/l. At 160°  $[\text{D}^+]$  should be higher because  $\Delta H_1 = +167$  cal/mol; hence  $l_{160} > l_{25}$ .<sup>8</sup>

(7) (a) A. J. Kresge and A. L. Allred, *J. Amer. Chem. Soc.*, **85**, 1541 (1963); (b) V. Gold, *Proc. Chem. Soc. London*, 141 (1963).

(8)  $\Delta H_1$  was calculated from a recently estimated value of the enthalpy of a related exchange equilibrium constant.<sup>9</sup>

(9) K. Heinzinger and R. E. Weston, Jr., *J. Phys. Chem.*, **68**, 744 (1964).

(10) E. Peters and E. A. von Hahn in "Unit Processes in Hydrometallurgy," M. E. Wadsworth and F. T. Davis, Ed., Gordon and Breach, New York, N. Y., 1964, pp 204-226.

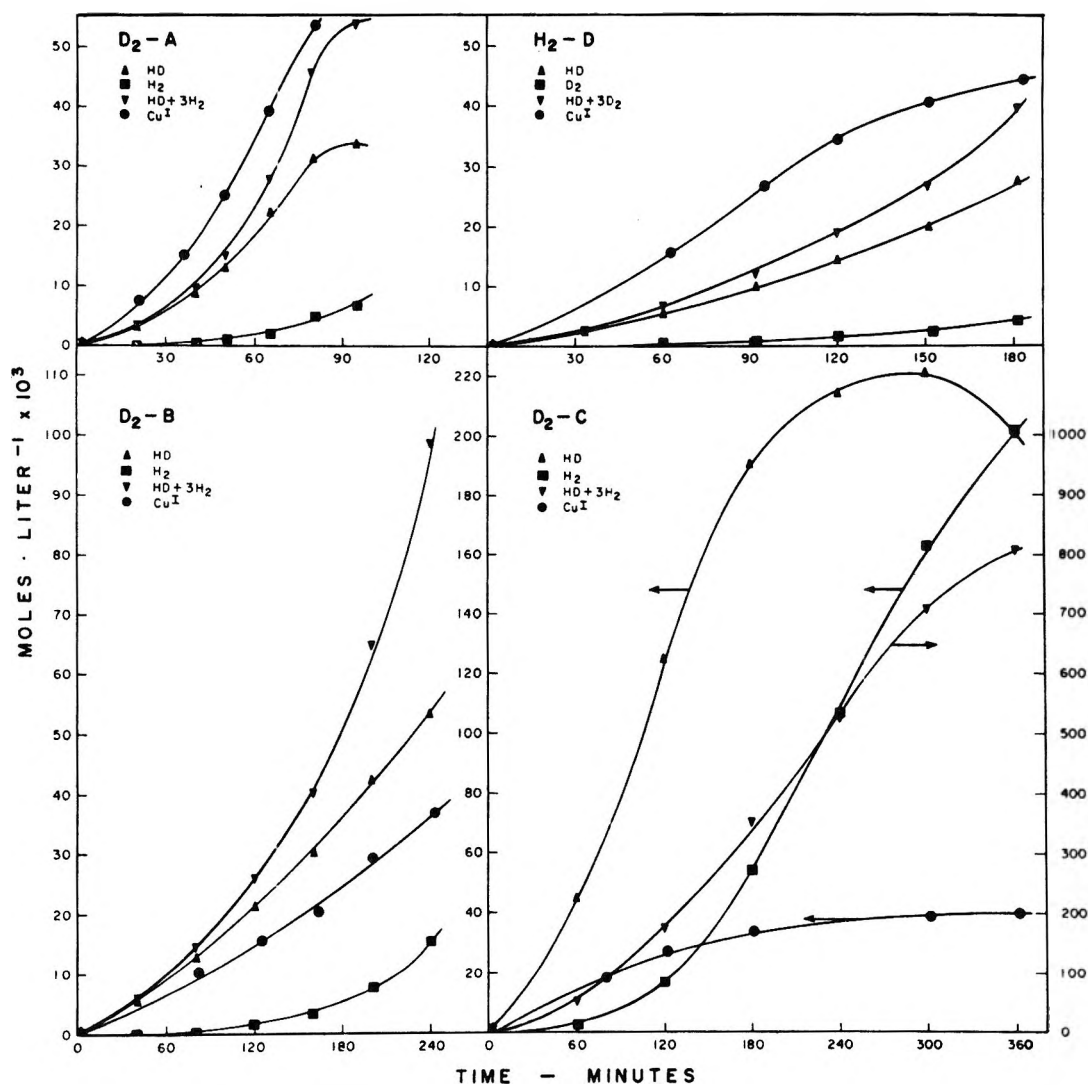
(11) These analyses were kindly done by J. A. Stone of the Research Chemistry Branch, Chemistry and Metallurgy Division, Atomic Energy of Canada Limited, Chalk River, Ontario.

(12) R. T. McAndrew, Ph.D. Thesis, The University of British Columbia, 1962.

Table I: Experimental Conditions for Exchange Experiments

Experiment no.	[Cu <sup>II</sup> ] <sub>0</sub> <sup>a</sup>	[H <sub>2</sub> SO <sub>4</sub> ] <sub>0</sub>	[HClO <sub>4</sub> ] <sub>0</sub>	Solvent	P <sub>D<sub>2</sub></sub> , atm	P <sub>H<sub>2</sub></sub> , atm	Temp, °C	[H <sup>+</sup> ] <sub>0</sub> <sup>b</sup> or [D <sup>+</sup> ] <sub>0</sub>
D <sub>2</sub> -A <sup>c</sup>	0.15	0.50		H <sub>2</sub> O	5		160	0.05
D <sub>2</sub> -B	0.15	0.85		H <sub>2</sub> O	5		160	0.71
D <sub>2</sub> -C	0.07		0.10	H <sub>2</sub> O	15		160	0.10
H <sub>2</sub> -D	0.15	0.85		D <sub>2</sub> O		5	160	0.71
D <sub>2</sub> -E <sup>d</sup>	0.00	0.50		H <sub>2</sub> O	5		160	0.05

<sup>a</sup> CuSO<sub>4</sub> except in experiment D<sub>2</sub>-C, in which Cu(ClO<sub>4</sub>)<sub>2</sub> was used. <sup>b</sup> The free initial [H<sup>+</sup>] ([D<sup>+</sup>] for experiment H<sub>2</sub>-D) for all experiments except D<sub>2</sub>-C, was calculated with a bisulfate dissociation constant  $K = 3 \times 10^{-3} M^{-1}$ . This  $K$  value was estimated by interpolation from recent molal high temperature values of the constant published by W. L. Marshall and E. V. Jones, *J. Phys. Chem.*, **70**, 4028 (1966). The effect of converting molal to molar values was small and was therefore disregarded. <sup>c</sup> Solution was 0.35  $M$  in MgSO<sub>4</sub>. <sup>d</sup> Solution was 0.50  $M$  in MgSO<sub>4</sub>.

Figure 1. Curves of exchange products and [Cu<sup>I</sup>] vs. time.

possibility of deuterium exchange taking place by base catalysis can be ruled out.

The experimental results are illustrated by the plots in Figure 1. The plots of HD and H<sub>2</sub> (or D<sub>2</sub>) vs. time are the exchange product curves given in units of moles

produced per liter of solution.<sup>13</sup> The plots of Cu<sup>I</sup> vs. time show the extent of Cu<sup>II</sup> reduction. The plots of HD + 3H<sub>2</sub> (or 3D<sub>2</sub>) vs. time give the total exchange that has taken place.<sup>14</sup>

The marked upward curvatures of the exchange

product plots illustrate the enhancing effect of cuprous ions on the exchange rates. The cuprous effect is predicted by reaction -3 in the mechanism of  $\text{Cu}^{\text{II}}$  reduction. It is evident in all four exchange experiments. The downward curvature of the HD plot of experiment  $\text{D}_2\text{-C}$  toward the end is caused by HD consumption from secondary exchange and from oxidation by  $\text{Cu}^{\text{II}}$ .

The enhancing effect of cuprous ions on the rates of  $\text{Cu}^{\text{II}}$  reduction in sulfuric acid solutions is illustrated by the upward curvatures of the  $[\text{Cu}^{\text{I}}]$  vs. time plots of experiments  $\text{D}_2\text{-A}$ ,  $\text{D}_2\text{-B}$ , and  $\text{H}_2\text{-D}$ . This effect does not appear in the perchloric acid experiment  $\text{D}_2\text{-C}$ . The results obtained here are analogous to those of the earlier  $\text{Cu}^{\text{II}}$  reduction studies in sulfuric<sup>2</sup> and perchloric<sup>10</sup> acid solutions.

Two noteworthy effects were revealed by the exchange experiments. The first one is the large cuprous ion effect on the deuterium exchange in the perchloric acid solution experiment  $\text{D}_2\text{-C}$ . The second one is the anomalously large extent of deuterium exchange obtained in the low sulfuric acid experiment  $\text{D}_2\text{-A}$ .

The large cuprous effect on the exchange reactions in experiment  $\text{D}_2\text{-C}$  was surprising in view of the very slight cuprous effect on the  $\text{Cu}^{\text{II}}$  reduction reaction in perchloric acid solutions as observed previously.<sup>10</sup> This result means that the exchange studies have revealed a hitherto unobserved fast reaction between cuprous ions and dissolved hydrogens in these solutions. This reaction is then followed by a similarly fast back reaction in which the reactants are regenerated, and by which the deuterium exchange probably takes place.

These findings suggest that the mechanism of  $\text{Cu}^{\text{II}}$  reduction (or hydrogen activation) in perchloric acid solutions is analogous to that found for sulfuric acid solutions, as given by eq 1-4. The fact that the cuprous ion effect on the rate of  $\text{Cu}^{\text{II}}$  reduction is only slight in perchloric acid solutions indicates that the rate of reaction 4 must be considerably slower than the rate of reaction -3. In sulfuric acid solutions the opposite is the case.

The anomalously large extent of deuterium exchange obtained in the low sulfuric acid experiment  $\text{D}_2\text{-A}$  was surprising, particularly since the extent of exchange was greater than that in the high sulfuric acid experiment  $\text{D}_2\text{-B}$ . The opposite to this result would have been expected, because according to reactions -1 and -3 the exchange rates are first order with respect to  $[\text{H}^+]$  and therefore should decrease with decreasing acidity.

Since no exchange was found to take place at low acidity in the absence of copper ions (experiment  $\text{D}_2\text{-E}$ ), the possibility that base-catalyzed exchange can account for this effect must be ruled out. One plausible explanation for this effect is that the cupric and cuprous ions exist in low sulfuric acid solutions mainly as sulfato complexes and that these complexes are more reactive toward dissolved hydrogen species than the corre-

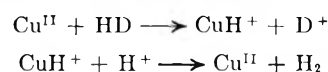
sponding aquo complexes. At low acidity the sulfato complexes should be more predominant because of the greater extent of dissociation of bisulfate ions.

**Reaction Rates.** Values of the total exchange rates,  $d(\text{HD} + 3\text{H}_2)/dt$ , and the net forward rates,  $-d[\text{D}_2 \text{ or } \text{H}_2]/dt = -1/2d[\text{Cu}^{\text{II}}]/dt = 1/2d[\text{Cu}^{\text{I}}]/dt$ , were measured at several points along the initial parts of the appropriate curves. Slope measurements were made by the mirror image method at  $[\text{Cu}^{\text{I}}]$  levels ranging from 5 to  $30 \times 10^{-3}$ . The rate values thus obtained were plotted against  $[\text{Cu}^{\text{I}}]$  for each exchange experiment, as shown in Figure 2. The total exchange rates are designated by  $r_{\text{T}}$  and the net forward rates by  $R_{\text{T}}$ . The  $R_{\text{T}}$  values for experiment  $\text{D}_2\text{-C}$  were corrected to take into account an error resulting from the slow oxidation of cuprous ions by perchlorate ions at the experimental temperature.<sup>15</sup>

These rate measurements were made for the purpose of obtaining data required to calculate values of  $k_1$ ,  $k_{-1}/k_2$ ,  $k_3$ , and  $k_{-3}/k_4$  for each exchange experiment. These calculations are shown below.

The apparently linear relationships between  $r_{\text{T}}$ ,  $R_{\text{T}}$ , and  $[\text{Cu}^{\text{I}}]$ , evident in Figure 2, indicate a first-order effect of  $[\text{Cu}^{\text{I}}]$  on the total exchange rates and the net forward rates. For the net forward rates this is in accordance with the rate law (eq 5) and agrees with the previous results for sulfuric acid solutions.<sup>2</sup> For the total exchange rates a first-order  $[\text{Cu}^{\text{I}}]$  effect is indicated by eq 14 (see below) because  $R_{\text{Cu}^{\text{I}}}$  in the second

(13)  $\text{H}_2$  (or  $\text{D}_2$ ) will appear as a result of secondary exchange, as illustrated by the following example for the  $\text{D}_2\text{-H}_2\text{O}$  system



This scheme applies when  $\text{H}^+$  is the dominant acid species in solution. When  $\text{D}^+$  is the dominant acid species, *i.e.*, when  $\text{D}_2\text{O}$  is the solvent,  $\text{D}_2$  will appear as a result of secondary exchange. A similar set of reactions applies in the activation of HD by  $\text{Cu}^{\text{I}}$ .

(14) The net reaction of a primary exchange event between deuterium and light water is



Two kinds of secondary events take place, namely



For each  $\text{H}_2$  molecule produced there are four events in all, two primary and two secondary events. One of the secondary events generates an HD molecule by reaction b and therefore has been counted once (but not twice) in the HD analysis. Thus, each  $\text{H}_2$  molecule represents three events that have not been counted by HD molecules, and the total exchange (neglecting tertiary and higher exchange) is  $[\text{HD} + 3\text{H}_2]$ .

(15) This reaction was observed in the earlier studies and an equation developed to correct for the resulting errors.<sup>10</sup> This equation has the form

$$R_{\text{T}} = \frac{-d[\text{D}_2]}{dt} = 1/2 \frac{d[\text{Cu}^{\text{I}}]}{dt} + 4k_{\text{Cl}}[\text{Cu}^{\text{I}}][\text{H}^+][\text{ClO}_4^-]$$

$k_{\text{Cl}} = (2.07 \times 10^{-4} \pm 7\%) \text{ M}^{-2} \text{ sec}^{-1}$  at  $160^\circ$ . The rates actually measured along the  $[\text{Cu}^{\text{I}}]$  vs. time curve in Figure 1 for experiment  $\text{D}_2\text{-C}$  are designated by

$$1/2d[\text{Cu}^{\text{I}}]/dt$$

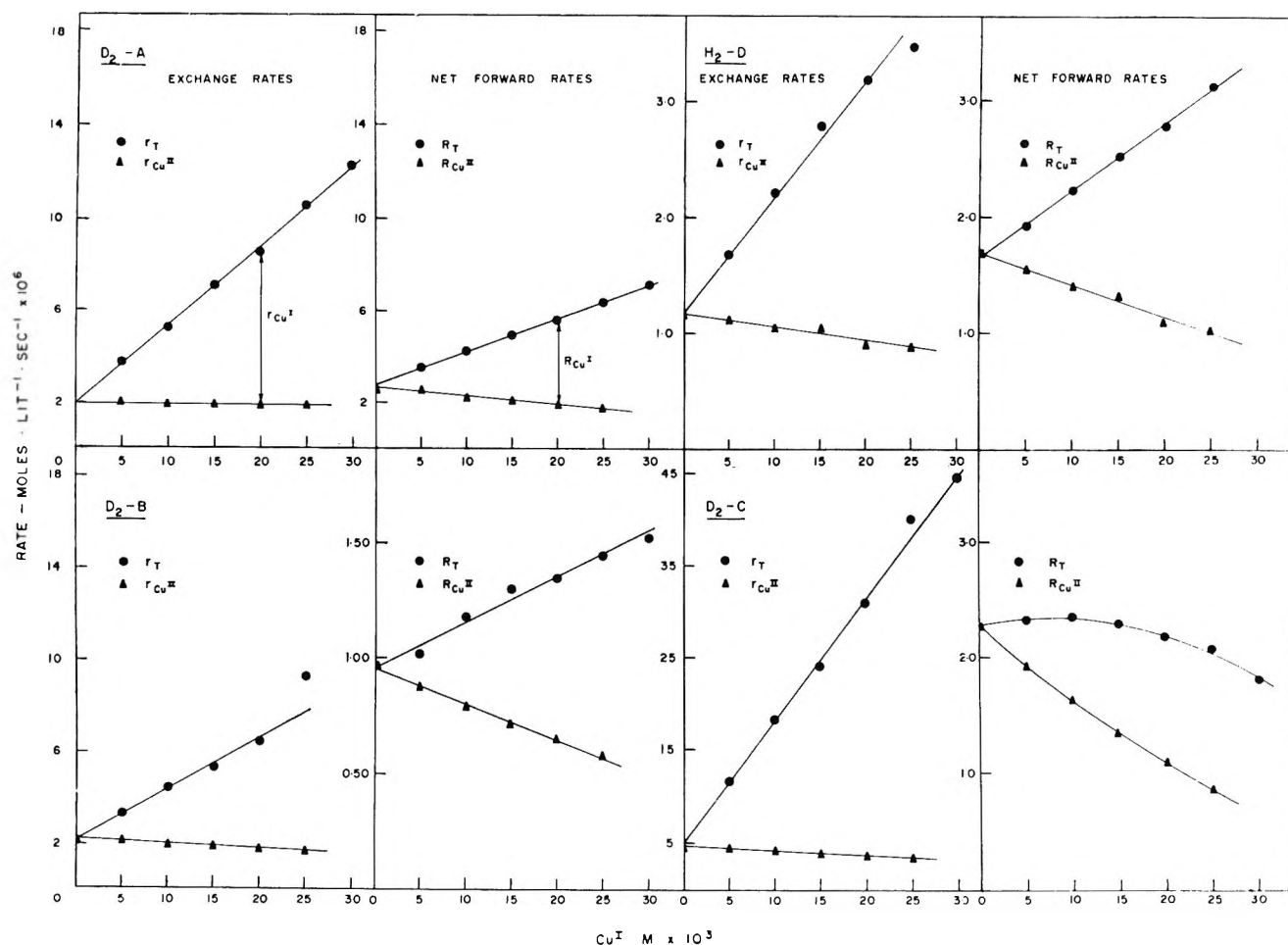


Figure 2. Plots of total exchange rates and net forward rates vs.  $[Cu^I]$ .

right-hand-side term of this equation is a first-order function of  $[Cu^I]$ .

For experiment  $D_2-C$  no linear relationship between  $R_T$  and  $[Cu^I]$  is evident, and the slope of the  $R_T$  plot decreases with increasing  $[Cu^I]$ . This again reflects the low cuprous ion effect on the net forward rates in perchloric acid solutions.

*Calculations of  $k_1$ ,  $k_{-1}/k_2$ ,  $k_3$ , and  $k_{-3}/k_4$ .* These rate constants and ratios were calculated for each exchange experiment using the measured values of the total exchange rates,  $r_T$ , the net forward rates,  $R_T$ , and suitable equations derived from the mechanism of  $Cu^{II}$  reduction (eq 1-4). It was assumed that this mechanism is also valid for perchloric acid solutions (experiment  $D_2-C$ ).

In the following the necessary equations used for each constant are derived and the method of calculation given. To begin with, the following relationships based on the reaction mechanism are defined.

$$\text{total exchange rate} = r_T = r_{Cu^{II}} + r_{Cu^I} \quad (6)$$

$$\text{total net forward rate} = R_T = R_{Cu^{II}} + R_{Cu^I} \quad (7)$$

where

$$r_{Cu^{II}} = \text{Cu}^{II}\text{-dependent exchange rate}$$

$$r_{Cu^I} = \text{Cu}^I\text{-dependent exchange rate}$$

$$R_{Cu^{II}} = \text{Cu}^{II}\text{-dependent net forward rate}$$

$$R_{Cu^I} = \text{Cu}^I\text{-dependent net forward rate}$$

We also have

$$r_{Cu^{II}} + R_{Cu^{II}} = k_1[Cu^{II}][H_2] \quad (8)$$

$$r_{Cu^I} + R_{Cu^I} = k_3[Cu^I][H_2] \quad (9)$$

Equations 8 and 9 represent, respectively, the  $Cu^{II}$ - and the  $Cu^I$ -dependent rates of hydrogen activation.

By adding eq 6 and 7 and eq 8 and 9, and equating the resultant sums, we obtain the total rate of hydrogen activation

$$r_T + R_T = r_{Cu^{II}} + R_{Cu^{II}} + r_{Cu^I} + R_{Cu^I} = k_1[Cu^{II}][H_2] + k_3[Cu^I][H_2] \quad (10)$$

For the sake of convenience,  $H^+$  and  $H_2$  are used in all equations even though  $D^+$ ,  $D_2$ , or  $HD$  would be appropriate.

$k_1$ . At the beginning of the experiments when  $[Cu^I] = 0$ ,  $r_{Cu^I} = R_{Cu^I} = 0$ , and eq 10 reduces to

$$r_T + R_T = r_{Cu^{II}_0} + R_{Cu^{II}_0} = k_1[Cu^{II}]_0[H_2] \quad (11)$$

whence

**Table II:** Values of  $k_1$  and  $k_{-1}/k_2$ 

Experiment no.	$k_1$ l. mol <sup>-1</sup> sec <sup>-1</sup>	$k_{-1}/k_2$	Acidity	Moles l. <sup>-1</sup>
(a) Sulfuric Acid Solutions				
D <sub>2</sub> -A	$5.3 \times 10^{-3} \pm 10\%$	$1.09 \pm 20\%$	Low	~0.05
<sup>a</sup>	$4.5 \times 10^{-3}$		Low	~0.01
D <sub>2</sub> -B	$3.6 \times 10^{-3} \pm 10\%$	$0.49 \pm 20\%$	High	0.71
H <sub>2</sub> -D	$3.1 \times 10^{-3} \pm 10\%$	$0.14 \pm 20\%$	High	0.71
<sup>b</sup>	$3.2 \times 10^{-3} \pm 10\%$	$0.13 \pm 30\%$		0.05 to 0.71
(b) Perchloric Acid Solutions				
D <sub>2</sub> -C	$5.5 \times 10^{-3} \pm 10\%$	$1.40 \pm 20\%$		0.07
<sup>c</sup>	$5.4 \times 10^{-3} \pm 15\%$	$0.37 \pm 30\%$		0.01 to 0.05

<sup>a</sup> See ref 5. <sup>b</sup> See ref 2. <sup>c</sup> E. A. Hahn and E. Peters, *Can. J. Chem.*, **39**, 162 (1961).

$$k_1 = \frac{r_{\text{Cu}^{II}_0} + R_{\text{Cu}^{II}_0}}{[\text{Cu}^{II}]_0[\text{H}_2]} \quad (12)$$

Values of  $r_{\text{Cu}^{II}_0}$  and  $R_{\text{Cu}^{II}_0}$  were obtained from the intercepts (at  $[\text{Cu}^I] = 0$ ) of the  $r_T$  and  $R_T$  plots in Figure 2. Values of  $[\text{Cu}^{II}]_0$  were taken from Table I; the values of  $[\text{H}_2]$  or  $[\text{D}_2]$  were calculated, using the partial pressures of these gases and the solubility coefficient  $\alpha$  for  $\text{H}_2$  in  $\text{H}_2\text{O}$  at  $160^\circ$ .<sup>12</sup> The values of  $k_1$  calculated with these data for each exchange experiment are listed in Table II.

$k_{-1}/k_2$ . To calculate this ratio, the following equation for the total exchange rate was first developed.

$$r_T = \frac{k_{-1}[\text{H}^+]}{k_2} \times \frac{k_1[\text{Cu}^{II}][\text{H}_2]}{\left[\frac{k_{-1}}{k_2}[\text{H}^+] + [\text{Cu}^{II}]\right]} + \frac{k_{-1}[\text{H}^+]}{k_2} \times \frac{k_2[\text{Cu}^I][\text{Cu}^{II}][\text{H}_2]}{\left[\frac{k_{-1}}{k_2}[\text{H}^+] + [\text{Cu}^{II}]\right] \left[\frac{k_{-3}}{k_4}[\text{H}^+] + [\text{Cu}^{II}]\right]} + \frac{k_{-3}[\text{H}^+]}{k_4} \times \frac{k_3[\text{Cu}^I][\text{H}_2]}{\left[\frac{k_{-3}}{k_4}[\text{H}^+] + [\text{Cu}^{II}]\right]} \quad (13)$$

This equation is derived from the mechanism of  $\text{Cu}^{II}$  reduction (eq 1-4) by using the steady-state approximation for the hydride intermediates  $\text{CuH}^+$  and  $\text{CuH}$ . A form more convenient for calculating  $k_{-1}/k_2$  is obtained when the first two right-hand-side terms are multiplied by  $[\text{Cu}^{II}]$  in both numerator and denominator and the third term is multiplied by  $[\text{Cu}^{II}]^2$  ( $(k_{-1}/k_2)[\text{H}^+] + [\text{Cu}^{II}]$ ) also in both numerator and denominator. After rearrangement, the following expression is obtained

$$r_T = \frac{k_{-1}[\text{H}^+]}{k_2[\text{Cu}^{II}]} \times R_{\text{Cu}^{II}} + \left[ \frac{k_{-1}[\text{H}^+]}{k_2[\text{Cu}^{II}]} + \frac{k_{-3}}{k_4} \frac{[\text{H}^+]}{[\text{Cu}^{II}]} \left( \frac{k_{-1}}{k_2} \frac{[\text{H}^+]}{[\text{Cu}^{II}]} + 1 \right) \right] \times R_{\text{Cu}^I} = r_{\text{Cu}^{II}} + r_{\text{Cu}^I} \quad (14)$$

$R_{\text{Cu}^{II}}$  and  $R_{\text{Cu}^I}$  are, respectively, the first and second right-hand-side terms of eq 5.

At the beginning of an experiment when  $[\text{Cu}^I] = 0$ , eq 14 reduces to

$$r_T = r_{\text{Cu}^{II}_0} = \frac{k_{-1}}{k_2} \frac{[\text{H}^+]_0}{[\text{Cu}^{II}]_0} R_{\text{Cu}^{II}} \quad (15)$$

and rearrangement yields

$$\frac{k_{-1}}{k_2} = \frac{r_{\text{Cu}^{II}_0}}{R_{\text{Cu}^{II}_0}} \frac{[\text{Cu}^{II}]_0}{[\text{H}^+]_0} \quad (16)$$

Values of  $k_{-1}/k_2$  were calculated for each exchange experiment with eq 16 and the same values of  $r_{\text{Cu}^{II}_0}$ ,  $R_{\text{Cu}^{II}_0}$ , and  $[\text{Cu}^{II}]_0$  that were used in calculating  $k_1$ . The  $[\text{H}^+]_0$  values were taken from Table I. The  $k_{-1}/k_2$  values obtained are listed in Table II.

$k_{-3}/k_4$ . Since the second right-hand-side term of eq 14 is equal to  $r_{\text{Cu}^I}$ , the following expression for  $k_{-3}/k_4$  can be derived

$$\frac{k_{-3}}{k_4} = \frac{[\text{Cu}^{II}]}{[\text{H}^+]} \left[ \frac{r_{\text{Cu}^I}}{R_{\text{Cu}^I}} - \frac{k_{-1}}{k_2} \frac{[\text{H}^+]}{[\text{Cu}^{II}]} \right] \frac{k_{-1}}{k_2} \frac{[\text{H}^+]}{[\text{Cu}^{II}]} + 1 \quad (17)$$

To calculate  $k_{-3}/k_4$ , values of  $R_{\text{Cu}^I}$  and  $r_{\text{Cu}^I}$  are required. They were calculated, respectively, with the equations

$$R_{\text{Cu}^I} = R_T - R_{\text{Cu}^{II}} \quad (18)$$

and

$$r_{\text{Cu}^I} = r_T - r_{\text{Cu}^{II}} \quad (19)$$

The  $R_T$  and  $r_T$  values were obtained from the appropriate plots in Figure 2. The  $R_{\text{Cu}^{II}}$  values were calculated with the equation

$$R_{\text{Cu}^{II}} = \frac{k_1[\text{Cu}^{II}]^2[\text{H}_2]}{\frac{k_{-1}}{k_2}[\text{H}^+] + [\text{Cu}^{II}]} \quad (20)$$

and the  $r_{\text{Cu}^{II}}$  values with the equation

$$r_{\text{Cu}^{\text{II}}} = \frac{k_{-1}}{k_2} \frac{[\text{H}^+]}{[\text{Cu}^{\text{II}}]} R_{\text{Cu}^{\text{II}}} \quad (21)$$

The values of  $k_1$  and  $k_{-1}/k_2$  used were those obtained earlier for each exchange experiment. The values of  $[\text{Cu}^{\text{II}}]$  and  $[\text{H}^+]$  (or  $[\text{D}^+]$ ) were calculated with  $[\text{Cu}^{\text{II}}] = [\text{Cu}^{\text{II}}]_0 - [\text{Cu}^{\text{I}}]$  and  $[\text{H}^+] = [\text{H}^+]_0 + [\text{Cu}^{\text{I}}]$ .  $[\text{H}_2]$  (or  $[\text{D}_2]$ ) values were calculated as above from the partial pressures of these gases and the solubility coefficient  $\alpha$  for  $\text{H}_2$  in  $\text{H}_2\text{O}$  at  $160^\circ$ .<sup>12</sup>

Figure 2 shows the plots of the calculated values of  $R_{\text{Cu}^{\text{II}}}$  and  $r_{\text{Cu}^{\text{II}}}$  vs.  $[\text{Cu}^{\text{I}}]$  for each exchange experiment at five levels of  $[\text{Cu}^{\text{I}}]$  ranging from  $5 \times 10^{-3}$  to  $25 \times 10^{-3}$ .

From these data, values of  $R_{\text{Cu}^{\text{I}}}$  and  $r_{\text{Cu}^{\text{I}}}$  were calculated at four levels of  $[\text{Cu}^{\text{I}}]$  ( $5 \times 10^{-3}$  to  $20 \times 10^{-3}$ ) with eq 18 and 19. They were used in eq 17 to calculate  $k_{-3}/k_4$ . Table III lists for each exchange experiment the values of  $k_{-3}/k_4$  obtained at each  $[\text{Cu}^{\text{I}}]$  level, together with the average values.

$k_3$ . This constant is calculated with the equation

$$k_3 = \frac{r_{\text{Cu}^{\text{I}}} + R_{\text{Cu}^{\text{I}}}}{[\text{Cu}^{\text{I}}][\text{H}_2]} \quad (22)$$

obtained by rearranging eq 9. Values of  $k_3$  were calculated for each exchange experiment at the four levels of  $[\text{Cu}^{\text{I}}]$ , using the values of  $r_{\text{Cu}^{\text{I}}}$  and  $R_{\text{Cu}^{\text{I}}}$  obtained above and the appropriate values of  $[\text{H}_2]$  (or  $[\text{D}_2]$ ). They are also listed in Table III together with their average values.

The above calculations have shown that with the kinetic data obtained from a single exchange experiment it is possible to calculate the four rate parameters,  $k_1$ ,  $k_{-1}/k_2$ ,  $k_3$ , and  $k_{-3}/k_4$ , occurring in the rate law of  $\text{Cu}^{\text{II}}$  reduction (eq 5). This method thus offers the possibility of considerably reducing the experimental work required for obtaining these rate parameters and also allowing the evaluation of secondary effects on the rate parameters, such as the low acid effect, that would otherwise be difficult or impossible to do.

**Errors.** Estimates were made of the errors of precision in the values of  $k_1$ ,  $k_{-1}/k_2$ ,  $k_3$ , and  $k_{-3}/k_4$ . For  $k_1$  and  $k_{-1}/k_2$  these errors were determined by drawing lines of maximum and minimum slope through the plotted points of  $r_{\text{T}}$  and  $R_{\text{T}}$  in Figure 2 and measuring the intercepts of these lines at  $[\text{Cu}^{\text{I}}] = 0$ . With these intercepts the maximum and minimum values of  $k_1$  and  $k_{-1}/k_2$  were calculated. The error limits obtained were  $\pm 10\%$  for  $k_1$  and  $\pm 20\%$  for  $k_{-1}/k_2$ .

The values of  $k_3$  and  $k_{-3}/k_4$  are influenced by the errors in  $k_1$  and  $k_{-1}/k_2$ . The calculations for determining the effects of these errors are lengthy. Hence only one estimate was made of these effects, namely for experiment D<sub>2</sub>-B at one  $\text{Cu}^{\text{I}}$  concentration level ( $10 \times 10^{-3}$  mol/l.). The variations obtained were  $\pm 10\%$  for  $k_3$  and  $\pm 60\%$  for  $k_{-3}/k_4$ . These variations are assumed to represent the errors in  $k_3$  and in  $k_{-3}/k_4$  in all exchange

Table III: Values of  $k_3$  and  $k_{-3}/k_4$

	$[\text{Cu}^{\text{I}}]$ level	$k_3$ , l. mol <sup>-1</sup> sec <sup>-1</sup>	$\frac{k_{-3}}{k_4}$
(a) Sulfuric Acid Solutions			
Experiment D <sub>2</sub> -A	$5 \times 10^{-3}$	$10.4 \times 10^{-2}$	0.69
	$10 \times 10^{-3}$	$9.50 \times 10^{-2}$	0.63
	$15 \times 10^{-3}$	$9.96 \times 10^{-2}$	0.52
	$20 \times 10^{-3}$	$10.0 \times 10^{-2}$	0.44
Average values		$10.0 \times 10^{-2}$ $\pm 10\%$	$\pm 60\%$
$\sim 0.01 M \text{H}_2\text{SO}_4^a$		$9.3 \times 10^{-2}$	
Experiment D <sub>2</sub> -B	$5 \times 10^{-3}$	$4.90 \times 10^{-2}$	0.21
	$10 \times 10^{-3}$	$5.16 \times 10^{-2}$	0.20
	$15 \times 10^{-3}$	$5.02 \times 10^{-2}$	0.18
	$20 \times 10^{-3}$	$5.24 \times 10^{-2}$	0.18
Average values		$5.1 \times 10^{-2}$ $\pm 10\%$	$\pm 60\%$
0.05 to 0.71 M $\text{H}_2\text{SO}_4^b$		$6.4 \times 10^{-2}$ $\pm 25\%$	$\pm 40\%$
Experiment H <sub>2</sub> -D	$5 \times 10^{-3}$	$3.15 \times 10^{-2}$	0.09
	$10 \times 10^{-3}$	$3.67 \times 10^{-2}$	0.07
	$15 \times 10^{-3}$	$3.60 \times 10^{-2}$	0.07
	$20 \times 10^{-3}$	$4.13 \times 10^{-2}$	0.05
Average values		$3.6 \times 10^{-2}$ $\pm 10\%$	$\pm 60\%$
(b) Perchloric Acid Solutions			
Experiment D <sub>2</sub> -C	$5 \times 10^{-3}$	$8.42 \times 10^{-2}$	2.80
	$10 \times 10^{-3}$	$8.43 \times 10^{-2}$	2.59
	$15 \times 10^{-3}$	$8.30 \times 10^{-2}$	2.35
	$20 \times 10^{-3}$	$8.40 \times 10^{-2}$	2.10
Average values		$8.39 \times 10^{-2}$ $\pm 10\%$	$\pm 60\%$

<sup>a</sup> See ref 5. <sup>b</sup> See ref 2.

experiments, because they are larger than those assignable to errors in rate measurements.

The reason for the large error in  $k_{-3}/k_4$  is evident from the form of eq 17, which shows that small changes in  $k_{-1}/k_2$  will cause large changes in  $k_{-3}/k_4$ . For  $k_3$  (calculated with eq 22) the opposite situation applies. The reason is that the values of  $r_{\text{Cu}^{\text{I}}}$  and of  $R_{\text{Cu}^{\text{I}}}$  change in opposite directions for a given change in  $k_{-1}/k_2$ . The influence of changes in  $k_1$  is smaller than that of changes in  $k_{-1}/k_2$ .

Errors of reproducibility of the rate constants and ratios are not available, because duplicate exchange experiments were not made.

Table III shows that the values of  $k_{-3}/k_4$  decrease with increasing  $\text{Cu}^{\text{I}}$  concentration, particularly in experiments D<sub>2</sub>-A and D<sub>2</sub>-C. Probable reasons for this shift are that the amounts of HD and  $\text{H}_2$  consumed in  $\text{Cu}^{\text{II}}$  reduction as well as the amounts of HD and  $\text{H}_2$  produced in tertiary and higher order exchange were ignored in calculating the points for the ( $\text{HD} + 3\text{H}_2$ )

curves in Figure 1. This neglect will cause the  $r_T$  values and hence the  $r_{Cu^I}$  values to be lower than the "true" values, which, according to eq 17, will cause the values of  $k_{-3}/k_4$  to be lower. This effect will increase with increasing  $Cu^I$ -concentration.  $k_3$  is not as much influenced by these effects because this constant is less sensitive to changes in  $r_{Cu^I}$  (eq 22).

*Comparison of Rate Constants and Ratios.* The values of the constants obtained in the exchange experiments are now compared with corresponding values obtained in previous studies. For this purpose the latter are also listed in Tables II and III.

$k_1$ . The values of this constant obtained in experiments D<sub>2</sub>-B, D<sub>2</sub>-C, and H<sub>2</sub>-D are in good agreement with the corresponding earlier values obtained for both sulfuric and perchloric acid solutions.

$k_{-1}/k_2$ . The values of this ratio obtained in experiments D<sub>2</sub>-B and D<sub>2</sub>-C are larger than the respective earlier values in sulfuric and perchloric acid solutions. This difference is considered to be related to isotope effects, as discussed in detail below. The value of the heavy water experiment D<sub>2</sub>-B agrees well with the earlier value.

$k_3$ . The average values of this constant obtained for experiments D<sub>2</sub>-B and H<sub>2</sub>-D are smaller than the corresponding previous value. For experiment D<sub>2</sub>-B the difference is within the limits of the assigned experimental errors; for experiment H<sub>2</sub>-D it is greater.

$k_{-3}/k_4$ . The average values of this ratio obtained in experiments D<sub>2</sub>-B and H<sub>2</sub>-D are both smaller than the corresponding previous value for sulfuric acid solutions. The value of experiment D<sub>2</sub>-B can be considered to be the same as the previous value within limits of the assigned experimental errors. The value of experiment H<sub>2</sub>-D is smaller than allowed by the limits of the assigned experimental errors.

*Experiment D<sub>2</sub>-A.* The anomalously large values of  $k_1$ ,  $k_{-1}/k_2$ ,  $k_3$ , and  $k_{-3}/k_4$  obtained in this experiment reflect the high exchange rates obtained therein. These are attributed to the presence of cupric and cuprous sulfato complexes of high reactivity, as discussed under Experimental Results. It is noteworthy that the values of  $k_1$  and  $k_3$  agree closely with corresponding previous limiting values obtained at low acidity and high free sulfate ion concentration (see Tables II and III). No corresponding previous  $k_{-1}/k_2$  and  $k_{-3}/k_4$  values are available for comparison.

$k_3$  and  $k_{-3}/k_4$  of Experiment D<sub>2</sub>-C. The average values of these constants obtained in the perchloric acid experiment are not comparable because no previous values exist for perchloric acid solutions. They are, however, both large in comparison to the values for sulfuric acid solutions.

The fact that  $k_{-3}/k_4$  for perchloric acid solutions is greater than any  $k_{-3}/k_4$  obtained for sulfuric acid solutions suggests the possibility that  $k_{4\text{perchloric}}$  is smaller than  $k_{4\text{sulfuric}}$ . This could explain the low cuprous ion

effect on the net forward rates in perchloric acid solutions. Since reaction 4 is an electron-transfer reaction its rate will be influenced by anion effects. According to recent findings by Bächmann and Lieser<sup>16</sup> for a number of redox reactions, the rates of electron transfer in the presence of sulfate ions were always higher than the rates in the presence of only perchlorate ions.

*Isotope Effects.* The isotope effects resulting from substitution of D<sub>2</sub> for H<sub>2</sub> or of D<sub>2</sub>O for H<sub>2</sub>O will influence the rates of the reactions in equations 1 to 4, and hence the values of the rate constants and ratios obtained in the exchange experiments. Comparison of these values with those obtained in the previous studies should therefore allow conclusions to be made regarding these isotope effects.

*Reaction 1.* The good agreement of the  $k_1$  values obtained in the exchange experiments with the corresponding previous values indicates that isotope effects are small or nonexistent in reaction 1, regardless of whether D<sub>2</sub> is substituted for H<sub>2</sub> or D<sub>2</sub>O for H<sub>2</sub>O, in both sulfuric and perchloric acid solutions at low and high acidity.

*Reactions -1 and 2.* The fact that the  $k_{-1}/k_2$  values of experiments D<sub>2</sub>-B and D<sub>2</sub>-C are markedly larger than the corresponding previous values indicates that reactions -1 and 2 are both influenced by isotope effects when D<sub>2</sub> is substituted for H<sub>2</sub>. On the other hand, the good agreement of the  $k_{-1}/k_2$  value of experiment H<sub>2</sub>-D with the corresponding previous value suggests that isotope effects are small or nonexistent in these reactions when D<sub>2</sub>O is substituted for H<sub>2</sub>O. The large  $k_{-1}/k_2$  value of experiment D<sub>2</sub>-A suggests also the presence of isotope effects. However, the magnitudes of these effects cannot be ascertained in this experiment because they are masked by the earlier discussed low acid effect on the rate constants and ratios.

The  $k_{-1}/k_2$  values of experiments D<sub>2</sub>-B and D<sub>2</sub>-C are larger than the corresponding previous values by nearly the same factor, namely about 3.8, which indicates that the isotope effects are essentially the same in sulfuric and perchloric acid solutions.

It was considered worthwhile to obtain a measure of specific isotope effects on reactions -1 and 2. For this purpose the values of the initial exchange and net forward rates ( $r_{Cu^{II}_0}$  and  $R_{Cu^{II}_0}$ ) were taken from the intercepts of the  $r_T$  and  $R_T$  plots of experiments D<sub>2</sub>-B, H<sub>2</sub>-D, and D<sub>2</sub>-C (Figure 2) and listed in Table IV together with the corresponding calculated values for the H<sub>2</sub>-H<sub>2</sub>O system. The initial rates were used in order to eliminate the cuprous ion effect.

It is evident from the  $r_{Cu^{II}_0}$  values that the rates of reaction -1 are about twice as great in the D<sub>2</sub>-H<sub>2</sub>O system as in the H<sub>2</sub>-H<sub>2</sub>O system. The  $R_{Cu^{II}_0}$  values, however, indicate that the rates of reaction 2 are only

(16) K. Bächmann and K. H. Lieser, *Ber. Bunsenges. Phys. Chem.*, 69 (6), 522 (1965).

Table IV: Illustration of Isotope Effects on Reactions -1 and 2

Experiment →	D <sub>2</sub> -B	Calcd <sup>a</sup>	H <sub>2</sub> -D	D <sub>2</sub> -C	Calcd <sup>b</sup>
Acid →	H <sub>2</sub> SO <sub>4</sub>	H <sub>2</sub> SO <sub>4</sub>	D <sub>2</sub> SO <sub>4</sub>	HClO <sub>4</sub>	HClO <sub>4</sub>
Isotope system →	D <sub>2</sub> -H <sub>2</sub> O	H <sub>2</sub> -H <sub>2</sub> O	H <sub>2</sub> -D <sub>2</sub> O	D <sub>2</sub> -H <sub>2</sub> O	H <sub>2</sub> -H <sub>2</sub> O
$r_{\text{Cu}^{II}_0} \times 10^6$ (reaction -1)	2.2	1.1 <sup>c</sup>	1.1	4.6	2.3 <sup>c</sup>
$R_{\text{Cu}^{II}_0} \times 10^6$ (reaction 2)	0.96	1.8 <sup>e</sup>	1.6	2.3	4.4 <sup>e</sup>

<sup>a</sup> Same solution composition, temperature, and gas pressures as those in experiments D<sub>2</sub>-B and H<sub>2</sub>-D. <sup>b</sup> Same solution composition, temperature, and gas pressures as those in experiment D<sub>2</sub>-C. <sup>c</sup> These  $r_{\text{Cu}^{II}_0}$  values were calculated with the expression

$$r_{\text{Cu}^{II}_0} = \frac{k_{-1}}{k_2} \times \frac{[\text{H}^+]_0}{[\text{Cu}^{II}]_0} \times R_{\text{Cu}^{II}_0}$$

(eq 21). <sup>d</sup> Units: mol l.<sup>-1</sup> sec<sup>-1</sup>. <sup>e</sup> These  $R_{\text{Cu}^{II}_0}$  values were calculated with eq 20. The appropriate values of  $k_1$  and  $k_{-1}/k_2$ , obtained in the previous studies (see Table II), were used in calculating  $R_{\text{Cu}^{II}_0}$  as well as  $r_{\text{Cu}^{II}_0}$ .

about half as great in the D<sub>2</sub>-H<sub>2</sub>O system as in the H<sub>2</sub>-H<sub>2</sub>O system. This applies to both sulfuric and perchloric acid solutions (experiments D<sub>2</sub>-B and D<sub>2</sub>-C).

From the  $r_{\text{Cu}^{II}_0}$  and  $R_{\text{Cu}^{II}_0}$  values of experiment H<sub>2</sub>-D it is evident that the rates of reactions -1 and 2 are nearly the same in the H<sub>2</sub>-D<sub>2</sub>O system as in the H<sub>2</sub>-H<sub>2</sub>O system. This confirms the above indicated absence of isotope effects on these reactions in heavy water.

The isotope effect on reaction 2 caused by D<sub>2</sub> for H<sub>2</sub> substitution is as would be expected. It is caused by an increase in the activation energy for the formation of the (CuD<sup>+</sup> ... Cu<sup>II</sup>)<sup>‡</sup> transition state complex relative to the activation energy for the formation of the (CuH<sup>+</sup> ... Cu<sup>II</sup>)<sup>‡</sup> transition state complex. This increase is related to the changes in the zero point energies of the reactants and the saddle point energy of the transition state complex, resulting from the substitution of D<sub>2</sub> for H<sub>2</sub>.

The doubling of the rate of reaction -1 resulting from D<sub>2</sub> for H<sub>2</sub> substitution is surprising. It indicates that the activation energy for the formation of the (CuD<sup>+</sup> ... H<sup>+</sup>)<sup>‡</sup> transition state complex is lower than that of the (CuH<sup>+</sup> ... H<sup>+</sup>)<sup>‡</sup> transition state complex. A possible explanation for this anomalous isotope effect is that the DH product molecule of reaction -1 has a lower zero point energy than the HH product molecule.

*Reactions 3, -3, and 4.* The evaluation of the isotope effects on these reactions from the values of  $k_3$  and  $k_{-3}/k_4$  obtained in the exchange experiments is uncertain, because of the fact that these constants are sensitive to errors in  $k_1$  and  $k_{-1}/k_2$ . Also, the average values of these constants are not considered to be sufficiently different from those obtained in the previous studies, when allowance is made for experimental errors, to allow definite conclusions to be drawn regarding the

existence of possible isotope effects. An exception is the low value of  $k_{-3}/k_4$  obtained in the heavy water experiment H<sub>2</sub>-D which can be attributed to solvent isotope effects on reactions -3 and 4, most likely on reaction -3 because reaction 4 involves electron transfer only.

### General Conclusions

In previously published studies of the precipitation of copper from acid solutions of copper sulfate,<sup>1,2</sup> the mechanism proposed for the reaction postulated steady-state intermediates having the properties of cupric or cuprous hydrides (CuH<sup>+</sup> or CuH) transiently present in solution. These either react further to precipitate copper metal or go back to original reactants, one of which is hydrogen gas.

The mechanism, if correct, predicts that a deuterium-hydrogen exchange would take place between the gas phase and the solution during hydrogen reduction, and the derived rate law permits calculation of the predicted rate of exchange.

In this paper the exchange experiments are described, and the observed exchange rates are tested against the rates predicted from the derived rate law. The exchange rates, using either deuterium and light water, or hydrogen and heavy water, were found to be consistent with the predicted rates, when isotope effects are taken into consideration. Thus, these exchange experiments support the validity of the copper reduction mechanism as well as substantiating the derived rate law.

*Acknowledgment.* Support for this work by a grant from the National Research Council of Canada and by a National Research Council Studentship to H. E. A. von Hahn is gratefully acknowledged.

## NOTES

## Photochemical Behavior of Isocyanides

by B. K. Dunning, D. H. Shaw, and H. O. Pritchard

Centre for Research in Experimental Space Science,  
York University, Downsview, Ontario, Canada  
(Received May 6, 1970)

Publication costs assisted by the National Research Council of Canada

Previous photochemical studies<sup>1,2</sup> have shown that at 2537 Å, gaseous methyl isocyanide isomerizes to methyl cyanide without the involvement of radicals; further, that the limiting low-pressure quantum yield is close to 2, and that the isomerization is strongly quenched by inert diluents such as nitrogen or ethane, but readily sensitized by other molecules such as benzene, carbon dioxide, nitrous oxide, and possibly acetone. This note describes some exploratory quantum-yield studies for gaseous ethyl and phenyl isocyanides and for methyl, ethyl, and phenyl isocyanides in the liquid phase, all experiments being conducted at a wavelength of 2537 Å.

## Experimental Section

**Materials and Experimental Technique.** Methyl, ethyl, and phenyl isocyanides were prepared by standard methods<sup>3</sup> and quantum yields ( $\Phi$ ) for isomerization to cyanide at 2537 Å were measured in the gas phase at 60° or in the liquid phase at room temperature. The general procedures have been described already;<sup>1,2</sup> the systems were mercury-free, and no thermal isomerization occurred under the conditions used in any of the experiments; light intensities were determined by ferrioxalate actinometry.<sup>4</sup> The minimum detectable quantum yield is governed by various experimental parameters such as the light intensity, irradiation time, extinction coefficient, chromatograph sensitivity, and so on; in these experiments, the minimum detectable quantum yields are shown in column five of Table I, and yields less than these are reported as nil in this note.

**Absorption Spectra.** Methyl isocyanide exhibits a simple continuous absorption beginning<sup>1,2</sup> around 260 nm with  $\epsilon \approx 0.3$  l. mol<sup>-1</sup> cm<sup>-1</sup> at 2537 Å; the absorption of ethyl isocyanide begins at slightly longer wavelengths, and at 2537 Å,  $\epsilon \approx 1.9$  l. mol<sup>-1</sup> cm<sup>-1</sup>. Phenyl isocyanide, on the other hand, exhibits a typical aromatic absorption spectrum, beginning at 300 nm with maxima as follow:  $\lambda_{\max}$  274, 271, 264, 257, 231, 227, 223, and 219 nm;  $\epsilon$ : 84, 138, 146, 118, 4900, 4700,

6300, and 4900 l. mol<sup>-1</sup> cm<sup>-1</sup>; at 2537 Å,  $\epsilon = 100$  l. mol<sup>-1</sup> cm<sup>-1</sup>.

**Liquid-Phase Photolyses at 25°.** All three isocyanides were photolyzed in hydrocarbon solution (pentane or hexane); also, MeNC and EtNC were photolyzed as neat liquids. In all cases, no isomerization could be detected, consistent with the gas-phase observation

**Table I:** Quantum Yields for Photoisomerization of Gaseous Isocyanides at 2537 Å

Mole- cule	T, °K	$\Phi$ (10 mm)	$\Phi$ (1 atm)	Detection limit
MeNC <sup>a</sup>	356	1.4 ± 0.2	Nil	2 × 10 <sup>-3</sup>
EtNC <sup>b</sup>	333	(1.5 ± 0.5) × 10 <sup>-1</sup>	Nil	1 × 10 <sup>-3</sup>
PhNC <sup>b</sup>	333	(1.1 ± 0.3) × 10 <sup>-2</sup>	(3.6 ± 1.0) × 10 <sup>-3</sup>	4 × 10 <sup>-4</sup>

<sup>a</sup> From ref 1. <sup>b</sup> This work; incident light intensity 2.0 × 10<sup>14</sup> quanta cm<sup>-2</sup> sec<sup>-1</sup>.

(see ref 1 and Table I) that collisional deactivation is a very efficient process for alkyl isocyanides and moderately efficient for phenyl isocyanide. Further, it is known that for the alkyl isocyanides (as opposed to the phenyl compound), the isomerization is catalyzed by methyl radicals,<sup>5</sup> and in all probability, photosensitized by acetone;<sup>1</sup> surprisingly cophotolysis of acetone with MeNC or EtNC either in hydrocarbon solution or as neat liquids yielded no isomerization, indicating highly efficient mutual deactivation processes in these systems. The only isocyanide which to our knowledge photoisomerizes in the liquid phase is *o*-biphenyl isocyanide,<sup>6</sup> but in this case the reaction is the formation of another ring rather than the formation of the cyanide.

**Gas-Phase Photolyses at 60°.** Previous work<sup>1,2</sup> on MeNC has shown that at 83° and 10 mm total pressure,  $\Phi$  at 2537 Å is about 1.4, but that the isomerization is very strongly quenched by the addition of inert gas; for example,  $\Phi$  was reduced by a factor of 10

(1) D. H. Shaw and H. O. Pritchard, *J. Phys. Chem.*, **70**, 1230 (1966).

(2) D. H. Shaw, Ph.D. Thesis, Manchester, 1966.

(3) I. Ugi, U. Fetzer, U. Eholzer, H. Knapfer, and K. Offermann, *Angew. Chem., Int. Ed. Engl.*, **4**, 472 (1965).

(4) J. H. Baxendale and N. K. Bridge, *J. Phys. Chem.*, **59**, 783 (1955).

(5) D. H. Shaw and H. O. Pritchard, *Can. J. Chem.*, **45**, 2749 (1967).

(6) J. H. Boyer and J. DeJong, *J. Amer. Chem. Soc.*, **91**, 5929 (1969).

in the presence of 100 mm of ethane<sup>2</sup> and no reaction could be detected at 1 atm total pressure.<sup>1</sup> Similar measurements at 2537 Å and 60° using 10 mm of EtNC gave  $\Phi \approx 0.15$ , and the addition of 1 atm of ethane quenched the photolysis completely. Under the same conditions the quantum yield for isomerization of PhNC at 10 mm pressure is about  $10^{-2}$ , but in contrast, this isomerization is not strongly quenched by foreign gas, and  $\Phi$  falls only about  $4 \times 10^{-3}$  upon addition of just under 1 atm (650 mm) ethane. However, in common with MeNC, neither EtNC nor PhNC showed any evidence of the presence of free radicals in these photolyses.

### Conclusions

The gas-phase results are summarized in Table I, and they show MeNC and EtNC to be similar in their general behavior, except that the former gives a somewhat larger quantum yield; however, since energy chains have been suspected in both photochemical<sup>1</sup> and chemically activated<sup>7</sup> systems containing MeNC, it is possible that EtNC may more nearly represent the norm for the photochemical behavior of alkyl isocyanides. The temperature coefficient for the MeNC photolysis observed in our earlier work<sup>1</sup> is insufficient to account for the quantum-yield difference between the two molecules.

In the gas phase PhNC differs from alkyl isocyanides in two respects: that the quantum yield for isomerization is rather low, and that the isomerization is less efficiently quenched by added gases. The low quantum yield could be the consequence of a greater fluorescence yield, but phenyl isocyanide is a rather unstable substance, and fluorescence measurements in the gas phase may prove difficult. The difference in quenching efficiency could be symptomatic of a difference in mechanism, perhaps that in the PhNC case the energy resides initially in the aromatic chromophore, whereas in the aliphatic molecules, it *must* initially enter *via* the isocyanide group chromophore (it being understood that the language of chromophores corresponds to a very oversimplified description of the electronic excitation process); if this were the case, an intramolecular conversion to a highly excited vibrational state of PhNC would have to occur, and this state would require a number of collisions before its energy was reduced below that of the thermal threshold. The position of the thermal threshold is not known precisely, but, more so than with the alkyl isocyanides, thermal isomerization takes place very readily indeed upon distillation, and it seems likely that the threshold could lie a little below the value of 38 kcal/mol found for the alkyl compounds.<sup>8,9</sup> Thus, with a primary excitation of 112 kcal/mol, the amount of vibrational energy that would have to be removed would be of the order of 70–80 kcal/mol; the removal of such a large excess of vibra-

tional energy would not take place with unit collision efficiency.

(7) D. H. Shaw, B. K. Dunning, and H. O. Pritchard, *Can. J. Chem.*, **47**, 669 (1969).

(8) F. W. Schneider and B. S. Rabinovitch, *J. Amer. Chem. Soc.*, **84**, 4215 (1962).

(9) K. M. Maloney and B. S. Rabinovitch, *J. Phys. Chem.*, **73**, 1652 (1969).

### Spectra and Cis-Trans Isomerism in Highly Bipolar Derivatives of Azobenzene

by G. Gabor\* and E. Fischer

*Department of Chemistry, The Weizmann Institute of Science, Rehovoth, Israel (Received July 27, 1970)*

*Publication costs borne completely by the Journal of Physical Chemistry*

The absorption spectra and the thermal and photochemical isomerization of aromatic azo compounds have been studied extensively.<sup>1-8</sup> For azobenzene (AB) the maximum of the  $\pi-\pi^*$  band is at 313 nm and is red-shifted on substitution of one or two hydroxyl or methoxyl groups.<sup>4-6</sup>

The trans isomer of AB is planar and therefore more stable than the cis isomer.<sup>7</sup> The activation energy of the cis  $\rightarrow$  trans thermal conversion is about 23 kcal/mol for azobenzene and its derivatives,<sup>3,8</sup> except for those containing substituents which cause intramolecular changes, such as production of tautomeric species or internal hydrogen bonds<sup>4,5</sup> and thereby lower the energy of the activated intermediate. Even in these derivatives the thermal isomerization can be "frozen out" at sufficiently low temperatures and the thermodynamic equilibrium which is 100% trans can be changed by irradiation.<sup>3-6</sup>

Similar isomerization processes in stilbenes<sup>9</sup> and in

(1) E. Fischer, *J. Amer. Chem. Soc.*, **82**, 3249 (1960), and earlier references quoted therein.

(2) G. Zimmerman, L. Chow, and U. Paik, *ibid.*, **80**, 3528 (1958).

(3) (a) D. Gegiou, K. A. Muszkat, and E. Fischer, *ibid.*, **90**, 3907 (1968); (b) J. Saltiel and E. D. Megarity, *ibid.*, **91**, 1265 (1969); **90**, 4759 (1968).

(4) (a) G. Gabor, Ph.D. Thesis, Rehovoth, 1964; (b) G. Gabor, Y. Frei, D. Gegiou, M. Kaganowitch, and E. Fischer, *Isr. J. Chem.*, **5**, 193 (1967).

(5) G. Gabor and K. Bar-Eli, *J. Phys. Chem.*, **72**, 153 (1958).

(6) (a) G. Gabor, Y. Frei, and E. Fischer, *ibid.*, **72**, 3266 (1968); (b) G. Gabor and E. Fischer, *ibid.*, **66**, 2478 (1962).

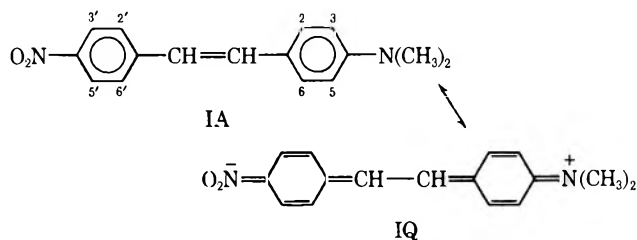
(7) (a) G. S. Hartley, *J. Chem. Soc.*, 633 (1938); (b) R. J. Corrucini and E. C. Gilbert, *J. Amer. Chem. Soc.*, **61**, 2925 (1939).

(8) (a) J. Halpern, G. W. Brady, and C. A. Winkler, *Can. J. Res.*, **28B**, 140 (1950); (b) E. R. Talaty, Ph.D. Thesis, Ohio State University, 1957.

(9) (a) Sh. Malkin, *Bull. Res. Council. Isr.*, **A11**, 208 (1962); (b) G. S. Hammond, M. J. Turro, and P. A. Leermakers, *J. Phys. Chem.*, **66**, 1144 (1962).

azo compounds<sup>10</sup> could be attained *via* energy transfer from triplet sensitizers. It is therefore generally accepted that these photoisomerization processes may occur *via* the triplet state of the molecule, though the role of the triplet state in the direct photoisomerization of stilbene is controversial.<sup>3</sup>

We now wish to report an investigation of the temperature dependence of the absorption spectra and of the thermal and the photochemical *cis-trans* isomerization of 4-dimethylamino-4'-nitroazobenzene (IA). This study was briefly mentioned in an earlier report,<sup>3a,4a</sup> and is again based on low-temperature techniques. (I) has a high dipole moment<sup>11</sup> which is probably due to the contribution of bipolar mesomeric structures (IQ).



Data about the spectra of AB, its 4-NO<sub>2</sub> and 4-N-(CH<sub>3</sub>)<sub>2</sub> derivatives, and of compound I and its 3-methyl derivative (II) are given in Table I. The red

**Table I:** Absorption Peaks of AB and Several Derivatives in Various Solvents at 25°

Compd	Solvent <sup>c</sup>	$n-\pi^*$ nm	$\pi-\pi^*$ nm
AB	1-p/2-p	430	315
AB	MCH/MCP	430	313
4-Nitro-AB	1-p/2-p	430	330
4-Nitro-AB	MCH/MCP	440	328
4-N(CH <sub>3</sub> ) <sub>2</sub> -AB	1-p/2-p		407
4-N(CH <sub>3</sub> ) <sub>2</sub> -AB	MCH/MCP		400
4-N(CH <sub>3</sub> ) <sub>2</sub> -4'-NO <sub>2</sub> -AB	1-p/2-p		470 (500°)
4-N(CH <sub>3</sub> ) <sub>2</sub> -4'-NO <sub>2</sub> -AB	MCH/MCP	480 (?)	445 (453°)
3-CH <sub>3</sub> -4-N(CH <sub>3</sub> ) <sub>2</sub> -4'-NO <sub>2</sub> -AB	1-p/2-p		420
3-CH <sub>3</sub> -4-N(CH <sub>3</sub> ) <sub>2</sub> -4'-NO <sub>2</sub> -AB	MCH/MCP		410

<sup>a</sup> In 1-propanol/H<sub>2</sub>O (3:1). <sup>b</sup> In MCH/toluene (1:1). <sup>c</sup> MCH = methylcyclohexane, MCP = methylcyclopentane, 1-p = 1-propanol, and 2-p = 2-propanol.

shift of the  $\pi-\pi^*$  band, due to substitution of polar groups, is pronounced. In I and II in nonpolar solvents a shoulder appears at somewhat longer wavelengths. It may perhaps be assigned to the  $n-\pi^*$  transitions which in polar solvents are blue-shifted and completely overlapped by the strong  $\pi-\pi^*$  band, which in turn is red-shifted in polar solvents.

The very big red shift of the  $\pi-\pi^*$  band in I, as compared with AB, is further increased in polar solvents, but decreases considerably when a methyl group

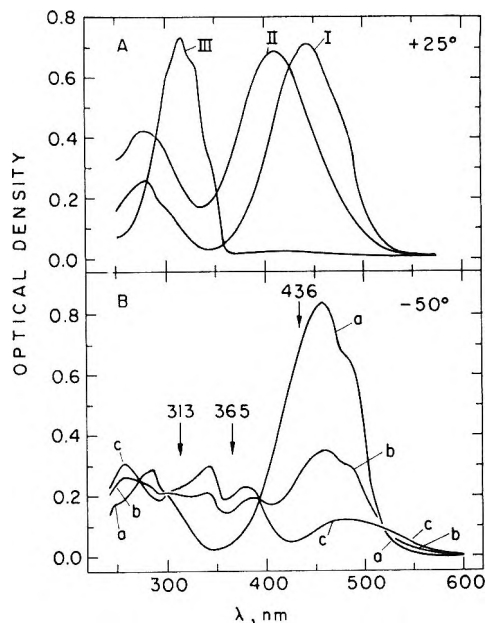


Figure 1. A, Absorption spectra of AB, III, 4-dimethylamino-4'-nitro-AB (I) and 3-methyl-I in MCH. The respective concentrations were  $3.6 \times 10^{-5} M$ ,  $1.9 \times 10^{-5} M$ , and  $3.3 \times 10^{-5} M$ . B, Absorption spectra of I in MCH/decalin, *ca.*  $2 \times 10^{-5} M$ , at  $-50^\circ C$ : (a) *trans* isomer; (b) photoequilibrium attained by irradiation at 436 nm; (c) *cis* isomer, extrapolated assuming that solution b contains 66% *cis* isomer.

is introduced at the 3 position, while the extinction coefficient is decreased by this methyl group (Figure 1A). A reasonable explanation is that the contribution of the bipolar mesomers IQ is increased in polar solvents and is higher in the excited state (as shown also for the analogous stilbene derivative<sup>12</sup>). On the other hand, since mesomer IQ demands coplanarity of the dimethylamino group with the rest of the conjugated system, any steric interference with such coplanarity should lower the contribution of this mesomer. This explains the effect of the methyl group in II.

Other anomalies of compounds I and II are the enormous red shift of the  $\pi-\pi^*$  peak on cooling, 23 nm/100° for I in methylcyclohexane-toluene, 15 nm/100° for I in 1-propanol-2-propanol, and 12 nm/100° for II in 1-propanol-2-propanol, as compared with about 4-7 nm/100° in AB, 4-NO<sub>2</sub>-AB, and 4-N-(CH<sub>3</sub>)<sub>2</sub>-AB. In 4-nitro-4'-dimethylaminostilbene<sup>3a</sup> it is about 15 nm, and the large extinction coefficient of I, about 38,000, which is about twice as big as those of other azo compounds at the respective peaks.<sup>2</sup>

Photoisomerization was induced by irradiation with monochromatic light at temperatures low enough to stop thermal *cis* → *trans* isomerization (*cf.* later).

(10) E. Fischer, *J. Amer. Chem. Soc.*, **90**, 796 (1968).

(11) A. L. McClellan, "Tables of Experimental Dipole Moments," Freeman and Co., London, 1963.

(12) E. Lippert, *Angew. Chem.*, **73**, 695 (1962).

The photoequilibria obtained were found to be a function of the wavelength of the exciting light and of the temperature, as reported in other cases.<sup>1,3a</sup> Figure 1B shows the absorption spectra of the two isomers of I, as well as the photoequilibrium obtained by irradiation at 436 nm, at  $-50^\circ$ , of a solution in a 1:1 mixture of methylcyclohexane and decalin. However, this mixture is a rather poor solvent, and I precipitated below this temperature. Quantum yields of the photoisomerization, and their temperature dependence for compounds I and II were therefore measured in 1:1 mixtures of methylcyclohexane-toluene and 1-propanol-2-propanol. The quantum yields of the photoisomerizations of I and II, calculated as described elsewhere<sup>6b,13</sup> are summarized in Table II. The

**Table II:** Quantum Yields of the cis  $\rightarrow$  trans ( $\phi_c$ ) and the trans  $\rightarrow$  cis ( $\phi_t$ ) Photoisomerization in the Temperature Range  $-100$  to  $-180^\circ$  (Solvents as in Table I)

Compd	Solvent	Wavelength of photoactive light, nm		Quantum yields at		
				$-110^\circ$	$-130^\circ$	$-150^\circ$
II	1-p/2-p (1:1)	313	$\phi_c$	0.62	0.56	0.41
			$\phi_t$	0.02	0.01	0.008
		436	$\phi_c$	0.71	0.50	0.48
			$\phi_t$	0.027	0.009	0.0035
I	1-p/2-p (1:1)	313	$\phi_c$	0.70	0.60	0.55
			$\phi_t$	0.16	0.12	0.073
	436	$\phi_c$	0.84	0.82	0.84	
		$\phi_t$	0.20	0.15	0.06	
	MCH/toluene (1:1)	436	$\phi_c$	0.72	0.77	0.73
			$\phi_t$	0.24	0.20	0.09

trans  $\rightarrow$  cis quantum yields  $\phi_t$  of II are essentially the same as those of azobenzene and its derivatives,<sup>2,13</sup> while those of I are much higher. The observed temperature dependence of the quantum yield  $\phi_t$  of the trans  $\rightarrow$  cis photoconversion indicates that this process has an activation energy in the excited state. The activation energies  $E_a^*$ , calculated as described previously,<sup>6b,13</sup> were about 2 kcal/mol for both compounds at 436 nm. It thus seems that the higher quantum yields in I do not result from a lower activation energy, since the present values are roughly similar to those calculated for other azo compounds.<sup>4,6b,13</sup> Without speculating about the actual mechanism of the photoisomerization in these compounds (singlet or triplet, etc.), one may conclude that in the donor-acceptor-substituted azobenzene the probability of transition to the state responsible for the isomerization is increased substantially. Possibly this results from the large contribution of highly bipolar mesomers in the excited state. However, the actual role of ionic and radical-like valence structures in determining the positions of the ground and excited states along the reaction coordinate is still an open question. (The

authors are indebted to one of the referees for stressing this fact.)

The thermal cis  $\rightarrow$  trans conversion was measured spectrophotometrically<sup>1</sup> (Cary 14) in polar and non-polar solvents for I and II, following photoenrichment of the cis isomer. Typical temperature ranges were  $15$ – $35^\circ$  for I in methylcyclohexane-decalin,  $-50$  to  $-75^\circ$  for I in 1-propanol-2-propanol, and  $-40$  to  $-65^\circ$  for II in 1-propanol-2-propanol. The corresponding activation energies calculated from the kinetic data were 16.5, 11.4, and 9.2 kcal/mol.

As mentioned earlier,<sup>3a,14</sup> amino derivatives of azobenzene are prone to catalyzed cis  $\rightarrow$  trans thermal isomerization, and the above data should therefore be treated with caution. However, we believe that at least the activation energy observed in methylcyclohexane/decalin may be ascribed to the actual first-order cis  $\rightarrow$  trans conversion.

We conclude that the contribution of a highly bipolar structure (IQ) in I: (1) lowers the energy of the first excited singlet state, (2) increases the probability of transition into the state responsible for isomerization in the excited state, and (3) decreases the energy of the transition state in the thermal isomerization. By attenuating the interaction of the electron donor group with the  $\pi$ -electron system we interfere with the first two effects which involve changes in the energy levels of the excited states and the transition probabilities, but do not influence the production of a low-energy transition state in the thermal isomerization.

*Acknowledgments.* The authors wish to thank Mr. M. Kaganowitch for synthesizing the compounds and Mrs. N. Castel for technical assistance.

(13) S. Malkin and E. Fischer, *J. Phys. Chem.*, **66**, 2482 (1962).

(14) E. Fischer and Y. F. Frei, *J. Chem. Phys.*, **27**, 328 (1957).

## On the Liquid Film Which Occurs in a Draining Vessel

by John A. Tallmadge

Department of Chemical Engineering, Drexel University, Philadelphia, Pennsylvania 19104 (Received August 21, 1970)

Publication costs borne completely by The Journal of Physical Chemistry

It is of interest to have a theoretical estimate for the thickness of the film that remains on the wall of a vessel (a) as the level of the wetting liquid is lowered and (b) after the motion of the liquid level has stopped. These two cases may be called liquid lowering and postlowering drainage. Concus<sup>1</sup> considered a steady

(1) P. Concus, *J. Phys. Chem.*, **74**, 1818 (1970).

draining case (constant thickness) of the first problem for a number of conditions. Consider a vessel with a radius  $R$  so much larger than the capillary length of the fluid ( $a \equiv \sqrt{2\sigma/\rho g}$ ) that the surface may be considered to be flat. In this note, we consider both curved and flat portions of the film to develop profiles general for all drain times. We also consider the second problem of postlowering drainage.

The two problems are related to those of unsteady withdrawal<sup>2</sup> and postwithdrawal drainage. The film profile for unsteady withdrawal (of a short vertical flat plate from a wetting liquid) has been approximated by two regions,<sup>3</sup> as given by

$$\begin{aligned} \text{at } x/L < T_0^2, h &= \sqrt{\frac{x}{L}} \sqrt{\frac{\mu U_w}{\rho g}} \\ \text{at } x/L > T_0^2, h &= T_0 \sqrt{\frac{\mu U_w}{\rho g}} \end{aligned} \quad (1)$$

Here  $x$  is the distance from the top of the film,  $L$  the height of the film at any instant,  $h$  the local film thickness,  $U_w$  withdrawal speed,  $g$  gravitational acceleration,  $\rho$  density,  $\mu$  viscosity, and  $T_0$  is a nondimensional constant for any given speed, viscosity, and surface tension  $\sigma$ . Equation 1 applies where the plate maintains contact with the liquid bath. Equation 1 applies for constant speed but is called unsteady withdrawal because the film thickness is a transient in general. The parameter  $T_0$  is a function of  $Ca \equiv U_w(\mu/\sigma)$  according to a steady-state, continuous withdrawal expression. One such expression is<sup>4</sup>

$$T_0 = 0.946Ca^{1/6}(1 - T_0^2)^{2/3} \quad (2)$$

Using eq 2, eq 1 has been verified experimentally; a  $Ca$  of 4 was used.

When withdrawal motion is stopped, the film continues to drain. In this case of postwithdrawal drainage, the junction between the curved and flat portions of the film travels downward and the  $x/L$  junction increases toward unity at a velocity  $U_j$ ,

$$U_j = T_0^2 U_w \quad (3)$$

After a critical drain time  $t_d^*$ , the entire postwithdrawal film will be curved, as in the asymptotic, long time solution.<sup>5</sup> Here critical drain time<sup>3</sup> is

$$t_d^* = t_w \left[ \frac{1 - T_0^2}{T_0^2} \right] = \frac{L}{U_w} \left[ \frac{1 - T_0^2}{T_0^2} \right] \quad (4)$$

Assuming that capillary forces in liquid lowering behave similarly to those in unsteady withdrawal, the above equations may be applied to liquid lowering. First we replace  $U_w$  by the liquid lowering velocity  $U_L$ . Thus for a  $Ca \equiv U_L(\mu/\sigma)$ , the film profile during lowering is given as

$$\begin{aligned} \text{at } x/L < T_0^2, h &= \sqrt{\frac{x}{L}} \sqrt{\frac{\mu U_L}{\rho g}} \\ \text{at } x/L > T_0^2, h &= T_0 \sqrt{\frac{\mu U_L}{\rho g}} \end{aligned} \quad (5)$$

After lowering is stopped, the critical drain time for the entire profile to become curved is

$$t_d^* = t_L \left[ \frac{1 - T_0^2}{T_0^2} \right] = \frac{L}{U_L} \left[ \frac{1 - T_0^2}{T_0^2} \right] \quad (6)$$

The  $x/L$  junction and film profile for the first portion of postlowering drainage (up to  $t_d^*$ ) is given by

$$\left( \frac{x}{L} \right)_j = T_0^2 + T_0^2 \left( \frac{t_d}{t_L} \right) \quad (7)$$

$$\text{at } \frac{x}{L} < \left( \frac{x}{L} \right)_j, h = \sqrt{\frac{x}{L}} \sqrt{\frac{\mu L}{\rho g(t_L + t_d)}} \quad (8)$$

$$\text{at } \frac{x}{L} > \left( \frac{x}{L} \right)_j, h = T_0 \sqrt{\frac{\mu U_L}{\rho g}}$$

The reference thickness  $h_R$  of the film is taken as

$$h_R = \sqrt{\frac{\mu L}{\rho g(t_L + t_d)}} \quad (9)$$

The shape of the entire film after the critical drain time  $t_d^*$  is

$$h = h_R \sqrt{\frac{x}{L}} = \sqrt{\frac{(x/L)}{(t_L + t_d)}} \sqrt{\frac{\mu L}{\rho g}} \quad (10)$$

Thus after  $t_d^*$ , the entire profile is curved, as predicted by the asymptotic Jeffreys equation for drainage at long times.<sup>5</sup>

All the above equations are useful for a wide range of speed. Equation 2 has been verified experimentally within 20% for all  $Ca$  tested; the range tested was from  $10^{-4}$  to  $4 \times 10^1$ .

Consider the low  $Ca$  case where  $T_0^2 \ll 1$ . Thus  $T_0 = 0.946Ca^{1/6}$  and eq 5 becomes

$$\begin{aligned} \text{at } x/L < 0.9 Ca^{1/3}, h &= \sqrt{\frac{x}{L}} \sqrt{\frac{\mu U_L}{\rho g}} \\ \text{at } x/L > 0.9 Ca^{1/3}, h &= 0.946 Ca^{1/6} \sqrt{\frac{\mu U_L}{\rho g}} \end{aligned} \quad (11)$$

For comparison with the steady draining asymptote, for which thickness is constant, we present some numerical examples. At a  $Ca$  of  $10^{-4}$ ,  $T_0 = 0.2$ . Thus the curved part of the profile ( $x/L$ ) occupies only the top 4% of the film here and the critical drain time is 25

(2) J. A. Tallmadge and C. Gutfinger, *Ind. Eng. Chem.*, **57** (11), 18 (1967).

(3) J. A. Tallmadge, "Draining Films in Unsteady Withdrawal," *A.I.Ch.E. J.*, in press.

(4) D. A. White and J. A. Tallmadge, *Chem. Eng. Sci.*, **20**, 33 (1965).

(5) H. Jeffreys, *Proc. Cambridge Phil. Soc.*, **26**, 204 (1930).

times the lowering time. At a  $Ca$  of  $10^{-2}$ ,  $T_0 = 0.39$ . Thus the curved part of the profiles occupies 15% of the film and  $t_d^*$  is about  $6t_L$ .

At a  $Ca$  of  $10^0$ , however,  $T_0 = 0.65$ . Thus the curved portion is 42% for this case and  $t_d^*$  is only  $1.4t_L$ . At a  $Ca$  of  $10^2$ ,  $T_0 = 0.85$ , for which the curved portion is 72% of the film and the critical drain time is only 40% of the lowering time.

To consider a dimensional example for velocities that were not too large, we select  $U_L = 1.0$  cm/sec as a low velocity. Also selecting  $\mu = 30$  poises and  $\sigma = 30$  dyn/cm, we have  $Ca = 1$ . For this case the flat profile holds only for about 60% of the total film. Furthermore, if  $L$  were 10 cm, the entire flat portion of the profile would disappear 14 sec after lowering has stopped. Thus neglecting the curved region may be serious if  $Ca$  is above  $10^{-2}$ .

The Concus note<sup>1</sup> was apparently concerned with an asymptotic film thickness for slow draining inside a tube and how it varies with a wide range of tube radius and contact angle. It was not concerned with the more general time-dependent problem, the top end effect of the film, a wide range of draining speeds, or postlowering draining, all of which are described by eq 5–10 above. Comparison of these equations with the Concus note indicates that the latter describes the constant thickness region suggested by Jeffrey (where  $\partial h/\partial x = 0$  and mass flow rate  $w$  is locally steady ( $\partial w/\partial t = 0$ )).

As indicated by the above numerical examples, eq 8 shows that the constant thickness assumption applies for a larger  $x$  region when  $Ca$  is small. The small  $Ca$  condition confirms and clarifies the condition referred to as a "velocity that is not too large."<sup>1</sup>

It is now clear that there are two asymptotic solutions for film thickness in drainage. The asymptotic solution of Jeffreys<sup>5</sup> describes the influence of position and time; it is best for long times in drainage and the top region in liquid lowering. The asymptotic solution of Concus<sup>1</sup> describes the influence of surface tension; it is best for short times in drainage and the lower region in liquid lowering. The equations presented above reduce to the long time asymptote as a special case and show for what  $x$  positions the short time asymptote is applicable.

Concus<sup>1</sup> presented a continuous withdrawal prediction for the effect of radius and contact angle on the inside of a tube. It is interesting to note that the prediction<sup>6</sup> for the effect of radius on the outside of a tube (which has been verified experimentally for wide  $Ca$ ) implies that only the zero contact angle is required.

These two radius theories can easily be compared for a cylinder of a small radius  $R < \sqrt{\sigma/\rho g}$ . For small  $R$  and zero contact angle, we note that both theories<sup>1,6</sup> reduce to

$$\frac{h_0}{R} = 1.34 \left( \frac{\mu U_w}{\sigma} \right)^{2/3} \quad (12)$$

Equation 12 was apparently first developed by Deryagin and is described in book form.<sup>7</sup>

We note parenthetically that the constant 0.946 in eq 2 and other equations is more precise than the 0.944 value used earlier. This is because the constant on which these numbers are based has been found to be 0.643<sup>8</sup> rather than 0.642.<sup>4</sup>

In summary, an equation has been developed for liquid lowering film profile (eq 5) which is general for all  $Ca$ , all times, and all  $x/L$  except the meniscus itself. General equations also are presented for postlowering drainage (eq 6–10). These equations are applicable for a wider range of  $Ca$  than those of Groenveld. A form of eq 11 was previously developed by Groenveld.

(6) J. A. Tallmadge and D. A. White, *Ing. Eng. Chem. Process Des. Develop.*, **7**, 503 (1968).

(7) B. V. Deryagin and S. M. Levi, "Film Coating Theory," Focal Press, New York, N. Y., 1964.

(8) C. Gutfinger and J. A. Tallmadge, *A.I.Ch.E. J.*, **11**, 403 (1965).

## Dipolar Contributions to Carbon-13 Relaxation Times

by James R. Lyerla, Jr., David M. Grant,\* and Robin K. Harris

Department of Chemistry, University of Utah, Salt Lake City, Utah 84112 (Received August 26, 1970)

Publication costs assisted by The National Institutes of Health

Information about molecular dynamics may be obtained from studies of nuclear spin relaxation. However, it is imperative to separate the contributions of the various relaxation mechanisms (*i.e.*, dipolar, spin-rotation, chemical shift anisotropy, quadrupole effects, etc.). Recently, Kuhlmann, Grant, and Harris<sup>1</sup> illustrated that quantitative evaluation of the <sup>13</sup>C-<sup>1</sup>H nuclear Overhauser effect (NOE) in conjunction with nuclear spin-lattice relaxation times ( $T_1$ ) allows separation of the dipolar mechanism from other  $T_1$  processes. As the existence of the NOE is solely dependent upon the nuclear dipolar coupling relaxation mechanism, the inherent relationship between the NOE parameter and  $T_1$  is readily apparent.

For a heteronuclear two-spin system of spin  $-1/2$  nuclei in the region of extreme narrowing, the Overhauser effect on the resonance of spin  $I$  when irradiating spin  $S$  is given by

(1) K. F. Kuhlmann, D. M. Grant, and R. K. Harris, *J. Chem. Phys.*, **52**, 3439 (1970).

**Table I:** NOE and  $T_1$  Values for the Methyl Group of Several Organic Molecules

Molecule	$\eta_{C-\{H\}}$	$T_1$ , sec	$T_{1D}^C$ , sec	$T_{10}^C$ , sec
CH <sub>3</sub> I	$0.42 \pm 0.05$	$11.1 \pm 0.4$	$52.5 \pm 6.5$	$14.1 \pm 1.7$
CH <sub>3</sub> CN	$0.53 \pm 0.07$	$13.1 \pm 1.0$	$49.1 \pm 7.5$	$17.9 \pm 2.7$
CH <sub>3</sub> OH	$0.73 \pm 0.07$	$13.4 \pm 0.8$	$36.5 \pm 4.1$	$21.2 \pm 2.4^a$
CH <sub>3</sub> COOH	$1.40 \pm 0.13$	$10.5 \pm 0.5$	$14.9 \pm 1.5$	$35.5 \pm 3.7$

<sup>a</sup> It is interesting to note that  $T_{10}^C$  for methyl alcohol is the same as  $T_1$  (23 sec) in CD<sub>3</sub>OD as might be expected. A. Olivson, E. Lippmaa, and J. Past, *Est. NSV Tead. Aka. Toim., Fuus.-Mat.*, **16**, 390 (1967).

$$\eta_{I-\{S\}} = \frac{1}{2} \frac{\gamma_S T_{1D}^{-1}}{\gamma_I T_1^{-1}} \quad (1)$$

where the spin-lattice relaxation time for nucleus I is  $T_1^{-1} = T_{1D}^{-1} + T_{10}^{-1}$ , with  $T_{1D}^{-1}$  being the heteronuclear dipolar relaxation rate and with  $T_{10}^{-1}$  the rate for all other relaxation processes. The overall enhancement factor equals  $1 + \eta_{I-\{S\}}$ . If spin  $S$  is a hydrogen and  $I$  is carbon-13 and if the dipolar mechanism is the dominant contributor to  $T_1$  ( $T_{1D}^{-1} \gg T_{10}^{-1}$ ) the maximum value of the <sup>13</sup>C-<sup>1</sup>H NOE becomes  $\eta = 1.988$  or  $1 + \eta = 2.988$ .<sup>3</sup> However, if relaxation mechanisms other than the heteronuclear dipolar process effectively contribute to the relaxation of spin  $I$ , the measured NOE will be less than the maximum value.<sup>1</sup> Thus, from  $T_1$  and NOE data, eq 1 permits the evaluation of  $T_{1D}$ . While the NOE does not distinguish between inter- and intramolecular dipolar effects, arguments have been advanced<sup>1</sup> that suggest intermolecular dipolar relaxation is relatively unimportant for <sup>13</sup>C nuclei directly bonded to a hydrogen atom. Also, it should be pointed out that eq 1 is valid only for the situation in which all protons are saturated and no other spin  $-1/2$  nuclei are present. Under these conditions, the relaxation of the enhanced <sup>13</sup>C lines is governed by a single exponential time constant  $T_1$ .

Herein are reported the <sup>13</sup>C-<sup>1</sup>H NOE and the <sup>13</sup>C spin-lattice relaxation times under decoupled conditions for the methyl carbon of methyl iodide, methanol, acetonitrile, and acetic acid. All the samples were degassed using at least five freeze-pump-thaw cycles on a vacuum line before sealing. The experiments were run using a Varian AFS-60 spectrometer operating at 14.1 kG field with decoupling accomplished *via* a Hewlett-Packard 5105A frequency synthesizer. Each relaxation time and NOE value was determined at least three times. The operating temperature of the probe under the conditions of the experiments was approximately 35°. The enhancement factor was determined from the ratio of the integrated <sup>13</sup>C-decoupled peak to that of the coupled spectrum. The relaxation times were determined by adiabatic fast passage as detailed in ref 1. The dipolar relaxation times calculated from the experimental quantities  $\eta$  and  $T_1$  are reported in Table I.

The less than maximum Overhauser enhancements

for CH<sub>3</sub>CN, CH<sub>3</sub>OH, and CH<sub>3</sub>I indicate that other relaxation mechanisms are effectively competing with the dipolar mechanism. In view of the supposed facility of rotational motion about the top axis, spin-rotation effects may be a major relaxation contributor. Woessner<sup>4</sup> has found spin-rotation to be the dominant relaxation process for the protons in acetonitrile above 25°. The higher NOE value of acetic acid may arise from extensive dimerization which leads to slower molecular reorientation rates, thereby increasing the effectiveness of the internal dipolar relaxation process.

Woessner<sup>5</sup> has accounted for the effect of motional anisotropies on dipolar spin relaxation in ellipsoidal molecules. For symmetric top molecules these effects are dependent upon the angle between the dipole-dipole vector and the top axis. The CH bond angle in a methyl group allows for an adequate test of this effect. The explicit form of the intramolecular dipolar relaxation time  $T_{1D}^C$  for carbon-13 relaxation in a methyl group is

$$\frac{1}{T_{1D}^C} = (3) \cdot \gamma_H^2 \gamma_C^2 \hbar^2 r_{CH}^{-6} R_{\perp}^{-1} \times [A/6 + B/(5 + \sigma) + C/(2 + 4\sigma)] \quad (2)$$

where (3) represents the number of CH interactions,  $\sigma$  the ratio of the rotational diffusion constants of the ellipsoid parallel and perpendicular to the major axis, and  $R_{\perp}$  the rotational diffusion constant perpendicular to the top axis. Values for  $A$ ,  $B$ , and  $C$ , geometric constants dependent upon the angle of the proton-carbon internuclear vector relative to the top axis, are given in ref 5.

Working independently, Woessner<sup>4</sup> and Bopp<sup>6</sup> have carried out extensive investigations on deuterated acetonitrile and determined  $T_1$  for the two quadrupolar nuclei, <sup>2</sup>H and <sup>14</sup>N. As electric quadrupole interactions provide the dominant relaxation mechanism for the nuclei, separation of other contributing relaxation ef-

(2) I. Solomon, *Phys. Rev.*, **99**, 559 (1955).

(3) K. F. Kuhlmann and D. M. Grant, *J. Amer. Chem. Soc.*, **90**, 7355 (1968).

(4) D. E. Woessner, B. S. Snowden, and E. T. Strom, *Mol. Phys.*, **14**, 265 (1968).

(5) D. E. Woessner, *J. Chem. Phys.*, **37**, 647 (1962).

(6) T. T. Bopp, *ibid.*, **47**, 3621 (1967).

facts is not necessary and values of  $\sigma$  and  $R_{\perp}^{-1}$  were ascertained directly from combination of the relaxation results. The relaxation time of  $^{14}\text{N}$  in acetonitrile is dependent only upon reorientational motion perpendicular to the symmetry axis and thus allows direct determination of  $R_{\perp}^{-1}$  via the equation

$$\frac{1}{T_{1\text{N}}} = \frac{3}{8} \left( 2\pi \frac{e^2qQ}{h} \right)^2 R_{\perp}^{-1} (A'/6) \quad (3)$$

where  $e^2qQ/h$  is the quadrupole coupling constant for  $^{14}\text{N}$  and  $A'$  specifies the geometry of the  $\text{C}\equiv\text{N}$  bond ( $B'$  and  $C'$  being zero along this vector). Interpretation of the temperature dependence of  $T_{1\text{N}}$  given in ref 6 allows  $R_{\perp}^{-1}$  to be calculated at  $35^\circ$  via eq 3. Using this value of  $R_{\perp}^{-1}$  ( $6.77 \times 10^{-12}$  sec),  $T_{1\text{D}}^{\text{C}}$  data from Table I, and appropriate geometric constants, a value of  $\sigma = 9.2$  is calculated from eq 1. This is in good agreement with those reported by Bopp (8.9) and Woessner (10.4) at room temperature. Owing to the different temperature dependence of  $R_{\parallel}(E_a \sim 0.8 \text{ kcal}^6)$  and  $R_{\perp}(E_a \sim 1.7 \text{ kcal}^6)$ , the values of  $\sigma$  determined by Bopp and Woessner should be slightly less at  $35^\circ$  than the room temperature values given above; however, in light of the magnitude of experimental errors, values at  $25^\circ$  are adequate for comparison purposes. The authors appreciate that reorientation about the parallel axis may not be diffusion controlled<sup>6,7</sup> and hence strict application of a diffusion equation may not be warranted for acetonitrile; however, our purpose is to point out that the  $^{13}\text{C}$  relaxation datum is compatible with those reported for  $^{14}\text{N}$  and  $^2\text{H}$ .

The unusually good correlation between the  $^2\text{H}$ ,  $^{13}\text{C}$ , and  $^{14}\text{N}$  relaxation data for acetonitrile substantiates the use of the  $^{13}\text{C}$ - $\{^1\text{H}\}$  NOE and  $^{13}\text{C}$  relaxation data to evaluate dipolar relaxation rates and lends credence to the other  $T_{1\text{D}}^{\text{C}}$  values in Table I. While the other molecules cannot be treated in the same manner as acetonitrile owing to the absence of two quadrupolar nuclei, an equation similar to eq 2 can be written<sup>5</sup> for the intramolecular proton dipolar relaxation time in a methyl group (neglecting the effect of the 1% abundant  $^{13}\text{C}$ ) as

$$\frac{1}{T_{1\text{D}}^{\text{H}}} = (2) \cdot \frac{3}{2} \gamma_{\text{H}}^4 \hbar^2 r_{\text{HH}}^{-6} R_{\perp}^{-1} \times [A''/6 + B''/(5 + \sigma) + C''/(2 + 4\sigma)] \quad (4)$$

where the double primes denote the geometry of the proton-proton vector and (2) the number of H-H interactions. Simultaneous solution of eq 2 and 4 if  $T_{1\text{D}}^{\text{H}}$  and  $T_{1\text{D}}^{\text{C}}$  are known thus allows calculation of  $\sigma$  and  $R_{\perp}$ . However, values of  $T_{1\text{D}}$  are not generally available as spin-rotation effects upon reported proton intramolecular relaxation times ( $T_{1\text{intra}}^{\text{H}}$ ) have not usually been characterized. Since the spin-rotation contribution to  $T_{1\text{intra}}^{\text{H}}$  for methyl protons can be dominant at room temperature (e.g., acetonitrile),

equating  $T_{1\text{intra}}^{\text{H}}$  values with  $T_{1\text{D}}^{\text{H}}$  could be hazardous. The use of reasonable estimates of  $\sigma$  in eq 2 and 4 along with  $T_{1\text{D}}^{\text{C}}$  data does allow one to calculate an approximate value for  $T_{1\text{D}}^{\text{H}}$ . For acetic acid, methyl iodide, and methanol,  $T_{1\text{D}}^{\text{H}}$  and  $R_{\perp}$  values have been calculated for  $\sigma = 2$  and 20 (these values were presumed to bracket the correct value) and the results are reported in Table II. The calculations indicate that while  $\sigma$  varies by tenfold, the change in  $T_{1\text{D}}^{\text{H}}$  is only 20–30%. Thus when  $\sigma$  gets very large both eq 2 and 4 become insensitive to the  $\sigma$  parameter and only the  $R_{\perp}^{-1}$  term will have any significant effect upon either  $T_{1\text{D}}^{\text{C}}$  or  $T_{1\text{D}}^{\text{H}}$ . Under these conditions reorientation of these molecules about their symmetry axis with rate  $R_{\parallel}$  becomes relatively ineffective in causing dipolar relaxation.

Table II: Predicted  $T_{1\text{D}}^{\text{H}}$  for Various Methyl Groups

Molecule	$T_{1\text{intra}}^{\text{H}}$ , sec	$\sigma$	$T_{1\text{D}}^{\text{H}}$ , sec	$R_{\perp}$ , sec <sup>-1</sup> $\times 10^{11}$
$\text{CH}_3\text{CN}$	48.1 <sup>a</sup>	9.2 <sup>b</sup>	52.2 <sup>c</sup>	1.48
$\text{CH}_3\text{I}$	20.2 <sup>d</sup>	$\left\{ \begin{array}{l} 2 \\ 20 \end{array} \right\}$	$\left\{ \begin{array}{l} 69.0 \\ 52.0 \end{array} \right\}$ <sup>f</sup>	$\left\{ \begin{array}{l} 3.48 \\ 1.16 \end{array} \right\}$ <sup>g</sup>
$\text{CH}_3\text{OH}$	21.3 <sup>e</sup>	$\left\{ \begin{array}{l} 2 \\ 20 \end{array} \right\}$	$\left\{ \begin{array}{l} 45.2 \\ 32.6 \end{array} \right\}$ <sup>f</sup>	$\left\{ \begin{array}{l} 2.64 \\ 0.83 \end{array} \right\}$ <sup>g</sup>
$\text{CH}_3\text{COOH}$	10.2 <sup>e</sup>	$\left\{ \begin{array}{l} 2 \\ 20 \end{array} \right\}$	$\left\{ \begin{array}{l} 18.5 \\ 13.3 \end{array} \right\}$ <sup>f</sup>	$\left\{ \begin{array}{l} 1.08 \\ 0.34 \end{array} \right\}$ <sup>g</sup>

<sup>a</sup> Calculated by Woessner (ref 4) from proton, deuterium, and nitrogen relaxation data. <sup>b</sup> Calculated value from eq 2 using carbon-13 data and  $R_{\perp} = 1.48 \times 10^{11}$ . <sup>c</sup> Calculated from eq 4 using  $\sigma = 9.2$  and  $R_{\perp} = 1.48 \times 10^{11}$ . <sup>d</sup> T. L. Pendred, A. M. Pritchard, and R. E. Richards, *J. Chem. Soc. A*, 1009 (1968). <sup>e</sup> H. G. Hertz, *Nucl. Magn. Spectrosc.*, **3**, (1967). <sup>f</sup> Calculated from eq 2 and 4 using indicated  $\sigma$  values and  $T_{1\text{D}}^{\text{C}}$  data. <sup>g</sup> Calculated from eq 2 using indicated  $\sigma$  values and  $T_{1\text{D}}^{\text{C}}$  data from Table I.

In all three compounds,  $\text{CH}_3\text{OH}$ ,  $\text{CH}_3\text{I}$ , and  $\text{CH}_3\text{COOH}$ , the calculated range of  $T_{1\text{D}}^{\text{H}}$  generally lies above the reported values of  $T_{1\text{intra}}^{\text{H}}$ . This result tends to suggest the importance of other mechanisms in  $T_{1\text{intra}}^{\text{H}}$  other than the proton-proton dipolar process. In fact, recent results on  $\text{CH}_3\text{I}$  on which the proton-proton dipolar and spin-rotation contributions to  $T_{1\text{intra}}^{\text{H}}$  have been separated indicate  $T_{1\text{D}}^{\text{H}}$  to be 50.5 sec at  $25^\circ$  with  $\sigma$  approximately 12–15, which is in substantial agreement with the results reported in Table II.<sup>8</sup> For acetic acid and methanol, it is not unreasonable to assume that  $\sigma$  could also be as large as 20 in view of the extensive dimerization and hydrogen bonding in these systems. If this is the case, the calculated values of  $T_{1\text{D}}^{\text{H}}$  for these molecules should

(7) K. T. Gillen and J. H. Noggle, *J. Chem. Phys.*, **53**, 801 (1970).

(8) K. T. Gillen, M. Schwartz, and J. H. Noggle, private communication.

agree more closely with the corresponding measured  $T_{1\text{intra}}^{\text{H}}$  than for  $\text{CH}_3\text{I}$  at the same  $\sigma$  value as spin-rotation effects upon  $T_{1\text{intra}}^{\text{H}}$  should be reduced relative to the more efficient homonuclear-dipolar process; the results in Table II for  $\sigma = 20$  support this position.

While a complete analysis of molecular motion in liquids requires the relaxation times and  $\eta$  values of more than one magnetic nuclei in a molecule, the above study does illustrate the facility with which the dipolar contribution to  $^{13}\text{C}$  relaxation times can be evaluated from  $T_1$  and NOE data and suggests a manner in which  $T_{1\text{D}}^{\text{C}}$  can be used to discuss molecular reorientation processes, as well as to estimate proton-proton dipolar contributions to intramolecular proton relaxation rates.

*Acknowledgment.* This research was supported by the National Institutes of Health under Grant No. GM-08521.

## The Photochemistry of Solid Layers.

### Reaction Rates

by E. L. Simmons

*Department of Chemistry, University of Houston, Houston, Texas 77004 (Received August 31, 1970)*

*Publication costs borne completely by The Journal of Physical Chemistry*

Recently there has been some interest shown in the photochemical reactions of solids in the form of thin films or layers.<sup>1-5</sup> As yet, however, the mathematical description of the rate of such a process has not been completely developed. Such a description is complicated by the fact that the reactant molecules cannot readily diffuse in a solid sample and a concentration gradient is therefore created by the photochemical reaction. The problem of the variation of the reactant concentration with the distance across a solid layer during a reaction in which there is no radiation intensity gradient has been theoretically treated for special cases in which the diffusion of gaseous reactants or products in the layer is important.<sup>1</sup> Approximate solutions have also been obtained for the case in which both the reactant concentration and the radiation intensity vary across the sample layer.<sup>3-5</sup>

In the treatment reported here an exact solution is obtained which describes the rate of the photochemical reaction of a solid layer for the case in which the photoproducts are transparent. An approximate solution is obtained for the case in which the photoproducts absorb radiation, and a method for determining the quantum yield is described.

*Case 1. Transparent Photoproducts.* Consider a solid layer of thickness  $d$  containing a reactant, A, which reacts photochemically to give transparent products. The initial concentration of A is  $C_0$  (in mol/cm<sup>3</sup>) while the concentration at a distance,  $x$ , across the layer after a time of reaction,  $t$ , is  $C$ . Monochromatic radiation of intensity,  $I_0$  (in einstein/cm<sup>2</sup> sec), at the surface of the layer is passed through the sample. After time,  $t$ , at a distance,  $x$ , across the layer, the intensity is  $I$ . The dependent variables,  $I$  and  $C$ , are to be related to the independent variables,  $x$  and  $t$ . Only two equations relating the variables are known, the Beer-Lambert equation which is valid in the differential form

$$dI/dx = -aCI \quad (1)$$

and the local rate equation

$$dC/dt = -\phi aCI \quad (2)$$

where  $a$  is the absorption coefficient and  $\phi$  the quantum yield. Solutions which satisfy eq 1 and 2 are<sup>6</sup>

$$I = I_0 \times \frac{\exp(-aC_0x)}{\exp(-\phi aI_0t)[1 - \exp(-aC_0x)] + \exp(-aC_0x)} \quad (3)$$

and

$$C = C_0 \times \frac{\exp(-\phi aI_0t)}{\exp(-\phi aI_0t)[1 - \exp(-aC_0x)] + \exp(-aC_0x)} \quad (4)$$

These solutions are obtained by combining eq 1 and 2 to obtain

$$-\phi dI = -(dC/dt) dx \quad (5)$$

Integration of eq 5 over  $x$  making use of the condition that  $I = I_0$  when  $x = 0$  gives

$$\phi(I_0 - I) = -d \left[ \int_0^x C dx \right] / dt \quad (6)$$

An expression for  $I$  is obtained by integrating eq 1

$$I = I_0 \exp\left(-a \int_0^x C dx\right) \quad (7)$$

An expression for the parameter  $\int_0^x C dx$  is obtained by substituting eq 7 into eq 6 and integrating making use of the condition that  $\int_0^x C dx = C_0x$  when  $t = 0$

(1) J. E. Wilson, *J. Chem. Phys.*, **22**, 334 (1954).

(2) P. G. Barker, M. P. Halstead, and J. H. Purnell, *Trans. Faraday Soc.*, **65**, 2389 (1969).

(3) T. R. Sliker, *J. Opt. Soc. Amer.*, **53**, 454 (1963).

(4) P. G. Barker, M. P. Halstead, and J. H. Purnell, *Trans. Faraday Soc.*, **65**, 2404 (1969).

(5) H. E. Spencer and M. W. Schmidt, *J. Phys. Chem.*, **74**, 3472 (1970).

(6) NOTE ADDED IN PROOF. It has come to the attention of the author that Mauser [H. Mauser, *Z. Naturforsch.*, **22b**, 569 (1967)] previously obtained similar equations by a different method for viscous samples.

$$\int_0^x C \, dx = (a^{-1}) \times \ln \left\{ \frac{\exp(-\phi a I_0 t) [1 - \exp(-a C_0 x)] + \exp(-a C_0 x)}{\exp(-a C_0 x)} \right\} \quad (8)$$

Differentiation of eq 8 with respect to  $x$  along with the proper algebraic rearrangements gives eq 4. Substitution of eq 8 into eq 7 gives eq 3.

Figure 1 illustrates the intensity and reactant concentration profiles across a layer. These curves were obtained using eq 3 and 4 and by arbitrarily choosing  $a = 10^4$ ,  $C_0 = 10^{-3}$ ,  $I_0 = 10^{-4}$ , and  $\phi = 1$ . Curves are given for various reaction times. The concentration gradient created by the photochemical reaction is evident. The gradient causes deviations from the exponential decrease of the radiation intensity across the layer predicted by the Beer-Lambert equation as can be seen in the lower part of Figure 1.

*Case 2. Photoproducts Absorb Radiation.* Although an exact solution for the case in which the photoproducts also absorb radiation was not obtained, an approximate solution which is valid for short reaction times was derived. For this case, eq 2 is valid, but

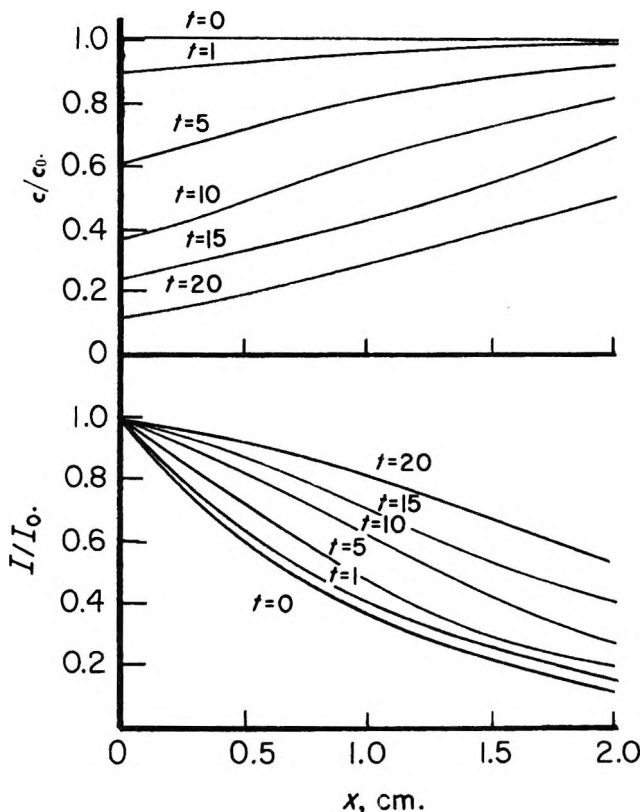


Figure 1. Radiation intensity and reactant concentration at various distances across the layer and various reaction times. The curves were obtained using eq 3 and 4 and arbitrarily choosing the following values:  $a = 10^4 \text{ cm}^2 \text{ mol}^{-1}$ ,  $C_0 = 10^{-3} \text{ mol/cm}^3$ ,  $I_0 = 10^{-4} \text{ einstein cm}^{-2} \text{ sec}^{-1}$ , and  $\phi = 1 \text{ mol einstein}^{-1}$ . Reaction times given are seconds.

eq 1 must be modified by adding to the right-hand side the term  $-\sum_j a_j g_j C_j$  where  $a_j$  is the absorption coefficient of the  $j$ th product,  $g_j$  the stoichiometry coefficient of the  $j$ th product, and  $C_j$  the concentration of the  $j$ th product. Since

$$C_0 = C + (g_j)^{-1} C_j \quad (9)$$

eq 1 may be written as

$$dI/dx = -(a - b)CI - bC_0I \quad (10)$$

where  $b = \sum_j a_j g_j^2$ . By carrying out the same procedures using eq 2 and 10 as for case 1 given in the previous section (eq 5) the following equation is obtained

$$\phi(I_0 - I) = -[(a - b)/a]d \left[ \int_0^x C \, dx \right] / dt - [bC_0/a]d \left[ \int_0^x \ln(C/C_0) \, dx \right] / dt \quad (11)$$

For small  $t$  when  $C/C_0$  does not differ greatly from one, the logarithmic term in eq 11 may be approximated by the first term of the series expansion

$$\ln(C/C_0) \cong C/C_0 - 1 \quad (12)$$

On substituting eq 12 into eq 11, eq 10 and 11 may be treated in a manner similar to that for eq 1 and 6 in the previous section to obtain the following solutions

$$I \cong I_0 \times \frac{\exp(-aC_0x)}{\exp[-(a - b)\phi I_0 t] [1 - \exp(-aC_0x)] + \exp(-aC_0x)} \quad (13)$$

and

$$C \cong C_0 \left\{ 1 + [a/(a - b)] \times \frac{\exp[-(a - b)\phi I_0 t] \exp(-aC_0x) - \exp(-aC_0x)}{\exp[-(a - b)\phi I_0 t] [1 - \exp(-aC_0x)] + \exp(-aC_0x)} \right\} \quad (14)$$

As expected, eq 13 and 14 reduce to eq 3 and 4 when  $b = 0$ . On varying  $b$ , there is a discontinuity in eq 14 when  $b = a$ ; thus, for this case, eq 14 cannot be used to calculate the reactant concentration.

*Applications.* The most apparent application for the equations obtained in the previous sections is connected with the quantum yield determination of the photochemical reaction of a solid layer. To determine the quantum yield it is convenient to have some easily measured parameter related to the reaction time. For solid layers the most easily measured parameter is usually the transmittance,  $T = I/I_0$ , of the layer. Equation 3 may be written in terms of the transmittance as

$$T = T_0[(1 - T_0) \exp(-\phi a I_0 t) + T_0]^{-1} \quad (15)$$

where  $T_0 = \exp(-aC_0d)$  ( $x$  is replaced by the total layer thickness,  $d$ ). By rearranging eq 15 and converting it to the logarithmic form, eq 16 may be obtained

$$\ln [(1 - T)T_0/(1 - T_0)T] = -\phi a I_0 t \quad (16)$$

Thus, a plot of  $\ln [(1 - T)/T]$  vs.  $t$  is a straight line with a slope related to the quantum yield. If  $a$  and  $I_0$  are known, the quantum yield can be determined from such a plot.

For the case in which the photoproducts absorb radiation, eq 14 may be treated in the same fashion to obtain

$$\ln [(1 - T)T_0/(1 - T_0)T] \cong -\phi(a - b)I_0 t \quad (17)$$

which is valid for small reaction times.

It is therefore apparently possible to determine the quantum yield of the photochemical reaction of a solid layer by measuring the transmittance of the layer as a function of time. Proof of the applicability of the method must, however, await experimental evidence.

*Acknowledgment.* The author wishes to thank the Science Research Council, London, England, and the Sandia Corporation, Albuquerque, New Mexico, for financial support during a large portion of this work.

## Kinetics of Chemical Ionization. I.

### Reaction of *tert*-C<sub>4</sub>H<sub>9</sub><sup>+</sup> with Benzyl Acetate

by S. Vredenberg, L. Wojcik, and J. H. Futrell\*<sup>1,2</sup>

*Department of Chemistry, The University of Utah, Salt Lake City, Utah 84112 (Received September 14, 1970)*

*Publication costs assisted by the Air Force Materials Laboratory, United States Air Force, Wright-Patterson Air Force Base, Ohio*

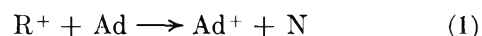
Recently, Field reported a study of the kinetics of reaction of *tert*-C<sub>4</sub>H<sub>9</sub><sup>+</sup> generated in a high-pressure ion source with benzyl acetate.<sup>3</sup> This pioneering attempt to measure rate parameters quantitatively under the conditions of chemical ionization mass spectrometry provided evidence that the rate constant was larger by a factor of 10 under certain conditions than could be rationalized on the basis of simple models for ion-molecule reactions<sup>4</sup> and that the rate constant exhibited a negative temperature coefficient. Using methane reagent gas to generate CH<sub>3</sub><sup>+</sup> and C<sub>2</sub>H<sub>5</sub><sup>+</sup>, Field also found a rate about five times larger than could be justified theoretically; this system, however, exhibited no variation of rate with temperature. Since there is no ready explanation for these phenomena, we have repeated the measurements using a high-resolution chemical ionization mass spectrometer of rather different design.<sup>5</sup>

## Experimental Section

Our experiments were carried out using a CEC Model 21-110B mass spectrometer which was modified for chemical ionization studies as described previously.<sup>5</sup> The gas-liquid inlet system is further modified by the addition of a septum inlet so that samples may be introduced directly into the expansion volume with a micro-liter syringe, ensuring precise sample measurement and good reproducibility. The samples are injected into a calibrated 3-l. volume maintained at 130°. The sample pressure is then increased to several Torr with reagent gas; a rather dilute mixture of benzyl acetate provides better sample control. It is also necessary to use enough pressure for the gas to flow into the source which is at 0.5 Torr pressure. Typical sample sizes are approximately 15 μl, and backing pressure is about 70 Torr. The required amount of sample is introduced into the source from the reservoir through a manual leak valve, and the pressure of sample-reagent gas mixture is measured with an MKS Baratron capacitance manometer. Additional reagent gas is then added from the high-pressure reservoir to establish and maintain the total pressure at 0.5 Torr. Source temperature is controlled in the normal fashion.

## Results and Discussion

Chemical ionization experiments are carried out using a sufficiently high pressure of the reagent gas so that hundreds of ion-neutral collisions occur.<sup>6</sup> A reagent gas is chosen whose primary ions react in a series of fast ion-molecule reactions to generate one or a small number of ions which are unreactive toward the reagent gas. These reagent ions react efficiently with the additive molecules in the manner indicated schematically by the reaction



A host of reactions are possible: charge transfer, proton transfer, condensation, dissociative proton transfer, etc. In the particular example under consideration, with *i*-C<sub>4</sub>H<sub>9</sub><sup>+</sup> as R<sup>+</sup> and benzyl acetate as Ad, the product ions are 91 (PhCH<sub>2</sub><sup>+</sup>), 107 (PhCH<sub>2</sub>O<sup>+</sup>), 108 (PhCH<sub>2</sub>OH<sup>+</sup>), 147 (PhCH<sub>2</sub>OC<sub>4</sub>H<sub>9</sub><sup>+</sup>), 151 (PhCH<sub>2</sub>OAcH<sup>+</sup>), 181 (protonated dimer less 2CH<sub>3</sub>COOH?), 241 (protonated dimer less CH<sub>3</sub>COOH?), and 301 ([PhCH<sub>2</sub>OAc]<sub>2</sub>H<sup>+</sup>). The distribution of products is a fairly strong function of temperature and at a given temperature our results are in generally good agreement with

(1) Alfred P. Sloan Fellow.

(2) This investigation was supported in part by a Public Health Service Research Career Development Award, No. 1 K04 GM4239001, from the National Institutes of General Medical Sciences.

(3) F. H. Field, *J. Amer. Chem. Soc.*, **91**, 2827 (1969).

(4) S. K. Gupta, E. G. Jones, A. G. Harrison, and J. J. Myher, *Can. J. Chem.*, **45**, 3107 (1967).

(5) L. H. Wojcik and J. H. Futrell, *Rev. Sci. Instrum.*, in press.

(6) F. H. Field, *Accounts Chem. Res.*, **1**, 42 (1968).

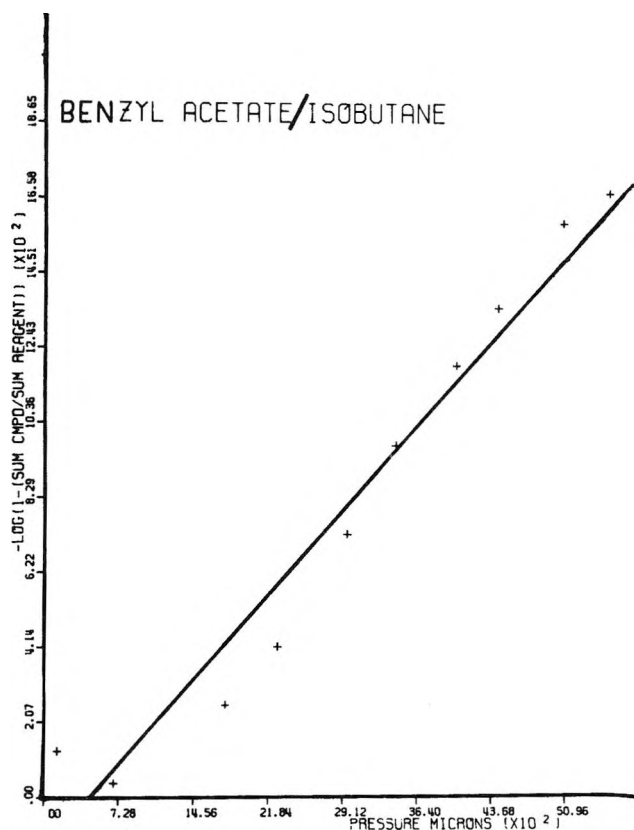


Figure 1. Rate constant plot for the reaction  $\text{tert-C}_4\text{H}_9^+$  with benzyl acetate at  $100^\circ$ . Line is least-squares fit of data from which a rate constant of  $1.2 \times 10^{-9} \text{ cm}^3 \text{ mol}^{-1} \text{ sec}^{-1}$  is deduced.

Field's.<sup>3</sup> The minor ions 107, 108, and 181 were not reported by him, while small intensities of ions at  $m/q$  150, 169, and 189 which he reported were not observed in the present work. Inclusion or exclusion of these relatively minor peaks in the summation of product ions does not significantly affect rate constants deduced from the data.

Under typical conditions where the concentration of additive is very much less than that of reactive ions, pseudo-first-order kinetics are followed. The integrated rate expression is therefore

$$\ln \left( 1 - \frac{\sum \text{Ad}^+}{I_{\text{R}^+}^0} \right) = -k[\text{Ad}]\tau \quad (2)$$

where  $\sum \text{Ad}^+$  is the summation of chemical ionization product ions,  $I_{\text{R}^+}^0$  is the ion intensity of reagent ions with no additive present,  $[\text{Ad}]$  is the concentration of additive molecules,  $k$  the rate constant, and  $\tau$  the source residence time of  $\text{R}^+$ .

Consequently, a plot of the logarithmic expression as a function of the partial pressure of additive should yield a straight line of slope  $k\tau$ . A typical plot of our data for the reaction of  $\text{tert-C}_4\text{H}_9^+$  with benzyl acetate is given in Figure 1. Since  $\tau$  can be calculated from ion mobility theory,<sup>6-8</sup> the rate constant is readily deduced. The residence time in seconds is

$$\tau = \frac{L(\alpha\mu)^{1/2}(273)P}{(25.9)(760)T_g E} \quad (3)$$

where  $L$  = distance from point of ion formation to exit slit in cm,  $E$  = electric field strength in V/cm,  $\alpha$  = polarizability of neutral and atomic units,  $\mu$  = reduced mass of neutral and ion reactants,  $T_g$  = absolute temperature of gas, and  $P$  = source pressure in Torr.

Before using this approach to deduce rate constants for the benzyl acetate system, we felt it necessary to establish source parameters for which the residence time is properly described using this formalism. Accordingly, we carried out a series of experiments with He- $\text{CH}_4$  mixtures. The rate constants for the principal ion-molecule reactions in methane are well known,<sup>9-11</sup> and this may be used as a test for the approach outlined above. Helium serves merely as a scatter gas of known polarizability in these experiments rather than a reagent gas. Ions produced by dissociative transfer with  $\text{He}^+$  do not interfere with the methane reactions.<sup>12</sup>

The apparent rate constants for the methane reaction



ranged from  $1.8 \times 10^{-10} \text{ cm}^3 \text{ mol}^{-1} \text{ sec}^{-1}$  at  $1 \text{ V cm}^{-1} \text{ Torr}^{-1}$  to  $3.0 \times 10^{-9} \text{ cm}^3 \text{ mol}^{-1} \text{ sec}^{-1}$  at  $40 \text{ V cm}^{-1} \text{ Torr}^{-1}$ . Over the range  $5\text{--}20 \text{ V cm}^{-1} \text{ Torr}^{-1}$  at pressures from 0.5 to 1 Torr the observed rate constant was within  $\pm 30\%$  of the accepted rate constant of  $1.18 \times 10^{-9} \text{ cm}^3 \text{ mol}^{-1} \text{ sec}^{-1}$ .<sup>5-7</sup> At higher field strength/pressure ratios the slow ion mobility theory breaks down,<sup>8</sup> and the lower repeller field measurements appear to suffer from as yet uncharacterized artifacts. At a repeller field of  $10 \text{ V cm}^{-1}$  and a pressure of 0.5 Torr our experimental rate constant for reaction 4 was  $1.2 \pm 0.2 \times 10^{-9} \text{ cm}^3 \text{ mol}^{-1} \text{ sec}^{-1}$ , and these conditions were used for subsequent measurements.

Figure 1 illustrates the typical precision of an experiment carried out under these conditions for the isobutane-benzyl acetate system at a temperature of  $100^\circ$ . The displayed least-squares line gives a fit of 0.999 and a rate constant of  $1.2 \times 10^{-9} \text{ cm}^3 \text{ mol}^{-1} \text{ sec}^{-1}$ . These measurements were then repeated at several temperatures and plotted in Figure 2.

The results obtained by Field for the same system<sup>3</sup> are displayed as the upper curve of Figure 2, which may

(7) Y. Kaneko, L. R. Megill, and J. B. Hasted, *J. Chem. Phys.*, **45**, 3741 (1966).

(8) J. B. Hasted, "Physics of Atomic Collisions," Butterworth, London, 1964.

(9) J. K. Gupta, E. G. Jones, A. G. Harrison, and J. J. Myher, *Can. J. Chem.*, **45**, 3107 (1967).

(10) C. W. Hand and H. von Weissenhoff, *ibid.*, **42**, 195 (1964).

(11) J. H. Futrell, T. O. Tiernan, F. P. Abramson, and C. D. Miller, *Rev. Sci. Instrum.*, **39**, 300 (1968).

(12) H. Sjögen, *Ark. Fys.*, **31**, 159 (1966).

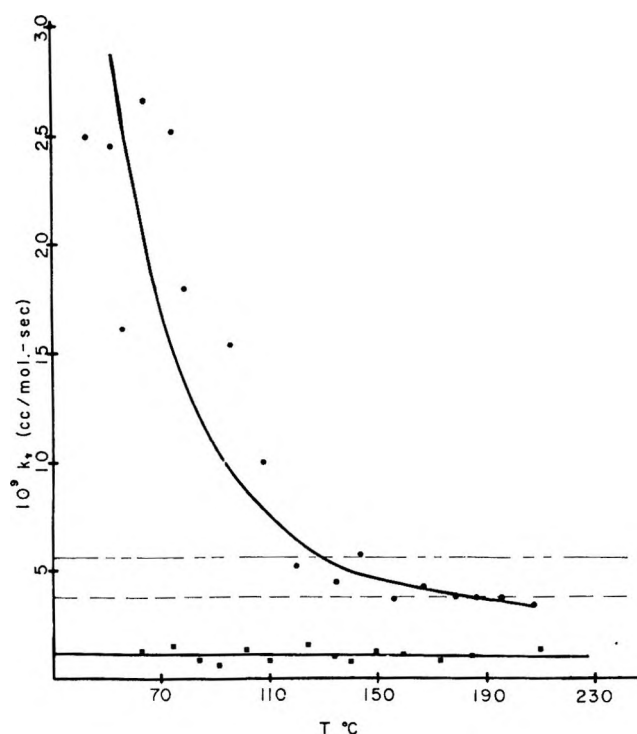


Figure 2. Temperature dependence of rate constants for the reaction of  $tert\text{-C}_4\text{H}_9^+$  with benzyl acetate. The upper solid line and associated data points are from ref 3, while the present results are shown in the lower part of the figure. Dashed lines show theoretical rates calculated from eq 5 (---) and 6 (— — —) of the text.

be contrasted with the lower solid line which summarizes the present results. We also show as dashed lines the theoretical rates computed from the expressions

$$k = 2\pi e(\alpha/\mu)^{1/2} \quad (5)$$

$$k = 2\pi e(\alpha/\mu)^{1/2} + 2\pi e\mu_D/v\mu \quad (6)$$

where  $e$  is the electronic charge,  $\alpha$  the polarizability of the molecule,  $\mu$  the reduced mass,  $\mu_D$  the dipole moment, and  $v$  the relative velocity. The former is the simple hard-collision Langevin rate constant deduced for a point charge-induced dipole interaction potential, while the latter is the maximum rate for a point charge-locked dipole interaction.<sup>4</sup> The rate constant deduced from our experiments is temperature-invariant and equal to  $1.1 \times 10^{-9} \text{ cm}^3 \text{ mol}^{-1} \text{ sec}^{-1}$ . As shown in the figure, it may also be rationalized in terms of either of these simple models, and it is not necessary to invoke any special properties for the reaction of *tert*-butyl ions with benzyl acetate.

We have also carried out a brief investigation of the kinetics of reaction of methane reagent ions with benzyl acetate. The rate constant did not exhibit any temperature dependence, in agreement with Field's results for this system,<sup>3</sup> and a rate constant of  $2.9 \pm 0.3 \times 10^{-9} \text{ cm}^3 \text{ mol}^{-1} \text{ sec}^{-1}$  was deduced from our data.

The ion source parameters used in Field's work and in ours are very similar and we are unable to suggest

plausible explanations for the discrepancies in either set of experiments. Final resolution of the question of temperature dependence of rates of chemical ionization reactions will require additional research by other investigators. Nevertheless, since the present results do not support any appreciable temperature dependence, and since the rate constant deduced is readily rationalized on the basis of the usual models for ion-molecule reactions, we believe that these reactions do not display any extraordinary kinetic behavior.

*Acknowledgments.* The authors wish to acknowledge helpful discussions of this and related problems with Professors Frank Field and John Hasted. The financial support of the Air Force Materials Laboratory through Contract F33615-70-C-1182 is also gratefully acknowledged.

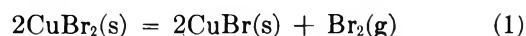
### Spectrophotometric Study of the Equilibrium between Copper(I) Bromide, Copper(II) Bromide, and Bromine

by David L. Hilden and N. W. Gregory\*

Department of Chemistry, University of Washington, Seattle, Washington 98105 (Received October 2, 1970)

Publication costs assisted by the National Science Foundation

Relative thermodynamic properties of  $\text{CuBr}_2(\text{s})$  and  $\text{CuBr}(\text{s})$  have been derived by a number of workers<sup>1-4</sup> from studies of the reaction



Results of diaphragm gauge studies<sup>1-3</sup> have been compared recently with those based on torsion effusion experiments performed in this laboratory.<sup>4</sup> In the latter, steady-state bromine pressures generated by reaction 1 were found to depend on the effusion cell orifice diameter. Furthermore, consistent values were obtained from a given cell only during the initial stages (decomposition of the first 10% of a sample of  $\text{CuBr}_2$ ) of the reaction, after which pressures fell with time. Extrapolation of the initial steady-state pressures to zero orifice area gave apparent equilibrium values for (1) generally consistent with the higher temperature diaphragm gauge study of Jackson.<sup>1</sup> However, independent van't Hoff values for the enthalpy and entropy

(1) C. G. Jackson, *J. Chem. Soc.*, **99**, 1066 (1911).

(2) S. A. Shchukarev and M. A. Oranskaya, *Zh. Obshch. Khim.*, **24**, 1926 (1954).

(3) P. Barrett and N. Guenebaut-Thevenot, *Bull. Soc. Chim. Fr.*, 409 (1957).

(4) R. R. Hammer and N. W. Gregory, *J. Phys. Chem.*, **68**, 314 (1964).

of reaction from the two studies did not agree closely with each other or with the results of the other workers,<sup>2,3</sup> which also differ significantly.

The relatively slow rate of the decomposition reaction and the resultant need for an extrapolation procedure make the uncertainty in the equilibrium properties derived from the effusion experiments larger than desired. Also, it was not possible by this method to determine if decomposition pressures varied with the relative amounts of CuBr and CuBr<sub>2</sub> over a wide composition range, particularly near pure CuBr. In addition, recent work of Ward, *et al.*,<sup>5</sup> and of others raises questions concerning the basic reliability of the effusion method and shows clearly a need for reexamination of its applicability.

In the present study equilibrium constants for (1) have been derived from vapor-phase absorbance measurements in sealed quartz cells over the temperature interval 170–260°. The molar absorptivities of bromine as a function of temperature are well established.<sup>6,7</sup> Neither of the copper bromides is sufficiently volatile at temperatures of interest to contribute significantly to the absorption in the wavelength range of the spectrophotometer. The results derived provide a test of conclusions based on the effusion study<sup>4</sup> as well as evidence for assignment of thermodynamic properties of the copper bromides.

### Experimental Section

The absorption spectra (700–300  $m\mu$ ) of the vapor developed over samples no. 1, 2, and 3 were obtained with a Beckman DU spectrophotometer. The standard cell compartment of this instrument was replaced by a larger one containing furnaces designed to heat custom-made fused silica cells (5-cm path length; volume *ca.* 15 cm<sup>3</sup>) to the desired temperatures.<sup>8</sup> Spectra of sample no. 4 were obtained with a Cary Model 14H spectrophotometer.<sup>9</sup> A T-shaped clam shell furnace was constructed to heat the sample cell; matched fused silica cells (Pyrocell Manufacturing Company, Westwood, N. J.) were used in the sample and reference beams. Temperatures were determined with chromel-alumel thermocouples, calibrated against NBS freezing point standards (Sn, Pb, Zn, Al).

Sample no. 1 was prepared in the spectrophotometer cell by reaction of copper with Baker's Analyzed Reagent Br<sub>2</sub>, vacuum distilled off F<sub>2</sub>O<sub>5</sub>, and NaBr. Bromine gas, in equilibrium with liquid bromine held at room temperature, was treated with the copper at *ca.* 450° to form CuBr; the mixture was then cooled to *ca.* 240° to form CuBr<sub>2</sub>. Free bromine was removed by vacuum evaporation prior to sealing off the cell at room temperature. This sample (*ca.* 0.5 g) was believed to approximate CuBr<sub>2</sub> in composition. Sample no. 2 was prepared by addition of vacuum-distilled Br<sub>2</sub> to an excess of Baker's analyzed CuBr which had been purified by three successive vacuum sublimations. The

mixture reacted to form CuBr<sub>2</sub> as the cell was brought to the temperatures at which equilibrium measurements were made. In neither of these cases was a quantitative measure of the composition of the brominated sample attempted.

Sample no. 3 was prepared in a manner similar to sample no. 1 except that the amount of copper foil was weighed and a limited amount of bromine was used. From the measured bromine concentration at temperatures sufficient to complete the decomposition of the CuBr<sub>2</sub>, and the known cell volume, the initial mole per cent of CuBr<sub>2</sub> was calculated to be 11% (89% CuBr). Sample no. 4 was prepared in a manner similar to sample no. 3 except the copper foil was preheated in the presence of hydrogen and the cell evacuated, and this treatment repeated twice to ensure removal of surface oxide. After bromination the initial mole per cent of CuBr<sub>2</sub> in this sample was determined (as for sample no. 3) to be 87% (13% CuBr).

### Results and Discussion

The pressure of bromine was determined by the relationship

$$P = cRT = A(RT/\epsilon b)$$

where  $A$ ,  $\epsilon$ , and  $b$  are the absorbance, the molar absorptivity of Br<sub>2</sub> vapor at the particular wavelength and temperature, and the cell path length, respectively. The molar absorptivity was calculated from an equation developed by Sulzer and Wieland.<sup>6</sup> This equation is based on the assumption of harmonic oscillator wave functions and gaussian curves of constant area. The necessary parameters have been supplied by Passchier, Christian, and Gregory.<sup>7</sup> In practice, many measurements of the bromine absorbance were made at various wavelengths for each temperature and the apparent concentrations averaged. The calculated pressure was taken equal to the equilibrium constant of (1).

The lack of significant miscibility between solid CuBr and solid CuBr<sub>2</sub> is suggested by the observation that sample no. 3, initially rich in CuBr (>89 mol %), gave results indistinguishable from those obtained with no. 1 and 2. Further, in sample no. 4 the composition of the solid changed during the measurements from 72 to 0 mol % CuBr<sub>2</sub> with observed equilibrium bromine pressures in good agreement with the other three samples. Hence, the activities of the solids did not show

(5) J. W. Ward, R. N. R. Mulford, and M. Kahn, *J. Chem. Phys.*, **47**, 1710 (1967).

(6) P. Sulzer and K. Wieland, *Helv. Phys. Acta*, **25**, 653 (1952).

(7) A. A. Passchier, J. D. Christian, and N. W. Gregory, *J. Phys. Chem.*, **71**, 937 (1967).

(8) For details see the Ph.D. Thesis of J. D. Christian, University of Washington, 1965; University Microfilms Publ. No. 66-5850, Ann Arbor, Mich.

(9) Instrumentation procured with assistance of NSF Grant GP-10506.

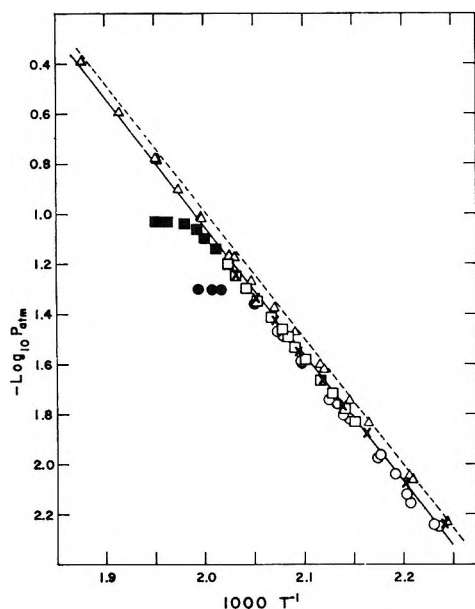


Figure 1. Equilibrium bromine pressures for reaction 1. The solid line represents the linear least-squares correlation in the form  $\log P_{\text{atm}} = -5101T^{-1} + 9.157$ . The dashed line is an extrapolation of a similar equation based on earlier effusion experiments:<sup>4</sup>  $\times$ , sample 1;  $\Delta$ , sample 2;  $\circ$ , sample 3;  $\square$ , sample 4. The filled symbol points, not included in the least-squares treatment, demonstrate the experimental evidence that all the  $\text{CuBr}_2(\text{s})$  was decomposed at the highest temperatures for these samples.

dependence on the relative amounts present and were taken as unity.

With the recording Cary 14H spectrophotometer the bromine pressure associated with sample no. 4 could easily be determined both from the absorbance at the maximum of the absorbance peak (*ca.* 420  $m\mu$ ) as well as from the integrated absorbance. In the latter case the Sulzer-Wieland expression for  $\epsilon$  was integrated over the wavelength range of the absorbance. The integrated  $\epsilon$  times the path length  $b$  was divided into the graphically integrated absorbance to determine the concentration at each temperature. The results of the two approaches were in excellent agreement. Since the theory assumes absorption peaks of constant area, the use of the integrated absorbance eliminates the necessity of specific knowledge regarding the temperature dependence of the molar absorptivity of bromine at a particular wavelength.

The data, Figure 1, have been correlated in the form  $\log P_{\text{atm}} = A'T^{-1} + B$ . For samples no. 3 and 4 the four and six data points, respectively, at the highest temperatures have not been included in the correlation. These points correspond to samples either close to or completely decomposed into  $\text{CuBr}(\text{s})$  and  $\text{Br}_2$ . Results from sample no. 2 appear to be consistently above those of the other three. The deviation suggests some systematic effect which we cannot explain. Since the difference is not clearly beyond experimental error, all

results were used with equal weight in a least-squares treatment to derive values of  $A'$  and  $B$ ,  $-5101$  and  $9.157$ , with a standard deviation of  $0.030$ . These constants yield values of  $\Delta H^\circ = 23.3 \pm 0.3$  kcal/mol and  $\Delta S^\circ = 41.9 \pm 0.6$  eu, taken as the mean for the temperature range  $170$ – $260^\circ$ . The listed uncertainties correspond to the standard errors of the slope and intercept of the least-squares line<sup>10</sup> and are not expected to reflect systematic errors in the data. The absolute uncertainty is estimated as about twice the standard error. Results of earlier workers are shown in Table I.

Table I: Thermodynamic Constants for the Reaction  $2\text{CuBr}_2(\text{s}) = 2\text{CuBr}(\text{s}) + \text{Br}_2(\text{g})$

Ref	$\Delta H^\circ$ , kcal/mol	$\Delta S^\circ$ , eu	$\Delta H^\circ_{298}$ , kcal/mol	Tem- perature range, $^\circ\text{C}$
1	21.7	38		166–281
2	16.5	28		130–316
3	19.3	34		151–250
4	23.2	41.8	23.4	50–110
a	23.3	41.9	23.6	170–260

<sup>a</sup> This work.

The value of  $\Delta H^\circ_{298}$  for (1) may be derived using free energy functions. Lewis, *et al.*,<sup>11</sup> give  $S^\circ_{298}$  as 23 and estimate  $-(G^\circ - H^\circ_{298})/T$  as 24 for  $\text{CuBr}(\text{s})$  at  $500^\circ\text{K}$ . Brewer, Somayajulu, and Brackett<sup>12</sup> estimate  $-(G^\circ - H^\circ_{298})/T$  for  $\text{CuBr}_2(\text{s})$  as 32 at  $298^\circ\text{K}$  and 34 at  $500^\circ\text{K}$ . Data for  $\text{Br}_2$  has been tabulated in the "JANAF Thermochemical Tables."<sup>13</sup>

The above data may be combined with  $\Delta G^\circ_T$ , determined in this work, to yield  $\Delta H^\circ_{298}$  for eq 1 at each experimental temperature. The results show an apparent temperature dependence, with  $\Delta H^\circ_{298}$  steadily decreasing as the temperature increases. As observed earlier in the effusion study,<sup>4</sup> this trend disappears if the values of  $-(G^\circ - H^\circ_{298})/T$  estimated for  $\text{CuBr}_2(\text{s})$  are lowered by *ca.* 1 eu; we have used 30.8 and 32.6 at 298 and  $500^\circ\text{K}$ , respectively. Alternatively, part of this adjustment could be ascribed to  $\text{CuBr}$ . The  $\Delta H^\circ_{298}$  calculated with the new free energy functions is independent of the experimental temperature and averages 23.6 kcal/mol. Tabulated enthalpy data,<sup>11,14</sup>

(10) J. Topping, "Errors of Observation and their Treatment," 3rd ed, Chapman and Hall, London, 1962, p 106.

(11) G. N. Lewis, M. Randall, K. Pitzer, and L. Brewer, "Thermodynamics," 2nd ed, McGraw-Hill, New York, N. Y., 1961.

(12) L. Brewer, G. R. Somayajulu, and E. Brackett, *Chem. Rev.*, **63**, 111 (1963).

(13) "JANAF Thermochemical Tables," Dow Chemical Co., Midland, Mich., Dec 31, 1961 Supplement.

(14) F. D. Rossini, D. D. Wagman, W. H. Evans, S. Levine, and I. Jaffe, *Nat. Bur. Stand. (U. S.) Circ.*, 500 (1952).

based on very early work, also give  $\Delta H^\circ_{298} = 23.6$  kcal/mol.

As seen in Figure 1, an extrapolation of the effusion results compares very favorably with the present studies. One concludes that the assumptions made in interpreting the effusion data were reasonable and the method is suitable for deriving equilibrium data for this particular decomposition reaction in spite of the kinetic problems.

With the choice of free energy functions selected in the present work one calculates  $\Delta S^\circ_{298} = 43.0$  eu for (1), which gives 7.8 eu for the difference between the standard entropies of  $\text{CuBr}_2(\text{s})$  and  $\text{CuBr}(\text{s})$  at  $298^\circ\text{K}$ . This value is approximately two-thirds of that predicted by Latimer's rule.<sup>11</sup>

*Acknowledgment.* Support for this research under NSF Grant GP 6608X is acknowledged with thanks.

### Solvent Effect on Anthracene Monosulfonates in the First Excited State

by K. K. Rohatgi\* and B. P. Singh

*Physical Chemistry Laboratories, Jadavpur University, Calcutta-32, India (Received March 16, 1970)*

*Publication costs borne completely by The Journal of Physical Chemistry*

Polar solvents are known to shift the absorption spectra of anthracene toward the red.<sup>1-3</sup> The difference between the 0-0 vibrational bands in absorption and emission also increases. The changes have been explained as due to dispersion force interaction between the solute and the solvent molecules. When the anthracene molecule is sulfonated it becomes water soluble. We have observed that the solvent effects on absorption and emission spectra of these compounds depend on the position of substitution and on the number of sulfonate groups introduced. Here we report some observations on the effect of solvents, especially water, on the fluorescence spectra of 1- and 2-anthracene sulfonates.

#### Experimental Section

Anthracene 1-, 2-mono, and 1,5-disodium sulfonates were prepared by reducing corresponding anthraquinones (BDH) with Zn dust and 20%  $\text{NH}_4\text{OH}$  for 4-6 hr. The products were treated with active animal charcoal to remove traces of anthraquinones and other impurities and were recrystallized three times from water.

Ethyl alcohol (100%) was prepared by treating the commercially available 99.5% alcohol with quicklime and subsequent distillation. Commercially available

(BDH) ethylene glycol was allowed to stand for 48 hr over anhydrous sodium sulfate and was then distilled twice. Acetonitrile (BDH) was first dehydrated over  $\text{CaCl}_2$  and then distilled twice. AR quality tetrahydrofuran (BDH) was shaken with 1% NaOH solution to free it from unstable peroxide (if any) and distilled twice. E. Merck chromatographically pure formamide was distilled once under low pressure before use. The refractive index was taken as a criterion of the purity of these solvents.

Uv absorption spectra were measured by a Beckman (DU) spectrophotometer Model 4700 provided with a blue-sensitive photomultiplier tube. Emission spectra were measured with the same instrument with a spectrofluorimetric attachment. A 1-cm silica cell was used and measurements were made at  $45^\circ$  to the normal, at high sensitivity of the instrument. An Hg vapor lamp with standard filter to isolate 365 nm was used as the source for excitation. For fluorescence studies, solutions at a constant solute concentration of  $8.0 \times 10^{-5} M$  were taken and fluorescence spectra were measured manually using 1-nm resolution. Solutions contained dissolved oxygen owing to the difficulty in estimating relative solvent losses on degassing samples.

#### Results and Discussion

The absorption and fluorescence spectra of anthracene in benzene and anthracene-1-sulfonate (1-AS), anthracene-2-sulfonate (2-AS), and anthracene-1,5-disulfonate (1,5-AS) in water are given in Figures 1 and 2, respectively. It is evident that whereas the absorption spectra are not much affected on sulfonation except for minor details in vibrational structures and small variation in molar extinction values between 1- and 2-sulfonates, the fluorescence spectra are completely changed for monosulfonates. The monosulfonate spectra are red-shifted by 5-10 nm as compared to 1,5-anthracene disulfonate in water. The absorption spectra are independent of pH or high acidity. The emission spectra also are not much affected by pH changes or by high acidity except for a red shift of 10 nm for solutions in between 1 and 2 N HCl.

The vibrational fine structure in the fluorescence spectra is lost in aqueous solution, more completely for 1-AS for which a smoothed out spectrum is obtained, but the same returns gradually on addition of solvents like acetonitrile (ACN), tetrahydrofuran (THF), formamide (FMD), ethyl alcohol (EtOH), and ethylene glycol (EG). The wavelength of the fluorescence maximum,  $\lambda_{\text{max}}$ <sup>11</sup> gradually shifts toward the blue and the fluorescence intensity decreases simultaneously. Addition of urea up to a concentration of 4 M has no observ-

(1) G. Körtum and B. Finckh, *Z. Phys. Chem.*, **B52**, 263 (1942).

(2) S. Sambursky and G. Wolfson, *Trans. Faraday Soc.*, **36**, 427 (1940).

(3) K. Lauer and M. S. Horio, *Ber.*, **69B**, 130-37 (1936).

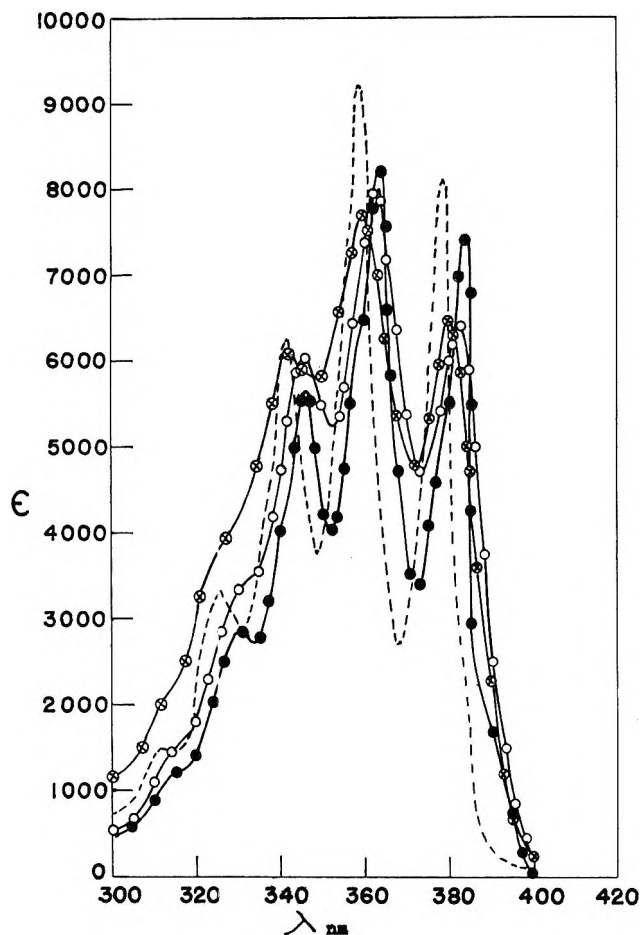


Figure 1. Absorption spectra: ---, anthracene in benzene; O, 1-AS in water;  $\odot$ , 2-AS in water;  $\bullet$ , 1,5-AS in water.

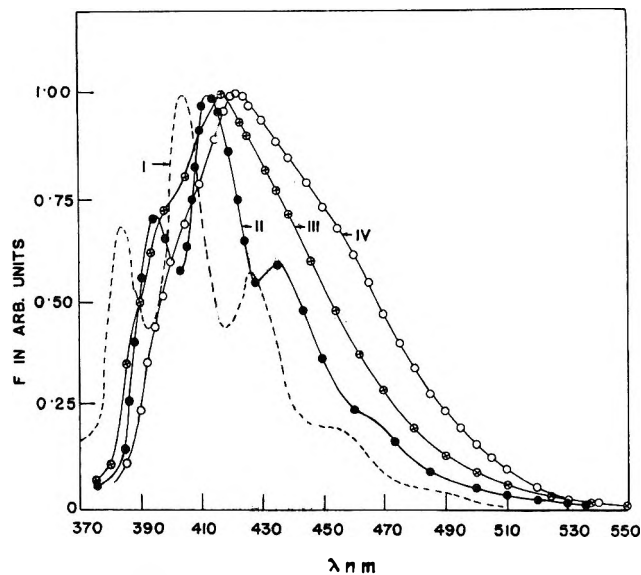


Figure 2. Normalized fluorescence spectra: I, anthracene in benzene; II, 1,5-AS in water; III, 2-AS in water; and IV, 1-AS in water.

able effect on the fluorescence spectrum in aqueous solution. The efficiency with which the unperturbed spectrum is recovered depends on the nature of the sol-

vent, the order being  $\text{H}_2\text{O} = \text{urea} < \text{FMD} \ll \text{EtOH}$ ,  $\text{ACN}$ ,  $\text{THF}$ . When the intensity of fluorescence for 1-AS at the wavelength of the maximum in aqueous solution is plotted as a function of solvent composition, the variation is linear and small for water-FMD and water-EG mixtures. For all other solvent mixtures, the value drops initially for 20 mol % solution and varies insignificantly for higher proportions of the nonaqueous solvents. It is difficult to explain this result completely, but it may be noted that the solvents of the first category are of a strongly associating type and also possess higher dielectric constants, whereas those of the second category do not associate much (except for EtOH) and have dielectric constants on the low side.

The polar solvent induced loss in vibrational structure and pronounced red shift of the fluorescence spectra without corresponding shift in absorption spectra have been observed for indole and substituted indoles by Van Duuren,<sup>4</sup> Walker and coworkers,<sup>5</sup> and Longworth.<sup>6</sup> Although Van Duuren had attributed this fluorescence red shift to generalized dipole-dipole interaction between solvent and solute in the excited state, the latter workers were able to establish the formation of exciplexes or specific solute-solvent complexes in the excited state. The fluorescence spectra of the exciplexes between methyl indole and alcohols like propanol, butanol, etc. were found to be featureless and broad with  $\lambda_{\text{max}}$ <sup>11</sup> shifted to longer wavelengths. The existence of such excited-state complexes between solute and polar solvents has been established mostly from studies in nonpolar media in the presence of small amounts of reactive solvent. However, in the present study, the spectra shift continuously on increasing addition of water; therefore a complex with one or two solvent molecules cannot be visualized. Solute-solvent exciplexes and also excimers are known to have structureless spectra. For excimer formation, a shift of about  $6000 \text{ cm}^{-1}$  and a dependence of the spectrum on solute concentration is expected. Such small shifts, and no effect of solute concentration on the spectrum, suggest a weak interaction with the solvent.

When frequency differences between absorption and fluorescence maxima for the anthracene sulfonates are plotted against the macroscopic properties of the solvents, such as dielectric constant ( $D$ ), and refractive index ( $n$ ), according to the formula of Lippert<sup>7</sup> and Mataga,<sup>8</sup> *et al.*, correlation is not good for 1-AS and 2-AS (all solvents taken were 80% mixtures in water because of poor solubility of the solute in pure solvents).

(4) B. L. Van Duuren, *J. Org. Chem.*, **20**, 2954 (1961).

(5) M. S. Walker, T. W. Bednar, and R. Lumry, *J. Chem. Phys.*, **45**, 3455 (1966); **47**, 1020 (1967).

(6) J. W. Longworth, *Photochem. Photobiol.*, **7**, 587 (1968).

(7) E. Lippert, *Z. Elektrochem.*, **58**, 714 (1954); **61**, 962 (1957).

(8) N. Mataga, *et al.*, *Bull. Chem. Soc. Jap.*, **29**, 465 (1956).

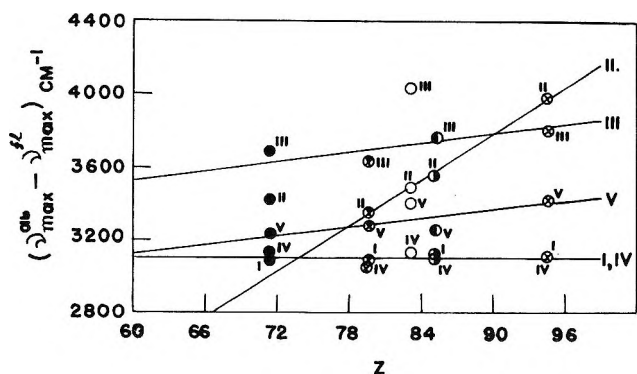


Figure 3. Stoke's red shifts as a function of Kosower's  $Z$  values for: I, anthracene; II, 1-AS; III, 2-AS; IV, 1,5-AS; and V, 1,8-AS; ●, ACN; ○, EtOH; ○, FMD; ○, EG; and ⊗, water.

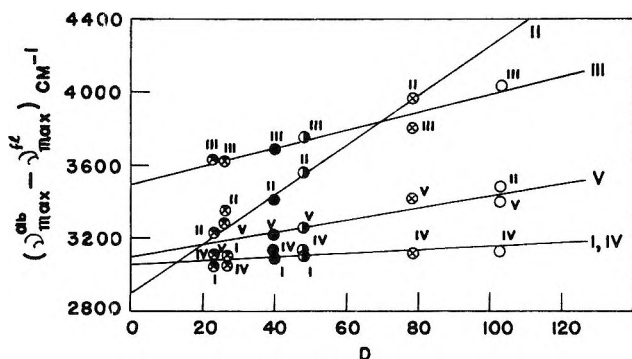


Figure 4. Stoke's red shifts as a function of the dielectric constant ( $D$ ) of solvents for: I, anthracene; II, 1-AS; III, 2-AS; IV, 1,5-AS; and V, 1,8-AS; ●, THF; ○, EtOH; ●, ACN; ○, EG; ⊗, water; and ○, FMD.

Only totally symmetric 1,5-disulfonate gave a good straight line with zero slope. On the other hand, good correlation is obtained with Kosower's  $z$  values<sup>9</sup> which measure the microscopic dielectric constant and are a better measure of solvent polarity. The points for 1-AS in ACN and 2-AS in FMD deviate considerably (Figure 3) although 2-AS correlates linearly with variation in dielectric constant  $D$  only (Figure 4). Now the point for 1-AS in FMD is completely off the line.

A series of fluorescence spectra obtained for water-ACN mixtures in different proportions show an isoemissive point at 390 nm for 1-AS (Figure 5) and at 387 nm for 2-AS (Figure 6). The solute concentration was kept constant for a given series. Due to poor solubility, the fluorescence spectrum for solutions in 100% ACN was obtained by preparing a saturated solution and estimating the concentration of the solute. The spectrum was adjusted for the concentration as used for the mixed solvents. The existence of an isoemissive point in fluorescence is an indication of a two-component equilibrium in the excited state.<sup>10,11</sup> Therefore, we should look for the complex formed in the excited state only, since the absorption spectra are not much affected.

The first excited state of anthracene is the  $\pi-\pi^*$

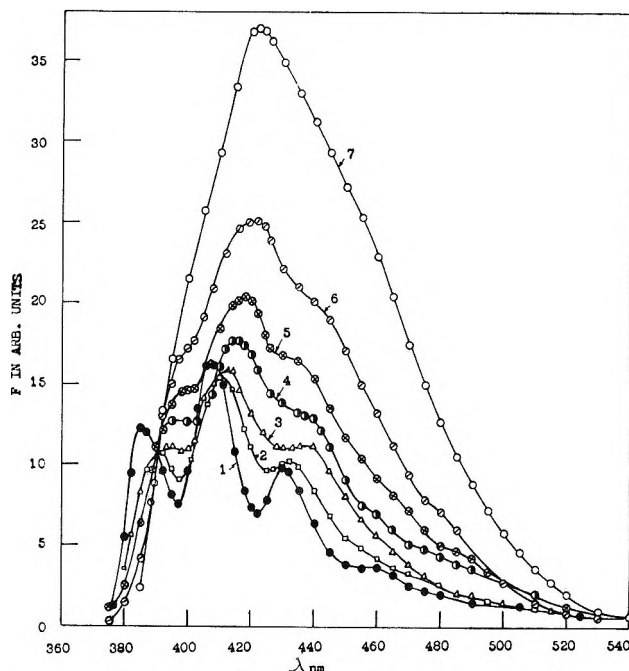


Figure 5. Fluorescence spectra of 1-AS in water-ACN mixtures ( $c = 8.0 \times 10^{-5} M$ ): 1 in ACN; 2 to 7 in 20; 40; 60; 80; 90; and 100% water, respectively.

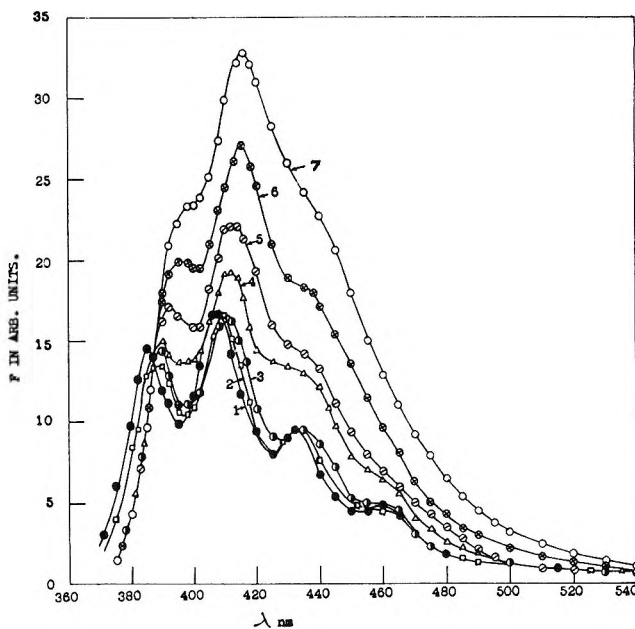


Figure 6. Fluorescence spectra of 2-AS in water-ACN mixtures ( $c = 1.2 \times 10^{-4} M$ ): 1 in ACN; 2 to 7 in 20; 40; 60; 80; 90; and 100% water, respectively.

state and is designated as  ${}^1L_a$  whose vibrational modes are totally symmetric with fundamental vibration frequencies of 1400 and 390  $\text{cm}^{-1}$ . Substitution of

(9) E. M. Kosower, *J. Amer. Chem. Soc.*, **80**, 3253, 3267 (1958).

(10) J. W. Longworth and R. O. Rahn, *Biochem. Biophys. Acta*, **147**, 526 (1967).

(11) J. W. Longworth, *Photochem. Photobiol.*, **7**, 587 (1968).

sulfonic acid group in the 1 and 2 positions introduces considerable asymmetry in the anthracene molecule. The ground-state energy is not much affected because  $-\text{SO}_3^-$  group interacts to only a small extent.<sup>12</sup> In the excited state,  $-\text{SO}_3^-$  does interact since the  $\lambda_{\text{max}}^{\text{fl}}$  in an inactive solvent like ACN is shifted by about 8–10 nm for all sulfonates relative to anthracene. The dipolar interaction with the solvent will also increase. However, since specific hydrogen bonding does not seem probable and the red shift follows the common polarity scale of Kosower, the interaction seems to be of rather a collective type. Solvent structure definitely has some part to play. In the present systems, such interaction is accompanied by activation of fluorescence rather than quenching. Förster and Rokos<sup>13</sup> had observed a decrease in the fluorescence quantum yield,  $\phi_{\text{fl}}$ , with anomalous Stokes shift for *N,N*-dimethyl-1-amino-5-naphthalene sulfonate in water in contrast to "inactive" solvents like dimethyl formamide. Thus any explanation of the solvent effect on anthracene monosulfonates should take into consideration the following points: (i) solvent red shift, (ii) loss of vibrational structure with enhancement of  $\phi_{\text{fl}}$ , and (iii) the existence of isoemissive point.

The points (i) and (ii) do not seem to be necessarily correlated. Further studies on 1,8-disulfonate in aqueous solution reveal that the  $\lambda_{\text{max}}^{\text{fl}}$  lies in the same region (421 nm) as that for 1-AS (422 nm). The former has definite vibrational pattern but much reduced fluorescence yield. From this fact and also from the behavior of 1-AS and 2-AS in  $\text{H}_2\text{O}$ -ACN mixed solvents, it appears that the enhancement of fluorescence yield is in some way associated with loss in vibrational fine structure. The slope of Kosower type plot decreases in the order 1-AS  $\gg$  1,8-AS  $\approx$  2-AS  $\gg$  1,5-AS  $\approx$  A. (Figure 3) anthracene (A) and 1,5-anthracene (1,5-AS) have zero slope. The development of dipole moment in the excited state is evident for the other three compounds. Since the spectral effects are not concentration dependent, the possibility of intramolecular charge transfer in the excited state from the  $\pi$ -electronic ring system of anthracene moiety to the sulfonic acid group (or the other way round) may be considered. The dipole direction appears to be along the short axis, since 1,5-AS with a center of symmetry behaves similar to anthracene, whereas 1,8-AS develops a dipole moment in the excited state.

A tentative explanation, for most of the observations, may be put forward as follows. The sulfonic acid group undergoes some kind of intramolecular bonding interaction with the excited electronic system of the ring. Such a complex has been recently reported by Lippert<sup>14</sup> for 9-methoxy-10-phenanthrene carboxanil. This kind of interaction will be geometry dependent. The geometry seems to be ideal for 1-AS but not so good for 2-AS. For 1,8-AS, steric distortion due to bulky substituents with a negative charge will prevent

internal complex formation. Such distortion is actually responsible for the low extinction value of this compound. If a donor-acceptor type complex, with  $-\text{SO}_3^-$  group as the acceptor, is considered, the absence of polarity of 1,5-compound can be accounted for. This mechanism also admits of an isoemissive point and enhanced emission intensity. The internal charge-transfer complex so obtained will be a function of the solvent polarity in the immediate neighborhood of the molecule. The nonconformity for the solvent formamide and the absence of any change on addition of urea suggests that the density of the hydroxyl groups may also have some part to play. A study at low temperatures may throw more light on the problem.

*Acknowledgment.* Helpful comments by Professor B. Stevens, University of S. Florida, Tampa are acknowledged. The financial assistance provided by the Council of Scientific and Industrial Research, India, for this work and maintenance grant to one of us (B. P. S.) are also gratefully acknowledged.

(12) A. Bryson, *Trans. Faraday Soc.*, **47**, 528 (1951).

(13) Th. Förster and K. Rokos, *Chem. Phys. Lett.*, **1**, 279 (1967).

(14) J. Muszik, Ph.D. Thesis, Stuttgart, 1966.

### Correlation between Translational and Rotational Relaxation Times for Ion Pairs in Solution

by Govind S. Darbari and Sergio Petrucci\*

*Department of Chemistry, Polytechnic Institute of Brooklyn, New York 11201 (Received July 20, 1970)*

*Publication costs borne completely by The Journal of Physical Chemistry*

We wish to report a correlation between two phenomena, the ultrasonic longitudinal relaxation and the dielectric orientational relaxation of ion pairs in electrolyte solutions.

Consider the ion pair process



This equilibrium can be studied by a perturbation method such as ultrasonic longitudinal relaxation. At sufficiently high frequencies the degree of freedom of translation for the formation and dissociation of the ion pair will be frozen out and the system will relax.

According to Eigen<sup>1</sup> the relaxation time is related to the forward and reverse rate constants by

(1) M. Eigen and L. DeMaeyer in "Investigation of Rates and Mechanism of Reaction," A. Weissberger, Ed., Wiley, New York, N. Y., 1963.

$$\tau_L^{-1} = k_f\theta + k_R \quad (\text{II})$$

where  $\tau_L$  is the longitudinal ultrasonic relaxation time

$$\theta = \alpha c \gamma^2 \pm \left( 2 + \frac{\partial \ln \gamma_{\pm}^2}{\partial \ln \alpha} \right)$$

$\alpha$  is the degree of dissociation, and  $\gamma_{\pm}$  is the mean activity coefficient of the electrolyte. If the forward process is diffusion controlled its rate constant may be calculated by the Smoluchowski-Debye<sup>2</sup> formula modified<sup>3</sup> by the introduction of the Stokes-Einstein relation

$$k_f = \frac{SNkT}{3000\eta} \left( \frac{-b}{e^{-b} - 1} \right) \quad (\text{III})$$

where  $N$  is the Avogadro number,  $k$  the Boltzmann constant,  $\eta$  the solvent viscosity,  $b$  the Bjerrum parameter

$$b = \frac{|Z_A Z_B| e^2}{a D k T} \quad (\text{IV})$$

$Z_A$  and  $Z_B$  the ionic charges,  $e$  the electronic charge,  $D$  the dielectric constant of the solvent, and  $a$  the distance of approach of the two ions in the ion pair. Then

$$\tau_L^{-1} = \frac{SNkT}{3000} \left[ \frac{b}{1 - e^{-b}} \right] \left( \theta + \frac{1}{K(\Lambda)} \right) \frac{1}{\eta} \quad (\text{V})$$

where  $K(\Lambda)$  is the association constant for ion pair formation, determined for instance by conductance measurements ( $K(\Lambda) = k_f/k_R$ ). On the other hand, the dielectric relaxation time associated with the dipolar orientation of the ion pair is given by the Debye relation<sup>4</sup>

$$\tau_D = \frac{4\pi a^3}{kT} \eta \quad (\text{VI})$$

Introducing (IV) and (VI) into (V), and neglecting  $e^{-b}$  in comparison to 1 gives

$$\tau_L^{-1} = \frac{32\pi N a^3}{3000} \frac{|Z_A Z_B| e^2}{D k T} \left[ \theta + \frac{1}{K(\Lambda)} \right] \tau_D^{-1} \quad (\text{VII})$$

In the above, it is assumed that the ions' center to center distance  $a$  (according to the Debye-Hückel definition of contact distance of the two spheres of radius  $a/2$ ) is equal to the radius of the dipole taken as a sphere.

We may test eq VII by applying it to a case where both  $\tau_L$  and  $\tau_D$  have been reported, namely, the system  $\text{Bu}_4\text{NBr}$  in acetone at 25°. Ultrasonic measurements<sup>5</sup> were interpreted in terms of diffusion-controlled ion pair formation. Dielectric relaxation data<sup>6</sup> were interpreted in terms of dipolar orientation of the ion pairs. Since both the ionic translation for ion pair formation and dipolar orientation are presumed to be opposed in this case by the activation energy barrier for viscous flow, eq VII should be applicable.

Using  $K(\Lambda) = 264 M^{-1}$  from conductance data<sup>7</sup> an

estimation of the distance of approach of ions can be made through the Fuoss formula,<sup>8</sup>  $K_A = K(\Lambda) = (4\pi N a^3/3000)e^b$ . This gives  $a = 3.41 \text{ \AA}$ . [It is believed<sup>9</sup> that the  $a$  value obtained from the  $J$  parameter of the conductance equation ( $a_J = 5 \text{ \AA}$ ) is less reliable, since the  $J_2 c^{3/2}$  term was not considered in the analysis and its neglect may affect the determination of  $J$ .]

With the above parameters, using  $D = 20.7$ ,  $\eta = 0.00302 \text{ P}$ , the determined  $\tau_D = 0.77 \times 10^{-10} \text{ sec}$ ,<sup>6</sup> and calculating  $\theta = 3.9 \times 10^{-3} M$ , for  $c = 0.05 M$ , one can obtain from eq VII  $\tau_L = 1.6 \times 10^{-9} \text{ sec}$ . The ultrasonic experimental value,  $\tau_L(\text{exp})$ , is  $2.0 \times 10^{-9} \text{ sec}$ . On the other hand, by retaining  $a_J = a = 5.0 \text{ \AA}$ ,  $\theta$  becomes  $5.7 \times 10^{-3} M$  for  $c = 0.05 M$ , and the calculated value of  $\tau_L$  becomes  $0.5 \times 10^{-9} \text{ sec}$ .

The agreement between these two results is rather good considering the approximations involved in the Debye relation,<sup>10</sup> in the Smoluchowski-Debye relation,<sup>5</sup> and in the evaluation of  $\theta$  (as pointed out elsewhere<sup>5</sup>).

The above results, while reinforcing the interpretation based on ionic association of our previous ultrasonic work,<sup>5</sup> more generally indicate an interesting correlation between the relaxation times of two molecular motions, valid when the common energy barrier is the one for viscous flow.

(2) M. von Smoluchowski, *Z. Phys. Chem. (Frankfurt am Main)*, **92**, 179 (1917); P. Debye, *Trans. Electrochem. Soc.*, **82**, 265 (1942).

(3) S. Petrucci, *J. Phys. Chem.*, **71**, 1174 (1967).

(4) P. Debye, "Polar Molecules," Chemical Catalog, New York, N. Y., 1929, Chapter V.

(5) G. S. Darbari and S. Petrucci, *J. Phys. Chem.*, **74**, 268 (1970).

(6) E. A. S. Cavell, *Trans. Faraday Soc.*, **61**, 1578 (1965).

(7) M. B. Reynolds and C. A. Kraus, *J. Amer. Chem. Soc.*, **70**, 1709 (1948); M. J. McDowell and C. A. Kraus, *ibid.*, **73**, 3293 (1951).

(8) R. M. Fuoss, *ibid.*, **80**, 5059 (1958).

(9) J. C. Justice, *J. Chim. Phys.*, **65**, 353 (1968); R. M. Fuoss and K. L. Hsia, *Proc. Nat. Acad. Sci.*, **57**, 1550 (1966); **58**, 1818 (1967).

(10) C. P. Smyth, "Dielectric Constant and Structure," McGraw-Hill, New York, N. Y., 1955, Chapter 11.

## Axial Coordination in the Vanadyl Ion

by Amos J. Leffler

*Department of Chemistry, Villanova University, Villanova, Pennsylvania 19085 (Received September 17, 1970)*

*Publication costs assisted by Villanova University*

The nature of the aqueous solvation sheath around the vanadyl ion has been the subject of considerable recent investigation.<sup>1-4</sup> It has been shown conclusively

(1) R. Hausser and G. Laukien, *Z. Phys.*, **153**, 394 (1959).

(2) R. K. Mazitov and A. I. Rivkind, *Dokl. Akad. Nauk SSSR*, **166**, 654 (1966).

(3) J. Reuben and D. Fiat, *Inorg. Chem.*, **6**, 579 (1967).

that below ambient temperature the four equatorial water molecules are comparatively tightly bound. However, it is uncertain whether  $^1\text{H}$  and  $^{17}\text{O}$  shift and relaxation effects in the bulk solution are due to weak coordination in the axial position opposite the vanadyl oxygen or on the four faces of the pyramid formed by  $\text{VO}^{2+}$  and the four more tightly bound equatorial water molecules. The purpose of this note is to describe the application of a recently reported technique<sup>5</sup> for the study of the second coordination sphere to this problem.

In the earlier work it was found that methylene chloride dissolved in deuterium oxide did not enter the first coordination sphere of hexaquo metal ions. Proton peak broadenings were due to dipolar coupling between the unpaired electrons and the protons, and only bulk susceptibility shifts were observed. From the data an estimated distance of approach of the methylene chloride to the metal ion of 0.354 nm was found. In the present work the peak broadenings of methylene chloride and  $\text{H}_2\text{O}$  were measured in a 0.115 *M* solution of  $\text{VOSO}_4 \cdot 2\text{H}_2\text{O}$  dissolved in deuterium oxide between 4 and 32°. Using the second coordination sphere distance measured earlier and assuming the axial proton distance of 0.314 nm estimated in ref 4, values of the correlation times were calculated assuming dipolar coupling. The values of  $T_{2M}$  were calculated from the relation

$$\frac{1}{T_2} = \frac{N_{\text{CH}_2\text{Cl}_2} \cdot n \cdot [\text{VO}^{2+}]}{N_{\text{D}_2\text{O}} + N_{\text{CH}_2\text{Cl}_2}} \frac{1}{T_{2M}} \quad (1)$$

where the  $N$  values are the numbers of moles of each substance present and  $n$  is the number of positions of each type. The values of  $N_{\text{CH}_2\text{Cl}_2}$  were those determined earlier<sup>5</sup> while  $N_{\text{D}_2\text{O}}$  was corrected from pure deuterium oxide for the amounts of vanadyl sulfate and methylene chloride present. Values of  $n$  were taken to be 1 for the axial position and 4 for second coordination sites as in ref 4. The values of  $T_2$  were those measured by peak broadenings corrected for the broadening observed in pure deuterium oxide. Using the calculated values of  $T_{2M}$  the correlation times were calculated from the equation

$$\frac{1}{T_{2M}} = \frac{4}{3} \frac{S(S+1)g^2\beta^2g_N^2\beta_N^2\tau_c}{\hbar^2\tau^6} \quad (2)$$

where the terms have their usual meanings. These are shown in Table I.

**Table I:** Calculated Correlation Times of Methylene Chloride As a Function of Temperature in Seconds<sup>a</sup>

Temp, °C	Axial	Second coord sphere
4	3.82	1.38
10	3.89	1.43
18	3.51	1.27
32	2.21	0.80

<sup>a</sup> All values are  $\times 10^{-10}$  sec.

All of the correlation time values are within a factor of 3 of each other and therefore they do not serve to indicate the site of relaxation in themselves. A comparison with the correlation times of hexaquo metal ions measured earlier<sup>5</sup> shows that the present second coordination sphere values are approximately an order of magnitude greater. Since there appears to be no reason to expect methylene chloride molecules in the second coordination sphere to behave differently in the presence of vanadyl ion compared with other species, the results tend to rule out second coordination sphere sites as important in the peak broadening mechanism.

Based on the present measurements the axial position is open to both bulk water and methylene chloride molecules. The calculated axial correlation time values are a function of the chosen distance of approach of the proton to the vanadium ion, and the latter value is undoubtedly too great. A similar conclusion was reached in the earlier work where second coordination sphere distance of 0.383 nm was estimated for the V-H distance for water. We can estimate an axial V-H distance for methylene chloride by assuming a correlation time of  $2 \times 10^{-11}$  sec found in the earlier work. The value is 0.208 nm, which is unreasonably short on geometrical grounds. Therefore the true correlation time must be between the two values, and it can be inferred that some type of interaction occurs between the vanadyl ion and methylene chloride. A possible mechanism is a dipolar interaction between the vanadium and chloride atoms. This would have the proper temperature dependence since the thermal motion of the molecules would increase with increasing temperature resulting in shortened correlation times.

(4) K. Wüthrich and R. E. Connick, *Inorg. Chem.*, **6**, 583 (1967); **7**, 1377 (1968).

(5) A. J. Leffler, *J. Phys. Chem.*, **74**, 2810 (1970).

# COMMUNICATIONS TO THE EDITOR

## Scavenging of the Molecular Hydrogen Yield from Water Irradiated with Tritium $\beta$ Particles<sup>1</sup>

Publication costs assisted by Department of Environmental Sciences, Rutgers University

*Sir:* It is well established that the yield of molecular products,  $H_2$  and  $H_2O_2$ , from  $\gamma$ -irradiated aqueous solutions is lowered in the presence of certain reactive scavengers.<sup>2</sup> This effect is usually attributed to reactions of the scavenger with free radical precursors of the molecular product within the "spur." Recently,<sup>3</sup> it has been suggested on theoretical grounds that a major fraction of the energy deposited in water by low-energy electrons gives rise to "short tracks" rather than spurs. In an attempt to distinguish experimentally the properties of spurs and short tracks, we have measured the scavengeability by copper ions of the molecular  $H_2$  yield produced by tritium  $\beta$  radiolysis (average energy of tritium  $\beta = 5.69$  keV). We find that this molecular  $H_2$  yield is significantly less scavengeable than that produced by  $^{60}Co$   $\gamma$  radiolysis.

Solutions containing approximately 40 mCi ml<sup>-1</sup> of tritiated water were used. The water was purified by standard techniques involving multiple distillation,  $\gamma$  irradiation, and uv photolysis.<sup>2</sup> The solutions all contained 10<sup>-3</sup> M KBr as OH scavenger and were deoxygenated by bubbling with argon. In dilute bromide solutions the measured yield of hydrogen  $G(H_2)$  is equal to the molecular yield  $G_{H_2}$  ( $G =$  molecules produced per 100 eV). Hydrogen evolved was analyzed by sweeping out with argon into a gas chromatograph.<sup>4</sup> In order to obtain efficient sweeping action, a wetting agent (10<sup>-4</sup> M tertiary butyl alcohol) was used which was found to be without effect on the hydrogen yields from  $\gamma$ -irradiated  $CuSO_4$  solution.  $Cu^{2+}$  reacts sufficiently rapidly with hydrogen atoms<sup>5</sup> so that the lowest concentration used (10<sup>-4</sup> M) is enough to prevent the formation of additional  $H_2$  through hydrogen abstraction from the alcohol. After each analysis, accumulated hydrogen peroxide was removed by uv photolysis and the oxygen which was evolved was swept out with argon. The solution was then left to accumulate hydrogen for a further period. In this way the solution was exposed for times ranging from 5 to 18 hr (2550 to 9200 rads) and a plot of hydrogen evolved as a function of dose was obtained at each  $CuSO_4$  concentration. The plots, each consisting of at least five points, were all linear with dose and passed through the origin. Dosimetry was by calculation from the specific activity of

the tritiated water used, as measured by serial dilutions and liquid scintillation counting.

The results are shown in Figure 1 where the ordinate is the ratio of the observed  $G_{H_2}$  to  $G_{H_2}^0$  (the extrapolated value at zero  $Cu^{2+}$  concentration, 0.575). Figure 1 also shows the same ratio for  $^{60}Co$   $\gamma$ -irradiated solutions containing  $Cu^{2+}$ .<sup>6</sup> The cube root of the  $Cu^{2+}$  con-

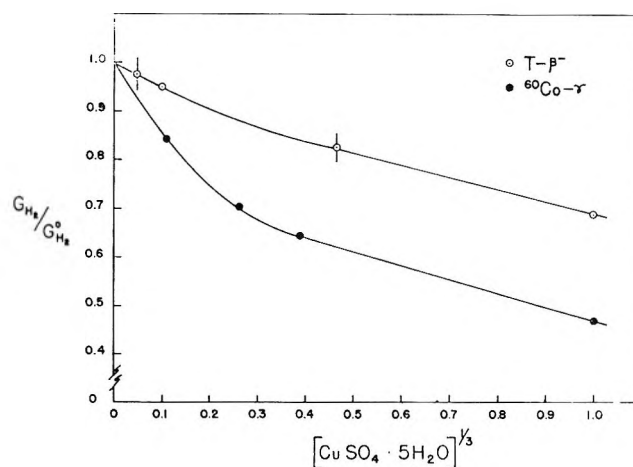
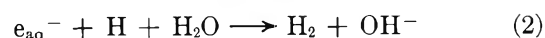
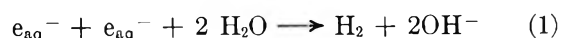


Figure 1. Decrease in  $G_{H_2}/G_{H_2}^0$  with concentration of copper sulfate:  $\circ$ , tritium  $\beta$  radiolysis;  $\bullet$ ,  $\gamma$  radiolysis, ref 6.

centration is used for the abscissa to spread the data. A distinct quantitative difference is apparent in the efficiency with which copper ions scavenge the molecular hydrogen yield produced by tritium  $\beta$  radiolysis as compared with cobalt  $\gamma$  radiolysis.

Three spur processes are important in hydrogen formation. They are



together with an initial molecular yield of  $H_2$ .<sup>7</sup> At pH

(1) Paper of the Journal Series, New Jersey Agricultural Experiment Station. Rutgers—The State University of New Jersey, Department of Environmental Sciences, New Brunswick, N. J.

(2) See, e.g., A. O. Allen, "The Radiation Chemistry of Water and Aqueous Solutions," Van Nostrand, New York, N. Y., 1961.

(3) A. Mozumder and J. L. Magee, *Radiat. Res.*, **28**, 203 (1966).

(4) J. W. Swinnerton, V. J. Linnenbom, and C. H. Cheek, *Anal. Chem.*, **34**, 483 (1962).

(5) M. Anbar and P. Neta, *Int. J. Appl. Radiat. Isotop.*, **18**, 493 (1967).

(6) H. A. Schwarz, *J. Amer. Chem. Soc.*, **77**, 4960 (1955).

(7) H. A. Schwarz, *J. Phys. Chem.*, **73**, 1928 (1969).

7, the relative contributions to the total molecular hydrogen yield of these four processes have been calculated to be, respectively, 31.6%, 29.7%, 3.9%, and 34.8%.<sup>7</sup> It is possible that the large difference in scavengeability of the molecular H<sub>2</sub> yield when it originates from radiations giving predominantly short tracks rather than spurs is due to a change in the relative importance of these four processes, and hence a change in the nature of the major precursor. It is noteworthy that our data can be brought into coincidence with the  $\gamma$ -ray data if a constant normalizing factor of 0.02 is applied to the Cu<sup>2+</sup> concentration even though this varies over four orders of magnitude. The value of 0.02 is very close to the relative reactivities of Cu<sup>2+</sup> with hydrogen atoms and with electrons.<sup>5</sup>

An increased contribution of spur reactions involving H atoms has been suggested to explain the observed low yield of H atoms at high LET;<sup>8</sup> our results, if explicable on the same basis, would lend support to a picture of tritium  $\beta$  radiolysis in terms of short tracks of high local LET. Further work is in progress to establish the generality of the effect reported here.

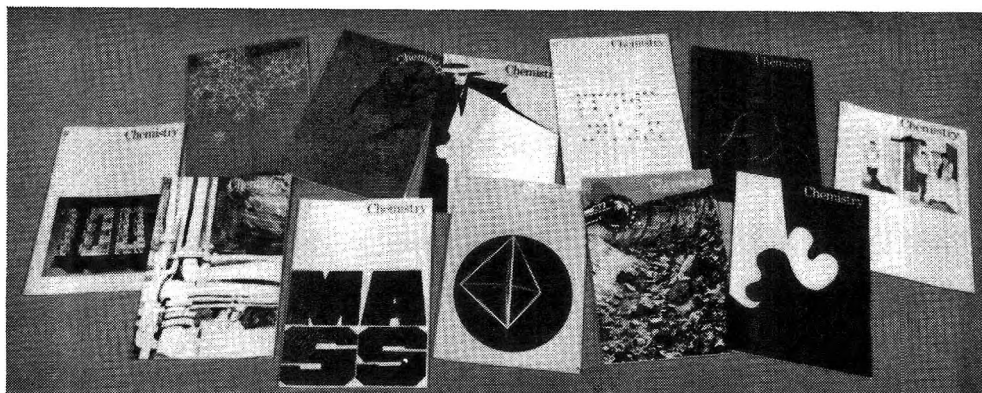
(8) A. Appleby and H. A. Schwarz, *J. Phys. Chem.*, **73**, 1937 (1969).

DEPARTMENT OF ENVIRONMENTAL SCIENCES  
RUTGERS—THE STATE UNIVERSITY  
NEW BRUNSWICK, NEW JERSEY 08903

A. APPLEBY\*  
W. F. GAGNON

RECEIVED OCTOBER 19, 1970

Designed for  
the potential  
scientist  
in your  
family . . .



**Chemistry** magazine—for the high school or college student whose curiosity of chemistry extends *beyond* required course work.

Eleven issues a year, including a special Summer issue, bring the reader

- experimental projects and investigations
- news items on recent research developments
- feature articles on theoretical and applied science
- book reviews
- chemical puzzles
- reader's column.

All adding up to an exciting opportunity to see chemistry in *action*—out of the textbook and in the real laboratory!

Each issue of *Chemistry* is as broad as the science itself. It delves into the past . . . reports the present . . . relates to the future.

Below is a sample of the interesting and timely articles offered in *Chemistry* . . .

"Why Should Anyone Study Chemistry" . . .  
 "The DDT Story" . . . "Conformational Analysis or How Some Molecules Wiggle" . . .  
 "Chemistry in Language and Literature" . . . "The George Washington Carver Story" . . .  
 "Schizophrenia—the Body's Chemical Mistake"

Each issue of *Chemistry* is unusual in its attractiveness and diversity of subject matter. The student can enter through many doors with a choice of reading from the rather general to the relatively technical, all informative . . . entertaining . . . useful in academic work.

Order *Chemistry* now and start an exciting adventure for a young member in your family!

**American Chemical Society  
 Publications  
 1155 Sixteenth Street, N.W.  
 Washington, D.C. 20036**

Yes—start a subscription to *Chemistry* at the low yearly rate of \$6.

Canada, PUAS \$7.00\*  Foreign \$7.50\*

\* Payment must be made in U.S. currency, by international money order, UNESCO coupons, or U.S. bank draft, or order through your book dealer.

Send *Chemistry* to:

Name \_\_\_\_\_

Check enclosed (payable to American Chemical Society)

Address \_\_\_\_\_

Send bill to

City \_\_\_\_\_ State \_\_\_\_\_ Zip \_\_\_\_\_

Recipient is a  student  teacher.

Address \_\_\_\_\_

other \_\_\_\_\_

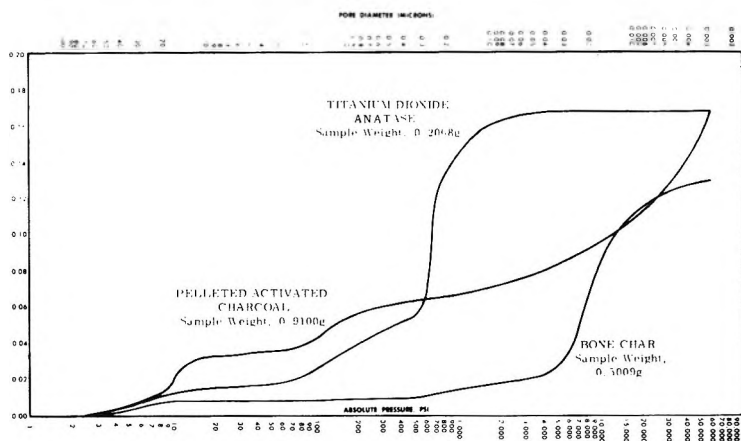
State \_\_\_\_\_ City \_\_\_\_\_ Zip \_\_\_\_\_

Only Aminco® Offers A Complete Line of Porosimeters

# MEASURE PORE VOLUME DISTRIBUTION AND PORE DIAMETERS FROM 1 mm to 30 Å IN LESS THAN 30 MINUTES

Only Aminco offers five models of Porosimeters: a 1.5 psi model for pore diameters from .011 mm to 1 mm; 5,000 psi for 350 Å to .180 mm; 15,000 psi for 120 Å to .180 mm; 30,000 psi for 60 Å to .180 mm; and 60,000 psi for 30 Å to .180 mm. All operate on the mercury intrusion principle and feature: ■ Completely hydraulic operation for maximum safety ■ Rupture discs to prevent excessive pressurization. ■ A unique filling device that permits vacuum preconditioning and sub-atmospheric measurements of a second sample while the first is being pressurized and tested, thus making possible an increased number of analyses per day. ■ Real density determination obtained simultaneously. ■ Isostatic pressing capability in the 60,000 psi model.

Penetrometers supplied with each instrument will accommodate solid or powder samples up to 6 cc (standard), to 1.5 cc, or to 35 cc (optional).



Typical pore analyses performed with Aminco Porosimeter



AMERICAN INSTRUMENT COMPANY  
DIVISION OF TRAVENOL LABORATORIES, INC.  
Silver Spring, Maryland 20910

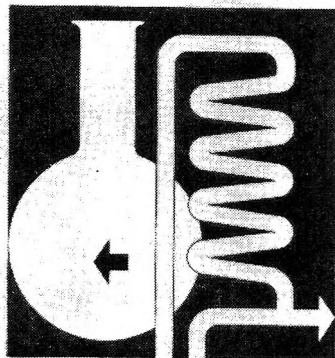


For details on Aminco Porosimeters,  
send for Portfolio RD2.

## ISOTOPE EFFECTS IN CHEMICAL PROCESSES

ADVANCES IN CHEMISTRY SERIES NO. 89

### Isotope Effects in Chemical Processes



ADVANCES IN CHEMISTRY SERIES 89

Thirteen papers from a symposium by the Division of Nuclear Chemistry and Technology of the American Chemical Society, chaired by William Spindel. Includes:

- Separating isotopes by chemical exchange, distillation, gas chromatography, electromigration, and photochemical processes
- Methods for fractionating isotopes of hydrogen, lithium, boron, carbon, and nitrogen
- Thermotransport in monatomic and ionic liquids
- Statistical-mechanical theory determining isotope effects

278 pages with index

Clothbound

(1969)

\$13.00

Postpaid in U.S. and Canada; plus 30 cents elsewhere.

Free set of L. C. cards with library orders upon request.

Order from:

SPECIAL ISSUES SALES  
AMERICAN CHEMICAL SOCIETY  
1155 SIXTEENTH ST., N.W.  
WASHINGTON, D.C. 20036